

Electrokinetics and Iron Precipitation for Ground Engineering and Metal Removal

David W. S. Faulkner

*Thesis Submitted In Partial Fulfilment of the Requirements of the
University of Brighton, for the Degree of
Doctor of Philosophy*

2010

The University of Brighton

Abstract

Passing an electric current through a wet mass of soil results in the net movement of pore water, and charged species in solution, whose direction of movement is controlled by the polarisation of the electrodes, and the charge on the dissolved species. The use of electric fields for the movement of soil components is termed electrokinetics.

The research presented here is concerned with the electrokinetic remediation of contaminants through the harnessing of electrochemically induced dissolution of iron-rich electrodes. The addition of iron compounds from the dissolving electrodes aids in the strategic precipitation of any contaminants and in fixing them in place in a stable form. This method was conceived at the universities of Brighton and Sussex and termed FIRS: Ferric Iron Remediation and Stabilisation. In addition to the remediation of contaminated soils, the addition and subsequent precipitation of iron is investigated for the improvement of the strength and for the modification of the soil's hydraulic properties.

This research is a development of the ideas presented by Cundy and Hopkinson, increasing the scale of previous experiments, designing new electrode arrays and presenting new data on metal mobility and the effects of hydraulic gradients. This thesis shows the response of a number of metal species to the treatment is significant and the process has shown to be useful for the isolation of arsenic in sediments and some other elements on scales of 0.5 m in estuarine sediment. The use of the technique for the stabilisation of unconsolidated sands is demonstrated as is its use for the reduction of the hydraulic permeabilities of quartz sand, loamy top-soil and estuarine sediment.

This work represents a contribution to the body knowledge through the successful use of novel electrode design and arrangement for the creation of a number of precipitated iron geometries including a horizontal iron-pan and presents results on the use of the technique for the mobilisation of metal species in estuarine sediment in both static groundwater conditions and under an imposed hydraulic gradient.

DWSF 2010

Declaration

I declare that the research contained in this thesis, unless otherwise formally indicated within the text, is the original work of the author. This thesis has not been previously submitted to this or any other university for a degree, and does not incorporate any material already submitted for a degree.

Signed

Date

Contents

Abstract	i
Index of Figures	viii
Index of Tables.....	xix
Dedication and Acknowledgements.....	xxi
1 Introduction	1
1.1 Rationale	1
1.2 Overview	4
1.3 Contaminated Land	7
1.4 Contaminated Land Management	9
1.5 Electrokinetic Approaches	17
1.6 Scope of Thesis	19
1.7 Aims and Objectives	20
1.8 Organisation of Thesis	22
2 Literature Review	23
2.1 Electrokinetics: Early Work	23
2.2 Electrokinetic Approaches	26
2.3 Electrokinetics: An Overview	27
2.4 Applications of Electrokinetics	30
2.5 Electroosmosis	36
2.5.1 Helmholtz Model	40
2.5.2 Helmholtz-Smoluchowski Equation:	41
2.6 Electrokinetics: The Soil/Solution Interface	44
2.6.1 Soil Chemistry and Composition	45
2.6.2 Zeta Potential	53
2.6.3 Gouy-Chapman Electrical Double Layer Model	54
2.6.4 The Stern Model.....	54
2.6.5 Electromigration.....	57
2.6.6 Cation Exchange Capacity	58
2.6.7 Joule Heating.....	60
2.7 Environmental Analogies.....	61
2.8 Electrokinetic Stabilisation	62
2.8.1 Electrokinetics and Barriers	63

2.9	Iron Electrochemistry and the FIRS Process	65
2.9.1	The FIRS Process	67
2.10	Economic Considerations.....	72
2.11	Electrode Arrangement Considerations	74
2.12	Electrode Composition Considerations.....	75
3	Precipitates as Barriers	79
3.1	Predetermined Geometry of Precipitates	80
3.1.1	Creation of Barriers.....	80
3.2	Investigative Outline	83
3.3	Voltage Experiments.....	83
3.3.1	Role of Applied Voltage	83
3.3.2	Discussion	85
3.4	Horizontal Barrier Experiment.....	87
3.5	Method	87
3.5.1	Horizontal Barrier Results.....	88
3.5.2	Resealing the Iron-rich Barrier.....	90
3.5.3	Iron-rich Barrier Analysis	92
3.5.4	Iron-rich Barrier Mineralogy.....	92
3.5.5	Geotechnical Characteristics	94
3.6	Bowl Experiment	95
3.6.1	Method	97
3.6.2	Discussion	99
3.7	Grid Experiment.....	100
3.7.1	Method	102
3.7.2	Results	103
3.7.3	Horizontal Barrier Experiment.....	104
3.7.4	Discussion	105
4	Barrier Formation Against an Imposed Hydraulic Gradient	108
4.1	Introduction	108
4.2	Experiment Design.....	109
4.3	Theoretical Considerations.....	111
4.4	Method	113
4.5	Results: Quartz Sand Experiment	114
4.5.1	Screened Topsoil Experiments.....	121

4.5.2	Estuarine Sediment Experiment	123
4.6	Discussion	126
4.7	Conclusions	129
5	The FIRS Process for Metals Mobilisation	132
5.1	Overview	133
5.1.1	Soils and Sediments: Composition and Physicochemical Concepts	135
5.1.2	Remediation Experiments	136
5.2	Estuarine Sediment Experiments	137
5.3	Method	138
5.3.1	pH Measurements.....	143
5.3.2	Sampling	143
5.3.3	XRF Analysis	144
5.3.4	XRD Analysis	145
5.3.5	Uncertainty and Error.....	145
5.3.6	Acetic Acid versus Tap Water Influent.....	152
5.4	Results	153
5.4.1	Physical and Mineralogical Characteristics of Starting Material.....	153
5.4.2	Electrical Current Measurements	156
5.4.3	Estuarine Sediment Metals Analysis.....	157
5.4.4	Iron Mineralised Region and Associated Elements.	158
5.4.5	Arsenic	160
5.4.6	Bromine.....	163
5.4.7	Calcium	165
5.4.8	Strontium.....	167
5.4.9	Cobalt	170
5.4.10	Manganese.....	172
5.4.11	Copper	174
5.4.12	Zinc	178
5.4.13	Vanadium	180
5.4.14	Zirconium.....	181
5.4.15	Titanium	183
5.5	Discussion	184
5.6	Metals Analysis for Estuarine Sediment Subjected to a Hydraulic Gradient.	191

5.6.1	Iron Data Hydraulic Head Experiment	192
5.6.2	Arsenic Hydraulic Head Experiment	193
5.6.3	Bromine Hydraulic Head Experiment.....	195
5.6.4	Calcium Hydraulic Head Experiment	196
5.6.5	Strontium Hydraulic Head Experiment.....	197
5.6.6	Cobalt Hydraulic Head Experiment	198
5.6.7	Manganese Hydraulic Head Experiment	199
5.6.8	Copper Hydraulic Head Experiment.....	200
5.6.9	Zinc Hydraulic Head Experiment	201
5.6.10	Vanadium Hydraulic Head Experiment	202
5.6.11	Zirconium Hydraulic Head Experiment.....	203
5.6.12	Titanium Hydraulic Head Experiment.....	204
5.7	Comparison of Applied Hydraulic Head and Static and Static Head Experiments with Tap Water Influent on Estuarine Sediment	205
5.7.1	Iron	207
5.7.2	Arsenic	207
5.7.3	Bromine.....	208
5.7.4	Calcium	209
5.7.5	Strontium.....	210
5.7.6	Cobalt	212
5.7.7	Manganese.....	213
5.7.8	Copper.....	214
5.7.9	Zinc	215
5.7.10	Vanadium	216
5.7.11	Zirconium.....	217
5.7.12	Titanium	218
5.8	Metal Mobilisation Discussion and Conclusions.....	219
6	Discussion.....	221
6.1	Limitations and Scope.....	221
6.1.1	Analysis.....	226
6.1.2	Stabilisation.....	227
6.2	Further Work	228
7	Conclusions	237
8	References and Bibliography.....	242

9	Appendix 1	259
10	Appendix 2- Experimental Data.....	278

Index of Figures

Figure 1: Flow chart showing the possible fates and accumulation sites of an inorganic ground pollutant (Adapted from, Alloway and Ayres, 1997)	3
Figure 2: Environment Agency UK flow chart describing the decision making process for the implementation of contaminated land management.....	16
Figure 3: Diagrammatic representation of electrokinetic phenomena achieved experimentally.....	24
Figure 4: Graphical representation of the charge distribution on and around a clay surface The edge of the slip plane is located at the edge of the Stern layer furthest from the clay surface (diagram adapted from, Mitchell and Soga, 2005)	40
Figure 5: Helmholtz-Smoluchowski model for electroosmosis in a capillary showing flow distribution (adapted from, Mitchell, 1976; and, Mohamed and Antia, 1998).	43
Figure 6: Relative proportions of soil components by volume. These may vary widely but generally lie within the ranges indicated (White, 2006).	47
Figure 7: Soil colloids grouped on the basis of their charge characteristics. 2:1 clay minerals have both a permanent and a variable charge, whereas 1:1 clay minerals, humus and oxides of iron and aluminium have a (pH influenced) variable charge (taken from, Ashman and Puri, 2002).	49
Figure 8: An illustration of material ion sorption reactions on a (hydr)oxide particle. (a) At low surface coverage, isolated site binding (adsorption) is the dominant sorption mechanism; (b) with increased metal loading, M hydroxide nucleation begins. Further increases in metal loadings results in (c) surface precipitation or (d) surface clusters (Fendorf, 1992).	52
Figure 9: Electrical potential distribution on a clay particle surface. The distance delta defines the Stern layer characterised by a linear reduction in potential, typically δ will have a value $\geq 10\text{nm}$ (e.g. Masliyah and Bhattacharjee, 2006).	55
Figure 10: Charge distribution around a colloid particle showing the named layers.....	56
Figure 11: Comparison of the net negative surface charge of soils as determined by potentiometric titration using point of zero salt effect (PZSE), with that	

calculated by Gouy–Chapman and Stern theories (taken from, Sparks, 1995).	57
Figure 12: Graphical representation of the relationship between the voltage and current in terms of electrokinetics and joule heating (adapted from, Pamukcu, 2005).	60
Figure 13: The principle electrochemical reactions and processes taking place during FIRS treatment. The electrolysis of water takes place at the electrodes, the oxidation of the iron from the anode electrode releases Fe^{2+} into solution, and the electromigration of charged species takes place as they are attracted to the electrode of opposite charge. M^+ represents a positively charged species (a metal ion for example) R^- represents a negatively charged species. Electroosmosis (not shown) occurs as the net movement of water towards the cathode.	68
Figure 14: Simple Iron speciation Eh pH diagram (Pourbaix diagram) at 25 degrees and 1atm pressure. The innermost dashed lines represent the oxidation/reduction limits for water, the outermost lines approximate for the ‘over voltage’ required for actual oxidation or reduction of water (Krauskopf, 1979).	70
Figure 15: The range of colours of iron present indicating the range of speciation determined by local small-scale variations in conditions.	71
Figure 16: Schematic showing an approximation of the field distribution for different linear electrode configurations for a constant area. Corrected and adapted from Alshawabkeh et al. (1999a).	75
Figure 17: Parallel linear electrode arrangement of the FIRS set up showing mechanism of precipitate formation (Taken from, Faulkner <i>et al.</i> , 2005).	79
Figure 18: simple voltage experiments conducted in sand with a seawater electrolyte conducted with different voltages to look at the effects of the voltage on the iron precipitate formed.	84
Figure 19: Relationship between applied voltage and measurement of visible portion of the iron-rich precipitate as measured through the transparent Perspex™ test cell.	84
Figure 20: Excavated iron-rich bands showing the size and shape of the precipitates formed.	86

Figure 21: Apparatus and experiment design schematic for the development of a horizontal iron-rich precipitate barrier (adapted from, Faulkner <i>et al.</i> , 2005). Top left shows the electrode arrangement and spacing. Top right shows the anode electrode design. Bottom left shows the electrodes in place in the sand medium. Bottom right shows the assembled apparatus with location of iron band formation.	88
Figure 22: Horizontal iron-rich band formed over 300h at 3V in quartz sand using sheathed anode electrodes and a surface mesh cathode electrode with a separation between electrodes of 20cm, (Faulkner <i>et al.</i> , 2005).....	89
Figure 23: Current values over the course of the iron-rich band formation with increase in current caused by deliberate point rupture of precipitate fabric, (Faulkner <i>et al.</i> , 2005) The arrows indicate the time at which the barrier was ruptured.	90
Figure 24: The iron-rich band, the top picture shows the band immediately after rupture is induced with a 4mm glass rod. The bottom picture shows the same region 24 hours later. The point rupture is shown to be blocked with freshly precipitated iron compounds, demonstrating the ‘self-healing’ process. The additional mineralisation either side of the rupture is due to ion migration (Taken from Faulkner et.al 2005).	91
Figure 25: XRD trace of the iron-rich barrier formed in quartz sand showing the composition of the mineralised region. C=calcite, Fe=elemental iron, G=goethite, K=k-feldspar, L= Lepidocrocite, M=maghemite and/magnetite, Mi = mica, P= plagioclase feldspar, Q= quartz (Faulkner <i>et al.</i> , 2005)	93
Figure 26: An excavated iron rich precipitate region. This was formed in high purity, unconsolidated quartz sand with sea water electrolyte, at 6 volts over a period of 16 days with an electrode separation of 15cm.....	94
Figure 27: Schematic diagram of a cross sectional view of conceptual electrode positioning in the 'bowl' experiment (not to scale). This diagram shows the postulated method of how to manipulate the geometry towards the formation of a bowl shaped continuous iron-rich barrier.	96
Figure 28: Revised experimental apparatus with both cathodes and anodes inserted at staggered depths to create the desired bowl shaped geometry. Dimensions are in millimetres.	97

Figure 29: Iron mineralisation in bowl experiment with the proposed formation location indicated in blue.	98
Figure 30: Experimental schematic for continuous grid stabilisation experiment. Viewed from above, the test cell consists of a Perspex tank 25 cm deep filled with the quartz sand to a depth of 15cm. The electrodes were connected to the power supply using standard domestic terminal blocks and the connection between them verified using a test meter to confirm continuity of the connections.....	102
Figure 31: Current change for the duration of the experiment to stabilise a continuous unconsolidated sand area using grid electrode array.	103
Figure 32: Mass stabilisation of a quartz sand using grid electrode arrangement, 50% sea water 50% fresh water electrolyte, diagram showing experimental set up and precipitate formation.....	104
Figure 33: Experimental set up for the generation of a constant hydraulic gradient across a test medium. The electrodes are at a separation of 45 cm with a maximum test material volume of 56350 cc. The anode electrodes are at the downstream end of the experiment since the electroosmotic effect and iron migration direction when the electric field is applied induces movement from anode to cathode. Note the flow is towards the anode electrode, contrary to the electroosmotic flow, which acts from anode to cathode.	110
Figure 34: Linear gravity flow distribution, sketch giving the definitions of the variables used to describe Dupuit's parabola and discharge (adapted from Raudkivi and Callander, 1976).	111
Figure 35: Theoretical water table height across test cell with an input head of 0.35 m and an output of 0.1 m also showing theoretical seepage velocity, calculated from empirical porosity and hydraulic conductivity measurements performed on quartz sand.....	115
Figure 36: Outflow measurements for quartz sand under a hydraulic gradient. The flow rate shows a significant drop over the first 10 days before stabilising at circa 140 ml/h.	116
Figure 37: Determination of Hydraulic conductivity from constant head test. Quartz sand.	117
Figure 38: Current measurements for quartz sand under a hydraulic gradient.....	118

Figure 39: Iron precipitation visible around and between the anode electrodes in the sand experiment excavated at the end of the experiment (furthest right anode electrode has been removed).	118
Figure 40: Loosely consolidated regions around the cathode electrodes extending in the direction of groundwater flow to form these 'fin' like protrusions (top). The structures had enough structural integrity to be removed from the test tank and retain their form (bottom). The electrodes are 35 cm long.	119
Figure 41: Volumetric flow rate measurements with time as measured at the out flow for loamy topsoil material. The voltage was dropped from 150 V to 75V after 48hours due to Joule heating. A trend line describing a power relationship has been included which might be expected from the relationship between the current flow and the precipitate formation.	121
Figure 42: This shows the increase in UCS of the loamy soil by region. Ten measurements were made across the surface of the test cell at the end of the experiment showing the significantly greater strength at the point of iron mineralisation. The cathode, anode and mid point areas gave considerably lower values.	122
Figure 43: Visual appearance of iron-rich precipitate forming close to the anode electrodes in loamy top soil.	122
Figure 44: Out flow measurements for estuarine sediment with time. The experiment was allowed to stabilise for four days with the electrodes inserted before the current was applied.....	123
Figure 45: Current with time showing the characteristic decay as seen in previous experiments. Day 9 the current was limited to a maximum of 3 Amps due to significant Joule heating of the material.	124
Figure 46: Precipitation of the iron-rich mineral phase in the Hythe sediment hydraulic head experiment with the region of iron enrichment highlighted in the bottom image.....	125
Figure 47: The location of the sample site from where the estuarine sediment was obtained. The sample site itself consisted of mud flats close to salt marsh (Aerial imagery from Google Earth™ and Microsoft™ Virtual Earth™ accessed June 2006).....	137

Figure 48: The experimental set up for the estuarine sediment experiments. The reservoir area is labelled ‘a’ the dashed line represents the mesh partition and the region labelled b is the sediment section.....	139
Figure 49: Example spectrum output for estuarine sediment analysis using minipal analysis software.....	145
Figure 50: Schematic of the balanced experimental design for the calculation of an estimate of the uncertainty for the sampling and analysis; the random error (Taken from, Ramsey, 2004).	146
Figure 51: Example regression analysis of measured against certified concentration for four different reference materials for the element Strontium. In this case the reference materials were GSS-3, GSS-4, GSS-6, and GSS-8. This is used to quantify the systematic error (bias) in the analysis.....	147
Figure 52: Textural classification (limiting percentage of sand silt and clay sized particles for the mineral texture class. The Hythe sediment was identified as ‘Silty clay loam’ as highlighted (Diagram adapted from, British Standards Institution, 1994).....	154
Figure 53: Particle size distribution for Hythe sediment sample as determined by laser particle size analysis.	155
Figure 54: Data output from XRD analysis of the mineral composition of estuarine sediment.....	155
Figure 55: Current measurements with time in the acetic and tap water experiments conducted on the Hythe sediment.....	156
Figure 56: Iron concentration across treated material in the experiments conducted with acetic acid and with tap water electrolyte. Error bars derived from table 19. Dashed line indicates the average starting concentration, from table 22.....	158
Figure 57: pH distributions measurements taken after day one of the experiment and at the end of the experiment for both the tap water and the acetic acid influent.	159
Figure 58: Arsenic concentration across treated material in the experiments conducted with acetic acid and with tap water electrolyte. Dashed line indicates the average starting concentration, table 22. Error bars derived from table 19.....	161

Figure 59: graph of the iron and arsenic concentration distributions in the acetic acid experiment.....	162
Figure 60: Bromine concentration across treated material in the experiments conducted with acetic acid and with tap water electrolyte. Dashed line indicates the average starting concentration, table 22. Error bars derived from table 19.....	164
Figure 61: Calcium concentration across treated material in the experiments conducted with acetic acid and with tap water electrolyte. Dashed line indicates the average starting concentration, table 22. Error bars derived from table 19.....	166
Figure 62: Strontium concentration across treated material in the experiments conducted with acetic acid and with tap water electrolyte. Dashed line indicates the average starting concentration, table 22. Error bars derived from table 19.....	168
Figure 63: Cobalt concentration across treated material in the experiments conducted with acetic acid and with tap water electrolyte. Dashed line indicates the average starting concentration, table 22. Error bars derived from table 19.....	170
Figure 64: Manganese concentration across treated material in the experiments conducted with acetic acid and with tap water electrolyte. Dashed line indicates the average starting concentration, table 22. Error bars derived from table 19.....	172
Figure 65: Mean iron and manganese plots for acetic acid influent experiment	173
Figure 66: Copper concentration across treated material in the experiments conducted with acetic acid and with tap water electrolyte. Dashed line indicates the average starting concentration, table 22. Error bars derived from table 19.....	175
Figure 67: Copper concentration in pore fluid of saline sediment after electrokinetic treatment with the application of 7 volts and an electrode separation of 19 cm, (Taken from, Altaee <i>et al.</i> , 2007).	177
Figure 68: Zinc concentration across treated material in the experiments conducted with acetic acid and with tap water electrolyte. Dashed line indicates the average starting concentration, table 22. Error bars derived from table 19.....	179

Figure 69: Vanadium concentration across treated material in the experiments conducted with acetic acid and with tap water electrolyte. Dashed line indicates the average starting concentration, table 22. Error bars derived from table 19.....	180
Figure 70: Zirconium concentration across treated material in the experiments conducted with acetic acid and with tap water electrolyte. Dashed line indicates the average starting concentration, table 22. Error bars derived from table 19.....	182
Figure 71: Titanium concentration across treated material in the experiments conducted with acetic acid and with tap water electrolyte. Dashed line indicates the average starting concentration, table 22. Error bars derived from table 19.....	183
Figure 72: Diagram showing the way the iron mineralised region's orientation can give a shift in maximum concentration values with distance from the anode, for elements associated with the iron mineralised zone, with a longitudinal sampling protocol. a, b, and c represent the bottom, middle and top portions of the treatment area respectively.	185
Figure 73: Combined graph of the concentration of Iron and cobalt across the cell with acetic acid influent.	186
Figure 74: Diagram to describe a theoretical geometry of the precipitated iron region which would give a concentration distribution similar to that shown for the iron and arsenic results.	187
Figure 75: manganese and iron tap water values for the mean of the three depths at each distance from the anode.	188
Figure 76: Arsenic and iron: tap water influent and the arsenic concentration for the top section of the treated material and the mean iron concentration. Data plotted on separate axes for concentration, and a shared axis for the distance from the anode.	189
Figure 77: Fe concentration distribution post-treatment in the hydraulic gradient experiment. Dashed line indicates the average starting concentration, table 22. Error bars derived from table 19.....	192
Figure 78: As concentration distribution post treatment in the hydraulic gradient experiment. Dashed line indicates the average starting concentration, table 22. Error bars derived from table 19.....	193

Figure 79: Arsenic and iron concentrations post experiment in the hydraulic head experiments.	194
Figure 80: Br concentration distribution post treatment in the hydraulic gradient experiment. Dashed line indicates the average starting concentration, table 22. Error bars derived from table 19.	195
Figure 81: Ca concentration distribution post treatment in the hydraulic gradient experiment. Dashed line indicates the average starting concentration, table 22. Error bars derived from table 19.	196
Figure 82: Sr concentration distribution post treatment in the hydraulic gradient experiment the dashed line indicates the mean pre-treatment concentration. Dashed line indicates the average starting concentration, table 22. Error bars derived from table 19.	197
Figure 83: Co concentration distribution post treatment in the hydraulic gradient experiment. Dashed line indicates the average starting concentration, table 22. Error bars derived from table 19.	198
Figure 84: Mn concentration distribution post treatment in the hydraulic gradient experiment. Dashed line indicates the average starting concentration, table 22. Error bars derived from table 19.	199
Figure 85: Cu concentration distribution post treatment in the hydraulic gradient experiment. Dashed line indicates the average starting concentration, table 22. Error bars derived from table 19.	200
Figure 86: Zn concentration distribution post treatment in the hydraulic gradient experiment. Dashed line indicates the average starting concentration, table 22. Error bars derived from table 19.	201
Figure 87: V concentration distribution post treatment in the hydraulic gradient experiment. Dashed line indicates the average starting concentration, table 22. Error bars derived from table 19.	202
Figure 88: Zr concentration distribution post treatment in the hydraulic gradient experiment. Dashed line indicates the average starting concentration, table 22. Error bars derived from table 19.	203
Figure 89: Ti concentration distribution post treatment in the hydraulic gradient experiment. Dashed line indicates the average starting concentration, table 22. Error bars derived from table 19.	204

Figure 90: Iron concentration across the hydraulic head and static tap water experiments. Dashed line indicates the mean starting concentration, table 22. Error bars derived from table 19.	207
Figure 91: Arsenic concentration across the hydraulic head and static tap water experiments. Dashed line indicates the mean starting concentration, table 22. Error bars derived from table 19.	208
Figure 92: Bromine distribution in experiments conducted with and without hydraulic head. The dashed line represents the mean starting concentration, table 22. Error bars derived from table 19.	209
Figure 93: Calcium distribution in experiments conducted with and without hydraulic head. Green dashed line indicates mean pre-treatment concentration, table 22. Error bars derived from table 19.	210
Figure 94: Strontium concentration across the hydraulic head and static tap water experiments. Dashed line indicates the mean starting concentration, table 22. Error bars derived from table 19.	211
Figure 95: Cobalt distribution in experiments conducted with and without hydraulic head. Green dashed line indicates mean pre-treatment concentration, table 22. Error bars derived from table 19.	212
Figure 96: Manganese distribution in experiments conducted with and without hydraulic head. Green dashed line indicates mean pre-treatment concentration, table 22. Error bars derived from table 19.	213
Figure 97: Copper distribution in experiments conducted with and without hydraulic head. Green dashed line indicates mean pre-treatment concentration, table 22. Error bars derived from table 19.	214
Figure 98: Zinc distribution in experiments conducted with and without hydraulic head. Green dashed line indicates mean pre-treatment concentration, table 22. Error bars derived from table 19.	215
Figure 99: distribution in experiments conducted with and without hydraulic head. Green dashed line indicates mean pre-treatment concentration, table 22. Error bars derived from table 19.	216
Figure 100: Zirconium distribution in experiments conducted with and without hydraulic head.	217

Figure 101: Titanium distribution in experiments conducted with and without hydraulic head. Green dashed line indicates mean pre-treatment concentration, table 22. Error bars derived from table 19.218

Figure 102: Cross section of a proposed composite electrode design. The solid black represents the inert portion, e.g. graphite. The circular iron portions are entirely enclosed within the inert portion except for a narrow extension to the exterior. This provides a limited surface area for the reaction of iron initially but a relatively large inert surface area; the available iron surface will increase when the narrow portions exposed to the exterior dissolve and expose the larger inner portions as the iron dissolves.....229

Figure 103: Proposed application of the point source electrode array.....232

Index of Tables

Table 1: Soil guideline values (SGVs) for some common contaminants. The threshold varies for different land uses. Concentrations are in mg kg ⁻¹ (DEFRA, 2002a, b, c, d, e, f, g) it should be noted that at the time of writing some of these values are under review as part of the on-going CLEA (Contaminated Land Exposure Assessment) program along with the addition of Health Criteria Values (HCVs) for the purpose of risk assessment of a contaminated site (Hopkins and Hosford, 2009a, b; Hopkins <i>et al.</i> , 2009; Watts and Hosford, 2009).	10
Table 2: Industrial sources of potential contamination (Adapted from Hester and Harrison, 2001)	12
Table 3: Some major environmental incidents in recent history due to hazardous chemicals (adapted from Rajeshwar and Ibanez, 1997).	14
Table 4: Some key developments in early understanding of electrokinetics (adapted from Lyklema, 2003).....	23
Table 5: Electrokinetic Phenomena	25
Table 6: Comparison of Electroosmotic permeability and hydraulic conductivity for various materials (adapted from, Mitchell, 1976).	39
Table 7: Outline description of the Major Groups of soil classification for soil survey in England and Wales. Within these major groups there are 41 groups, and 109 sub-groups (Taken from, White, 2006).	48
Table 8: The pH values for ‘zero point of charge’ of selected minerals. At pH lower than these values, the mineral will have a positive surface charge; and at higher pH values the charge will be negative.	50
Table 9: Some naturally occurring oxides, oxyhydroxides, and hydroxides found in soils (Sparks, 1995).....	51
Table 10: Cation exchange capacities of some typical soil components.	59
Table 11: Major classes of organic matter in soils, (Manahan, 2000).	59
Table 12: Some typical iron oxide, hydroxide and oxyhydroxide compounds which may be formed from iron in solution.	66
Table 13: Estimates of cost breakdown for electrokinetic remediation.....	72

Table 14: Selected costs associated with methods of electrokinetic remediation, (from, Virkutyte <i>et al.</i> , 2002; Yuan and Weng, 2004).....	73
Table 15: XRD analyses of pre treatment quartz sand and the post treatment iron-rich barrier region (Faulkner <i>et al.</i> , 2005).....	93
Table 16: Rough classification of ground improvement techniques (Otsuki <i>et al.</i> , 2007)	101
Table 17: Measurements and calculated value for porosity of quartz fibre sand.....	114
Table 18: Estuarine sediment starting conditions in the two experiments.....	140
Table 19: Table of the calculation of measurement uncertainty and percentage uncertainty calculated from the balanced experimental design in mg/kg	150
Table 20: Calculated detection limits from replicate analyses of reagent blanks (boric acid).	151
Table 21: Lower limit of detection values provided by the equipment manufacturer (PANalytical, 2006).....	151
Table 22: Calculation of mean starting concentrations in the estuarine sediment.	152
Table 23: LOI calculation for estuarine sediment calculated from five random samples labelled A,B,C,D and E.....	154
Table 24: Calculated ‘r’ values for Spearman's rank correlation coefficient for selected elements to indicate a correlation with the iron comparing mean values. The shaded values indicate a correlation at the 5% significance level. n=25 critical value= 0.337	190
Table 25: Spearman's rank correlation coefficient matrices for elemental means in estuarine sediment for tap water and acetic acid experiments. Shaded values indicate significant correlation either negative (light grey) or positive (dark grey). 5% confidence interval, critical value = 0.337 n=25.....	191
Table 26: experimental parameters for the two tap water experiments.	205
Table 27: Table showing the P values from the ANOVA tests. P values ≤ 0.05 are shaded green. P values > 0.05 are shaded red.....	220

Dedication and Acknowledgements

I am indebted to the friends I have made at Brighton University, including but not limited to, Dr. Stewart Ulllyott, Dr. Conor Ryan, Professor Rory Mortimer, Dr. Maureen Berg, Dr. Katherine King, Dr. Jenna Truder, Dr. Joanna Sage, Dr. Hannah Wood, Neil Hadlow, Aline Da Silva, Ray Ward, Benjamin Kyambbade, Professor Phil Ashworth, Dr. David Nash, Dr. Chris Joyce, Dr. Martin Smith, Thomas Hawkins, Dr. Norman Moles, Edward Rhodes... The list goes on...

Without the help and support of my family I would have been unable to see this thesis through to the end, thanks to my Mum for all the help and for believing in me, and thanks to my Dad for the late night sessions and the endless encouragement. Also thanks to my Grandparents, Bre and Frank, for their kindness and ability to always cheer me up. I am also grateful to Pat and Michael for their wise words and generosity.

This thesis is dedicated to Amy, without whom, I never would have got back to university, and who has since been a constant source of encouragement and reassurance. She has put up with the late nights, the weekends, the bad moods and the financial hardships. Without her unflagging patience, understanding and support, I would have given up countless times. *“When you’re finished...”*

Thanks Ames.

1 Introduction

This thesis is the outcome of research funded by the UK's Engineering and Physical Sciences Research Council (grant number GR/S27924/01) conducted to perform a 'baseline study' of the process developed at the University of Brighton and the University of Sussex, known as FIRS, Ferric Iron Remediation and Stabilisation, (see Appendix 1, for research council grant abstract).

Research was conducted to deliver to the research council the results of investigations into specified aspects of the technique as described in the funding description, with flexibility in the remit for independently identified avenues of research appropriate to the production of a doctoral thesis.

This chapter introduces and outlines some of the fundamental aspects of the FIRS technology, and puts the research into context in terms of the environmental and engineering situations the technique aims to address.

1.1 Rationale

Pollution is arguably the most serious problem humanity has had to face in modern times (e.g. McNeill, 2000; Rees, 2003). Whether this is directly, by damaging the health of people exposed to harmful substances or in terms of reducing the global biodiversity through harm to ecosystems, pollution has far reaching consequences. The ecological damage that pollution can inflict ranges in scale from highly localised, right up to damage affecting countries or even on the scale of continents e.g. the Chernobyl disaster, or CFC induced ozone destruction (Lovelock, 1974; Yu and Neretnieks, 1997). Indeed, pollution in the form of 'greenhouse gasses' is accepted to be the main contributing factor in global climate change which is predicted to have potentially disastrous consequences (e.g. Rees, 2003; Chiras, 2006 etc.).

Severe environmental consequences such as these have raised the profile of environmental issues in recent times and have led to a rapidly growing public awareness of the potential impacts of environmental recklessness. This awareness has had a knock-on effect towards all aspects of environmental concern; including contaminated land.

Pollution of the ground is a complex issue due to the way in which environmental pollution tends not to remain in one medium; or even in one phase. For instance a contaminated land problem may, through leaching, become a ground water or surface water problem; micro-organisms may volatilise some contaminants in the ground, resulting in air pollution, (Figure 1).

Ecosystem interactions and bio-accumulation may bio-magnify very low concentrations of hazardous substances up the food-chain as they are sequestered in body tissues, damaging sensitive species populations, food chain stability, as well as potentially risking human health (Meharg, 2004; Pendergrass and Butcher, 2006). This can mean that levels of a pollutant at concentrations at the limits of detection in the environment; might be accumulated in body tissues of an organism to hazardous levels. It is in this climate of public and political environmental awareness that this thesis is presented.

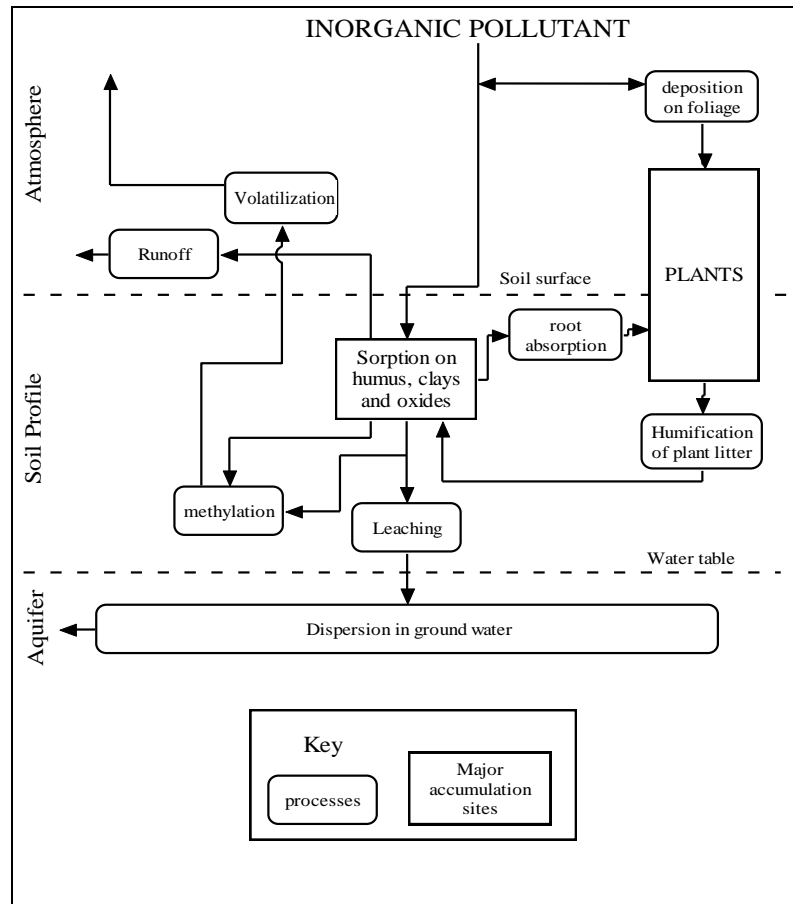


Figure 1: Flow chart showing the possible fates and accumulation sites of an inorganic ground pollutant (Adapted from, Alloway and Ayres, 1997) .

The wide and varied consequences of all kinds of pollution have only relatively recently been appreciated by policymakers and the growing legislation and regulation requires a more detailed understanding of the behaviour of contaminants in the ground (Meyer *et al.*, 1995).

It is in the light of these considerations that the concept described here is investigated as a potential development to contaminated land remediation/management strategies along with additional potential for ground engineering applications.

1.2 Overview

Contamination of the environment is a major concern across the industrialised world. Its associated hazards are receiving growing recognition as receptor pathways of toxins become better understood, and the liability for operators and landowners increases in terms of both damage to health and to the environment. The threat of litigation has inevitably led to increased pressure on operators to restore, remediate or otherwise manage contaminated land. Often, the simplest solution to a contaminated land situation is to displace the problem by transferring the contaminated material to another site by dumping to landfill. Space in suitable landfill sites is finite and the cost of disposal has been steadily increasing; as a result, the dumping of hazardous material is no longer necessarily the cheapest option.

Improved analytical technologies, such as portable XRF equipment and portable gas analysers, can identify hazardous material easier, faster and more reliably (Argyaki *et al.*, 1997; Kalnicky and Singhvi, 2001; Potts *et al.*, 2002) resulting in the rapid indication of contamination in an area, increased demand for landfill sites, and site operators inevitably charging an increased premium.

Governments are also encouraging alternatives to the dumping of contaminated land by making it more expensive to dispose of material in this way and making other changes to policy to dissuade operators from this method of disposal. The introduction of the Landfill Directive (EU, 1999), implemented in the UK in 2004, dictates that there will no longer be the option to co-dispose of hazardous with non-hazardous waste. All hazardous waste will therefore have to be disposed to a limited number of approved sites (Eaton, 2004). This is designed to reduce the negative environmental impact of landfill sites. The picture is similar on the international stage as well as domestically. Financial and political pressures mean the demand for cost effective and reliable measures to deal with contaminated sites has never been greater.

The UK government's additional measures designed to reduce the amount of waste disposed to landfill have taken the form of taxes levied per ton of waste, as an incentive for more responsible waste disposal and to encourage increased recycling activity whilst generating revenue at the same time. These taxes are increasing annually, landfill tax in

the UK as of 2006 was set at £24 per tonne rising by £3 per tonne per financial year until it reaches £35 per ton; in 2008 this has increased annually by £8 per ton until 2010 where it is expected to be subject to yet more increases (UK-Treasury, 2006) . This appears to be having the desired effect:

“The tax – working alongside other measures – has been successful with overall quantities of waste recorded at landfill sites registered for the tax falling from around 96 million tonnes in 1997-98 to around 72 million tonnes in 2005-06, a reduction of around 25 per cent.”

(HM Treasury, 2007)

This fall in disposal volume indicates that the hazardous material is being treated rather than simply dumped. Any technological or procedural advances that enable contaminants to be removed from contaminated land sites, such that the levels of contaminants are brought below thresholds considered hazardous, in a more cost-effective way, are much in demand.

This translates into the requirement for a method for reducing a given volume of contaminated material into a smaller volume by concentrating the contamination into a fraction of the material and reducing the contaminant concentration in the remainder to an acceptable level, thus reducing the volume of waste that must be disposed of to a designated hazardous landfill. This is highly sought after, especially in the case of metals contamination which, unlike other hazardous materials; such as organic pollutants, cannot easily be chemically altered or broken down since they are usually harmful in their elemental form.

With the ever growing global population, the requirement for building-land is always increasing; sites which, if it wasn't for contamination, would be prime development locations, may be economically unattractive due to the remediation/waste disposal costs. In situations such as these, a technique which can reduce the remediation costs or reduce the volume and therefore disposal costs, can transform an uneconomical development proposal into an economically viable one.

In the developed world, the modern climate of environmental responsibility, litigation and accountability, means industrial operators and landowners are increasingly aware of their responsibilities in terms of minimising environmental impact and eliminating human health hazards. In this regard, containing hazardous materials in the ground within a defined area, and preventing the movement of hazardous substances to areas where there may be exposure pathways to sensitive receptors, is another area of increasing interest. The hazard associated with a contaminated site is a function of the likelihood of the pollutant reaching a receptor; be that a person or a sensitive ecological entity. If the mobility is prevented and therefore the prospect of reaching a receptor is negated, the hazard is eliminated. Reliable and cost effective containment strategies are therefore an avenue receiving growing interest. In addition to the remediation of affected areas, site owners are also looking for means to contain contaminants in a given location. It may often be the case that it is cheaper to contain contaminants on a site rather than risk the migration of contamination to a neighbouring site given the 'polluter pays' principle enforced in many countries.

It is in the light of these considerations that this thesis considers a novel means of tackling these concerns using electrokinetically controlled migration and fixation of metal contaminants, and the generation of low permeability regions in the ground to control contaminant migration and to concentrate contaminants into a reduced volume for more cost effective disposal. This technique is called FIRS (Ferric Iron Remediation and Stabilisation)

The FIRS technique described in this thesis also has the benefit of being applicable to non-contamination related soil improvement methods. There are many instances where the properties of the ground are not suitable in their natural state for a proposed engineering project; or indeed the properties of the ground change over time and require modification to maintain their properties within acceptable parameters. Many soil engineering techniques have been developed to tackle a range of encountered materials, building requirements and locations. This thesis explores the possibility of the same technique which is applied to contaminated soils to be used for the improvement of the strength properties of different materials and the extent to which the technique can be controlled to achieve specific outcomes in terms of ground engineering through a

combination of de-watering and the strategic precipitation of metal oxides in soils and unconsolidated sands.

The technique is therefore to be investigated in terms of its potential usefulness in the following three areas:

1. For causing the migration, concentration and fixation of metal contaminants in a mass of soil or sediment.
2. Producing a reduction of the permeability and hydraulic conductivity of a soil or sediment as a means to manage groundwater or contaminant mobility.
3. Preliminary investigations into the technique as a means to augment the strength and engineering properties of the ground.

1.3 Contaminated Land

The pollution of the environment has a history almost as long as the history of mankind itself (Hong *et al.*, 1994). For instance, Roman smelting sites, more than 2000 years later, remain an environmental concern in the UK and abroad (e.g. Pyatt *et al.*, 2002).

The start of the Industrial Revolution at the end of the 18th century saw the truly large-scale, anthropogenic introduction of contaminants into the environment as mineral wealth was exploited and industrial scale processing began (Candelone *et al.*, 1995; Gribbin, 2002). Initially this was in Great Britain but quickly spread to mainland Europe, North America, Russia and Japan. Between 1875 and 1975, lead and cadmium emissions increased about 20 fold (McNeill, 2000), primarily as a result of metallurgical and smelting activity, with large quantities released to the atmosphere. Often this kind of aerial release results in localised surface deposition which, coupled with the release of sulphurous by-products of the smelting process, acidifies the location and mobilises the metal contaminants into the soil profile (e.g. Walker, 1996).

Short-sighted production techniques, accidents and irresponsible practices as well as plain ignorance, have left a persistent legacy of land contamination on a global scale

with sometimes horrifying effects on the environment and people (e.g. Blacksmith Institute, 2007). In the UK, the Environment Agency calculate that around 325,000 sites (300,000 ha) have had some form of current or previous use that could have lead to contamination (Environment Agency, 2004, 2007).

Awareness of the hazards of certain contaminants along with increased demands on the land in terms of use such as: land development, resource exploitation, food production and leisure; mean that pressures on the environment have never been higher with the problem all the more acute in densely populated regions (Korolev, 2006).

In the former USSR and the countries making up what used to be known as the 'Eastern Bloc' e.g. Poland, Hungary, the Czech Republic and Slovakia etc. often recklessly practiced the exploitation of their mineral resources and development of their industrial activities, and environmental issues were, at best, a minor concern. But now these countries are member states of the European Union and must conform to strict EU directives on contaminated land management, as laid out in, to use but one example, *The Thematic Strategy for Soil Protection* (Van Camp, 2004). This has led to a great deal of activity, in industry and in academia, geared towards the development of cost effective methods to tackle the extensive contamination problems in these areas (e.g. Rose, 1993). The problem is not just a European one, and it does not only affect the more economically developed countries, the less economically developed countries with their current rapid rate of expansion are the hosts to some of the most severely polluted sites in the world (e.g. Blacksmith Institute, 2007).

The scale of the extent of land contamination is truly enormous and the effects on the health of people exposed to damaging concentrations of pollutants can be terrible, there are also ecological and environmental impacts.

In the UK, the designation 'contaminated' when referring to land, has a strict definition. According to the CLEA (Contaminated Land Exposure Assessment) which is the framework constructed by the Environment Agency, and the Department of Environment Food and Rural Affairs (DEFRA), under Part IIA of EU Directive, 2004/35/CE on environmental liability with regard to the prevention and remedying of environmental damage, the statutory definition of contaminated land is:

“Land which appears to the local authority in whose area it is situated to be in such a condition, by reason of substances in, on or under the land, that –

- (a) Significant harm is being caused or there is a significant possibility of such harm being caused; or
- (b) Pollution of controlled waters is being, or is likely to be, caused.”

(Great Britain Dept. of the Environment Transport and the Regions, 1999)

‘Significant harm’ for humans is defined in this context as:

“Death, disease, serious injury, genetic mutation, birth defects or the impairment of reproductive functions.”

(Great Britain Dept. of the Environment Transport and the Regions, 1999)

This part of the framework does not consider risks to other receptors such as plants, wild animals or buildings. The practical implications of contaminated land management and the associated concerns are considered in the following section.

1.4 Contaminated Land Management

Once an area of land has been identified as contaminated and in need of remedial action, then the options for treatment may be evaluated. Many factors need to be considered before a decision on the best course of action is reached and the proposed approach administered, these factors include the soil chemistry, type and concentration of contaminant, the proposed use of the site and the likely cost of remediation or disposal versus available budget. Table 1 shows the UK soil guideline values for some typical metal (and metalloid) contaminants.

Table 1: Soil guideline values (SGVs) for some common contaminants. The threshold varies for different land uses. Concentrations are in mg kg⁻¹ (DEFRA, 2002a, b, c, d, e, f, g) it should be noted that at the time of writing some of these values are under review as part of the on-going CLEA (Contaminated Land Exposure Assessment) program along with the addition of Health Criteria Values (HCVs) for the purpose of risk assessment of a contaminated site (Hopkins and Hosford, 2009a, b; Hopkins *et al.*, 2009; Watts and Hosford, 2009).

Substance	Residential with plant uptake	Residential without plant uptake	Allotments	Commercial/ industrial
Lead	450	450	450	750
Selenium	35	260	35	8000
Nickel	50	75	50	5000
Mercury	8	15	8	480
Chromium	130	200	130	5000
Cadmium	1,2,8 (for pH 6,7,8)	30	1,2,8 (for pH 6,7,8)	1400
Arsenic	20	20	20	500

These are the prescribed limits for some inorganic soil contaminants for specified land-uses based on investigations into the likely receptor pathways and associated hazard assessments. The actual classification of land as being ‘contaminated’ is a complicated issue; not least because of uncertainty associated with the sampling and analysis of a site which may affect the classification of a site which is at or near a threshold concentration (e.g. Ramsey *et al.*, 1995; Ramsey and Argyraki, 1997; Ramsey, 1998, 2004).

This can have significant implications for the economics of the development of a site. Studies have shown that the major source of uncertainty in the classification of contaminated land is associated with the sampling protocol employed on the site with uncertainty due to analysis contributing a much less significant portion of the measurement uncertainty (e.g. Ramsey *et al.*, 1995; Ramsey and Argyraki, 1997).

In spite of these difficulties, this is the current legislation which site operators must follow, and once a site has been designated as contaminated then remediation strategies can be considered.

Generally, remediation technologies may be broadly classified into three categories:

Removal: a process that physically removes the contaminant or contaminated medium (or both) from the site without the need for a separate separation step.

Separation: a process that removes the contaminant from the host medium (soil or water) either entirely or by reduction to an acceptable concentration.

Destruction: a process that chemically or biologically destroys or neutralizes the contaminant to produce less toxic compounds this is mostly applicable to organics.

Since metal contaminants are often toxic in their elemental form, it is not possible to break them down further so removal or separation are the only options. Some of the available and developing technologies for tackling contaminated land usually involve one or more of the following approaches:

Containment: a process that stabilises or immobilizes contamination preventing further migration of the contaminant.

Bioremediation: Used for the removal of organics (halogenated and non-halogenated volatiles and semi-volatiles including pesticides) but is not suitable for heavy metals or metalloids, this would fall into the destruction category according to the classification criteria above.

Thermal de-sorption: This technique is also only useful for hydrocarbons including petrochemicals. This is a separation technique.

Soil Vapour extraction: Can be effective for the removal of a range of organic and inorganic contaminants but is only applicable to suitable sites in terms of hydrogeology and soil permeabilities. This is a separation technique.

Soil Washing: works effectively only on high permeability, coarse grained soils. This is particularly useful for removing surface adsorbed heavy metals. This is a separation technique.

Soil flushing (pump and treat): can be effective for heavy metal contamination, again, low permeability soils are problematic. This is a separation technique.

Electrokinetic Soil Remediation: Suitable for fine grained, low permeability soils with adsorbed metal contamination. This is a separation technique.

(adapted from Virkutyte *et al.*, 2002)

It is the electrokinetic approach which is investigated for the purposes of this thesis. Contaminants which have been shown to be amenable to electrokinetic processes (to a greater or lesser extent) include:

Heavy metals	Cyanides
Radioactive species	Toxic anions
Explosives	Dense non-aqueous phase liquids
Mixed organic/ionic contaminants non halogenated organic pollutants	Halogenated hydrocarbons
Petroleum hydrocarbons (diesel fuel, gasoline, kerosene and lubricating oils)	

(Van Cauwenberghe, 1997)

This description of amenable contaminants covers most of the substances likely to be encountered in a variety of contaminated land situations. The likely contaminants associated with particular industries or industrial processes are outlined in Table 2.

Table 2: Industrial sources of potential contamination (Adapted from Hester and Harrison, 2001)

Sector	Contaminant type	Example
<i>Gasworks</i>	Coal tar	creosote
	Phenols	phenol
	Cyanide	free / complex
	Sulphur	sulphide / sulphate
<i>Iron + Steel works</i>	Metals	copper, nickel, lead
	Acids	sulphuric, hydrochloric
	Coking works residues	(as for gasworks)
<i>Metal finishing</i>	Metals	cadmium, chromium, copper, nickel, zinc
	Acids	sulphuric, hydrochloric
	Plating salts	cyanide
	Aromatic hydrocarbons	benzene
	Chlorinated hydrocarbons	1,1,1-Trichloroethane
<i>Oil refineries</i>	Hydrocarbons	various fractions
	Acids, alkalis	sulphuric, caustic soda
	Lagging, insulation	asbestos
	Spent catalysts	lead, nickel, chromium
<i>Petrochemical plants</i>	Acids, alkalis	sulphuric, caustic soda
	Metals	copper, cadmium, mercury
	Reactive monomers	styrene, acrylate, VCM
	Cyanide	toluene di-isocyanate
	Amines	aniline
	Aromatic hydrocarbons	benzene, Toluene
<i>Petrol stations</i>	Metals	copper, cadmium, lead, nickel, zinc
	Aromatic hydrocarbons	benzene
	Octane boosters	lead, MTBE
	Chlorinated hydrocarbons	trichloroethylene
	Paint, plastic residues	barium, cadmium, lead
	Metals	copper, nickel, cadmium
<i>Semi-conductors</i>	Metalloids	arsenic, antimony, zinc
	Acids	nitric, hydrofluoric
	Chlorinated hydrocarbons	trichloroethylene
	Alcohols	methanol
	Aromatic hydrocarbons	xylene, Toluene
	Metals	aluminium, tin, titanium, zinc
<i>Wood processing</i>	Chlorinated hydrocarbons	pentachlorophenol
	Metalloids / metals	arsenic, copper, chromium

Also of vital importance is information as to the way in which the contaminant was released, over what timescales, or the speciation of the contamination, which are important factors in the assessment of hazard. In some instances the concentrations or speciation of a contaminant may be modified in the environment from a stable or non-toxic form to a more hazardous form. Some metals, such as mercury, can be methylated (addition of a methyl group) by micro-organisms in the environment. This methylation makes the mercury much more readily absorbed by organisms termed 'bio-available' and therefore more hazardous (e.g. Chiras, 2006). Despite some fairly high profile mercury related incidents affecting large numbers of peoples' health e.g. Minamata Bay, Japan (Harada, 1995), there is a paucity of literature describing the attempted remediation of mercury contaminated soils with some exceptions, e.g. Reddy *et al.* (2003) and Cox *et al.* (1996), due in part to the relatively low solubility of mercury and the tendency towards natural attenuation, given sufficient time.

The contaminants associated with a particular source may take an extended period of time to reach concentrations which pose a significant hazard, indeed, generation of contaminants may not be typical of every instance of an industrial process – they may only be a result of badly maintained examples of a procedure or accidental releases or indeed unscrupulous deliberate releases to the environment. The other scenario for contamination of the environment is the sudden unexpected and potentially catastrophic release of contaminants. These types of release can result in rapid mass transport of contamination and sudden, dramatic, localised contaminant concentrations. These may be short-lived, exacting acute damage but rapidly diluted or dispersed, such as was seen with the 'Wheal Jane' acid mine drainage incident in the UK (e.g. Younger, 2000, 2007). An example of a more chronic release of contamination is the Norilsk smelter plant in Siberia, Russia. Founded in 1935, and still the site of the worlds largest smelter, it is estimated to release 4 million tons of atmospheric pollution annually (Allen-Gil *et al.*, 2003), the pollution locally is so severe that surface soils are enriched in palladium and platinum to the point that they are mined as an economic grade resource.

Table 3: Some major environmental incidents in recent history due to hazardous chemicals (adapted from Rajeshwar and Ibanez, 1997).

Incident	Period	Comment
Love Canal	1942-1953	Approximately 23,000 tons of chemical wastes were dumped in this canal in Niagara Falls, New York. A health emergency was declared by the state in 1978 and cleanup efforts began.
The Reed Paper controversy	1962-1970	About 10 tons of mercury lost from the chlor-alkali plant into the Wabigoon-English River system. This plant supplied the chemicals needed to bleach the pulp at the pulp mill in Dryden, Ontario.
Lekkerkerk	1986	The Rhine river drains a vast basin in four countries (France, Germany, Switzerland, and the Netherlands) as it runs from the Alps to the North sea. The basin is heavily industrialised and the river accumulates and transports to the Netherlands a heavy load of pollutants.
Minamata Bay	1956	Minamata disease was first discovered in Minamata city in Kumamoto prefecture, Japan in 1956. It was caused by the release of methyl mercury in the industrial wastewater from the Chisso Corporation's chemical factory. This highly toxic chemical bioaccumulated in shellfish and fish in Minamata Bay and the Shiranui Sea, which when eaten by the local populace resulted in mercury poisoning. While cat, dog, pig and human deaths continued over more than 30 years, the government and company did little to prevent the pollution.

Large scale releases can have a legacy of chronic contamination, such as has been seen from the release of radioactive material from nuclear weapons testing (e.g. Robison *et al.*, 2003). Table 3, shows some other noteworthy examples of large scale hazardous

material released into the environment resulting in severe environmental damage and harmful effects on health.

These types of contamination event are often obvious in their occurrence and extent, but more commonly a suspected contaminated site has to be subjected to extensive testing and monitoring to ascertain the source and nature of the contamination.

Figure 2, shows the decision making process required to assess the need and nature of remediation of a suspected contaminated site according to current UK best practice. There are many factors to be considered and many decisions have to be made on the basis of fairly extensive research including the investigation of historical records for land use at the site, as well as field-work assessments, sampling strategies and laboratory analyses.

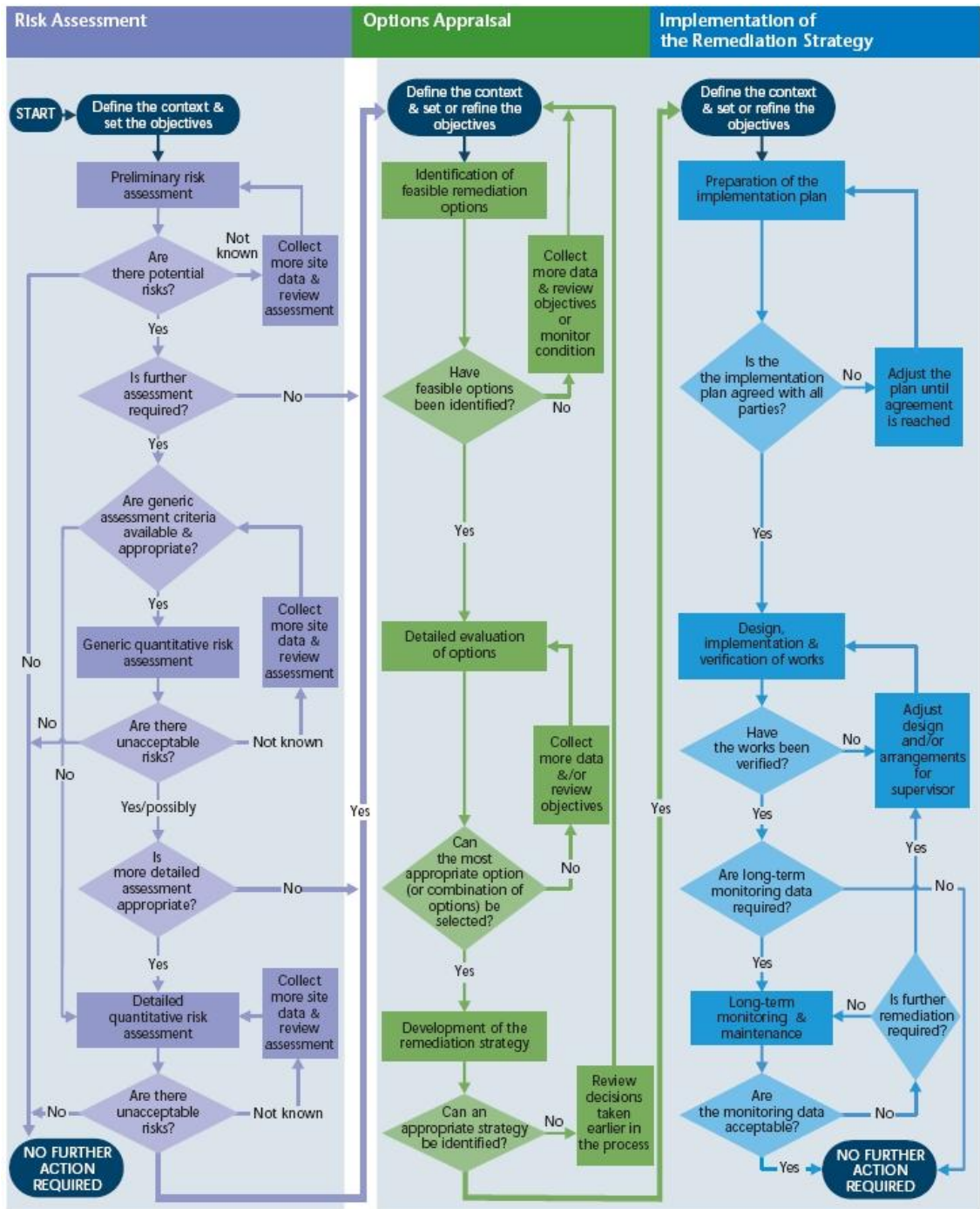


Figure 2: Environment Agency UK flow chart describing the decision making process for the implementation of contaminated land management.

Note: The process may apply to one or more pollutant linkages, each of which may follow a different route. For some linkages, it may be possible to stop at an early stage – others will progress all the way through the process. The level of complexity of each stage may also vary and in some cases may be very simple (adapted from, Environment Agency and DEFRA, 2004).

The range of fates and exposure routes for any particular contaminant are many and varied. The removal of common heavy metal contaminants from low permeability

(often clay-rich) material is an example of a difficult to treat contaminated land situation- as the material is not easy to process due to the physical and chemical characteristics of the material (these will be discussed in detail). They can hold a relatively large amount of water which can make them bulky and heavy, which also makes them expensive to transport and to dispose of to landfill. These considerations are dealt with in the context of this thesis and it is with these factors and types of material and contaminants in mind that this research is conducted.

1.5 Electrokinetic Approaches

In soils and sediments of low hydraulic permeabilities with metal contamination the remediation options are limited as these materials are difficult to treat by existing methods, such as pump and treat, physical separation etc. and often have to be dumped to landfill. This is because they have a low hydraulic permeability which makes pump and treat impossible and the clay fraction may be aggregated, but the clay particles themselves are of the micron scale, this makes a physical separation by mechanical means unfeasible, the energy to make a separation is not worth the level of fractionation that can realistically be expected to be achieved. Electrokinetic remediation has been receiving growing interest for the treatment of very fine grained or clay-rich low permeability materials (e.g. Martin and Ruby, 2004) due to its ready applicability to materials of this nature.

Electrokinetic remediation involves the passing of an electric current through a wet soil mass to cause the movement of contaminants adsorbed to the surface of soil particles or in the pore water. The mobilised contaminants are then normally removed from the soil by an appropriate flushing system (Acar and Alshawabkeh, 1993; Probststein and Hicks, 1993; Shapiro and Probststein, 1993) or by electroplating directly onto the electrode (e.g. Lee and Yang, 2000).

By passing a current between electrodes inserted into wet soil either side of the mass of material to be treated, three distinct phenomena occur:

- Electromigration: movement of ions towards the electrode of opposite charge.
- Electroosmosis: net movement of water and dissolved species towards the cathode (negative electrode).
- Electrophoresis: movement of charged particles or colloids towards the oppositely charged electrode.

(e.g. Acar and Alshwabkeh, 1993; Acar *et al.*, 1995; Choi and Lui, 1995; Alshwabkeh and Acar, 1996; Page and Page, 2002; Yeung, 2006a etc.)

Most conventional electrokinetic methods would tend to fall under the ‘separation’ classification according to the definitions given in Section 1.4, although the technique described in this thesis satisfies both the separation and the containment categories as shall be discussed.

As well as remediation and pollution control, electrokinetics has been explored for a great variety of other purposes. Electroosmotic dewatering of football pitches has been achieved by the application of an electric field to the near-surface of the pitch via buried conductive geo-textiles which utilises the movement of water through the soil under the influence of an applied voltage to prevent water logging of the playing surface (Lamont-Black, 2001). A similar set up has been used for sewage sludge dewatering to be used as an alternative to mechanical methods (Lamont-Black, 2001).

The electrokinetic transport of nutrients for plant growth has also been investigated and the incorporation of phytoremediation (utilising plants to take up and concentrate metals in their tissues) with electrokinetics has been investigated (Hodko *et al.*, 2000). Transport of bacteria and bacterial nutrients to stimulate the activity of contaminant metabolising microorganisms for bioremediation applications has also been investigated (DeFlaun and Condee, 1997). In civil engineering applications, electrokinetics has been utilised for the manipulation of injected grouts for sub-soil barrier formation for added control of the development and geometry of sub-surface grouting projects (Bell, 1975).

In petroleum exploration electrokinetics has been incorporated to aid with oil extraction (Sacuta, 1980). There has also been the successful implementation of ‘electro-fences’ using electrokinetic phenomena for groundwater control (Godschalk and Lageman, 2005; Lynch *et al.*, 2007; Lynch, 2009), and also as a combined approach termed a ‘biofence’ (Lageman and Pool, 2009). Another important area of research into applications of electrokinetics is in the improvement of ground characteristics for engineering purposes using a variety of electrokinetic approaches etc. (Bjerrum *et al.*, 1967; Bell, 1975; Trushinskii, 1993, 1996; DeFlaun and Condee, 1997; Kiely, 1997; Lamont-Black, 2001; Pyatt *et al.*, 2002; McGuire *et al.*, 2003; Lear *et al.*, 2004).

1.6 Scope of Thesis

The FIRS (Ferric Iron Remediation and Stabilisation) method for mobilising and concentrating soil contaminants provided in Hopkinson and Cundy (2003), and Cundy and Hopkinson (2005) describes the initial phase of development of this electrokinetic technique with preliminary experiments conducted on a small scale, electrode separation of ~15 cm, along with some preliminary geotechnical tests. (The FIRS process is described in full technical detail in Section 2.9. Cundy and Hopkinson conducted experiments in 2003 on the remediation of two contaminated materials (radionuclide, and heavy metal/hydrocarbon) at this scale, with encouraging data obtained. The method is covered by international patent number WO2004028717 (Cundy and Hopkinson, 2004).

The electrode arrangements in the experiments conducted by Cundy and Hopkinson were all parallel linear, and although alluded to, there are no experimental data on strategic barrier geometry formations by Cundy and Hopkinson.

This thesis represents the continuation of the investigation and development of the FIRS technique as a tool for contaminated land management. The feasibility of the method is assessed in terms of potential up-scaling and the use of the technique for the reduction in volume of contaminated material by concentrating and stabilising contaminants (primarily metals/metalloid contamination but also non-metals) within, or concentrated

around, iron-rich mineral phases. Additionally, the generation of a low permeability, iron enriched region within the soil is addressed as a method of groundwater management, whether or not in a contaminated land or ground engineering scenario.

The iron-rich mineral phases also augment the strength properties of an unconsolidated material and may prove useful for soil improvement and engineering applications (Cundy and Hopkinson, 2005) and data is also presented on this aspect as well as the strategic creation of iron mineral fabrics to predetermined geometries.

1.7 Aims and Objectives

The objectives of the work conducted fall into three distinct areas: Remediation experiments, groundwater effects and stabilisation experiments (with some overlap regarding the remediation and groundwater areas), and these can be further sub-divided.

In a general sense the remediation experiments were conducted to:

1. To evaluate the performance of the system described in Cundy and Hopkinson (2003; 2004) on an estuarine sediment and on a larger scale than previous experiments (between 2 and 4 times the size).
2. To compare the results in one medium for different electrolytes (tap water and dilute acetic acid 2M).
3. To compare the effectiveness of the technique with and without an imposed hydraulic head.

For the stabilisation experiments the objectives were:

1. To find useful electrode configurations and designs to create novel strategic iron pan geometries in the sub-surface.
2. To characterise the composition and physical properties of the iron-rich precipitates formed in terms of the potential for groundwater management applications.

For the groundwater management experiments the objectives were:

1. To ascertain whether the technique can be used to manipulate groundwater flow in different materials (sand, loamy soil, estuarine sediment).
2. To investigate whether a robust iron-rich mineral barrier might be generated in a moving groundwater flow in different materials.

The work was conducted to investigate the FIRS technique for the remediation, in terms of its use as a strategy to localise contamination into a narrow region of the soil, of some common metal and metalloid contaminants through experimentation on selected materials. The imposed movement of contaminants and subsequent stabilisation capacity of the approach along with other experimental considerations were then appraised. The findings from these experiments provide information useful for working towards the optimisation of the technique, and for the purpose of providing recommendations for the issues to be addressed in future work.

Additional experiments were designed to attempt to strategically control the precipitation of the iron mineral phases to form a useful manipulation of the hydro-permeable properties of the soil for the creation of iron-rich barrier geometries and to evaluate the applicability of these to environmental and engineering problems.

This was tackled by the design and experimentation of custom electrode design and geometric arrangements. The hydraulic flow limits to which the electrokinetically induced migration and precipitation of iron might be subjected were tested with experiments on the creation of precipitate barriers against an artificially imposed hydraulic head.

1.8 Organisation of Thesis

Now that an overview of the research has been given and the scientific, environmental and political landscape defined, the thesis can be laid out.

The thesis is structured to give a contextualisation of the research in terms of the state of the art and the existing literature, and how this thesis fits into the body of knowledge. Also the chemical concepts are reviewed and the relevant processes are outlined in section 2. With the context defined, the experimental work is introduced in the next chapter. This describes the strategic formation of barrier experiments, including the horizontal barrier formation, and mass-stabilisation experiments. It also discusses the potential commercial applications and addresses the strengths and weaknesses of existing barrier construction methods.

Section 3 deals with the formation of barriers against an imposed hydraulic head; to investigate the effects of dynamic groundwater situations encountered in the natural environment. This includes barriers created in estuarine sediment with elevated metals/metalloid concentrations. This completes the experiments and findings of the investigations into the formation of subsurface, iron-rich, low permeability barriers.

Section 4 deals with another set of remediation experiments conducted this time on a fine grained, low hydraulic permeability, estuarine sediment collected from Hythe, UK to evaluate the efficacy of the mobilisation of metals in tap water electrolyte compared with an acetic acid conditioning solution in this medium. The use of this material in both the remediation and the hydraulic head experiments allows the comparison of results from both sets of experiments.

The discussion follows with the findings discussed and the relevance and applicability of the technique to existing environmental concerns appraised. The conclusions follow; with recommendations for the direction and methods that future work might utilise, and with ideas for improved technical designs for specific purposes and the use of a composite electrode design as well as other design and implementation improvements.

2 Literature Review

Scientific research into electrokinetic phenomena has been conducted since the beginning of the 19th century, more or less continuously, up to the present day. There have been some periods of increased activity, notably the 1940s then the 1960s and the mid to late 1990s proved particularly fruitful, and currently the first decade of the 21st century is providing something of a resurgence in activity in the field. This chapter is concerned with presenting the relevant literature with respect to the development of this thesis, and gives context to the research work carried out in terms of the existing body of work.

2.1 Electrokinetics: Early Work

The early explanations for the observed phenomena associated with electrokinetics, as discussed in the previous chapter, are based on empirical studies carried out in the early nineteenth century. As science progressed and the phenomena of electromagnetism and the atomic theory of matter became understood, as well as improvements in analytical technology, theoretical models developed and improved. Table 4 shows some of the early theorists and scientists and important milestones in the understanding of electrokinetic phenomena.

Table 4: Some key developments in early understanding of electrokinetics (adapted from Lyklema, 2003).

Year	Author	Observation / Theory
1808	Reuss	Electrophoresis of clay particles, electroosmosis
1861	Quincke	Electroosmosis through glass capillaries
1879	von Helmholtz	Equations for mobilities, streaming currents/potentials
1880	Dorn	Dorn effect (sedimentation potential)
1882	Schulze	Coagulation efficiency increase with ion valency
1892	Saxen	Correlation with electroosmotic volume flow and streaming current
1905	Smoluchowski	Theorem for plugs of arbitrary geometry
1909	Gouy	Diffuse double layer theory
1911	Smoluchowski	Coagulation kinetics theory
1913	Smoluchowski	Forced Brownian motion
1924	Stern	Stern Layers
1932	Verway	Recognition of charge determining ions.

Reuss (1808) recorded the first observations of the electroosmotic effect after experiments carried out with clay, utilising electrodes made up of a conductor in a glass tube surrounded by the electrolyte (water). These were emplaced in a mass of wet clay or other porous material. Reuss noted that when a current was passed between the electrodes, the water level in the cathode tube increased, while the level in the anode dropped, up to a maximum height difference for a constant voltage (at this point the hydraulic pressure on the cathode side equals the electroosmotic pressure and this height is a function of the applied electrical gradient, Reuss, 1808).

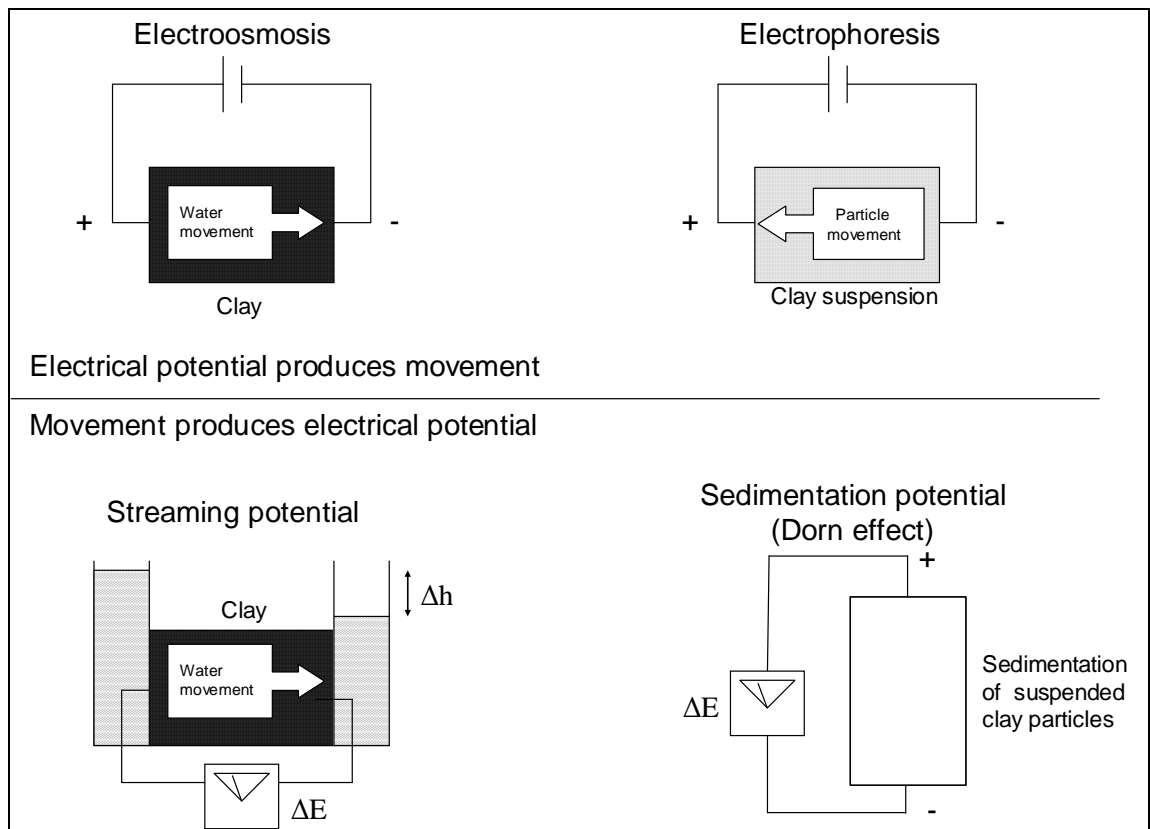


Figure 3: Diagrammatic representation of electrokinetic phenomena achieved experimentally. Electroosmotic and electrophoretic movement arises from the application of an electric current to a mass of clay and a clay suspension. Streaming potential refers to electric potential (ΔE) produced between upstream and downstream electrodes by the forced movement of water (or other electrolyte) through a mass of clay, this may be achieved by a head difference (Δh) across the clay mass. The gravitationally (or any acceleration) induced movement of particles in a suspension produces an electrical potential between the upper and lower electrodes (adapted from, Mitchell, 1976).

Quincke in (1861) observed electrophoresis of clay suspensions through glass capillaries in water using platinum electrodes (capillary tubes were used to allow only two dimensional movement of the suspension). He observed that the clay particles moved towards the anode. He postulated that at the interface of the clay surface and the

surrounding liquid, opposite charges are present. This explained the observed movement of the suspended particles, since the application of an electric field would cause positively charged species to move in the opposite direction to the negatively charged species; he went on to note that this implied that if the solid portion was fixed (i.e. not a suspension or colloidal fraction) then the liquid portion alone would migrate, which supported Reuss' observations. The main processes and terminology associated with electrokinetics are summarised in Table 5 and graphically in Figure 3.

Table 5: Electrokinetic Phenomena

Phenomenon	Description	Explanation
Electroosmosis	Movement of a solution through a stationary solid phase.	Application of an electric field induces the net movement of the electrolyte from anode to cathode.
Electromigration	The movement of an ion or dipole from electrostatic attraction to a region of opposite charge.	An externally applied electric field induces the movement of charged species towards the electrode of opposite charge.
Electrophoresis	Movement of colloids, or micelles with a net surface charge through a liquid medium due to electrostatic attraction.	An externally applied electric field induces the movement of charged species towards the electrode of opposite charge.
Streaming potential	Potential difference induced in stationary solid phase by the through movement of a liquid phase.	A hydraulic gradient forcing liquid through a solid phase or fine capillary results in a voltage potential between upstream and downstream regions.
Sedimentation potential	Potential difference due to sedimentation of particles under the influence of acceleration (normally gravity).	Also known as the Dorn effect, the electrical potential arising between electrodes at different heights from the action of gravity (or analogous forces such as may be generated in a centrifuge) causing sedimentation.

Helmholtz (1879) contributed a mathematical description of the experimental observations that agreed with Quincke's hypotheses, yet there was no robust theoretical explanation for the formation of a double layer resulting in the observed phenomenon. Smoluchowski and Gouy, in the early twentieth century added to the existing mathematical basis and developed the theoretical aspects further. A more complete picture thus emerged. The particulars of the theoretical development and mathematical description of electrokinetic phenomena are dealt with in detail in section 2.6.

2.2 Electrokinetic Approaches

Electrokinetic phenomena have been applied to numerous situations, predominantly in environmental and engineering applications, but also in medical science. Indeed research was conducted to investigate electroosmosis for the introduction of dissolved substances into living tissue (Barratt and Harris, 1912). It is also commonly used for the electrophoretic separation of organic molecules, particularly DNA. This electrophoretic separation on treated DNA is the method used for genetic fingerprinting for forensic identification of suspected criminals and for paternity disputes.

The electrochemically induced dissolution of metals has been used extensively for diverse applications such as the precision machining of metal components (McGeough, 1974), as well as investigated for the manipulation of metals for the creation of novel surface applications of metal species (e.g. Peulon *et al.*, 2004).

Electrokinetic phenomena have also been investigated for the delivery of nutrients for microbes in microbially enhanced degradation of organic (hydrocarbon) based contamination, (Jackman *et al.*, 2001; Luo *et al.*, 2005) and for the delivery and transport of microorganisms themselves (DeFlaun and Condee, 1997). The degradation of organics chlorinated, halogenated, and petrochemical, has been investigated using electrokinetic processes directly (Röhrs *et al.*, 2002; Saichek and Reddy, 2003a, b; Reddy and Cameselle, 2009).

In addition, the investigation of electrokinetic remediation for use on radionuclide contaminated sites is an area of growing interest (e.g. Maes *et al.*, 1999), but it comes with inherent difficulties associated with working with such materials as well as specific safety demands on the facilities undertaking work with radioactive materials. Electrokinetics have been applied to non-metal inorganic contamination, for instance removal of nitrates (e.g. Manokarajah and Ranjan, 2005).

These diverse applications lie outside the scope of this thesis, so only environmental and selected engineering applications will be considered here. For the purposes of this thesis the term electrokinetic is used only to refer to the application and effects in the context of soils sands and sediments.

2.3 Electrokinetics: An Overview

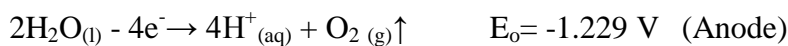
Electrokinetics describes any process whereby movement of a species (ion, electrolyte, charged particle, or colloid) is induced by the application of an electric field. This term actually refers to a number of distinct processes. In the context of this thesis, the effect has been applied to contaminated land remediation and to physical strengthening of soils and sediments by electroosmotic dewatering and electrochemically induced cementation.

The general electrokinetic approach involves the forced movement of contaminants under the influence of an electric field, and has been demonstrated to be effective for the removal of both organic and inorganic species (including radionuclides) from soils and sediments (Acar and Alshawabkeh, 1993; Beskid *et al.*, 1993; Probststein and Hicks, 1993; Yeung and Mitchell, 1993; Acar *et al.*, 1994; Alshawabkeh and Acar, 1994; Acar *et al.*, 1995; Kovalick, 1995b; Acar and Alshawabkeh, 1996; Alshawabkeh and Acar, 1996; Puppala *et al.*, 1997; Alshawabkeh, 2001; Mulligan *et al.*, 2001; Virkutyte *et al.*, 2002; Yeung, 2006a; b etc.).

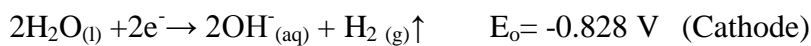
By passing a current between electrodes inserted into the soil or sediment either side of a mass of wet soil; three of the phenomena presented in Table 5 above, occur:

- **electromigration**- movement of ions in the pore water towards the electrode of opposite charge.
- **electroosmosis**- net movement of water (normally towards the cathode but flow may be reversed in extremes of pH, this is covered in more depth in Section 2.6.2).
- **electrophoresis** - movement of charged particles (e.g. micelles) or colloids in the pore water towards the oppositely charged electrode (Van Cauwenberghe, 1997).

The dissociation of water by electrolysis at the electrodes forms H⁺ ions and oxygen gas at the anode, (Equation 1), and OH⁻ ions and hydrogen gas at the cathode, (Equation 2). The acidification of the soil due to the production of H⁺ ions at the anode lowers the pH and generally increases the mobility of metal species in the soil. This advancing region, the part of the electrolyte at or near the anode that is changed in composition by the reactions at the anode is sometimes termed the *anolyte* (e.g. Lageman *et al.*, 2005). The H⁺ ions also tend to displace metal ions adsorbed on to the surface of clay particles, thus aiding the solubilisation and mobilisation of these types of contaminant.



Equation 1



Equation 2

Where E_o is the standard reduction potential at 25°C, 1 atm, pH 7 (Acar and Alshwabkeh, 1993).

Existing electrokinetic methods deal mainly with remediation of low permeability soils and sediments and have demonstrated considerable success- often removing up to 90% of a specific contaminant (e.g. Probstin and Hicks, 1993; Shapiro and Probstin, 1993; Virkutyte *et al.*, 2002 etc.). However these levels of removal efficiency commonly involve the use of complicated pH management systems and high voltage equipment (Acar and Alshwabkeh, 1993; Virkutyte *et al.*, 2002 etc.). In addition, high

remediation efficiencies are often achieved under strictly controlled laboratory conditions, using purified clays which have been artificially ‘spiked’ (e.g. Shapiro and Probst, 1993; Denisov *et al.*, 1996; Reddy and Chinthamreddy, 1999 etc.). It follows that frequently, these conditions do not necessarily reflect those which actually exist in contaminated environments.

The existing body of literature is weighted towards laboratory investigation rather than application in the field (with a few notable exceptions, see section 2.4). There is also some dogma regarding certain aspects of the typical apparatus e.g. The existing literature is heavily biased towards:

- The use of inert electrodes (graphite, ceramic etc.)
- Avoidance of precipitation of metals in the soil mass.
- Suppression of alkali front (or of both acid and alkali fronts)

(e.g. Pamukcu and Wittle, 1992; Acar *et al.*, 1993; Probst and Hicks, 1993; Shapiro and Probst, 1993; Hicks and Tondorf, 1994; Acar *et al.*, 1995; Acar *et al.*, 1997; Pamukcu *et al.*, 1997; Reddy *et al.*, 1997; Wong *et al.*, 1997; Yeung *et al.*, 1997b; Sogorka *et al.*, 1998; Alshwabkeh *et al.*, 1999a; Alshwabkeh *et al.*, 1999b; Reddy and Chinthamreddy, 1999; Pamukcu *et al.*, 2003; Alshwabkeh *et al.*, 2004; Pamukcu *et al.*, 2004; Reddy and Ala, 2005)

It has also been strongly stated in the literature that some of these recommendations should be strictly adhered to:

“... putting electrodes directly into soil will fail, as found by earlier workers...
managing the electrolyte is essential, in fact it is a “conditio sine qua non”.

(Lageman, 1993)

Since the work presented in this thesis complies with none of the directives above, explicitly: sacrificial electrodes are emplaced directly in the soil, no suppression of the acid or alkali fronts is attempted i.e. no electrolyte management, and the deliberate precipitation of metal compounds in the soil mass is encouraged, it contradicts many of the recommendations found in the literature:

“Of the adverse effects of OH^- and H^+ on remediation, the immobilization of toxic metal ions by precipitation in soils alkalinized by OH^- is considered the most debilitating.”

(Leinz *et al.*, 1998)

One of the main reasons for this is due to the objective of much of the research reported in the literature commonly being to remove the contaminants in solution at the electrodes.

This thesis advocates the idea outlined in Cundy and Hopkinson (2005), that a reduction in volume of contaminated material, coupled with a stabilisation effect, may be a viable alternative. The more recent literature shows gathering support for this approach (e.g. Kimura *et al.*, 2007a).

This approach treats the soil mass being remediated as an indivisible unit, thus any significant concentration of contaminant remaining in the soil renders the treatment a failure according to this view.

2.4 Applications of Electrokinetics

Environmental applications and research into electrokinetics has consisted of:

1. Electroosmotic dewatering of clayey soils for the stabilising and consolidating effect this has (e.g. Lamont-Black, 2001).
2. Electrochemical alteration of the soil by the addition of metallic species by electrodisolution of the anode electrodes (e.g. Casagrande, 1947; Casagrande, 1949).
3. Dissolution and or removal of contaminants from soils via electromigration and electroosmosis

Leo Casagrande working in Germany in the 1930s was a pioneer of the practical application of electroosmosis to building projects. Whilst not concerned with clean-up of contaminated land; his was the first documented full-scale application. His work

included soil engineering applications of electrokinetics through the use of mass-dewatering projects on clay soils; and stabilisation by anodic aluminium dissolution and re-precipitation.

Many of the practical considerations when using field-scale electrokinetics (electrode decomposition, precipitation around the electrodes, joule heating, and expected flow rates, energy requirements etc.) were first elucidated and disseminated by Casagrande (e.g. Casagrande, 1947, 1949) and he was still applying the technique to civil engineering problems more than thirty years later.

“The electro-osmotic stabilization of a 2800 foot long depressed section of the main line of the Canadian Pacific Railway at Clan William, British Columbia, Canada, and the electro-osmotic stabilization of the slope for a 250 foot deep excavation for the core trench of the British Columbia Hydro and Power Authority's Revelstoke Dam at Revelstoke, British Columbia, are described. The two projects, located within five miles of each other, involved extensive excavations through sensitive silts that required stabilization during construction.”

(Casagrande *et al.*, 1981)

There was other research being conducted utilising the electro-dissolution and reprecipitation of sacrificial electrodes by other groups and individuals (e.g. Endell and Hoffmann, 1936), albeit on a much smaller scale. Much of this early work was developed further during the 1960s where ground engineering applications were explored further including the use of different electrode materials and an assortment of conditioning solutions with many successful full scale applications. For example, experiments were conducted which included the introduction of calcium chloride, followed by aluminium sulphate to enhance the strengthening effect of the procedure as well as improving the conductivity of the electrolyte (Bjerrum *et al.*, 1967; Harton *et al.*, 1967; Gray and Schlocker, 1969).

The stabilisation of clayey soils with electrochemically introduced species was also achieved (Adamson *et al.*, 1966a; Adamson *et al.*, 1966b; Adamson *et al.*, 1967). However, the assumption at this time was that the only significant transport mechanism taking place was electroosmosis, and did not take into account the electrostatic

migration of ionic species (cations in particular) in the pore water and adsorbed on the soil surface, the movement of these was found to be primarily influenced by such factors as electric field effects, soil properties and pore water chemistry (Probstein and Hicks, 1993; Eykholt and Daniel, 1994; Baraud *et al.*, 1997; Yeung *et al.*, 1997a; Yeung *et al.*, 1997b etc.).

In the 1980s Reinout Lageman *et al.* at the Geokinetics Company in the Netherlands, conducted some large scale remediation projects using electric currents passed between electrodes emplaced in the soil, coupled with an electrolyte flushing system, they termed the process 'Electroreclamation' (Lageman *et al.*, 1989; Lageman, 1993; Lageman *et al.*, 2005 etc.).

Mixed successes led to both a growth in interest in electrokinetic approaches to contaminated land remediation, and to a return to laboratory based investigations in order to improve the techniques and to better understand the controlling factors for the electrokinetic transport of contaminants in soils. It was in the 1990s that research in the field gathered pace. Yalcin Acar, Akram Alshawabkeh, Robert Gale *et al.* formed a core of researchers working together and with others who published numerous papers throughout the 1990's. Primarily at Louisiana State University, USA, they produced a wealth of laboratory based research using pure clays spiked with a variety of contaminants. Their work forms a significant portion of the key literature for commercial application of electrokinetics for removal of contaminants from the ground from laboratory based experimentation (e.g. Acar and Alshawabkeh, 1993; Acar *et al.*, 1995; Acar *et al.*, 1997; Puppala *et al.*, 1997; Alshawabkeh *et al.*, 1999a; Alshawabkeh *et al.*, 1999b; Alshawabkeh *et al.*, 2004).

Probstein and Hicks (1993) published their research on electrokinetic remediation in the world renowned journal, *Science*. This can be regarded as another key paper in the theoretical/practical development of electrokinetic remediation of contaminated land, and in the dissemination of the electrokinetic approach's potential. It also draws a parallel with the work conducted regarding this thesis, albeit from a different strategic standpoint. The paper describes the precipitation of metal hydroxides and oxyhydroxides at a point between electrodes of opposite charge, but despite being acknowledged as a potential remediation strategy, it is ultimately dismissed, as shall be

discussed later, this kind of precipitation is key to the technique investigated in this thesis.

“Although these tests showed that a metal pollutant can be concentrated at some intermediate region between the electrodes and so can subsequently be removed by excavation of a relatively small amount of soil, true in situ removal at the electrodes is the desired objective. To accomplish this removal, the formation of a focusing region must be eliminated by flushing of the cathode with tap water to remove the hydroxyl ions generated there.”

(Probstein and Hicks, 1993)

The removal of contaminants at the electrode thus became the method of choice for the majority of researchers working in the field, illustrated by this statement from a later scientific paper:

“Successful decontamination depends on maintaining metal ion solubility with either a low or a high pH throughout the soil and avoiding the conditions resulting in precipitation.”

(Page and Page, 2002)

Much experimentation has been conducted, and there is what might be described as a ‘main stream’ approach to laboratory investigations. The common factors tend to be:

- Small scale- typically less than 30 cm electrode separation with a soil volume of 2000 cm^3 (Sometimes *much* less).
- A sealed test vessel (excluding gas vents) with electrode flushing apparatus or constant electrolyte supply/overflow.
- Laboratory grade clay samples (often Montmorillonite, Kaolinite or Bentonite etc.).
- The material is spiked with a laboratory prepared contaminant or contaminants solution.
- Inert electrodes, usually graphite.
- Attempt 100% removal of contaminant at the electrode(s).

(e.g. Pamukcu and Wittle, 1992; Acar *et al.*, 1993; Probstein and Hicks, 1993; Shapiro and Probstein, 1993; Hicks and Tondorf, 1994; Acar *et al.*, 1995; Acar *et al.*, 1997;

Pamukcu *et al.*, 1997; Reddy *et al.*, 1997; Wong *et al.*, 1997; Yeung *et al.*, 1997b; Sogorka *et al.*, 1998; Alshawabkeh *et al.*, 1999a; Alshawabkeh *et al.*, 1999b; Reddy and Chinthamreddy, 1999; Pamukcu *et al.*, 2003; Alshawabkeh *et al.*, 2004; Pamukcu *et al.*, 2004; Reddy and Ala, 2005)

There are exceptions, such as seen in the work of, Haran and Ho, and Mukhopadhyay *et al.* (Haran *et al.*, 1996, 1997; Ho *et al.*, 1997; Ho *et al.*, 1999; Mukhopadhyay *et al.*, 2007). For instance, Haran *et al.* (1996) shun inert electrodes and utilise an alpha-pure sacrificial iron electrode to exploit the reductive properties of electrochemically dispersed divalent iron for the reduction of Cr(VI), Mukhopadhyay *et al.* (2007) describe a similar system and other applications of Fe(II) also exist (Eary and Rai, 1988; Beskid *et al.*, 1993; Pamukcu *et al.*, 2003).

The range of scales is also extremely varied with some workers, perhaps surprisingly, working on experiments measuring just millimetres (Otsuki *et al.*, 2007) while at the other end of the scale, Yu and Neretnieks, (1997), utilise a 3m treatment cell with 100 volts applied. This is an unusually large electrode separation compared to the bulk of the literature which tend to be smaller bench-scale experiments.

Another distinct approach involves chromium contamination specifically hexavalent chromium. Work has been conducted which is very similar to some of the research presented here, where iron anode electrodes are used as a source of iron for the reduction of Cr(VI) to the less dangerous Cr(III). Hexavalent chromium typically forms an oxy-anion in solution causing it to electromigrate towards the anode and therefore the zone of highest ferrous iron concentration (Haran *et al.*, 1996, 1997; Mukhopadhyay *et al.*, 2007). Some encouraging results have been achieved. It is nonetheless difficult to find examples of research where the controlled precipitation of any species in the soil mass is not dismissed as an adversity to the process (e.g. Lageman *et al.*, 2005) in terms of remediation.

Examples of precipitation of electrochemically concentrated materials for engineering purposes are more readily come by (e.g. Endell and Hoffmann, 1936; Bjerrum *et al.*, 1967; Harton *et al.*, 1967; Gray and Schlocker, 1969; Trushinskii, 1993; Trushinskii, 1996).

Through the study of the existing literature, the work presented in this thesis is seen to occupy an otherwise vacant niche in the novel application of established (but not commonly adopted) practises in ground engineering for the purpose of management of contaminated land and ground stabilisation.

In an un-buffered soil material with inert electrodes where the dissociation of water is the sole reaction taking part at the electrodes the formation and migration of the H^+ and the OH^- ions is controlled by the relative mobilities of these ions in a constant electric field and these have been established theoretically with good agreement empirically (Acar *et al.*, 1997; Baraud *et al.*, 1997) these values are given in the Appendix.

Shapiro *et al.* conducted experiments using inert (platinum) electrodes in an agar gel containing a dilute sodium chloride solution to model the development of the pH fronts as a current is applied. Agar was used rather than a soil so that a chromatic pH indicator solution could be used to identify the development and progression of the acid and alkali fronts. These experiments and models have shown that the progress of the acid and alkali fronts is determined by the buffering properties of the medium, and other species in the soil.

A model was also run in the same conditions using an iron anode electrode with an interesting prediction of a narrow region of the soil to show a sharp increase in pH on the boundary where the creation of ferrous hydroxide in the conditions at that part of the pH front development acts as a base, absorbing the available H^+ ions. In an inert substrate with inert electrodes the point of pH jump would be determined purely by the relative rates of diffusion coefficients/ionic mobilities with H^+ having a value of $362.5 \text{ cm}^2 \text{ V}^{-1} \text{ sec}^{-1}$ compared with OH^- , $205.8 \text{ cm}^2 \text{ V}^{-1} \text{ sec}^{-1}$, in free solution (Acar *et al.*, 1997). The values for diffusion coefficient and ionic mobilities are listed in Appendix 1 (Taken from, Acar *et al.*, 1997).

2.5 Electroosmosis

The most visible effect of passing a current through a wet soil mass is that of electroosmosis, whereby the application of an electric field causes the mass movement of water through the soil.

The movement of the water content of a soil in the pore water solution and the bulk movement of water through fissures etc. controls the rate of movement of many types of contamination and the extent and likely fate of land contamination (e.g. Yong and Thomas, 1997; Casey *et al.*, 1998). Electroosmosis therefore is the action of inducing the movement of pore water solution using an electric field, with the obvious implications for the managed movement of contamination.

Darcy's Law describes the flow of water through a medium under a hydraulic head. In his experiments, Darcy introduced water into a sealed container filled with the test medium via an in-flow, and an out-flow of water at each end; incorporating two manometers, to measure the hydraulic head at two points, Δl distance apart.

Darcy's experiments identified, v , the specific discharge of fluid passing through the test medium (a sand or soil for instance) as the rate of in-flow, Q (m^3s^{-1}) per unit cross sectional area of the sample, A , m^2 , (e.g. Freeze and Cherry, 1979; Mitchell and Soga, 2005).

$$v = \frac{Q}{A}$$

Equation 3

Where:

v = specific discharge (ms^{-1})

Q = rate of in-flow (m^3s^{-1})

A = cross sectional area of the sample (m^2)

Darcy's experiments found that, v , was proportional to the applied hydraulic head, Δh , (by convention this is arbitrarily a negative value) when the length of the sample cell (Δl) was constant, and inversely proportional to (Δl) when the hydraulic head was constant.

This is what is now referred to as ‘Darcy’s law’, and is generally written as:

$$v = -K \frac{\Delta h}{\Delta l}$$

Equation 4

Where:

v	=	specific discharge (ms^{-1})
K	=	hydraulic conductivity (ms^{-1})
$\Delta h/\Delta l$	=	hydraulic gradient

The coefficient K (a constant of proportionality) is a property of the medium being tested. It is known as the ‘hydraulic conductivity’, K has higher values for gravel and coarse sands and lower values for clay and rock. It has the same dimensions as v , (ms^{-1}) since the hydraulic gradient term is dimensionless.

By combining Equation 3 and Equation 4 we obtain:

$$Q = -K \frac{\Delta h}{\Delta l} A$$

Equation 5

The hydraulic gradient ($\Delta h/\Delta l$) may be condensed into a single term, i , giving:

$$Q = -KiA$$

Equation 6

This is analogous to the equation for the electroosmotic flow rate, q_A , (Equation 7) from the Helmholtz-Smoluchowski Theory (see Section 2.5.2, Equation 9 and Equation 10) for the prediction of electroosmotic flow velocity per unit of electrical gradient.

$$q_A = -k_e i_e A$$

Equation 7

Where k_e = coefficient of electro-osmotic flow rate (conductivity).
 i_e = electrical field strength or negative potential gradient.
 A = total cross sectional area normal to the direction of flow.

In this model, k_e is defined as:

$$k_e = \frac{\zeta D}{\eta} n$$

Equation 8

Where ζ = zeta potential (see section 2.6.2 below)
 D = relative permittivity (dielectric constant) ¹
 η = viscosity of fluid
 n = porosity

(Mitchell and Soga, 2005; Reddy and Cameselle, 2009)

Here, k_e is analogous to the hydraulic conductivity but is independent of pore size, and it is this factor which gives electrokinetic movement of water in a fine grained soil its advantage over pressure induced movement (Page and Page, 2002).

This demonstrates the theory behind one of the most important properties of electroosmosis in the scope of this thesis; *i.e.* that electroosmosis is a more effective method of inducing movement of solution through a very fine grained medium, than is applying a hydraulic gradient (e.g. Mitchell and Soga, 2005) due to the conductivity not being dependent on pore size, and explains why good electroosmotic flux is achieved in clays due to their high porosity yet small pore size.

This is the theoretical foundation for the interest electrokinetics is gaining as a means for the treatment of materials with low hydraulic conductivities (Kovalick, 1995a;

¹ The permittivity is the measure of the work required to polarize and orientate molecules in an electric field $\varepsilon = \varepsilon_0 D$ taken from, Mitchell, J.K., and Soga, K.B. (2005) *Fundamentals of soil behavior*. xiii, 577 p. p. Wiley, New York ; Chichester.

Kovalick and Kingscott, 1996; Eykholt, 1997). This might include remediation or dewatering of slurries or other dewatering applications- such as stabilisation/consolidation. More recently research has been conducted on the successful dewatering and consolidation of an artificially created, leaking dyke, using electrokinetic methods (Wittle *et al.*, 2008).

A number of terms have been introduced in this section which will be elaborated on in later sections. This section serves to explain the importance of electroosmosis for overcoming the hydraulic properties of low permeability contaminated materials. Terms like ‘zeta potential’ and the Helmholtz-Smulowchowski theory are treated individually in more depth in sections to follow.

Table 6: Comparison of Electroosmotic permeability and hydraulic conductivity for various materials (adapted from, Mitchell, 1976).

Material	Water Content %	K_e $10^{-5} \text{ cm}^2(\text{sV})^{-1}$	K_h cm s^{-1} (approximate)
London Clay	52.3	5.8	10^{-8}
Boston Blue Clay	50.8	5.1	10^{-8}
Kaolin	67.7	5.7	10^{-7}
Clayey silt	31.7	5.0	10^{-6}
Rock flour	27.2	4.5	10^{-7}
Na- Montmorillonite	17.0	2.0	10^{-9}
Mica Powder	49.7	6.9	10^{-8}
Fine Sand	26.0	4.1	10^{-4}
Quartz Powder	23.5	4.3	10^{-4}
Clayey silt, (Little Pic River, Ontario)	26.0	1.5	2×10^{-5}

Table 6, shows the general relationship between electroosmosis and hydraulic conductivity in fresh water. Empirically K_e is normally in the range of 10^{-5} and $10^{-4} \text{ cm}^2(\text{sV})^{-1}$ (Mitchell, 1976) showing that for many clay rich/fine grained materials, K_e is significantly greater than K_h .

Other studies have addressed the relationship between electric field intensity and pore size, finding that the relationship is such that increasing field strength and reduced pore size and fissures improves the electroosmotic effect (Moreau *et al.*, 1997).

2.5.1 Helmholtz Model

This theory describes the phenomena of electroosmosis arising from the charge distribution at the solid/liquid interface. Particles are treated as point charges and form a continuous single layer on a charged surface such as an electrode or a clay particle.

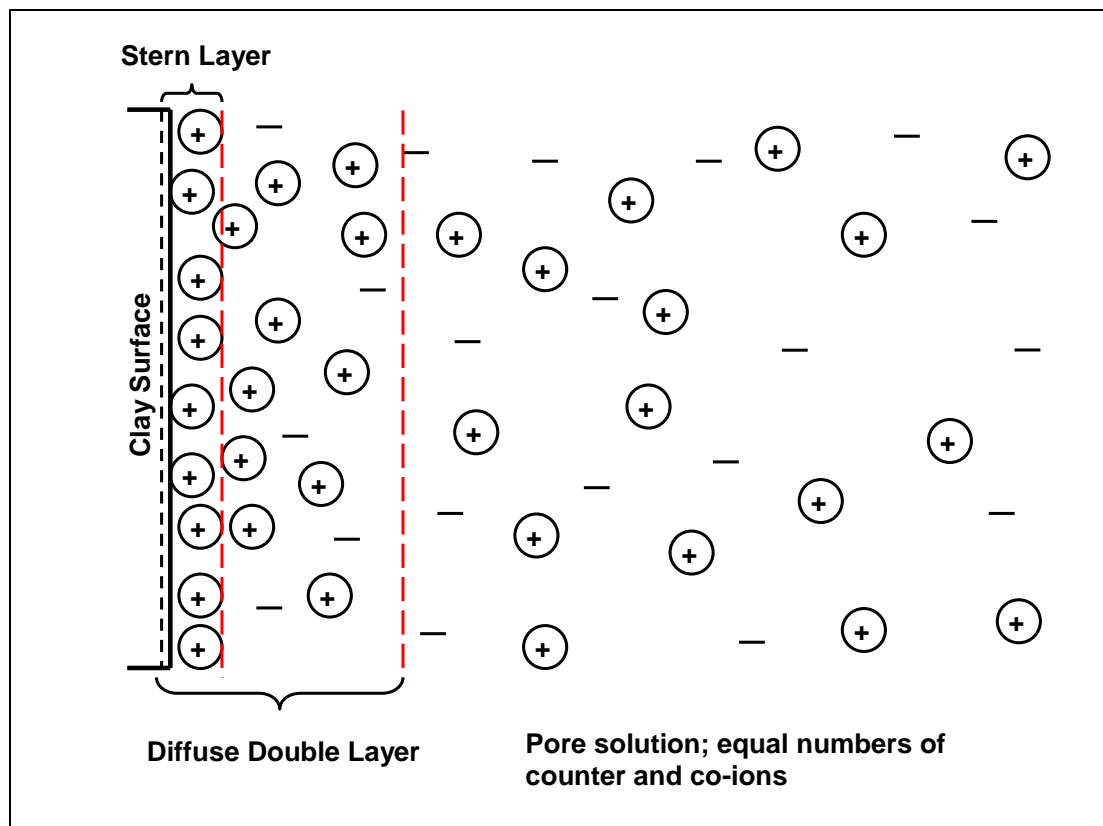


Figure 4: Graphical representation of the charge distribution on and around a clay surface The edge of the slip plane is located at the edge of the Stern layer furthest from the clay surface (diagram adapted from, Mitchell and Soga, 2005)

This model is considered to be the first theory to deal with what is now termed the ‘diffuse double layer’ and underwent a number of reincarnations following this initial form. Helmholtz used a mathematical model based on that of a capacitor and applied it

to the electrokinetic problem. Since the charged particles are considered to be dimensionless point charges, the Helmholtz model overestimates the surface charge-density, Figure 4.

2.5.2 Helmholtz-Smoluchowski Equation:

The Smoluchowski equation describes the relationship between the electrophoretic mobility, the zeta potential (related to surface charge conditions, see section 2.6.1), and the pore solution properties. Since electrophoresis is the inverse of electroosmosis (in electroosmosis the liquid phase moves relative to the solid phase, and in electrophoresis, the solid phase moves relative to the liquid phase), both are controlled by the interaction between the applied electric field and the charge on the diffuse double layer and the same mathematical expression describes both. The common form of the equation is:

$$\mu = \frac{\zeta \varepsilon}{\eta}$$

Equation 9

Where:

ζ	= Zeta potential
μ	= Electrophoretic/electroosmotic mobility
ε	= Electric permittivity of liquid
η	= Viscosity of liquid

And, as was seen in Equation 7, and Equation 8

$$q_A = -\frac{\zeta \varepsilon}{\eta} n i_e A$$

Equation 10

Where:

q_A	=Electroosmotic flow rate
n	=Porosity
i_e	=Electrical gradient
A	=Cross sectional area

Thus the surface charge characteristics, the applied electric field and the porosity and the viscosity of the liquid are combined to describe the rate of electroosmosis. This

formula, although somewhat simplified, agrees well with most empirical studies, and measurements made in the field (e.g. Casagrande, 1949).

Derived from the original Helmholtz model (1879), the Helmholtz-Smoluchowski model relates the rate of electroosmosis to the electrical gradient applied and was developed from Quinke's work on the effects of electric fields on clay particles in a glass capillary.

Its derivation is such that the velocity of the liquid is assumed to be constant across the diameter of the capillary. This assumption is feasible when the diffuse double layer is very small compared to the diameter of the capillary. The Helmholtz-Smoluchowski equation in its common form is as shown below, (Equation 11):

$$v_{eo} = -\frac{\zeta \epsilon}{\eta} \cdot \frac{\delta \phi}{\delta x}$$

Equation 11

Where:

v_{eo} = Electroosmotic (electrophoretic) velocity

ϵ = Dielectric constant of pore fluid

ζ = Zeta potential

η = Viscosity of fluid

$\partial \phi / \partial x$ = Electrical gradient.

(Lyklema, 2003; Mitchell and Soga, 2005; Pamukcu, 2009)

The Helmholtz Smoluchowski equation links the electric gradient, the dielectric constant (which is 80 for pure water under standard conditions, although the dielectric constant will vary for different conditions it is often taken to be a constant (Mitchell and Soga, 2005)) and the electroosmotic velocity.

Since the zeta potential for similar soils will be of similar magnitude, the controlling factor becomes the electric gradient, for most common environmental conditions the dielectric constant will not vary to a significant degree (Mitchell, 1976; Mohamed and Antia, 1998; Mitchell and Soga, 2005; Masliyah and Bhattacharjee, 2006).

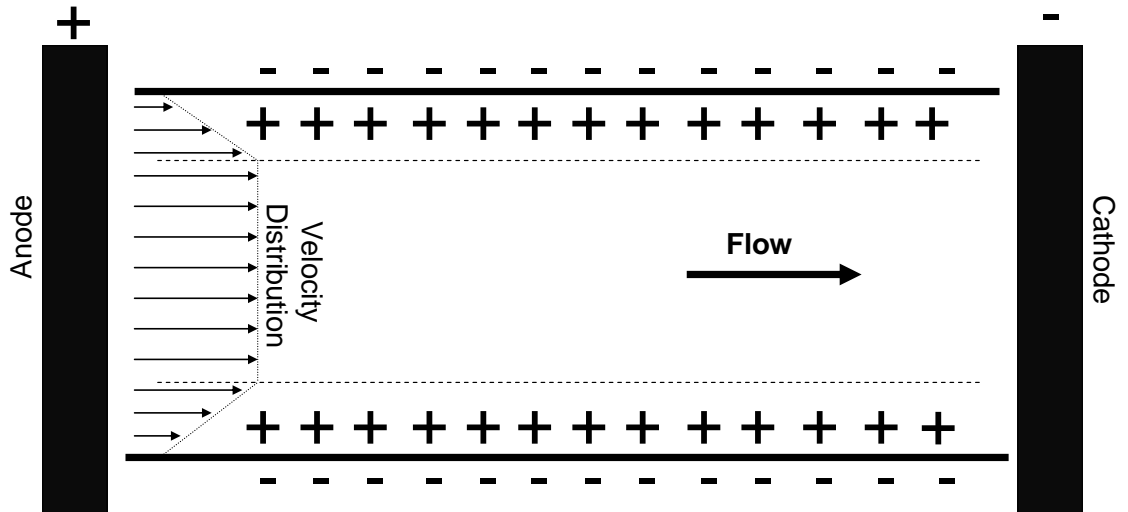


Figure 5: Helmholtz-Smoluchowski model for electroosmosis in a capillary showing flow distribution (adapted from, Mitchell, 1976; and, Mohamed and Antia, 1998).

Figure 5 shows the theoretical conditions arising from the flow of mobile cations in a capillary tube with net negative charge used to simulate electroosmosis through a clay with net negative charge, there is a steep velocity gradient between the two planes of the condenser (the opposite sides of the capillary as shown in the diagram). The rate of flow is determined by the proportionate influence of the electrical gradient versus the friction between the electrolyte and the containing wall.

The Helmholtz-Smoluchowski should be independent of pore size, as opposed to the hydraulic conductivity which is not. Mitchell (1976) illustrates this with a straightforward example which is adapted below:

“Two materials: Fine sand and a clay with values of hydraulic conductivity K_h of:

clay: $K_h = 1 \times 10^{-8} \text{ cm s}^{-1}$

fine sand $K_h = 1 \times 10^{-3} \text{ cm s}^{-1}$

both have equal k_e of $5 \times 10^{-5} \text{ cm}^2(\text{sV})^{-1}$ So for equal flow rates

$$k_h i_h = k_e i_e$$

or

$$i_h = \frac{k_e}{k_h} i_e$$

If we apply a potential gradient of 0.2 V cm^{-1} then for the fine sand

$$i_h = \frac{5 \times 10^{-5}}{1 \times 10^{-3}} \times 0.2 = 0.01$$

and for the clay,

$$i_h = \frac{5 \times 10^{-5}}{1 \times 10^{-8}} \times 0.2 = 1000$$

Thus for the sand, a hydraulic gradient of only 0.01 can move water as effectively as an electrical gradient of only 0.2 V cm⁻¹. But for the clay; a hydraulic gradient of 1000 would be needed to offset the electroosmotic flow.”

(Taken from, Mitchell, 1976)

This gives a numerical perspective on relationship between hydraulic flow and electroosmotic flow in sands and clays.

However, as Mitchell points out, there are no energy considerations here and the implied efficiency of the electroosmotic process does not account for the technical and physical processes implicit in orchestrating actual electroosmosis through a soil medium- factors such as the power expenditure required to deliver the necessary electrical potential, for instance. Now that some of the theory of electrokinetic approaches has been discussed the environmental factors and soil properties will be considered.

2.6 Electrokinetics: The Soil/Solution Interface

The observed electrokinetic phenomena associated with electrokinetic remediation depend on the interaction at the interface of solid and liquid on a soil particle. The phenomena arise due to interactions between the applied charge from the electrodes and the charge developed on the soil particle surface. This charge tends to develop due to a combination of irregularities in the crystal lattice and/or the presence of variable ionisation compounds at the surface. It is the presence of a net negative surface charge

on clay minerals, and dissolved charged species in the pore fluid that account for most of the electrokinetic effects observed when a current is applied.

2.6.1 Soil Chemistry and Composition

There is a growing appreciation of soil as a finite resource which has to be conserved, protected and retained as the need for fertile and productive soil is ever growing (Montgomery, 2007). The need for good healthy soil for agricultural purposes is obvious; but there is added pressure from the growing importance of energy production from bio-fuels, which puts extra demand on soil resources since the competing demand for land for growing fuel crops compete directly with the demand for land dedicated to food and fibre crops (Giampietro *et al.*, 1997). Research has been conducted on the possibility of the creation of synthetic soils derived from ‘waste’ materials produced as a by-product of industrial processes; an organic fraction is combined with mineral components (Guest *et al.*, 2001). The difficulty lies in that good soil is not just a mixture of mineral content and organic matter in the appropriate proportions.

Mature soils are developed over hundreds of years (e.g. Montgomery, 2007; Ponting, 2007) and the result is a material with a highly complex composition, a vast and varied microbial population and comprises a habitat supporting a range of organisms and ecosystems. The basic general description of a soil identifies a number of discrete regions within the profile of the soil. The uppermost layer is the organic layer (referred to O horizon with an overlying L layer or litter region) consisting of plant matter from the freshly deposited through to the more decayed material beneath. The A horizon is below this and consists of a zone of mixed mineral and organic matter. This is sometimes underlain by the E horizon, identified as a region depleted in certain components (E comes from *elluvial* meaning that the soil components have been transported out of this region.) The B horizon is below this in the profile and is the *illuvial* region where the components transported from the E horizon accumulate and is characterised by the accumulation of organic matter, minerals and inorganic chemicals. The C horizon consists of unconsolidated parent material and lies directly above the consolidated parent bedrock material, the R horizon. Different soils will not necessarily

have all of these layers present and the extent and characteristics of each layer displays an enormous variability across different soils (e.g. White, 2006).

In a temperate climate a typical soil is a *podzol* which has distinctive horizons clearly differentiated, see Table 7. Below the *elluvial* zone in the accumulation zone acidic soils may result in the formation of ‘iron pans’ (see Section 2.6 for a description of environmental generation of iron pans and environmental analogies).

The loss or destruction of soil resources has historically has been implicated in the fall of various civilisations in antiquity (Montgomery, 2007), and there is growing realisation that the soil is a fragile and finite resource which is squandered at great peril. It has been estimated that the current rate of disappearance of useful soil resources is more than twenty times the rate at which it is being created (Montgomery, 2007). Slowly, appreciation and action is being taken to assess and properly manage the soil as the fundamental resource that it is and government policy is moving on the right direction (e.g. Environment Agency, 2004).

There are difficulties in the classification of soils since there are many and diverse properties to consider. Due to the variety in soil horizon development, composition and physical properties a taxonomical approach, comparable to that used for the classification of organisms used in biology, with soils belonging to a nested position within a system of divisions and subdivisions has been adopted. There are a number of classification systems in existence; this is due in part to the existence of soils which are fairly unique to a particular country as well as the lack of other types of soil which makes a pan-global system somewhat unwieldy in some cases. However, there have been commissioned global soil surveys, such as the FAO (Food and Agricultural Organisation) global survey of soil resources. A generalised composition of a generic soil is given in Figure 6.

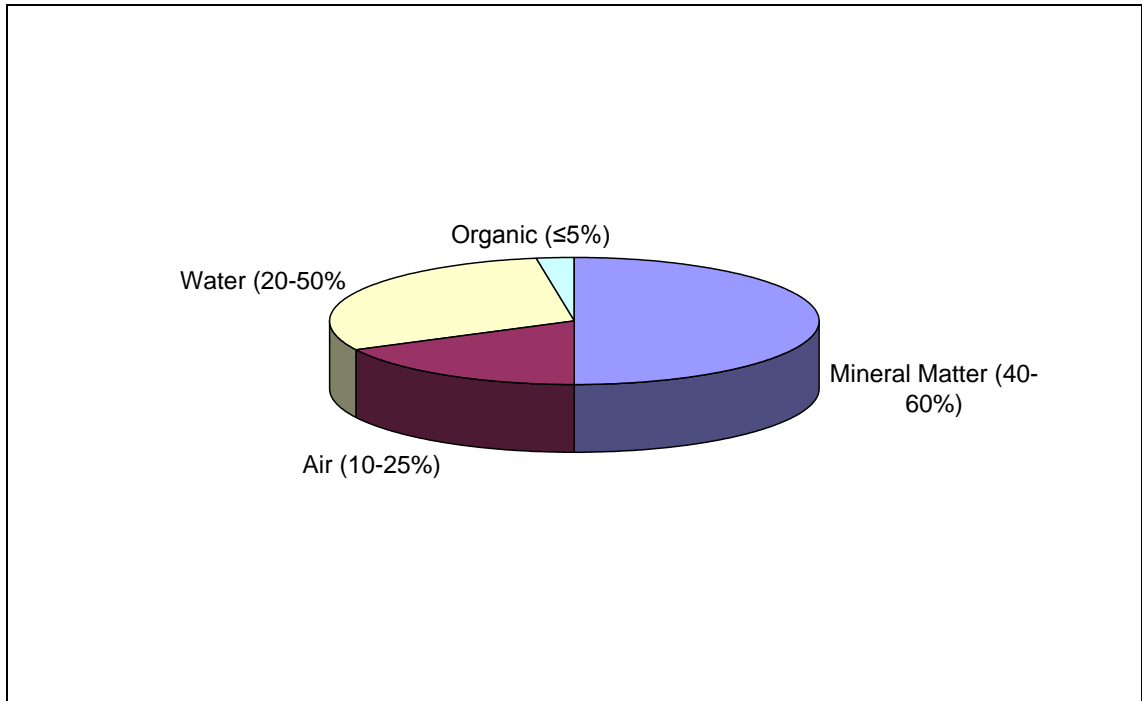


Figure 6: Relative proportions of soil components by volume. These may vary widely but generally lie within the ranges indicated (White, 2006).

The formation of a soil begins with the weathering of bare rock by wind rain and the action of organisms. This follows with pioneer plant species- lichen, liverworts, mosses etc) colonising the weathered material. Some lichens also fix atmospheric nitrogen which is incorporated into complex organic compounds, along with species extracted from the rock material, which are then returned to the proto-soil (lithosol) when the plant dies or sheds leaves. Organisms feeding on the plants may also add to the mix with the deposition of their faeces. These compounds are then further acted on by soil microbes which synthesise and metabolise these organic compounds.

As the soil continues to develop, more varied plants and trees are able to colonise the soil and as well as increasing the rate of weathering with their root action, the volume and rate of addition of organic material also increases. For a calcareous soil developing in a temperate climate this soil might mature into a brown forest soil with a deep dark-brown organic horizon with a gradual merging into a lighter coloured mineral soil over altered parent material (e.g. White, 2006).

Table 7: Outline description of the Major Groups of soil classification for soil survey in England and Wales. Within these major groups there are 41 groups, and 109 sub-groups (Taken from, White, 2006).

Soil Group	Description
Gley Soils	Soils which are subjected to long periods of water logging. Horizons can be grey-coloured with mottling.
Lithomorphic soils	Soils with shallow profiles, characterized by organic horizons overlying bedrock
Pelosols	Soils with high clay concentrations which crack when dry.
Brown soils	Well-drained soils with no gleyed features above 40cm. Good agricultural soils which are divided further into subgroups on the basis of degree of lessivage and mottling, below 40 cm.
Podzolic soils	Soils generally formed under acidic environments showing accumulations of organic matter and accumulations of iron and iron oxides. There may be the development of an iron pan in the B horizon.
Man-made soils	Self explanatory, examples include soils formed from remediation processes following mining and quarrying.
Peat soils	Soils rich in organic matter, with organic matter accumulations at least 40cm thick.

The formation and composition of a particular soil is therefore dependent on a number of factors; initially the type and characteristics of the inert rock, but also the climate the topography and the organisms present all play an important role in the development of the soil and the resulting physical and chemical properties (Darmawan and Wada, 2002).

Charge development in soils is primarily due to two phenomena: isomorphic substitution in the crystal lattice (permanent surface charge, not pH dependent) and ionisation of functional groups on the surface of solids making up the soil matrix (pH dependent). These result in the constant surface charge of some minerals (notably in clays) and the pH dependant charge on the surface of clays and other minerals (Andrews, 1996). The charge characteristics of some common soil components are illustrated in, Figure 7.

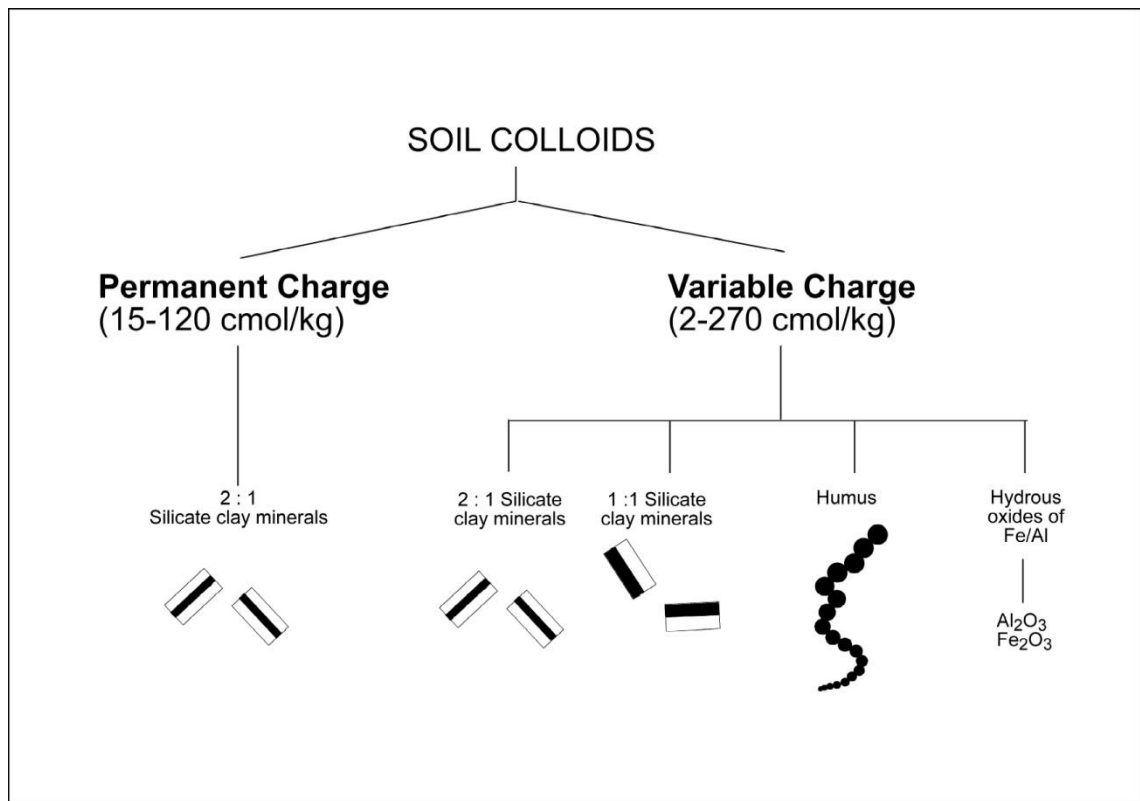


Figure 7: Soil colloids grouped on the basis of their charge characteristics. 2:1 clay minerals have both a permanent and a variable charge, whereas 1:1 clay minerals, humus and oxides of iron and aluminium have a (pH influenced) variable charge (taken from, Ashman and Puri, 2002).

Isomorphic substitution occurs when an ion in the crystal matrix is substituted for another of a different valence. Since the charge distribution is altered within the matrix this is not influenced by ions in solution (or pH) and results in what is known as a *constant surface charge* mineral (e.g. Alloway and Ayres, 1997). The presence of counter-ions in solution means that these become adsorbed to the surface of these minerals (Mohamed and Antia, 1998).

The second type of charge in soils is the pH dependant type termed *constant surface potential*, in these the charge depends on the concentration of H⁺ ions (the charge determining ions), associated with functional groups on the surface of the soil particles. The functional groups concerned are typically carboxyl, hydroxyl, phenol and amine groups. It is the protonation or deprotonation of these functional groups (hence pH dependency) that determines the charge on the functional group. The fractions of the soil which have associated functional groups such as these include sheet silicates, metal oxides, hydrous oxides, and organics (Mohamed and Antia, 1998; Altaee, 2004; Mitchell and Soga, 2005; Altaee *et al.*, 2007) and all influence the retention or mobility of dissolved species (Potter and Yong, 1997, 1999). This is also related to the cation exchange capacity discussed in section 2.6.2.

One of the implications of environmentally controlled charge development is the concept of zero point of charge. This is the pH (H⁺ concentration) for which the net charge on the surface of the clay mineral is zero, Table 8. This reduces the electrostatic repulsion between particles, and coagulation of small particles into larger aggregations in the pore water takes place; therefore the potential mobility of contaminants may be increased due to the relative increase in pore space and associated hydraulic conductivity.

Table 8: The pH values for ‘zero point of charge’ of selected minerals. At pH lower than these values, the mineral will have a positive surface charge; and at higher pH values the charge will be negative.

Mineral	pH
Haematite	2.1
Kaolinite	4.2
Gibbsite	4.8
Amorphous Iron	8.5

(Adapted from, Mohamed and Antia, 1998)

There are a number of theoretical models which have been formulated and refined to deal with the soil/solute interface and interactions under an electric field; these are discussed in, Section 2.6.4.

The importance of the development of such surface charge is significant due to the effect it has on the adsorption of species in the soil. Adsorption is one of the most important chemical processes in soils controlling the availability of nutrients for plant uptake, the mobility of metals, hydrocarbons and other organic species. It is thus responsible for the mobility and availability of species essential for plant growth and the distribution and mobility of contaminants as well as the electrostatic properties of a soil which might include the coagulation and precipitation of species in the soil.

Table 9: Some naturally occurring oxides, oxyhydroxides, and hydroxides found in soils (Sparks, 1995)

Aluminium oxides	Bayerite α -Al(OH) ₃ Boehmite γ -AlOOH Diaspore α -AlOOH Gibbsite γ -Al(OH) ₃
Iron oxides	Akaganite β -FeOOH Ferrihydrite Fe ₁₀ O ₁₅ .9H ₂ O Feroxyhyte δ -FeOOH Goethite α -FeOOH Hematite α -Fe ₂ O ₃ Lepidocrocite γ -FeOOH Maghemite γ -Fe ₂ O ₃ Magnetite Fe ₃ O ₄
Manganese oxides	Birnessite δ -MnO ₂ Pyrolusite β -MnO ₂
Titanium oxides	Anatase TiO ₂ Rutile TiO ₂

Naturally occurring metal oxides, oxyhydroxides and hydrous oxides are an important component of many soils. Of these, those of aluminium, iron and manganese are the most important (Sparks, 1995). Not the most abundant of the soil components, the oxides, as they can be generally referred to, are important because of their relatively high surface areas and reactivity. The oxides may exist as discrete crystals, as coatings

on phyllosilicate and humic substances, and as mixed gels, and are collectively part of the secondary soil minerals group, some of these are listed in Table 9.

Of the iron oxides Goethite is the most stable and the most common oxide found.

The extent to which any particular metal ion is labile in the soil environment is dependent on a number of factors, pH being the most significant of these (Selim and Amacher, 1997) due to the relatively wide range of pH values which can be encountered in a soil system.

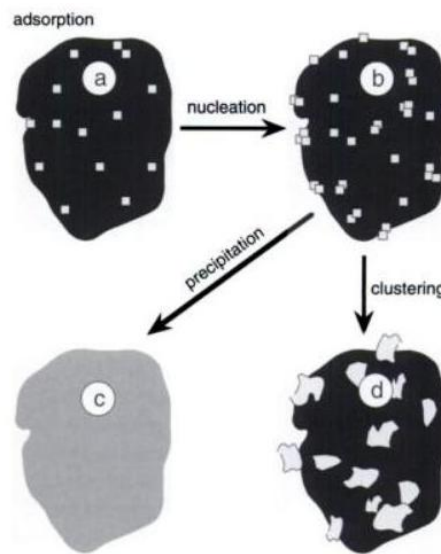


Figure 8: An illustration of material ion sorption reactions on a (hydr)oxide particle. (a) At low surface coverage, isolated site binding (adsorption) is the dominant sorption mechanism; (b) with increased metal loading, M hydroxide nucleation begins. Further increases in metal loadings results in (c) surface precipitation or (d) surface clusters (Fendorf, 1992).

Another phenomenon, related to adsorption, is surface precipitation, Figure 8, this occurs when sorption results in a high level of surface coverage and the cation or anion forms a precipitate with the mineral (Fendorf, 1992; Fendorf, 1995).

Part of the terminology of adsorption and of importance at the soil solution interface is the concept of ‘zeta potential’ which will be addressed in the next section.

2.6.2 Zeta Potential

At the interface between a solid surface and a liquid solution, a potential develops due to the differential separation of charged species. This charge is known as zeta potential (Greek letter zeta- ζ) and its development influences the charge distribution in the vicinity of the interface region, giving rise to what is termed the double layer (see Section 2.5.1). The solid surface may be a clay particle, or electrode surface or any solid present in the liquid medium.

The zeta potential is electrical potential, usually measured in millivolts, and is the primary factor influencing electrophoresis and electroosmosis. Since the surface of clay particles in a solution in a moderate pH range can be considered to have a net negative charge (recall the zero point of charge in Section 2.6.1), the double layer tends to consist of cations and positively charged species, or (less commonly) exteriorly positive micelles. It is essentially an empirical measurement of the electrical potential associated with the charge surrounding a solid in an electrolyte solution.

The application of an electric field causes the migration of charged species such as ions, micelles and colloidal clays etc. The exact composition of a soil in terms of the mobile species and the ratio of cations to anions will be subject to variation between different soil types. Generally there will be an excess of cations and the net movement of these from anode to cathode exerts a frictional effect on the solution, observable as electroosmotic flow in the same direction.

Under extreme conditions this flow may reverse, acidification of the anode region due to the creation of protons from the dissociation of water may reverse the zeta potential from negative to positive due to the cation (proton) saturation on the soil particles surfaces resulting in a positive surface charge (related to zero point of charge, Table 8). In soils with a low buffering capacity, reversal of the electroosmotic flow has been observed in electrokinetic remediation experiments (e.g. Eykholt and Daniel, 1994; Virkutyte *et al.*, 2002; Mitchell and Soga, 2005; Garcia-Gutierrez *et al.*, 2007). This is due the pH at the anode becoming less than the point of zero charge (PZC) resulting in a positive zeta potential, the opposite takes place at the cathode and the PZC becomes

more negative. This reversal of the usual direction of electroosmotic flow is termed *electroendosmosis* (Reddy and Cameselle, 2009)

2.6.3 Gouy-Chapman Electrical Double Layer Model

By addressing some of the limitations of the Helmholtz model the work of Gouy and Chapman developed a more robust model of the double layer. When a flat surface is considered, the charge on that surface influences the ion distribution in the electrolyte in the vicinity (Figure 4). The resulting arrangement consists of the negatively charged clay surface attracting and adsorbing the diffuse double layer arrangement of positively charged species. The Gouy Chapman model makes a number of assumptions, namely:

- The adsorbent surface is a uniform plane of charge density (despite the fact that the structure of sheet silicates in clays have ‘*constant surface charge*’ on the flat surfaces and pH dependent, ‘*constant surface potential*’ regions on the sheet silicate edges due to broken chemical bonds).
- The adsorptive ions only interact with the charged surface and each other through electrostatic attraction and repulsion and this is manifest in the formation of the diffuse double layer.
- The aqueous solution has a uniform dielectric constant.

(Mohamed and Antia, 1998)

The treatment of the cations as dimensionless point charges in the Gouy-Chapman model over estimates the amount of counter ions adsorbed to a charged surface for a given charge. In addition, the dielectric is known to vary close to the charged surface due to the increased concentration of cations compared to anions (e.g. Sparks, 1995).

2.6.4 The Stern Model

The Stern layer model addresses the limitations of the Gouy-Chapman diffuse double layer and is sometimes referred to as the Gouy-Chapman-Stern model. This model still

assumes that the charged particles are infinitely small but attempts to correct the deficiency in the Gouy-Chapman model by introducing a minimum distance ' δ ' where the adsorbed species form a layer between the charged surface and the first layer of the adsorbed counter ions (Mohamed and Antia, 1998). This compact layer close to the surface is termed the Stern layer. There is a linear decrease in the electrical potential across the Stern layer, Figure 9.

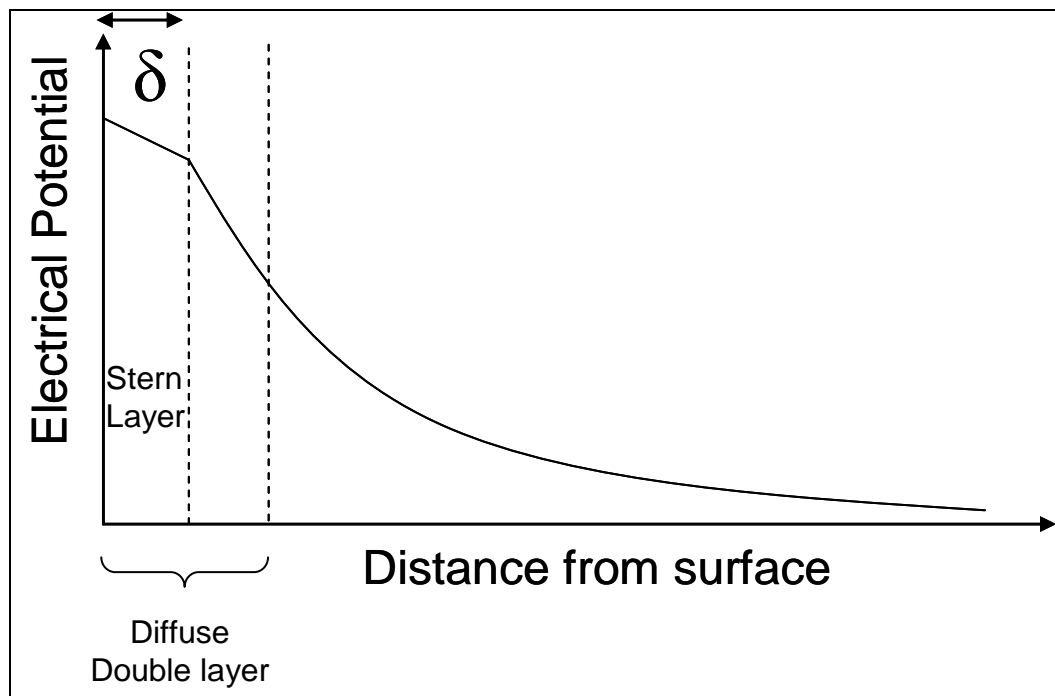


Figure 9: Electrical potential distribution on a clay particle surface. The distance delta defines the Stern layer characterised by a linear reduction in potential, typically δ will have a value $\geq 10\text{nm}$ (e.g. Masliyah and Bhattacharjee, 2006).

Beyond the Stern layer there is an exponential decrease in electrical potential moving away from the particle surface through the diffuse double layer. The boundary between the Helmholtz layer and the Stern Layer is called the shear zone (Masliyah and Bhattacharjee, 2006). The layer distribution (not to scale) around a theoretical particle is shown in, Figure 10 .

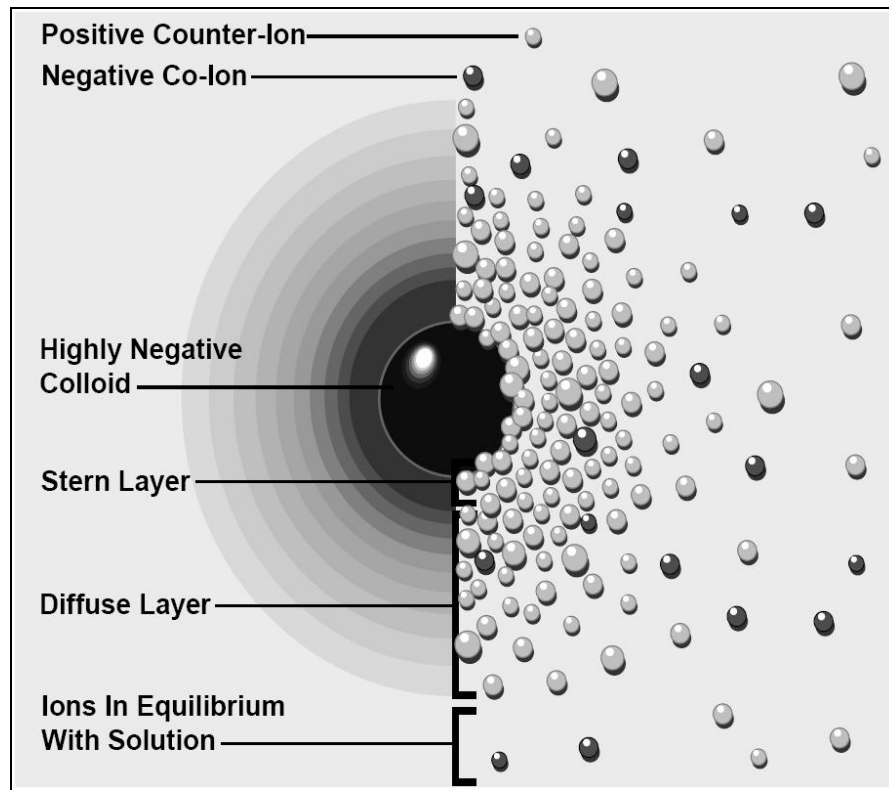


Figure 10: Charge distribution around a colloid particle showing the named layers.

The ‘Stern Layer’ is characterised by strongly associated counter-ions and a linear drop in electrical potential with distance. The diffuse double layer, also known as the Helmholtz plane is next to this. The zeta potential is a measure of the voltage or potential difference between this region and the general pore-water solution, see section 2.6.2 above. Outside of this area the charge distribution equalises with no net charge in the pore solution. The Stern theory allows for changes in the dielectric constant as well as for bonding other than by purely electrostatic forces. (Mohamed and Antia, 1998; Mitchell and Soga, 2005)

The stern model has shown greater experimental accuracy when compared to the Gouy Chapman model although there is comparable agreement at lower surface potentials, Figure 11. This shows that there is better agreement between experimentally measured values and the Stern model compared to the Gouy-Chapman model (the ratio δ/ϵ' where δ is the thickness of the Stern layer and ϵ' is the average dielectric constant, used in calculating the net surface charge was 0.015 (Sparks, 1995)).

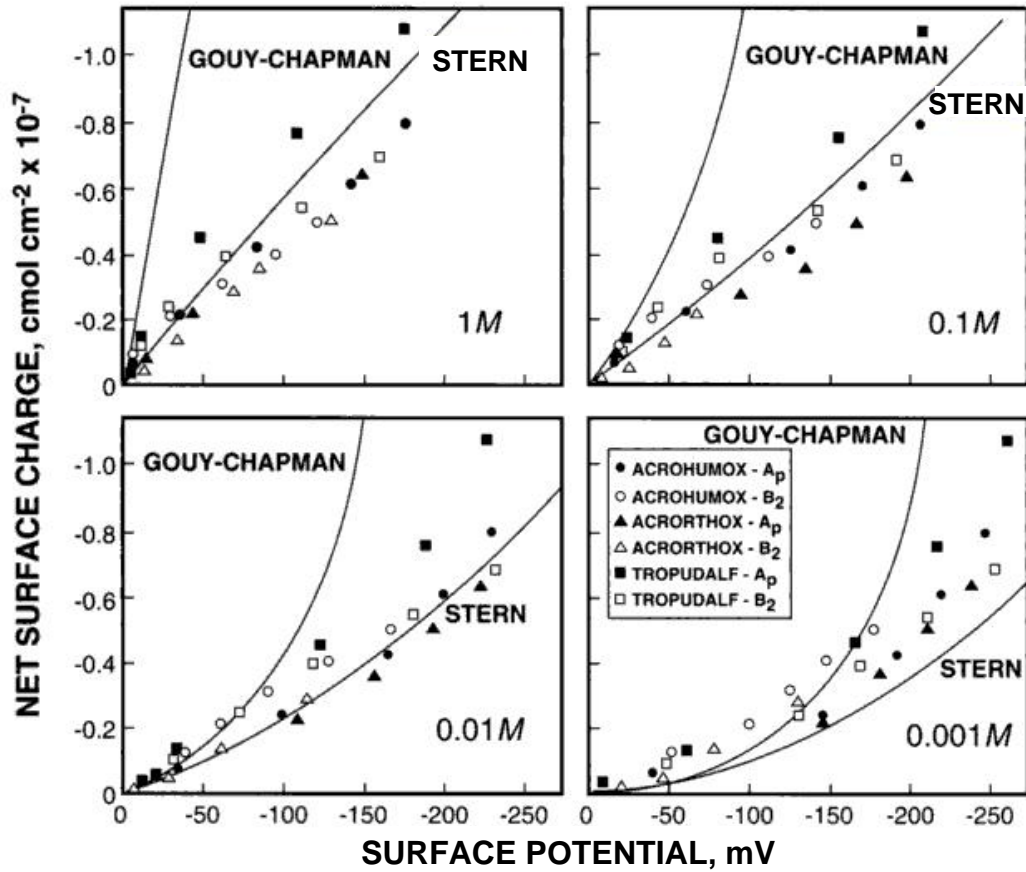


Figure 11: Comparison of the net negative surface charge of soils as determined by potentiometric titration using point of zero salt effect (PZSE), with that calculated by Gouy–Chapman and Stern theories (taken from, Sparks, 1995).

2.6.5 Electromigration

This is the movement of charged species through a medium under the influence of electrostatic attraction. In a solution species are able to move relatively unimpeded but in a soil or clay the path taken must go around the particles resulting in a tortuous path. The ionic velocity is given by, Equation 12 (Acar and Alshwabkeh, 1993; Narasimhan and Sri Ranjan, 2000; Lynch, 2009).

$$v_{ion} = u \frac{dV}{dL} n \tau$$

Equation 12

Where

dV/dL is the electrical gradient

n is the porosity of the medium

τ is the tortuosity

u is the ionic mobility and is defined in Equation 13 (Narasimhan and Sri Ranjan, 2000; Lynch *et al.*, 2007; Lynch, 2009)

$$u = \frac{D_i z F}{RT}$$

Equation 13

Where

D_i is the diffusion coefficient of species i in solution

z is the ionic charge

F is the Faraday constant

R is the gas constant

T is temperature in Kelvin

A list of ionic mobilities and diffusion coefficients is included in Appendix 1.

2.6.6 Cation Exchange Capacity

Since the surfaces of soil colloids; defined as the fraction less than 0.001 mm in size- colloidal clays, humic substances, inorganic colloids such as Mn oxides etc., tend to be negatively charged, their counter ions are thereby normally cations, and therefore the exchange occurs between those cations forming the diffuse double layer, and those free in solution. The cation exchange capacity (CEC) is a measure of the exchangeable charge per unit mass, usually measured in cmol kg^{-1} (centimoles per kilogram). The soil fraction with the highest CEC is soil organic matter, Table 10.

Table 10: Cation exchange capacities of some typical soil components.

Soil constituent	CEC cmol kg ⁻¹
Organic Matter	150-300
Kaolinite	2-5
Montmorillonite	80-100
Illite	15-40
Vermiculite	150
Hydrous oxides	4

(Alloway and Ayres, 1997)

Cation exchange is dependent on the cation concerned. An ion with a higher valence will replace one of a lower valence (e.g. Al³⁺ will be more strongly adsorbed than K⁺). Ionic radius is also important, a smaller hydrated ionic radius will be more readily adsorbed than a larger one (Alloway and Ayres, 1997). Organic compounds in the soil may only make up a relatively small fraction of the soil, typically less than 5%, but they play a major role in the adsorption reactions and therefore the CEC of a soil. The typical constituents making up the organic fraction of a soil are shown in Table 11.

Table 11: Major classes of organic matter in soils, (Manahan, 2000).

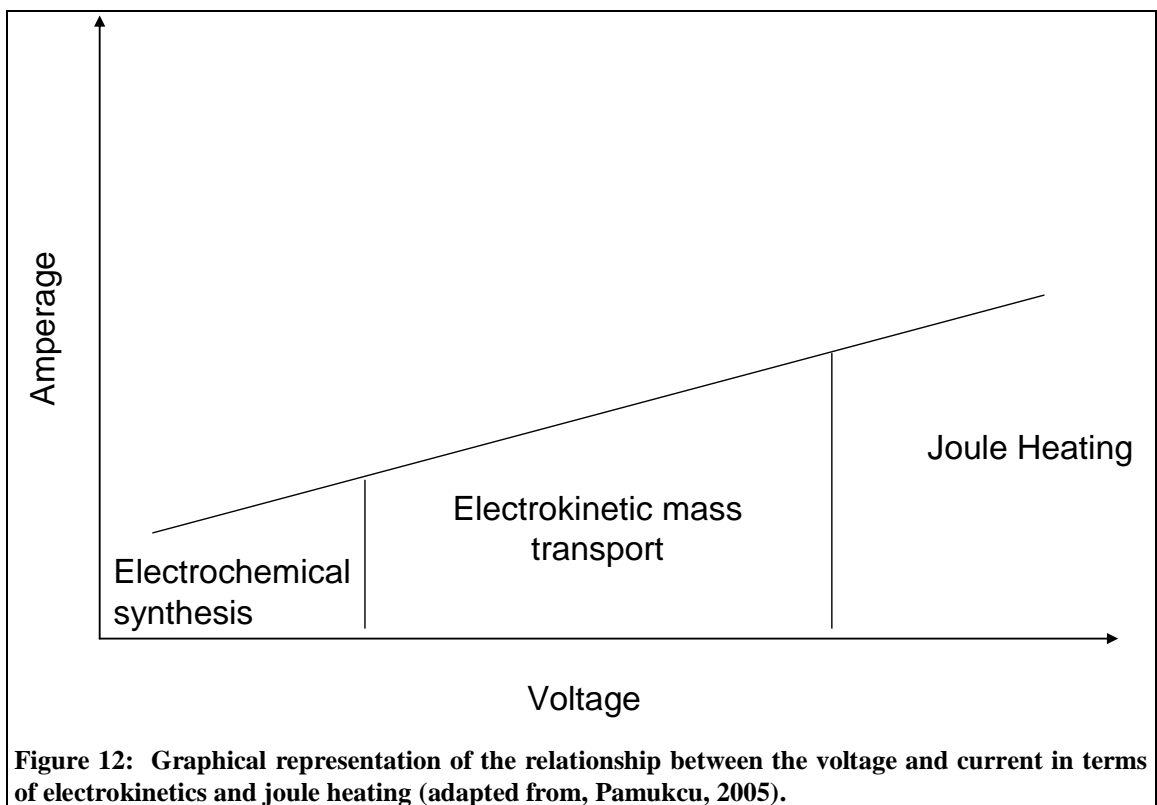
COMPOUND TYPE	COMPOSITION	SIGNIFICANCE
Humus	Degradation resistant residue from plant decay largely C, H and O	Most abundant organic component, improves soil physical properties, exchanges nutrients, reservoir of fixed N.
Fats, resins, and waxes	Lipids extractable by organic solvents.	Generally, only several percent of soil organic matter, may adversely affect soil physical properties by repelling water, perhaps phytotoxic.
Saccharides	Cellulose, starches, hemicelluloses, gums.	Major food group source for soil micro-organisms, help stabilize soil aggregates.
Nitrogen containing organics	Nitrogen bound to humus, amino acids, amino sugars, other compounds.	Provide nitrogen for soil fertility.
Phosphorous compounds	Phosphate esters, inositol phosphates (phylic acid) phospholipids.	Sources of plant phosphate.

Anion exchange may also take place, though it is usually much less significant than cation exchange. Certain materials (especially hydrous oxides of Fe and Al) can have positive sites on their surfaces which hold anions in exchangeable positions (Manahan, 2000). Again, the charge on these materials are dependent on the counter ion concentration and are therefore pH dependent with an associated zero point of charge.

2.6.7 Joule Heating

A number of phenomena occur when an electrical current is passed through a soil or sediment as has already been discussed; another factor which has not yet been introduced is that of joule heating.

Joule heating is the term used to describe the temperature change induced by passing an electric current through a material. The amount of heat expressed in joules is related to the current applied in amps, the resistance of the medium in Ohms and the duration of the application of the current measured in seconds



Joule's law is expressed as

$$Q = I^2 R t$$

Where Q is the heat generated, I, is a constant current flowing through a medium of electrical resistance, R, for a time, t. When these coefficients are all expressed in SI units, Q is given in Joules.

Temperature effects have obvious implications in terms of making an electrokinetic process as energy efficient as possible, Figure 12, but significant heating can also have an effect on the migration of contaminants and detrimentally affect the remediation efficiency (Baraud *et al.*, 1999).

In the circumstances considered in this thesis, the conducting medium is the 'soil' which may have a variable resistance. This variation might be due to changes in water content, with a drop in saturation leading to an increase in resistance. The migration of ions may result in an increase in resistance as there are fewer charge carrying ions present to carry current. Conversely there might be an initial decrease in resistance as the breakdown of the pore water initially increases the number of charge carrying ions present in the soil. This effect has been observed with an initial increase in current flow at the beginning of an experiment, before the exponential decay of the current value begins.

2.7 Environmental Analogies

The formation of iron precipitates from the artificial manipulation of redox and pH conditions, i.e. by electrical means, has an analogue in open systems found in the lithosphere (Jacob *et al.*, 1994). In the laboratory, flux is maintained by supplying electrical potential to the electrodes, preventing a thermodynamic equilibrium occurring

and imparting a continuous supply of iron into the system, from the dissolution of an iron electrode..

Thermodynamic conditions in the lithosphere may also provide sufficient energy gradients to produce analogous metal hydroxide precipitates as may be found in quartz sand basins such as the Lower Greensands in the Folkestone Beds, UK.

According to Klein, (1990), natural processes resulting in the generation of an electrical potential can be grouped into six categories:

- Electrochemical potentials (Eh/pH)
- Tensor induced potentials (pressure/temperature gradients)
- Potentials as a function of phase transformation (phase boundary)
- Potentials produced by induction (polarization)
- Electrokinetic potentials (electrophoresis/electroosmosis Dorn effect etc.)
- Electropotentials produced by radioactivity

In soils the migration and subsequent precipitation can result in the formation of what are known as ‘iron pans’ from the translocation of substances in the upper regions of the soil to the lower horizons. Conditions in the lower portions of the soil can be substantially different from those encountered near to the surface. There may be flocculation of clays and precipitation of metals which may coat ped faces (White, 2006). If there is significant iron present this can result in a continuous precipitated region or horizon, typical of a ferruginous sand as described above.

2.8 Electrokinetic Stabilisation

Electrokinetic methods are already being used on a large scale for the stabilisation of soils, either by utilising the a strength improvements from the de-watering of the area around the anode (e.g. Lamont-Black, 2001; Micic *et al.*, 2003; Burnotte *et al.*, 2004),

or by mobilising additives such as cements and grouts to the required areas (e.g. Ingles and Metcalf, 1972).

Stabilisation of soils through controlled electroosmosis or by dissolving and re-precipitating aluminium electrodes to induce cementation of soils electrokinetically has been successfully demonstrated (Endell and Hoffmann, 1936; Casagrande, 1947, 1952; Farmer, 1975; Casagrande, 1983; Masliyah, 1994; Lamont-Black, 2001); and has been achieved on a relatively large scale (e.g. the stabilisation of a 850 m railway cutting, Casagrande *et al.*, 1981) and the strengthening and dewatering of an artificial levee made from harbour dredgings (Wittle *et al.*, 2008).

Ground stabilisation using electrokinetics has also been accomplished by the addition of metal salt solutions or the decomposition of the anode electrode: usually iron or aluminium but copper electrodes have also been used (e.g. Endell and Hoffmann, 1936; Casagrande, 1947, 1949; Adamson *et al.*, 1966a; Adamson *et al.*, 1967; Bjerrum *et al.*, 1967; Harton *et al.*, 1967; Gray and Schlocker, 1969; Mukhopadhyay *et al.*, 2007).

Electrokinetic methods of ground stabilisation have been around for decades and have been used successfully on a number of different applications they have not become generally adopted as mainstream approaches. In some cases the materials and additives used have often proved problematic in environmental terms (for instance, aluminium is toxic and can be quite readily bio-available and mobile under certain redox/pH conditions) in addition the perceived high energy costs plus a likelihood for site engineers to be suspicious of less traditional approaches to groundwork, have limited the more widespread adoption of electrokinetic techniques for soil strengthening and cementation.

2.8.1 Electrokinetics and Barriers

Rather than removal, in many situations effective *containment* by constructing physical barriers or electrochemical stabilisation may be a more realistic and cost effective method to deal with contaminated land. Another approach has been to utilise

electroosmotic flow to counter or redirect a groundwater flow in the opposite direction (e.g. Narasimhan and Sri Ranjan, 2000). By positioning the anode electrodes downstream, in the path of a contaminant plume, such that the electroosmotic flow is acting contrary to the groundwater flow, the contaminant plume may be diverted. This may act to protect a sensitive receptor down-stream from the contaminant plume or prevent the contamination from entering a site belonging to another owner and the legal ramifications that this might have. There is limited information regarding the cost of such approaches versus more conventional approaches; such as a bentonite wall or installation of an impermeable membrane (Reddy and Cameselle, 2009).

There have been other novel investigations which have utilised the precipitation of iron rich material as a method of reducing leaching and isolating potentially hazardous material by creating an interface where acidic waste jarosite is placed in contact with high pH coal fly ash waste. At the point of contact the iron and mobile metals from the jarosite encounter the high pH and precipitate a low permeability iron-rich material which appears to self-seal, stabilise and contain the migration of the acidified fraction and self-stabilises the waste material mass (Ding *et al.*, 2002).

Another novel approach has been to use the phenomena associated with electrokinetics to stabilise dykes and levees by dewatering and barriering water ingress (Wittle *et al.*, 2008), and even *in situ* beneath rivers (White, 2000). Wittle (2008) revisits Casagrande's methods by combining the electro-fence concept (using electroosmosis to dewater/barrier) with the electrochemical dissolution of sacrificial aluminium electrodes to stabilize a working dyke. A dyke was created across a pool of 2 m depth, designed to behave as a failing dam i.e. there was significant seepage. Electrodes were installed in the dyke and the dyke material was successfully stabilised and de-watered, unfortunately there is no characterisation of the material the dyke is made from in the research.

Mainstream technology for the production of barriers for contaminant containment may be classified broadly into three categories:

1. Driven barriers are formed when steel or concrete barriers are driven into the soil and are joined to form a suitably impermeable wall. These may also provide structural support.
2. Injected barriers are formed when grout is injected into the subsurface. This technique tends to be relatively high cost and may result in a discontinuous grout curtain that leaves un-grouted flow paths, along which contaminants may preferentially migrate.
3. Cut and fill barriers are constructed by excavating a trench and filling it with concrete, grout or other material so that a suitable aquitard is reached

(Cairney and Hobson, 1998).

It is very labour intensive and often expensive to install a *horizontal* barrier beneath an existing contaminated site (such as a landfill), because these generally require large-scale excavations or horizontal drilling, which may also be unfeasible if surface structures are close by. For this reason the development of a method for the creation of a sub-surface barrier to any required geometry is an important avenue of research, which is described in relation to the FIRS process in Section 3.

2.9 Iron Electrochemistry and the FIRS Process

Iron has low biological toxicity and is widespread throughout the environment (Schwertmann, 1991; Gurzau *et al.*, 2003), indeed, iron is an essential biological component for plants and animals, which, among other things, forms an essential component of haemoglobin, the oxygen carrying molecule in blood (Walker, 1996). In the soil it is involved in co-precipitation in many metal species and the iron containing compounds formed cement other species present.

Due to its multiple oxidation states it can form numerous complexes and compounds (Table 12), and can act as both a reducing and an oxidising agent. This is observed in the environment where iron and manganese oxides form coatings on soil particles and cement and bind particulates together (e.g. Fendorf, 1992; Alloway and Ayres, 1997). It also serves as an adsorbent surface to reduce the mobility of ions in soils (Hartley *et*

al., 2004). Iron is ubiquitously found in soils since almost all soil forming rocks contain at least some iron, in the oxidising conditions at the surface (due to atmospheric oxygen) the typically divalent iron becomes an Fe(III) oxide, although microbially mediated reduction may result in reduction once more to the Fe(II) state (Schwertmann, 1991), typically at depths below the immediate surface particularly in waterlogged conditions.

Iron compounds have also been used in semi-permeable reactive barriers, and for the treatment and de-chlorination of pesticides and other hazardous chlorinated hydrocarbons as well as other organic compounds (e.g. Helland *et al.*, 1995; Chew and Zhang, 1998; Ye and Chiu, 2005; Chien *et al.*, 2006; Yuan and Chiang, 2007) and as a reactive substrate for the removal of arsenic from water supplies (Meng *et al.*, 2001; Meng *et al.*, 2002; Leupin and Hug, 2005; Yuan and Chiang, 2007).

It is these properties and others which are utilised in the FIRS process.

Table 12: Some typical iron oxide, hydroxide and oxyhydroxide compounds which may be formed from iron in solution.

FORMULA	COLOUR	VALENCY	MINERAL/COMPOUND NAME
Fe ₂ O ₃ .H ₂ O or Fe(OH) ₃	Red/Brown	Fe ³⁺	Haematite or Ferric(III)Hydroxide
Fe ₃ O ₄	Black	Fe ^{2+/3+}	Magnetite or Iron(II,III)Oxide
Fe(OH) ₂	Blue/Green	Fe ²⁺	Iron(II)Hydroxide/ Ferrous hydroxide (Soluble)
FeO	Black	Fe ²⁺	Iron(II)Oxide/ Ferrous oxide (Pyrophoric)
FeO(OH) FeOOH	Red/Brown	Fe ³⁺	Lepidocrocite/ Goethite.
FeO(OH).nH ₂ O	Yellow/Brown	Fe ³⁺	Limonite

2.9.1 The FIRS Process

FIRS uses iron anodes to introduce iron into the medium which migrates in solution towards the cathodes. The opposite pH conditions developed at the electrodes of opposite charge develops a boundary zone of rapid pH change. This causes the iron in solution to precipitate out of solution and form an iron oxide/oxyhydroxide mineral fabric.

The FIRS technique employs directly emplaced iron-rich electrodes. This is significant as it allows for the electro-dissolution of the anode electrodes as a means of introducing iron species into the system. It is this input of iron which allows for the co-precipitation of iron containing species along with any contaminants, and cements them in place. It is this precipitated material which also modifies the physical properties, the permeability and strength, of the material.

By facilitating the electro-dissolution of the iron electrode, iron as an active ionic species is introduced directly into the soil and is mobilised. It is then able to interact with other species in the soil or directly modify the physical properties of the soil or sediment. Figure 13 shows a simplified schematic of the processes taking place in a typical bench scale FIRS treatment tank. The reaction at the anode for a pure iron electrode is:



Equation 14

e.g. Shapiro *et al.* (1996) as shown in Figure 13, however the high carbon content and other impurities provide sites for the electrolysis of water and the generation of the acid and alkali fronts as well as the gaseous by-products; hydrogen and oxygen (Acar and Alshawabkeh, 1993).

At the anode there may be a single step oxidation of the zero valent iron into ferric iron



or alternatively a two step process where the initial oxidation is to ferrous iron



and then secondary oxidation to ferric iron



(Cifuentes *et al.*, 2001)

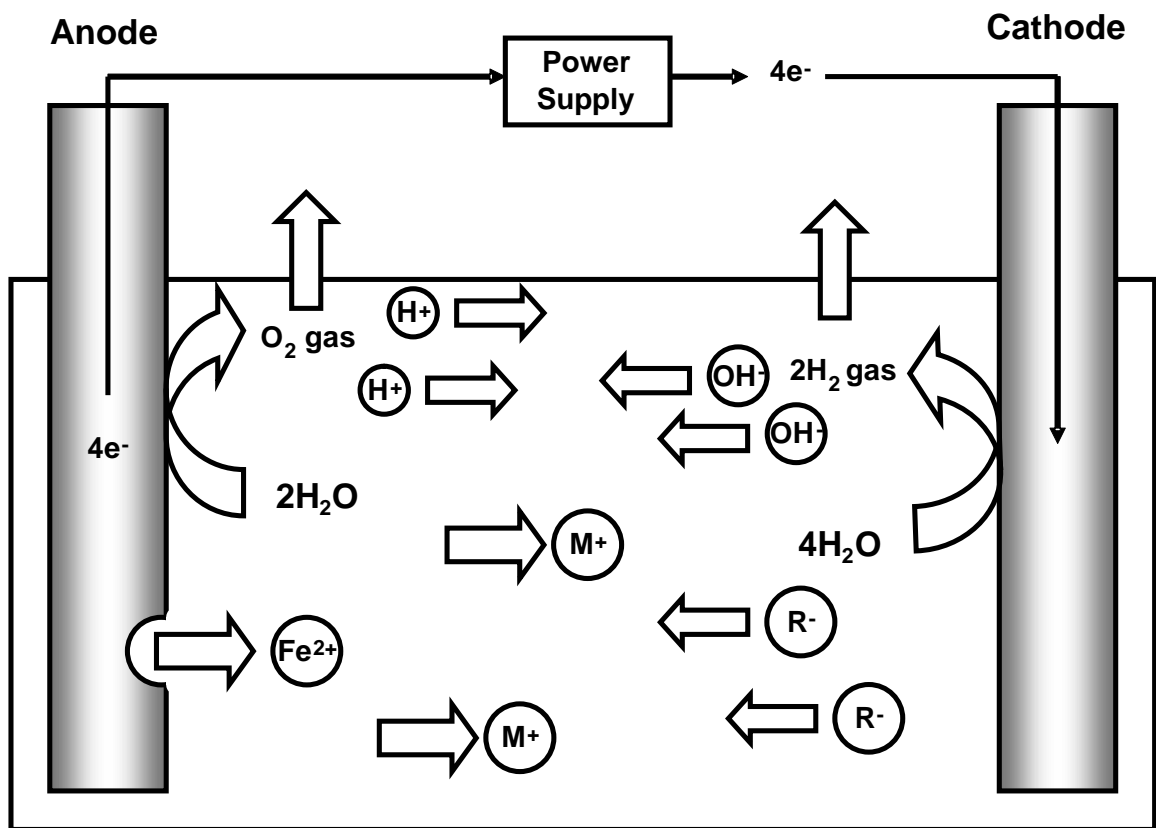


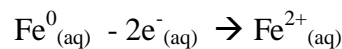
Figure 13: The principle electrochemical reactions and processes taking place during FIRS treatment. The electrolysis of water takes place at the electrodes, the oxidation of the iron from the anode electrode releases Fe²⁺ into solution, and the electromigration of charged species takes place as they are attracted to the electrode of opposite charge. M⁺ represents a positively charged species (a metal ion for example) R⁻ represents a negatively charged species. Electroosmosis (not shown) occurs as the net movement of water towards the cathode.

In terms of remediation, the propagation of H⁺ ions at the anode lowers the pH and helps desorption of metal ions or dipoles adsorbed to soil particles.

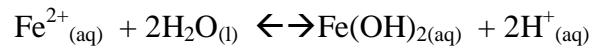
The mechanisms and theories involving the soil/solution interface are considered in detail in section 2.6.

The electrochemical dissolution of iron from the anode into the pore water solution and subsequent precipitation is responsible for the co-precipitation of contaminants on and around this narrow band of iron-rich precipitate. In addition to the cementation of contaminants, this iron-rich precipitate dramatically changes the strength and permeability of the soil in this region. The nature of the way this precipitate is formed means that it creates a continuous layer or curtain of low permeability in the soil or sediment mass. This is because the acid and alkali fronts, upon meeting, form the precipitated region at the interface. As the precipitated region begins to form, the remaining unprecipitated regions become the areas of least resistance for the movement of not just the acid and alkali fronts, but for electroosmosis, and the electromigration of charge carrying species which accelerates the formation of the precipitated material in these remaining areas. The result is a continuous mineral fabric. This phenomenon is discussed in more detail in section 3.1, page 80.

When a current is applied to electrodes immersed in a wet soil mass, the iron at the surface of the anode electrode becomes oxidised to the ferrous divalent ion and passes into solution (e.g. Trushinskii, 1993) as shown in the redox reaction below.



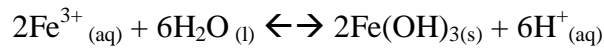
In the aqueous environment electrolysis of water also takes place at the anode; generating oxygen gas and protons. The divalent iron will normally undergo further equilibrium reactions, e.g.



This further yields protons, lowering the pH. An alternative reaction which may also be expected in the oxygen enriched locale of the anode electrode may be the further oxidation of the ferrous ion to the trivalent ferric ion:



This consumes two protons; however this is not a stable species in solution and may react further:



(e.g. Younger, 2000)

Liberating yet more protons, consuming water, and forming the insoluble precipitate ferric(III)hydroxide which is stable for a range of pH under mildly to highly oxidising conditions (see Figure 14).

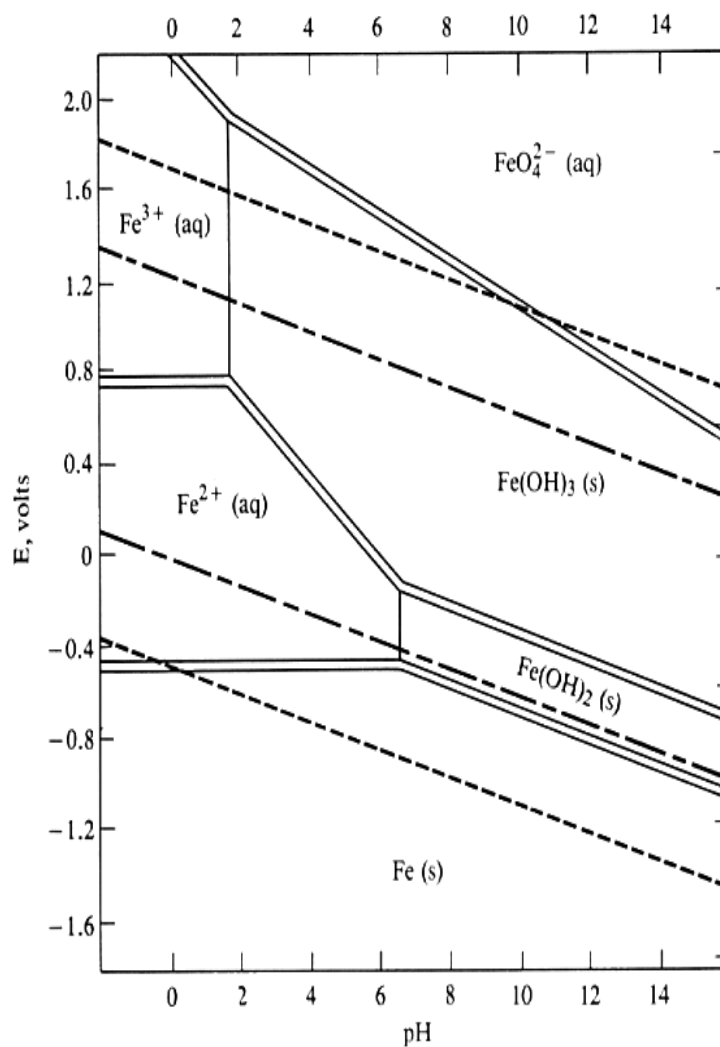


Figure 14: Simple Iron speciation Eh pH diagram (Pourbaix diagram) at 25 degrees and 1atm pressure. The innermost dashed lines represent the oxidation/reduction limits for water, the outermost lines approximate for the 'over voltage' required for actual oxidation or reduction of water (Krauskopf, 1979) .

Most of the compounds observed in the FIRS process as the iron-rich precipitate begins to form are orange/brown, indicating iron in the Fe^{3+} state but some of the blue/green compounds are also seen as the conditions favour the ferrous iron compounds, Figure 14, Figure 15.



Figure 15: The range of colours of iron present indicating the range of speciation determined by local small-scale variations in conditions.

This gives a visual indication of the speciation of the iron by the colour of the iron in the medium. Closer study of the cross-section of the iron band formed shows the different valency state of the iron in the compounds formed due to the rapid change in pH conditions at the point of meeting of the acid and alkali fronts. A carbonate rich material is likely to neutralise the acid front while allowing the alkali front to propagate, conversely sulphate rich material will neutralise the alkali front and favour the

generation of the acid front. Chlorides will also influence the composition of precipitates formed.

Findings from preliminary investigations were of the scale of <20cm electrode separation (Cundy and Hopkinson, 2004, 2005,) and have showed metals responding to the treatment process. Investigations appear to show good response to the treatment for some elements particularly for the mobilisation/fixation of arsenic, but data is presented for a limited number of elements only.

2.10 Economic Considerations

There have been numerous estimations of costing for electroosmotic/electrokinetic remediation techniques. Virkutyte *et al.* (2002) identifies the factors controlling the cost of an in-situ electrokinetic treatment to be:

- Soil properties
- Depth of contamination
- Cost of accommodating electrodes and placing treatment zones
- Clean-up time
- Cost of labour and electrical power

Athmer (2009) goes further, and breaks down the proportional component costs of an electrokinetic remediation system (in situ) Table 13:

Table 13: Estimates of cost breakdown for electrokinetic remediation

Item	Typical Range (%)	Average (%)
Electricity	7-25	15
Site preparations	5-25	10
Installation (labour, equipment, materials)	10-60	40
Operation, less electricity (labour expendables	15-50	25
Waste management, permits, oversight	5-20	10

Schultz calculated that for a system incorporating a fluid handling system and pH management, for a low permeability soil to be USD \$78 m⁻³ (1997) with \$15 of this calculated as fixed costs and the remainder made up by energy costs, electrode materials and installation costs. An earlier study estimates energy costs to be in the region of \$15 to \$30 m⁻³ (Acar *et al.*, 1995). Yuan and Weng (2004), estimate their costs to be between \$5.15 and \$12.65 m⁻³ (Ho *et al.*, 1997; Schultz, 1997; Ho *et al.*, 1999).

Table 14: Selected costs associated with methods of electrokinetic remediation, (from, Virkutyte *et al.*, 2002; Yuan and Weng, 2004).

Technique	Costs	Remarks
SAEKa	\$ 17–42 m ⁻³ approximate	5 day treatment periods surfactant concentration: 0.1–2.0%
Lasagna	\$50–120 m ⁻³	Mandrel/tremie-tube method of emplacement is used instead of earlier proposed steel plate. Electrodes with wick drains and carbon-filled treatment zone
Soil heating/vapour extraction technology	\$65–123 yd ⁻³	
Chemical oxidation (with potassium permanganate or hydrogen peroxide)	\$130–200 m ⁻³	Technique was mostly used to remove Dense Non-aqueous Phase Liquid in situ

Other studies have compiled detailed methods for costing electrokinetic remediation strategies (U.S. Environmental Protection Agency, 1997; Alshwabkeh *et al.*, 1999b), the usefulness of these estimates have limited ‘shelf life’ due to the changing costs of energy and materials as well as the licences and other variables. This thesis deals with a technology which is still at the bench scale and at best, rough approximations are provided for the costs involved. Table 14 shows some of the cost estimates for some different techniques compiled from the literature.

More recently researchers have arrived at more expensive estimates of costs of an average of \$200/m³ for inorganic and organic pollution which equates to approximately \$90 per ton (Athmer, 2009). It should be remembered that even if the costs may be higher than certain other treatment methods, electrokinetics is often the only alternative to landfill when the material is of a low enough permeability that there is no existing method suitable for its treatment.

The ideal energy expenditure is in the region where electrokinetic mass transport occurs without significant joule heating. Joule heating is often a result of increased resistance, usually from drying. It can also be a result of excessive voltage; either situation results in unnecessarily high energy costs.

2.11 Electrode Arrangement Considerations

The general rule concerning the number and spacing of electrodes is that the more electrodes that can be incorporated will result in a denser and more evenly distributed field, see Figure 16. The advantages of increasing the number of electrodes may be offset by the increase in time and cost of providing, installing and powering a greater number of electrodes as detailed by Alshawabkeh (1999b).

Sheet electrodes have been used in other work (Ho *et al.*, 1997; Ho *et al.*, 1999 etc.), but improvements in the electric field generated are somewhat offset by the increased difficulties in the installation of a large single sheet electrode compared to the relatively straightforward round bar type or sheet pile. Relatively large currents and or voltages may be employed and when using sheet electrodes the current entry and exit junctions must be sufficient in number and or capacity to cope. In addition to this, differences in the soil mass, due to heterogeneity in composition or saturation, may result in differential rates of dissolution of the electrode material. Individual electrodes which have corroded away can be easily replaced; this is more problematic with a large sheet arrangement if part of it corrodes before the rest. For inert electrodes the problem of ensuring even contact between the electrode and the soil remains.

Indeed, on a field scale installation, the technical considerations for the installation of a large sheet electrode are more complicated. Sheet electrodes also obstruct flow of pore water whereas flow can take place around cylindrical electrodes (Rasmussen and Budhu, 1996; Alshawabkeh *et al.*, 1999a). For these reasons, whilst they were considered, sheet electrodes were rejected for the experiments conducted for this thesis.

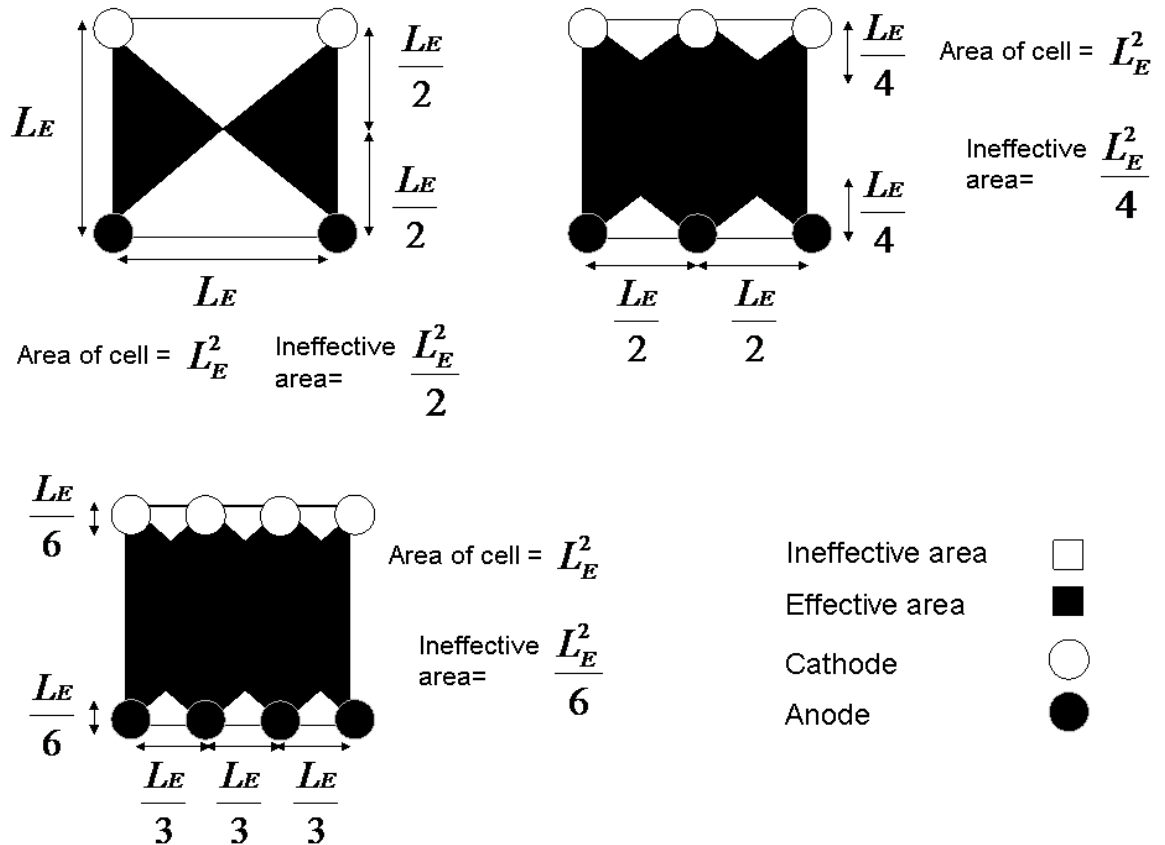


Figure 16: Schematic showing an approximation of the field distribution for different linear electrode configurations for a constant area. Corrected and adapted from Alshawabkeh *et al.* (1999a).

2.12 Electrode Composition Considerations

The electrodes used throughout the experiments were made of cast-iron (grade 250). This was chosen in the first instance by Cundy and Hopkinson (2003) for its ready availability and relative ease of machining to rod shapes of required diameter for use as

electrodes. The composition of the cast iron used is given in full in Appendix 1. The significant factor in its composition is its relatively high carbon content (2.5%- 3.5%).

It is really only the composition of the anode that is significant since the cathode could be made of any suitable conductor e.g. Graphite or Aluminium or Copper etc. This is because there are no reaction products generated from the cathode electrode material (hydroxide ions are formed but these are not formed from the electrode material); it is simply an electron source for the introduction of charge to the soil mass and the electrolysis of water generating hydroxide ions and hydrogen gas.

The high carbon content of the anode has an unforeseen benefit since it increases the hydrolysis of water to take place as well as the oxidative dissolution of the iron. This is because the carbon, in the form of carbon flakes which form as a result of the casting process, does not break down into solution but acts as an oxidation site for the electrolysis of water to generate protons.

Simultaneously, the iron component in contact with the soil solution is oxidised into solution and the acid conditions which have been propagated mean that it stays in solution and is able to migrate under electrostatic attraction towards the cathode. This can be compared for instance with Haran *et al.* (1996) who utilised 99.99% alpha pure iron for the anode electrodes and found that the alkali region was much greater in extent than the acid region in experiments conducted in a saturated sand.

This is discussed in more detail; see section 3.3, since this is the opposite of what was found in some of the experiments conducted here.

“The high pH in the major portion of all the cells leads to enhanced movement of chromate ions towards the anode. The pH in most part of the tube (up to 60cm from the cathode) remains around [pH] 10-12 due to the advection of the OH⁻ because of the competing anodic dissolution reaction producing Fe²⁺ ... Further the rate of production of H⁺ is less compared to OH⁻ because of the competing anodic dissolution reaction producing Fe²⁺.”

(Haran *et al.*, 1996)

The longer term experiments conducted here on sands in seawater resulted in the almost complete dissolution of the anode electrodes leaving a friable carbon-rich relic. Similar reactions occur in the corrosion of carbon steel used in marine applications. A galvanic circuit is created between the iron component and the carbon component due to their significantly different electro-negativity with the seawater as an effective electrolyte, accelerating the dissolution of the iron and revealing a fragile carbon skeleton.

Cast iron was used initially as a source of cheaply available and workable material but some of its properties have been beneficial for the purpose of electrokinetics. It should also be borne in mind that there may also be less desirable components making up the composition of cast iron- elements such as copper, molybdenum, chromium may also be present at varying concentrations (Marukawa and Edwards, 2001). The presence of these potentially hazardous elements in the anode electrodes in a remediation scenario could be problematic if they are introduced to a site where previously they were not present.

This could conceivably result in a remediation procedure resulting in what amounts to dumping of hazardous material! It should be said that the concentrations of these species are typically at trace levels but the grade of cast iron used should be carefully considered as much of it is produced from recycled material and some sources of iron (e.g. that obtained from scrapped automobiles) has the potential to contain significant concentrations of a variety of undesirable species (e.g. Marukawa and Edwards, 2001; Kim *et al.*, 2004). Indeed some of the data presented in this thesis suggest the introduction of some elements sourced from the anode electrode material (Section 5)

Since the anode electrodes are expected to dissolve with time there is a theoretical minimum diameter determined by the rate of dissolution versus the duration of the treatment. Studies using iron anodes for the development of the Lasagna™ process (Shapiro, 1996) have determined the minimum cross sectional area A_e , per unit length, b given by:

$$\frac{A_e}{b} = \frac{M_w}{\rho} \cdot \frac{i}{Fz} t_r \quad \text{Equation 15} \quad (\text{from, Shapiro, 1996})$$

Where:

M_w = molecular weight of iron (=55.8 g/mol)

ρ = density of iron (7.6 g/cc)

i = current density, A/m²

F = Faraday's constant (96000 C/mol)

z = valence change in the electrode reaction (=2 from $\text{Fe}^0 \rightarrow \text{Fe}^{2+} + 2e^-$)

t_r = remediation time, days

The theoretical considerations have been addressed and the state of the art and relevant body of knowledge addressed. The niche that the research conducted here is to occupy has been established. The following chapters deal with the experiments and results obtained.

3 Precipitates as Barriers

As described in the previous section the FIRS process involves the electrokinetic dissolution of iron-rich anode electrodes and the associated reactions which take place, Figure 17. The generation of an acid and alkali front, iron migration and consequent iron-rich precipitate formation using the FIRS method has been demonstrated in various natural media, including estuarine sediments and a range of contaminated soils, using both high ionic strength electrolyte (seawater) and tap water (Hopkinson and Cundy, 2003; Cundy and Hopkinson, 2004; Cundy and Hopkinson, 2005; Faulkner *et al.*, 2005). The implications of this for the controlled migration of metals and radionuclides for remediation purposes has been discussed (Hopkinson and Cundy, 2003; Cundy and Hopkinson, 2005; Faulkner *et al.*, 2005). However, strategic precipitation of iron for the purposes of *in situ* barrier formation and contaminant containment are an additional avenue of research.

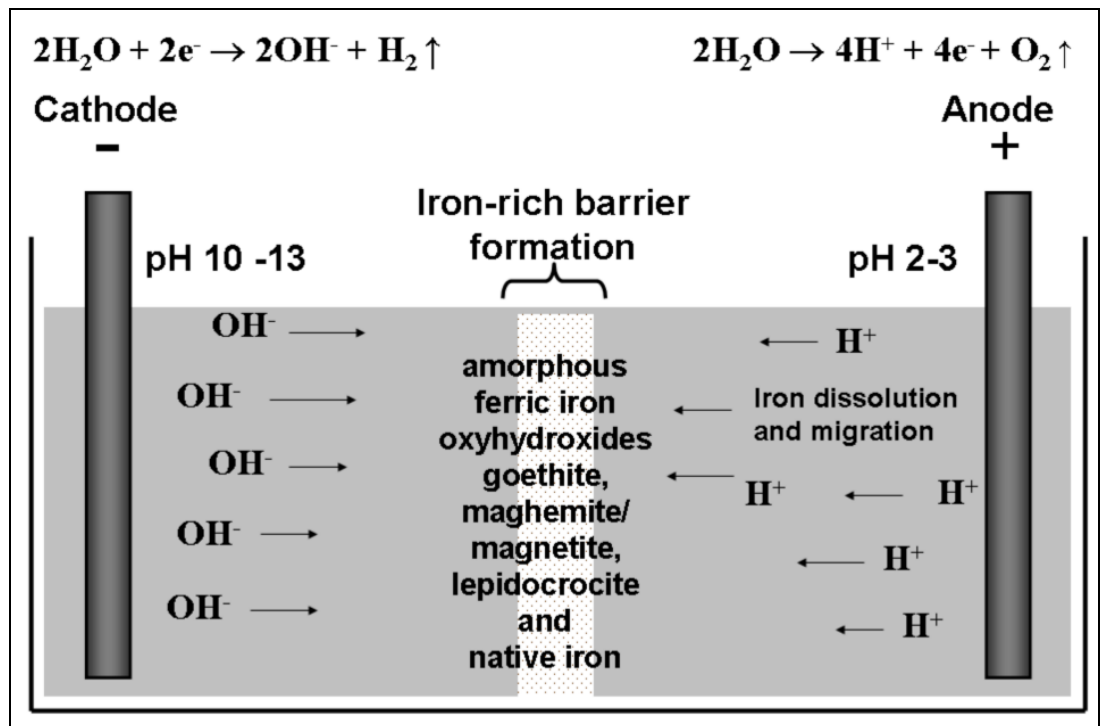


Figure 17: Parallel linear electrode arrangement of the FIRS set up showing mechanism of precipitate formation (Taken from, Faulkner *et al.*, 2005).

This section describes experiments utilising the precipitation reactions, outlined in section 2.8.1 above to form useful barriers in the subsurface. The barriers are investigated in terms of physical characteristics, methods of formation and factors controlling the geometry of the mineral fabrics formed. Experiments were conducted to assess the usefulness of the precipitated iron mineral phases as a means for the control of ground water flow and hence the potential control of contaminant migration. The composition and geotechnical properties of the precipitated phases were also analysed.

3.1 Predetermined Geometry of Precipitates

The introduction of iron by way of electrochemical dissolution into the subsurface to form local mineralised fabrics has been achieved previously, Jacob et al. (1994) describe the generation of ‘dissipative structures’ by electrochemical introduction of iron:

“Fine quartz sand, as a homogeneous and non-structured medium, was placed between vertical iron electrodes in cylindrical or square cross-section test vessels 15 to 20cm across. The pore space was occupied by seawater. A direct electric potential of 1.0 to 1.5 volts was applied; a potential of this order might be present also in many natural processes... As a consequence of the potential difference, a sharp boundary zone is developed in which anions and cations encounter and form a boundary zone at which a sudden change in pH from 2.5 up to 8 occurs. After reaching super-saturation conditions in this boundary zone, spontaneous precipitation of insoluble metal hydroxides and metal chlorides occurs at the isoelectric point.”

(Jacob *et al.*, 1994)

3.1.1 Creation of Barriers

The principles of the FIRS process have been described as a means of producing an iron-rich mineral precipitate which has very low permeability. This has been investigated as a means of reducing the permeability across a section of material to act as a barrier to the movement of pore water (Hopkinson and Cundy, 2003; Cundy and Hopkinson, 2004; Cundy and Hopkinson, 2005; Faulkner *et al.*, 2005; Hopkinson *et al.*,

2009). The strategic precipitation of continuous and impermeable iron-rich precipitates has obvious potential uses for the formation of subsurface barriers to groundwater flow. Additionally, iron compounds, particularly zero-valent iron, are known to be active in the dechlorination of chlorinated hydrocarbons and degradation of hydrocarbons (Helland *et al.*, 1995; Johnson *et al.*, 1998; Harbottle, 2003; McGuire *et al.*, 2003; Oh *et al.*, 2003). Thus the dual benefits of controlling the flow of a contaminated groundwater plume may also employ the reactive properties of iron compounds to deliver a certain amount of treatment to a contamination situation (For the purposes of this thesis, only metals will be considered.).

The ability to form the small circum-vertical barriers is limited in its usefulness since a barrier of this nature simply directs groundwater in a flow-path around the generated obstruction. Continuous ‘curtains’ of iron-rich precipitate in the ground would be more able to facilitate the separation of one region of ground from another, for instance to re-direct a contaminant plume away from an aquifer (e.g. as described by, Nyer, 2001; Lynch, 2009)

These continuous curtains may be formed by thinking of the small scale electrode arrays already described, as repeatable units, allowing the electrode array to be extended to the desired length. To avoid a flow-path under the precipitated barrier, the electrodes would have to be of sufficient depth that a suitable aquiclude is reached. Despite such limitations the successful generation of such barriers may prove useful for directing ground water or leachate flow, or for directing contaminant plumes to a treatment zone such as a permeable reactive barrier.

A possible useful formation for the barrier would be to create a continuous ‘bowl-shaped’ barrier. This would allow contaminants to be entirely contained within a region of the ground, or give added protection to underground storage tanks or to landfill sites. The problem with this concept is that in order to generate a vertical pH gradient, the electrodes need to be emplaced at depth i.e. below the point where the barrier needs to be formed. This would entail disrupting the site in order to install electrodes beneath the contaminated region or the region below which the barrier is to be created. This is problematic due to the possibly very large volumes of material which might have to be excavated and also, if the material is already contaminated there is a risk of spreading

the contamination as a side effect of the excavation process (e.g. drying followed by wind dispersion, surface run off etc.).

Other electrokinetic methods install laminar electrodes at depth to facilitate a vertical electrokinetic effect; such as the lasagne process (Shapiro, 1996; Ho *et al.*, 1997; Ho *et al.*, 1999 etc.) or electroosmotic de-watering of the ground for engineering purposes (e.g. Lamont-Black, 2001 installing 'geotextiles' below the surface.), but these methods require excavation to install the electrodes at depth. If an excavation must be carried out to install the electrodes then the option exists to use something relatively cheap, and readily available, such as synthetic polymer sheeting, or concrete lining for instance. Difficulties arise where excavation is problematic or unfeasible; perhaps due to buildings or other structures in close proximity or on the site, or if the ground material is of a hazardous nature.

One likely scenario is a leaking landfill site which is passing leachates into the surroundings (Holzlohner *et al.*, 1997; Islam and Singhal, 2004). To find and re-line the leaking region of the site would be hugely expensive and potentially hazardous. Current government legislation also means that once the contents are excavated, the owners may be forced to obtain new licenses, since when excavated, the waste is once more classified a hazardous waste which requires a new license for disposal, even if this is only to replace the excavated material back into the excavation. With this in mind an electrode design was devised to allow the emplacement of an electrode array at depth *without the need for excavation*. The following sections deal with the FIRS system for the generation of sub surface barrier formation and the characterisation of the iron-rich mineralised region.

The iron precipitates also cement and consolidate unconsolidated material (Hopkinson and Cundy, 2003; Cundy and Hopkinson, 2004; Cundy and Hopkinson, 2005; Faulkner *et al.*, 2005) and this feature may be utilised for improving the mechanical properties of a material, for instance to more easily facilitate an excavation in a loose sandy material.

The full journal paper (Faulkner *et al.*, 2005) as it appeared in print is included in Appendix 1, which details investigations into this aspect. This journal paper is also cited a number of times in Reddy and Camesell (2009).

3.2 Investigative Outline

A series of bench-scale experiments were carried out to examine the formation, mechanical strength and mineralogy of electrokinetically-generated iron-rich barriers in wet sands, the role of applied voltage on iron-barrier formation, and the potential for growth of continuous iron barriers to a desired geometry (specifically, the growth of a horizontal iron barrier and a parabolic precipitate). All experiments were conducted using electrodes fabricated from cast iron rods (grade 250) composition: C 3.48%, Si 2.87%, Mn 0.812%, S 0.099, P 0.364%, and Fe 92.38% within British Standard parameters (see Appendix 1). Experiments were conducted on siliciclastic sand, with 90% quartz, and accessory clays, feldspars and carbonates.

3.3 Voltage Experiments

Six identical Perspex cells (dimensions 200 x150 x180 mm) were filled with sand, and seawater added to saturation as an electrolyte. Two cast iron electrodes were inserted into each cell at 15cm electrode separation, and a range of voltages (between 2 and 8 Volts DC) applied for ca. 300 hours, to examine iron-barrier growth under different applied voltages. The resultant iron-rich bands were measured at four points as viewed through the Perspex cell (0, 2, 4 and 6cm from the base of the cell).

3.3.1 Role of Applied Voltage

Data from the six Perspex cells, run over 300 hours at a range of voltages, indicate a clear, directly proportional relationship between the voltages applied and iron-rich band thickness as measured at different vertical heights through the visible portion through the Perspex container, Figure 18 and Figure 19.

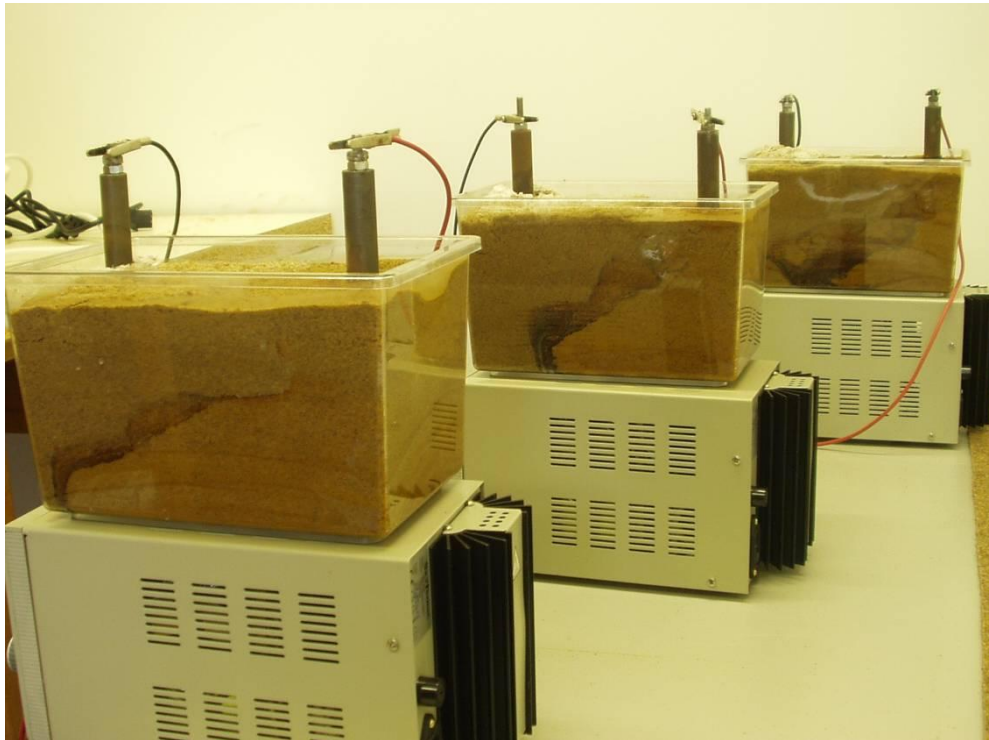


Figure 18: simple voltage experiments conducted in sand with a seawater electrolyte conducted with different voltages to look at the effects of the voltage on the iron precipitate formed.

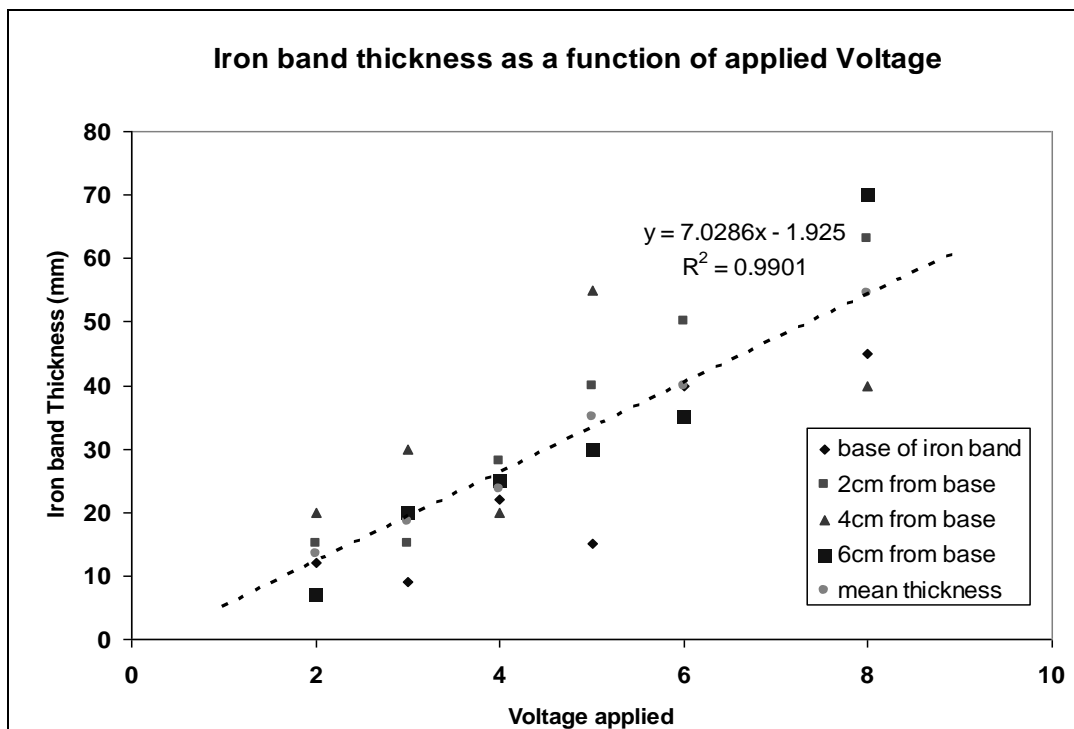


Figure 19: Relationship between applied voltage and measurement of visible portion of the iron-rich precipitate as measured through the transparent Perspex™ test cell.

Increasing the voltage apparently increases the input of iron into the system due to accelerated dissolution of the cast iron anode electrode, suggesting that increasing the applied voltage may be an effective means of increasing the formation rate of the iron barrier. However, at higher voltages (>100 volts) soil heating and the formation of significant amounts of hydrogen gas at the cathode becomes problematic (e.g. Virkutyte *et al.*, 2002).

Increasing the input energy also introduces additional problems with drying. The increased rate of dissociation of water requires frequent topping up of the experiment. In fine grained soils, with higher electrical resistance, increasing the applied voltage may lead to joule heating of the soil which will exacerbate drying and might present a hazard. Increasing the energy input for the experiment also increases the energy costs.

These results represent some preliminary experiments to look at the effect of increased voltage on the formation of the iron mineralised region, and also as a means to generate some iron-rich precipitate in clean quartz-sand in order to analyse its composition.

Influence of current density and pH on electrokinetics has also been studied in laboratory conditions, (Hamed and Bhadra, 1997). The findings indicate that increasing the current density increases the speed of migration of the acid front and that high pH influent increases the electroosmotic flow (by increasing the zeta potential of the kaolinite).

3.3.2 Discussion

The barrier geometries which were obtained through the measurement of the visible iron precipitate as viewed through the transparent Perspex tank that initially indicated the physical thickness of the precipitate formed was directly controlled by the voltage applied (Faulkner *et al.*, 2005), Figure 19. The cemented region had enough structural integrity to be completely removed from the test tanks. It was the measurement of the excavated iron precipitates which successfully removed in one piece that allowed the

measurements to be revealed as not in fact the thickness of the precipitate layer, but the measurement of the part of the precipitate running next to the side of the Perspex tank, much like the arm of a horse-shoe.



Figure 20: Excavated iron-rich bands showing the size and shape of the precipitates formed.

This is likely to be due to a combination of the higher requirement of water for the experiments conducted at higher voltages; due to the increased rate of dissociation of water contributing to an accelerated rate of drying. The increased input of water seems to have resulted in the more eccentric shape of the precipitate formed since in the relatively coarse grained sand medium, with its lower zeta potential, electroosmosis is negligible.

In addition at higher voltages the migration of the acid front would be more rapid and since the experiments were constructed with a single, centrally placed electrode, the field

effects would explain the more eccentric parabola shape observed in the higher voltage experiments.

3.4 Horizontal Barrier Experiment

Following on from the previous experiments where circum-vertical precipitate structures were created an experimental apparatus and electrode design was created with the intention of creating a horizontal iron precipitated region, without the need for excavation. This design consisted of asymmetrical electrode arrays – a surface mesh for the cathode and sleeved anode electrodes with iron tips exposed. The concept was to allow for the anode electrodes to be driven to a required depth from the surface where the exposed tips act as a continuous anode array. This arrangement means that all the electrodes can be installed without the need for any excavation. The iron precipitated region was expected to form continuously in the sand medium and surround the sleeved portion of the anodes creating a continuous barrier at depth.

3.5 Method

The potential for the growth of a continuous horizontal barrier was examined using a 400 x 200 x 150 mm cell, filled with siliciclastic sand. A potential difference of 3 Volts DC was applied between: (a) a vertically emplaced anodic electrodes partially sheathed with PU insulation, emplaced into seawater soaked sand such that the exposed electrode tips act as a single anode layer at a depth of 20 cm, and (b), a cathode layer constructed from steel mesh, positioned at approximately 5 mm depth, see Figure 21. Current was monitored throughout. Following iron-band growth (after 400 hours), a secondary investigation into the ability of the iron-rich band to re-heal when damaged was carried out whereby the iron-rich band was deliberately point ruptured using a glass rod, see Section 3.5.2 below.

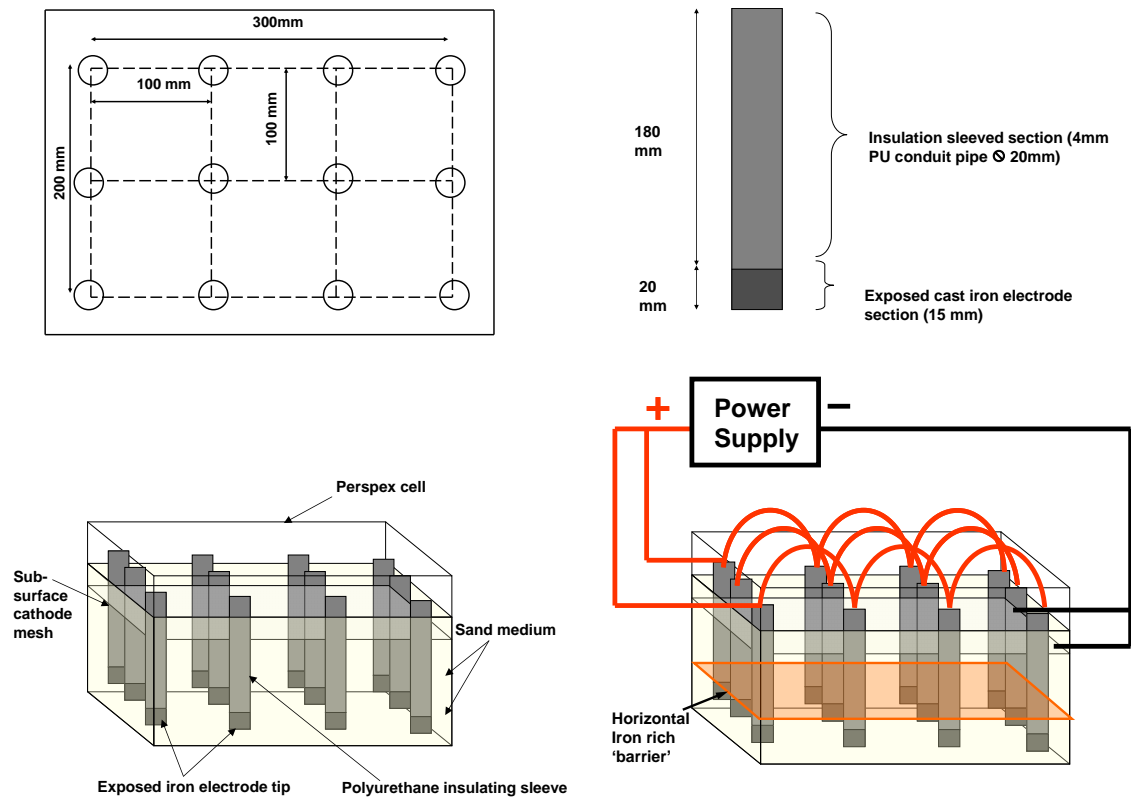


Figure 21: Apparatus and experiment design schematic for the development of a horizontal iron-rich precipitate barrier (adapted from, Faulkner *et al.*, 2005). Top left shows the electrode arrangement and spacing. Top right shows the anode electrode design. Bottom left shows the electrodes in place in the sand medium. Bottom right shows the assembled apparatus with location of iron band formation.

3.5.1 Horizontal Barrier Results

The straightforward parallel linear electrode arrangement of oppositely charged electrodes on either side of the sand results in the generation of a continuous, circum-vertical iron-rich barrier approximately half way between the two sets of electrodes of opposite polarity. However, by insulating the upper section of the anode electrodes and incorporating a shallow surface cathode electrode, a continuous horizontal iron-rich barrier of approximately 5 mm was generated in the sub-surface over a ≈ 400 hour period, without any excavation for installation of electrodes required, Figure 22.

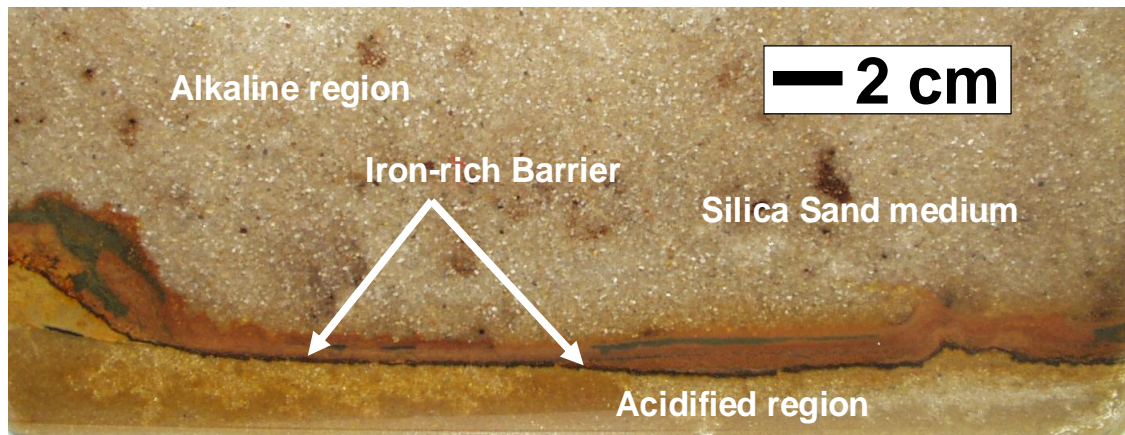


Figure 22: Horizontal iron-rich band formed over 300h at 3V in quartz sand using sheathed anode electrodes and a surface mesh cathode electrode with a separation between electrodes of 20cm, (Faulkner *et al.*, 2005).

The current flow shows an initial increase from 0.48 Amps to 0.74 Amps within the first ~20 hours, since the water is unevenly distributed throughout the sand profile at the beginning of the experiment (it is gravitationally influenced causing a saturated water table at depth, with a drier upper region) in addition, the initial input of ions from the dissolution of the anodes and the dissociation of water improves current flow, Figure 23.

When the current is switched on, the water becomes more evenly distributed as it is electroosmotically mobilised towards the surface cathode, allowing for more efficient ion movement and thus increased current flow. This is observed in all the experiments conducted and is due to the initial reduction in resistance due to the production of charge carrying ions at the electrodes.

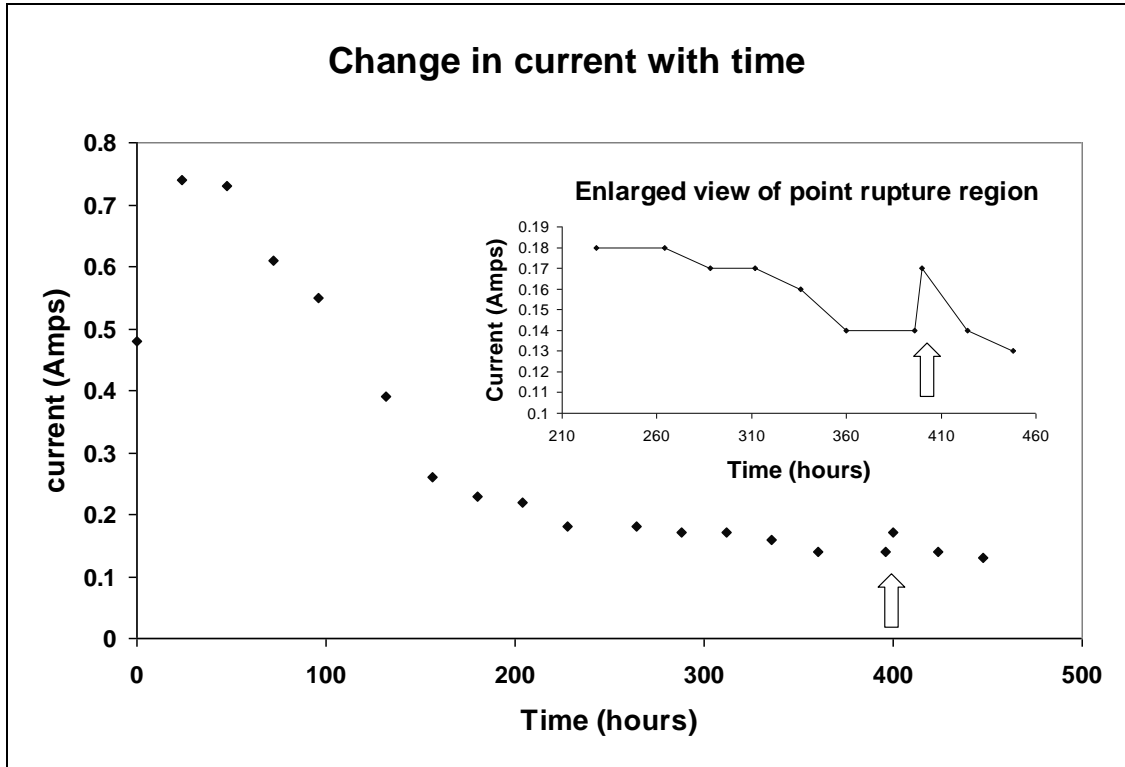


Figure 23: Current values over the course of the iron-rich band formation with increase in current caused by deliberate point rupture of precipitate fabric, (Faulkner *et al.*, 2005) The arrows indicate the time at which the barrier was ruptured.

The current shows a progressive drop from a maximum of 0.74 Amps down to 0.14 Amps, Figure 23, as the iron-rich barrier forms, due to impedance of ion flow by the precipitated iron phases (Faulkner *et al.*, 2005).

3.5.2 Resealing the Iron-rich Barrier

The theory was tested that by creating a flow path once a continuous precipitated fabric had formed would result in new precipitation occurring effectively self-healing the rupture (with continued current applied).

After 400 hours, the fully developed horizontal iron-rich layer was ruptured using a glass rod (diameter 4 mm). The current immediately increased from a steady 0.14 Amps, to 0.17Amps. Over the course of the next few hours the current gradually decreased until it returned to its pre-damage level of 0.14 Amps, Figure 23.

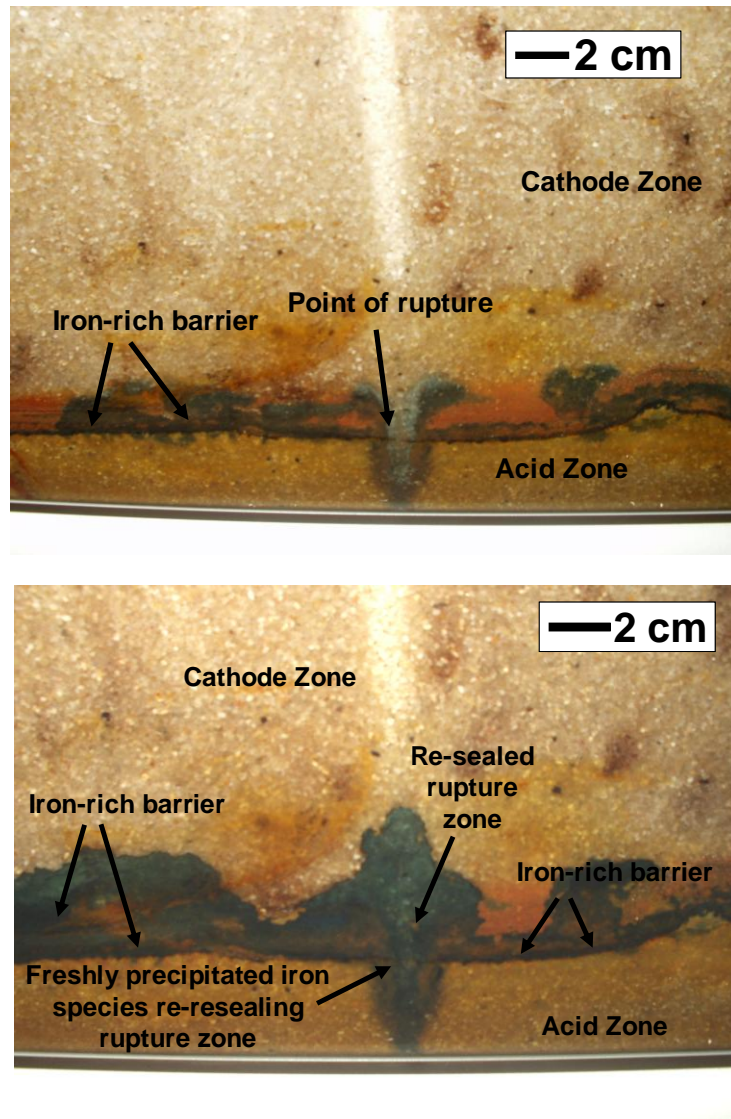


Figure 24: The iron-rich band, the top picture shows the band immediately after rupture is induced with a 4mm glass rod. The bottom picture shows the same region 24 hours later. The point rupture is shown to be blocked with freshly precipitated iron compounds, demonstrating the ‘self-healing’ process. The additional mineralisation either side of the rupture is due to ion migration (Taken from Faulkner et.al 2005).

Within 24 hours the damaged section had visibly reformed, indicating that the barriers can self-heal due to the opening of a flow path between opposite polarity electrodes created by the rupture, Figure 24. Iron speciation, determined by the change in redox and pH conditions at the boundary, gives rise to distinctive green/blue colour indicating the presence of iron (II) as it migrates into the alkaline cathode region.

3.5.3 Iron-rich Barrier Analysis

Samples were removed from the iron-rich bands from all three experiments for geotechnical testing and mineralogical characterisation. The point load and uniaxial compressive strength (UCS) of the precipitated iron band, and its permeability compared to the untreated sand, were determined following Franklin and Brook (1985) and Head (1982). Four samples from the iron-rich barriers, and the sand test medium itself, were analyzed by X-ray diffraction (XRD) at the Southampton Oceanography Centre, University of Southampton using a Philips PANalytical X'Pert Diffractometer. Semi-quantitative analysis was performed using the internal standard method. Three grams of the sample and one gram of the internal standard (corundum) were ground together under iso-propanol for 8 minutes in a micronising mill. The sample was side-loaded into a rotating sample holder and scanned from 3° to 76° 2θ at 1.2° 2θ per minute using Fe-filtered $\text{CoK}\alpha$ radiation. Areas of selected peaks were ratioed to the areas of the peaks of the internal standard, and the values compared with those obtained for a pure mineral standard (Faulkner *et al.*, 2005).

Because of preferred orientation, clay minerals were not determined individually, but were estimated on the basis of 'total phyllosilicates' using non basal 020 and 060 reflections. Error is estimated to be 5% of the amount present or 2% absolute, whichever is the larger, except for 'total phyllosilicates' where the error is estimated in house at 10%. The lack of appropriate mineral standards and the likelihood that poorly crystalline and x-ray amorphous iron phases are generated by the electrokinetic process (Hopkinson and Cundy, 2003) prohibited quantitative analyses of the iron mineral phases in the iron-rich barriers.

3.5.4 Iron-rich Barrier Mineralogy

XRD analyses of the iron-rich bands revealed the presence of goethite, lepidocrocite, maghemite/magnetite and native iron, Figure 25. Quantitative analyses of iron mineralogy were not possible. However, based on the sizes of peaks the iron-rich barriers have an approximate composition of ~65% cemented quartz (and feldspar),

with ~4% goethite, ~5% native iron, 5% maghemite/magnetite, 5% lepidocrocite, and ~15% x-ray amorphous ferric iron oxyhydroxides, Table 15.

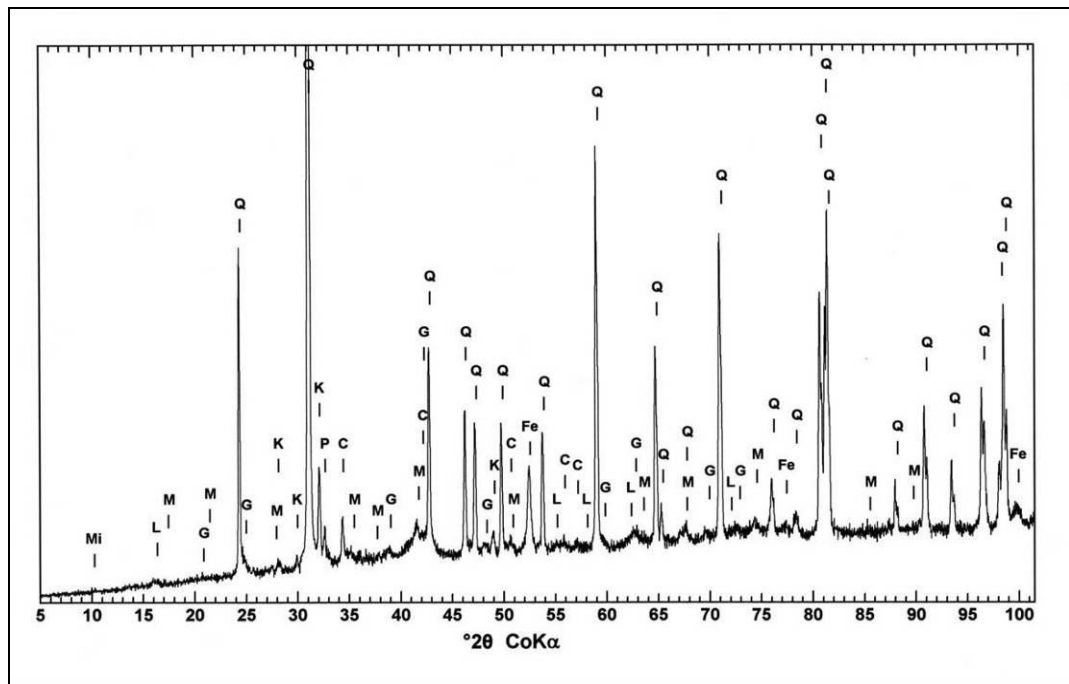


Figure 25: XRD trace of the iron-rich barrier formed in quartz sand showing the composition of the mineralised region. C=calcite, Fe=elemental iron, G= goethite, K=k-feldspar, L= Lepidocrocite, M=maghemite and/magnetite, Mi = mica, P= plagioclase feldspar, Q= quartz (Faulkner *et al.*, 2005)

Table 15: XRD analyses of pre treatment quartz sand and the post treatment iron-rich barrier region (Faulkner *et al.*, 2005).

PRE-TREATMENT SILICICLASTIC SAND MINERALOGY	MODAL ABUNDANCE	POST-TREATMENT IRON-RICH BARRIER MINERALOGY	MODAL ABUNDANCE
Quartz	90%	Quartz & Feldspar	65%
Clay(mica)	3.5%	Goethite	4%
K-Feldspar	3.5%	Native Iron	5%
Plagioclase	1.5%	Maghemite/magnetite	5%
Calcite	1%	Lepidocrocite	5%
Dolomite	0.5%	Amorphous ferric iron oxyhydroxides	As much as 20%

It is interesting that these results suggest the presence of native iron since this elemental iron is of interest for the dechlorination of polychlorinated hydrocarbons such as

pesticides and dioxins. Iron compounds have also been successfully utilised in permeable reactive barriers (PRBs) to passively treat contaminated groundwater plumes (e.g. Younger *et al.*, 2002). Goethite and magnetite are also established as important scavengers for heavy metals in the soil and for their association with a number of key contaminants in terms of co-precipitation.

3.5.5 Geotechnical Characteristics

By inserting cast iron electrodes vertically into the wetted sand and applying a current, the dissolution and re-precipitation of iron from the electrodes results in a continuous band or curtain of iron precipitates that form a distinct cemented zone within the sand or sediment, Figure 26. The coefficient of permeability, (k) of this iron-rich barrier was tested using a falling head permeability test and found to be 10^{-9} ms^{-1} (Faulkner *et al.*, 2005)



Figure 26: An excavated iron rich precipitate region. This was formed in high purity, unconsolidated quartz sand with sea water electrolyte, at 6 volts over a period of 16 days with an electrode separation of 15cm.

This is classified according to Terzaghi and Peck (1967) as ‘practically impermeable’. The co-efficient (k), for the clean, untreated sand, was measured as 10^{-2} ms^{-1} (Faulkner *et al.*, 2005), demonstrating a dramatic decrease in the permeability of the material.

The approximate uniaxial compressive strength of the iron-rich band was measured as 10.8 N/mm^2 comparable to, for example, a strong chalk or moderately lithified sandstone (Cundy and Hopkinson, 2005).

The measured physical properties of the precipitated material indicate that it is suitably impermeable for use as a barrier to groundwater migration. This concept is returned to in Section 4.

3.6 Bowl Experiment

Having successfully generated substantial iron precipitated regions in both vertical and horizontal orientations the next set of experiments were designed to modify the precipitated material's geometry to form more complex shapes. A novel variation of the horizontal barrier electrode array using a parabolic rather than linear arrangement of electrodes was invented. The initial design was based on the arrangement used for the horizontal barrier experiment, Figure 27, however the limitation of this approach for larger scale installations was acknowledged. This is because of the practical difficulties of installing a large sheet electrode on a larger scale due to possible obstructions and surface irregularities making a sheet type electrode impractical. To address these issues an alternative system was devised whereby both the anodes and the cathodes are emplaced at depth, Figure 28.

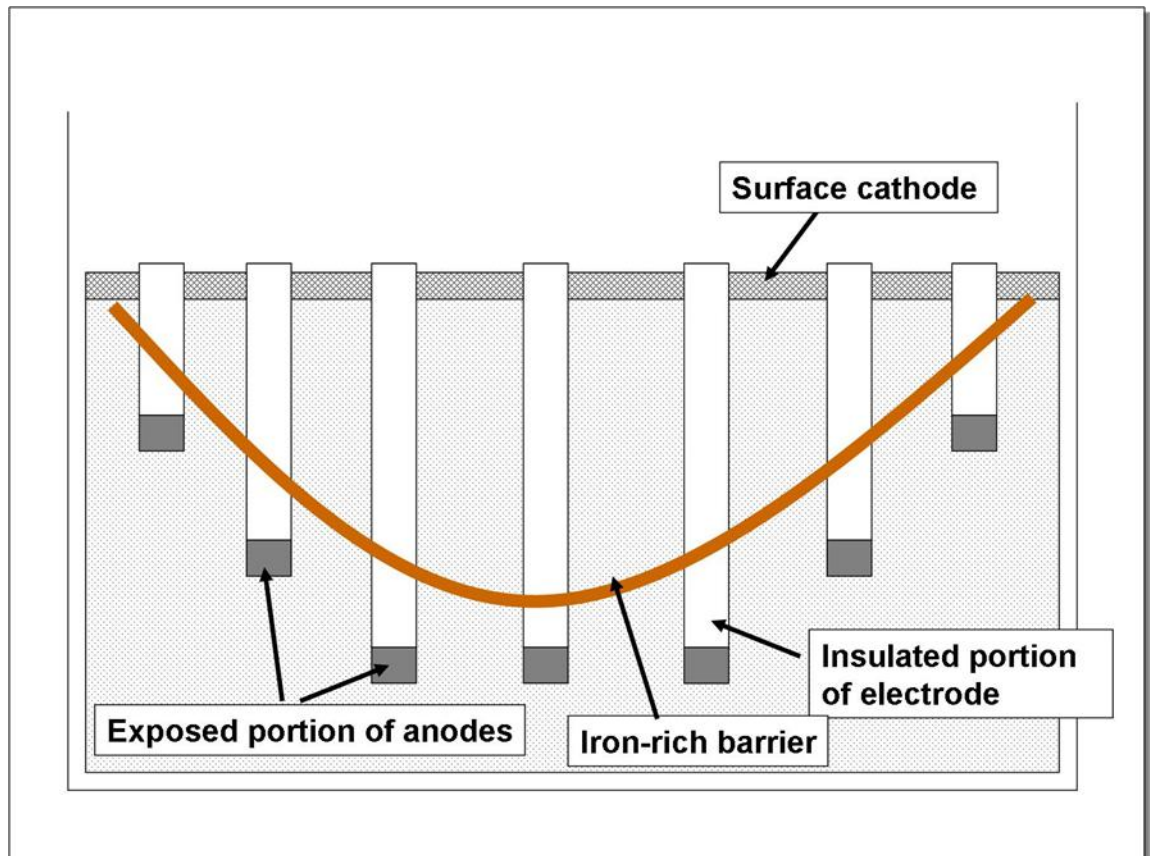
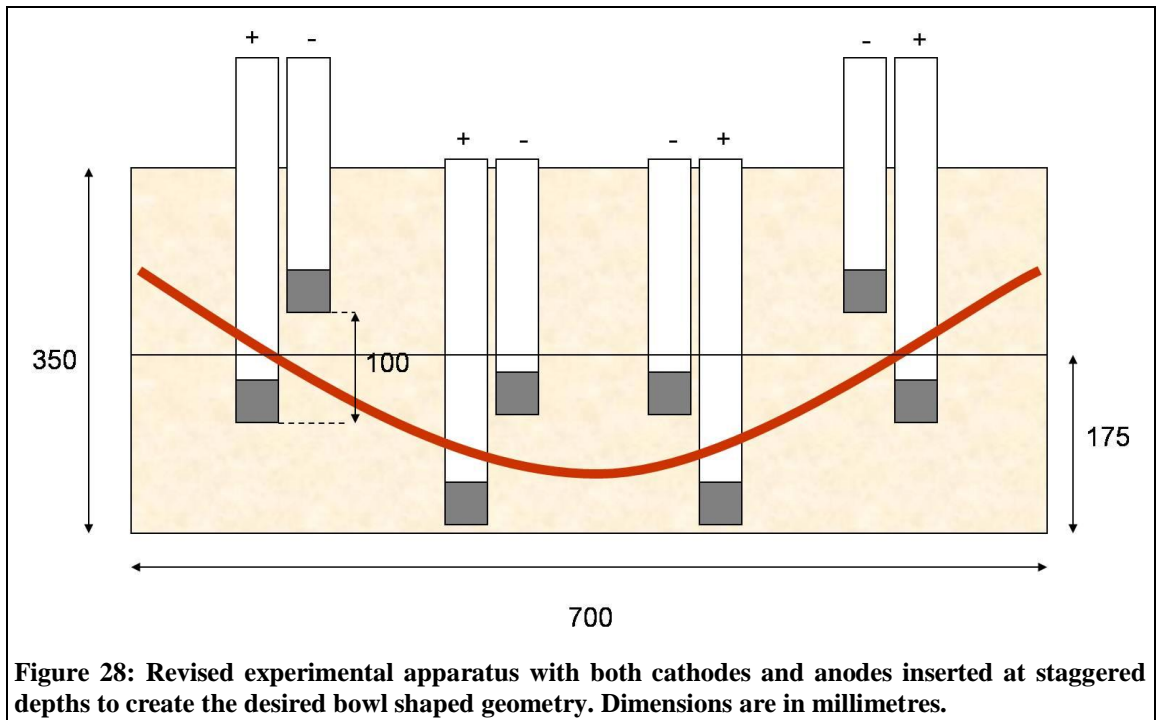


Figure 27: Schematic diagram of a cross sectional view of conceptual electrode positioning in the 'bowl' experiment (not to scale). This diagram shows the postulated method of how to manipulate the geometry towards the formation of a bowl shaped continuous iron-rich barrier.

An experiment was set up as a means to test the hypothesis that iron-rich precipitates can be strategically produced to completely contain contaminants in a region of soil/sediment by producing a continuous bowl shaped iron-rich barrier.

This was intended to be developed as a possible means to contain contaminants being released from a leaking underground storage tank (sometimes referred to by the acronym, LUST) or to contain the movement or migration of a region of contaminated land from one region to another.

A preliminary 'test of concept' experiment was run with the objective to produce a 'U' shaped iron-rich precipitate in a bench top experiment operating in two dimensions,..The results of the pilot scale experiment highlighted the problems associated with the generation of gas at the electrodes.



A modification to the design of the electrodes and the way in which they are positioned was investigated where by both the anodes and the cathodes are partially insulated and both are emplaced at depth, this was done to improve the level of control over where the iron mineralised region forms. This is because the distance between the exposed portions of the electrodes is kept constant, Figure 28.

3.6.1 Method

Seawater was used as the electrolyte throughout. The initial horizontal iron-rich barrier experiment was modified in that both the anodes and the cathodes were constructed to consist of an insulated portion with a cast iron region exposed at the end. This allows for the depth of both the anodes and the cathodes to be independently controlled. This was a modification of the surface mesh approach used for the horizontal iron-rich barrier experiment. The separation between anodes and cathodes was 10 cm and the separation between pairs of electrodes was 15 cm.

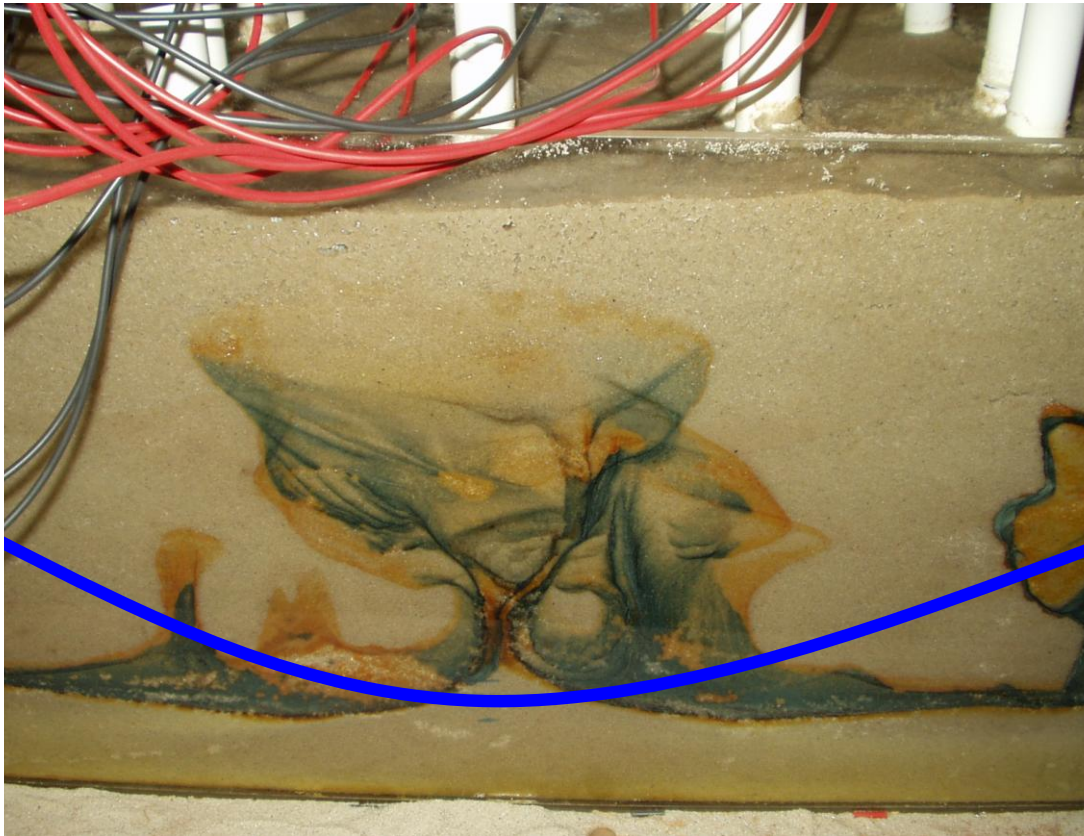


Figure 29: Iron mineralisation in bowl experiment with the proposed formation location indicated in blue.

The mineral fabric formed in the bowl experiment was designed to create a curved precipitated region as an intermediate step towards the creation of a bowl shaped precipitated mineral fabric to isolate a region from the groundwater system surrounding it. The sand medium was chosen as it had been successfully used for creating consolidated iron-rich mineral fabrics in previous experiments. This and the fact that the migration and precipitation of the iron species is clearly visible due to the contrasting colours makes the development of the precipitated region's progress easily monitored and identifiable. However, as seen in, Figure 29 the mineralisation did not occur as intended, the blue curved line represents the approximate location of the intended mineralisation. The swirled iron staining is suspected to be due to the generation of gases at the anode electrodes causing turbulent flow in the pore water and, thus interfering with the development of a regular mineralisation pattern.

3.6.2 Discussion

Some of the difficulties encountered were seemingly due to the production of gas at the electrodes causing turbulence in the pore water. A possible explanation is that the production of oxygen bubbles at the deeper anodes, rising upwards through the wet sand acts as a mechanism to draw the pore water upwards. This drives a circulation of pore water in the sand mass with pore water originating from nearer the surface being drawn down to replace the water that has risen resulting in a convection current. The difficulty is that the mixing of surface pore water which is more alkaline and the acidified water from around the anode results in somewhat unpredictable precipitation of the dissolved iron. Smaller scale pilot experiments have resulted in tubular iron precipitates forming upwards from the anode. This was not observed in the horizontal barrier experiment.

The other difficulty with the experiments as they were run was that the addition of water to the surface of the experiment to prevent drying also causes turbulence and the highly permeable sand in use is a difficulty in this respect. The sand was chosen as a test medium in the first instance due to the previous success in the formation of discrete regions of iron rich precipitates and also for its constancy of composition. The silver/white colour of the sand also allows the progress and colouration of the iron species to be seen. These properties meant that the experiments could be readily repeated with the variables controlled as much as possible, but in this case it seems the permeability is too high for the objective in this case. Some new designs of electrode have been devised to deal with this problem and are addressed in the discussion chapter.

The potential for the generation of a bowl shaped precipitate barrier has not been discounted despite the lack of success in the quartz sand. Modifications to the electrode design and to the method of emplacement and physical shape of the cathode(s) is likely to be required. The problems encountered seem to be due to the highly permeable nature of the material and the gas driven fluid flows, rather than due to the theory being unsound.

The formation of gas at depth with no venting incorporated into the system would pose a problem in any material. A proposed modification to the electrode design could accommodate this. One potential design consists of electrodes which are essentially a pipe with thick walls (i.e. instead of a solid electrode there is a small hole running through the length of it) and the entire outer surface is insulated. This is designed to remove the active region of the installed electrode to the inside of the body of the electrode. So the only electrochemically active surface is the interior surface of the pipe.

The beneficial effect that this would have is two fold, firstly the gas could dissipate straight up the electrode and vent to the surface without building up at depth or influencing the pore water flow or causing turbulence and secondly it means that all the iron in solution generated inside the body of the electrode is released from the opening at the end of the electrode, potentially a very small opening, thus improving the level of control. The same could be done for the cathode electrodes for the gas generation. By ensuring the rapid removal of the gasses, the electrode surface is not insulated by the gasses forming a barrier between the electrode surface and the pore solution, for instance if gas pockets develop close to the electrodes.

This particular problem has been described as a limiting factor and addressed by (Mattson, 1993) and is similar in construction to a lysimeter and allows the electrode be effective in the vadose zone however the level of complexity of the system (the attachment of a vacuum pump to every electrode) is likely to deter widespread adoption of the technique.

3.7 Grid Experiment

The next approach was to develop a method for the stabilising of a material using the precipitated iron-rich mineral fabric. This would obviously require more than an isolated vertical/circum-vertical precipitated region. The approach was to increase the scale of the experiments and to incorporate a repeating geometric electrode array as shall be described below.

In areas consisting of predominantly sedimentary deposits a method for mass stabilisation of a large area is in high demand. Especially as the presence of existing structures makes conventional methods problematic, for instance grout injection or cementation, (Bell, 1975). To produce a mass stabilisation of material beneath existing structures in these areas could prove highly beneficial in terms of liquefaction protection, slope stability improvements, consolidation of spoil heaps etc. The stabilisation approaches in the literature are concerned with the dewatering of saturated materials, (Lamont-Black, 2001) or those that have utilised electrochemical dissolution and precipitation have been concerned with more localised strengthening – for instance around ground anchors (Adamson *et al.*, 1966a; Trushinskii, 1996).

Table 16: Rough classification of ground improvement techniques (Otsuki *et al.*, 2007)

Type	Technique
compaction by static methods	Pre-loading Pre-loading with consolidation aid Compaction grouting. Influencing ground-water table
Compaction by dynamic methods	Vibro-compaction. Compaction using vibratory hammers. Dynamic compaction (drop-weight) Compaction by blasting. Air pulse compaction
Reinforcement with displacing effect	Vibro stone columns Sand compaction piles Lime/cement columns installed by displacing methods
Reinforcement without displacing effect	Mixed-in-place methods Jet grouting Permeation grouting Ground Freezing

3.7.1 Method

The electrodes (solid cylinders diameter 2.5cm length 25cm) were arranged in a regular grid spaced at 45 cm centres. The electrodes were arranged alternating between positive and negative such that each electrode is of opposite charge to that of its immediate neighbours, see Figure 32. The current was $\sim 4\text{A}$ which is close to the maximum of the power supply in use at a voltage of 10V. A pure quartz sand (industrial sand used for filtration of molten plastics before spinning, >99% quartz with no organic matter, see Appendix 1 for full specification) was used as the test medium. This was chosen for its constancy of composition to improve the repeatability of the experiments conducted. Drying, due to evaporation and the loss of water from electrolytic dissociation, was countered by regular watering using tap water.

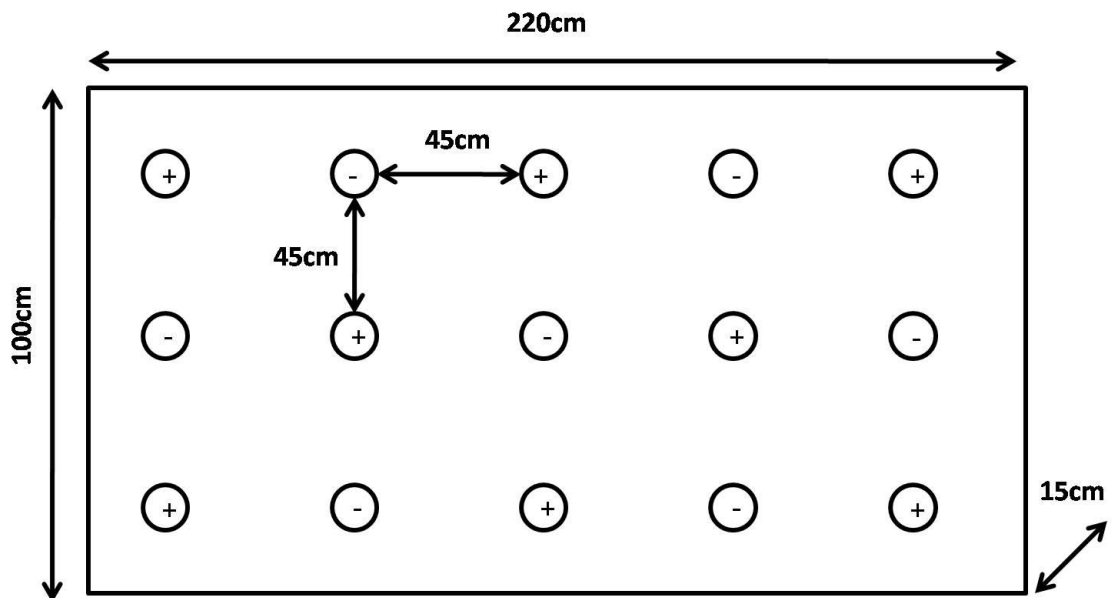


Figure 30: Experimental schematic for continuous grid stabilisation experiment. Viewed from above, the test cell consists of a Perspex tank 25 cm deep filled with the quartz sand to a depth of 15cm. The electrodes were connected to the power supply using standard domestic terminal blocks and the connection between them verified using a test meter to confirm continuity of the connections.

3.7.2 Results

The result was the mass-stabilisation of a 2 m² area of loose sand to the full depth of 15cm, Figure 32. The initially unconsolidated quartz sand was cemented to a continuous and regular geometry to the full depth of the material between the electrodes (represented by the solid lines in Figure 32 d) over a period of 30 days. Boundary effects at the edge of the experimental cell limit the formation of the precipitate there.

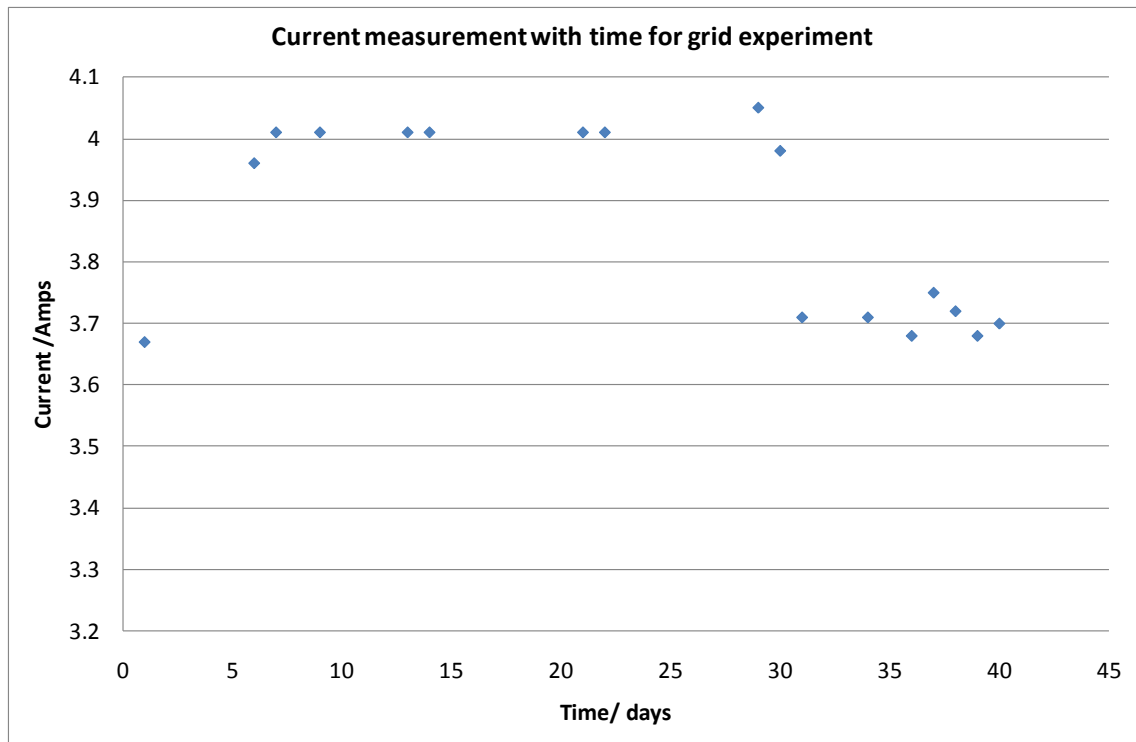


Figure 31: Current change for the duration of the experiment to stabilise a continuous unconsolidated sand area using grid electrode array.

In this experiment there was less of a pronounced drop in the current as the iron precipitation took place, and at the end of the experimental run the current was still at around 90% of the maximum current flow, Figure 31. This may be due to possible boundary effects taking place between the electrodes on the perimeter of the experiment. It may also be an electrical effect caused by the higher current flow and greater number of electrodes.

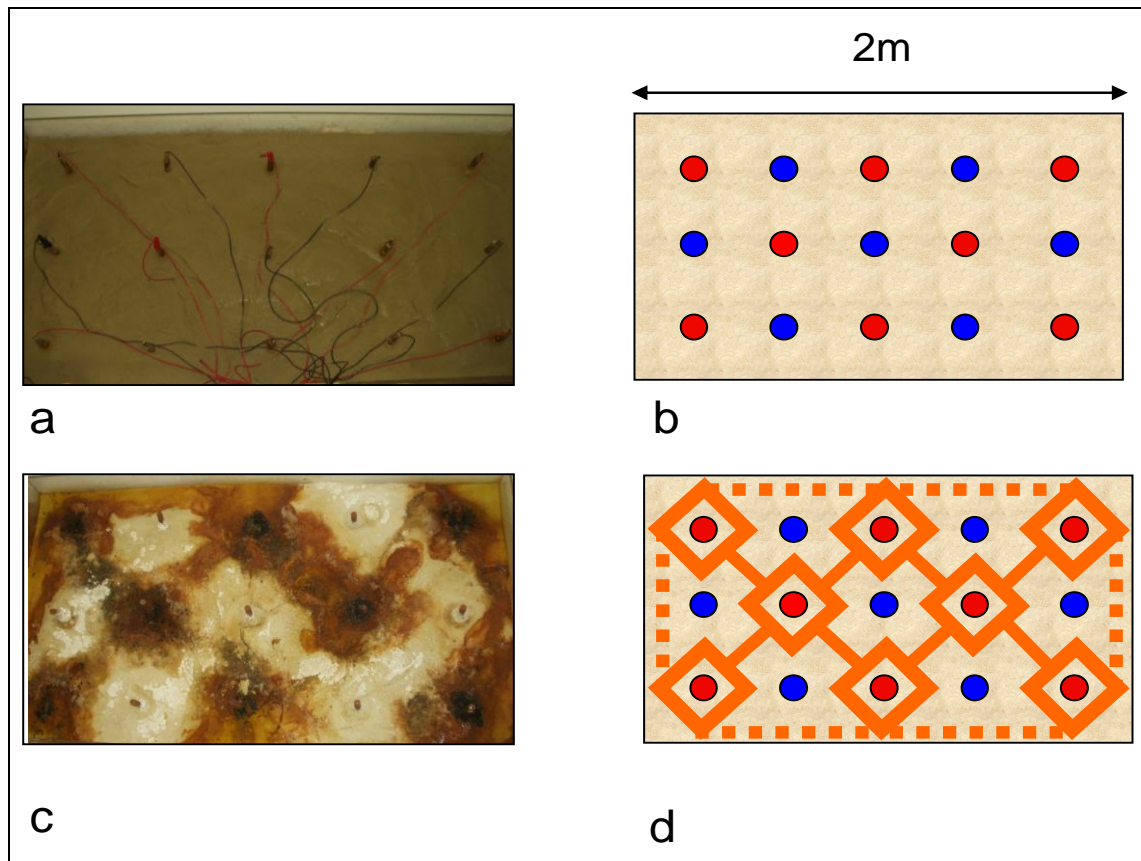


Figure 32: Mass stabilisation of a quartz sand using grid electrode arrangement, 50% sea water 50% fresh water electrolyte, diagram showing experimental set up and precipitate formation.

a) Starting conditions with the electrodes in place. b) Schematic with anodes coloured red and the cathodes in blue. c) Surface discolouration around the electrodes viewed from above. d) Schematic of the geometry of the iron precipitate formed.

3.7.3 Horizontal Barrier Experiment

By strategic insulation of the anode electrodes, such that only the lowermost portion is exposed, vertically emplaced electrodes can be made to function as would a continuous horizontally emplaced electrode at depth. By combining this with a porous cathode positioned on the surface a vertical voltage gradient between electrodes can be achieved. The anodes have been selected as the vertical electrodes but the polarities could be reversed. For the bench scale investigations it was decided that the uprights should be the anodes to make use of the electroosmotic flow from anode to cathode and prevent the water rapidly settling into a water-table with a dryer portion above. In a real

environment situation without boundaries it expected that water would continuously replace that displaced due to electroosmosis, reducing this problem, except in a very low hydraulic conductivity material where the rate of electroosmosis is likely to significantly exceed natural flow rates.

3.7.4 Discussion

The data presented here suggest that it is possible to electrokinetically generate an impermeable, re-sealable iron-rich barrier to a variety of three-dimensional geometries in wet sediments, at low voltages and using simple electrode arrangements. Whilst these experiments were conducted at bench scale, the system's potential for successful up-scaling is strengthened due to the use of low voltages and inexpensive sacrificial electrodes.

The apparent capacity of the system for *in situ* monitoring of barrier integrity, *in situ* self healing, combined with the ability to control iron-rich band geometry in three dimensions, as documented here, offer potential advantages over traditional physical barriering techniques by eliminating the need for excavations to emplace a barrier. The barrier could also be formed *beneath* existing structures. Since the method requires no chemical additives, and utilises relatively low toxicity iron as the strengthening material, environmental impacts are expected to be minimal. The experiments conducted so-far have an energy requirement in the region of 11 kW/m³ of soil. Up-scaled experiments will be required to establish the technique's energy requirements for application in real environment situations but the initial findings are that the technology offers a low cost approach.

In 'real' groundwater environments there is a net movement of water in a given direction. Typically, groundwater movement is slow, it moves at a rate of between 5 and 64 cm per day (Chiras, 2006). Since the rate of migration of the H⁺ and OH⁻ ions under the influence of the electric field is many orders of magnitude greater than typical groundwater flow-rates (Appendix 1, for table of ionic mobility values), the technique is expected to be applicable even under significant hydraulic gradients (see Section 4).

The use of seawater as a high ionic strength electrolyte improves current flow (e.g. Casagrande, 1947), but iron-rich barriers have also been created using distilled water, (Faulkner *et al.*, 2005).

In addition to providing a physical barrier, or indeed a method of locally stabilising and strengthening soil, the electrokinetically generated iron barrier also has the potential to act as a reactive surface for the adsorption of contaminants from leachates. The affinity of freshly-precipitated iron phases for sorption of a range of contaminants has been widely reported, (e.g. Bendell-Young and Harvey, 1992) and evidence of the sorptive capacity of iron barriers generated using electrokinetic techniques has been presented in Cundy and Hopkinson (2005) for a range of inorganic species. Other researchers have stated that in heterogeneous materials the presence of buried objects particularly metal objects would have a significant effect on the electrokinetic process and therefore the creation of sub-surface barriers.

Notably, it has also been shown that iron compounds are significant in the catalysis of the dechlorination of contaminants such as PCBs, organic pesticides and other chlorinated hydrocarbons by acting as electron donors (McGuire *et al.*, 2003). The apparent presence of zero-valent iron in the iron-rich barrier, Figure 25, as well as large amounts of Fe^{2+} , suggests that the technique may have important applications as a reactive surface for the degradation of chlorinated hydrocarbons through iron-mediated dechlorination of the hydrocarbon (Helland *et al.*, 1995; Johnson *et al.*, 1998).

Future work should include the large scale application of precipitated iron phases for ground engineering purposes. In instances of subsidence it may be possible to sufficiently improve the load-bearing properties of the ground material to stop or slow down the rate of subsidence.

The mass stabilisation of a significant area of unconsolidated sand represents a novel result not reported in the literature. Whilst labour intensive on the scale of this experiment the data encourages further work. The regular grid arrangement of electrodes could be extended indefinitely to theoretically stabilise an area of any size. This could be applied to slope stability problems with unconsolidated materials or as a method to retard the rate of erosion of a material susceptible to wind erosion or any

application where stabilisation is required over an extended area. There is a paucity of data describing stabilisation of a large area of unconsolidated material by this kind of 'cellular' stabilisation using electrokinetics. This experiment appears to represent a first for the use of electrochemical stabilisation on this scale and for the use of a continuous 2D electrode array for stabilisation purposes. The voltage and current required for this experiment indicate that the energy requirement for this experiment is around 40 Watts. And the experiment was allowed to run for 40 days which equals approximately 38.4 Kilowatt hours.

4 Barrier Formation Against an Imposed Hydraulic Gradient

This chapter deals with experiments conducted using apparatus to simulate a dynamic groundwater situation as may be encountered in a naturally occurring groundwater setting. These experiments were designed to evaluate the use of electroosmosis and the electrochemically produced iron mineral fabrics described in the previous chapter as a method for groundwater control and hence contaminated land management. This emerged out of the requirement to maintain a constant level of hydration of the material causing the adaptation of the experimental tanks which was then modified further to provide a means to add a controlled hydraulic head to the test medium. The FIRS technique is therefore investigated in terms of its ability to provide a possible method to protect aquifers and contain or control contaminant plumes in the sub-surface.

This section is a general introduction and description of the method along with some of the theoretical and practical aspects of the experiments considered. The results and discussion for each of the test materials: sand, loam, and estuarine sediment, are addressed separately.

4.1 Introduction

Groundwater is an extremely important resource for obtaining drinking water as well as for the irrigation of crops and the potential impacts of contamination of aquifers is huge. In the case of organic contaminants, a relatively small volume, a single drum of approximately 200 litres of trichloroethylene for instance; can result in a concentration rise from zero to the US threshold value of $5\mu\text{g/l}$, in 6×10^{10} litres of water (Pierzynski *et al.*, 2005). When just one leaking barrel has the potential to contaminate 60 *billion* litres of clean water; the protection of valuable water resources is an obvious concern.

There are added difficulties with groundwater in that it may exist at significant depth below the surface and the fact that groundwater is part of a dynamic system; capable of transporting contamination a significant distance from source. Groundwater management is therefore an important factor for the mitigation of remediation strategies. Typically, groundwater movement is slow, it moves at a rate of between 5 and 64 cm per day (Chiras, 2006) and hydraulic gradients are seldom greater than 0.1 m/m (Ranjan, 2009).

This section deals with an electrokinetic approach to the control and management of groundwater flow as a method for controlling the migration and mobility of contaminants. This may also have useful applications for ground excavations and other ground engineering approaches.

By purposely and strategically propagating this precipitation, the properties of permeability, chemical composition and structural/strength properties of the ground can be strategically manipulated to provide control over groundwater flow, contaminant plumes, soil strengthening and additionally providing a reactive surface within the soil for contaminant degradation.

Experiments were conducted to replicate groundwater flow in the laboratory to assess whether it was possible to cause migration and reprecipitation of iron dissolved from the positive electrode; against the flow of groundwater in soil, sediment and in purified sand; and to demonstrate the method as a means to form subsurface barriers to groundwater flow.

4.2 Experiment Design

The experiments were designed to mimic a near-surface groundwater flow, incorporating a saturated and a vadose zone, in a gravitationally induced flow system. In these mimicked natural conditions, counter-flow electroosmosis along with the production of an iron rich precipitate barrier formation was attempted.

Other workers have conducted electroosmotic experiments against a groundwater flow using a sealed unit with a pressurised flow, (e.g. Lynch *et al.*, 2007), these experiments have tended to be on a relatively small scale (10-20 cm) and concerned with preventing the migration of contaminants into an uncontaminated region of the test cell.

The apparatus was constructed to give a controllable hydraulic head to one side of a mass of soil/sediment. This allowed experiments to be conducted in a controlled groundwater situation with measurable groundwater flows, as might be encountered in a natural groundwater situation, replicated in the laboratory.

A Perspex container (dimensions 700 x 350 x 350 mm) - as used in the remediation experiments- was modified by the addition of nylon mesh partitions at 120 mm from each end, and provided with input and output connections for the supply and removal of electrolyte either side of the material. This produced a central compartment to contain the sand/sediment mass whilst allowing inflow/outflow of solution freely from each end. The electrodes are able to be inserted directly into the sand/sediment as in previous experiments, Figure 33.

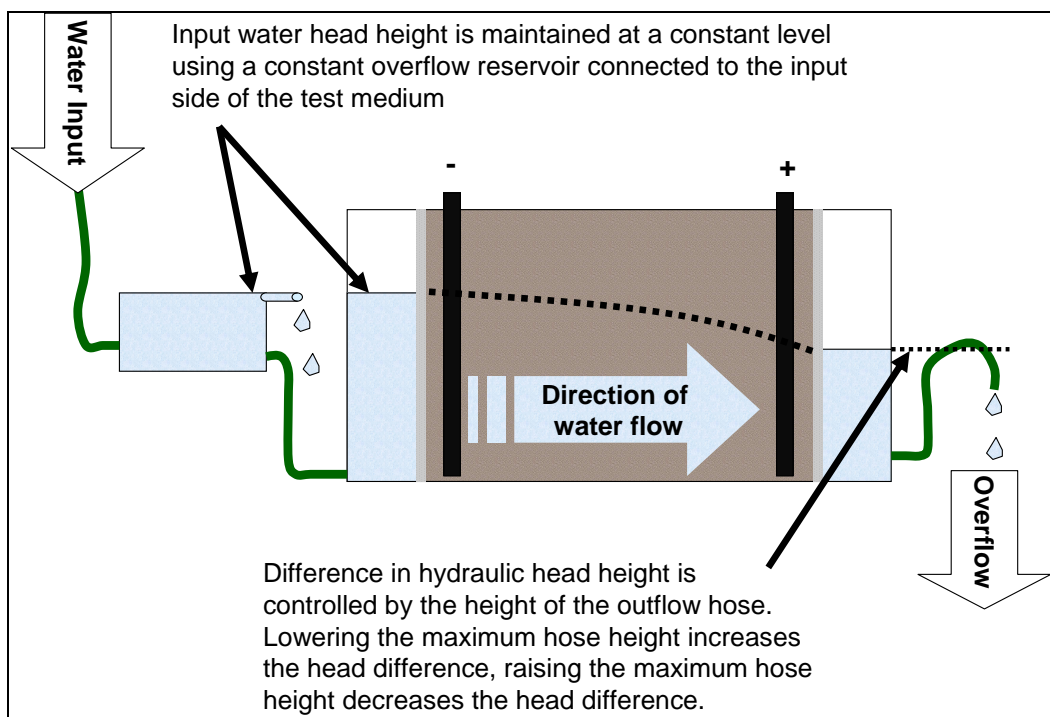


Figure 33: Experimental set up for the generation of a constant hydraulic gradient across a test medium. The electrodes are at a separation of 45 cm with a maximum test material volume of 56350 cc. The anode electrodes are at the downstream end of the experiment since the electroosmotic effect and iron migration direction when the electric field is applied induces movement from anode to cathode. Note the flow is towards the anode electrode, contrary to the electroosmotic flow, which acts from anode to cathode.

The height of water fill in the reservoir tank is kept constant due to the overflow system. The tank itself can be raised or lowered to provide the desired hydraulic head, Figure 33. The height of the outfall was also adjustable so that once set, any increase in water height on the output side is lost as overflow setting a maximum head height on the output side. This combination allows for a constant hydraulic gradient to be established across the material being treated.

4.3 Theoretical Considerations

The height of the outfall was made adjustable such that the hydraulic gradient can be finely controlled with the outfall lowered to increase the head difference and therefore the hydraulic gradient, or raised to decrease it. The rate of flow is calculated by volumetric measurement of the outflow for a specific time interval (ml/hour).

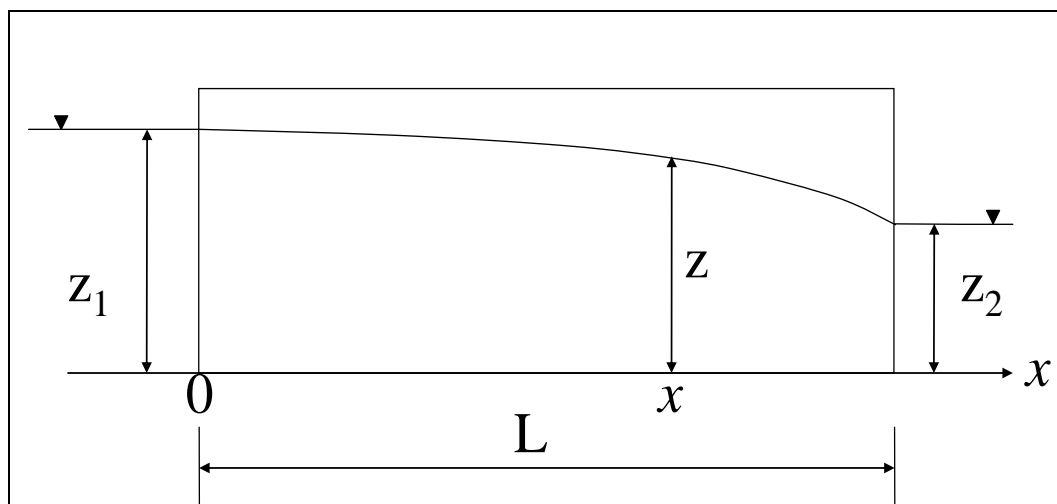


Figure 34: Linear gravity flow distribution, sketch giving the definitions of the variables used to describe Dupuit's parabola and discharge (adapted from Raudkivi and Callander, 1976).

The saturated zone/capillary zone interface forms a predictable boundary (termed the phreatic surface) shown in, Figure 33 (dashed line) and the definition sketch, Figure 34, determined by the input and output water levels and is described by a mathematical

expression and is. This distinctive profile is called Dupuit's parabola and is derived from solving the Laplace equation for flow over a horizontal impervious base (e.g. Raudkivi and Callander, 1976).

The apparatus used allows for some convenient assumptions, namely that K (coefficient of permeability) is constant and that flow is effectively only taking place in two dimensions. The variables are defined in, Figure 34 for the region between the mesh partitions containing the test medium. Derived from the Laplace equation, the parabola is described by, Equation 16

$$z^2 = z_1^2 - \frac{z_1^2 - z_2^2}{L} x$$

Equation 16

which gives:

$$\frac{x}{L} = \frac{z_1^2 - z^2}{z_1^2 - z_2^2}$$

Equation 17

From this, and incorporating the hydraulic conductivity, K , the theoretical rate of discharge, q , per unit area becomes:

$$q = -Kz \frac{dz}{dx} = \frac{K(z_1^2 - z_2^2)}{2L}$$

Equation 18

(Equations 16-18 taken from, Raudkivi and Callander, 1976).

The velocity of the water's movement through the test medium is determined experimentally by the measurement of the volume of fluid leaving the system; and is related to the cross sectional area of the mass of material, that measurement is termed the *Darcy Flux*.

This is a measure of the rate at which water is leaving the sample at the output side. This does not account for the fact that in the pore spaces of the test medium the water is actually following a tortuous path. This means that the local linear velocity may be higher than the Darcy Flux (Raudkivi and Callander, 1976). So at a particular point in the soil medium the actual pore water velocity may be significantly higher than the Darcy Flux measurement might indicate.

These factors need to be considered for the comparison between the ionic diffusion rates; of the iron in solution and the hydrogen and hydroxide ions produced at the electrodes; and the comparative rates of flow due to gravity and electroosmosis. This comparison will allow for the prediction of maximum hydraulic head against which ionic migration can be facilitated and will be essential for the production of a model for the prediction of the conditions under which a precipitated barrier may be formed in a material of known composition and physical characteristics.

4.4 Method

The experimental apparatus was the same in each case, Figure 33. The experiment was set up as described and a voltage of 150V applied between the two rows of electrodes. The outflow rate was periodically measured by recording the volume of effluent from the outflow per unit time, and repeating the measurement a number of times to obtain an average rate.

The flow rates were recorded and compared as the experiment progressed and, along with the electrical current reading, used as indicators for the extent of formation of the iron-rich precipitate barrier impeding water/ion flow. The pH measurements in both the anode and cathode compartments were also taken.

In the washed sand experiment the migration of the iron from the electrodes is clearly visible as an oxidised iron front, contrasting with the light coloured sand.

Significant joule-heating of the loamy soil experiment became evident after 48 hours of application and the voltage was dropped to 75 volts to avoid heat damage to the apparatus and based on this the experiment using the estuarine sediment was also run at 75V.

The progress of the experiments was also monitored with a visual record obtained by photographic recording of the experiment progress.

4.5 Results: Quartz Sand Experiment

The hydraulic conductivity of pure un-compacted sand was measured using a constant head permeability test and was found to be $5.8 \times 10^{-3} \text{ ms}^{-1}$ which is typical for a sand of this grain size and grade. The porosity was determined to have an average value of 0.365, Table 17.

Table 17: Measurements and calculated value for porosity of quartz fibre sand.

Sample	Container Mass /Kg	Container Diameter/ m	Container height/ m	Container Volume/ m ³	Container +dry sand mass /Kg	Mass sample/ Kg
S1	0.0272	0.0554	0.0554	0.0001335	0.239	0.2118
S2	0.0268	0.0556	0.0553	0.0001342	0.2401	0.2133
Dry density Kg/m ³	Container + Wet Sand mass /Kg	Mass water /Kg	Volume water /m ³	Wet density Kg/m ³	Volume Solid /m ³	Porosity
1586.0144	0.2878	0.0488	0.0000488	1951.4417	8.47423E-05	0.365
1588.6441	0.2892	0.0491	0.0000491	1954.3376	8.51654E-05	0.365
Average						0.365
Porosity						0.365 (3sf)

As seen in Figure 35, the water table profile has been modelled from theory. This shows the theoretical height and shape of the water table along with the seepage velocity for a given height difference between the input level and the outflow height. The seepage

velocity increases towards the outflow point as the cross sectional area of the saturated zone decreases due to the gravitational influence.

From Darcy's Law (see Section 2.4):

$$Q = -K \frac{dh}{dl} A$$

Equation 19

Where: Q is the rate of inflow/outflow (m^3s^{-1})

K is the hydraulic conductivity (ms^{-1})

dh/dl is the hydraulic gradient

A is the cross sectional area (m^2)

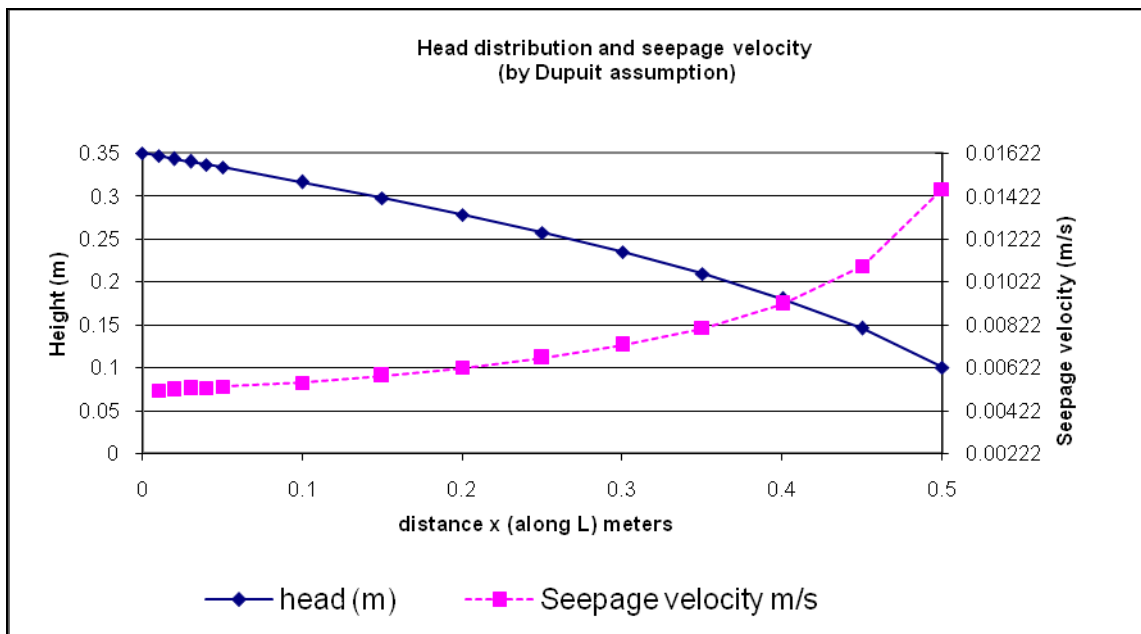


Figure 35: Theoretical water table height across test cell with an input head of 0.35 m and an output of 0.1 m also showing theoretical seepage velocity, calculated from empirical porosity and hydraulic conductivity measurements performed on quartz sand.

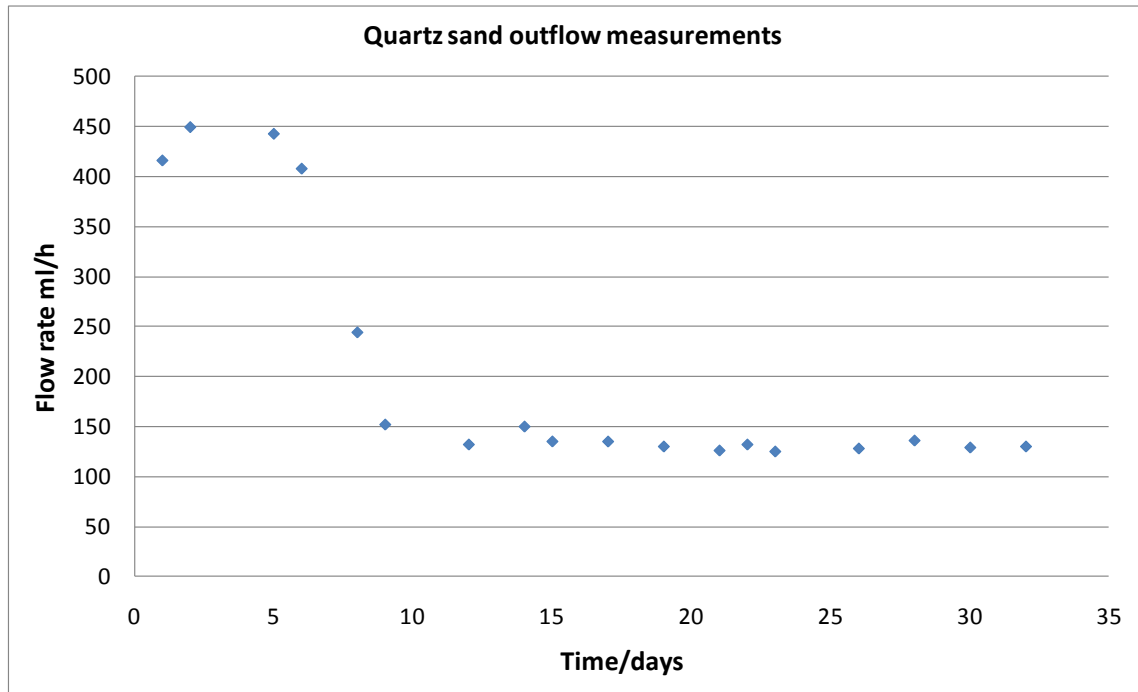


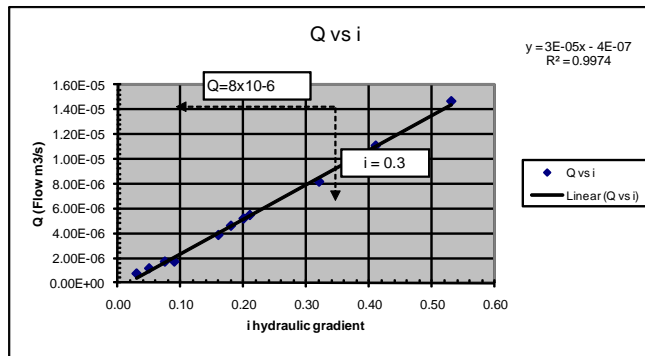
Figure 36: Outflow measurements for quartz sand under a hydraulic gradient. The flow rate shows a significant drop over the first 10 days before stabilising at circa 140 ml/h.

There was a visible formation of iron precipitate around and behind the anode electrodes, Figure 39. Measured outflow also showed a progressive reduction in rate of flow. This flow did not, however, fall to zero; possibly due to flow continuing along the flat edges or along the corners of the test cell where the vertical sides meet the bottom of the tank, rather than through the sand, sometimes called ‘piping’ (e.g. Lynch, 2009). There was a progressive drop in current as the iron-precipitate formed.

		h	t		Q		A	y	i	Rt
h1 (mm)	h2 (mm)	h1-h2 (m)	Time (sec)	Volum e (m3)	Flow Rate (m3s-1)	cell Diameter (mm)	XSA (mm2)	Length (m)	hydraulic gradient (h1-h2)/y	Temp. Correcti on Factor
252	146	0.106	34	0.0005	1.47E-05	0.08	0.00454	0.20	0.53	1.00
756	682	0.074	51	0.0005	9.80E-06	0.08	0.00454	0.20	0.37	1.00
428	346	0.082	45	0.0005	1.11E-05	0.08	0.00454	0.20	0.41	1.00
80	4	0.076	50	0.0005	1.00E-05	0.08	0.00454	0.20	0.38	1.00
848	806	0.042	91	0.0005	5.49E-06	0.08	0.00454	0.20	0.21	1.00
684	644	0.040	96	0.0005	5.21E-06	0.08	0.00454	0.20	0.20	1.00
132	68	0.064	61	0.0005	8.20E-06	0.08	0.00454	0.20	0.32	1.00
72	36	0.036	108	0.0005	4.63E-06	0.08	0.00454	0.20	0.18	1.00
372	340	0.032	129	0.0005	3.88E-06	0.08	0.00454	0.20	0.16	1.00
		0.010	85	0.0001	1.18E-06	0.08	0.00454	0.20	0.05	1.00
		0.006	132	0.0001	7.58E-07	0.08	0.00454	0.20	0.03	1.00
		0.018	58	0.0001	1.72E-06	0.08	0.00454	0.20	0.09	1.00
		0.015	145	0.0003	1.72E-06	0.08	0.00454	0.20	0.08	1.00

Rt/A	Q/i	k
220.436	2.77469E-05	0.0061
220.436	2.64971E-05	0.0058
220.436	2.71003E-05	0.0060
220.436	2.63158E-05	0.0058
220.436	2.61643E-05	0.0058
220.436	2.60417E-05	0.0057
220.436	2.56148E-05	0.0056
220.436	2.57202E-05	0.0057
220.436	2.42248E-05	0.0053
220.436	2.35294E-05	0.0052
220.436	2.52525E-05	0.0056
220.436	1.91571E-05	0.0042
220.436	2.29885E-05	0.0051

average = 0.0055



Hydraulic Conductivity

Gradient of line q vs $i = dQ/di = 8 \times 10^{-6} / 0.3$

=

$K = (dQ/di) \times (Rt/A)$

= 26.666×220.436

= 0.005878

= $5.8 \times 10^{-3} \text{ ms}^{-1}$

Figure 37: Determination of Hydraulic conductivity from constant head test. Quartz sand.

Due to the relatively high hydraulic conductivity of the sand being used, the hydraulic head gradient was necessarily small so that the out flow volume measurements were large enough to be measured yet the volumes involved were not so large that they could be dealt with in the laboratory.

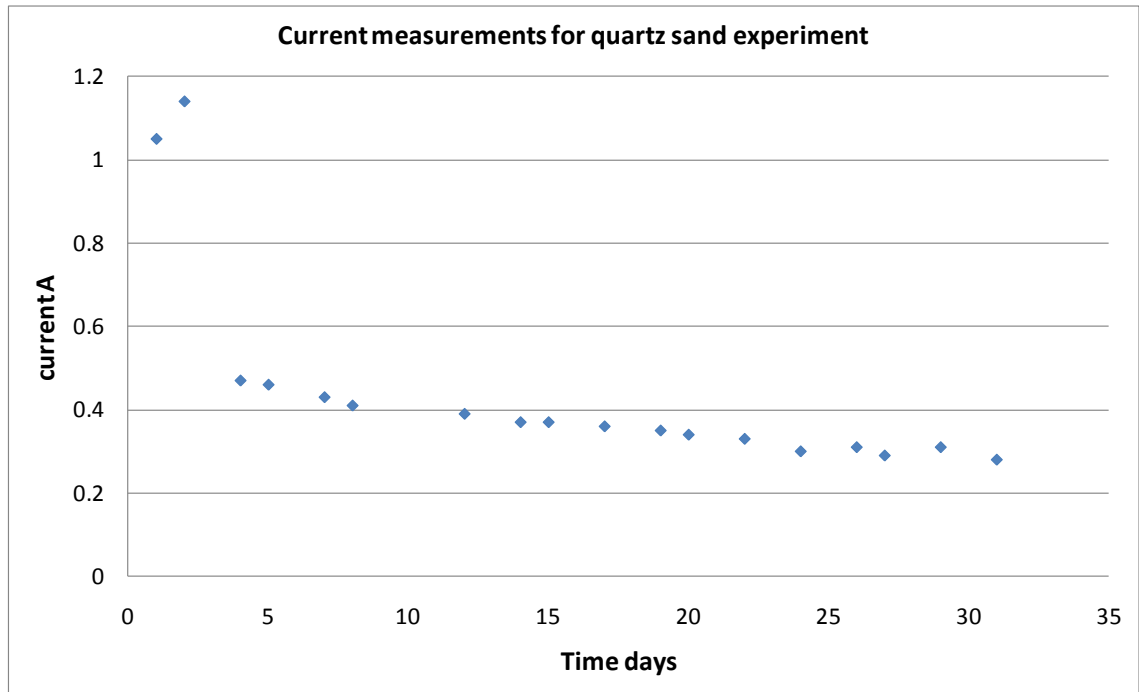


Figure 38: Current measurements for quartz sand under a hydraulic gradient.



Figure 39: Iron precipitation visible around and between the anode electrodes in the sand experiment excavated at the end of the experiment (furthest right anode electrode has been removed).



Figure 40: Loosely consolidated regions around the cathode electrodes extending in the direction of groundwater flow to form these 'fin' like protrusions (top). The structures had enough structural integrity to be removed from the test tank and retain their form (bottom). The electrodes are 35 cm long.

There was also additional calcification around the cathode electrodes which has not been observed in other experiments. This took the form of fin shaped regions of loosely consolidated sand which extended from each electrode in the direction of water flow, Figure 40.

This may have had an effect on the overall permeability of the test cell and also account for some of the measured out-flow drop and drop in current. The proposed mechanism for this cementation at and around the electrodes is expected to be due to the precipitation of the mineral content of the introduced tap-water which is sourced from a 'hard water' supply. This explains the fin like shape of the cemented regions under the

influence of the hydraulic gradient the cementation appears to have taken place in the form of a plume behind each cathode electrode. The cementation here is far less robust than the precipitated iron region at the anode and the fin structures are rather delicate and friable. It is however noteworthy that there is observable precipitation/cementation taking place at the cathode under these conditions and in this medium. Similar effects were not noted in the other materials tested, possibly due to the much smaller grain size which meant that the un-cemented regions did not fall away in the same way to reveal the cemented regions (if indeed they existed) and penetrometer testing did not demonstrate a measurable difference in the strength of the area directly behind the electrodes. There may have been some significant effects due to the reduction in flow rate that this may have caused but the way the experiment is set up only total permeability is measured.

The experimental setup could be modified to include a system of boreholes which would indicate the level of permeability across the length of the test cell which could be correlated with theoretical values and values obtained from untreated material. The effect of this cementation and resultant drop in hydraulic conductivity in terms of the generation of an impermeable barrier could be taken to be beneficial since it is likely to help the generation of the iron- rich mineral fabric by reducing the rate of flow through the medium allowing for the migration of the iron species to take place more effectively. This would require more work to establish the significance of this phenomenon. Re-running the experiment using distilled water rather than tap-water could establish whether the phenomenon is observed which would indicate whether the cementation is taking place due to the ionic content of the influent or if it is still observable when there is no salt content in the introduced electrolyte. This is likely due to the high purity of the sand used, containing very little calcite.

4.5.1 Screened Topsoil Experiments

The loamy soil was commercially available ‘topsoil’ purchased from a garden centre. It was certified to conform to British Standards BS 3882 (British Standards Institution, 1994, 2007) for chemical composition, organic content etc.

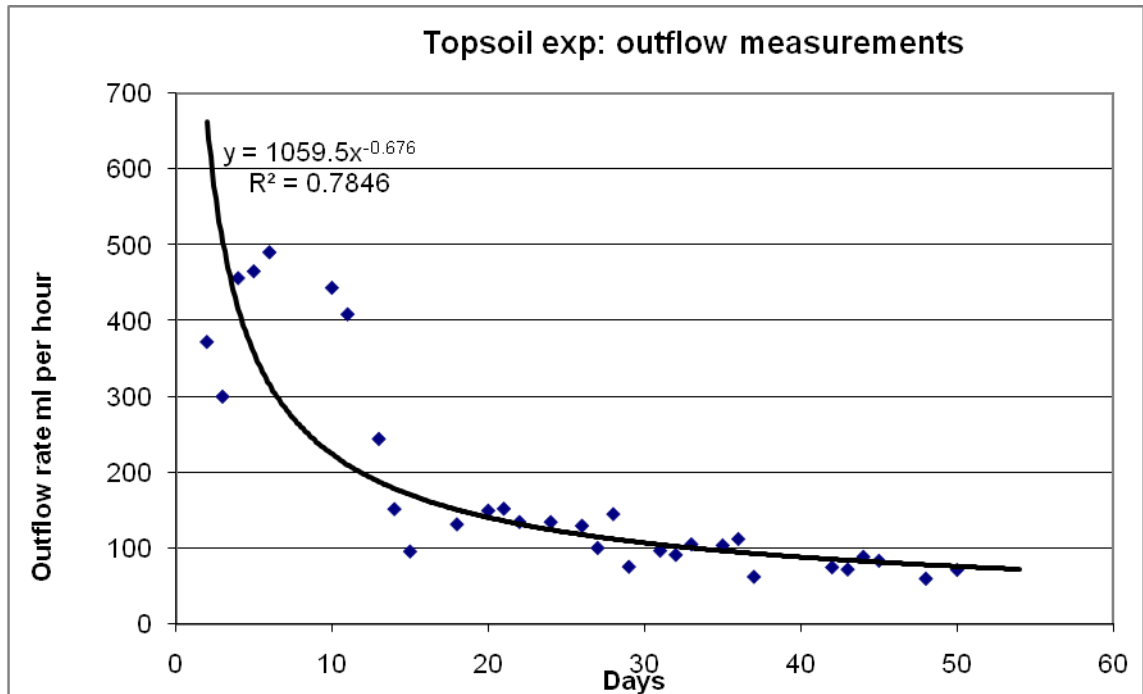


Figure 41: Volumetric flow rate measurements with time as measured at the out flow for loamy topsoil material. The voltage was dropped from 150 V to 75V after 48hours due to Joule heating. A trend line describing a power relationship has been included which might be expected from the relationship between the current flow and the precipitate formation.

The formation of the iron band resulted in significant reduction in flow rate (from almost 500ml h⁻¹ down to around 90ml h⁻¹) Figure 41. There was also a significant increase in the strength of the material. The consistency of the starting material was an unconsolidated and uncompacted material, rich in organic material; fragments of wood and plant material were visible, and there was elasticity in its structure: it would spring back after compression. The iron precipitated region in contrast was harder, and well consolidated. The physical strength of the iron enriched region was approximated using a hand penetrometer, Figure 42.

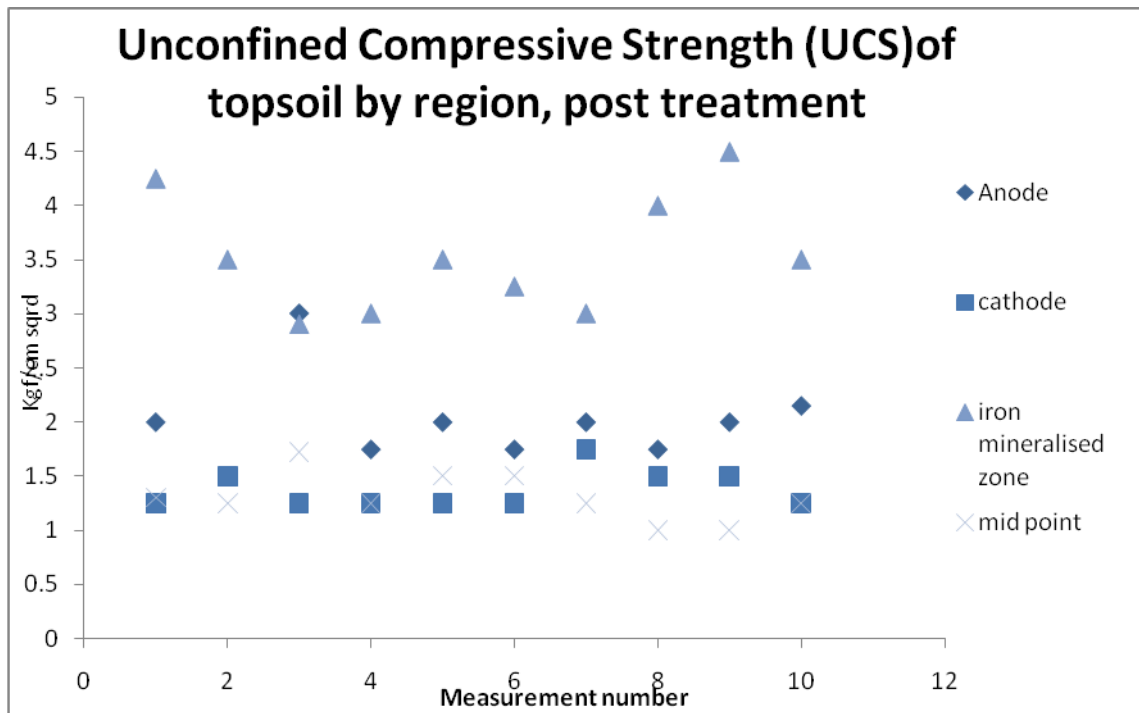


Figure 42: This shows the increase in UCS of the loamy soil by region. Ten measurements were made across the surface of the test cell at the end of the experiment showing the significantly greater strength at the point of iron mineralisation. The cathode, anode and mid point areas gave considerably lower values.



Figure 43: Visual appearance of iron-rich precipitate forming close to the anode electrodes in loamy top soil.

4.5.2 Estuarine Sediment Experiment

Within 72 hours of having applied the current, the outflow dropped to zero and stayed at zero for the remainder of the experiment. The formation of an iron precipitate barrier has been successfully achieved under a hydraulic head difference of 6cm across the cell. This is equivalent to a gradient of 0.12.

Measurements of the unconfined compressive strength using a hand penetrometer showed a significant increase in the strength of the sediment at the anode due to the dewatering and the chemical change due to the introduction of iron into this region, but particularly in the precipitated region with values that correspond quite closely with the values obtained by Cundy and Hopkinson (2005) see Figure 42

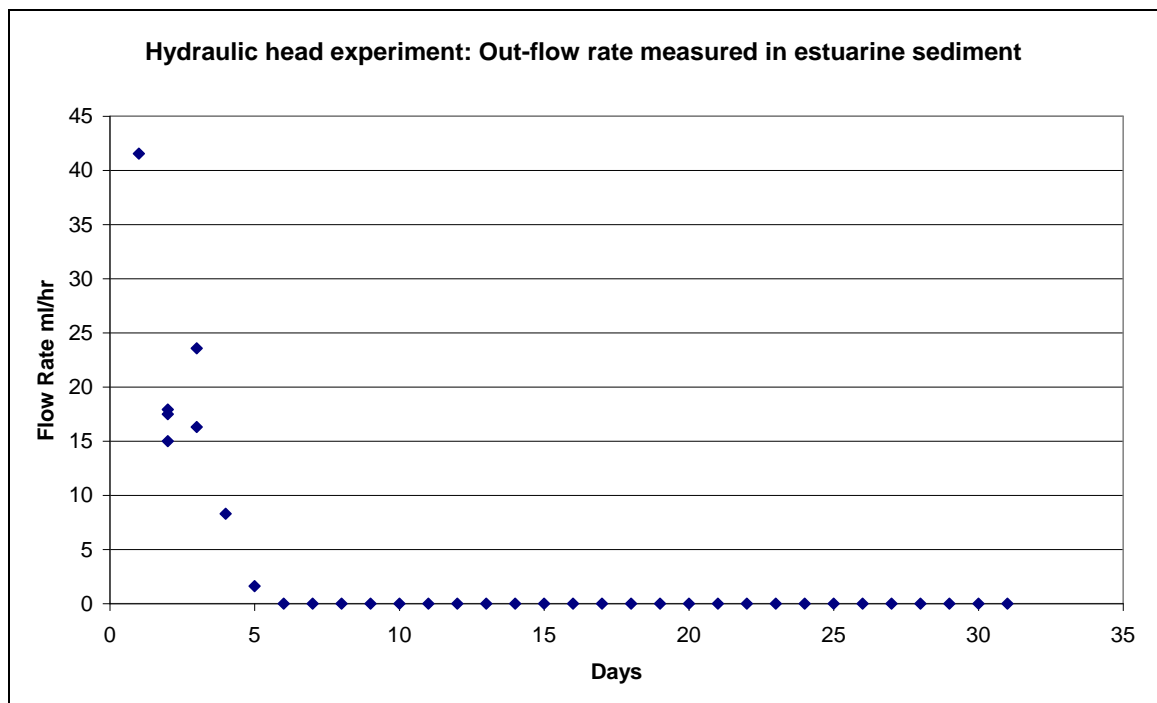


Figure 44: Out flow measurements for estuarine sediment with time. The experiment was allowed to stabilise for four days with the electrodes inserted before the current was applied.

There was a visible and substantial iron precipitated region, Figure 46. The experiment was terminated, i.e. the current was disconnected and the experiment was left with the head still applied to see if the barrier that had formed remained impermeable without the electric current and associated electroosmotic influence countering the gravitational flow.

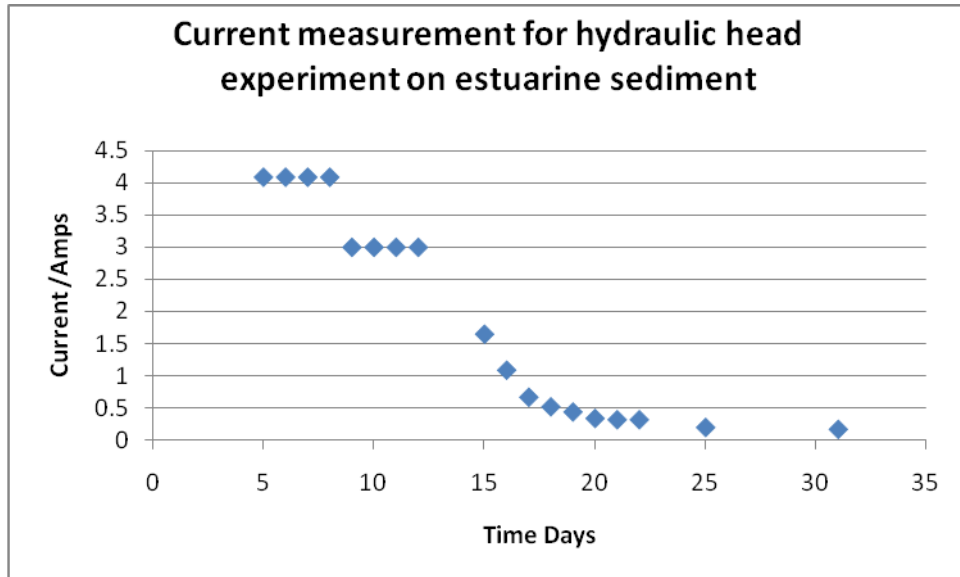


Figure 45: Current with time showing the characteristic decay as seen in previous experiments. Day 9 the current was limited to a maximum of 3 Amps due to significant Joule heating of the material.

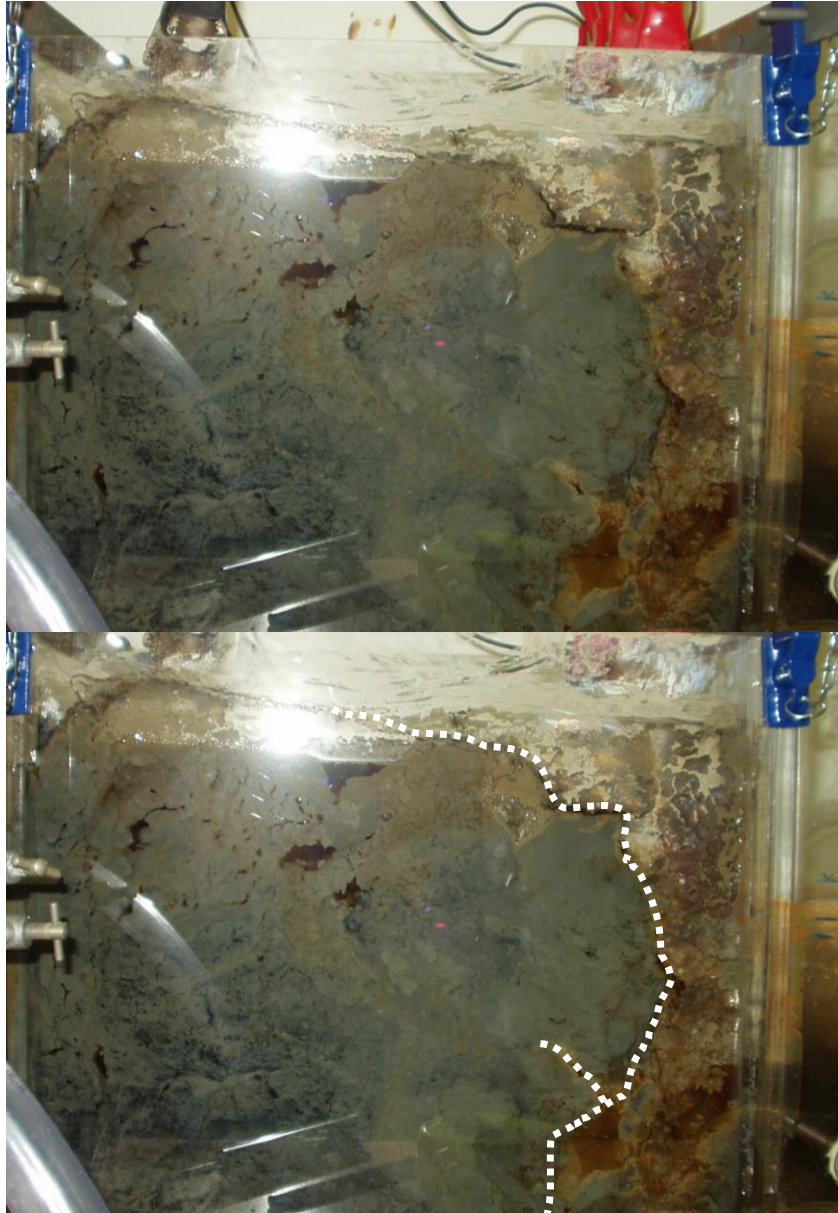


Figure 46: Precipitation of the iron-rich mineral phase in the Hythe sediment hydraulic head experiment with the region of iron enrichment highlighted in the bottom image.

Figure 46 shows the appearance of the iron-rich mineral phase forming as viewed through the side panel of the apparatus. The bottom picture has superimposed the apparent mineralised region responsible for the reduction in both the out flow through the test medium and the drop in current.

4.6 Discussion

In the sand experiment a limitation of the apparatus was exposed. The rate of flow through the medium exceeded the rate of migration of the iron from the electrode. This resulted in the iron migrating in the direction of water flow with viscous drag being the more dominant transport mechanism. The electrodes were positioned close to the mesh partition at each end of the test cell. The iron in solution precipitated out at the mesh partition, due to oxidation by atmospheric oxygen. This precipitate clogged the mesh and inhibited the out flow from the cell. This reduced the head difference and therefore the flow rate. The precipitation seen around the electrodes and the reduction in the volumetric output from the system therefore may have been the result of this clogging.

In the estuarine sediment experiment an unexpected result was observed. After the sample had been allowed to stabilise for four days, the current was applied, at this point an initial *increase* in out flow rate was measured. This was not predicted, in fact there was predicted to be an almost immediate drop in out-flow rate on application of the electric field due to electroosmosis (worm casts were observed forming during the stabilising period).

The initial increase in outflow observed was unexpected, however it is likely to be caused by volume changes in the test material (particularly in the case of the top soil and estuarine sediment). The application of the electric current and the associated phenomena would be expected to alter the saturation of the upper part of the material due to the electroosmosis as well as the generation of gasses at the electrodes displacing liquid.

Another contributing factor might be that the application of the electric current causes a sudden increase in invertebrate activity due to the change in conditions; resulting in increased burrowing. These burrows may have provided flow paths for the input water of significant diameter for gravitational flow but too wide for electroosmosis. As the experiment progressed, the competing fluxes of the hydraulic head flow and electroosmotic flow and the associated turbulence and transport of suspended solids quickly clogged and blocked these burrows and removed these flow paths. This is speculation and the argument could be tested for by comparing a biocidally treated

sample and a sample known to contain burrowing invertebrates. The isolation and identification of the soil fauna was decided to be outside of the scope of this thesis but could be addressed in future work.

The non-zero flow in the sand and in the loam suggest that there was either a non-continuous iron-mineral fabric formed, or that it did not develop sufficient integrity over the timescale of the experiment to completely stop the flow of water through the test medium or flow through void space..

For a low permeability soil under a low hydraulic gradient the electroosmotic effect may be of such magnitude in comparison to the rate of migration of water through the soil gravitationally, that backflow of the water after the current is no longer applied is so slow as to have the effect of having produced a temporary barrier (Narasimhan and Sri Ranjan, 2000; Lynch *et al.*, 2007). For instance if a temporary excavation is required it can be implemented without chemicals or structural installation simply using electrokinetic dewatering.

The apparatus could be modified to allow for this since it is conceivable that rather than forming the precipitate barrier at some point between the two electrode banks, the barrier could be formed downstream, or even behind the anode electrode array.

If the apparatus was extended in the downstream direction, to allow for the migration further in this direction before coming to the mesh partition, it might be possible that a precipitated barrier might begin to form behind the electrodes from the combination of oxidation from dissolved oxygen and the presence of hydroxide ions formed at the cathode. This is analogous to the oxidised iron deposits (ferric hydroxide) seen on river beds downstream from the introduction of acid mine drainage waters (Alloway and Ayres, 1997; Manahan, 2000), where the change in redox and pH cause the iron dissolved in mine drainage to drop out of solution as precipitate.

This deposit might be expected to be more diffuse in nature than the sharply defined iron-pans previously formed, but if it was able to develop to such an extent where it provides significant impedance to the groundwater flow under the influence of gravity, then the flow rate could become reduced enough that the electromigration towards the

cathode overcomes the opposing effect of the groundwater flow. At this point we might expect that a secondary iron pan may form more conventionally at some point between the anode and cathode electrode arrays.

This scenario is only likely to be valid for a sandy material with relatively high permeability as used in this experiment. In a more fine grained or clayey material the permeability will be lower; which makes electroosmosis and electromigration more significant transport mechanisms than the purely gravitationally induced flow. Another factor is that a fine grained material will be less well penetrated by atmospheric oxygen, indeed, if there was any significant organic fraction contained in the material these conditions would be expected to become reducing due to the action of micro-organisms. Only the uppermost surface of the material may be oxidised and any additional subsurface oxidation would probably be that associated with the burrows of soil invertebrates such as nematodes and annelids. This would mean that the iron introduced from the electro-dissolution of the anodes may stay in its reduced form and thus in solution indefinitely with no precipitation at all.

One possible criticism of the experimental set-up employed could be to do with the disruption to the sediment undergone by the collection and then transferral to the experimental cell. At the start of the experiment the sediment was lightly compacted and air pockets etc. were attempted to be kept to a minimum. The material was left to stabilise for 48 hours before the experiment was started. There was evidence of worm/invertebrate activity at the end of this period.

In undisturbed, in situ sediment, there may be expected to be a more uniform structure to the sediment and the profile of the sediment with depth would be expected to be slightly different. As the experiment was started, the flow rate may have been somewhat more than would be obtained from undisturbed and deposited in-situ sediment. However, these experiments were undertaken as a proof of concept, rather than as an accurate representation of an environmental material and as such, these factors are something to be addressed more rigorously in field scale trials in undisturbed materials (perhaps with and without hydraulic gradients).

It is also worth noting that in spite of the disruption of the material and the associated air pockets and other preferential flow paths, that might be expected to have introduced, the starting flow was reduced and eventually stopped on application of the electric current. The iron mineral precipitated remained intact after the current was removed so the experiment also suggests that the technique is promising for more than just the most homogenous of materials.

The experimental apparatus was acknowledged to have limitations introduced by the action of removing and transporting the material to the laboratory and the creation of the voids etc. However there is implicit heterogeneity in a natural soil.

“In practice, field soils are rarely structurally homogeneous due to the presence of old root channels, worm holes, and gaps between aggregates, so the downward movement of water is more erratic... Although the change in water content at the wetting front is sharp in this soil there is also evidence of water at some points moving ahead of the main transmission zone.” (White, 2006)

4.7 Conclusions

The experiments presented here have shown that the FIRS technique can be used for a number of applications which have not been previously demonstrated.

For the first time it has been demonstrated that it is possible to generate an iron-rich impermeable barrier against a hydraulic head and that the barrier remains impermeable after the current has been stopped.

The method is most successful for employment in fine grained and clay rich soils where the electroosmotic effect is dominant to gravitational flow. The electromigration and subsequent precipitation of iron proved to be able to work as a robust barrier to groundwater for the duration of the experiment and for four weeks afterwards. It can be noted that in the last experiment conducted; the estuarine sediment experiment was left undisturbed once the current was switched off. Six weeks later there was still no out-flow from the test cell proving suggesting that this may be a robust barrier to

groundwater flow for a significant period after the application of the electric current has ceased.

Further work might be directed towards the measurement of the working life of these barriers under a variety of different conditions.

There was evidence of the presence of invertebrate life (burrow casts etc.) in the test sample towards the beginning of the experiment but the conditions become rather extreme around the electrodes and they did not show evidence of their presence for the second half of the experiment. In a field scale experiment sufficiently mobile creatures would be able to relocate themselves away from the test zone as conditions became less favourable, but importantly, would be able to re-colonise the area once the current is disconnected. The activities of burrowing organisms or plant roots may damage the integrity of the cemented region making the lifespan of the barrier shorter lived than might be found in the lab. Equally the barrier may in fact prove resilient to such activity and remain intact. Further work including either field emplaced tests or large scale experiments in the lab would be required to assess these effects. Plant root systems may also present similar problems in terms of the lasting effectiveness of the barrier.

In addition to the effects of organisms on the macro scale, micro-organisms may also be an important consideration for the formation and longevity of the barrier. In deeper surface-sediments, significantly reducing conditions are often encountered due to the anoxic conditions and breakdown products of micro-organisms metabolising organic materials. As mentioned previously, this may prevent the oxidation of the iron from the anodes necessary to form the barriers from taking place. Contrary to this is the fact that free oxygen gas is generated at the anode, and if significant iron; or other metal species are present in solution, this oxygen enrichment is likely to cause them to drop out of solution in the vicinity of the anode. Again though, this raises questions in terms of the likely longevity of a barrier in these conditions.

It can however be born in mind that it has been shown possible to re-seal a damaged iron barrier ('Resealing the Iron-rich Barrier', Section 3.5.2) and that there may be information about the integrity of the barrier obtained by measuring the resistance

across a barrier in-situ. This allows for the possibility of a control mechanism which will apply the electric current when a drop in resistance (increase in electric current) across the barrier might indicate a loss of integrity. This would require some further investigation as a high resistance could indicate an intact barrier or equally, significant drying of the medium, or a change in the ionic strength of the electrolyte.

5 The FIRS Process for Metals Mobilisation

This section describes the FIRS process in more detail and its performance in terms of the remediation of metal contaminants via the mobilisation and localised concentration of metals. The precipitation of iron mineral fabrics has been discussed in, Section 3, in terms of augmentation of the strength properties of unconsolidated materials and for the localised reduction in hydraulic conductivity in a contaminated land management scenario. The FIRS technique has also been put forward for application to the more mainstream approach to contaminant management using electrokinetics as a method for causing the movement, concentration and subsequent removal of contaminants from the soil (Hopkinson and Cundy, 2003; Cundy and Hopkinson, 2004; Cundy and Hopkinson, 2005; Faulkner *et al.*, 2005; Hopkinson *et al.*, 2009).

The generalised concept consists of the cationic metal/metalloid species mobilised by the acidic anolyte, which migrate towards the cathode and the associated alkaline catholyte. At the 'pH junction', to use the phrase favoured by Kimura *et al.* (Kimura *et al.*, 2007a; Kimura *et al.*, 2007b), where the conditions rapidly change from acidic to alkaline, the iron mineral-fabric formation occurs. Other species present are also expected to precipitate out at this point, as previously discussed. The trace metals naturally associated with the co-precipitation of iron oxides in the environment are mainly, V, Mn, Ni, Cu, Zn, Mo (e.g. Alloway and Ayres, 1997; Cornell and Schwertmann, 2003). But in alkaline conditions metals in general (with some important exceptions) become immobile.

The remediation model is therefore as follows: the problem metals are removed from the anode region (and some specific species from the cathode region e.g. Cr and As) and concentrated at the iron mineralised point and the iron precipitate cements and stabilises the region, as well as identifying the area of precipitation for excavation by the visible presence of the iron mineralisation. The precipitation takes place due to the change in conditions and by co-precipitation with the iron phases. From a contaminated land perspective this would be intended to reduce the concentration of contaminants present to below a threshold value and fix them in a narrow and localised region of the soil. This small-volume region can then be excavated and disposed of or subjected to a secondary form of processing.

There may also be sufficient concentration of the contaminant to make the concentrated region an economical prospect for the subsequent recovery of the contaminant species; which may have an economic value depending on the metal, volumes and concentrations involved, along with the market value of the species in question.

Cundy and Hopkinson (2005) discuss this possibility. The success of this approach depends on the migration of the required species in a high proportion and into a narrow localised region, along with a significant overall reduction in concentration of contaminants in the treated area.

This chapter is concerned with the use of the FIRS technique to cause the movement and precipitation of metals along with the introduced iron and describes experiments conducted on estuarine sediment from close to a large oil refinery complex which has been found to contain elevated concentrations of a number of metals including copper and arsenic (Cundy and Croudace, 1995b). An experiment was carried out to evaluate the addition of acetic acid have on the remediation efficiency. The response of a selection of metal elements to the procedure was quantified by XRF analysis. The results of this appear in Section 5.4

5.1 Overview

The concept of using the electrodisolution of iron anodes to enhance metals remediation has been reported in the literature, but in the context of a system designed to remove contaminants at the electrode. The fixing in situ of contaminants has been considered undesirable or a failure in the literature.

“Although these tests showed that a metal pollutant can be concentrated at some intermediate region between the electrodes and so can subsequently be removed by excavation of a relatively small amount of soil, true in situ removal to the electrodes is the desired objective.”

(Probstein and Hicks, 1993)

“...the immobilization of contaminants in a narrow band in the soil, analogous to isoelectric focusing, was reproduced experimentally and simulated with a

mathematical model. It was shown that the focusing effect can be eliminated by controlling the pH at the cathode using a water rinse.”

(Hicks and Tondorf 1994)

There are other examples of research conducted with sacrificial iron electrodes and subsequent precipitation, for instance research conducted for the development of the Lasagna™ technology has utilised investigative experiments with iron anodes and precipitated iron hydroxide (Shapiro, 1996), the use of iron electrodes in this case is evaluated as an alternative to inert electrodes. The use of iron anodes in an agar medium compares empirical and theoretical results; with good agreement (Shapiro, 1996). Another interesting finding of these models and experiments was the discovery that the model predicted a 2mm pH spike of ~ pH 10 moving just ahead of the progressing acid front. This is postulated to be due to the formation of ferrous hydroxide at the boundary between the anolyte and the surrounding medium which continues to advance as the acid front propagates across the medium until it encounters the catholyte.

More recently, Kimura *et al.* (2007a) have conducted research which builds on the work conducted at MIT (e.g. Probstein and Hicks, 1993) where the focusing of contaminants at the point of rapid pH change as a remediation method with the addition of ethylenediaminetetraacetic acid (EDTA) to create an accumulation of the metal-EDTA complex. This is similar in its objectives to the research presented here whereby the contaminants are concentrated into a relatively narrow portion of the sub-soil and of conditioning agents to help to facilitate the movement of certain metals. The key difference is that the EDTA accumulates in a localised region due its ability to form either a positively or negatively charged species depending on the conditions rather than precipitating out of solution.

Eh/pH dependent speciation is the primary influence on the solubility and thus the mobility of most heavy metals found in soils (e.g. Alloway and Ayres, 1997). Speciation of some contaminants determines the toxicity and also the mobility of the contaminant. It is a property of iron, and other metal oxides, that they are very important in the adsorption of species to soil components. Iron oxides as well as manganese oxides have been used as soil additives to promote microbially generated

humic substances, and can also reduce the mobility and uptake of contaminants by plant species (e.g. Warren *et al.*, 2003; Kumpiene *et al.*, 2006; Mench *et al.*, 2006).

The remit of this research was to investigate the results of using the experimental set-up as outlined in Cundy and Hopkinson (2004).

5.1.1 Soils and Sediments: Composition and Physicochemical Concepts

Some of the theoretical physicochemical factors requiring consideration have been described in Section 2.3. In a real world environmental contamination situation, aspects beyond the physics of soil/contaminant interactions must be considered.

Materials that might be termed soils, whilst exhibiting some variety, generally share a number of similar properties in terms of profile, structure and basic composition. The distinction between what constitutes a soil rather than sediment is a somewhat arbitrary distinction due to the fact that in many cases the composition; such as organic matter, material derived from rock weathering and clays etc. may be very similar. From an environmental science point of view, sediment might be considered an accumulation of transported material, as opposed to a soil which develops in situ. A geologist might be more likely to use the term sediment to describe a peat (evolved in situ) since it is a precursor to the formation of a sedimentary rock: coal (Jones, 2000). The two terms, for the purpose of this thesis, may generally be used without leading to confusion.

There are additional complications aside from terminology which are caused by the nature and behaviour of different contaminants in a soil, due to the various means by which contaminants might be introduced to a soil environment. A pollutant may be introduced into a soil in a single event; such as a chemical spill, or by dumping of a waste material. Alternatively, it may be the case that a contaminant accumulates over many years, perhaps from a source some distance away, or by a progressive input at a limited rate; as may be found with a slowly leaking storage tank, or from the accumulation and concentration of a dilute or dispersed contaminant into a particular

‘sink’ e.g. Sellafield nuclear site, UK, radionuclide accumulations on surficial sediments (Charlesworth *et al.*, 2006).

This is where soil pollution is different from most other environmental pollution, in that generally sources of pollution are rapidly diluted in the environment; for instance by mixing in moving air or water. Soils, conversely, have the tendency to act as a ‘sink’, and accumulate and concentrate pollutants. The adsorptive properties of soil components mean that both inorganic and organic contaminants can be bound to the surfaces of soil particles due to the presence of humic substances, clays and sheet silicates, metal oxides etc.(Murphy *et al.*, 1990), some of these have already been outlined in Table 10 page 59. Amorphous iron oxides, oxides of aluminium, and other metal oxides and oxyhydroxides are also significant and are considered to be one of the dominant factors in retaining heavy metals by surface adsorption (Potter and Yong, 1997).

Rather than a mature soil in the formal sense of the word (with distinct horizons etc.), in many contaminated land scenarios, particularly heavy metal contamination from mining operations, what might be termed ‘soils’ turns out to be an umbrella term used to refer to any material found underfoot. This will often be an anthropogenic mixture, which may be an industrial or mining waste, or something which is commonly described using the blanket term: made-ground. This describes in-fill of material from outside the site, or from another part of the site. Typically this could include rubble, gravel, sand or any manner of waste materials. These waste materials can often prove to be sources of environmental contamination.

5.1.2 Remediation Experiments

Remediation experiments were conducted on a naturally occurring sediment. This was done to indicate the usefulness of the electrokinetic technique in terms of real-world situations and contamination scenarios as opposed to the use of pure samples artificially spiked with a particular contaminant (e.g. Acar and Alshawabkeh, 1996; Puppala *et al.*, 1997; Wong *et al.*, 1997; Reddy and Chinthamreddy, 1999; Reddy *et al.*, 2003; Reddy and Chinthamreddy, 2003; Vereda-Alonso *et al.*, 2004; Luo *et al.*, 2005; Reddy and

Ala, 2005). This provides a more robust approach in terms of tackling real environmental problems and with up-scaling of the process in terms of measuring the effectiveness of the procedure despite heterogeneity of materials, varying soil composition and a variety of contaminants.

5.2 Estuarine Sediment Experiments

The sediment samples were collected from Southampton Water near to the town of Hythe (map reference 50.51°56'N, 01.23°51'W). The sediment was collected from an area of salt marsh near to a large oil refinery complex at Fawley on the western side of Southampton Water. The samples were taken from the intertidal mud flats next to an area of salt marsh, Figure 47. Southampton Water is an area that has been consistently used by heavy tonnage shipping as well as being popular with pleasure craft and is the main access route to Cowes. The nearby petrochemicals refinery complex began operations in 1921 and was significantly expanded in the 1950s and is currently the largest in the UK (Cundy and Croudace, 1995a; Cundy and Croudace, 1995b).

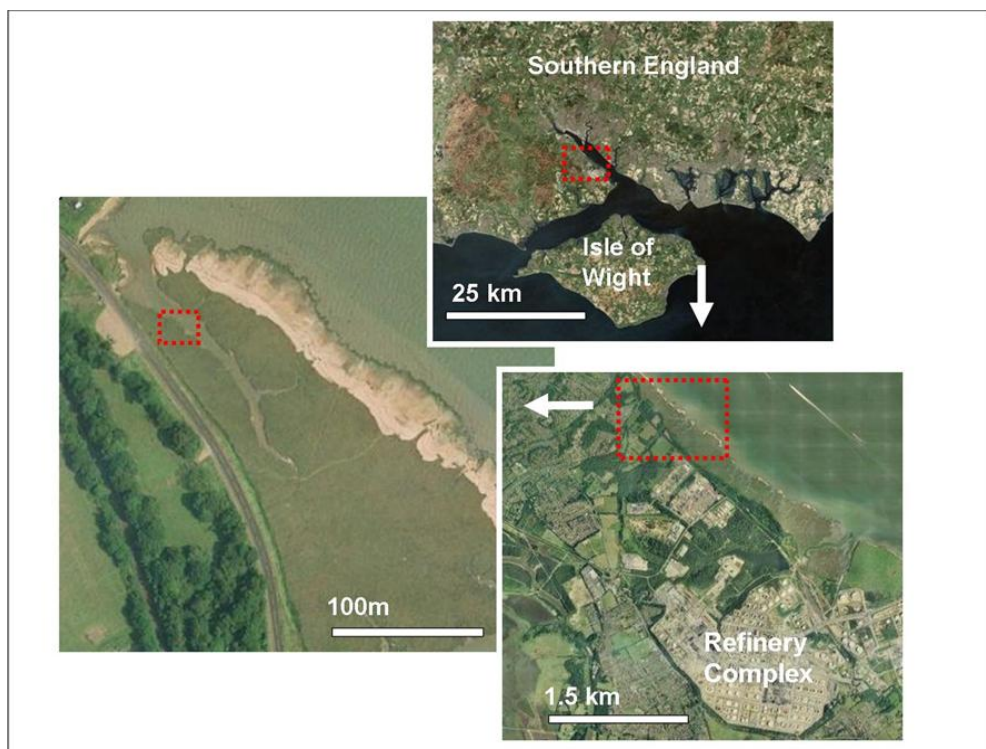


Figure 47: The location of the sample site from where the estuarine sediment was obtained. The sample site itself consisted of mud flats close to salt marsh (Aerial imagery from Google Earth™ and Microsoft™ Virtual Earth™ accessed June 2006).

Many possible contaminants are likely to have come from the refinery complex during its history of operation. This would consist of hydrocarbons but also the possibility of an assortment of heavy metals/metalloids including lead, cadmium and mercury (e.g. Hester and Harrison, 2001; Nadal *et al.*, 2004). The refinery complex is also thought to be responsible for releasing copper containing compounds into Southampton Water (e.g. Cundy and Croudace, 1995a; Cundy and Croudace, 1995b) although this release has been limited since the 1970s.

Salt marshes in inter-tidal environments are important sinks for heavy metals, metals and nutrients in the environment (Cundy and Croudace, 1995b; Cundy and Croudace, 1995a; Kershaw and Cundy, 2000; Cundy *et al.*, 2003; Cundy *et al.*, 2005). Metals present in rivers tend to be transferred from solution to sediment by adsorption on to suspended particulate matter which flocculates when it encounters the brackish conditions of the estuary. There is a relatively short time lag between the solution phase being transferred to the deposited phase and thus surface sediments may represent a good indicator of water quality (e.g. Spencer *et al.*, 2003).

5.3 Method

Intertidal sediment was removed from the sediment's surface to a depth of 30cm. It consisted of greyish brown very fine grained sediment at the surface layer with some organic material present including root material etc. This is indicative of a diagenic sediment containing sulphide minerals with permanently reduced sediment with significant sulphate reduction (Buckley *et al.*, 1995).

The removed sediment was transferred to black plastic sacks for transportation back to the laboratory in batches of approximately 25kg, with a total of ~100 kg removed. This was immediately transferred to the treatment apparatus.

Due to the nature of the transport and transfer to the experimental cell there was significant disruption to the sediment and the experiment could not be considered to have been conducted on a sediment as it exists *in situ*, there was some mechanical mixing of the material to reduce the amount of void space and air bubbles in the test

material. This resulted in the material being fairly well homogenised by the physical mixing of the material as a result of the sampling, transfer to the treatment vessel and the compaction/set-up of the experiment.

There was continued evidence of organisms active in the test medium so at least in this respect, that aspect of the in-situ conditions are maintained. This also raises new problems since the organisms in the test soil are effectively held captive and might re-locate if they were able- as they might be in a real-world scenario. The activity of burrowing by soil organisms is also an important aspect in the near-surface, since their burrows alter the near-surface chemistry of the sediment as the burrows are a means of introducing atmospheric oxygen to the material. This is evident by the coloration of the sediment around these burrows often taking on a reddish brown colour due to the presence of oxidised iron (Cornell and Schwertmann, 2003).

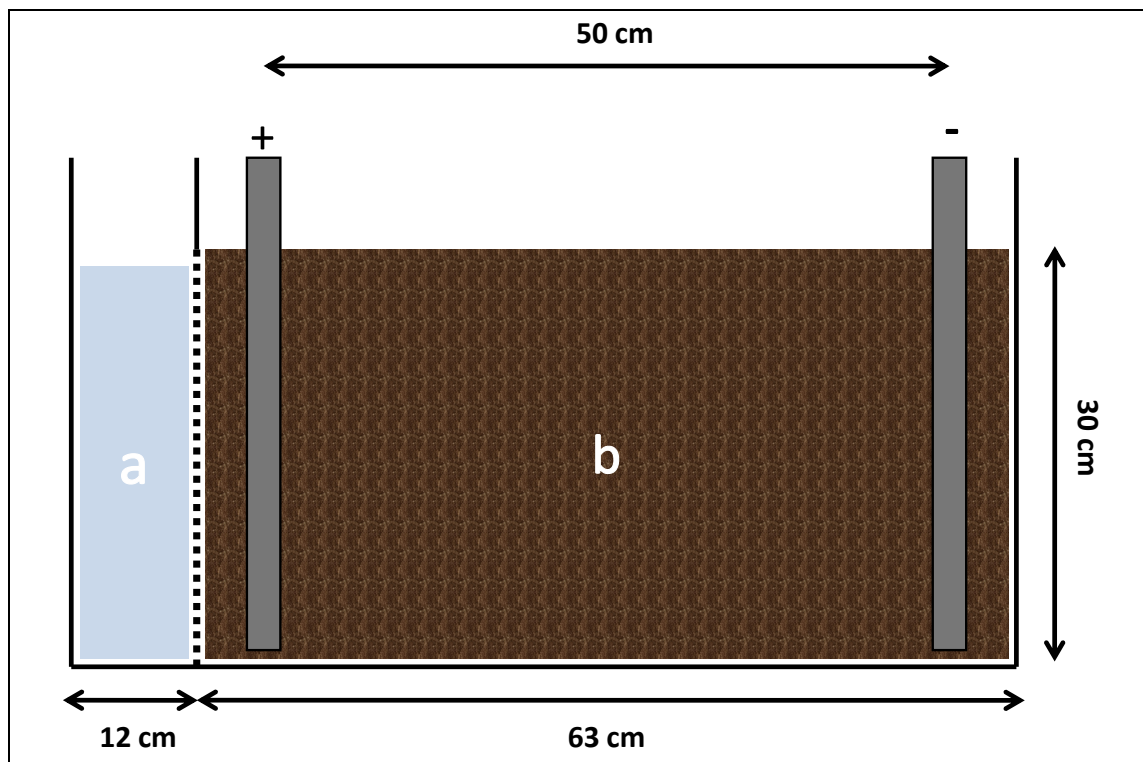


Figure 48: The experimental set up for the estuarine sediment experiments. The reservoir area is labelled 'a' the dashed line represents the mesh partition and the region labelled b is the sediment section.

The estuarine sediment experiments were set up in a similar fashion to the other remediation experiments, Figure 48, with an electrode separation of 50 cm between parallel linear electrode arrays consisting of five equally spaced electrodes. The only

modification was the inclusion of a mesh partition at the anode side designed to allow for better penetration of the influent into the test medium to counteract the rapid drying that takes place at the anode due to electroosmosis and to a lesser extent the dissociation of water (Hester and Harrison, 1997).

This was thought necessary due to the low permeability of the estuarine material which would make it more difficult to keep the material saturated by surface addition of the influent due to the large volume of material being tested. The mesh partition was inserted between the anode side of the tank wall and the test medium. This created space between the tank wall and the test medium to allow the penetration of the influent along the entire depth of the test volume. Two identical test tanks were set up, Tank A was run with tap-water as the influent solution and Tank B was run with a 2 molar acetic acid solution as the influent.

The inclusion of what is essentially an imposed hydraulic gradient through the sample due to the column of influent at the anode side might exert an additional influence on the movement of adsorbed species. For this reason the treated material was divided not just into samples according to distance from one or other of the electrode arrays, as was carried out in other experiments; but also into vertical sections to look into distribution of elements as a function of depth. The starting conditions for the experiments are given in Table 18.

Table 18: Estuarine sediment starting conditions in the two experiments.

Electrolyte added	Acetic acid 2M	Tap water
Electrode separation	50 cm	50 cm
Number of electrodes	5	5
Applied Voltage	10 V	10 V
Anode electrode material	Cast iron	Cast iron
Starting current	2.0 Amps	2.1Amps
Starting pH	7.5	7.5

After the experiment had run, i.e. the current had dropped to a negligible level; the sediment material was sampled using a stainless steel trowel. The soil mass was divided into 2 cm sections longitudinally and into three equal sections ‘top middle and

bottom' vertically. The samples consisting of approximately 200g were collected into paper bags for drying. They were dried in an oven at 60 °C for 48 hours. The entire sample was then transferred to the planetary mono-mill for grinding/homogenisation. The grinding was carried out until the entire sample was a fine powder and of uniform consistency. From this, approximately 10 g was removed and mixed thoroughly with 10 drops of 0.8 g l⁻¹ poly vinyl alcohol solution to act as a binder. The mixture was then transferred to a press assembly where it was subjected to 200 kN of pressure to form a consolidated 'tablet' ready to be loaded into the sample carousel of the XRF machine.

The Phillips PANalytical minipal 2 energy dispersive X-ray Fluorescence Spectrometer with 30 Rh tube (Appendix 1, for full specification details) was employed using a program set up to analyse a wide variety of elements using analysis settings suitable for use with a range of different soils, sediments and rocks. The XRF machine will give concentration data for the following elements: Mo, Zr, Y, Sr, Rb, Ga, Br, Se, Zn, Cu, Ni, Co, Fe₂O₃, MnO, Cr, V, TiO₂, CaO, K₂O, U, Th, Bi, Pb, Ba, W, Nb, As, Ce, La, Sn with the majors expressed as their oxides according to XRF convention . However, for a number of these elements there were no suitable standards available for soil/sediment analysis. So although included as part of the compositional readout, the data for these elements are included only for completeness. This is discussed further in section 5.3.3.

The machine has the capacity to analyse sequentially up to twelve prepared samples. The samples taken from the experiment were analysed in batches of eleven, the remaining space was filled in each analytical run by a certified reference material (CRM) or other standard reference material. The certified reference material was NIST 2710 Montana Soil with elevated metal content (see Appendix 1 for full compositional details). This was included in each batch to identify any analytical 'drift' as part of the analysis.

The samples were analysed in a pseudo-random fashion to reduce the influence of analytical 'drift' influencing any trends and suitable sample duplicates and analytical duplicates were taken to allow the level of uncertainty in both the sampling and analysis to be quantified (see Appendix 2). The elements selected for analysis were those tested for as part of the installed analysis program for trace elements. This program has been

set up and calibrated using a range of standards and reference materials and has been proven to yield reliable results for the elements selected in soils sediments and rocks (e.g. Cundy *et al.*, 2005).

The results of the error and uncertainty analysis indicate that for a number of the elements examined; the level of uncertainty was so large that the data obtained for them was unsuitable to draw any meaningful conclusions from. So this data was included only for completeness, (see Appendix 2).

By using a balanced experimental design (Ramsey *et al.*, 1995; Ramsey and Argyraki, 1997; Ramsey, 1998, 2004) the random uncertainty due to sampling and analysis was also addressed. The bias was calculated for the elements of interest which allows for the systematic error to be quantified and the data adjusted as demanded. There is no satisfactory method for the estimation of a bias incorporated into the sampling procedure designed for use in this situation. The random uncertainty estimate is indicated only on the mean measurement plots as error bars on all the data points reduces the clarity of the graphs. The uncertainty is indicative, since the actual concentrations present are less significant (for the purposes of this thesis) than the relative distribution of the elements across the treatment zone. Considering the relatively small scale of the experiments and correspondingly small distances involved in the sampling of the experimental material, the random component of the uncertainty was significantly higher than might have been expected. This issue is addressed in the discussion and conclusions, Section 5.8.

The experiment was conducted to look at the effect of increasing the acidification of the anode compartment so that the maximum acid purge can be facilitated and any buffering effects of the soil can be minimised. The alkali front was allowed to propagate unimpeded, The experimental set up was exactly the same in the control experiment with tap water used instead of the acetic acid.

5.3.1 pH Measurements

The pH measured across the material is very similar to other experiments conducted with the relatively rapid generation of both an acid and an alkali zone which, by the end of the experiment, show a steep region of pH change. The limitations of obtaining this data are due to the fact that, in order to avoid invasively disturbing the test medium, pH measurements were taken only at the surface. It would be possible, with sufficient resources to install pH meters across the length of a mass of sediment at a range of depths. The output from these meters could then be fed into a data logging system to give a continuous record of the pH developed within the material. Other researchers have incorporated pH indicator dyes into their experiments to give a visual display of the pH conditions in the material as the treatment progresses, (Probstein and Hicks, 1993), but in a dark coloured sediment this would be less clear.

In these experiments the introduction of significant pH indicator could influence the results and so duplicate experiments would need to be conducted with and without the pH indicator present to ascertain whether there is any significant difference in the behaviour and mobility of the metals. The reality is that there has been such a volume of work conducted containing measures of the development of the pH fronts which are mutually confirmatory that the development of these fronts is not expected to deliver any surprises. This aspect would not be a major consideration for most materials and only highly buffering soils are likely to be problematic.

5.3.2 Sampling

The sampling strategy, which consisted of the sectioning of a region across the entire cell and then homogenising it before then carrying out the analysis was selected at a resolution of 2cm to provide adequate information on the extent of migration of metals present. In these experiments, the required sample had to be of a significant size since the required volume of sample to form a pellet of suitable size and robustness to load into the spectrometer is 10g, but realistically it needs to be larger than this to allow for the sample lost as residue during the sample preparation; which includes transferring the sample to a vessel for drying, and then the sample is prepared further by grinding and

then mixing with a binder and is finally transferred to the pellet press assembly before loading into the XRF spectroscope (full details of sample preparation in Appendix 1).

It is good practise that more sample material should be taken than is required for a single sample pellet, as sometimes the pellet loses its integrity after the pressing stage and may crumble or break and have to be discarded. So as a contingency the preparation in terms of drying, grinding and the addition of the binder is done on a sample of sufficient size to allow for the preparation of a number of pellets. The number of replicates and duplicates taken was decided according to the balanced experimental design as described.

5.3.3 XRF Analysis

XRF analysis was utilised as a reliable and cost effective method for metals analysis of the treated materials. Since XRF analysis looks at the total content of the sample being analysed, without taking into account the speciation or molecular aspects, it supplies a good description of the migration of metals in a test sample. See Figure 49 for an example spectral output. The experiments were conducted to ascertain whether there has been an appreciable migration of adsorbed heavy metals from one region towards another. This approach was adopted as the objective was to demonstrate a net movement of metals many of which might be classed as contaminants.

Some elements which may have been of environmental significance include Pb, Cd and Hg, were analysed as part of the XRF analysis program but did not give useable data. This was suspected to be due to interference effects as a result of the cocktail of elements which were present, as well as the elevated concentrations of iron in the system.

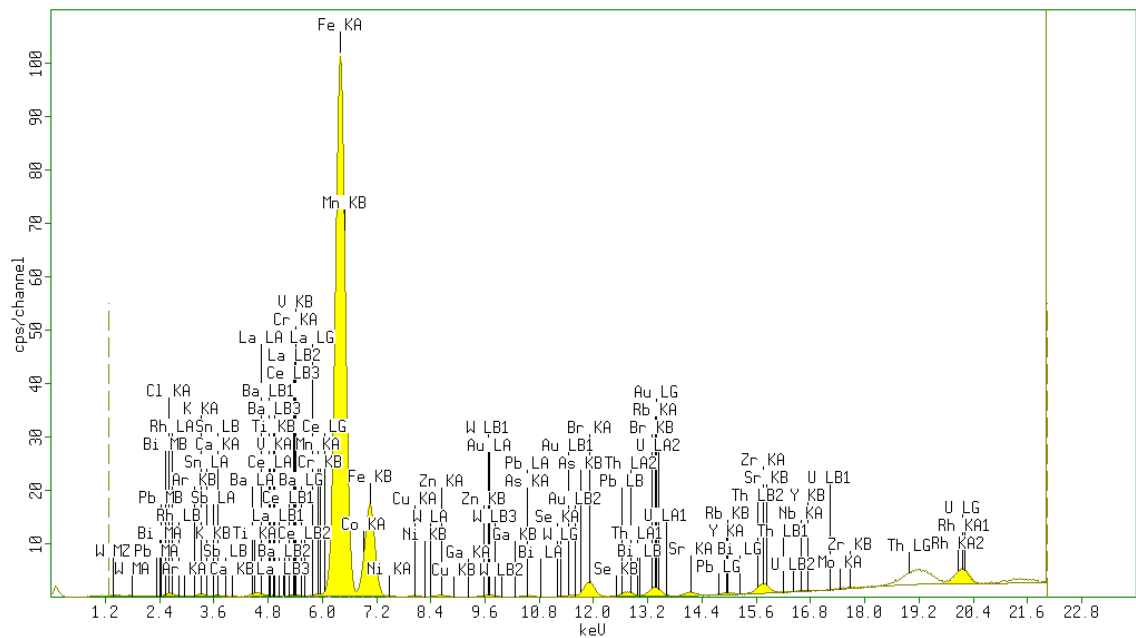


Figure 49: Example spectrum output for estuarine sediment analysis using minipal analysis software.

5.3.4 XRD Analysis

XRD analysis was carried out on the estuarine sediment using PANalytical X’pert Pro x ray diffractometer to establish the mineralogy of the Hythe material. The samples were dried and then ~5 g of this was ground using an agate pestle and mortar to a fine powder of uniform consistency. This was then transferred to a sample holder and lightly compressed. The sample holding assembly was then loaded into the spectroscope.

5.3.5 Uncertainty and Error

The uncertainty associated with a particular sampling and analysis method must also be quantified in order to ascertain the level of uncertainty associated with a particular measurement, which may have serious consequences for the classification of land as ‘contaminated’ or ‘not contaminated’ in terms of threshold values (e.g. Ramsey and Argyraki, 1997).

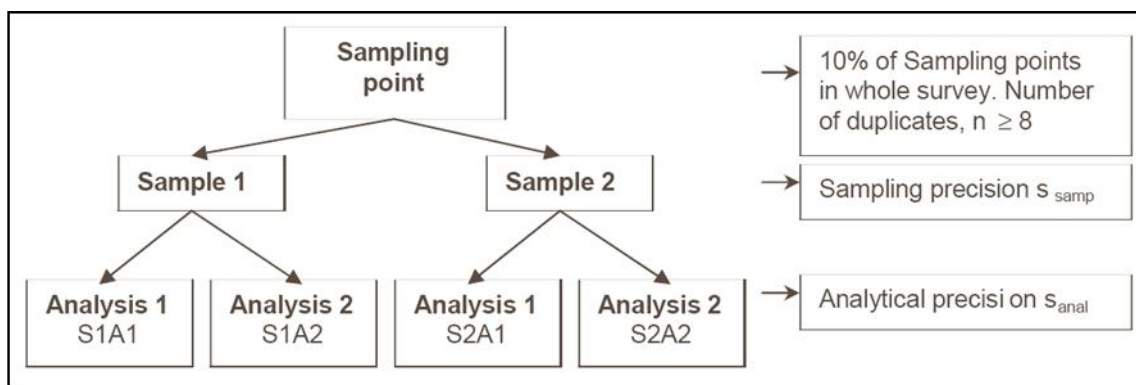


Figure 50: Schematic of the balanced experimental design for the calculation of an estimate of the uncertainty for the sampling and analysis; the random error (Taken from, Ramsey, 2004).

For this purpose and to indicate the reliability of the analysis, sampling and random error of the techniques employed, and a balanced experiment design was utilised, see Figure 50, above. This technique, coupled with a robust statistical analysis and use of traceable certified reference materials allows for the quantification of the level of uncertainty of the data obtained for different elements, and to establish the proportion of uncertainty associated with the analysis, the sampling and the systematic error the techniques employ. The sample resolution (2cm increments, at three depths) was selected to show a high level of resolution in the data with feasible sample numbers and preparation requirements.

The systematic error, or '*bias*', was established through the analysis of certified reference materials (IAEA, 2004; Ramsey, 2004) displayed as the output from the regression analysis of the measured values and the certified values. The experiments were conducted and the data processed in such a way that reasonable estimates could be made regarding the magnitude and influence of the uncertainty that is inherent in any measured quantity. The use of certified reference materials (CRMs) GSS-3, GSS-6, GSS-4, GSS-8, NIST 2710, reagent blanks and balanced experimental design were used to make appropriate estimates of the systematic and random errors that the experimental sampling and analysis introduces to the measurements made and the quality of data obtained. Using regression analysis of the data from the numerous standards that were used, the systematic error was quantified, Figure 51. The regression analyses for the other elements are given in Appendix 2.

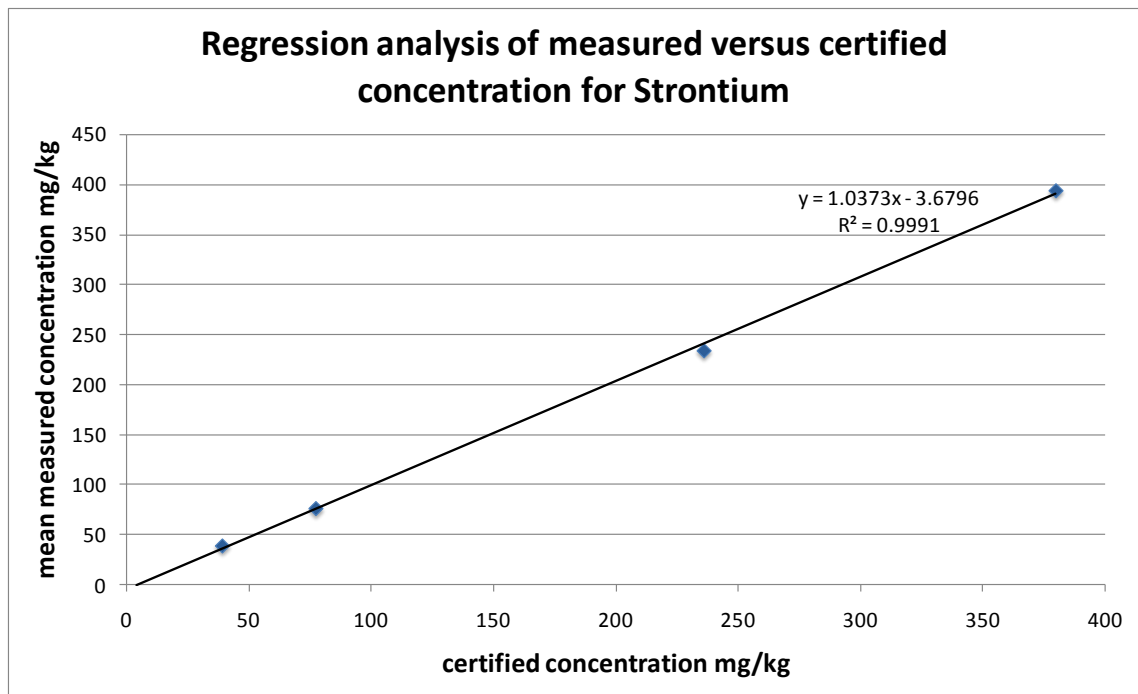


Figure 51: Example regression analysis of measured against certified concentration for four different reference materials for the element Strontium. In this case the reference materials were GSS-3, GSS-4, GSS-6, and GSS-8. This is used to quantify the systematic error (bias) in the analysis.

The balanced experimental design was applied to the tap water experiment only, and the uncertainty and bias taken to be indicative for all the experiments conducted in this material (tap-water, acetic acid and the hydraulic head experiments). Since the material and the procedures for sampling, sample preparation, and analysis were identical, this was deemed to be an acceptable compromise. The data indicates that for a number of the elements analysed as part of the ‘trace elements’ program on the XRF spectrometer the data is not reliable enough for meaningful interpretation and for some elements there was no significant relationship between the certified values for the CRMs and the measured values (at 95% confidence). The data for these elements appears in the appendices for completeness and are not included in the analysis section of this thesis.

The bias calculations give either a positive or negative value. A negative value indicates that the measured values are systematically less than the certified values and a positive bias indicates that the measured values are systematically greater than the certified values. In the case of bias the uncertainty cannot be reduced by increasing the number of observations since the bias is introduced *as* part of the observation. The bias estimation associated with each element is composed of a rotational component and

linear component. The data for these were analysed for their statistical significance. The calculated p value for each set of analyses indicates whether each component is significantly different from 0 at 95% confidence interval. A perfect analysis with no bias at all would have a coefficient of precisely 1 for the rotational bias and a linear component of 0 indicating a 1:1 relationship between the measured and certified values. These calculated bias estimates were applied to the raw data to give bias corrected values in the graphical representations, where there was a calculable bias from the available CRMs

5.3.5.1 Robust ANOVA

Robust ANOVA (ANalysis Of VAriance) statistical tests were conducted on the data obtained from the acetic acid experiment from the balanced experimental design sample duplicates. Robust analysis was conducted using a custom designed program called ROBCOOP4.EXE, available via the Royal Society of Chemistry website (Royal Society of Chemistry, 2008). The method and the details of the program's operation are available in, (Analytical Methods Committee, 1989a, b). Essentially the robust ANOVA is less sensitive to outliers and non-normal distributions than the classical ANOVA. The ROBCOOP4.EXE program outputs both classical and robust ANOVA results, the output from both the classical and robust ANOVA is given for comparison.

The percentage variance associated with the sampling and the analysis as well as the geochemical variance, is calculated in the following way:

$$S^2_{\text{total}} = S^2_{\text{geochem}} + S^2_{\text{sample}} + S^2_{\text{analysis}}$$

The measurement uncertainty can be estimated from the combination of the sampling and analytical variance, giving the measurement variance as:

$$u = S_{\text{meas}} = \sqrt{(S^2_{\text{sample}} + S^2_{\text{analysis}})}$$

For an increased confidence factor this is customarily multiplied by 2 (i.e. $k=2$ below), analogous to two standard deviations for 95% confidence (95.449974 % to 6dp, to be more precise).

$$U = k \cdot u = 2 s_{\text{meas}}$$

This gives an uncertainty estimate in the same units as the measurements e.g. mg/kg etc.

Relative uncertainty (relative to the concentration) becomes:

$$U\% = 200 s_{\text{meas}} / \bar{x}$$

(After, Ramsey, 1998)

The output for each element analysed is shown along with a visual representation in the form of a pie chart to illustrate the percentage uncertainties associated with the random error component (sampling etc.) of the experiment, see Appendix 2

This method of error quantification is applied to full-size contaminated land sites and the associated sampling protocol. In spite of the experiment size being so much smaller than field-scale experiments the general rules still apply, although we may expect the uncertainty associated with the sampling to be smaller, but this is not necessarily the case. It is useful to appreciate the level of uncertainty in a data set since claims and deductions from an experiment or a field investigation can be swiftly discounted if the errors are not quantified due to excessive uncertainty related to any and possibly all of the measured values.

The bias was established using the analysis of a number of certified reference materials. The measured results compared to the certified values allow for the calculation of the bias and percentage bias through regression of the measured concentration against the certified values. The regression equation coefficients can then be statistically analysed to establish (in this case, with 95% confidence) whether the slope and intercepts are statistically different from one and zero respectively (Moore and Cobby, 1998; Ramsey, 1998; IAEA, 2004). The percentage bias can then be calculated and incorporated into

the results in the form of bias-adjusted data plots, coupled with the error bars from the uncertainty calculations to properly acknowledge the measurement uncertainty.

The systematic error associated with the sampling procedure was not quantified due to no appropriate and established method for this without involving multiple samplers and methods. This was not practicable for these experiments.

Table 19: Table of the calculation of measurement uncertainty and percentage uncertainty calculated from the balanced experimental design in mg/kg. n=10

element	units	s geochem	s samp	s analy	mean conc.	v (samp sqrd + analy sqrd)	s meas	U	U%	s.e.m. (s meas/vn) %
As	ppm	15.18	4.65	2.03	22.10	25.76	5.08	10.15	45.93	26.52
Br	ppm	31.02	8.33	1.51	73.90	71.58	8.46	16.92	22.90	13.22
Ca	ppm	1.82	0.66	0.10	2.83	0.45	0.67	1.34	47.42	27.38
Co	ppm	25.87	6.27	6.20	44.21	77.84	8.82	17.65	39.91	23.04
Cr	ppm	35.86	0.00	31.49	224.71	991.81	31.49	62.99	28.03	16.18
Cu	ppm	12.05	5.09	7.14	43.67	76.85	8.77	17.53	40.15	23.18
Fe	wt%	10.16	1.20	0.16	15.67	1.46	1.21	2.42	15.43	8.91
K	ppm	0.56	0.11	0.04	2.01	0.01	0.12	0.23	11.63	6.71
Mn	wt%	0.05	0.02	0.01	0.09	0.00	0.02	0.03	36.31	20.96
Mo	ppm	0.09	0.00	0.13	1.54	0.02	0.13	0.26	16.88	9.75
Sr	ppm	54.89	12.29	2.51	102.54	157.24	12.54	25.08	24.46	14.12
Ti	ppm	0.14	0.04	0.01	0.69	0.00	0.04	0.08	11.28	6.51
V	ppm	32.40	7.76	16.77	102.73	341.58	18.48	36.96	35.98	20.78
Zn	ppm	0.68	8.65	3.96	133.02	90.51	9.51	19.03	14.30	8.26
Zr	ppm	44.30	8.20	4.63	126.95	88.64	9.41	18.83	14.83	8.56

Table 19, shows the measurement uncertainties calculated from the robust ANOVA. Both the percentage uncertainty, U%, and the S.E.M. (standard error on the mean) are given. The U% applies to any single measurement made on a particular sample. For the purpose of clarity, these are not displayed graphically on the graphs. Instead the mean concentration of the three depths that were sampled has the uncertainty of this value displayed as error bars, which is equivalent to the S.E.M. value. The data has already had the bias correction applied to all the data points. Full uncertainty, bias and ANOVA data is given in Appendix 2.

Table 20: Calculated detection limits from replicate analyses of reagent blanks (boric acid) n=5.

mg/Kg	1	2	3	4	5	mean	stdev	3s
Compound								
Zr	30.6	28.5	26.8	28.6	30.6	29.02	1.61	4.83
Sr	-4.1	-0.8	-2.5	-1.9	-0.2	-1.9	1.52	4.57
Br	-9.1	-8.5	-7.2	-7.1	-7.1	-7.8	0.94	2.81
Zn	1.6	8	8	9.9	9.9	7.48	3.42	10.26
Cu	7.7	11.5	10.3	8.5	11.8	9.96	1.81	5.43
Co	19.6	19.9	19	21	17.9	19.48	1.14	3.43
Fe2O3	0.57	0.57	0.57	0.57	0.57	0.57	0.00	0.00
MnO	0	0	0.01	0	0.01	0.004	0.01	0.02
V	74.6	99.2	82.5	85.2	87.9	85.88	8.95	26.86
TiO2	-0.01	0.01	0	0.01	0.01	0.004	0.01	0.03
CaO	-0.14	-0.13	-0.16	-0.17	-0.16	-0.152	0.02	0.05
As	12.6	9.6	12.2	10	10.6	11	1.33	4.00

The detection limit for the XRF Spectrometer was estimated by the analysis of reagent blanks; boric acid is an X-ray absorber and was used as a blank. Multiple analyses were carried out for each element and the detection limit was calculated, Table 20.

In addition to these calculations, the manufacturer of the XRF spectrometer provides details of the calculated detection limits and analytical precision for some toxic heavy metals/metalloids, Table 21.

Table 21: Lower limit of detection values provided by the equipment manufacturer (PANalytical, 2006).

Detection limit (ppm)	Fe	Ni	Cu	Zn	As	Pb
LLD (lower limit of detection 150s count time)	15	10	8	6.5	4	6

The lower limit of detection is calculated in this instance from:

$$LLD = \frac{3}{s} \sqrt{\frac{r_b}{t_b}}$$

Where:

s=sensitivity (cps/ppm)

r_b= background concentrate (cps)

t_b= counting time background (s)

For the selected elements there is good agreement between the manufacturer's detection limits and those found experimentally, Table 20 and Table 21.

Table 22: Calculation of mean starting concentrations in the estuarine sediment n=5

	start A1	start A2	hh start	start 1	start 2			adjusted
	Conc	Conc	Conc	Conc	Conc	st. dev.	Mean	for bias
As1	24	27	24.5	24.4	26.8	1.44	25.34	39.78 ppm
Br	158.8	158.5	147.2	165	167.6	7.88	159.42	159.42 ppm
CaO	0.92	0.97	2.49	1.86	1.85	0.67	1.618	1.80 %
Co	24.8	24.4	18.1	17.7	17	3.86	20.4	20.40 ppm
Cr	148.8	169.6	318.2	233.8	242.8	66.95	222.64	222.64 ppm
Cu	47.7	50.4	66.5	67.8	74.8	11.78	61.44	61.44 ppm
Fe2O3	4.72	4.88	5.61	5.6	5.72	0.47	5.306	4.93 %
K2O	0.74	0.86	2.27	2.33	2.43	0.85	1.726	1.83 %
MnO	0.02	0.02	0.02	0.02	0.02	0.00	0.02	0.02 %
Sr	105.6	104.1	103.6	97	99.5	3.58	101.96	105.73 ppm
TiO2	0.39	0.42	0.76	0.78	0.79	0.20	0.628	0.56 %
V	14.8	9	104.7	115.9	132.2	58.75	75.32	49.79 ppm
Zn	129.4	138.6	129.8	138.8	149.1	8.09	137.14	137.19 ppm
Zr	174.3	179.1	207.5	204	190.9	14.68	191.16	152.93 ppm

The sediment was also analysed pre-treatment to establish mean starting concentrations of metals in the material, Table 22. The figures obtained were then adjusted for the analytical bias that was calculated and it is these adjusted values which appear on the graphical representations of the data as dashed lines. There is expected to be variation in concentrations in the sediment due to heterogeneity of the Hythe material (e.g. Ármannsson *et al.*, 1985). There was mixing of the material prior to setting up the experiments and generally there seems to be good agreement between grab samples for the starting material.

5.3.6 Acetic Acid versus Tap Water Influent

Acetic acid was used as a conditioning agent as it has been associated with increased mobility of a number of metal species in other studies using electrokinetics, (e.g. Acar and Alshawabkeh, 1993; Puppala *et al.*, 1997; Reddy and Chinthamreddy, 2003; Giannis and Gidaracos, 2005; Altae *et al.*, 2007).

In other experiments the use of acetic acid is applied for the suppression of the alkali zone developed from the cathode zone. Since this process is concerned with the precipitation of the species of interest the acetic acid in this case was applied behind the anode zone in the partitioned space created using the nylon mesh. The purpose of this was to maximise the acidification of the anode zone and to utilise the electroosmotic flow from anode to cathode while preventing the anode zone from drying out. This was

done to amplify the acid purge while still achieving the precipitation and mineralisation at the point of pH jump to look at the co-precipitation characteristics. The experimental set-up is described in Table 18. The experiments conducted were of a scale that is unusual for lab based experiments which are generally on a scale an order of magnitude smaller than those described here. This builds on the experiments conducted by Cundy and Hopkinson and Hopkinson and Cundy (2003; 2005) which were significantly smaller experiments with correspondingly reduced sampling resolution. The greater size allows for more extensive sampling of the material since the volume of material is sufficient for suitably sized samples to be taken from different depths.

5.4 Results

This section begins with the results of the characterisation analysis of the starting material followed by the results of the electric current measurements. The iron mineralised region is analysed and then the other metals analysis post treatment follows.

5.4.1 Physical and Mineralogical Characteristics of Starting Material.

The material was fine grained and organic-rich (see Figure 53 for the particle size analysis results), Table 23 shows the loss on ignition analysis of the samples giving a mean organic content of 12.4% by mass.

This was discerned by mass loss from a set of samples air-dried for 72 hours at 40° Celsius (until no further drop in mass was obtained) followed by 2 hours at 220° Celsius to remove bound water, then ashed at 450° in a muffle-furnace to combust the soil organic matter.

Table 23: LOI calculation for estuarine sediment calculated from five random samples labelled A,B,C,D and E.

sample	vessel mass	dry sample and jar	Sample Mass	post furnace jar and sample	Loss on ignition	% loss
A	148.39	160.73	12.34	159.41	1.32	10.69
B	149.63	161.29	11.66	159.91	1.38	11.83
C	151.06	163.72	12.66	162.21	1.51	11.92
D	148.62	158.90	10.28	157.15	1.75	17.02
E	150.07	158.71	8.64	157.82	0.89	10.30
Mean (2dp)						12.36

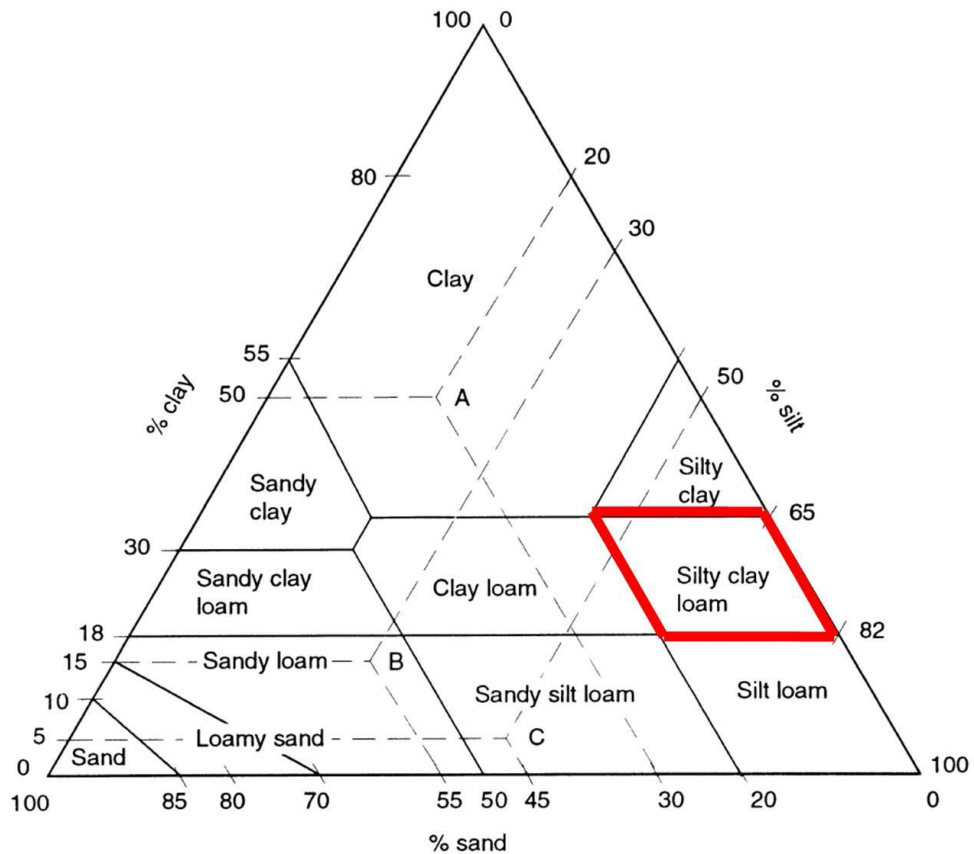


Figure 52: Textural classification (limiting percentage of sand silt and clay sized particles for the mineral texture class. The Hythe sediment was identified as ‘Silty clay loam’ as highlighted (Diagram adapted from, British Standards Institution, 1994)

The textural classification of the sample was identified as ‘silty clay loam’, see Figure 52, this is typical for an estuarine environment such as this (Cundy and Croudace, 1995b). The material was also subjected to laser particle size analysis, Figure 53.

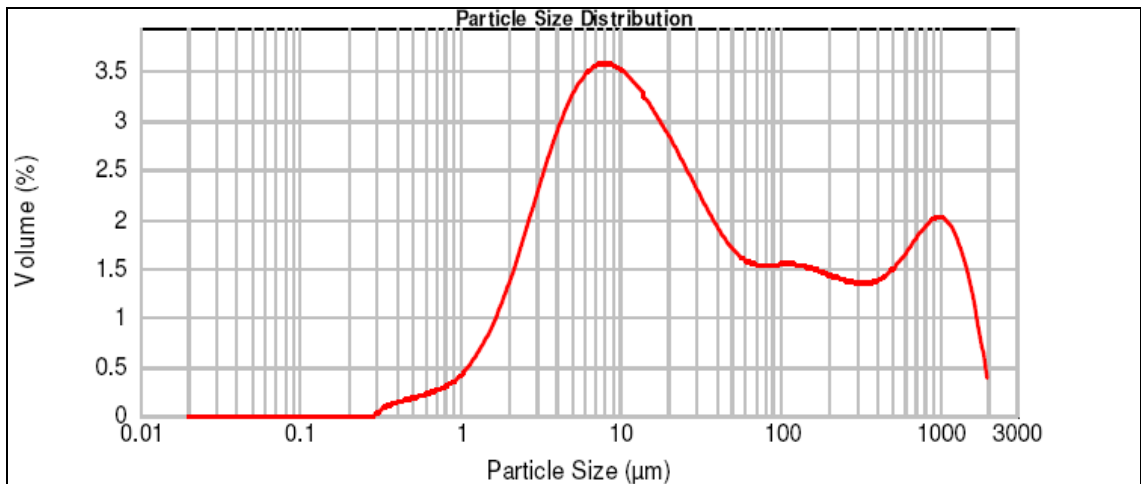


Figure 53: Particle size distribution for Hythe sediment sample as determined by laser particle size analysis.

The sediment was also analysed for its mineral components using a semi-quantitative XRD analysis, details in Appendix 2. This indicated that the sediment was primarily quartz (~65 %) with the clay component made up of Kaolinite and Muscovite (~21 %). The remainder was identified as gypsum (4 %), iron pyrite (3 %), calcite (3 %), and halite (3%), Figure 54. The halite and gypsum are assumed to be artefacts of the saline conditions and a result of the drying process since these readily soluble minerals would not be expected in an intertidal zone.

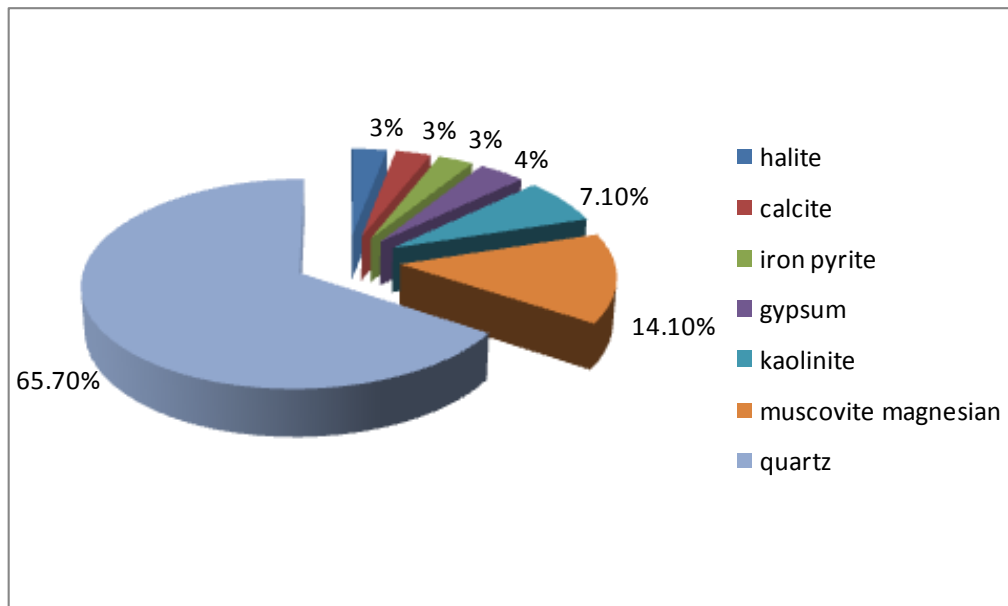


Figure 54: Data output from XRD analysis of the mineral composition of estuarine sediment.

The minerals of primary interest are the calcite due to its importance as a pH buffer, acting to neutralise the evolution of the acid front, and maintain the high pH in the cathode zone, and the sheet silicate minerals, muscovite and kaolinite since they constitute the fraction of the sediment that is involved in the adsorption of charged species and the electrokinetic phenomena previously described.

5.4.2 Electrical Current Measurements.

The current displays the familiar decay observed in previous experiments with an initial rise in current flow associated with the drop in resistance across the treatment cell as the generation of ions (protons and hydroxide ions) facilitates better current flow. Following this, there begins a steady drop in current due to the movement of ions, and the impedance of the precipitated zone, Figure 55.

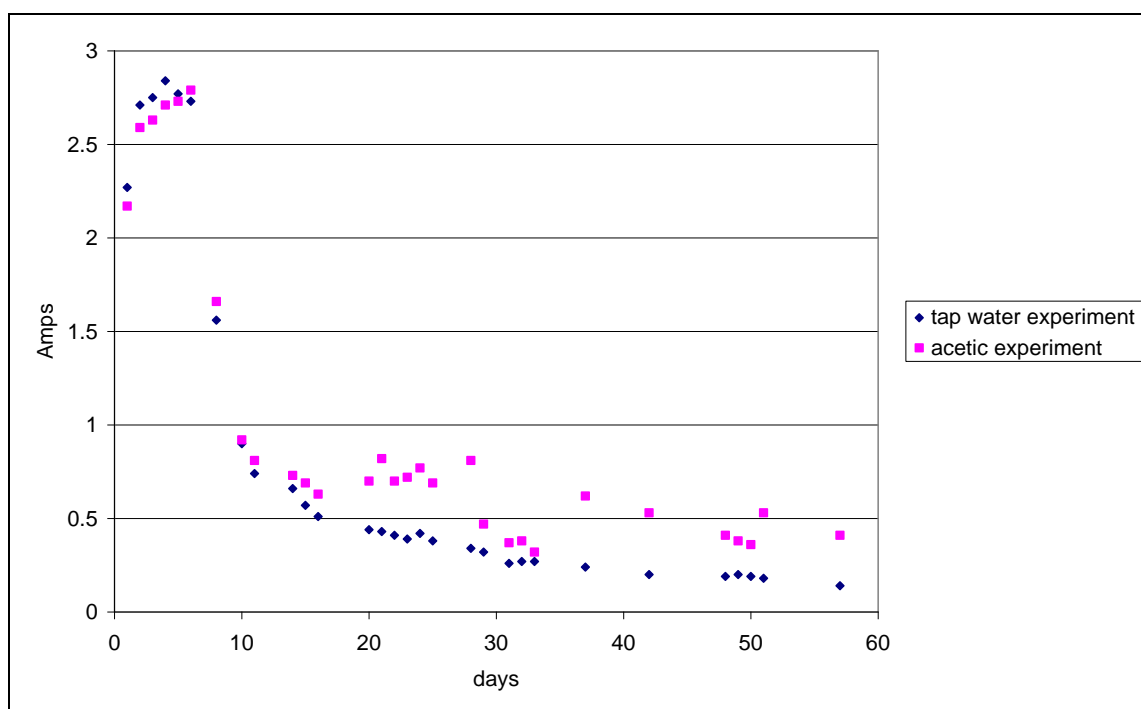


Figure 55: Current measurements with time in the acetic and tap water experiments conducted on the Hythe sediment.

The acetic acid experiment shows consistently higher values for the measured current, this is not surprising since it dissociates into an acetate ion and a proton in solution which would be expected to lower the ohmic resistance compared to the tap water experiment because of these charge carrying ions.

It is again noted that the current does not reach zero, this is postulated to be due to the exponential decay/reduction in current which would require infinite time to reach zero. See Section 6, where this aspect is dealt with in detail.

The current and therefore the energy expenditure is an important consideration for the possible implementation of the technique for future field scale use but is of less significance at this stage of research. The energy requirements of the technique have been discussed in detail in Section 2.10.

The data suggests that the acetic acid gives an appreciably higher current flow compared to the tap water influent. However, a two sample 't- test' carried out on the data shows that the difference between the values obtained for the current measurements are not statistically different from each other at 95% confidence (p value of 0.498). This shows that the use of acetic acid in this experiment does not affect the current, and therefore the energy requirement, to a statistically significant degree.

5.4.3 Estuarine Sediment Metals Analysis

In this section, elements of interest for both the tap water and acetic acid experiments are presented. Those metals which are most closely associated with the iron enriched regions are dealt with in detail. The elements which the XRF measured but for which the data was too poor to be usefully interpreted, are included in the appendix for completeness. At the beginning of this section the iron mineralised region is dealt with and the relationship between the region of maximum iron concentration and other elements present is evaluated.

The data is presented graphically with the concentrations across the treated material in the top middle and bottom thirds shown as well as the arithmetical mean of the top,

middle and bottom layer concentrations. The data points presented have been adjusted for the systematic errors calculated for each element as previously described

5.4.4 Iron Mineralised Region and Associated Elements.

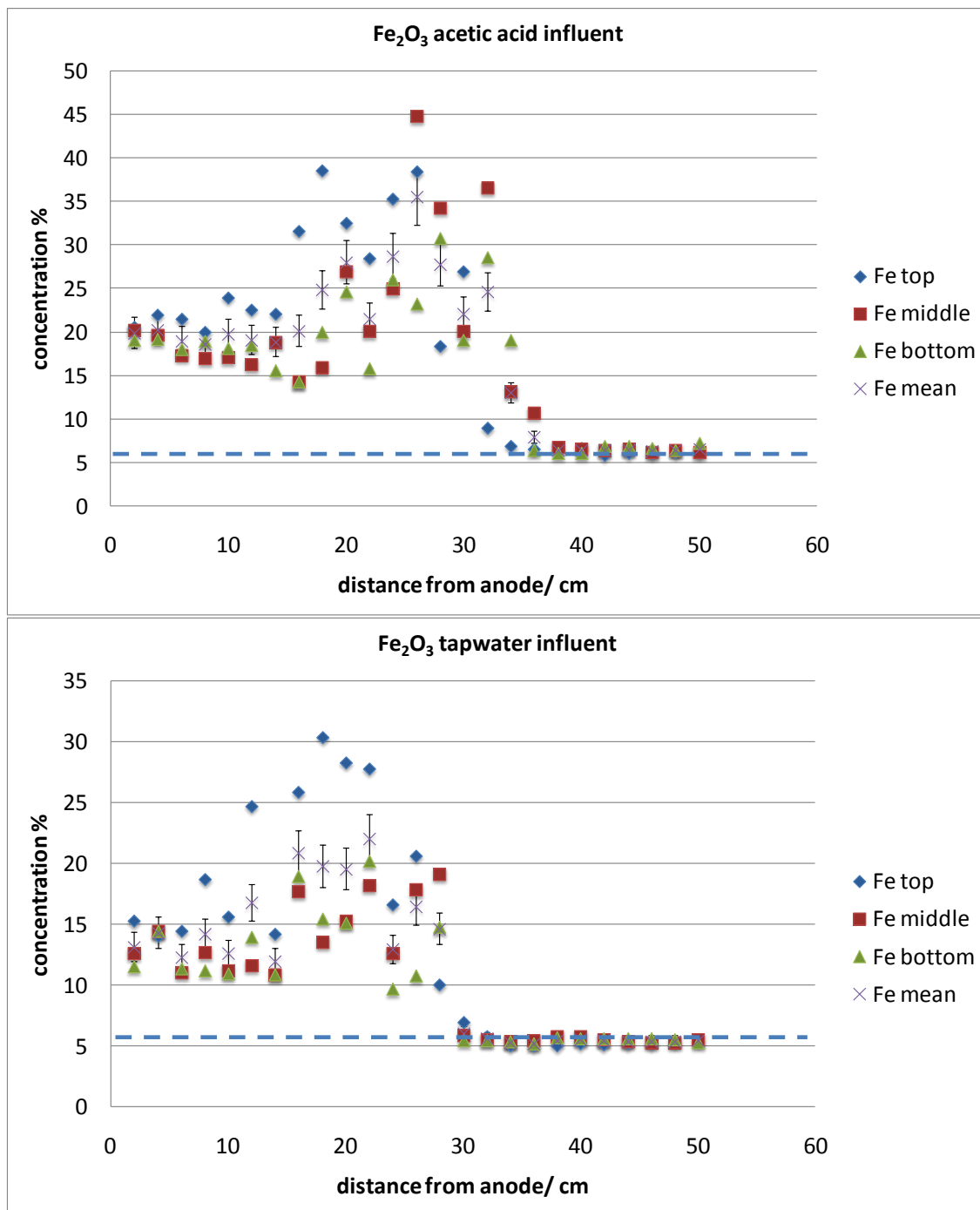


Figure 56: Iron concentration across treated material in the experiments conducted with acetic acid and with tap water electrolyte. Error bars derived from table 19. Dashed line indicates the average starting concentration, from table 22.

The following section deals with those elements which appear to be associated with the region of maximum iron mineralisation. The elements which appear to best show an affinity for the iron mineralised section are: manganese, arsenic and cobalt. The iron concentrations on the cathode sides are consistently low, circa 5%, and demonstrate very similar values for each depth: top, middle and bottom sections, Figure 56. This is a good indicator of the reliability of the sampling and the analysis procedure for this element. It is also consistent with the calculated mean starting concentration of iron indicating that the iron present in this part of the treatment cell has remained immobile.

As expected the iron concentration is much higher in the anode portion of the treated material due to the electro dissolution of the cast iron anode and subsequent migration towards the cathode electrode, as observed in previous experiments. It also matches very well with the pH profile at the end of the experiment (see Figure 57) whereby the iron is enriched with iron from the anode in the acidified region and remains immobile in the alkaline region, Figure 56. The distribution of the concentration of iron across the cell after treatment shows numerically what was evident visually. There are elevated iron concentrations on the anode side of the treated material with the maximum concentrations appearing in the region of maximum iron precipitation (between approx. 15 and 25 cm from anode). The data shows that on the cathode side of the region of iron precipitation, a significant drop in iron concentration taking place over a span of only 2-4 cm.

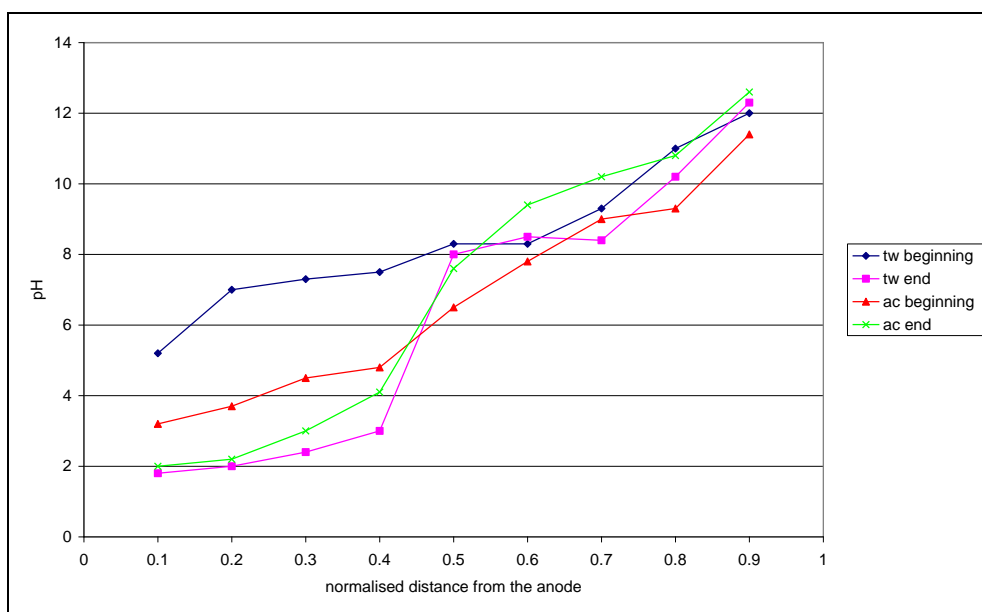


Figure 57: pH distributions measurements taken after day one of the experiment and at the end of the experiment for both the tap water and the acetic acid influent.

The normalised distance from the anode at which point the pH junction begins is between 0.4 and 0.5 which corresponds to between 20 cm and 25 cm from the anode which is also the point at which the highest concentrations of iron are observed.

This is measured at the surface so should only be considered indicative for the full depth profile of the material. The junction is more accurately mapped by the iron concentration distribution which looks at the concentrations in the top third the middle third and the bottom third. Since the precipitation of the iron will correspond to the pH jump (Hopkinson and Cundy, 2003; Cundy and Hopkinson, 2005; Faulkner *et al.*, 2005).

5.4.5 Arsenic

Perhaps the most environmentally interesting response to the treatment in these experiments is that demonstrated by arsenic. In both the tap water and acetic acid experiments the arsenic was associated with the iron precipitated region and appears to have been depleted in both the cathode and the anode side with significant enrichment in the precipitation zone, Figure 58.

In the acetic acid experiment the arsenic measurements on either side of the iron mineralised region were less than 20 ppm. The mean concentration of arsenic at 28 cm from the anode is over 80 ppm and the measured value for the middle section at this distance was greater than 140 ppm. But it should be acknowledged that there is a significant uncertainty factor for the higher concentrations. This is taken along with the fact that a visual inspection of the data shows a distribution consistent with an element associated with the iron mineralised zone, and that the lower concentrations measured at the far ends of the test cell agree well with each other, between depths, which is a strong indicator of the reliability of the data.

The distribution of arsenic shows a distinct region of enrichment at approximately half-way across the treatment cell. This is consistent with the surface measurements of where the pH jump is (between 20 and 25 cm from the anode).

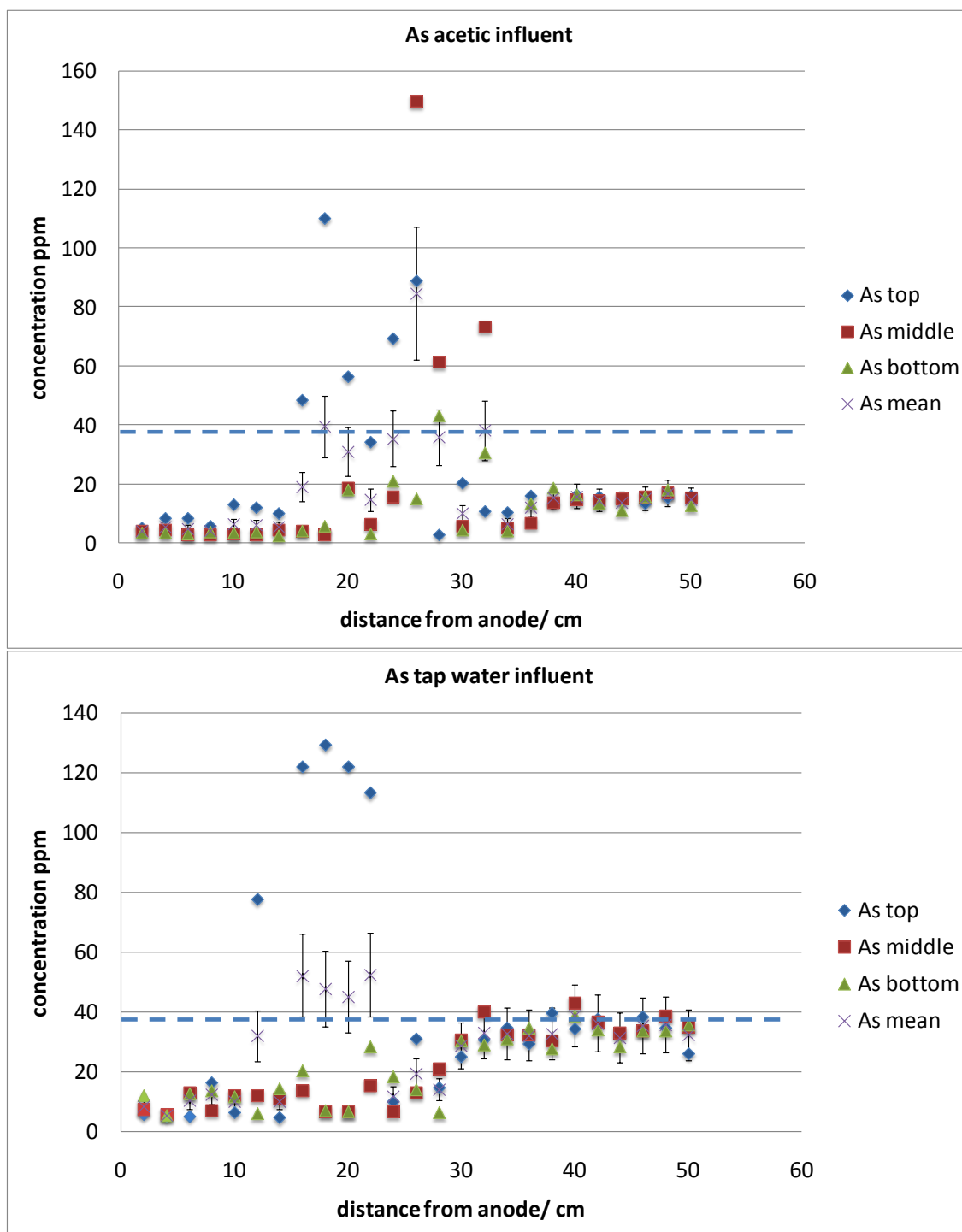


Figure 58: Arsenic concentration across treated material in the experiments conducted with acetic acid and with tap water electrolyte. Dashed line indicates the average starting concentration, table 22. Error bars derived from table 19.

The bias for the arsenic measurements was found to be + 50 % which is high but the regression analysis showed good agreement across a range of values and an R^2 value of 0.968 with a translational bias not significantly different from 0 (at 95% confidence). This means that although the true and measured values are significantly different they are different at a constant proportion and the data can be adjusted accordingly as has been applied here. This is a somewhat academic correction since the (re)distribution/relative concentrations rather than the effective concentrations are of primary concern here, but this analysis does allow for the distributions to be verified as actual; rather than artefacts of a faulty detector or analytical ‘drift’ for instance.

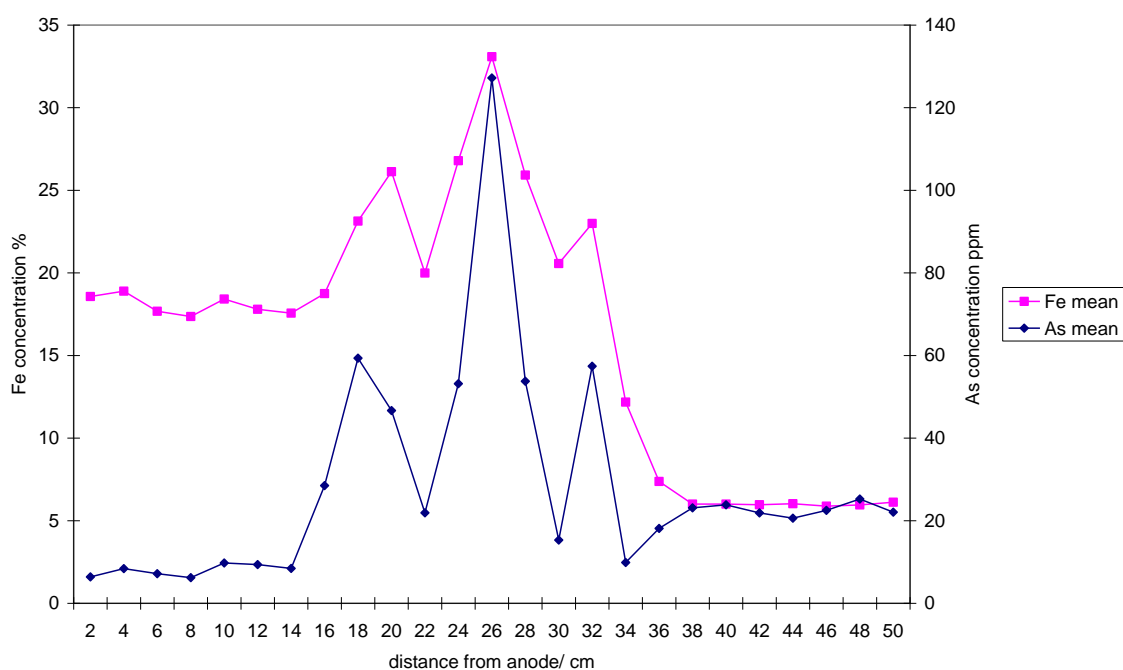


Figure 59: graph of the iron and arsenic concentration distributions in the acetic acid experiment.

Very good correlation is demonstrated between the distribution profiles of iron and arsenic, Figure 59, The reason for this distinctive three-peak profile is not immediately clear but the chance of it being an artefact of the analysis is unlikely due to the pseudo-random analysis procedure and the fact that the same distribution is observed between different elements (but importantly, not for *all* the elements analysed) The wavelength of the spectral lines associated with arsenic and measured by the XRF detector are also distinct, negating the possibility of an ‘overlap’ effect. This indicates a real correlation is present rather than an introduced effect.

An increase in the concentration of arsenic was shown in the top section in the region where the iron precipitation was most evident. However the bottom and middle sections show no rise in concentration at in this region, and in two data points, show a distinct drop below the trend for the same region.

Other than this peak in the top section at the iron enriched region, there is a general modest increase in concentration of arsenic from anode to cathode, from 5-10 ppm to 10-20 ppm. The DEFRA threshold values of arsenic concentration are 20 ppm for all types of land use. This suggests that the arsenic concentration has been concentrated up from well below threshold values to recorded values of greater than the recommended UK safe limits (the random error calculated means there should be some interpretation of the data since the uncertainty could indicate that the 'true' values could be just below the prescribed limits up to values well over the safe levels) or 'probably contaminated' according to the definition given by Ramsey *et al.* (1998).

The starting concentration of arsenic in the pre-treatment material had a mean concentration of 25 ppm. The cathodic concentrations in both the tap water and the acetic acid experiments were found to be below this level (10-18 ppm). This might indicate that there has been a concentration reduction on both sides of the treated material, not only the more pronounced reduction on the anode side. This is feasible since arsenic can exist in the environment in a number of valence states and associations; including both anions and cations (Meng *et al.*, 2002; Smedley and Kinniburgh, 2002).

5.4.6 Bromine

As demonstrated in previous experiments the anionic bromide ion is electrostatically attracted to the anode electrode, and shows marked depletion in the cathode zone and considerable enrichment in the anode zone, Figure 60.

The systematic error (bias) for bromine was not calculable with the available standard reference materials; the concentration of bromine in these was too low. However, the consistency of the data between neighbouring points and across the different depths

indicates that there is good precision and that the trend in concentration is a good representation of the distribution of the concentration change in the material. For these experiments this is not as important as it might be if, for example, the analysis was to classify land as contaminated, however this is unlikely to be the case for this element.

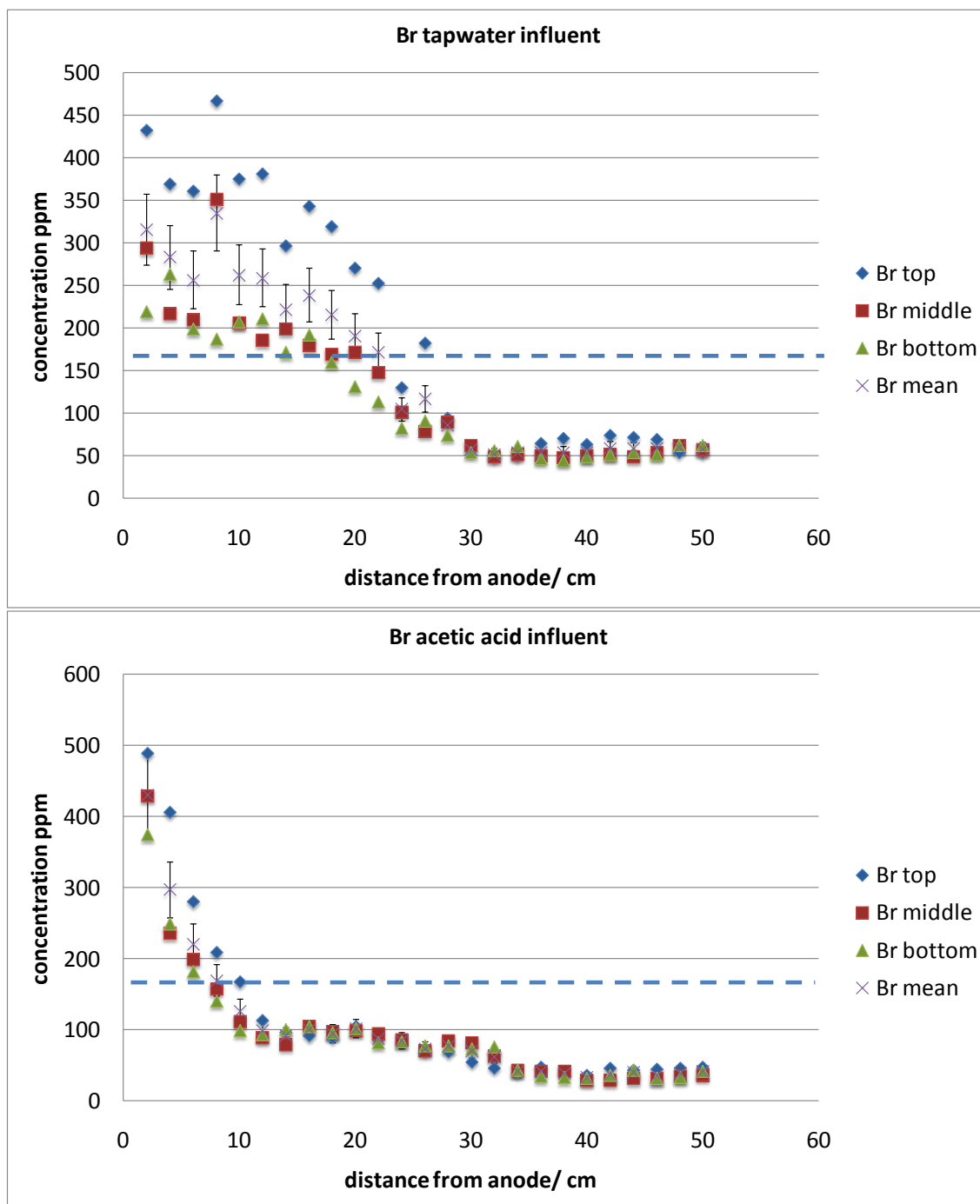


Figure 60: Bromine concentration across treated material in the experiments conducted with acetic acid and with tap water electrolyte. Dashed line indicates the average starting concentration, table 22. Error bars derived from table 19.

The distribution with depth shows a response in the top section with a lesser accumulation in the middle and bottom sections. The depth distribution profile for the tap water experiment gives consistently higher concentrations in the top section, compared to the middle and bottom sections.

The enrichment of the bromine concentration on the anode side of the treated material is high. The cathode half of the treatment cell shows measured concentrations of close to 50 ppm whereas the anode side has mean concentrations of over 250 ppm with two of the mean values greater than 300 ppm. In the acetic acid experiment the cathode side measurements are around 50 ppm and the anode side shows mean values as high as 430 ppm. These results again show that bromine has a strong response to the treatment, this confirms the findings of previous studies (Hopkinson and Cundy, 2003; Cundy and Hopkinson, 2004).

5.4.7 Calcium

Figure 61, shows the data obtained from the acetic acid experiment for calcium. The calcium shows a strong response to the treatment with the concentration at the anode reduced almost to zero, from a starting concentration of 1.62 %.

The maximum value recorded was 9 % with the data indicating a strong trend in increasing concentration towards the cathode although not a particularly strong association with the region of maximum iron mineralisation. The maximum concentration occurs at 28 cm from the anode for all depths.

Calcium is expected to be predominantly in the carbonate mineral calcite which was found by XRD analysis to constitute 1% of the sediment material. This calcium carbonate would be expected to be completely dissolved in the acid conditions generated around the anode and the introduction of the acetic acid will also facilitate the dissolution of calcite in the sediment. The calcite would also act to some extent as a buffer suppressing the generation of the acid front.

In the strong acid conditions developed in the anode zone there would be expected dissolution of the calcium present as calcite, (CaCO_3) in a neutralisation reaction with subsequent re-precipitation in the higher pH region.

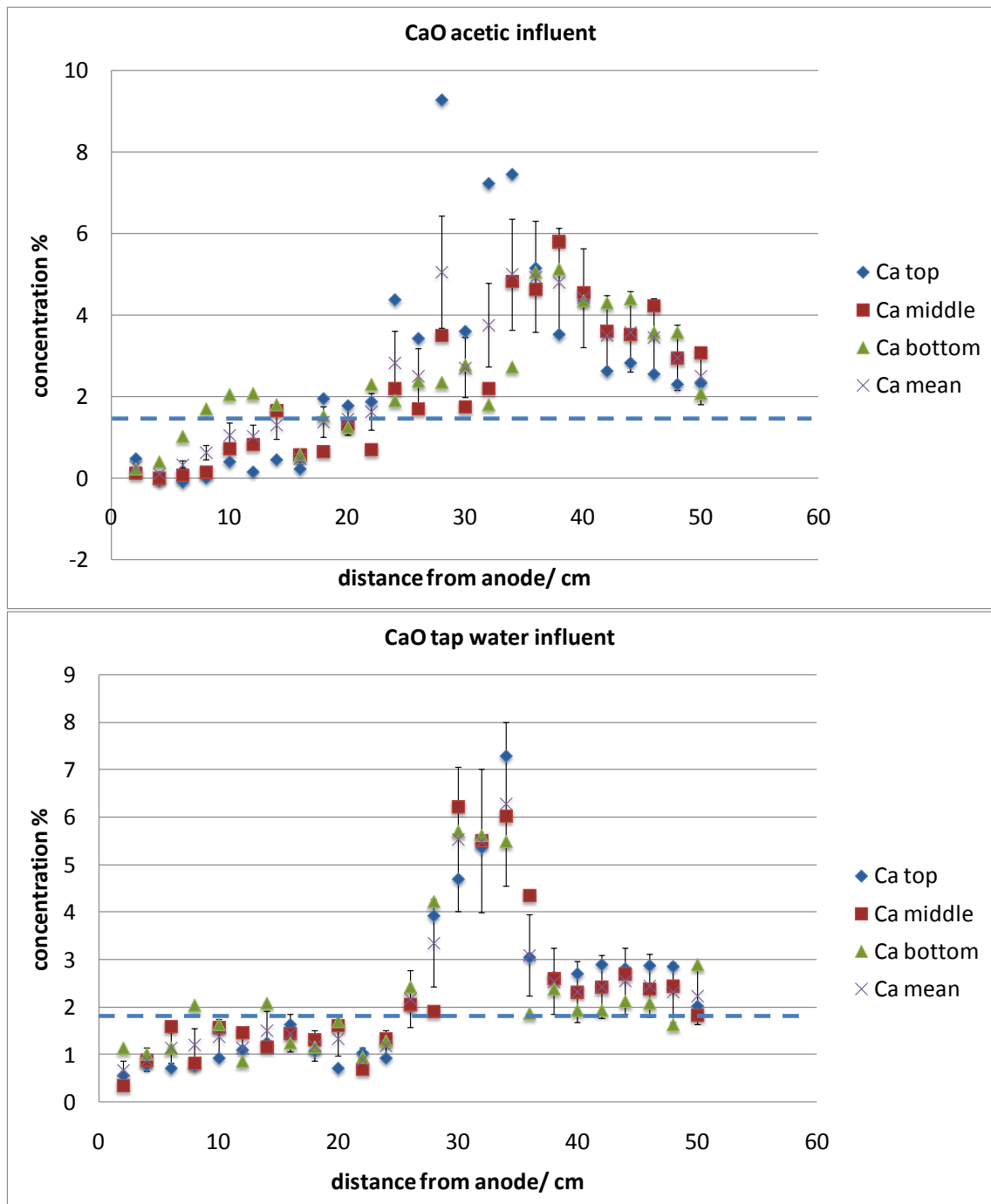


Figure 61: Calcium concentration across treated material in the experiments conducted with acetic acid and with tap water electrolyte. Dashed line indicates the average starting concentration, table 22. Error bars derived from table 19.

The calcium measurements for the tap water experiment show less variation between depths than in the acetic acid experiment.

Again though there is evident depletion in calcium concentration on the anode side as seen in the acetic experiment, as well as an enrichment beginning at around 30 cm from the anode. The measurements in the cathode zone are closer to the starting concentration than in the acetic acid experiment. This distribution indicates that there has been negligible migration from the cathode side whilst there has been significant migration from the acidified region with subsequent precipitation at 30 cm from anode region.

The percentage uncertainty was estimated as 47.42% and the systematic error was +11%. The systematic error was small due to a good range of concentrations in the certified reference materials and concentrations well above the detection limit of the detector. The random error is more substantial but a visual inspection of the data shows that although there is significant uncertainty with the measurements particularly the higher concentrations there is still a pronounced enough distribution profile to indicate a definite response to the process.

5.4.8 Strontium

The data indicates that strontium is extremely amenable to the electrokinetic process but behaves apparently independently of the iron mineralised region, Figure 62. In both the tap water and the acetic acid influent experiments the strontium concentration in the depleted anode zone is around 60 ppm and in the cathode zone it peaks at over 200 ppm. It is noteworthy that the distribution for the concentration of calcium is remarkably similar to that shown by strontium. This is due to the chemical similarity between strontium and calcium, i.e. same group and similar ionic radius etc.

In the tap water experiment the top middle and bottom sections agree closely with each other; the acetic acid experiment shows close agreement between the middle and bottom sections but the top section is slightly skewed towards the anode side- as observed in some of the other elements. The good agreement of the values obtained for all depths in

the anode zone again reinforces the good sampling and analysis precision as discussed in Section 5.3.3 and calculated for strontium in Section 0. Taking the arithmetical mean of the values obtained on the anode-side 25 cm (61.0 ppm) versus the 25 cm on the cathode side (134.9 ppm) shows an increase of more than double the concentration of the anode side. The average starting value was calculated to be 101.96 ppm.

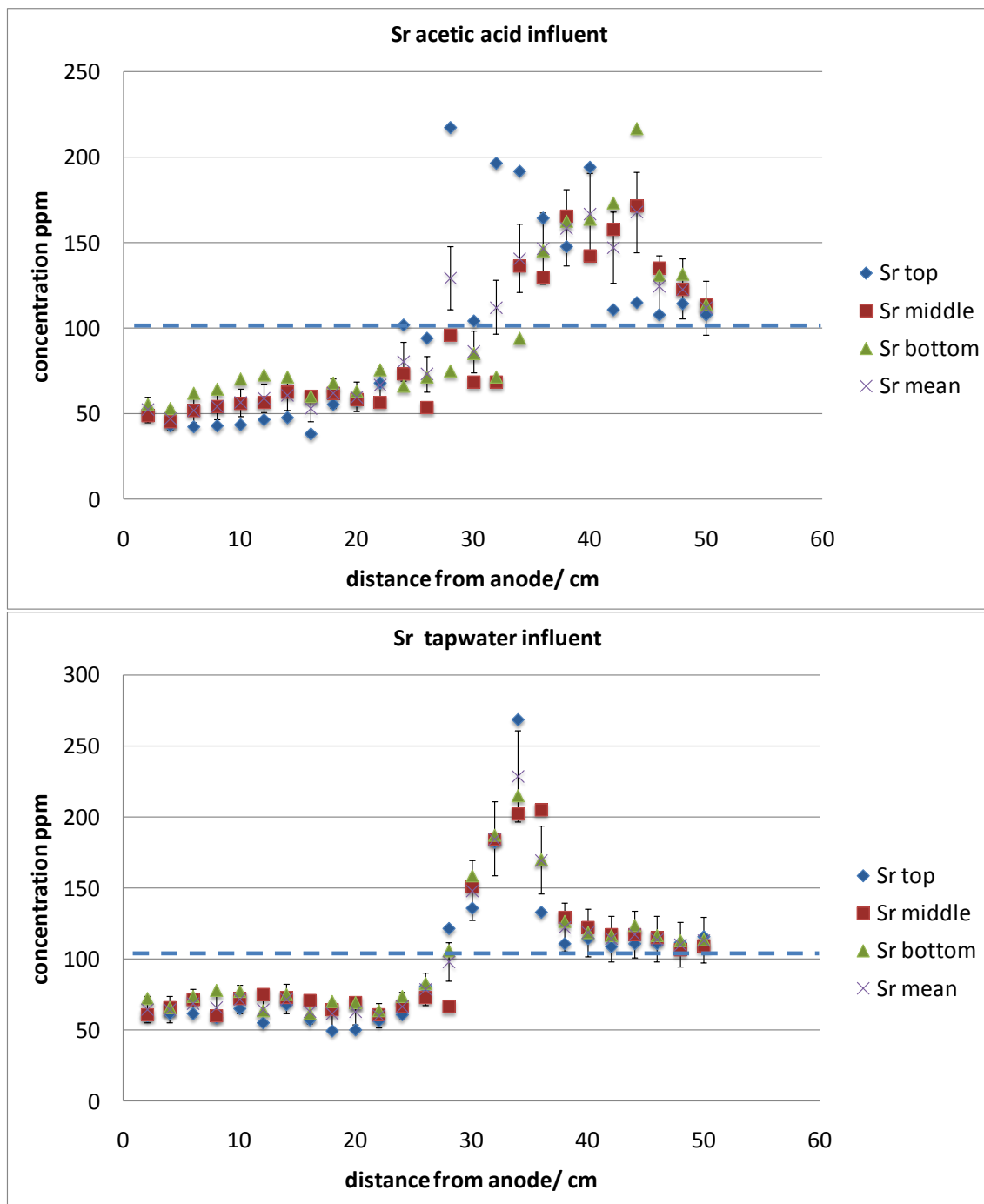


Figure 62: Strontium concentration across treated material in the experiments conducted with acetic acid and with tap water electrolyte. Dashed line indicates the average starting concentration, table 22. Error bars derived from table 19.

The measurements on the anode side of the cell are consistently around 60 ppm before rising to a distinct peak beginning at around 28 cm from the anode, peaking at nearly 260 ppm for the measurement at 34 cm from the anode in the top section before levelling off to just over 100ppm for the measurements at the cathode side of the cell, which is approximately the starting concentration of 101.9 ppm on average. This demonstrates considerable depletion on the anode side with localised enrichment in the 30 – 36 cm from anode region, returning to pre-treatment values closer to the cathode.

Strontium has been found to be associated with Fe and Mn oxides in the natural environment under conditions encountered in brackish estuarine sediment regions, (e.g. Andersson *et al.*, 1994).

Since there is no such association observed in these experiments it might indicate that the strontium is migrating in advance of the iron and magnesium. This hypothesis would account for the lack of association between the iron and manganese, and the strontium observed. In addition to this, strontium is likely to be associated with any carbonate fraction present (Xu and Marcantonio, 2004), which is apparent from its concentration distribution which is very similar to that seen for calcium above.

This is due to strontium carbonate being soluble in acidic conditions but insoluble in alkali conditions, both calcium and strontium will form carbonate minerals under alkaline conditions. It appears that dissolution, followed by electromigration is the transport mechanism followed by re-precipitation.

The bias calculated for strontium was +3.7 % and the percentage uncertainty estimated as 24.5 %. The concentration distribution of strontium across the cell is much less dispersed in the tap water experiment, but shows a region of maximum concentration which is not centred on the iron enriched region. There is consistency between the depth samples and the samples taken across the cell. The way that the samples show good agreement between samples, and between the depths, indicates good sampling protocol and a high level of analytical precision for this element.

Statistical tests showed no statistically significant difference between depths for tap water or acetic and no significant difference between tap water and acetic.

5.4.9 Cobalt

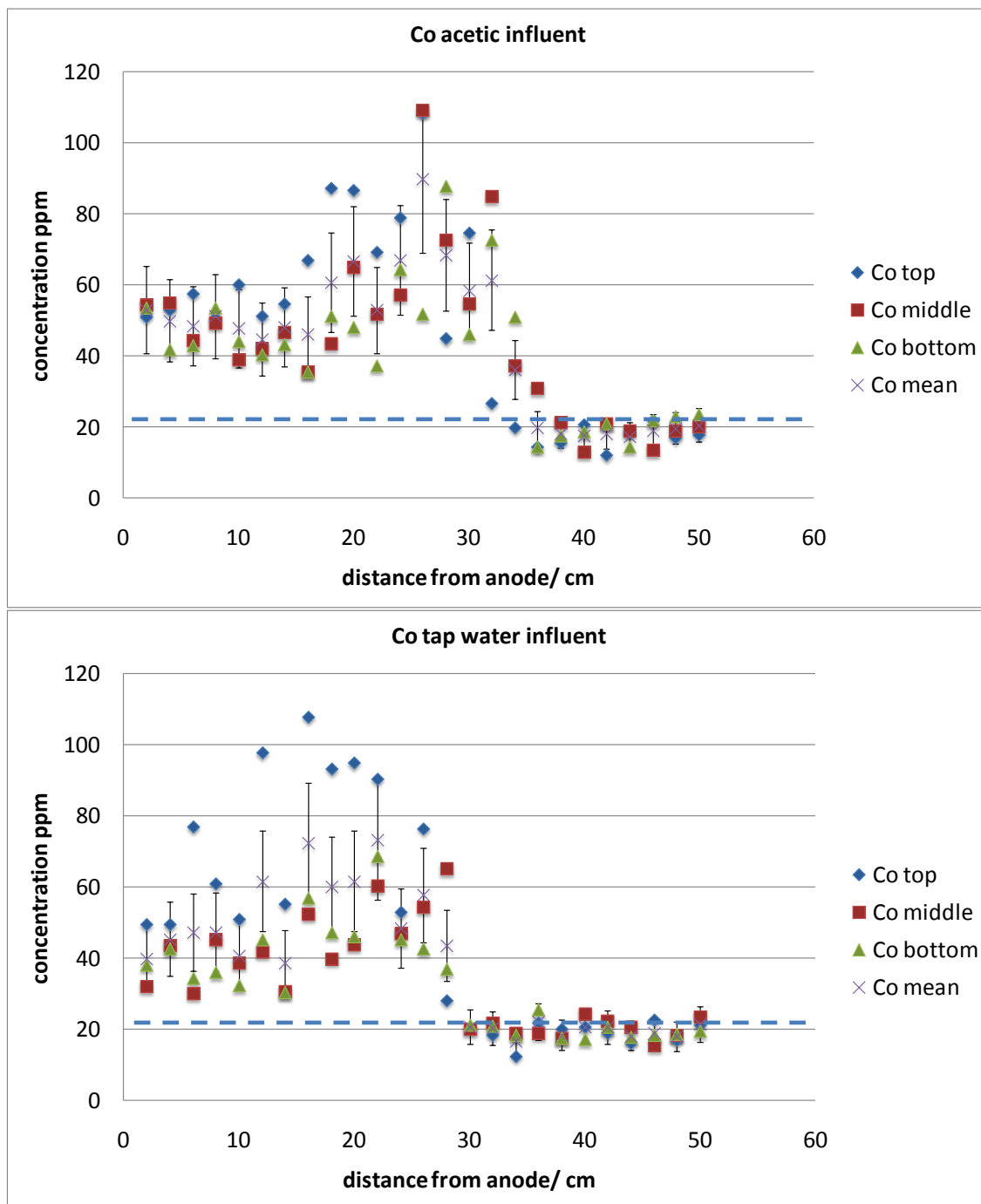


Figure 63: Cobalt concentration across treated material in the experiments conducted with acetic acid and with tap water electrolyte. Dashed line indicates the average starting concentration, table 22. Error bars derived from table 19.

The bias for the cobalt analysis was determined as having no statistically significant correlation between the measured and certified values. However, the concentrations in the certified reference materials were all well below the values in the sediment (bar one CRM, that being NIST 2710) so the reliability of the bias estimation incorporates this weakness and therefore the bias estimation is unrealistically high but is included in the Appendices Section 0 for completeness.

This is coupled with the visual inspection of the data, which shows good correlation between values at the top middle and bottom as well as between neighbouring values longitudinally indicating that the data is a reliable representation of the relative concentrations. This could be accounted for by future analyses of a more suitable range of certified reference materials. However, as mentioned previously, the absolute concentrations are of less significance than are the relative concentrations for the purposes of this investigation. The starting concentration measured pre-treatment for cobalt was calculated to have a mean concentration of 20.4 ppm so there is no evident reduction in the starting concentration since the cathode side values are close to the starting values. There is enrichment on the anode side, possibly indicating the introduction of cobalt from the anode electrode.

The cobalt concentration across the cell shows an interesting distribution, which requires some interpretation since the distribution seems to show a significant difference in concentration between the anode side and the cathode side with higher concentration at the anode and fairly constant cathode side measurements of around 20 ppm.

The anode side measurements are more dispersed with some of the higher measurements associated with the top layer of measurements. The middle and bottom depth measurements are more similar in their distribution. The mean concentrations show a correlation with the iron enriched region. The concentration distributions for both the tap water and the acetic acid experiments are very similar which suggests that they are not especially influenced by the acetic acid. The measurement uncertainty was estimated at 39.91% at 95% confidence interval, which is higher than ideal but as is

seen in the graphical presentation of the data, the error bars still accommodate the distribution which is predicted.

5.4.10 Manganese

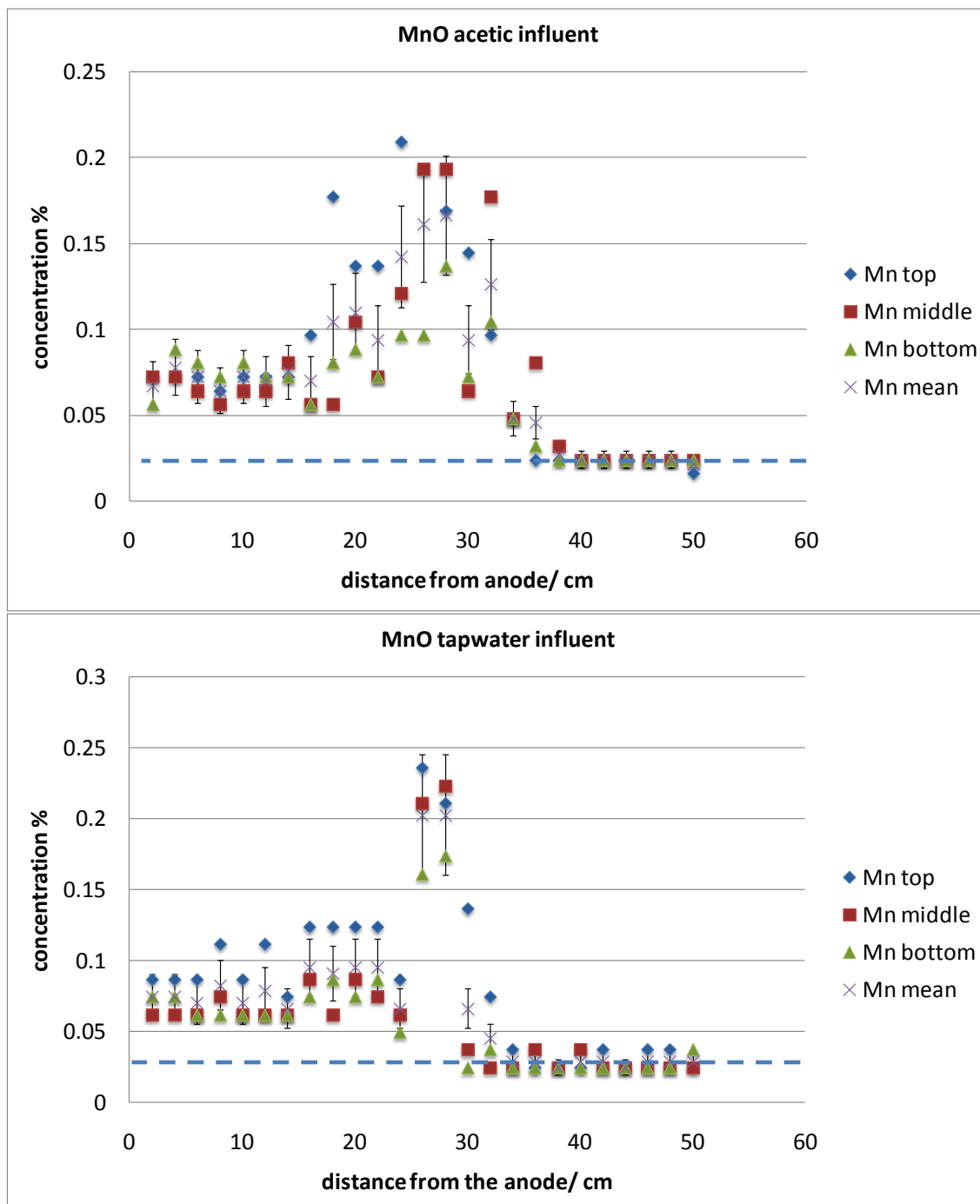


Figure 64: Manganese concentration across treated material in the experiments conducted with acetic acid and with tap water electrolyte. Dashed line indicates the average starting concentration, table 22. Error bars derived from table 19.

The movement of manganese shown by the data is what might be anticipated given that iron and manganese are chemically similar.

This trend is clearly shown in Figure 64. With the more oxidising conditions associated with the cathode side of the experiment the maximum migration of the manganese is approximately 5cm further towards the cathode side of the experiment at between 25 and 30 cm from the anode for the tap water experiment. It is noteworthy that the starting concentration of manganese in this experiment is only present at low concentrations (~0.02%).

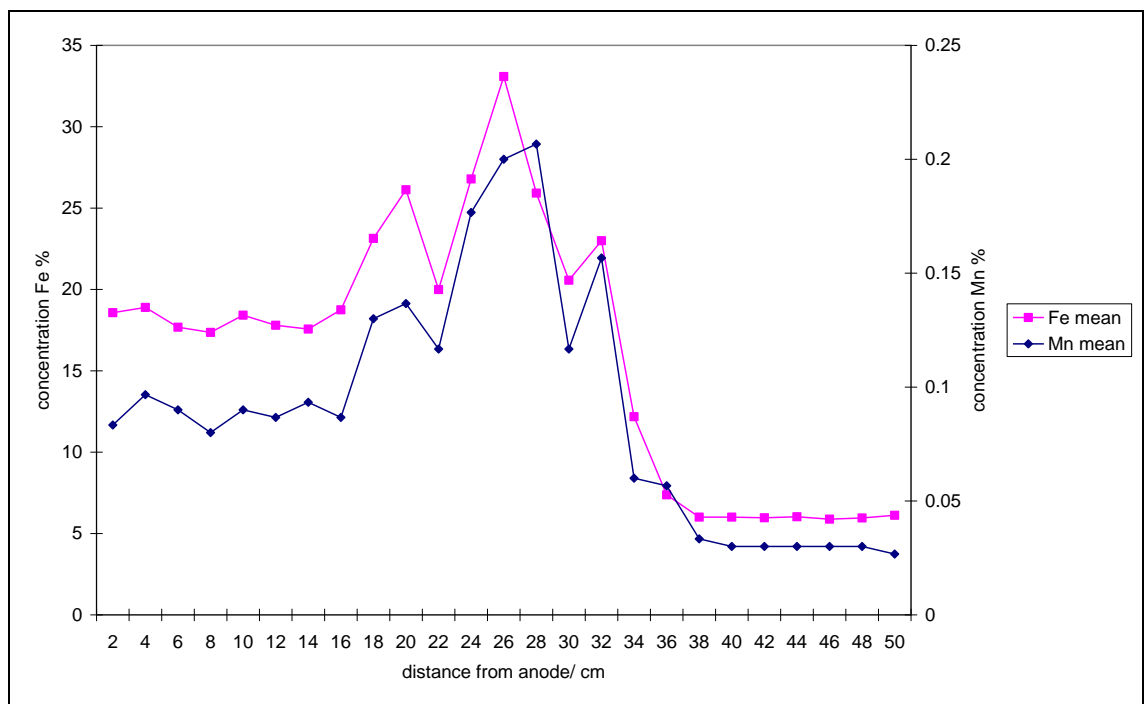


Figure 65: Mean iron and manganese plots for acetic acid influent experiment

It is noteworthy that the mean concentrations across the treated material for iron and some of the other elements show such a similar distribution, e.g. Figure 65 (and arsenic as already discussed). For instance the distribution of iron and manganese follow one another very closely and both display three peaks (or two troughs) in the region of the iron precipitation. The iron shows these high and low points at all depths, although there is some off-setting. The graph has lines joining the data points to make it easier to see the distribution shape; the lines do not represent presumed values between data points.

Possible explanations for this concentration distribution might be regions of lesser and greater mineralisation, possible voids or air pockets, or heterogeneity in the composition of material in the regions with lower overall concentrations. This would account for the good agreement between the values for the iron and the other species.

The manganese in the cathode region of the treatment cell shows a relatively constant concentration on the cathode side of the region of peak enrichment, again a good indication of reliable and repeatable sampling/analysis protocol. The narrow peak indicates that the manganese is greatly localised in its enrichment, to between 25 cm and 30 cm from anode.

The bias estimate for manganese was calculated as +24 % and the measurement uncertainty was calculated to be 36.3 %. These values would be considered high for many applications but are considered fit for purpose in this case. Visual inspection of the data shows good agreement between values on the cathode side, with neighbouring values showing strong agreement with one another as well as expected enrichment in the iron precipitated region and on the anode side. The starting concentration of the manganese was measured in the starting material as 0.02 % which is the approximate concentration of the eighteen measurements made on the cathode side after the experiment, indicating that the manganese has remained immobile in this area.

5.4.11 Copper

The copper concentrations in acetic and the tap water experiments are addressed separately due to the distinctly different responses in each experiment. Copper concentrations in the acetic acid enhanced electrolyte, despite being generally quite low, are higher close to the anode. This is in contrast to the distribution seen in the tap water experiment where there was significant migration towards the cathode, Figure 66.

The bias for the copper measurements was calculated to consist of a ‘rotational bias’ of + 16.5 % but there was also a significant ‘translational’ bias (at 95% confidence interval) of -14.05 mg/kg which was also applied to each of the measurement values.

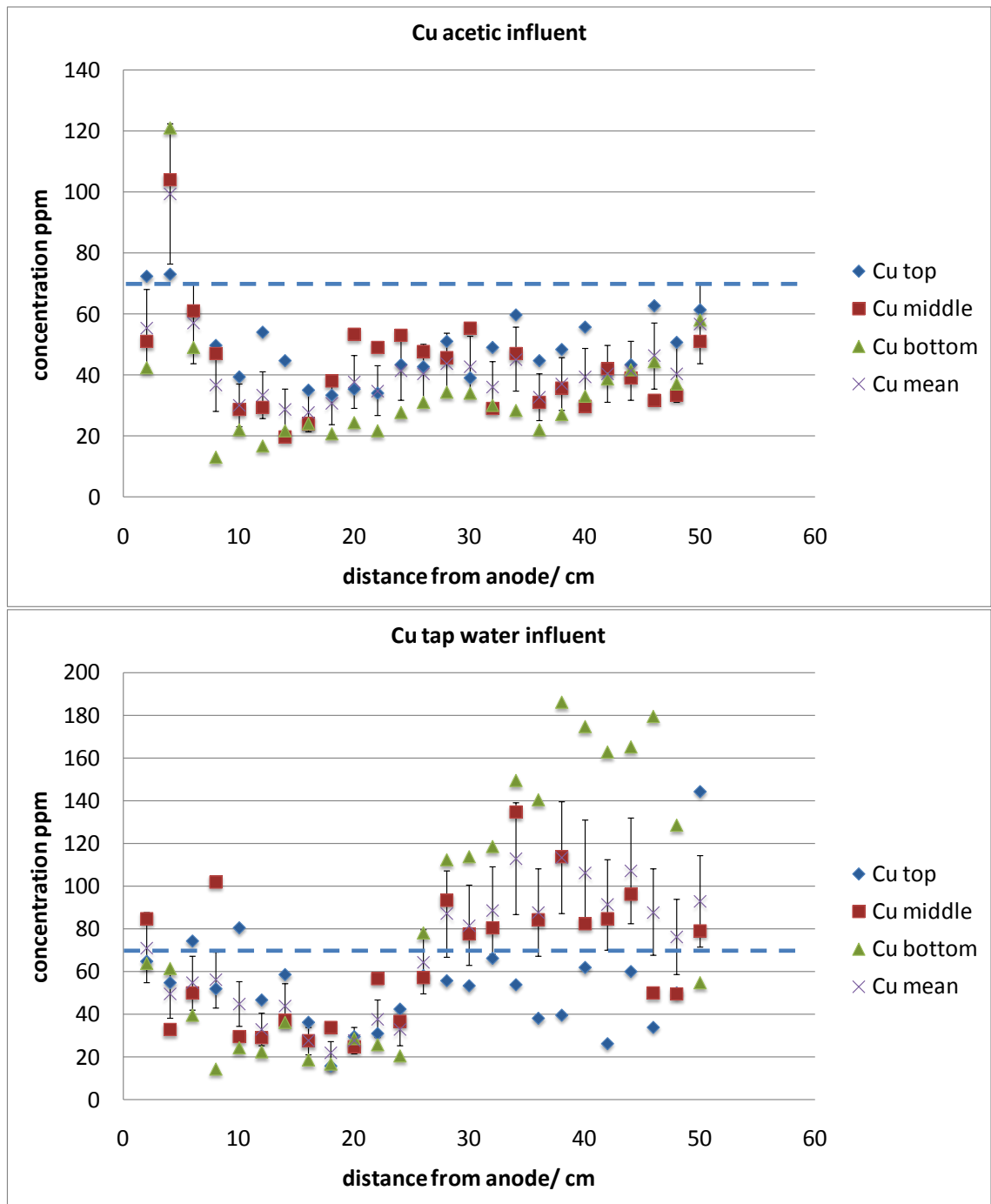


Figure 66: Copper concentration across treated material in the experiments conducted with acetic acid and with tap water electrolyte. Dashed line indicates the average starting concentration, table 22. Error bars derived from table 19.

The concentration of copper in the pre treatment material was calculated to have a mean concentration of 61.44 ppm; the standard deviation was 11.8 ppm. This might indicate that there is significant reduction in the concentration of the copper present on the cathode side. A ‘two sample t-test’ to compare the pre-treatment concentrations with the concentrations on the cathode side of the region of iron mineralisation (using the statistical software package, Minitab[®] version 15) for the measurements taken

between 22cm from anode and 50 cm from anode was carried out. This yielded a p-value of 0.011 indicating that the concentrations of copper on the cathode side are statistically different from the starting concentrations, for a confidence interval of 95% (See Appendix 2 for full output data). So there is a statistically significant difference between concentrations on the cathode side with those on the anode side indicating the copper concentrations have been influenced by the treatment.

This indicates that the copper concentration on the cathode side is significantly lower than the pre treatment levels. Since the copper concentration in this region is fairly uniform, it might be a result of a mobile and an immobile fraction of copper in the sediment. The mobile fraction has been mobilised towards the iron enriched region leaving the immobile fraction behind. This explains the reduced concentration of copper in the cathode side of the treated material whilst still showing a uniform concentration profile. The pre-treatment measurements are measuring both the mobile and the immobile fraction and therefore returning a higher value. To test this hypothesis, a species-selective analysis is required on a leachate test.

In the tap water experiment, distributions of copper concentrations appear to demonstrate an increased response to the treatment at depth with the samples taken from the bottom of the treatment tank demonstrating a greater degree of migration from the anode side to the cathode zone. There is a general depletion of the concentrations at the anode side and a marked increase in the measured concentrations at the cathode side. The samples from the bottom of the treatment cell showed the greatest response to the treatment and the samples taken from the top of the treatment cell showing the least response. The middle section's response to the treatment was between the two. The data suggests that there is a strong relationship between the depth of the sample and the movement of copper through the material. The samples at depth would be expected to be significantly more reducing in the natural environment.

The tap water experiment has generated a migration toward the cathode side of the treatment cell- indicating a positive ion or complex. Whilst the acetic acid experiment indicates that there is an increase in the concentration of copper close to the anode which would suggest that the copper is present in a negatively charged form i.e. as a negatively charged complex or ionic molecule.

This is likely to be due to the copper complexing with the acetate ion and forming a negative species which migrates towards the anode (Wong *et al.*, 1997) whereas the tap water experiment has the copper in solution as a cation which therefore migrates towards the cathode. The data supports this theoretical summary of the migration controls for copper. This brings into sharp relief the effect that the speciation/complexation of a metal determines the response to the process.

Another study using acetic acid as a conditioning agent has found a remarkably similar distributions in electrokinetic experiments; in similar sediments namely, Altaee *et al.* (2007) where the concentration of copper in the pore fluid was measured, Figure 67, found a distinct increase in copper concentration close to the anode.

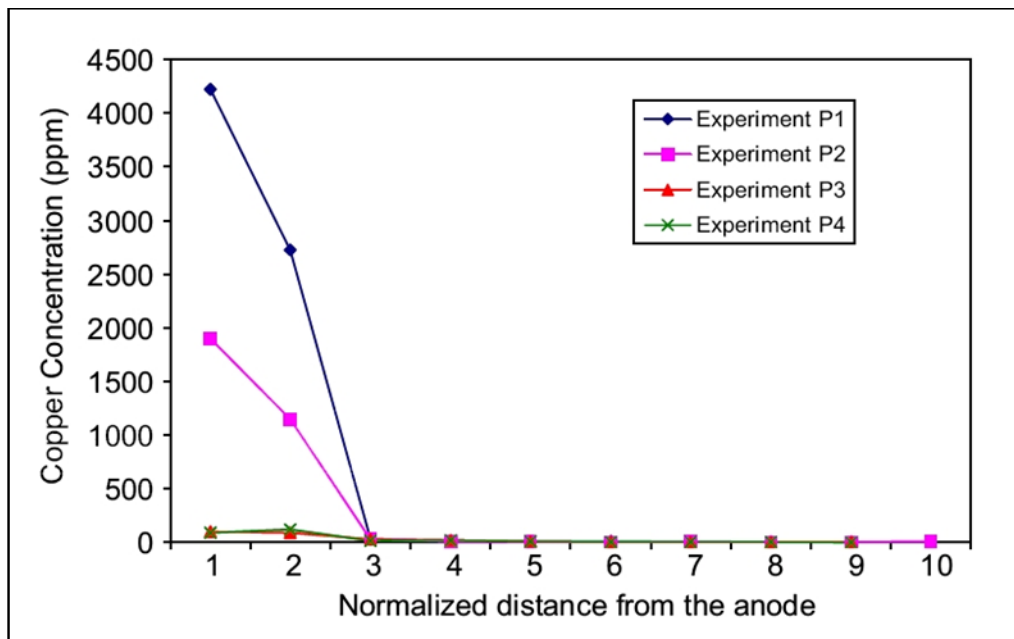


Figure 67: Copper concentration in pore fluid of saline sediment after electrokinetic treatment with the application of 7 volts and an electrode separation of 19 cm, (Taken from, Altaee *et al.*, 2007).

In this case there is unlikely to be significant amounts of copper being introduced from the cast iron electrodes, mostly because copper is not likely to be found in the cast iron since copper's high economic value means it is preferentially scavenged from waste materials, but also because the results obtained by, Altaee *et al.* (2007) were achieved using graphite electrodes where there would be no release of metals from the electrode material.

The concentration increase at the anode is postulated to be due to the formation of the anion CuOH^- in the cathode region (Acar *et al.*, 1995). The data obtained by Altaee *et al.* (2007) for the copper associated with the soil shows a less distinct relationship. But since the total copper was measured in the experiments conducted for this thesis it might be that the results do in fact correspond. The use of the acetic acid does indeed appear from these results to have exerted an influence on the behaviour, in terms of response, to the treatment.

There is a paucity of information in the literature which describes a depth dependent distribution of metals following electrokinetic treatment, primarily due to the fact that the scales of the experiments conducted in the laboratory tend to be too small to provide enough sample volume for analysis to be conducted on both longitudinal and vertical planes.

The majority of the experiments conducted in the literature use laboratory grade materials, often Kaolinite, rather than a natural and organic rich sediment. This means that the microbially induced reducing conditions which might be expected in the natural sediment are not developed in the laboratory apparatus which is the presumed explanation for the effect.

An additional factor which lends weight to the data being generated by the analysis being a reliable reflection of the concentrations present in the material is the depth dependent distribution in the tap water experiment. This shows a concentration gradient through the depth of the test material with consistently higher concentrations in the bottom section, followed by the middle section and the lowest concentrations observed in the top section for measurements on the anode side.

5.4.12 Zinc

The zinc data indicates a limited response to the treatment in both the tap water and acetic acid experiments, Figure 68. The data suggests a small depletion in concentration in the area close to the anode with a possible indication of enrichment close to the iron

precipitated area. The changes are limited with the vast majority of the measurements obtained lying between 100 and 200 ppm.

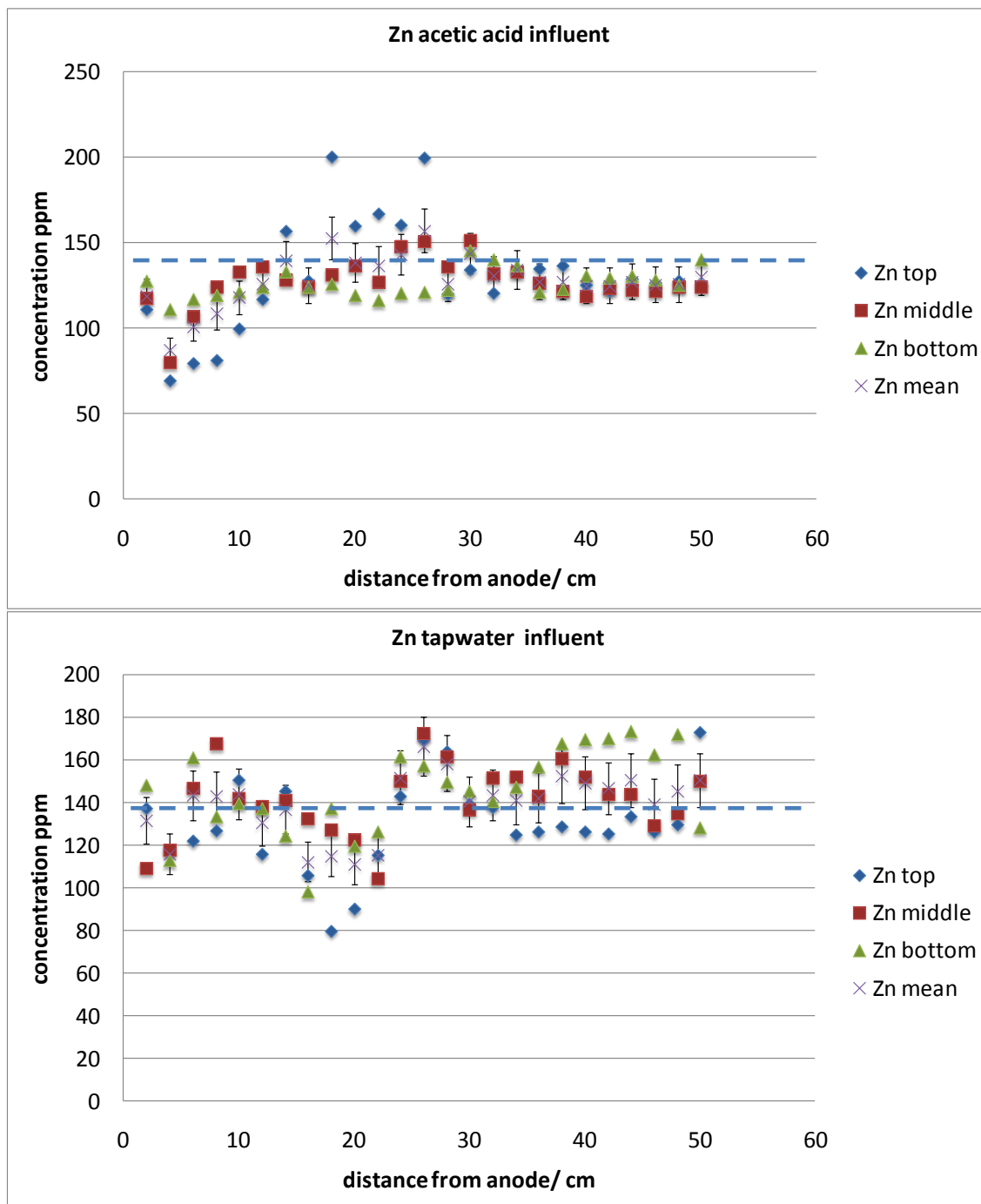


Figure 68: Zinc concentration across treated material in the experiments conducted with acetic acid and with tap water electrolyte. Dashed line indicates the average starting concentration, table 22. Error bars derived from table 19.

The region with the most iron rich precipitation seems to be significant (15-25 cm from anode), in this region there appears to be a depletion on the anode side of the iron enriched area and a concentration at the cathode side of the region of iron precipitation.

This corresponds broadly with the pH profile for the experiment. There does not seem to be an obvious depth profile relationship for zinc as observed for the other elements.

5.4.13 Vanadium

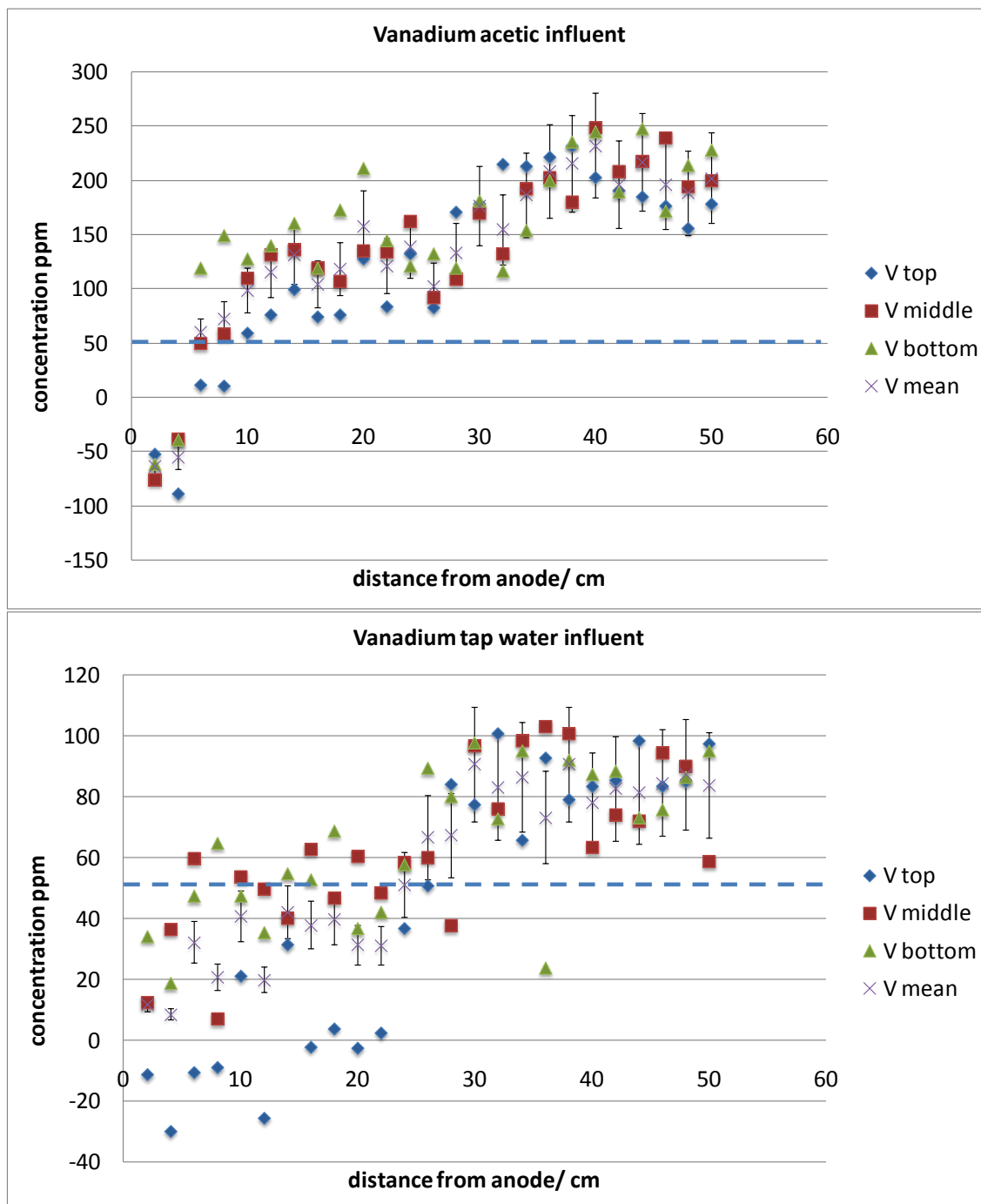


Figure 69: Vanadium concentration across treated material in the experiments conducted with acetic acid and with tap water electrolyte. Dashed line indicates the average starting concentration, table 22. Error bars derived from table 19.

The concentration profile for vanadium is distinctive in its very low values in the first four centimetres of the anode side, Figure 69. There is a similar but less pronounced distribution observed in the tap-water experiment.

Vanadium shows a gradual increase in concentration across the cell from anode to cathode, Figure 69. The lowest concentrations on the anode side of the treatment cell are below the detection limit of the instrument and result in negative values due to the algorithm used by the processor to subtract noise from the readings.

The bias of the data in this series was estimated at -33% and the measurement uncertainty estimated at 35.99% again, somewhat higher than desired for many applications but passable for the purposes of this thesis. The regression analysis gave an R^2 value of 0.887 indicating less than perfect linear relationship.

5.4.14 Zirconium

Zirconium and titanium in soils and sediments are often used as reference values to calculate an enrichment factor for another species which are suspected of being above background levels of concentration due to human activities. The reason for using these so called 'conservative elements' is that they are not part of the nutrient cycle i.e. not taken up by plants or animals and they are considered to be immobile and insoluble in the chemical environment of soils (Scalenghe *et al.*, 2006). It is for this reason that it is particularly surprising to see a response to the electrokinetic process for both zirconium and titanium in the tap water and acetic experiments, Figure 70.

The bias measurement was calculated as -20% and the measurement uncertainty was 14.83% indicating good quality data. There is apparent enrichment of the zirconium concentration towards the cathode side with a distribution profile very similar in the acetic acid experiment.

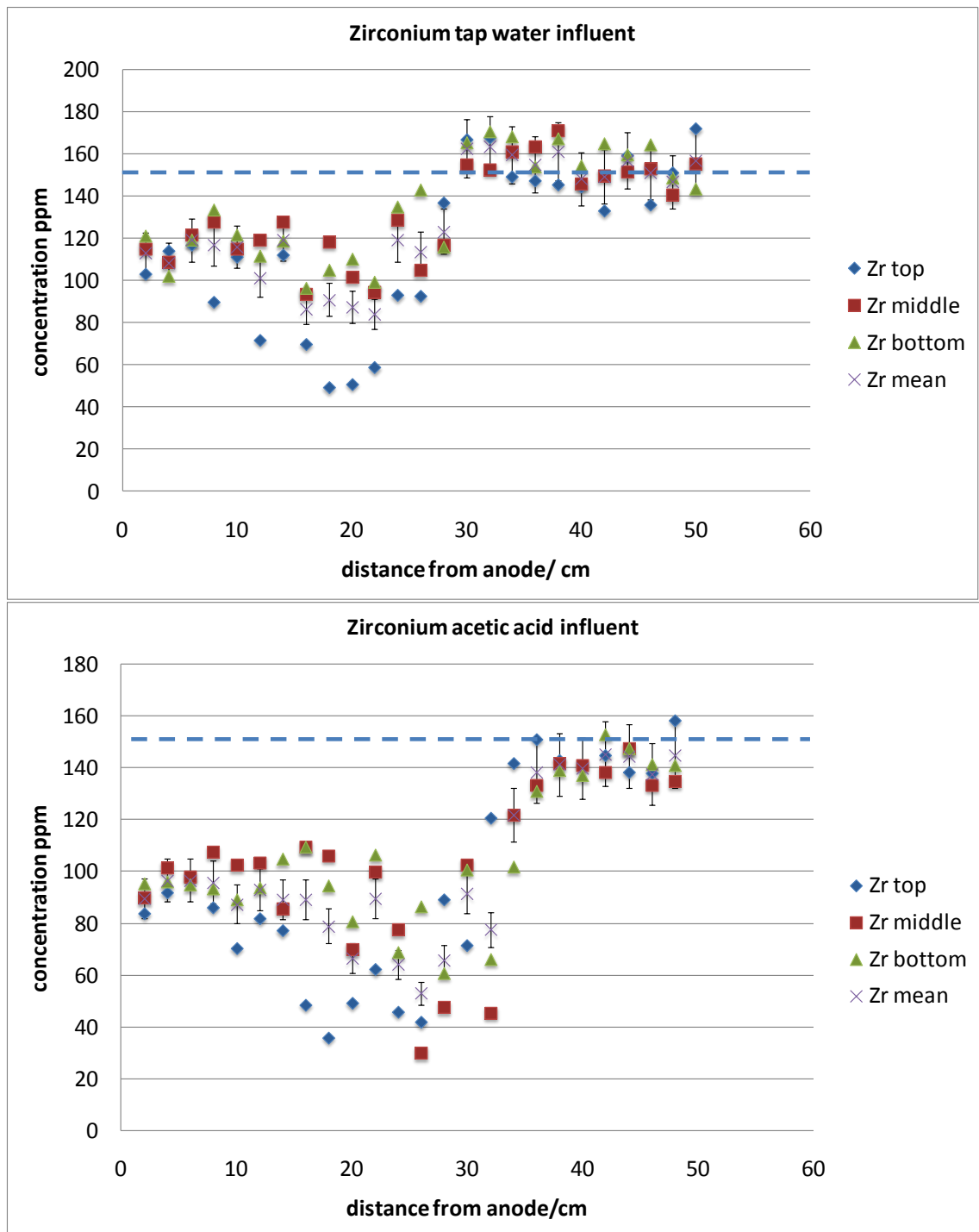


Figure 70: Zirconium concentration across treated material in the experiments conducted with acetic acid and with tap water electrolyte. Dashed line indicates the average starting concentration, table 22. Error bars derived from table 19.

The zirconium measurements show a distinct drop in concentration in the anode zone but there is no appreciable increase in concentration on the cathode side Figure 70. There seems to be an added depletion in the iron mineralised zone. This may be due to a lower than calculated starting concentration of Zr in the material pre-treatment since there is no obvious analytical reason for artificially low concentration measurements.

5.4.15 Titanium

The titanium distribution, Figure 71, shows a discernable difference between the concentrations measured at the anode side compared to that measured at the cathode side, with significant enrichment on the cathode side. The mean starting concentration of titanium in the sediment was 0.63 %.

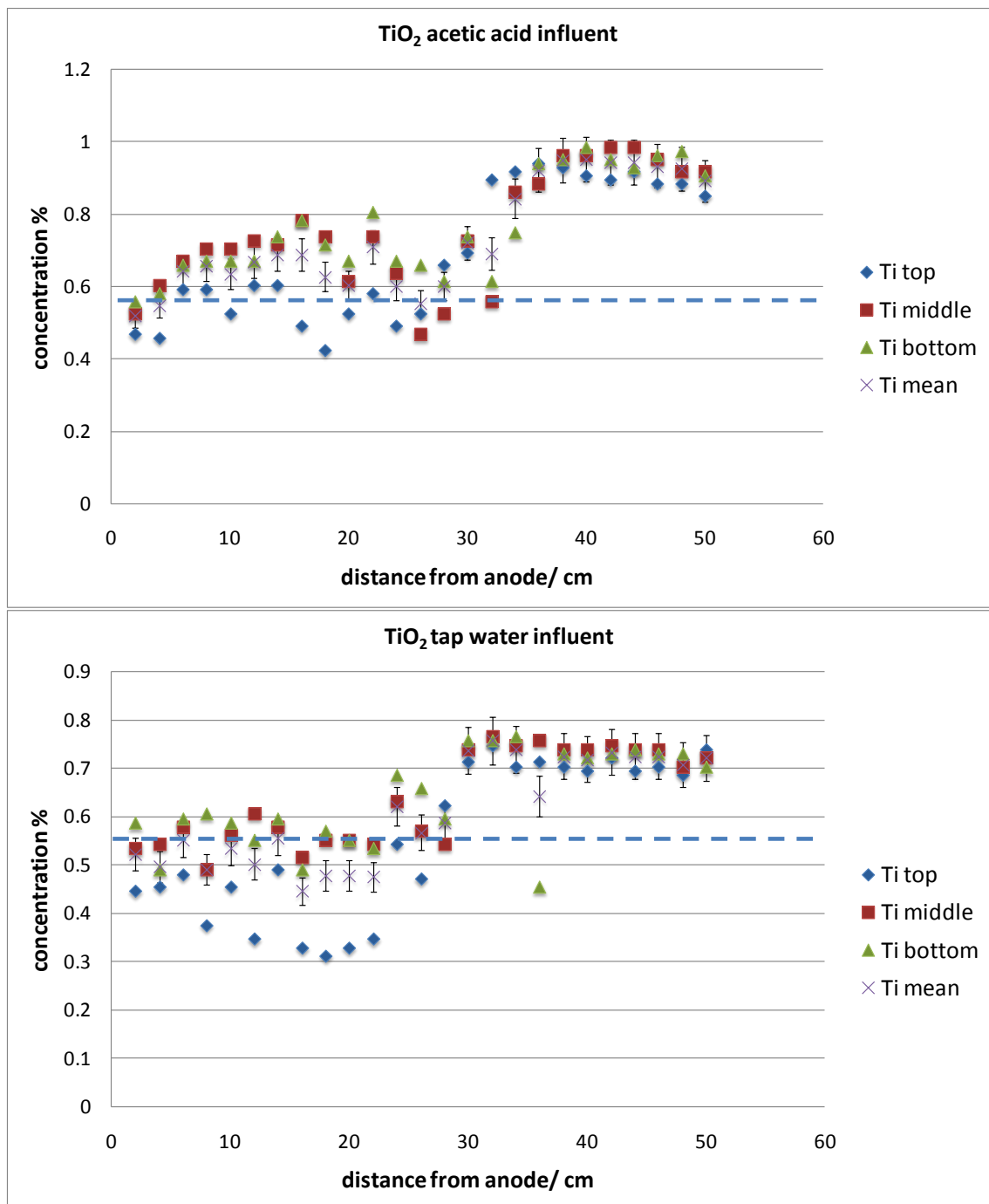


Figure 71: Titanium concentration across treated material in the experiments conducted with acetic acid and with tap water electrolyte. Dashed line indicates the average starting concentration, table 22. Error bars derived from table 19.

This indicates that there is considerable enrichment on the cathode side. The reduction in concentration on the anode side seems to be predominantly in the top layer, with lesser reduction in concentration in the middle and bottom layers. The bias calculated for the titanium measurements was -10.8% and the measurement uncertainty was 11.28%, again indicating a good level of reliability for this data.

5.5 Discussion

In general there has been a clear migration of species under the influence of the applied electric field. Some of the elements have also been associated with the region of iron precipitation, but not all of them. This indicates that there are elements which precipitate out in the same region as the iron either by co-precipitation, and/or due to the change in pH. There are the elements that show limited association with iron or any general response to the treatment such as zinc. Then there are the elements that show a response to the treatment (migration) but, like strontium and bromine, migrate and concentrate independent of the introduced iron.

Of these three types of response (or lack of) only those associating with the iron adhere to the remediation model set out by Cundy and Hopkinson in that elements are deposited on or around the region of iron precipitation. Since if the elements are acting independently of the iron then there is no purpose to introducing iron into the system by way of the sacrificial electrode.

Some of the depth dependent concentration distributions observed might involve the geometry of the iron mineralised region. This could cause the off-setting seen in the depth profile e.g. if the iron mineralisation is assumed to be a circum-vertical plane running through the sample at some shallow angle, then the off-setting would be explained by the bottom section, for instance, having the higher measurements where the iron has precipitated out at that point a certain distance from the anode.

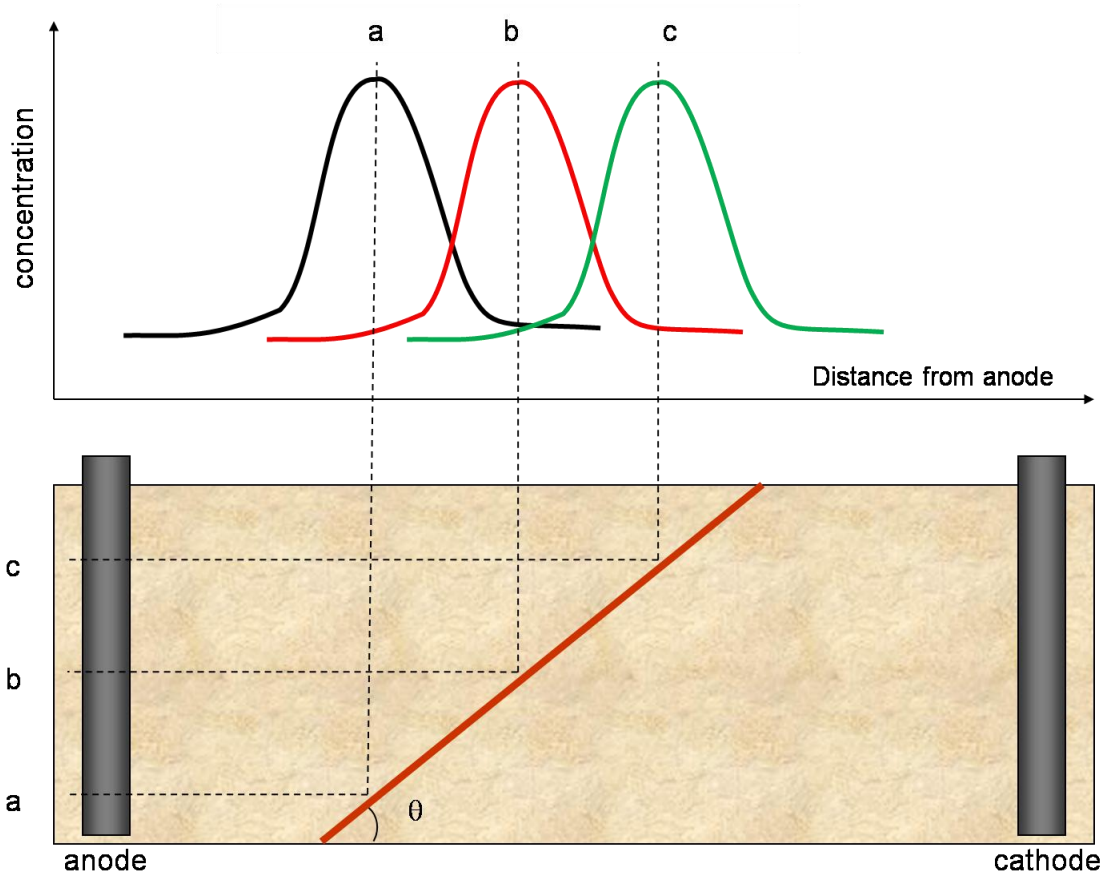


Figure 72: Diagram showing the way the iron mineralised region's orientation can give a shift in maximum concentration values with distance from the anode, for elements associated with the iron mineralised zone, with a longitudinal sampling protocol. a, b, and c represent the bottom, middle and top portions of the treatment area respectively.

Due to the slope of the iron precipitate the corresponding high value further up the soil profile will be found at a point further up the slope of the precipitated region, see Figure 72, where a, b and c represent samples from different depths. This model is assuming a uniform linear precipitate with the element in question being strongly associated with the iron-rich precipitate.

This demonstrates that the geometry and orientation of the iron mineralised region can affect the concentration distribution results obtained. However it is worth noting that the concentration shift generated by this model would give consistent shift in terms of the depth and direction of shift- this consistency is not observed for all elements in the data. A perfectly linear deposition is unlikely in practice and the actual mineralised regions observed in the various experiments conducted have tended to be either curved or quite irregular as seen in Section 3.

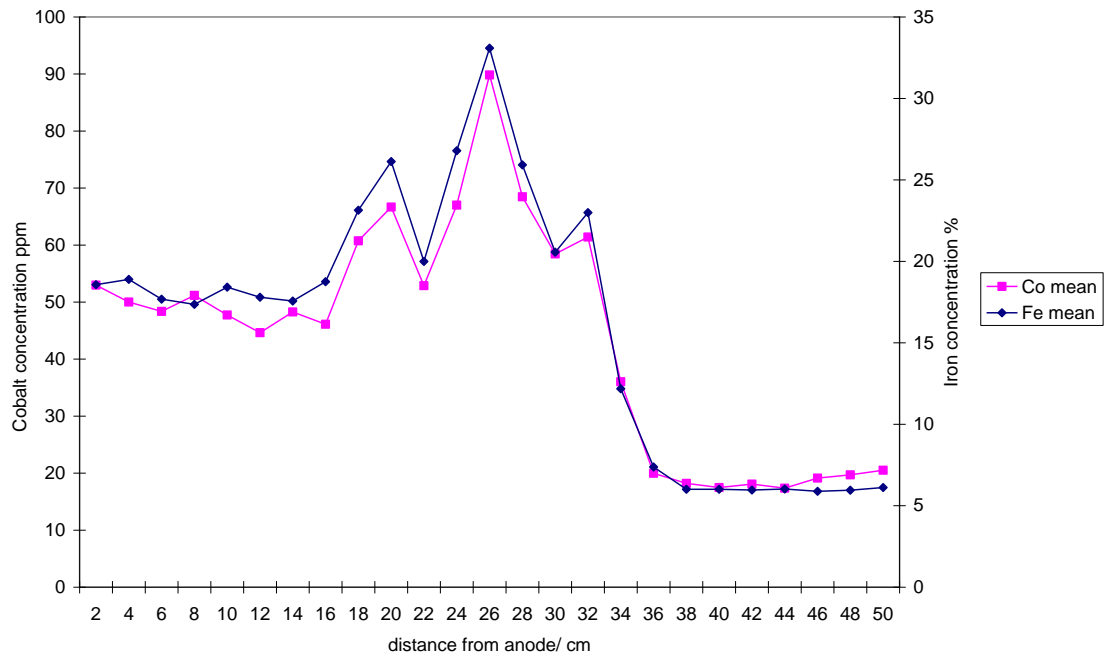


Figure 73: Combined graph of the concentration of Iron and cobalt across the cell with acetic acid influent.

Much better agreement between the iron mineralised zone and the concentration of certain elements is observed in the experiments conducted with acetic acid influent compared to that demonstrated by the tap water experiment, this is expected to be the case for elements which are coprecipitating with the iron and as predicted the acetic acid conditioning agent appears to enhance this effect. This is expected to be due to more effective mobilisation of these elements under the acidified conditions and a more localised region of pH jump.

Figure 74 illustrates how the geometry of a single and continuous iron mineralised fabric (with associated co-precipitation of the metal of interest) could theoretically give rise to a concentration distribution similar to that observed. This is not to say that this geometry was observed or expected, merely to demonstrate how iron band geometry might influence the observed concentrations of iron, and elements associated with the precipitation of iron, given that the treated material was sampled in sections longitudinally across the cell. A higher resolution three dimensional sampling strategy would remove any implied responses.

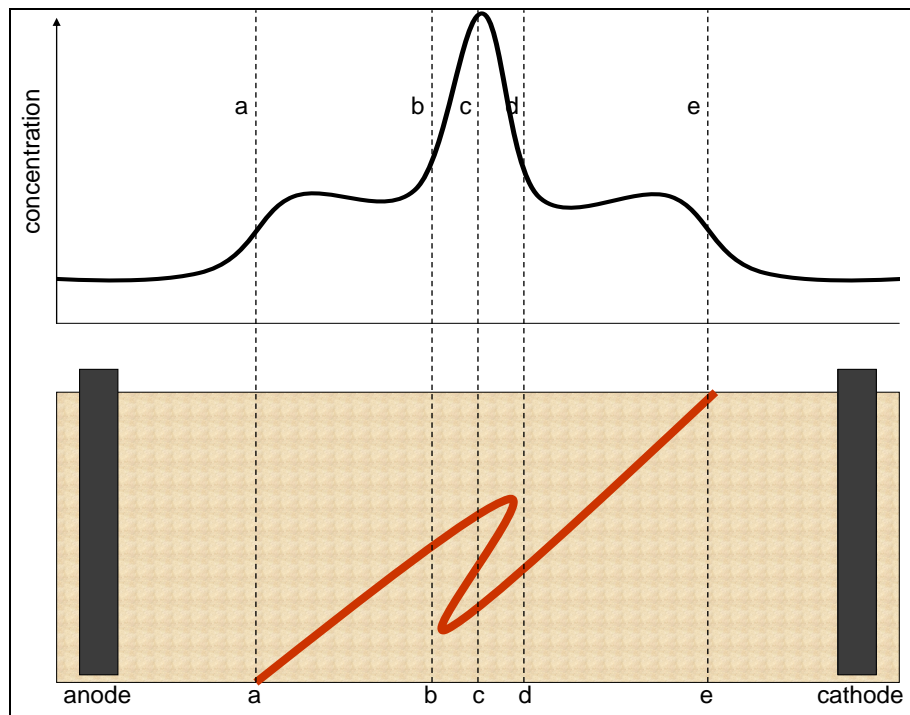


Figure 74: Diagram to describe a theoretical geometry of the precipitated iron region which would give a concentration distribution similar to that shown for the iron and arsenic results.

The iron mineralised boundary is a circum-vertical sigmoid shown in cross section thorough the treatment cell. The concentration curve is an approximation of what might be encountered in this situation. At distance (a) across the cell the mineralised region is first encountered giving a rise in the concentration for samples taken between this point and point (b). From point (b) to point (d) the geometry means that this section contains multiple mineralised regions and the measured concentrations rise further peaking in region (c). Continuing across the cell, symmetry makes points (d) and (e) equivalent to (a) and (b).

An alternative model would be that there is simply a non-uniform accumulation of the iron-rich precipitate in the treated material perhaps due to irregular composition of the material or to the existence of preferential flow paths generated as a result of electroosmosis or heterogeneity within the test material.

The overall enrichment on the anode side might indicate that at least some of the cobalt might have been introduced as an impurity in the anode material. Either that or some of the cobalt migrates past the region of primary iron precipitation, continuing into the

anode zone, the cobalt distribution is dealt with separately in, Section 5.4.8. Measurements taken at the start of the experiment gave pre-treatment values for iron of 5.03 percent, which is consistent with the cathode side values.

By mapping the iron distribution along with the other elements investigated the co-precipitation of expected elements can be assessed. There are certain metal ions which are often associated with iron in the environment, in particular: V, Mn, Ni, Cu, Zn, and Mo (e.g. Alloway and Ayres, 1997). However there is no discernable correlation observed for any of these elements and the region of maximum iron precipitation.

The distribution of these elements would be expected to match very closely the distribution of the iron precipitated region, which is in turn dictated by the location of the point of pH jump. For instance, if these metals are only present in significant concentrations within crystal matrices then there would be little or no movement expected.

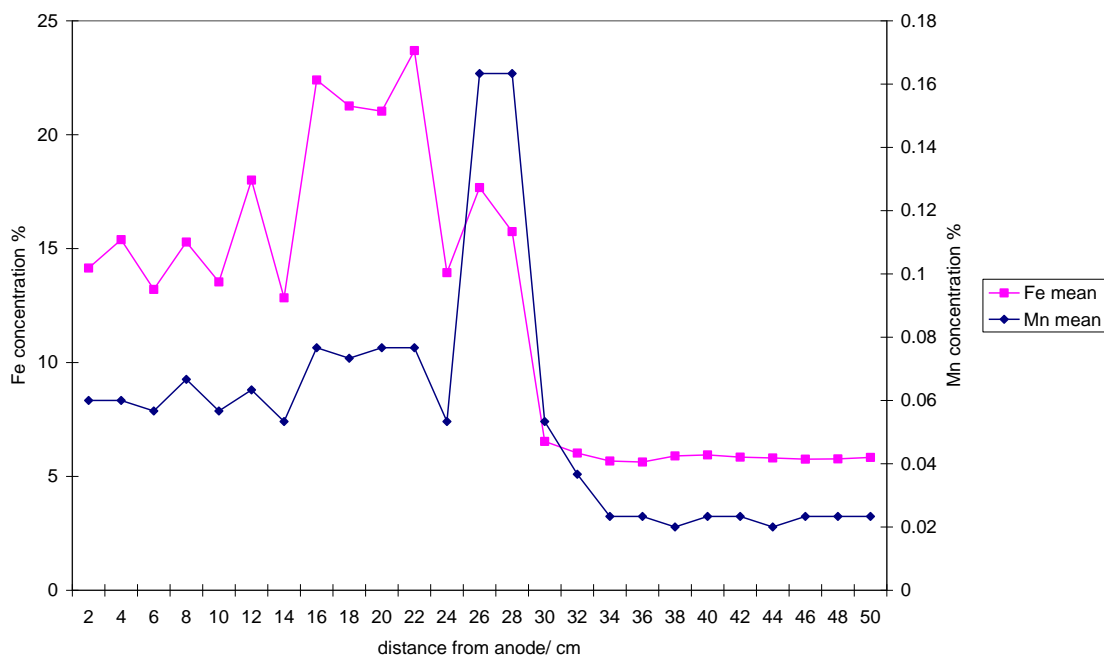


Figure 75: manganese and iron tap water values for the mean of the three depths at each distance from the anode.

There is an increased concentration of manganese at the anode side (0.05 – 0.07 % wt) and much lower concentrations on the cathode side (0.02% wt) since manganese in the sediment at the start of the experiment would be expected to become depleted in the

anode area and show a peak at the area of iron rich precipitate. The starting concentration of manganese averages 0.02 % so this does seem to indicate that manganese has been introduced to the anode zone.

This indicates that the manganese present in the sediment is being introduced from the anode electrode, the iron used can be expected to contain up to 1% manganese, Appendix 1. The manganese would be expected to precipitate out somewhat closer to the cathode than the iron; due to its slightly greater oxidising requirement to drop out of solution.

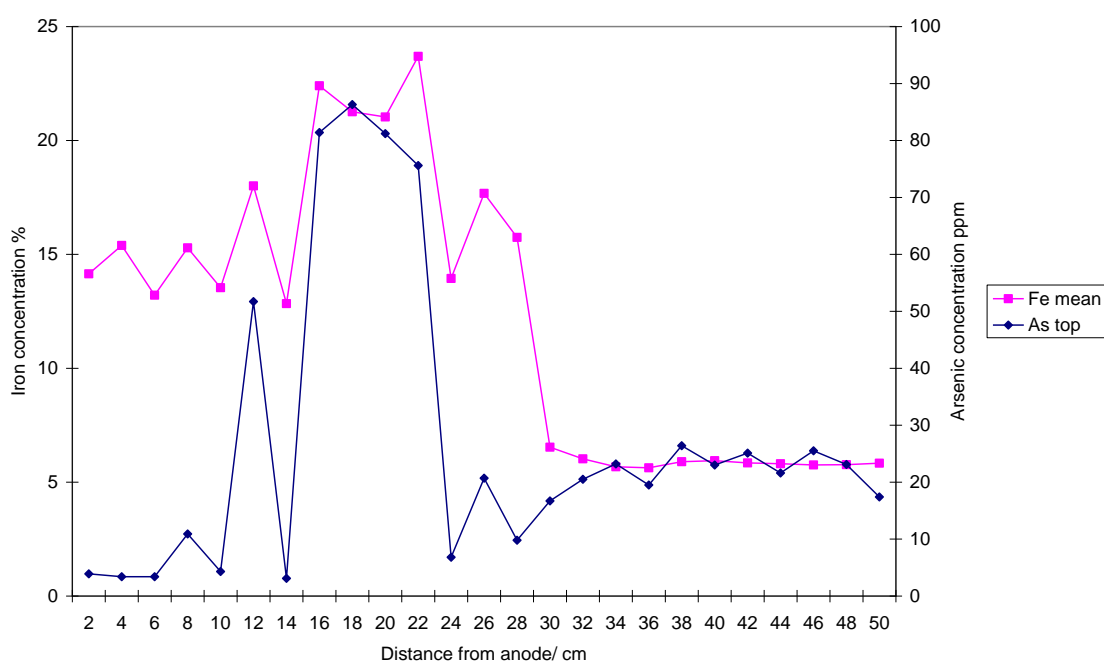


Figure 76: Arsenic and iron: tap water influent and the arsenic concentration for the top section of the treated material and the mean iron concentration. Data plotted on separate axes for concentration, and a shared axis for the distance from the anode.

The iron does seem to show some correlation with other species which may be present, for instance with arsenic, Figure 76. The regions of maximum concentrations of both species are in the 10 to 25 cm from anode region. Arsenic in the environment exists in a number of oxidation states and in a variety of complexes (e.g. Hartley *et al.*, 2004; Pendergrass and Butcher, 2006). And there is an abundance of literature associated with utilising iron containing compounds to remove arsenic from soils and particularly from groundwater (e.g. Meng *et al.*, 2001; Mulligan *et al.*, 2001; Meng *et al.*, 2002; Smedley and Kinniburgh, 2002; Smedley *et al.*, 2002; Warren *et al.*, 2003; Hartley *et*

al., 2004; Kumar *et al.*, 2004; Leupin and Hug, 2005; Mohan and Pittman, 2007; Yuan and Chiang, 2007).

Figure 76 shows the correlation between the iron concentration and the arsenic concentration. The concentration of the arsenic is apparently depleted in the anode zone (0-10 cm) to less than 5ppm whilst in the iron enriched region the maximum recorded value is over 80 ppm. The cathode zone values are consistently around 20 ppm, in the anode zone (0-10 cm from anode) enriching the 10-26 cm from anode region and leaving the remaining treatment area as was.

This shows a valid remediation scenario on this scale for this element. Although the effective treatment area as a percentage of the whole (~20%) is not as high as would be desirable and the enriched region is ~36% leaving the remainder unchanged in concentration relative to the starting concentration.

A Spearman rank correlation coefficient was calculated for each of the elements of interest to see which are statistically significantly correlated with the iron. This test was chosen due to the non-normal distribution of the data, where other correlation tests are not applicable. The results of this are shown in, Table 24. The results show that there is significant correlation for a number of elements, including negative correlations.

Table 24: Calculated ‘r’ values for Spearman's rank correlation coefficient for selected elements to indicate a correlation with the iron comparing mean values. The shaded values indicate a correlation at the 5% significance level. n=25 critical value= 0.337

	As	Br	Ca	Sr	Co	Mn	Cu	Zn	V	Zr	Ti
Tap water	0.025	0.669	-0.655	-0.848	0.910	0.910	0.802	-0.426	-0.751	-0.851	-0.828
Acetic	0.720	-0.070	0.232	0.072	0.610	0.634	-0.096	0.729	0.014	-0.626	-0.270

In both the acetic acid and the tap water experiments there are significant correlations between iron and cobalt and manganese. In the acetic acid experiment there is also significant correlation between iron and arsenic, and iron and zinc. In the tap water experiment there is significant positive correlation between iron and bromine and iron and copper. There is significant negative correlation between iron and calcium, strontium, zinc, vanadium, zirconium, and titanium in the tap water experiment. It is interesting to note that there is a significant positive correlation between iron and zinc in

the acetic acid experiment, and a significant negative correlation for the same elements in the tap water experiment. As expected from a visual inspection of the data, there are strong correlations indicated for manganese and cobalt in both the acetic acid influent and the tap water experiments.

A correlation matrix was also constructed using the Spearman's rank correlation coefficient test to look at correlations between all the elements of interest for the acetic acid and tap water experiments.

Table 25: Spearman's rank correlation coefficient matrices for elemental means in estuarine sediment for tap water and acetic acid experiments. Shaded values indicate significant correlation either negative (light grey) or positive (dark grey). 5% confidence interval, critical value = 0.337 n=25

Tap water	Fe	As	Br	Ca	Sr	Co	Mn	Cu	Zn	V	Zr	Ti
Fe		0.025	0.669	0.726	-0.848	0.910	0.910	0.802	-0.426	-0.751	-0.851	-0.828
As			-0.422	0.263	0.018	0.007	-0.074	0.033	-0.237	0.286	-0.039	0.023
Br				-0.831	-0.837	0.657	0.658	-0.732	-0.436	-0.848	-0.799	-0.809
Ca					0.885	-0.720	-0.529	0.722	0.431	0.856	0.828	0.809
Sr						-0.849	-0.751	0.867	0.556	0.843	0.948	0.936
Co							0.862	-0.858	-0.435	-0.808	-0.875	-0.877
Mn								-0.756	-0.381	-0.711	-0.792	-0.775
Cu									0.606	0.737	0.861	0.849
Zn										0.532	0.548	0.572
V											0.857	0.871
Zr												0.947
Ti												

Acetic acid	Fe	As	Br	Ca	Sr	Co	Mn	Cu	Zn	V	Zr	Ti
Fe		0.720	-0.070	0.232	0.072	0.610	0.634	-0.096	0.729	0.014	-0.626	-0.270
As			-0.404	0.462	0.385	0.276	0.333	-0.166	0.545	0.326	-0.362	0.032
Br				-0.831	-0.931	0.585	0.522	-0.056	-0.225	-0.907	-0.547	-0.835
Ca					0.938	-0.278	-0.181	0.046	0.333	0.807	0.239	0.587
Sr						-0.504	-0.414	0.045	0.268	0.915	0.457	0.756
Co							0.923	0.030	0.406	-0.609	-0.885	-0.833
Mn								-0.131	0.434	-0.542	-0.920	-0.750
Cu									-0.199	-0.012	0.258	-0.116
Zn										0.262	-0.389	-0.031
V											0.557	0.843
Zr												0.773
Ti												

5.6 Metals Analysis for Estuarine Sediment Subjected to a Hydraulic Gradient.

The barrier to groundwater flow experiment using the same Hythe estuarine sediment was sampled and analysed for the same elements as used in the remediation experiments using the same technique (XRF). This allowed the effect of a dynamic groundwater flow on the efficacy of the remediation to be considered. The experimental set-up was

not however identical; the electrodes were spaced at 30 cm rather than 50cm in the remediation experiments. This was due to the reduced capacity of the treatment cell due to the inflow/outflow apparatus, installed in the test tanks.

The details of the experimental set up for the hydraulic gradient experiments are given in Section 4.2. The sampling of the treated material was conducted as for the remediation experiments, that being in 2 cm sections between the electrodes divided into top, middle and bottom thirds vertically. The water influent was flowing from cathode to anode.

The elements which show a response to the electrokinetic treatment are shown below, the elements analysed but which show no result, or have measurement uncertainty too high for meaningful interpretation are included in the appendix for completeness

5.6.1 Iron Data Hydraulic Head Experiment

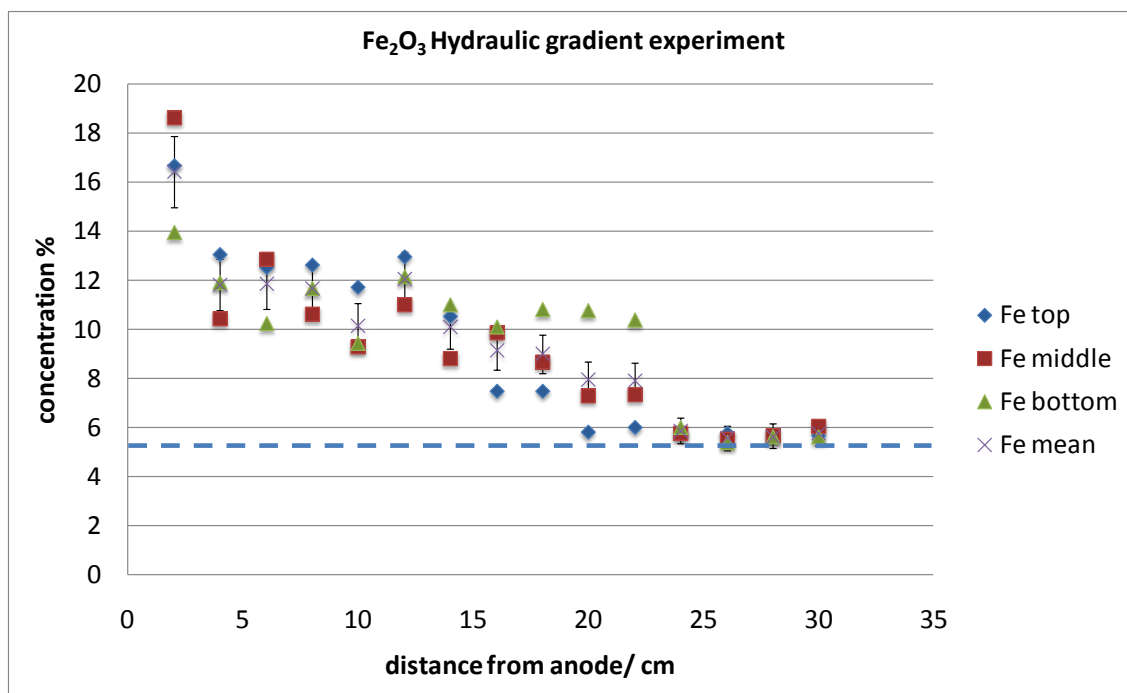


Figure 77: Fe concentration distribution post-treatment in the hydraulic gradient experiment. Dashed line indicates the average starting concentration, table 22. Error bars derived from table 19.

The iron distribution does not show the peak seen in previous experiments, there is a clear enrichment of the anode zone with the measurements taken from the cathode zone showing base-line concentration measurements similar to the pre-treatment levels. Observationally the iron enriched region formed close to the anodes as the graph suggests, (Figure 77), at between 2 and 4 cm from the anode electrodes. Given that there is not a more typical peak in the iron content this might affect the interpretation of the distribution of other elements which have been seen to be associated with the precipitation of the iron. There is obvious enrichment in iron concentration on the anode side from the electro-dissolution of the anode electrodes, despite the hydraulic head.

5.6.2 Arsenic Hydraulic Head Experiment

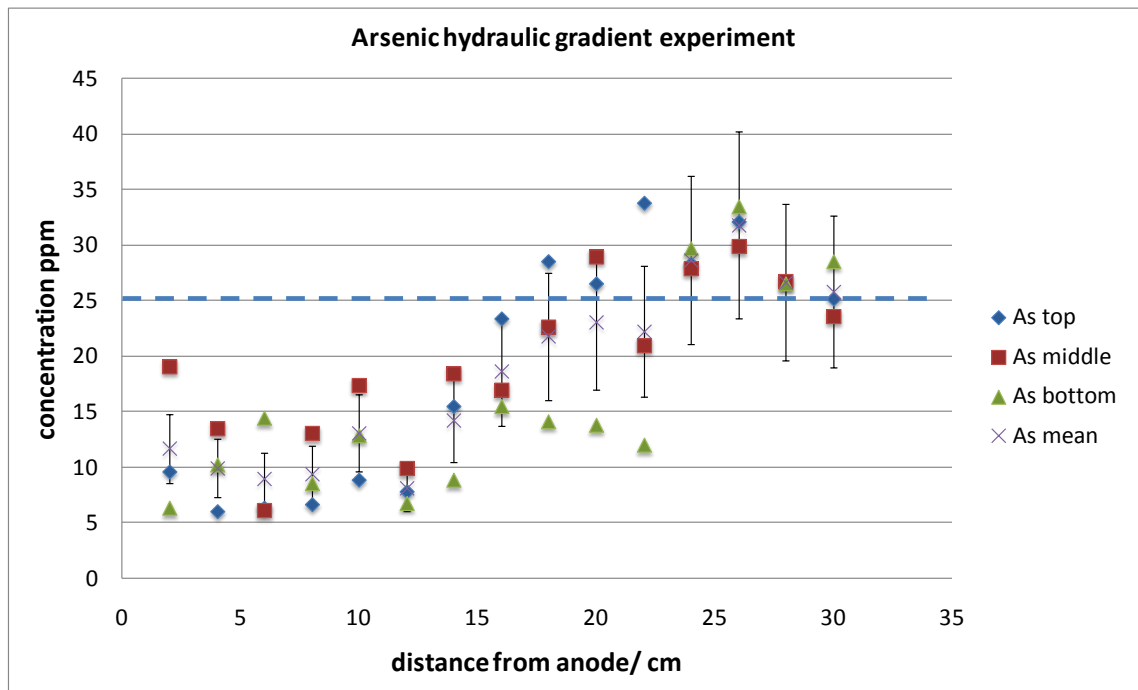


Figure 78: As concentration distribution post treatment in the hydraulic gradient experiment. Dashed line indicates the average starting concentration, table 22. Error bars derived from table 19.

The arsenic seems to have been influenced more by the hydraulic flow than some of the other elements studied, Figure 78. The concentration distributions in the other experiments showed a strong correlation between the arsenic concentration and the iron concentration.

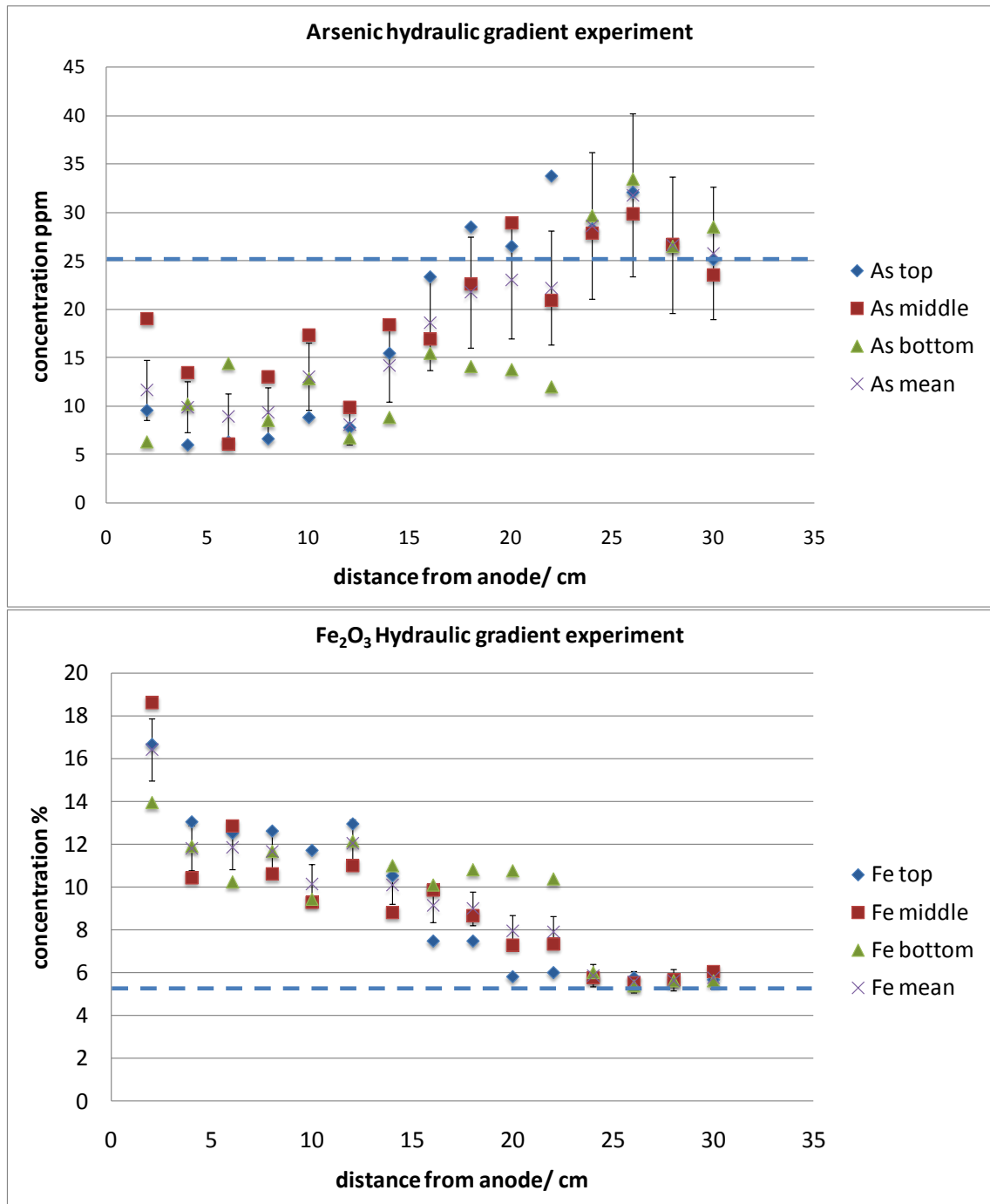


Figure 79: Arsenic and iron concentrations post experiment in the hydraulic head experiments.

The speciation of the arsenic in the sediment then is likely to be either in the form of a micelle or suspended in the pore water within the sediment as a neutral species or complex.

5.6.3 Bromine Hydraulic Head Experiment

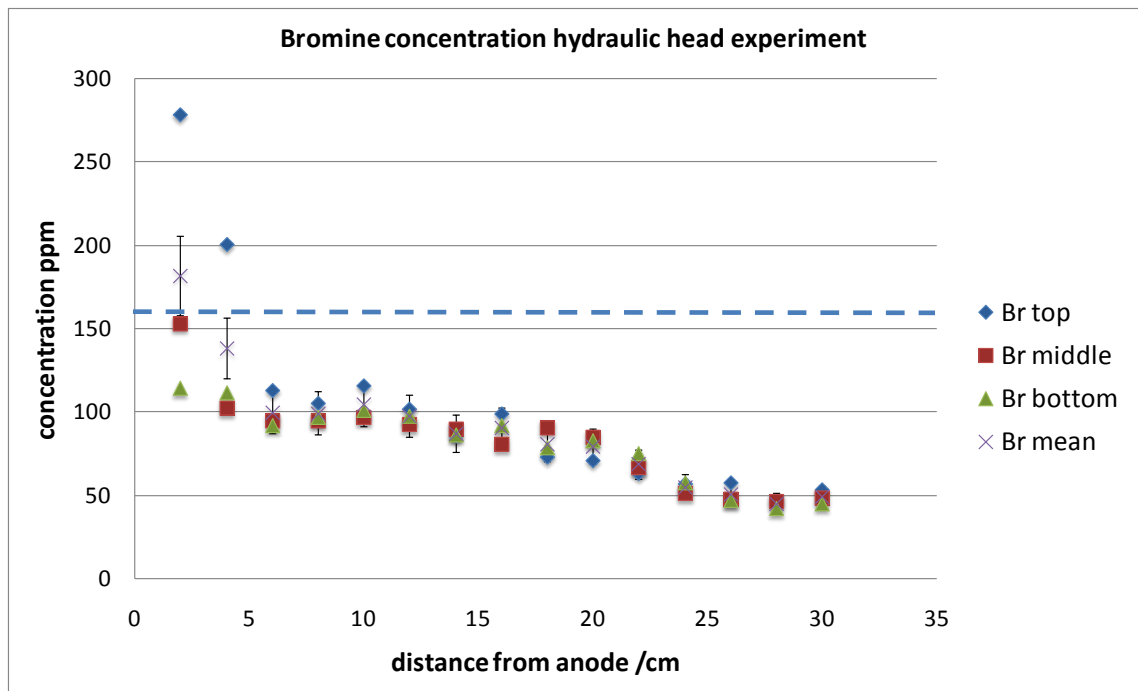


Figure 80: Br concentration distribution post treatment in the hydraulic gradient experiment. Dashed line indicates the average starting concentration, table 22. Error bars derived from table 19.

Bromine has again shown the response observed in the other experiments, Figure 80. It is noteworthy that as an anion, it is travelling against the flow direction relatively unhindered. This demonstrates that the distributions observed in the other experiments are confirmed with a comparable distribution in this experiment. The average starting concentration of bromine was 159.4 ppm pre-treatment, so there is a demonstrated depletion and enrichment taking place.

There appears to be a depth dependent response at the region closest to the anode with the highest values recorded for the top section of the depth profile. The values for the

samples taken on the cathode side are closely grouped with relatively small associated errors. The anionic bromine has shown the effectiveness of the electrostatic attraction mode of electrokinetics overcoming a net movement of the pore fluid in the opposite direction.

5.6.4 Calcium Hydraulic Head Experiment

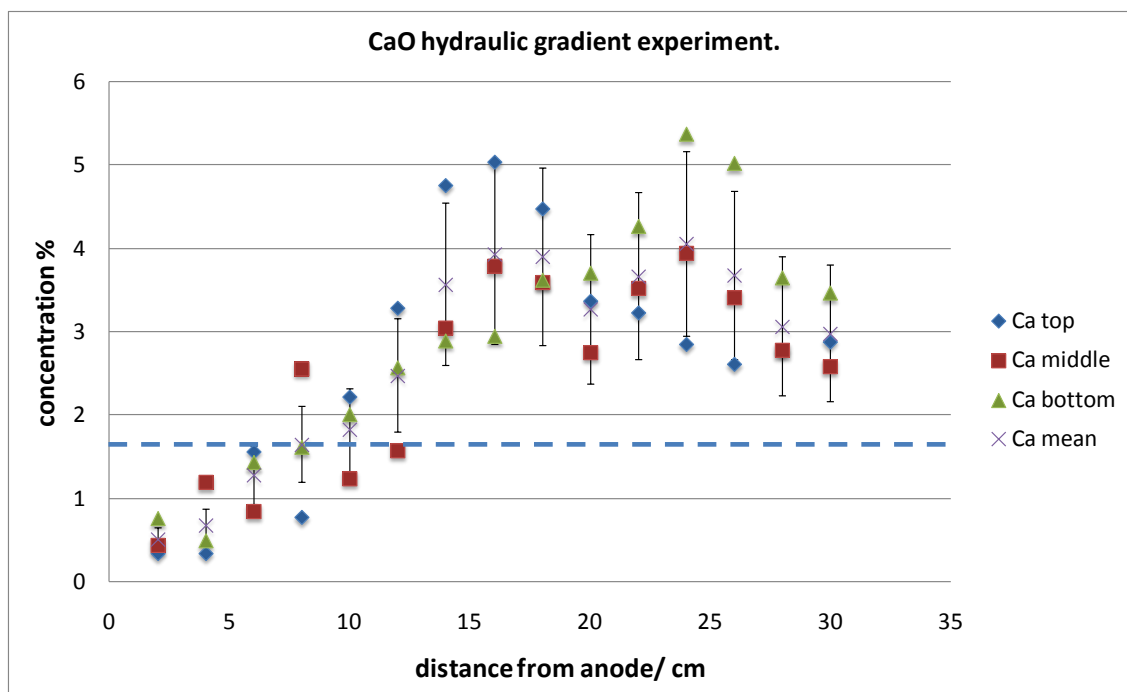


Figure 81: Ca concentration distribution post treatment in the hydraulic gradient experiment. Dashed line indicates the average starting concentration, table 22. Error bars derived from table 19.

Figure 81, shows the concentration distribution for calcium across the sediment. There is an unequivocal response to the treatment. The distribution shows a steady increase in concentration across the treatment area. The starting concentration was 1.618 % so there is also depletion in concentration in the anode zone. This is in spite of the fact that the experiments were conducted using tap-water in a hard-water area, so a certain amount of calcium would be expected to be introduced from the water supply. The calcium is also to be expected to be associated with the iron mineralised region, given the results of the previous experiments.

However this experiment did not produce the same continuous iron mineralised region observed in the previous experiments, thus there is a more generalised enrichment profile for this element, without the central peak seen in the static hydrology experiments. There does however appear to be a dissolution/re-precipitation of the calcium carbonate as previously observed.

5.6.5 Strontium Hydraulic Head Experiment

The strontium present, which as has been seen in the previous experiments, responds strongly to the treatment, shows a similarly strong response under a hydraulic gradient, Figure 82. There appears to be a more pronounced response in the middle and bottom thirds of the material. Theory predicts that the fluidic velocity would be greatest in the bottom and middle thirds (e.g. Figure 35, page 115). The mean starting concentration of strontium in the pre-treatment sediment was 101 ppm, so there can be seen a significant enrichment and depletion profile across the depths for this element.

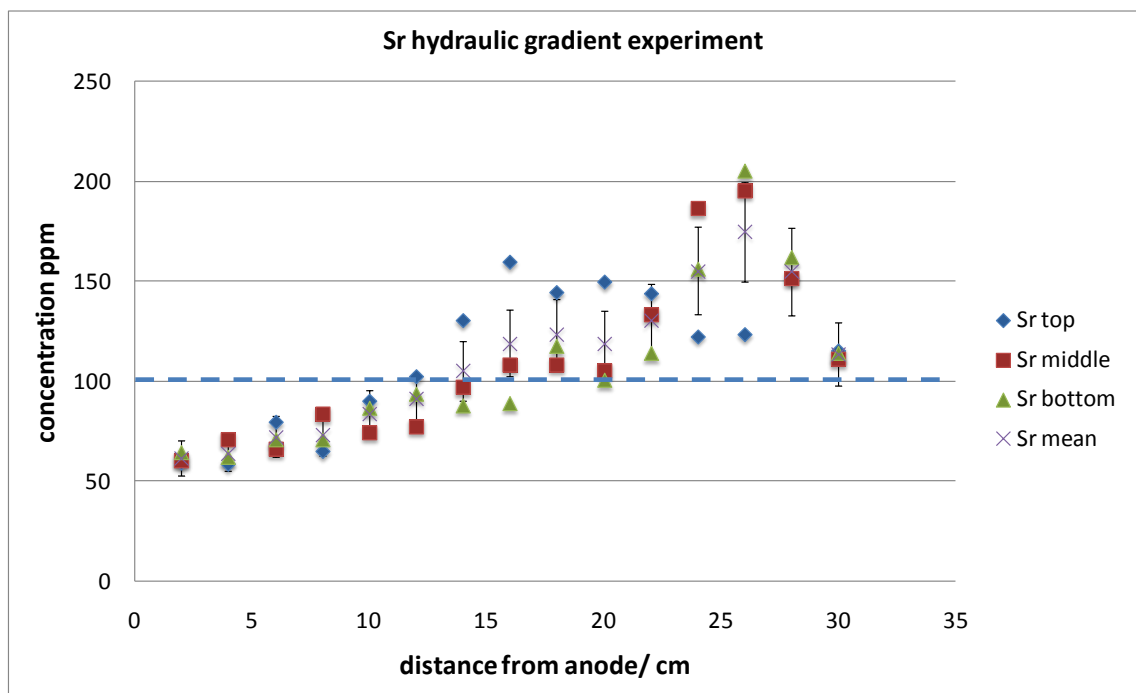


Figure 82: Sr concentration distribution post treatment in the hydraulic gradient experiment the dashed line indicates the mean pre-treatment concentration. Dashed line indicates the average starting concentration, table 22. Error bars derived from table 19.

There is a possible depth dependent shift in the concentration of strontium with the maximum concentration in the top layer at 15cm from the anode whereas the maximum concentration in the middle and bottom layers occurs at 27 cm from the anode. However as seen in the measurements of the iron concentration, there is no apparent distinct and localised region of iron enrichment such as was observed in the previously conducted experiments. So for this distribution to be contributable to an association with the iron then there would be a similar depth dependent distribution for the iron. This is further discredited by the fact that there has been no association between strontium and iron observed in the previous experiments. This would indicate that there is a depth dependent distribution independent of the iron but some other factor which is changing with depth such as redox conditions.

5.6.6 Cobalt Hydraulic Head Experiment

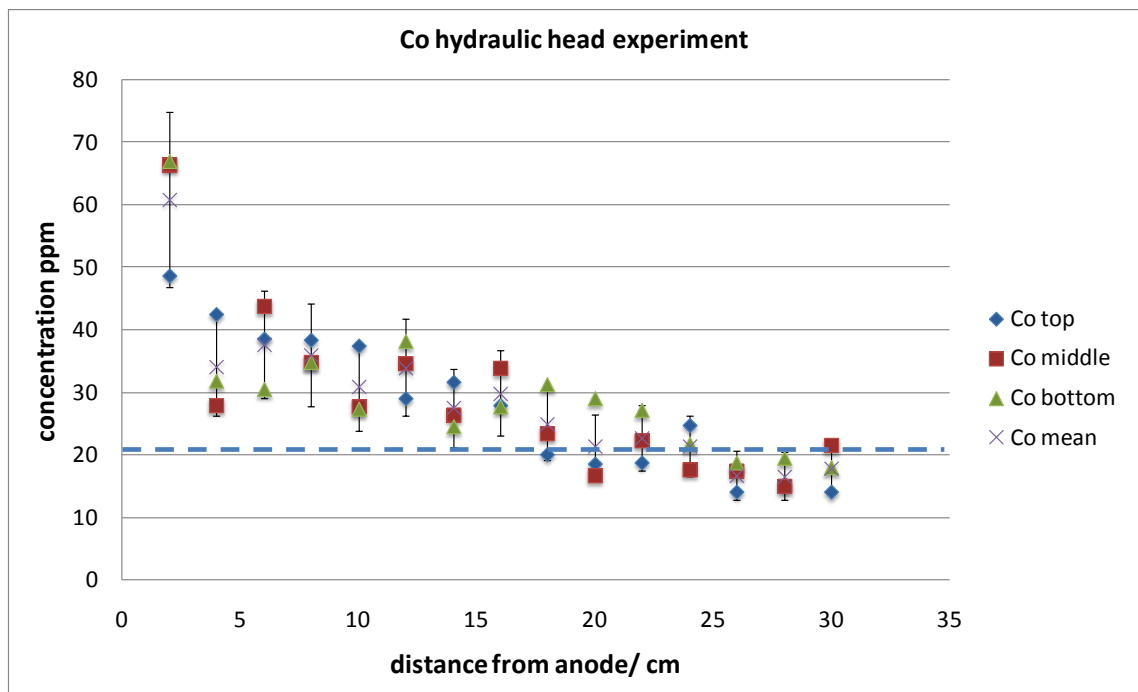


Figure 83: Co concentration distribution post treatment in the hydraulic gradient experiment. Dashed line indicates the average starting concentration, table 22. Error bars derived from table 19.

Figure 83 shows the cobalt concentration has a significant peak in concentration at the sample point 2 cm from the anode. There is a subtle enrichment in the direction of the anode but no association with the iron mineralised region. The cathode side is around the starting concentration of 20.4 ppm.

5.6.7 Manganese Hydraulic Head Experiment

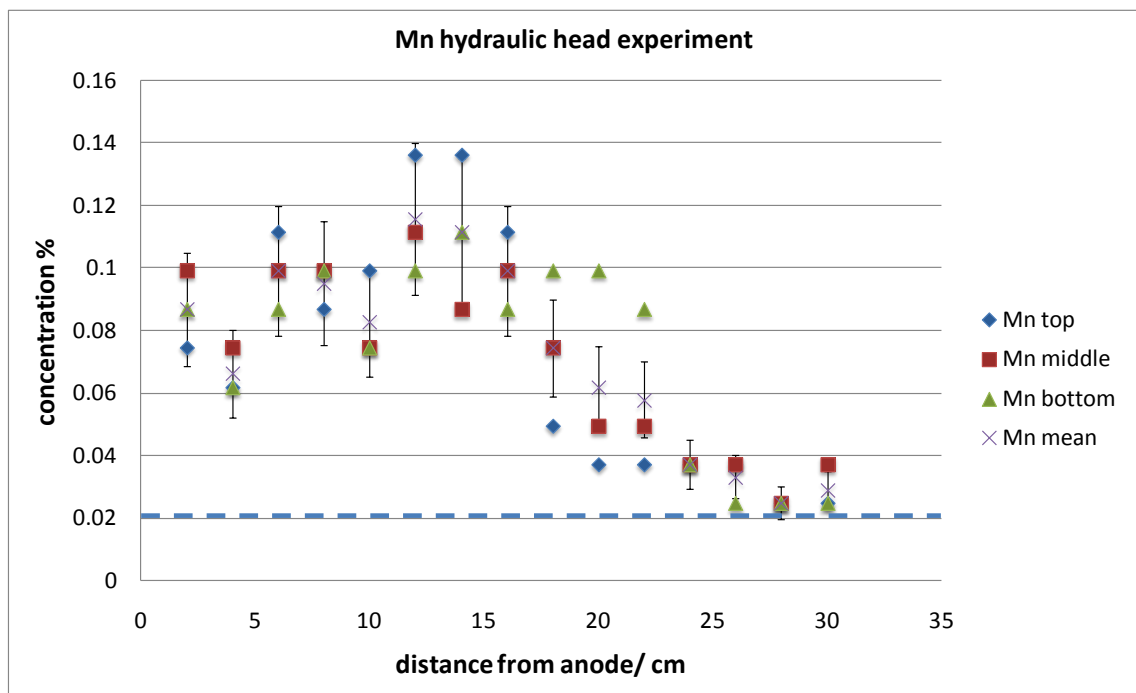


Figure 84: Mn concentration distribution post treatment in the hydraulic gradient experiment. Dashed line indicates the average starting concentration, table 22. Error bars derived from table 19.

The manganese shows a more familiar distribution with a discernable peak approximately half way between the electrodes, Figure 84. The measurements close to the cathode electrodes are at the starting concentration of 0.02 %. As recorded in the previously conducted experiments there appears to be significant manganese introduced from the anode electrode. This is evidenced by the starting concentration (0.02 %)

remaining at this level on the cathode side, with almost six times this concentration in the 12 to 15 cm from anode region.

5.6.8 Copper Hydraulic Head Experiment

Figure 85, shows the copper data. Interestingly the distribution is quite different to that seen in the static experiments. Overall the concentrations of copper across the treated material are higher than in the other experiments and are also higher than the average starting concentration which was found to be 61.44 ppm. It is conceivable that there is some introduction of copper to the material (a short length of copper tubing formed part of the test cell apparatus). However it is unlikely that this would provide such a rise in concentration.

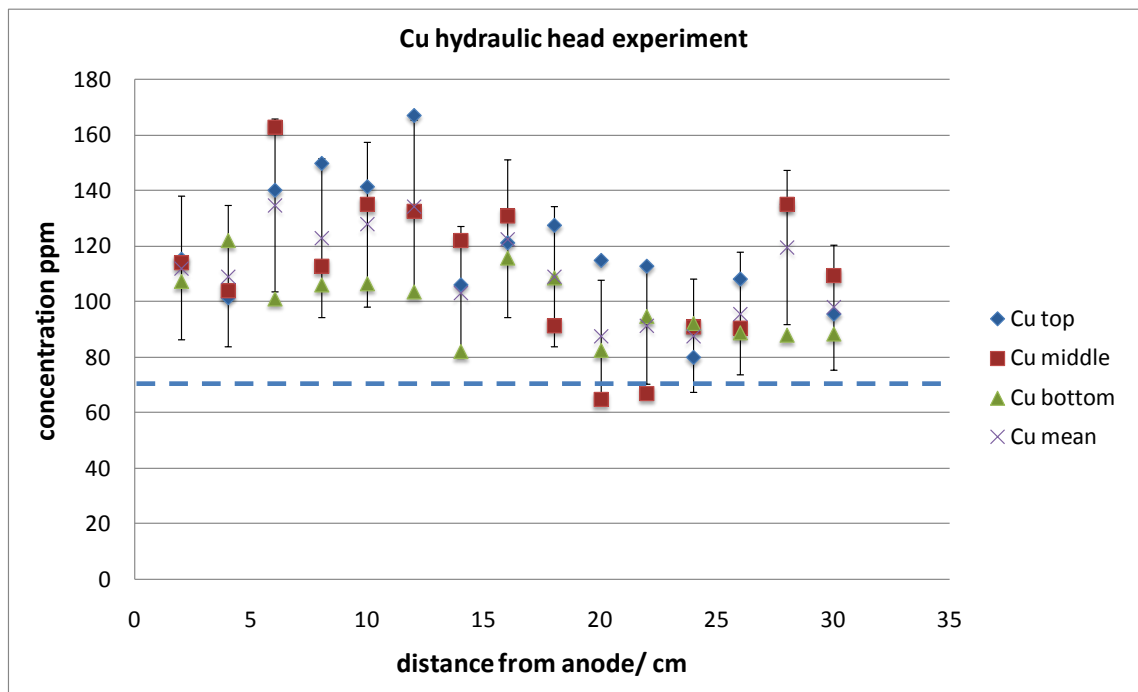


Figure 85: Cu concentration distribution post treatment in the hydraulic gradient experiment. Dashed line indicates the average starting concentration, table 22. Error bars derived from table 19.

There is a possible indication of enrichment on the anode side versus depletion on the cathode side. This is a minimal response compared to that seen in earlier experiments.

5.6.9 Zinc Hydraulic Head Experiment

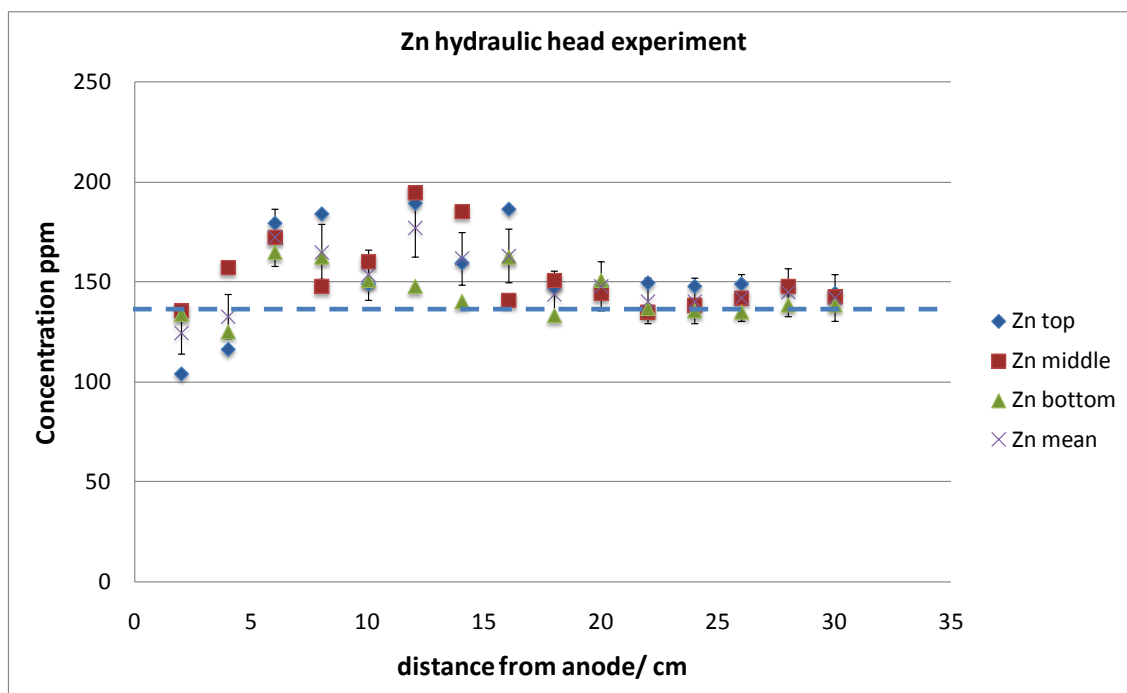


Figure 86: Zn concentration distribution post treatment in the hydraulic gradient experiment. Dashed line indicates the average starting concentration, table 22. Error bars derived from table 19.

The zinc present in the starting material shows a similar distribution to that observed for the lead and vanadium Figure 86. That being that there is a significant reduction in concentration close to the anode electrode. The average starting concentration for the zinc was found to be 137.14 ppm so the response limited but it does seem to have

affected the distribution in the treated material to a measurable extent, although not to the extent of being considered remediation.

5.6.10 Vanadium Hydraulic Head Experiment

Vanadium, Figure 87 appears to show a significant depletion in concentration in the section nearest to the anode for all depths. This was similarly observed in the previous experiments, the acetic acid treated experiments in particular. It is likely that this region of maximum acidity was required to mobilise the normally somewhat recalcitrant vanadium. There is considerable uncertainty for the vanadium measurements and significant geochemical heterogeneity. However, the starting concentration for vanadium of 75.32ppm indicates that there is no significant response to the treatment.

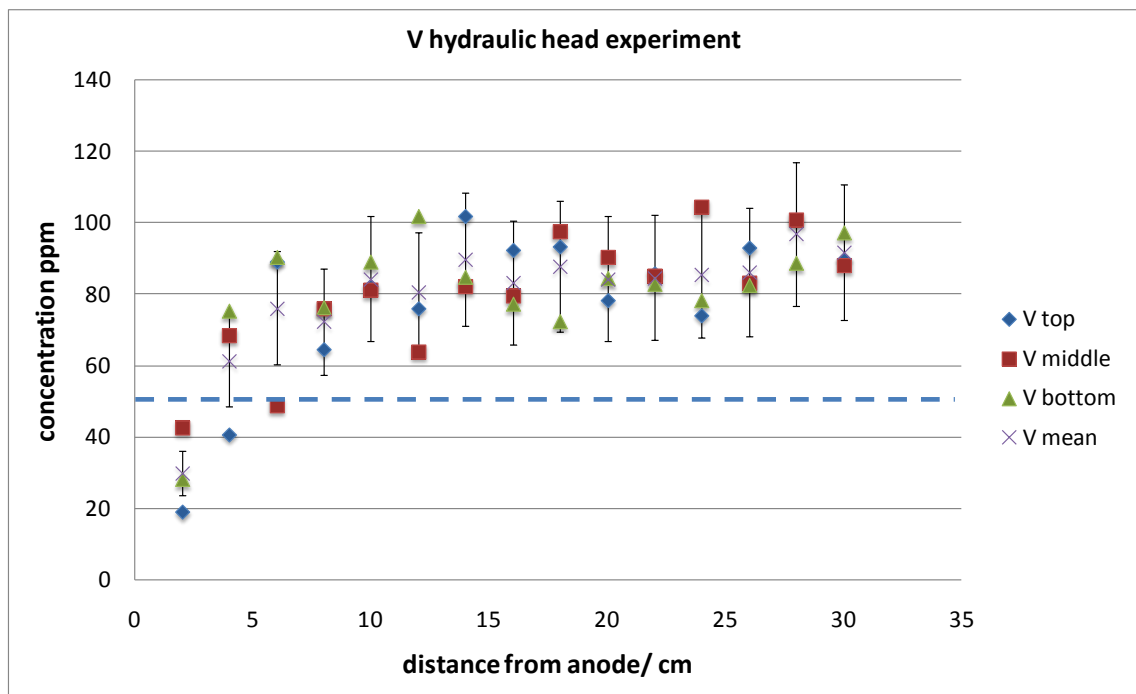


Figure 87: V concentration distribution post treatment in the hydraulic gradient experiment. Dashed line indicates the average starting concentration, table 22. Error bars derived from table 19.

5.6.11 Zirconium Hydraulic Head Experiment

Figure 88 shows the zirconium concentration to have a less pronounced response to the technique than that demonstrated in the previous experiments. The average starting concentration for the pre-treatment material was 191.2 ppm, so there could be a limited reduction at the anode side versus some enrichment towards the cathode although this is not confirmed by this data since the error bars and high starting concentration relative to the majority of the values obtained for this experiment. There is no apparent association with the iron mineralised region.

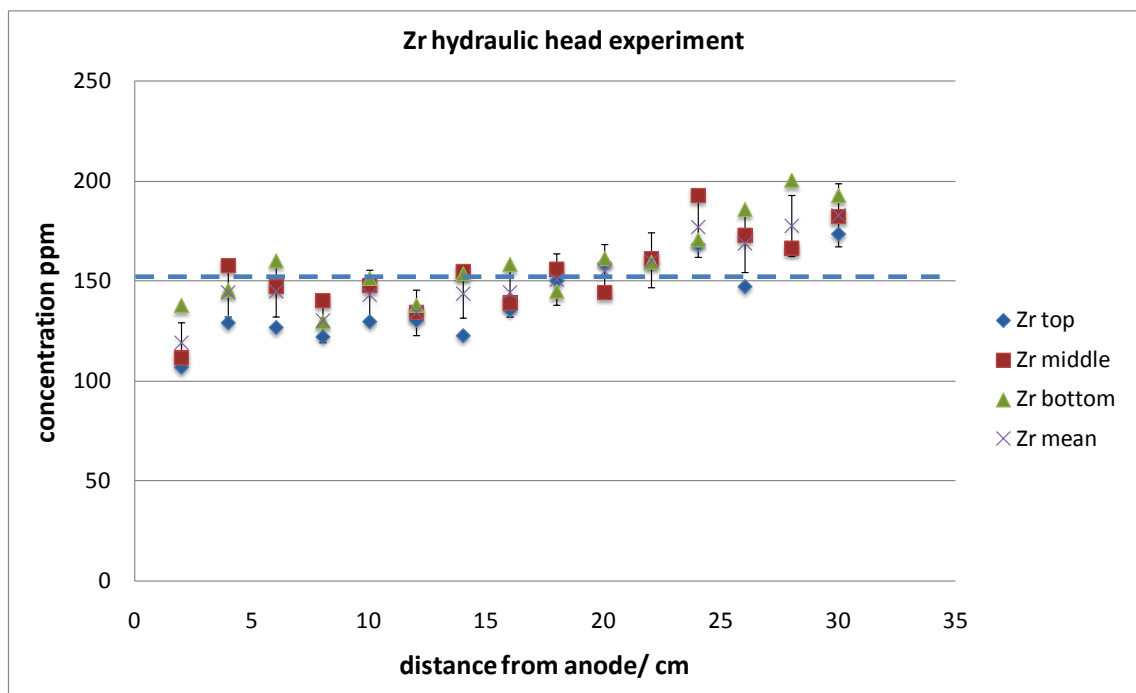


Figure 88: Zr concentration distribution post treatment in the hydraulic gradient experiment. Dashed line indicates the average starting concentration, table 22. Error bars derived from table 19.

The zirconium analysis shows a greatly reduced response to the electrokinetic process as compared to the static tap water experiment

5.6.12 Titanium Hydraulic Head Experiment

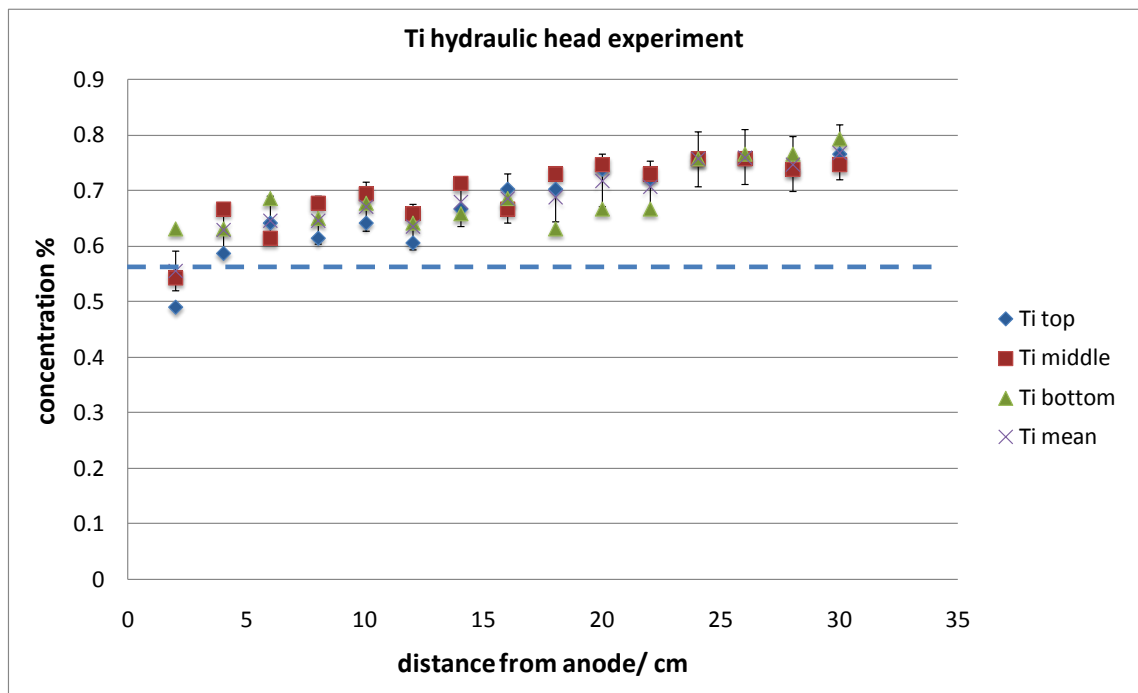


Figure 89: Ti concentration distribution post treatment in the hydraulic gradient experiment. Dashed line indicates the average starting concentration, table 22. Error bars derived from table 19.

Figure 89 shows the concentration distribution for titanium, with values between ~0.5 % and 0.8%. The starting concentration was found to be 0.628 % so no dramatic change in concentration across the material following the treatment. The data appears to display a slight trend in that the concentration increases steadily from anode to cathode.

5.7 Comparison of Applied Hydraulic Head and Static and Static Head Experiments with Tap Water Influent on Estuarine Sediment

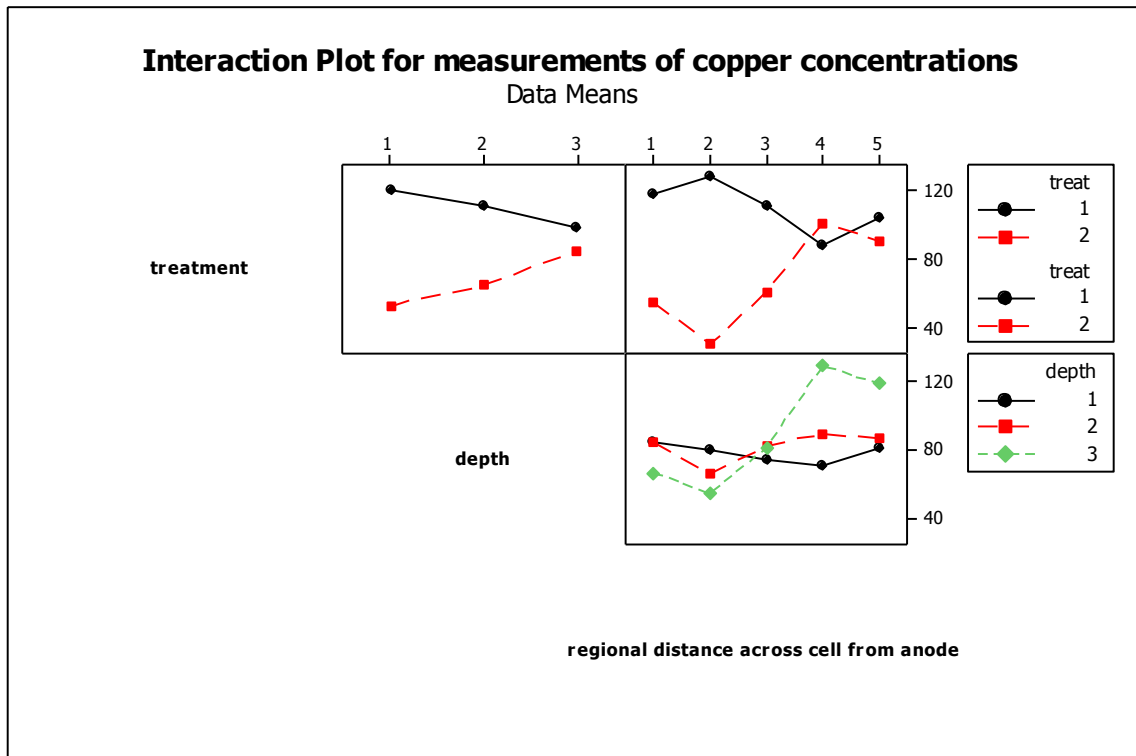
The experiments conducted with tap water on the estuarine sediment with no significant hydraulic gradient, and the experiment conducted with an imposed hydraulic gradient allow for the comparison of the metals response between the two. Because of the modification of the test tank to facilitate the generation of a controllable hydraulic gradient the hydraulic head experiment has the electrodes slightly closer together, Table 26 shows the comparison.

Table 26: experimental parameters for the two tap water experiments.

	Hydraulic head (hh)	No hydro head
Electrode separation	30 cm	50cm
Voltage	75V	75V
Electrolyte	Tap water	Tap water

The comparison is to evaluate any difference in the metals distribution due to the application of the hydraulic head.

The use of statistical analyses allows for the quantification of the likelihood that the results obtained would be obtained if there was or was not an interaction or association between the different factors i.e. between treatments (hydro head and no hydro head), between the different depths that were sampled and across the treated cells. The distance factor was simplified by the use of zoning where the total distance was divided into five regions and the concentrations of the samples in these zones were compared between treatments. Using this approach interaction plots were generated using Minitab[®] statistical software package.



This illustrates how the means of the values for the different variables interact in terms of: the depth of the samples, the treatment (hydraulic head or no hydraulic head), and the distance across the cell from the anode. Converging lines indicates that there is a significant interaction. Analysis of variance for the different variables were also carried out to look at whether there were statistically significant differences between these variables both within each experiment and also between the experiments at 95% confidence.

The following section compares the hydraulic head experiments with those conducted on with out the applied hydraulic head. The distances across the treated material have been normalised to allow the comparison between the two different electrode separations. Error bars are applied only to the mean concentrations for clarity. The abbreviations 'st' and 'hh' represent 'static head' and 'hydraulic head' respectively.

5.7.1 Iron

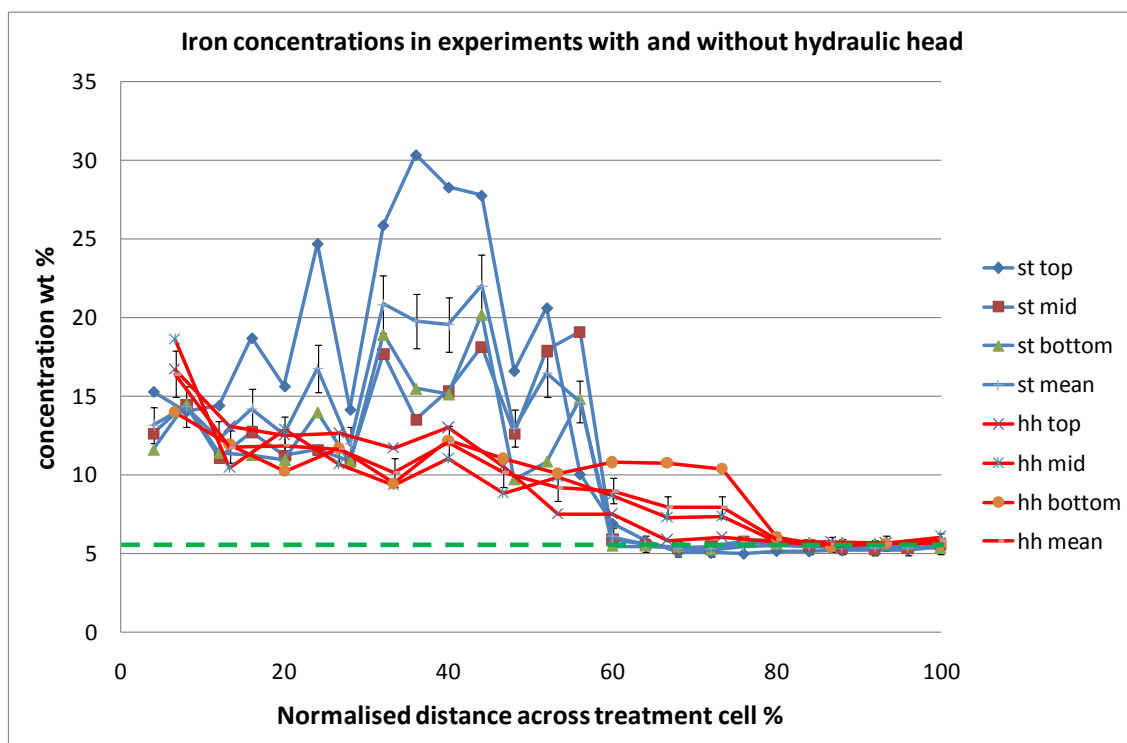


Figure 90: Iron concentration across the hydraulic head and static tap water experiments. Dashed line indicates the mean starting concentration, table 22. Error bars derived from table 19.

The iron concentration distribution for the hydraulic head experiment appears to show much less of an enrichment in a localised area compared to the static experiment Figure 90. Statistical analysis of the two data sets, head versus no head, indicates that this difference is significant at the 95% confidence interval. The iron accumulation/precipitation has been diffused by the action of the hydraulic gradient. There is no significant depth effect, but there is a significant distance (across the cell) effect.

5.7.2 Arsenic

The values obtained in the hydraulic head experiment show lower than starting values on the anode side yet no significant increase in concentration on the cathode side. This suggests that the concentration of arsenic was generally lower in this experiment. An alternative theory is that there may in fact have been some hydraulic ‘flushing’ whereby

the arsenic has been transported through the sediment and out the other side as a result of the movement of the pore water under the influence of the hydraulic gradient Figure 91, this might also have been the case with the bromine below.

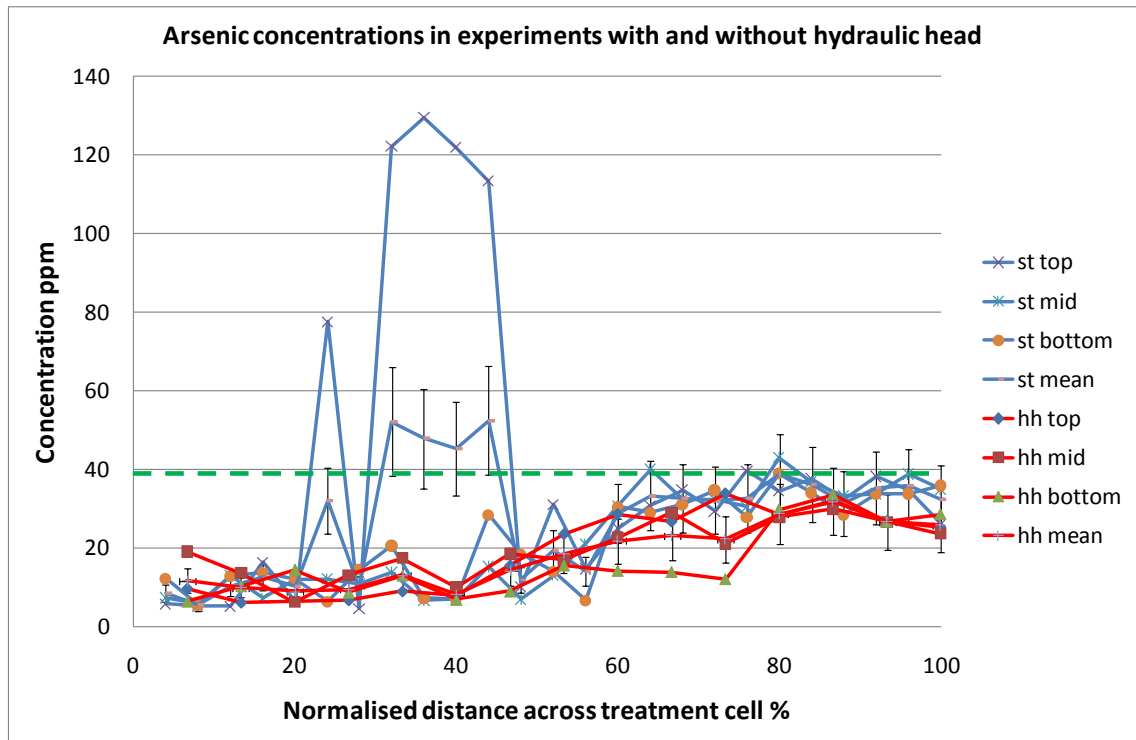


Figure 91: Arsenic concentration across the hydraulic head and static tap water experiments. Dashed line indicates the mean starting concentration, table 22. Error bars derived from table 19.

The data shows a significant depth/distance interaction and significant depth/treatment interaction as well as significant distance, depth, and treatment effects. Here the arsenic accumulation appears to be negatively affected by the application of a hydraulic head, resulting in a much less pronounced localised focusing.

5.7.3 Bromine

Shows a statistically significant difference in bromine response between the hydraulic head and the static conditions at 95% percent confidence interval. Statistically significant depth effect within treatments. But no correlation between the depths and treatments, Figure 92

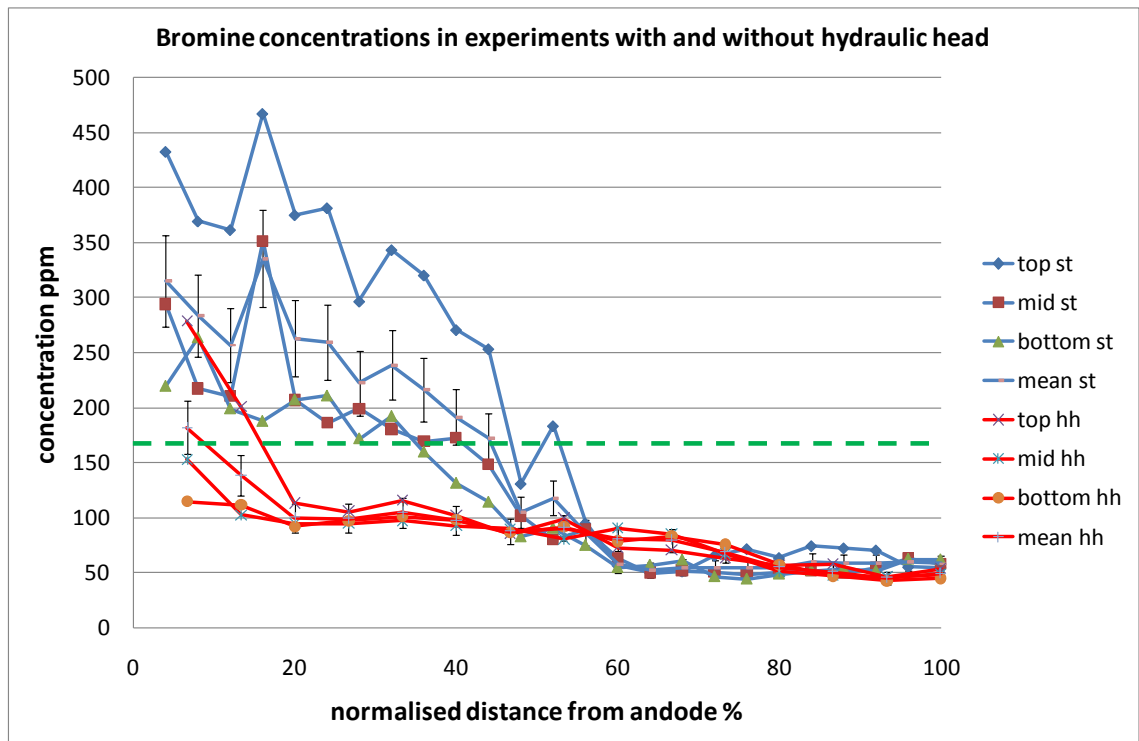


Figure 92: Bromine distribution in experiments conducted with and without hydraulic head. The dashed line represents the mean starting concentration, table 22. Error bars derived from table 19.

The bromine shows reduced enrichment at the anode. And the lower concentrations generally suggest that there may be some ‘flushing’ of the bromine out of the system by the action of the hydraulic gradient.

5.7.4 Calcium

Calcium and strontium show a comparable distribution or both sets of experiments, unsurprisingly due to their chemical similarity, Figure 93.

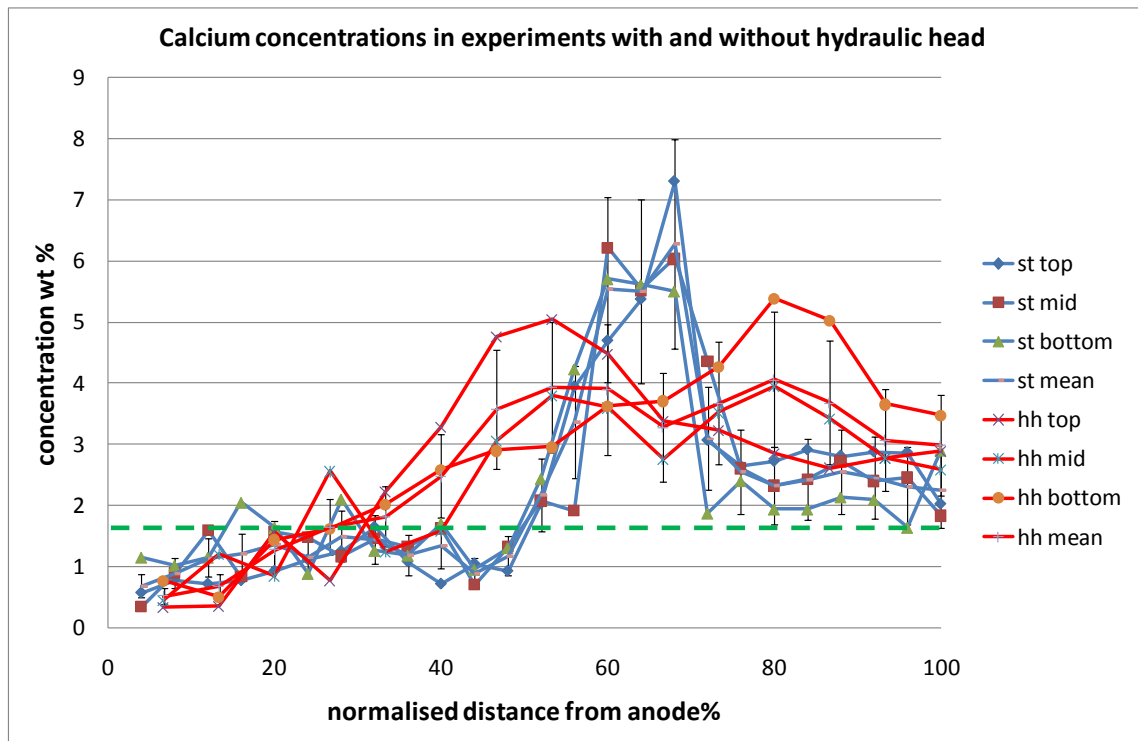


Figure 93: Calcium distribution in experiments conducted with and without hydraulic head. Green dashed line indicates mean pre-treatment concentration, table 22. Error bars derived from table 19.

Calcium shows no statistically significant difference between treatments with and without a hydraulic head. Although the graph suggests that there is a broader region of enrichment, it is not statistically significant at the 95% confidence interval. There is also no significant depth effect. This indicates that the application of the hydraulic head has not affected the movement and redistribution of the calcium in these experiments.

5.7.5 Strontium

Figure 94, shows the comparative concentrations of strontium across the material post treatment. The maximum concentrations of the strontium in the experiment conducted under an imposed hydraulic head are further into the cathode region than those for the experiment conducted under static conditions. This indicates that the hydraulic gradient offers no increased impediment to the migration of strontium ions (N.B. the tap-water is flowing from cathode to anode) and may also be affecting the development of the alkaline front causing the accelerated propagation of the alkali front.

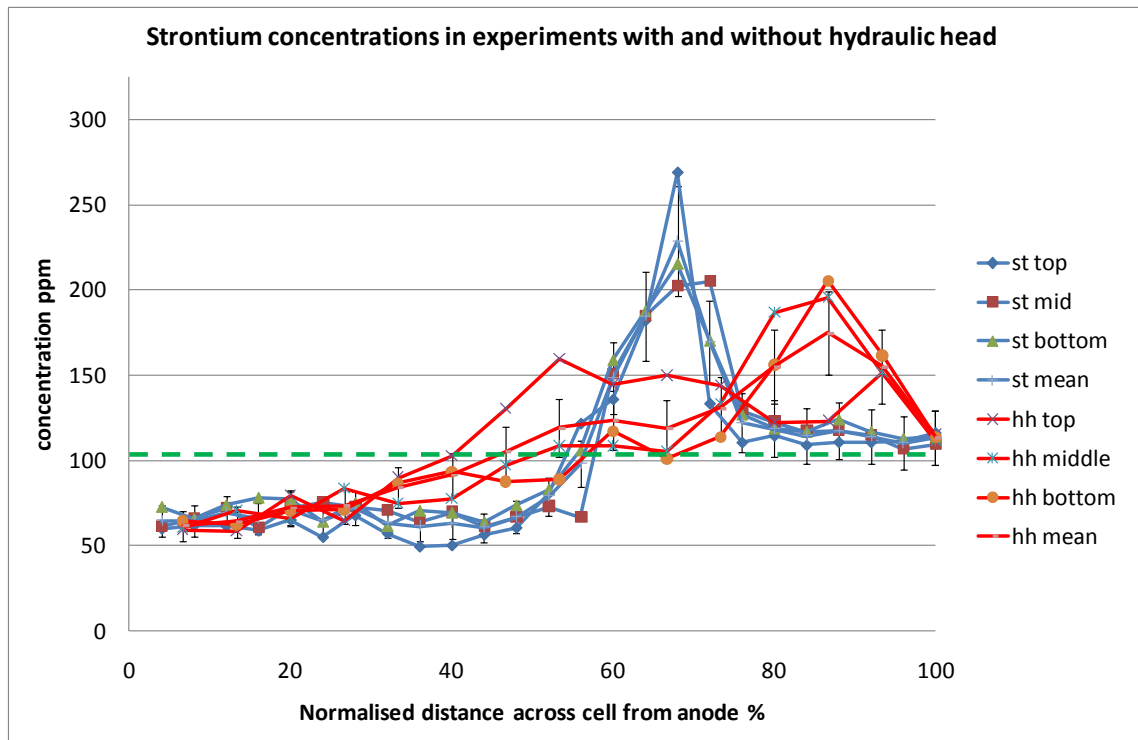


Figure 94: Strontium concentration across the hydraulic head and static tap water experiments. Dashed line indicates the mean starting concentration, table 22. Error bars derived from table 19.

Statistical analysis shows a significant treatment/distance interaction and a significant distance effect. Significant between treatments effect but no significant depth effect. So there is a statistically significant difference in the strontium distribution with and without an applied hydraulic head. However it is noteworthy that the highest concentration of strontium found in the hydraulic head experiments is further into the cathode zone than found in the static experiments, and this movement is acting against the direction of induced flow. This may be due to the dilution of the alkaline front due to the introduction of excess tap water allowing the strontium to remain mobile for a greater proportion of the distance between the electrodes.

5.7.6 Cobalt

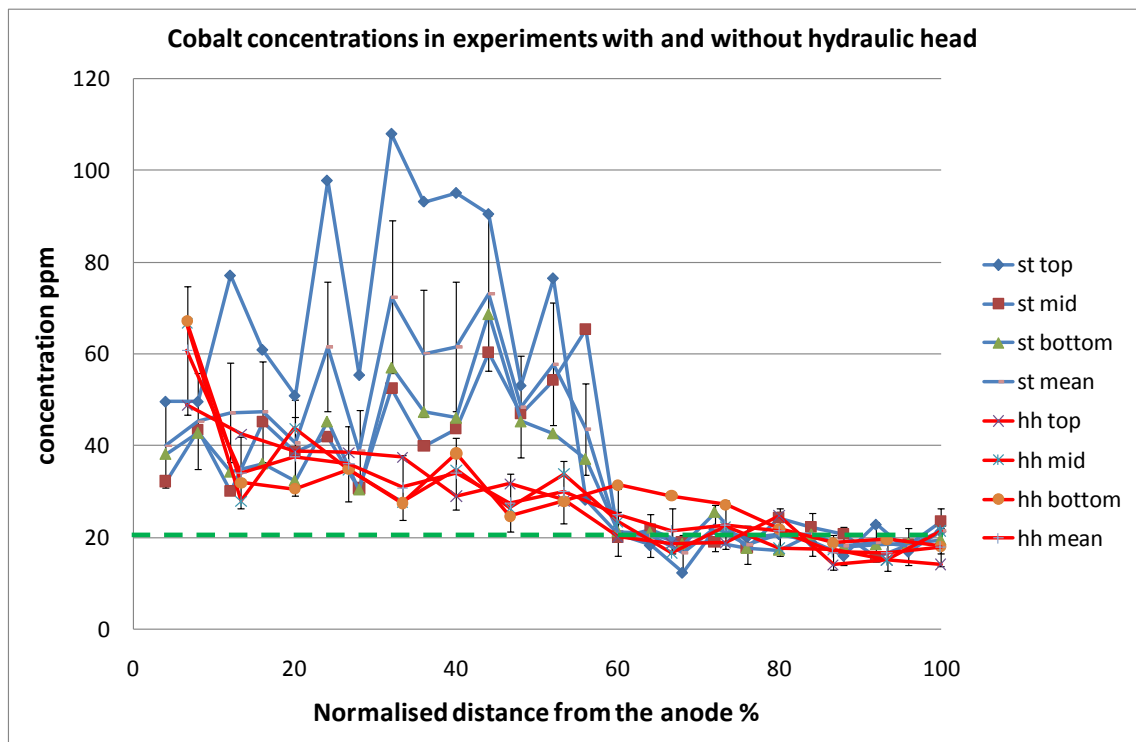


Figure 95: Cobalt distribution in experiments conducted with and without hydraulic head. Green dashed line indicates mean pre-treatment concentration, table 22. Error bars derived from table 19.

The graph indicates that the application of the hydraulic head to the material has an attenuating effect on the response of cobalt to the treatment, Figure 95. Statistical analysis shows no significant depth effects, and very significant difference in response between treatments (p value 0.009). Although both treatments result in enrichment towards the anode side, there is a statistically significant difference between them.

The concentrations found in both experiments on the cathode side remain at or close to the starting concentrations indicating that there is no mobilisation due to pore water flow for this element, the mobilisation only takes place in the acidified region. However, in order to achieve an overall enrichment then a reduction in concentration in another part of the cell would be expected.

5.7.7 Manganese

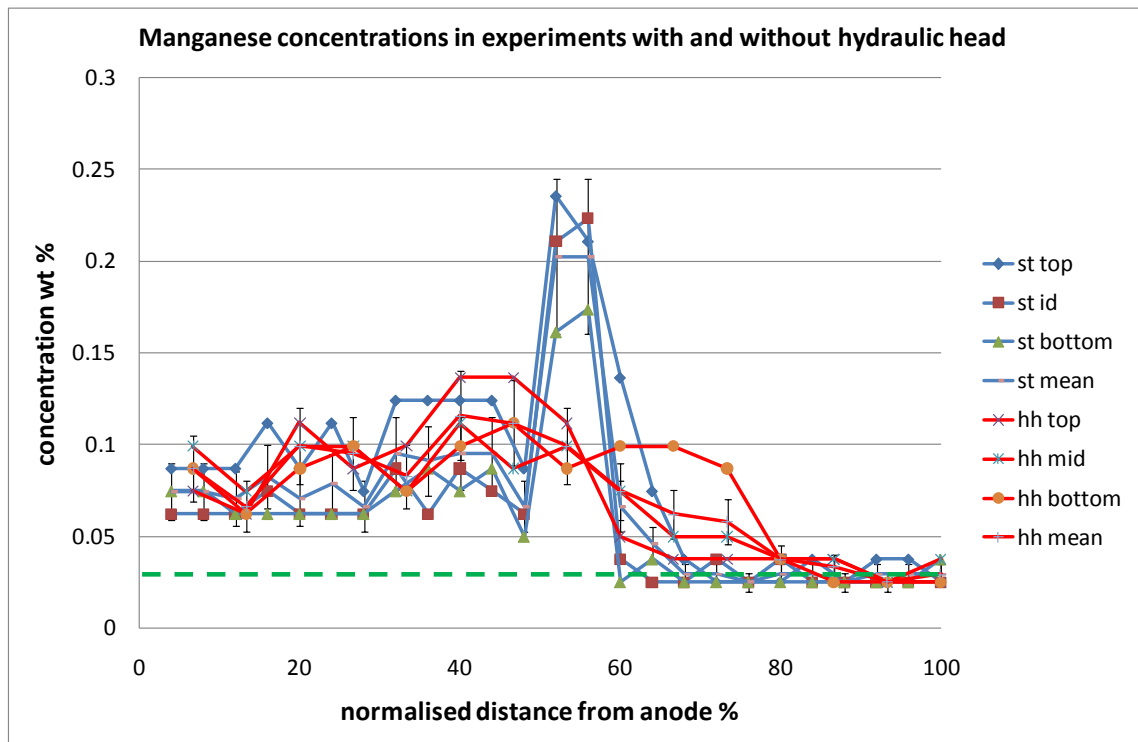


Figure 96: Manganese distribution in experiments conducted with and without hydraulic head. Green dashed line indicates mean pre-treatment concentration, table 22. Error bars derived from table 19.

The manganese concentration shows a significant difference between the two treatments and conspicuously does not show the localised concentration spike. There is no significant between depths effect. The effect of the hydraulic head again appears to diffuse the distribution profile encountered in the static head experiments. Once more the cathode side concentrations appear unchanged from the mean starting values, so for the enrichment that is shown to take place there should be a corresponding depletion. According to the model, the acid purge should reduce the concentration of this element up to a spike at the boundary zone where there is significant enrichment. Here the whole anode region is enriched.

5.7.8 Copper

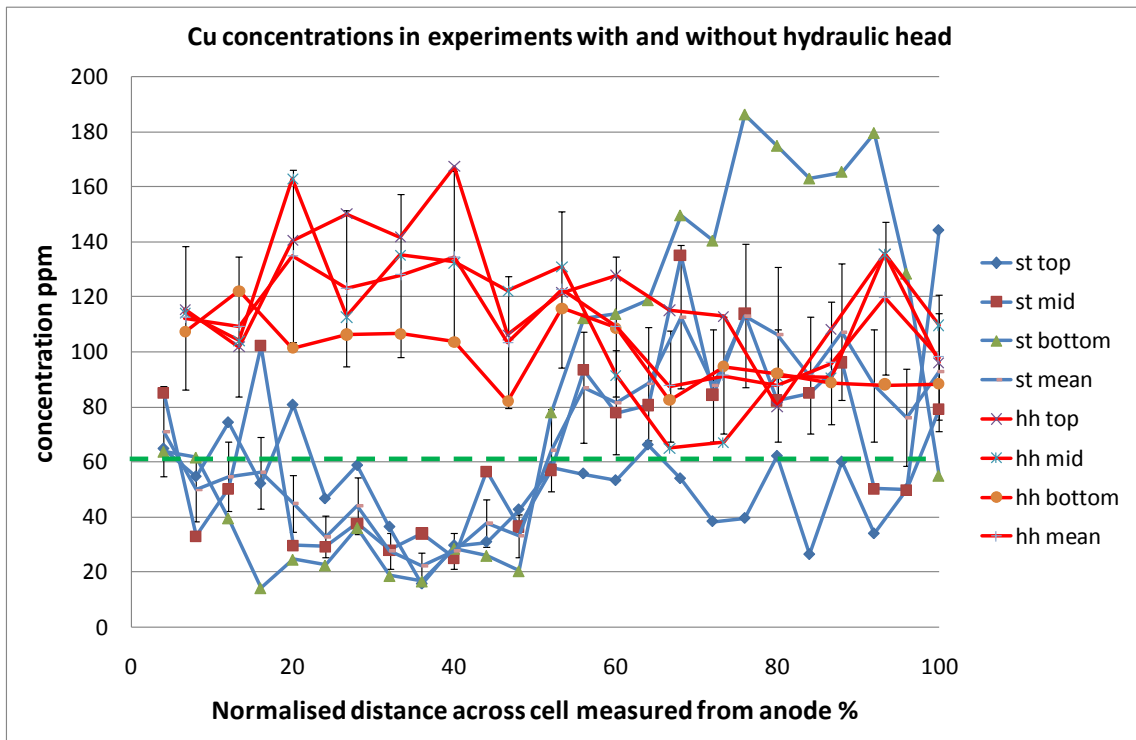


Figure 97: Copper distribution in experiments conducted with and without hydraulic head. Green dashed line indicates mean pre-treatment concentration, table 22. Error bars derived from table 19.

There is an apparent and confirmed significant difference between all aspects. The difference between the concentration profiles is very apparent and adds weight to the hypothesis that there is introduced copper from the dissolution of the cast iron electrode at least in the hydraulic head experiment. In the static head experiment there is a reduction below the starting concentration on the anode side with subsequent enrichment (in the bottom and middle sections) in the cathode zone; fitting the model. However the effect of the application of the hydraulic head in this instance appears to be to limit any sort of response at all. It should be noted though that all the measurements for copper concentration post treatment in the hydraulic head experiment are clearly above the mean starting concentration

5.7.9 Zinc

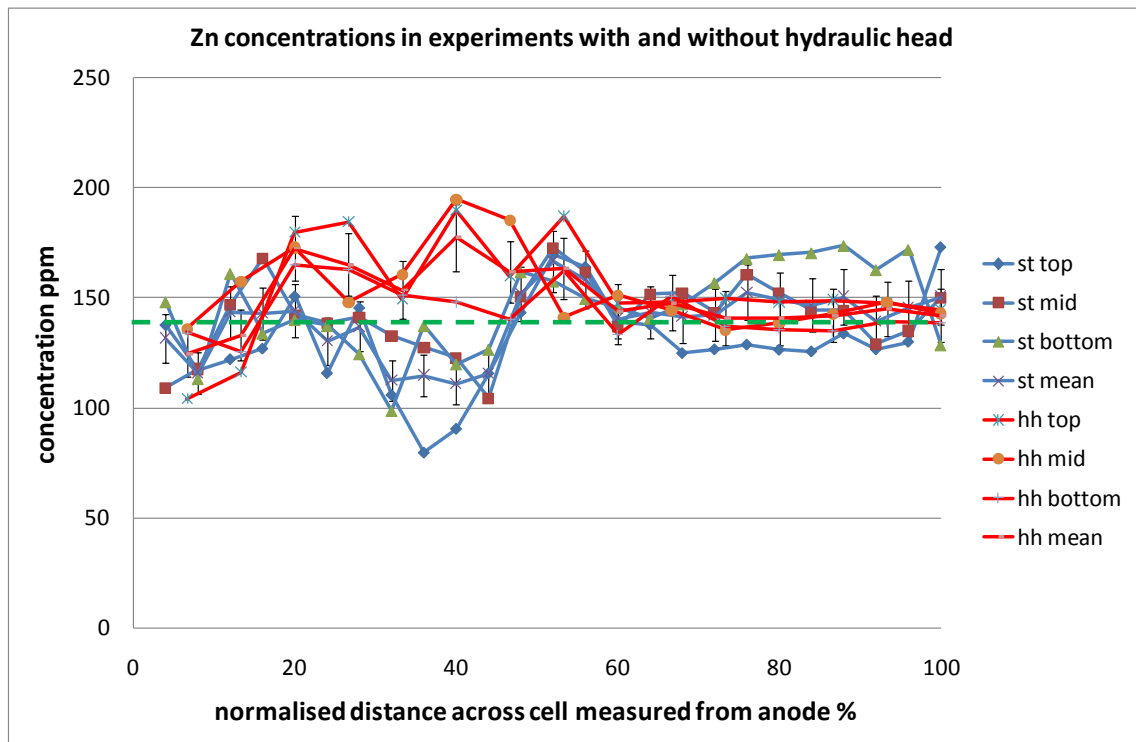


Figure 98: Zinc distribution in experiments conducted with and without hydraulic head. Green dashed line indicates mean pre-treatment concentration, table 22. Error bars derived from table 19.

The zinc concentration distribution in the static experiment shows more of the sigmoid distribution associated with a depletion/enrichment process compared to the hydraulic head experiment. The hydraulic head data show a limited depletion close to the anode and some enrichment in the precipitation zone, but is once again more diffuse than seen in the static head experiments. Statistical analysis shows a significant difference between treatments and there is a treatment*depth interaction ($p=0.02$). The distribution of the zinc appears to be adversely affected by the application of the hydraulic head in this case, from a remediation point of view.

5.7.10 Vanadium

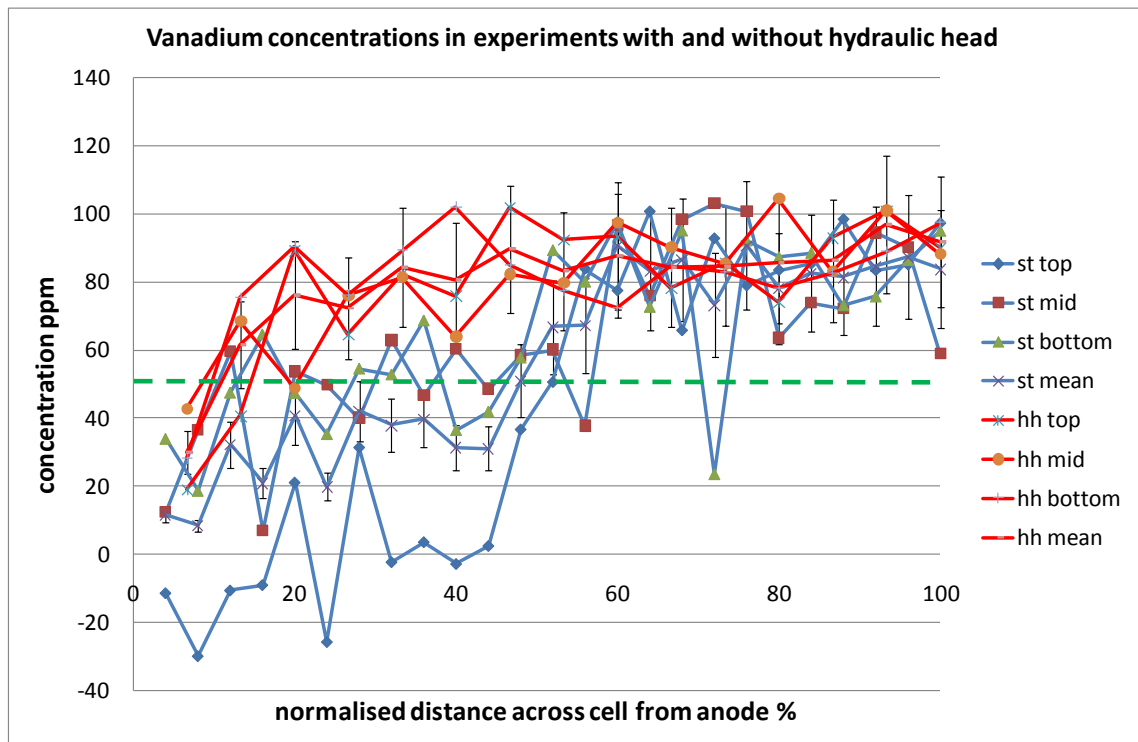


Figure 99: distribution in experiments conducted with and without hydraulic head. Green dashed line indicates mean pre-treatment concentration, table 22. Error bars derived from table 19.

The data for the vanadium shows statistically significant difference between treatments, and between depths. There is more of a depletion in concentration in the static head experiment compared to the hydraulic head experiment. There is no appreciable localised enrichment in either case, however both experiments yield concentrations in the cathode zone significantly higher (70-100 ppm) than the mean starting concentration (~50 ppm).

5.7.11 Zirconium

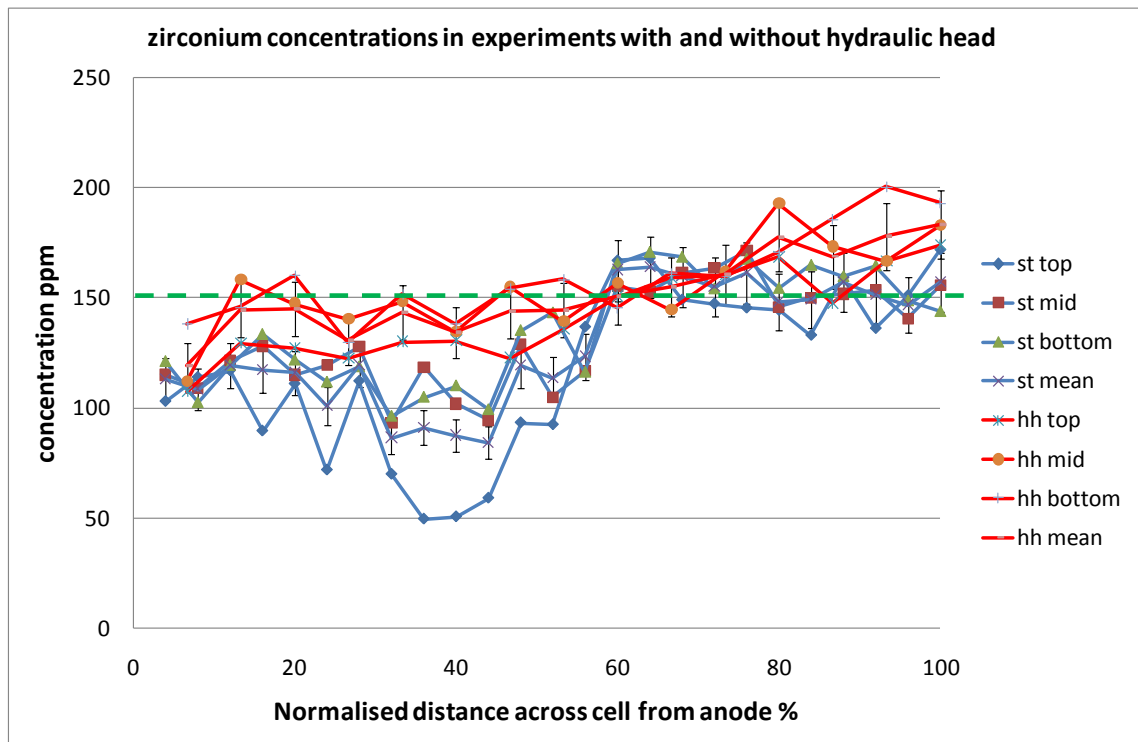


Figure 100: Zirconium distribution in experiments conducted with and without hydraulic head. Green dashed line indicates mean pre-treatment concentration, table 22. Error bars derived from table 19.

Significant difference between treatments and significant depth effects are shown. Although statistically different, it could be argued that the zirconium has responded positively in both treatments. There appears to be significant depletion in the case of the static head experiment but limited enrichment. The effect is even less defined in the hydraulic head experiment. This does suggest that the application of a hydraulic head in the case of zinc negatively affects the useful mobilisation of the metal.

5.7.12 Titanium

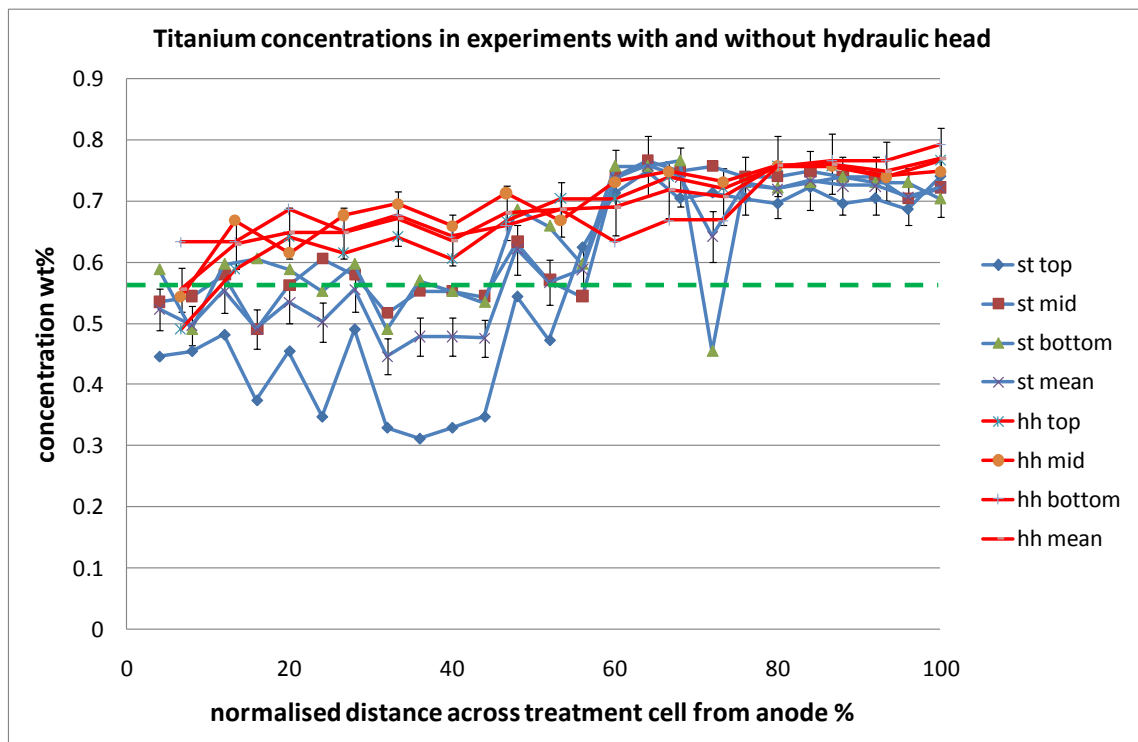


Figure 101: Titanium distribution in experiments conducted with and without hydraulic head. Green dashed line indicates mean pre-treatment concentration, table 22. Error bars derived from table 19.

The titanium distribution shows a sigmoid remediation response for the static head experiments but a much less striking effect for the hydraulic head experiment. There is a statistically significant difference between the treatments. Again the hydraulic head negatively impacts the mobilisation and redistribution of this element according to these experiments.

5.8 Metal Mobilisation Discussion and Conclusions

There has been demonstrated a considerable response to the process by a number of elements but not by all the elements looked at and not all the more environmentally sensitive elements. The response has been seen to be variably associated with the iron introduced into the system, as well as seemingly acting independently of the iron in some cases. The significant response by strontium – whilst not associated with the iron, showed a defined and localised enrichment at all depths, and also in the hydraulic head experiment.

Arsenic has proved to be particularly responsive to the treatment and appears to be one of the few elements which seem to be enriched in the region of iron mineralisation in both the tap-water and the acetic acid experiments. The correlation between the arsenic and the iron enriched region is encouraging in terms of remediation potential, especially since arsenic is such a hazardous environmental contaminant. This result is important because the arsenic found in the untreated material is at a concentration which is high enough that it might be considered to be contaminated with arsenic (for certain uses, according to UK threshold values) and thus the technique might be realistically employed (hypothetically, as a low permeability and fine grained material) as a method to deal with it.

Since the data indicates in most cases that the ‘remediated’ area only makes up 20% of the area between the electrodes, the efficiency is clearly not optimised. In addition to this limited treatment-area, the enriched region is less localised than in an ideal situation. The extent of the area between the electrodes in which the concentration of arsenic is elevated above background occupies approximately 36% of the total area between the electrodes. Or, conversely, ~44% of the area between the electrodes yields no response to the treatment. In spite of these limitations, the response of arsenic to the process would certainly warrant further development in material/contaminant combinations of this type.

The similarity between the results for the experiments conducted in static groundwater conditions and those obtained under the hydraulic gradient is such that the hydraulic

gradient in this material causes no detrimental effect to the efficacy of the technique. This is interesting since the gradient applied is not insignificant in terms of what might be expected to be encountered in the natural environment (e.g. Ranjan, 2009). It is noted that the permeability of the material is such that the hydraulic gradient applied is not enough to generate the levels of outflow seen for the sand and loamy soil experiments, but this was not the intention. The experiment was not designed to find the upper limit for the hydraulic gradient, rather to generate a hydraulic effect likely to be encountered in fairly typical natural conditions.

The inference that some elements (bromine, arsenic etc.) might be flushing through the system could be confirmed by capturing outflow liquid, and evaporating it down to a fraction of its original volume for subsequent analysis with atomic emission spectroscopy, the tap water should also be characterised to establish a baseline.

Table 27: Table showing the P values from the ANOVA tests. P values ≤ 0.05 are shaded green. P values > 0.05 are shaded red.

element	interactions				effects		
	depth*treatment*distance	treatment*distance	depth*distance	depth*treatment	distance	treatment	depth
strontium	0.691	0.000	0.484	0.109	0.000	0.001	0.795
arsenic	0.010	0.065	0.012	0.021	0.000	0.001	0.012
iron	0.695	0.004	0.095	0.096	0.000	0.001	0.805
bromine	0.700	0.000	0.479	0.120	0.000	0.000	0.000
calcium	0.879	0.006	0.494	0.930	0.000	0.146	0.246
cobalt	0.737	0.107	0.073	0.001	0.650	0.000	0.000
manganese	0.561	0.013	0.760	0.010	0.000	0.005	0.175
copper	0.016	0.000	0.010	0.001	0.021	0.000	0.803
zinc	0.621	0.000	0.693	0.009	0.243	0.001	0.415
vanadium	0.175	0.001	0.019	0.040	0.000	0.000	0.014
zirconium	0.556	0.030	0.663	0.964	0.000	0.000	0.000
titanium	0.763	0.008	0.072	0.119	0.000	0.000	0.003

Table 27, shows the output of the statistical tests to look at the interactions between factors and the significance of the different variables. A ‘p value’ of less than 0.05 (green) indicates a significant effect. A ‘p value’ of greater than 0.05 (red) indicates no significant effect. As expected there are significant effects between the treatments and across the cell.

6 Discussion

This section discusses issues encountered through the conduction of the investigations, along with some of the difficulties and recommendations for changes in approach for future work. New directions of research and suggested solutions to improve future research are also considered. The discussion is intended to serve as a reference to be reviewed for future undertakings in this topic, there is some referral to the findings of previous researchers which apply to the findings within this thesis, and are compared to the questions and issues raised as a result of the investigations undertaken here.

6.1 Limitations and Scope

As a baseline study of the FIRS technology, the investigations undertaken have revealed certain technical difficulties and limitations of the technique (as well as developing and proving potential of the technique). There have been successes as well, with new achievements having been made for the first time using the FIRS system. There have also been other avenues of research identified and technical modifications have been put forward.

A number of authors have already cited Faulkner *et al.* 2005 which was written as a result of research carried out for the production of this thesis (Cundy *et al.*, 2007; Cundy *et al.*, 2008; De Gioannis *et al.*, 2009; Lynch, 2009; Yeung, 2009; Andreottola *et al.*, 2010). This is encouraging as well as indicating that there is the possibility of collaborative research projects with other groups of researchers in the field.

One of the problems identified has been the competing benefits and difficulties associated with using iron anodes for remediation applications. The iron is important for the identification of the point of sudden pH change in the material and for fixing the contaminants in place. The downside of introducing the iron in this way is that the greater the iron content of the anode electrodes the greater the reduction in the

propagation of protons (due to the preferential oxidation of Fe^0 to Fe^{2+} occurring (Haran *et al.*, 1996)) resulting in less acidic conditions. If this is coupled with any significant buffering capacity of the material then there could easily be inadequate acidification of the material to desorb contaminants on soil particles, although other research has shown that this is not necessarily the case, for instance the removal of lead from a calcite rich soil, e.g. Amrate *et al.* (2005). Similarly, if the electrodes are replaced with inert or low reactivity electrodes, such as platinum or graphite, there may be improved acidification of the material but without the electrochemically introduced iron there may be difficulties in the identification of the region of localised concentration and secondary migration of any contaminants concentrated there due to the lack of cementation provided by the iron-rich precipitate. The goal therefore is to maximise acidification whilst simultaneously introducing the required amount of iron.

In cases where there is mixed contamination – cationic and anionic species, or dissolved contaminants along with immiscible hydrocarbon contamination, there are difficulties in diametric migration of some species. For example, if there is a mixture of chromium contamination with other metallic contaminants, such as zinc and nickel, the chromium would most likely form its chromate anion and tend to move from cathode to anode, whereas those contaminants which tend to exist in solution as metallic ions will be positively charged and migrate towards the cathode. The extent and degree of localisation of the various contaminants could result in nothing more than redistribution within the material of the various contaminants present, with no useful overall decontamination effect. It seems imperative that for useful remediation the iron-rich precipitate has to be as localised as possible and the pH jump as severe as possible to ensure that all species present are immobilised in the same narrow region. In materials with only one contaminant present this is less significant.

Another difficulty lies in the self-limiting nature of the procedure. As soon as the alkali and acid fronts meet, the precipitation begins, this decreases the rate at which electroosmosis and electromigration can occur due to the resultant precipitation and cementation occurring in the pore-spaces, which limits pore water flow and increases electrical resistance. This can be avoided only in a limited number of ways. One method would be to limit the formation and progression of one of the fronts- probably the alkali front in most cases. This could be achieved either with buffering solutions to

prevent the build up of an alkali front, as has been used by some workers, using a 'cation-selective membrane' (e.g. Puppala *et al.*, 1997). This is a physical membrane which is impermeable to hydroxide ions. This would have the effect of increasing the duration and the extent of the acid sweep of the treatment area, and preventing the reduction in pore space volume from the precipitated iron species. This of course removes one of the most significant aspects of the technology- that being, the strategic precipitation of iron species for the cementation and co-precipitation of species on and around the iron precipitate.

Another approach might be to incorporate a dual stage procedure whereby the first phase of the experiment would be conducted using inert electrodes to provide a low pH sweep of the anode side of the treatment area, since there is no anodically introduced iron, when the two fronts meet there might be expected to be some precipitation of dissolved species, but not as significant as that resulting from the electrodisolution of the iron anodes. The second stage would then consist of replacing or adding to the existing electrode array a proportion of iron rich electrodes. The theory being that there is still significant electroosmosis and electromigration taking place for the newly introduced iron to dissolve and migrate to the pH jump where it will then have its usual cementing effect. This approach would be expected to be less successful in materials which have a high dissolved species load, or those that already have high iron content. These materials might result in a significant iron or mixed-metals precipitated region forming and impeding migration before the second stage of the procedure is carried out.

Another approach might be to use a combination electrode array consisting of both iron rich and inert anode electrodes. The reason for this type of array would be to use the inert electrodes to maximise the proton production for an intensive acid sweep, whilst the iron electrodes are simultaneously electrochemically adding iron into the system. This approach does not remove the self-limiting aspect of the technique, because as soon as the iron begins to precipitate, the efficiency of the experiment immediately begins to reduce. However what this approach attempts to achieve is to make more effective the period between the start of the treatment and the point at which it begins to self-limit.

The FIRS technique, since its inception, has been posited to provide a cheap and simple, lo-tech approach to contaminated land management. This has been approached by avoiding harsh conditioning agents and expensive materials. The technique is an attempt at a renewable approach, using low-cost waste scrap iron. This has meant that some options which might have been pursued have been rejected. Notably, the use of electrode solution management systems has been avoided (Hopkinson and Cundy, 2003; Cundy and Hopkinson, 2005). There are numerous potential reasons to use a system which can maintain the properties and quantities of influent solution as well as the removal of excess effluent. pH management and the control of the development of the acid and alkali fronts is another area which may benefit from a greater level of control.

The argument against the use of electrolyte management is twofold. Firstly there is the commercialisation aspect; how to develop the technique so that it can be employed as a commercial proposition in a real-world contaminated land scenario. This has meant that a technology which is as cheap as possible to implement is preferable to one which has more technically challenging equipment, set-up, running and maintenance requirements. The other factor has been to make the technique appealing as a non-invasive, non-industrialised, low-energy, with what is sometimes termed 'secondary usage' of waste material (scrap iron) in its approach: in other words, to have the maximum in terms of 'green' credentials.

Another difference in the way this research has been carried out is that 'real world' materials have been used and on a bigger scale than usual when compared with much of the published work. This has both benefits and drawbacks. The benefits are that the techniques' credentials as a good prospect for use in the commercial sector is reinforced by having been already shown to have tackled material which might be encountered in an actual contaminated site. The difficulties lie in the fact that there are other factors introduced in a natural material in terms of heterogeneity and also of varied composition. The technique, whilst being a useful method for dealing with some contamination issues is not a 'magic wand' which can be used to deal with any instance of contaminated land. That said it may well prove to be a viable and successful approach for a specific range of material properties and contaminant combinations. Particularly low permeability metals/metalloid contaminated material.

There may be some benefit from continued bench scale investigations to establish the optimised parameters for the variables alongside the field-scale experiments. There is likely to be a ‘middle course’ steered whereby those improvements to the efficiency of the technique which also compromise the simplicity of the approach may have their potential benefits weighed against the complications they may add.

Another factor which may need to be considered further is the possible permanent changes to the material being treated during the course of the treatment. The extremes of pH generated can result in permanent and semi-permanent changes to the atomic structure. For instance under pH conditions of greater than 9, there is likely to be ionisation of the SiOH which is not significant at lower pH due to the pKa of silicic acid being so high (Sparks, 1995). It may also be noted that the created charge difference may persist after the current is switched off such that there could be opposite force generated due to the reversing of the polarity. The effect could be of significant magnitude on a larger field scale installation and it should be sufficiently hazard-assessed to ensure that there is consideration given to the possibility. The extremes of pH may also change the composition of the soil. The structure of clays are known to be degraded by extremes of pH either acid or alkali. This should be considered for the changes to the physical properties and the resulting changes in water retention and the strength properties for building applications (Yeung, 2009).

Whilst the successful use of real world soil and sediments lends weight to the argument in favour of the commercialised up-scaling of the technique, the same introduces uncertainty in terms of the prediction of the usefulness of the technique in a variety of conditions or compositions of the local material. There is little work conducted on real world contaminated soils, with a few exceptions (e.g. Giannis and Gidarakos, 2005). The experiments were conducted on what is expected to be fairly ‘typical’ composition for the area e.g. intertidal estuary deposits. This is hoped will allow for the results to be considered fairly robust when making predictions or planning of future work in comparable materials.

As has been found in other studies the bonding of the contaminant of interest is of major importance in the likely efficiency of the process in the successful removal of metal species. With the weakly bound exchangeable fraction, high removal efficiencies

might be achieved (Kim *et al.*, 2002), but if the primary association is more recalcitrant such as organically bound then removal efficiencies may be expected to be much less. Studies on a much bigger variety of different soil types/contaminant combinations will be required to establish the working parameters of the FIRS technique.

6.1.1 Analysis

The analysis methods employed might be reviewed in future work, in spite of XRF being a reliable and robust method of analysis. Batch analysis of conditions and the concentration of contaminants in the pore solution in a continuous and automated way (e.g. Reddy *et al.*, 2001) would have benefits in terms of the data being analysed continuously allowing for monitoring of the conditions as they change with time, the question of how this would be usefully implemented without a flushing or conditioning system.

XRF analysis gives a reliable and cost effective method for establishing the elemental distribution across a treated soil mass but does not account for elements which are the same but bonded in different compounds, or in a crystal matrix. The result is that it may appear that there has been little movement of a particular element, which might lead to the conclusion that the element/contaminant is not amenable to the process. The reality however is that the element in question is in fact associated as part of a compound or crystal structure which renders it practically inert since it is not affected by local conditions. A toxic element in this state would have a correspondingly low associated hazard, but the limitations of the criteria for identifying contaminated land might still categorise the material as 'hazardous'. This is a fundamental difficulty with any heavy metals contaminated land, initial investigations may show that there is a particular metal present but only if there is an appropriate chemical analyses to establish the form that the metal is in can an appropriate course of action be undertaken. A typical example might be chromium- as discussed in Section 2, previously the hexavalent form is both highly toxic and mobile, yet chromium present in its ore, chromite, is of limited toxicity and extremely immobile.

Heterogeneity of the starting material is an issue in experiments of the size presented here. The samples taken, particularly for the characterising of the starting material, have to be representative. Homogenising the material by extensive mixing would improve the reliability of the starting concentrations of metals measured, however, this disrupts the material and its inhabitants and part of this investigation was to look at possible performance of the technique as an *in situ* approach. The starting concentrations have been measured from multiple samples, table 22, and for the purposes of this thesis the relative migrations of the elements looked at is most significant, rather than the absolute concentrations. Therefore the starting concentrations shown are indicative.

6.1.2 Stabilisation

The stabilising ability of the technique when applied to unconsolidated materials has been demonstrated to significantly add to the strength of the treated area (Hopkinson and Cundy, 2003; Cundy and Hopkinson, 2004). The question that remains is whether this method is a viable alternative to existing approaches; such as the application of cements, or of grouts. The technique does offer a fairly unique set of characteristics which many existing approaches lack; these being:

- The ability to gain information on the extent of iron precipitate formation from the current/resistance measurements.
- The iron precipitation may theoretically be developed at any depth depending on the local conditions.
- The measurement of the current/ resistance can be used to detect ruptures in a precipitated region as demonstrated in Section 3.5.2 . And reapplication of the current used to repair the ruptures.

The combination of these features may find some specific use that the relatively high cost of installing and powering electrode arrays justifies. One proposed use is for the stabilisation of unconsolidated spoil heaps where the disturbance of applying a conventional binder or grout may de-stabilise a spoil heap whereas the relatively easy

insertion of iron/steel rods may be less disruptive. This would also give early indication of any movement of the spoil since the electrodes provide information about the integrity of the precipitated region. The emplacement of electrodes also provides a convenient means to determine the level of saturation of the spoil which may also give information about the likely stability of a heap for instance, during periods of prolonged or heavy rain.

The experiments conducted for the mass stabilisation using a grid formation of electrodes showed that the technique has potential for this kind of application. This could have uses for consolidation or to prevent liquefaction and erosion or unconsolidated materials.

6.2 Further Work

The investigations conducted have identified a number of key areas towards which future work might be directed as well as what might be considered technology development.

The FIRS technique could be evaluated for the purpose of converting low quality metal ores into economically viable ores. Many low grade ore deposits have been abandoned as they are unable to provide an economically competitive end product, but with the rapidly changing markets the difference between sub-economic and profitable can be small. If the electrokinetic effect can be harnessed to mobilise the metal of interest into a particular region, whereby increasing the concentration at this point to one which is economically viable for processing there may be significant returns.

One method which might be efficiently employed may combine the electrode array developed in section 3.4, for horizontal barrier formation with this approach. The electrode array is constructed as in the barrier experiment, the difference being that the objective is not barrier formation but is to concentrate the metal of interest in sufficient quantities as close to the surface as possible. This might be facilitated by the acidification of the cathode at the surface to suppress the alkali front as much as possible allowing the acid front to propagate from depth, right to the surface. The surface cathode electrodes could then be removed once the mobilisation is complete.

The result should be that the surface material is enriched in the species of interest and can be simply bulldozed up and collected for smelting/processing. There have been other researchers who have, since the publication of my own research on the technique, been independently looking at the benefits of comparable arrays (Wang *et al.*, 2006, 2007), but their work is focussed at this stage solely on remediation applications rather than any kind of groundwater control/barrier formation.

The material of interest would have to be some kind of secondary resource rather than a pure ore because of the electrokinetic process being most amenable to adsorbed metals on the surfaces of charged species in the soil. However there may be additional approaches to allow for the technique to be used on material where the metal of interest is in a mineral matrix. These approaches might include the addition of agents to bring the metals into solution, such as strong acids.

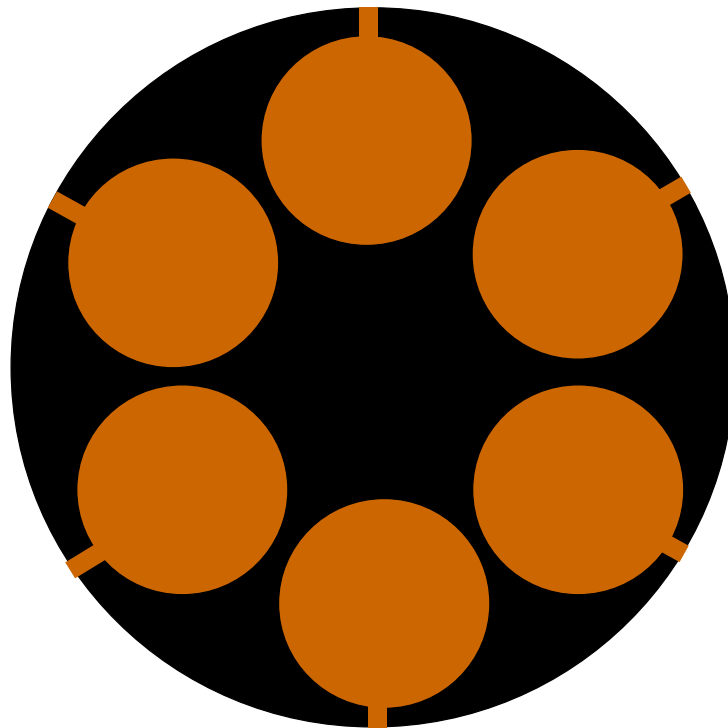


Figure 102: Cross section of a proposed composite electrode design. The solid black represents the inert portion, e.g. graphite. The circular iron portions are entirely enclosed within the inert portion except for a narrow extension to the exterior. This provides a limited surface area for the reaction of iron initially but a relatively large inert surface area; the available iron surface will increase when the narrow portions exposed to the exterior dissolve and expose the larger inner portions as the iron dissolves.

Increased levels of sophistication in terms of electrode design and function may also be considered but the effectiveness of these will need to be considered alongside increased costs of electrode construction due to the added complexity. Composite electrode design might allow for the two stage implementation of inert/iron electrode from a single electrode emplacement. This might be achieved for instance by coating an inert electrode in pure iron. This would allow for an initial introduction of iron into the system until the iron coating is all dissolved. This exposes the inert electrode underneath for an increased acidification (bearing in mind that the ionic diffusion rate of protons is six times greater than that for Fe^{2+} (Acar *et al.*, 1994)) such that the material being treated will benefit from increased acidification giving increased mobility of species and the increased de-sorption of species.

For increased acidification before the electrochemical introduction of the iron, for the purpose of prolonging the time that the acid front is developed before the electrokinetic effects begin to self-limit, another composite electrode design is suggested. The design of the electrode could be adapted to provide a minimal reactive surface area of iron at the start of the experiment, compared to the surface area of the inert portion, graphite for instance. As the iron portion begins to dissolve, it exposes a greater and greater reactive surface for the introduction of iron, Figure 102, up to a maximum iron versus graphite surface area ratio before it decreases as the iron dissolves away.

It might also be feasible to reverse the polarity of the electrode arrangement such that the movement of metal cations is downwards towards the cathodes emplaced at depth. The argument for this approach is that in many cases of environmental contamination where the hazard is due to windblown fine material or ingestion of metal contaminated soils with negligible threat to water courses, then capping of the contaminated region with clean topsoil is often the simplest and most cost effective approach. By causing the adsorbed metal to migrate down to a significant depth leaving the uppermost region theoretically relatively free of contamination, this has the same effect as capping but without the need to acquire transport and distribute a potentially large volume of clean topsoil to the area as would be required for capping.

Studies to compare the costs of the installation of an electrokinetic system versus the cost of capping will be necessary to establish the associated energy and financial costs.

Outside of costs though is the fact that soil is becoming increasingly recognised as a finite resource which requires conservation. Capping involves the harvesting of a suitable soil from one area for transportation to another, there are concerns that the rate at which soil is being eroded is 20 times greater than the rate it can regenerate, since it can take hundreds of years for soil to regenerate this is not a sustainable practice (Montgomery, 2007). For these reasons it may in fact prove cost effective, or at least more environmentally justified in utilising an electrokinetic approach. This process does not necessarily require iron anodes and as such falls outside of the description of the FIRS technique as outlined in (Cundy and Hopkinson, 2004).

This thesis has been concerned with the application of the technique to an inorganic contaminant. There is some data that the technique can result in the movement of organic compounds, in particular synthetic engine oil. These results have not been replicated. If there is a proposed mechanism for the movement of this kind of material it would be associated with an electroosmotic purge of the material since a mixture of high molecular weight, non-polar molecules as found in an engine oil would not be expected to exhibit any significant electromigration under the influence of an electric field due to electrostatic attraction unless significant dipole effects were encountered.

Point-Source Electrode Array

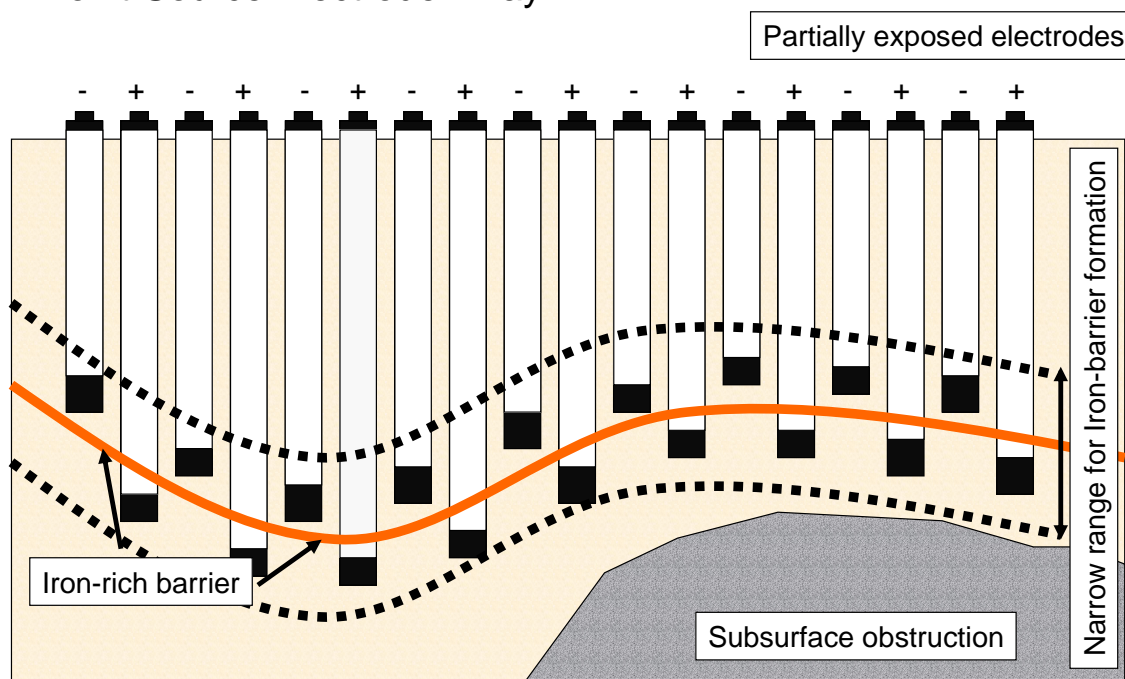


Figure 103: Proposed application of the point source electrode array.

Of additional interest is the use of the technique to deliver iron into a low permeability material which has chlorinated hydrocarbon content. Existing literature (e.g. Helland *et al.*, 1995; Johnson *et al.*, 1998; McGuire *et al.*, 2003 etc.), suggests that iron is a significant catalyst for the dechlorination/dehalogenation of such contaminants as pesticides, dioxins, PCBs and other chlorinated/halogenated hydrocarbons. The investigation of the ability and time scale for the dehalogenation of these types of compounds may prove a useful approach for so called ‘cocktail’ contamination issues where a site is contaminated with a combination of metal, non-metal and metalloid contamination where the non-metal component may consist of hydrocarbon (petrochemical), PAHs, or commonly pesticides and there has been some encouraging work conducted on such sites (Chinthamreddy and Reddy, 1999). Based on these findings the FIRS process could form part of a multi-stage remediation strategy.

There is probably benefit from this kind of approach which outweighs the added costs in terms of installing such a system and the additional maintenance requirements. However the improved efficiency of the process and the optimisation of the conditions may prove to make this a viable option. For the purposes of this thesis, the remit was to

test the limits of the procedure in its simplest form- that being the emplacement of electrodes directly into the material to be treated. There are numerous opportunities for the management of the moisture levels in the test material. The gas venting electrodes outlined above could serve the dual purpose of acting as an input/extraction-point for solutions.

An additional proposition is to perforate the electrodes so that any solutions introduced are able to enter the test material along the length of the electrode. In a coarse grained material with a high hydraulic conductivity the addition of solutions has been demonstrated to present conditions requiring consideration in terms of the precipitation of the introduced iron and other dissolved species. For controlled precipitation, the turbulence and gravitationally controlled movement of the pore water can lead to unpredictable precipitation behaviours. This is less of a consideration in the case of lower hydraulic conductivity materials.

The analysis of the treated areas consisted of the homogenisation of a section of the treatment zone. This consisted of a 2cm slice across the width of the treated area running parallel to the electrodes. This was used to gain information about the overall net movement of metal species in the treated soil. In large scale or full scale treatment applications the sampling and analysis would have to be done differently. There would be far too much material involved to proportionally carry out the same method. And the larger scale experiments might have more heterogeneity in terms of the composition of the treatment area and there may also be more variation in terms of preferential flow paths, possible physical obstructions and differences in hydraulic conductivities.

In these situations it is recommended that a sampling procedure used for the classification of a piece of land as being contaminated is employed. In that respect the goal would be to analyse the test zone according to an approved protocol before treatment and then to carry out the treatment on the area and carry out the second sampling and analysis procedure and the results would be hoped to prove that the technique can take a previously contaminated material and have it reclassified as not contaminated according to a recognised sampling/analysis procedure. There are existing difficulties in this respect due to the level of uncertainty associated with a particular sampling and analysis combination (Ramsey and Argyraki, 1997; Kurfurst *et*

al., 2004) as discussed previously. The essential difficulty being that no method allows for one hundred percent certainty and depending on the uncertainty associated with a given measurement or set of measurements can have repercussions for the classification of contaminated land (e.g. Ramsey *et al.*, 1995; Ramsey and Argyraki, 1997).

The apparatus used to generate the horizontal iron band (Section 3) could be modified in order to cause the iron mineralised region to form as close to the surface as possible. This could be used in a contaminated land scenario as a means to raise contaminants to the surface, where the top layer, containing the contaminants can be simply bulldozed away leaving the 'clean' material below. This might also prove to be an easier way to deal with the contaminated material. There would have to be contingencies to reduce any possibility of wind transportation to sensitive receptors, a similar approach has since been developed to cause upward migration of contaminants (Wang *et al.*, 2006, 2007).

The use of the technique has been applied to smelter waste and although in terms of remediation were not successful (due to the fact that the 'contaminants' were significantly associated with the mineral matrix rather than as adsorbed onto soil particles) there might be situations where the metal content of a mining spoil deposit or smelter waste might be of a threshold concentration that means that a minimal increase in concentration might result in an economically viable source of the metal in question for reprocessing. Quite recently, tin mines that have been dormant for decades in Cornwall, UK are preparing to re-open due the current high value of tin on the global markets (Lashmar, 2004; Buckley, 2007).

Another possibility is to combine the arrangement outlined above, where the contaminants are driven to the surface, with another process such as phytomining or phytoremediation. In both of these techniques a plant species is grown on the medium containing the metal of interest (this technique is applicable only to metals contamination) where the species of plant grown has the property of taking up the metal or metals of interest and accumulating it in its tissues (Hodko *et al.*, 2000; Mulligan *et al.*, 2001; Martin and Ruby, 2004; Pendergrass and Butcher, 2006). Some species of plant are capable of accumulating high concentrations of target metals in their tissues removed from the soil. In the case of phytomining the concentration and extraction of

metals from a substrate for processing to obtain the metal of interest, the plants are harvested and the metals in the plant tissues obtained through processing. The harvesting of the plants means that the metals depleted soil in the surface layer which the plant roots have scavenged may not have an economically viable volume of available metals present. This might be addressed by ploughing or bulldozing to reveal the layer of the deposit which was previously below the level of the plant root system.

The FIRS system could be utilised to drive up the metal of interest from below making it available to the root system of the plant. This could allow for the replanting of an area at the surface repeatedly since the metal of interest could be continuously driven upwards, this would also have the benefit of allowing the more efficient application of other growth factors such as fertilisers and pH buffers. Without this benefit it might be necessary to dump the surface layer and re-apply the growth factors between each planting cycle.

Further work on larger scale creation of sub-surface barriers should utilise geophysical surveying methods to detect and measure iron band development on a field scale trial: such as ground penetrating radar, magnetometry etc. The iron mineralised region has been demonstrated to contain magnetite (by XRD and by using a permanent magnet) so should be amenable to detection by these methods.

It would be interesting to conduct experiments to observe the formation of the iron pan in high resolution. This could help with the understanding of the way in which the iron-pan forms and give information on the way that the iron enriched region goes from a diffuse solution to a solid and continuous mineral fabric. For instance, there may be a way to modify the conditions such that instead of a mineral fabric forming, a more diffuse iron enriched region may be created (Zhou *et al.*, 2004; Zhou *et al.*, 2005a; Zhou *et al.*, 2005b).

Further investigations which utilise cast iron anode electrodes should include analysis of the trace metal composition of the anode material. It would also be useful to conduct future experiments with the incorporation of a means to obtain information about the development of redox conditions in real-time as the experiment progresses.

The demonstration of the feasibility of the technique to create an impermeable barrier under the influence of a hydraulic gradient has been achieved; future investigations may establish the upper threshold in terms of hydraulic gradient that a barrier can be formed for different materials.

To address the interference effects which affected some elements (Pb, Cd and Hg), additional analysis methods should also be employed to address these environmentally significant metals. AAS or ICP incorporating a suitable extraction/digestion procedure would be useful for this.

7 Conclusions

Some of the conclusions arising from the work carried out for the production of this thesis have been made as part of the relevant chapters so this section intends to summarise and condense these findings.

In terms of the objectives of the investigations these have been achieved summarised below:

To evaluate the performance of the system described in Cundy and Hopkinson (2003; 2004) on electrokinetic metal movement in estuarine sediment and on a larger scale than previous experiments: Experiments with an electrode separation of 0.5 m represent a significant increase in scale of the experiments and data on metals response in sediment from Hythe intertidal mud flats.

To compare the results in one medium using tap water and acetic acid (2M) electrolytes. The experiments conducted allow for the comparison of the migration of metals when using tap water and using acetic acid as the introduced electrolytes.

To investigate electrode configurations and designs to create novel strategic iron pan geometries in the sub surface. Novel arrays and designs of electrode have been used to generate predetermined iron-rich mineral fabrics and additional experimentation demonstrated the ability of the iron-rich mineral fabric to ‘heal’ a rupture.

To characterise the composition and physical properties of the iron-rich precipitates formed in terms of the potential for groundwater management applications. Geotechnical test of the permeability of the iron rich mineral fabric carried out and analysis by XRD for compositional information.

To compare the effectiveness of the technique with and without an imposed hydraulic gradient. The experiments on the estuarine sediment subjected to hydraulic gradient allow the comparison of the metals’ response to the treatment with and without the hydraulic gradient applied.

To ascertain whether the technique can be used to reduce groundwater flow in different materials (sand, top soil, estuarine sediment) and whether an iron pan might be induced to form in moving groundwater conditions. Experiments were conducted to measure flow through a test medium subjected to an electric field and the generation of an iron-rich barrier achieved.

Cundy and Hopkinson (2004) claim that The FIRS technique *can* be used to create an effectively impermeable region within a soil mass. By designing custom electrodes and experimenting with electrode arrays some of the potential for this side of the technology has been elucidated. In terms of the remediation of contaminated material there have been demonstrated mixed successes, with some materials being far more amenable to the process than others. It suggests that the technique is not a magic wand which can be waved at any remediation problem and indeed some of the premises of the technology fall short of the reality; particularly the co-precipitation of the contaminant with the iron into a narrow region. In many cases some of the species present which might be thought of as contaminants (but which may not be present in sufficient concentrations to be considered as hazardous) do not respond to the electrokinetic process to a significant degree or do not precipitate out of the pore solution in the same region of the test material as the iron has precipitated out. This is analogous to an electrophoretic separation of compounds as might be seen in a DNA separation. This effect has been referred to as ‘isoelectric focusing’ by Gray and Schlocker (1969), Probst and Hicks (1993) and Jacobs *et al.* (1994), and is assumed to be related to the relative ionic mobilities of different ions and complexes. As well as the redox and pH conditions across the treatment zone.

The main obstruction to more complete remediation is the self limiting nature of the technique which begins to reduce in effectiveness as soon as the two fronts meet. So that when the fastest moving ions meet, the protons and the hydroxide ions, the process is already reducing in effectiveness. Describing a similar situation where a pH jump is allowed to develop, Jacobs *et al.* (1994) speaks of the system’s tendency to “lock” itself because of the fact that where the electric field strength is large there are only a small number of ions, and where there are plenty of ions the field strength is small (Jacobs *et al.*, 1994). The speciation and complexation of the different species present is not

simple either, especially in materials with an organic fraction. There may be myriad compounds and complexes in the material which will have an associated effect on the mobility characteristics of the associated metal. For ordinary, non-exotic materials which have evolved by natural means and have a fairly homogenous composition the operation could have significantly less uncertainty and a higher predicted likelihood of a successful outcome. The problems increase with more problematic introduced materials and man-made materials perhaps on a site which has experienced multiple uses historically with associated variety of introduced compounds. The other difficulty arises in maintaining an optimal level of saturation over a large area perhaps in an arid or semi-arid area.

The key problem areas which have been identified are:

- Problems associated with the generation of gas at the electrodes leading to reduced efficiency of the conductors and or the generation of turbulent conditions in the pore water of a coarse grained medium leading to unpredictable precipitation formation.
- The effects of buffering capacity of a soil leading to minimal acidification of the material being treated and associated reduction in the mobilisation of adsorbed metals in the test medium.
- The optimisation of the energy expenditure versus effectiveness of the procedure.
- The compositional characteristics of cast iron in terms of the variability of composition, the possibility of exotic and or toxic elements in the anode material and the effect of the carbon content on the ratio between the production of divalent iron versus the electrolysis of pore water.
- Benefit or otherwise of the use of more controlled pH management systems which might enhance the process to a greater or lesser degree, coupled with the use of chelating agents or acids to enhance the removal efficiency of the process.
- The self limiting nature of the process as a result of the precipitation process.

There has been some encouraging work conducted within my own research team using the process to deal with hexavalent chromium by using the iron in solution to reduce it

to the trivalent form. It is not clear how this process is different from the technique used by Haran *et al.* (1996; 1997) since in essence the technique is identical. Haran *et al.* use alpha pure elemental iron for their anode and they have achieved good results. Chromium contamination seems particularly amenable to electrokinetic processing (Chinthamreddy and Reddy, 1999).

Whilst some studies have looked at the nature and function of the buffering capacity of naturally occurring soils in the context of electrokinetic remediation (Hernández-Luis *et al.*, 2004) there is still more work required in this area. One important difference between the work presented here and much of the existing research is the way the acetic acid was applied in the experiments here. The existing literature generally uses the addition of acid as a method to suppress the propagation of the alkali front. In the experiments conducted here the acid is used as a means to maximise the acid sweep of the anode side whilst still allowing for the precipitation of the metal and the introduced iron.

The addition of the acid is to act as a de-sorbent to the adsorbed fraction of the contaminants in the anode region and to facilitate the transport to the precipitation region where the iron/contaminant complex precipitates out. The reason for this approach- which may result in a smaller fraction of the treatment mass being effectively remediated is to test the premise as laid down in (Cundy and Hopkinson, 2004; Cundy and Hopkinson, 2005) that the iron mineralised region is an effective trap to isolate and stabilise the contaminants which are present. This requires that the iron and other ions present are required to precipitate within the treatment area. It may be a fruitful avenue of research to develop the technique further to perhaps suppress the alkali front and facilitate the removal of contaminants at the cathode electrode or via an electrolyte flushing system. However, this makes the addition of iron into the system somewhat redundant and the system becomes indistinguishable from other systems already described in the literature.

The research which was published in 2005 has been cited a number of times (Cundy *et al.*, 2008; De Gioannis *et al.*, 2009; Hopkinson *et al.*, 2009; Lynch, 2009; Yeung, 2009; Andreottola *et al.*, 2010) and clearly represents a contribution to the body of knowledge. Specifically, this consisted of the design and construction of the means to generate

horizontal iron pans below the surface without the need for excavation. Additionally, the demonstration of the ability of the generated iron pan to reseal a point rupture over a relatively short timescale. The metals migration experiments represent contributions in terms of the scale of the experiments, and has generated important new data on the comparison between electrolytes. The hydraulic head experiments have generated empirical data on the effects of ground water movement in a real world material and the formation of iron-rich barriers under dynamic conditions in different materials in custom designed and fabricated apparatus.

Although the general approach of using electrokinetic phenomena to implement the remediation from contaminated soils has many appealing possibilities, actual successful results in field scale applications are limited. Some of the pressure seems to be the cost effectiveness of the approach compared to more common mechanical means for general contaminated land issues. The benefits of moving solutions through relatively impermeable clay materials is a tantalising one and it certainly seems that the electrokinetic approach should be focused on these materials. The electrokinetic approach and FIRS (as a means of contaminant remediation) in particular, might be best considered as a specialised approach to a narrow range of soil/sediment types with a known set of chemico-physical properties and a contaminant or contaminants content which is demonstrably responsive to the treatment.

- Acar, Y.B., and Alshawabkeh, A.N. (1993) Principles of electrokinetic remediation. *Environmental Science & Technology*, **27**, 2638-+.
- . (1996) Electrokinetic remediation. I: Pilot-scale tests with lead-spiked kaolinite. *Journal of Geotechnical and Geoenvironmental Engineering*, **122**, 173-85.
- Acar, Y.B., Alshawabkeh, A.N., and Gale, R.J. (1993) Fundamentals of extracting species from soils by electrokinetics. *Waste Management*, **13**, 141-51.
- Acar, Y.B., Alshawabkeh, A.N., and Parker, R. (1997) Theoretical and experimental modelling of multi-species transport in soils under electric fields. US Environmental Protection Agency (USEPA), Office of Research and Development, Cincinnati, OH 45268.
- Acar, Y.B., Gale, R.J., Alshawabkeh, A.N., Marks, R.E., Puppala, S., Bricka, M., and Parker, R. (1995) Electrokinetic remediation: Basics and technology status. *Journal of Hazardous Materials*, **40**, 117-37.
- Acar, Y.B., Puppala, S., Marks, R.E., Gale, R.J., and Bricka, M. (1994) An assessment of selected enhancement techniques in electrokinetic remediation of inorganic species. *Abstracts of Papers of the American Chemical Society*, **207**, 116-ENVR.
- Adamson, L.G., Chilingar, G.V., Beeson, C.M., and Armstrong, R.A. (1966a) Electrokinetic dewatering, consolidation and stabilization of soils. *Engineering Geology*, **1**, 291-304.
- Adamson, L.G., Quigley, D.W., Ainsworth, H.R., and Chilingar, G.V. (1966b) Electrochemical strengthening of clayey sandy soils. *Engineering geology*, **1** (6), 451-9.
- Adamson, L.G., Rieke, H.H., Grey, R.R., and Chilingar, G.V. (1967) Electrochemical treatment of highly shrinking soils. *Engineering Geology*, **2**, 197-203.
- Allen-Gil, S.M., Ford, J., Lasorsa, B.K., Monetti, M., Vlasova, T., and Landers, D.H. (2003) Heavy metal contamination in the taimyr peninsula, siberian arctic. *The Science of The Total Environment*, **301**, 119-38.
- Alloway, B.J., and Ayres, D.C. (1997) *Chemical principles of environmental pollution*. xvii,395p. p. Blackie Academic & Professional, London.
- Alshawabkeh, A.N. (2001) Basics and applications of electrokinetic remediation: Handouts for a short course, p. pp 1-95. Federal university of Rio de Janero.
- Alshawabkeh, A.N., and Acar, Y.B. (1994) Electrokinetic remediation - modeling the process. *Abstracts of Papers of the American Chemical Society*, **207**, 115-ENVR.
- . (1996) Electrokinetic remediation .2. Theoretical model. *Journal of Geotechnical Engineering-Asce*, **122**, 186-96.
- Alshawabkeh, A.N., Gale, R.J., Ozsu-Acar, E.J., and Mark Bricka, R.J. (1999a) Optimization of 2-d electrode configuration for electrokinetic remediation. *Journal of Soil Contamination*, **8**, 617-35.
- Alshawabkeh, A.N., Sheahan, T.C., and Wu, X. (2004) Coupling of electrochemical and mechanical processes in soils under dc fields. *Mechanics of Materials*, **36**, 453-65.

- Alshawabkeh, A.N., Yeung, A.T., and Bricka, M.R. (1999b) Practical aspects of in-situ electrokinetic extraction. *Journal of Environmental Engineering-Asce*, **125**, 27-35.
- Altaee, A. (2004) Metal removal from soil by electrokinetic processes : The effects of inorganic soil components on the process. *School of the Environment*, **PhD**. University of Brighton, Brighton.
- Altaee, A., Smith, R., and Mikhalovsky, S. (2007) The feasibility of decontamination of reduced saline sediments from copper using the electrokinetic process. *Journal of Environmental Management*, **In Press, Corrected Proof**.
- Amrate, S., Akretche, D.E., Innocent, C., and Seta, P. (2005) Removal of pb from a calcareous soil during edta-enhanced electrokinetic extraction. *Science of The Total Environment*, **349**, 56-66.
- Analytical Methods Committee. (1989a) Robust statistics - how not to reject outliers .1. Basic concepts. *Analyst*, **114**, 1693-7.
- . (1989b) Robust statistics - how not to reject outliers .2. Inter-laboratory trials. *Analyst*, **114**, 1699-702.
- Andersson, P.S., Wasserburg, G.J., Ingri, J., and Stordal, M.C. (1994) Strontium, dissolved and particulate loads in fresh and brackish waters: The baltic sea and mississippi delta. *Earth and Planetary Science Letters*, **124**, 195-210.
- Andreottola, G., Bonomo, L., De Gioannis, G., Ferrarese, E., Muntoni, A., Poletini, A., Pomi, R., and Saponaro, S. (2010) Lab-scale feasibility tests for sediment treatment using different physico-chemical techniques. *Journal of Soils and Sediments*, **10**, 142-50.
- Andrews, J.E. (1996) *An introduction to environmental chemistry*. xviii,209p p. Blackwell Science, Oxford.
- Argyragi, A., Ramsey, M.H., and Potts, P.J. (1997) Evaluation of portable x-ray fluorescence instrumentation for in situ measurements of lead on contaminated land. *Analyst*, **122**, 743-9.
- Ármansson, H., Burton, J.D., Jones, G.B., and Knap, A.H. (1985) Trace metals and hydrocarbons in sediments from the southampton water region, with particular reference to the influence of oil refinery effluent. *Marine Environmental Research*, **15**, 31-44.
- Ashman, M.R., and Puri, G. (2002) *Essential soil science : A clear and concise introduction to soil science*. vi, 198 p. p. Blackwell Science, Oxford.
- Athmer, C.J. (2009) Cost estimates for electrokinetic remediation. In K.R. Reddy, and C. Cameselle, Eds. *Electrochemical remediation technologies for polluted soils, sediments and groundwater*, p. 583-8. Wiley, Hoboken.
- Baraud, F., Tellier, S., and Astruc, M. (1997) Ion velocity in soil solution during electrokinetic remediation. *Journal of Hazardous Materials*, **56**, 315-32.
- . (1999) Temperature effect on ionic transport during soil electrokinetic treatment at constant ph. *Journal of Hazardous Materials*, **64**, 263-81.
- Barratt, J.O., and Harris, A.B. (1912) Observations on electro-osmosis. *Biochemical Journal*, **6**, 315-0.
- Bell, F.G. (1975) *Methods of treatment of unstable ground*. [8],215p. p. Newnes-Butterworths, London.
- Bendell-Young, L., and Harvey, H.H. (1992) The relative importance of manganese and iron oxides and organic matter in the sorption of trace metals by surficial lake sediments. *Geochimica et Cosmochimica Acta*, **56**, 1175-86.
- Beskid, N.J., Devgun, J.S., Zielke, M.M., and Erickson, M.D. (1993) Applied research and development private sector developments. US Department of Energy, .

- Bjerrum, L., Moum, J., and Eide, O. (1967) Application of electro-osmosis to a foundation problem in a norwegian quick clay. *Geotechnique*, **17**, 214-35.
- Blacksmith Institute. (2007) The world's worst polluted places. The top ten of the dirty thirty. In B. Institute, Ed. *Blacksmith Institute*, New York.
- British Standards Institution. (1994) *Specification for topsoil*. BSI, London.
- . (2007) *Specification for topsoil and requirements for use*. BSI, London.
- Buckley, C. (2007) Devon tin mine to reopen as prices soar. *The Times*, UK.
- Buckley, D.E., Smith, J.N., and Winters, G.V. (1995) Accumulation of contaminant metals in marine sediments of halifax harbour, nova scotia: Environmental factors and historical trends. *Applied Geochemistry*, **10**, 175-95.
- Burnotte, F., Lefebvre, G., and Grondin, G. (2004) A case record of electroosmotic consolidation of soft clay with improved soil-electrode contact. *Canadian Geotechnical Journal*, **41**, 1038-53.
- Cairney, T., and Hobson, D.M. (1998) Contaminated land : Problems and solutions, p. xvi, 369p. E & FN Spon, London.
- Candelone, J.P., Hong, J.H., Pellone, C., and Boutron, C.F. (1995) Post-industrial revolution changes in large scale atmospheric pollution of the northern hemisphere by heavy metals as documented in central greenland snow and ice. *Journal of Geophysical Research*, 16605-16.
- Casagrande, L. (1947) *The application of electro-osmosis to practical problems in foundations and earthworks*. 8°. p. pp. iv. 15. London.
- . (1949) Electro-osmosis in soils. *Géotechnique*, **1**, 159-77.
- . (1983) Stabilization of soils by means of electro-osmosis the state-of-the-art. *Journal of the Boston Society of Civil Engineers Section, American Society of Civil Engineers*, **69**, 255-302.
- Casagrande, L., Wade, N., Wakely, M., and Loughney, R. (1981) Electro-osmosis projects, british columbia, canada. *Proceedings of the International Conference on Soil Mechanics and Foundation Engineering*, **3**, p. 607-10. A. A. Balkema, Stockholm, Swed.
- Casey, F.X.M., Logsdon, S.D., Horton, R., and Jaynes, D.B. (1998) Measurement of field soil hydraulic and solute transport parameters. *Soil Science Society of America Journal*, **62**, 1172-8.
- Charlesworth, M.E., Service, M., and Gibson, C.E. (2006) The distribution and transport of sellafield derived ¹³⁷cs and ²⁴¹am to western irish sea sediments. *Science of The Total Environment*, **354**, 83-92.
- Chew, C.F., and Zhang, T.C. (1998) In-situ remediation of nitrate-contaminated ground water by electrokinetics iron wall processes. *Water Science and Technology*, **38**, 135-42.
- Chien, C.C., Inyang, H.I., and Everett, L.G. (2006) *Barrier systems for enviromental contaminant containment and treatment*. 375 p. CRC ; London : Taylor & Francis, Boca Raton, Fla.
- Chinthamreddy, S., and Reddy, K.R. (1999) Oxidation and mobility of trivalent chromium in manganese-enriched clays during electrokinetic remediation. *Journal of Soil Contamination*, **8**, 197-216.
- Chiras, D.D. (2006) *Environmental science*. xxiii, 642, [30] p. p. Jones and Bartlett, Sudbury, Mass. ; London.
- Choi, Y.S., and Lui, R. (1995) A mathematical model for the electrokinetic remediation of contaminated soil. *Journal of Hazardous Materials*, **44**, 61-75.
- Cifuentes, L., Torrealba, J., Crisóstomo, G., and Bustamante, M. (2001) Production of ferric hydroxide by anodic dissolution of carbon steel. *Ciencia Abierta* **15**.

- Cornell, R.M., and Schwertmann, U. (2003) *The iron oxides : Structure, properties, reactions, occurrences and uses*. xxxix, 664 p. p. Wiley-VCH, Weinheim ; [Cambridge].
- Cox, C.D., Shoesmith, M.A., and Ghosh, M.M. (1996) Electrokinetic remediation of mercury-contaminated soils using iodine/iodide lixiviant. *Environ. Sci. Technol.*, **30**, 1933-8.
- Cundy, A.B., and Croudace, I.W. (1995a) Heavy metal and hydrocarbon pollution in recent sediments from southampton water, southern england: A geochemical and isotopic study. *Environ. Sci. Technol.*, **29**, 1288-96.
- . (1995b) Sedimentary and geochemical variations in a salt marsh/mud flat environment from the mesotidal hamble estuary, southern england. *Marine Chemistry*, **51**, 115-32.
- Cundy, A.B., Croudace, I.W., Cearreta, A., and Irabien, M.J. (2003) Reconstructing historical trends in metal input in heavily-disturbed, contaminated estuaries: Studies from bilbao, southampton water and sicily. *Applied Geochemistry*, **18**, 311-25.
- Cundy, A.B., and Hopkinson, L. (2005) Electrokinetic iron pan generation in unconsolidated sediments: Implications for contaminated land remediation and soil engineering. *Applied Geochemistry*, **20**, 841-8.
- Cundy, A.B., Hopkinson, L., Lafite, R., Spencer, K., Taylor, J.A., Ouddane, B., Heppell, C.M., Carey, P.J., Charman, R., Shell, D., and Ulliyott, S. (2005) Heavy metal distribution and accumulation in two spartina sp.-dominated macrotidal salt marshes from the seine estuary (france) and the medway estuary (uk). *Applied Geochemistry*, **20**, 1195-208.
- Cundy, A.B., Hopkinson, L., and Whitby, R.L.D. (2007) *From nano to macro: Utilising iron chemistry for contaminated land remediation and pollution control*. 1150-4 p. Science Press Beijing, Beijing.
- . (2008) Use of iron-based technologies in contaminated land and groundwater remediation: A review. *Science of The Total Environment*, **400**, 42-51.
- Cundy, A.B., and Hopkinson, L.J. (2004) Patent no wo2004028717: Method for soil remediation and engineering. In E.P. Office, Ed. University of Brighton, University of Sussex, United Kingdom.
- Darmawan, and Wada, S.I. (2002) Effect of clay mineralogy on the feasibility of electrokinetic soil decontamination technology. *Applied Clay Science*, **20**, 283-93.
- De Gioannis, G., Muntoni, A., Polettini, A., and Pomi, R. (2009) Electrokinetic treatment of contaminated marine sediments. In K.R. Reddy, and C. Cameselle, Eds. *Electrochemical remediation technologies for polluted soils, sediments and groundwater*, p. 149-79. Wiley, Haboken.
- DeFlaun, M.F., and Condee, C.W. (1997) Electrokinetic transport of bacteria. *Journal of Hazardous Materials*, **55**, 263-77.
- DEFRA. (2002a) *Soil guideline values for arsenic contamination*. Great Britain, Department for Environment, Food & Rural Affairs.
- . (2002b) *Soil guideline values for cadmium contamination*. Great Britain, Department for Environment, Food & Rural Affairs.
- . (2002c) *Soil guideline values for chromium contamination*. Great Britain, Department for Environment, Food & Rural Affairs.
- . (2002d) *Soil guideline values for inorganic mercury contamination*. Great Britain, Department for Environment, Food & Rural Affairs.

- (2002e) *Soil guideline values for lead contamination*. Great Britain, Department for Environment, Food & Rural Affairs.
- (2002f) *Soil guideline values for nickel contamination*. Great Britain, Department for Environment, Food & Rural Affairs.
- (2002g) *Soil guideline values for selenium contamination*. Great Britain, Department for Environment, Food & Rural Affairs.
- Denisov, G., Hicks, R.E., and Probst, R.F. (1996) On the kinetics of charged contaminant removal from soils using electric fields. *Journal of Colloid and Interface Science*, **178**, 309-23.
- Ding, M., Schuiling, R.D., and van der Sloot, H.A. (2002) Self-sealing isolation and immobilization: A geochemical approach to solve the environmental problem of waste acidic jarosite. *Applied Geochemistry*, **17**, 93-103.
- Eary, L.E., and Rai, D. (1988) Chromate removal from aqueous wastes by reduction with ferrous ion. *Environ. Sci. Technol.* ; Vol/Issue: 22:8, Pages: 972-7.
- Eaton, K. (2004) Is this the end of dig and dump? *Environ- Estates Review*, **1**, p. 190-2.
- Endell, K., and Hoffmann, U. (1936) Electrochemical hardening of clayey soils. *Proceedings of the 1st International Conference on Soil Mechanics and Foundation Engineering*, **1**, p. 273-5, Cambridge, Massachusetts.
- Environment Agency. (2004) *The state of soils in england and wales*. 28 p. p. Environment Agency, Bristol.
- (2007) Environment agency : Main contaminants at reported contaminated land sites in england and wales, 2007.
- Environment Agency, and DEFRA. (2004) *Model procedures for the management of land contamination*. Environment Agency, Bristol.
- EU. (1999) Council directive 1999/31/ec of 26 april 1999 on the landfill of waste *OJ L 182 of 16.07.1999*. Coucil Directive.
- Eykholt, G.R. (1997) Development of pore pressures by nonuniform electroosmosis in clays. *Journal of Hazardous Materials*, **55**, 171-86.
- Eykholt, G.R., and Daniel, D.E. (1994) Impact of system chemistry on electroosmosis in contaminated soil. *Journal of Geotechnical Engineering-Asce*, **120**, 797-815.
- Farmer, I.W. (1975) Electroosmosis and electrochemical stabilisation. In F.G. Bell, Ed. *Methods of treatment of unstable ground*, p. 26-36. Newnes-Butterworths, London.
- Faulkner, D.W.S., Hopkinson, L., and Cundy, A.B. (2005) Electrokinetic generation of reactive iron-rich barriers in wet sediments: Implications for contaminated land management. *Mineralogical Magazine*, **69**, 749-57.
- Fendorf, S.E. (1992) Oxidation and sorption mechanisms of hydrolyzable metal ions on oxide surface. *Department of Plant and Soil Sciences, PhD Dissertation*, p. 251. University of Delaware, Delaware, USA.
- (1995) Surface reactions of chromium in soils and waters. *Geoderma*, **67**, 55-71.
- Franklin, J.A., and Brook, N. (1985) Method for determining point load strength index. International society for rock mechanics commission on testing methods (revision of the point load test method). *International Journal of Rock Mechanics and Mining Science*, **22**, 51-60.
- Freeze, R.A., and Cherry, J.A. (1979) *Groundwater*. xv,604p. p. Prentice-Hall, Englewood Cliffs ; London.
- Garcia-Gutierrez, M.D., Gomez-Lahoz, C., Rodriguez-Maroto, J.M., Vereda-Alonso, C., and Garcia-Herruzo, F. (2007) Electrokinetic remediation of a soil contaminated by the pyritic sludge spill of aznalcollar (sw, spain). *Electrochimica Acta*, **52**, 3372-9.

- Giampietro, M., Ulgiati, S., and Pimentel, D. (1997) Feasibility of large-scale biofuel production. *BioScience*, **v47**, p587(14).
- Giannis, A., and Gidarakos, E. (2005) Washing enhanced electrokinetic remediation for removal of cadmium from real contaminated soil. *Journal of Hazardous Materials*, **123**, 165-75.
- Godschalk, M.S., and Lageman, R. (2005) Electrokinetic biofence, remediation of vocs with solar energy and bacteria. *Engineering Geology*, **77**, 225-31.
- Gray, D.H., and Schlocker, J. (1969) Electrochemical alteration of clay soils. *Clays and Minerals*, **17**, 309-22.
- Great Britain Dept. of the Environment Transport and the Regions. (1999) *Contaminated land : Implementation of part iia of the environmental protection act 1990*. Great Britain, Department of the Environment, Transport and the Regions.
- Gribbin, J.R. (2002) *Science: A history, 1543-2001*. xxii, 646 p. p. Allen Lane, London.
- Guest, C.A., Johnson, C.T., King, J.J., Alleman, J.E., Tishmack, J.K., and Norton, L.D. (2001) Chemical characterization of synthetic soil from composting coal combustion and pharmaceutical by-products. *Journal of Environmental Quality*, **30**, 246-53.
- Gurzau, E.S., Neagu, C., and Gurzau, A.E. (2003) Essential metals - case study on iron. *Ecotoxicology and Environmental Safety*, **56**, 190-200.
- Hamed, J.T., and Bhadra, A. (1997) Influence of current density and ph on electrokinetics. *Journal of Hazardous Materials*, **55**, 279-94.
- Harada, M. (1995) Minamata disease: Methylmercury poisoning in japan caused by environmental pollution. *Critical Review of Toxicology*, **25**, 1-24.
- Haran, B.S., Popov, B.N., Zheng, G.H., and White, R.E. (1996) Development of a new electrokinetic technique for decontamination of hexavalent chromium from low surface charged soils. *Environmental Progress*, **15**, 166-72.
- . (1997) Mathematical modeling of hexavalent chromium decontamination from low surface charged soils. *Journal of Hazardous Materials*, **55**, 93-107.
- Harbottle, M.J. (2003) The use of electrokinetics to enhance the degradation of organic contaminants in soils. *Department of Engineering Science*, , **Doctor of Philosophy**, p. 255. University of Oxford, Oxford.
- Hartley, W., Edwards, R., and Lepp, N.W. (2004) Arsenic and heavy metal mobility in iron oxide-amended contaminated soils as evaluated by short- and long-term leaching tests. *Environmental Pollution*, **131**, 495-504.
- Harton, J.H., Suliman, H., Abi-Chedid, E., and Chilingar, G. (1967) Effects of electrochemical treatment on selected physical properties of a clayey silt. *Engineering Geology*, **2**, 191-6.
- Head, K.H. (1982) *Manual of soil laboratory testing*. p450-5 p. Pentech, London.
- Helland, B.R., Alvarez, P.J.J., and Schnoor, J.L. (1995) Reductive dechlorination of carbon-tetrachloride with elemental iron. *Journal of Hazardous Materials*, **41**, 205-16.
- Helmholtz, H. (1879) Studien über electrische grenzsichten. *Annalen der Physik und Chemie*, **243**, 337-82.
- Hernández-Luis, F., Domingo, M.L., V., G.M., and Arbelo, V.C.D. (2004) Electroremediation: A study of the influence of buffering behavior in contaminated soils. *Remediation Journal*, **14**, 105-12.
- Hester, R.E., and Harrison, R.M. (1997) *Contaminated land and its reclamation*. xv,145p. p. Telford, London.

- . (2001) *Assessment and reclamation of contaminated land*. xiii, 164 p. p. Royal Society of Chemistry, Cambridge.
- Hicks, R.E., and Tondorf, S. (1994) Electrorestoration of metal-contaminated soils. *Environmental Science & Technology*, **28**, 2203-10.
- HM Treasury. (2007) *Budget 2007. Building Britain's long-term future. Prosperity and fairness for families*. The Stationary Office, London.
- Ho, S.V., Athmer, C., Sheridan, P.W., Hughes, B.M., Orth, R., McKenzie, D., Brodsky, P.H., Shapiro, A., Thornton, R., Salvo, J., Schultz, D., Landis, R., Griffith, R., and Shoemaker, S. (1999) The lasagna technology for in situ soil remediation. 1. Small field test. *Environ. Sci. Technol.*, **33**, 1086-91.
- Ho, S.V., Athmer, C.J., Sheridan, P.W., and Shapiro, A.P. (1997) Scale-up aspects of the lasagna process for in situ soil decontamination. *Journal of Hazardous Materials*, **55**, 39-60.
- Hodko, D., Van Hyfe, J., Denvir, A., and Magnuson, J. (2000) Methods for enhancing phytoextraction of contaminants from porous media using electrokinetic phenomena In U.P. Office, Ed, USA.
- Holzlohner, U., August, H., and Meggyes, T. (1997) *Advanced landfill liner systems*. 389p. p. Thomas Telford Publishing, London.
- Hong, S., Candelone, J.P., Patterson, C.C., and Boutron, C.F. (1994) Greenland ice evidence of hemispheric lead pollution two millennia ago by Greek and Roman civilizations. *Science*, **265**, 1841-3.
- Hopkins, J., and Hosford, M. (2009a) *Contaminants in soil : Updated collation of toxicological data and intake values for humans - mercury*. vii, 45 p. p. Environment Agency, Bristol.
- . (2009b) *Contaminants in soil : Updated collation of toxicological data and intake values for humans : Cadmium*. ix, 43 p. p. Environment Agency, Bristol.
- Hopkins, J., Watts, P., and Hosford, M. (2009) *Contaminants in soil : Updated collation of toxicological data and intake values for humans : Inorganic arsenic*. viii, 40 p. p. Environment Agency, Bristol.
- Hopkinson, L., and Cundy, A.B. (2003) Firs (ferric iron remediation and stabilisation): A novel electrokinetic technique for soil remediation and engineering. *Claire Research Bulletin RB2*.
- Hopkinson, L., Cundy, A.B., Faulkner, D.W.S., Hansen, A., and Pollock, R. (2009) Electrokinetic stabilization of chromium (vi)-contaminated soils. In K.R. Reddy, and C. Cameselle, Eds. *Electrochemical remediation technologies for polluted soils, sediments, and groundwater*, p. 1 v. Wiley-Blackwell, Oxford.
- IAEA. (2004) Soil sampling for environmental contaminants. International Atomic Energy Agency, Vienna.
- Ingles, O.G., and Metcalf, J.B. (1972) *Soil stabilization : Principles and practice*. 381p. p. Butterworths, Sydney ; London.
- Islam, J., and Singhal, N. (2004) A laboratory study of landfill-leachate transport in soils. *Water Research*, **38**, 2035-42.
- Jackman, S.A., Maini, G., Sharman, A.K., Sunderland, G., and Knowles, C.J. (2001) Electrokinetic movement and biodegradation of 2,4-dichlorophenoxyacetic acid in silt soil. *Biotechnology and Bioengineering*, **74**, 40-8.
- Jacob, K., Dietrich, S., and Krug, H.J. (1994) *Self organisation of mineral fabrics*. 259-68 p. Springer Verlag, Berlin.
- Jacobs, R.A., Sengun, M.Z., Hicks, R.E., and Probst, R.F. (1994) Model and experiments on soil remediation by electric-fields. *Journal of Environmental*

- Science and Health Part a-Environmental Science and Engineering & Toxic and Hazardous Substance Control*, **29**, 1933-55.
- Johnson, T.L., Fish, W., Gorby, Y.A., and Tratnyek, P.G. (1998) Degradation of carbon tetrachloride by iron metal: Complexation effects on the oxide surface. *Journal of Contaminant Hydrology*, **29**, 379-98.
- Jones, A. (2000) *Practical skills in environmental science*. x, 290 p. p. Prentice-Hall, [London].
- Kalnicky, D.J., and Singhvi, R. (2001) Field portable xrf analysis of environmental samples. *Journal of Hazardous Materials*, **83**, 93-122.
- Kershaw, S., and Cundy, A. (2000) *Oceanography : An earth science perspective*. xii, 276 p. p. Stanley Thornes, Cheltenham.
- Kiely, G. (1997) *Environmental engineering*. xx, 979p. p. McGraw-Hill, London.
- Kim, K.H., Joung, H.T., Nam, H., Seo, Y.C., Hong, J.H., Yoo, T.W., Lim, B.S., and Park, J.H. (2004) Management status of end-of-life vehicles and characteristics of automobile shredder residues in korea. *Waste Management*, **24**, 533-40.
- Kim, S.O., Kim, K.W., and Stuben, D. (2002) Evaluation of electrokinetic removal of heavy metals from tailing soils. *Journal of Environmental Engineering-Asce*, **128**, 705-15.
- Kimura, T., Takase, K.-I., and Tanaka, S. (2007a) Concentration of copper and a copper-edta complex at the ph junction formed in soil by an electrokinetic remediation process. *Journal of Hazardous Materials*, **143**, 668-72.
- Kimura, T., Takase, K.-I., Terui, N., and Tanaka, S. (2007b) Ferritization treatment of copper in soil by electrokinetic remediation. *Journal of Hazardous Materials*, **143**, 662-7.
- Klein. (1990) Dissipative gefugebildungen in lockersedimenten durch einwirkung elektrischer felder ein beitrag zur bedeutung des thermodynamischen nichtgleichgewichts fur lagerstattengenetische vorgange. Diss tu berlin, berlin. Quoted in: Jacob, K.H., Dietrich, S. and Krug, H.J. (1994) *Self organised mineral fabrics*. Pp. 259-268 in: *Fractals and Dynamic Systems in Geoscience* (J.H. Kruhl, editor). Springer Verlag, Berlin.
- Korolev, V.A. (2006) Electrokinetic remediation of a contaminated land in cities. *IAEG 2006: Engineering geology for tomorrow's cities*, Nottingham, UK.
- Kovalick, W.W. (1995a) In situ remediation technology status report: Electrokinetics. In W. Environmental Protection Agency, DC (United States). Office of Solid Waste and Emergency Response, Ed, p. 27 p. ; PL:.
- . (1995b) Remediation technologies for us hazardous-waste sites. *Chemistry & Industry*, 500-3.
- Kovalick, W.W., and Kingscott, J. (1996) Emerging issues and technology in site remediation. *Hazardous Waste & Hazardous Materials*, **13**, U2-U6.
- Krauskopf, K.B. (1979) *Introduction to geochemistry*. xv,617p. p. McGraw-Hill, New York ; London.
- Kumar, P.R., Chaudhari, S., Khilar, K.C., and Mahajan, S.P. (2004) Removal of arsenic from water by electrocoagulation. *Chemosphere*, **55**, 1245-52.
- Kumpiene, J., Ore, S., Renella, G., Mench, M., Lagerkvist, A., and Maurice, C. (2006) Assessment of zerovalent iron for stabilization of chromium, copper, and arsenic in soil. *Environmental Pollution*, **144**, 62-9.
- Kurfurst, U., Desauls, A., Rehnert, A., and Muntau, H. (2004) Estimation of measurement uncertainty by the budget approach for heavy metal content in soils under different land use. *Accreditation and Quality Assurance*, **9**, 64-75.

- Lageman, R. (1993) Electroreclamation. *Environmental Science & Technology*, **27**, 2648-50.
- Lageman, R., Clarke, R.L., and Pool, W. (2005) Electro-reclamation, a versatile soil remediation solution. *Engineering Geology*, **77**, 191-201.
- Lageman, R., and Pool, W. (2009) Electrokinetic biofences. In K.R. Reddy, and C. Cameselle, Eds. *Electrochemical remediation technologies for polluted soils, sediments, and groundwater*. Wiley, New Jersey.
- Lageman, R., Pool, W., and Seffinga, G. (1989) Electro-reclamation - theory and practice. *Chemistry & Industry*, 585-90.
- Lamont-Black, J. (2001) E.K.G.: The next generation of geosynthetics. *Ground Engineering*, **34**, 22-3.
- Lashmar, P. (2004) Cornwall goes back down the tin mine as fresh demand puts a shine on. *Independent on Sunday*.
- Lear, G., Harbottle, M.J., van der Gast, C.J., Jackman, S.A., Knowles, C.J., Sills, G., and Thompson, I.P. (2004) The effect of electrokinetics on soil microbial communities. *Soil Biology & Biochemistry*, **36**, 1751-60.
- Lee, H.-H., and Yang, J.-W. (2000) A new method to control electrolytes ph by circulation system in electrokinetic soil remediation. *Journal of Hazardous Materials*, **77**, 227-40.
- Leinz, R.W., Hoover, D.B., and Meier, A.L. (1998) Neochim: An electrochemical method for environmental application. *Journal of Geochemical Exploration*, **64**, 421-34.
- Leupin, O.X., and Hug, S.J. (2005) Oxidation and removal of arsenic (iii) from aerated groundwater by filtration through sand and zero-valent iron. *Water Research*, **39**, 1729-40.
- Lovelock, J.E. (1974) Atmospheric halocarbons and stratospheric ozone. *Nature*, **252**, 292-4.
- Luo, Q.S., Zhang, X.H., Wang, H., and Qian, Y. (2005) The use of non-uniform electrokinetics to enhance in situ bioremediation of phenol-contaminated soil. *Journal of Hazardous Materials*, **121**, 187-94.
- Lyklema, J. (2003) Electrokinetics after smoluchowski. *Colloids and Surfaces A: Physicochemical and Engineering Aspects*, **222**, 5-14.
- Lynch, R. (2009) Electorkinetic barriers for prevention of groundwater pollution. In K.R. Reddy, and C. Cameselle, Eds. *Electrochemical remediation technologies for polluted soils, sediments, and groundwater*. Wiley-Blackwell, Oxford.
- Lynch, R.J., Muntoni, A., Ruggeri, R., and Winfield, K.C. (2007) Preliminary tests of an electrokinetic barrier to prevent heavy metal pollution of soils. *Electrochimica Acta*, **52**, 3432-40.
- Maes, N., Moors, H., Dierckx, A., De Canniere, P., and Put, M. (1999) The assessment of electromigration as a new technique to study diffusion of radionuclides in clayey soils. *Journal of Contaminant Hydrology*, **36**, 231-47.
- Manahan, S.E. (2000) *Fundamentals of environmental chemistry*. Lewis Publishers, Boca Raton, FL.
- Manokararajah, K., and Ranjan, R.S. (2005) Electrokinetic retention, migration and remediation of nitrates in silty loam soil under hydraulic gradients. *Engineering Geology*, **77**, 263-72.
- Martin, T.A., and Ruby, M.V. (2004) Review of in situ remediation technologies for lead, zinc, and cadmium in soil. *Remediation Journal*, **14**, 35-53.
- Marukawa, K., and Edwards, K.L. (2001) Development of iron and steel into eco-material. *Materials & Design*, **22**, 133-6.

- Masliyah, J.H. (1994) *Electrokinetic transport phenomena*. Alberta Oil Sands Technology & Research Authority, Edmonton.
- Masliyah, J.H., and Bhattacharjee, S. (2006) *Electrokinetic and colloid transport phenomena*. xxiv, 707 p. p. Wiley-Interscience, Hoboken, N.J.
- Mattson, E.D. (1993) Electrokinetic extraction of chromate from unsaturated soils. In U.S Department of Energy, Ed.
- McGeough, J.A. (1974) *Principles of electrochemical machining*. xv,255p. p. Chapman and Hall, London.
- McGuire, M.M., Carlson, D.L., Vikesland, P.J., Kohn, T., Grenier, A.C., Langley, L.A., Roberts, A.L., and Fairbrother, D.H. (2003) Applications of surface analysis in the environmental sciences: Dehalogenation of chlorocarbons with zero-valent iron and iron-containing mineral surfaces. *Analytica Chimica Acta*, **496**, 301-13.
- McNeill, F.E., Stokes, L., Brito, J.A.A., Chettle, D.R., and Kaye, W.E. (2000) 109cd k x ray fluorescence measurements of tibial lead content in young adults exposed to lead in early childhood. *Occup Environ Med*, **57**, 465-71.
- McNeill, J.R. (2000) *Something new under the sun : An environmental history of the world in the 20th century*. xxiv, 421 p. p. Penguin, 2001, London.
- Meharg, A.A. (2004) Arsenic in rice - understanding a new disaster for south-east asia. *Trends in Plant Science*, **9**, 415-7.
- Mench, M., Vangronsveld, J., Beckx, C., and Ruttens, A. (2006) Progress in assisted natural remediation of an arsenic contaminated agricultural soil. *Environmental Pollution*, **144**, 51-61.
- Meng, X.G., Korfiatis, G.P., Bang, S.B., and Bang, K.W. (2002) Combined effects of anions on arsenic removal by iron hydroxides. *Toxicology Letters*, **133**, 103-11.
- Meng, Z.G., Korfiatis, G.P., Christodoulatos, C., and Bang, S. (2001) Treatment of arsenic in bangladesh well water using a household co-precipitation and filtration system. *Water Research*, **35**, 2805-10.
- Meyer, P.B., Williams, R.H., and Yount, K.R. (1995) *Contaminated land : Reclamation, redevelopment and re-use in the united states and the european union*. x, 223 p. p. E. Elgar, Aldershot.
- Micic, S., Shang, J.Q., and Lo, K.Y. (2003) Electro cementation of a marine clay induced by electrokinetics. *International Journal of Offshore and Polar Engineering*, **13**, 308-15.
- Mitchell, J.K. (1976) *Fundamentals of soil behavior*. xvii,422p. p. Wiley, New York ; London.
- Mitchell, J.K., and Soga, K.B. (2005) *Fundamentals of soil behavior*. xiii, 577 p. p. Wiley, New York ; Chichester.
- Mohamed, A.M.O., and Antia, H.E. (1998) *Geoenvironmental engineering*. xxi, 707p. p. Elsevier, Amsterdam ; Oxford.
- Mohan, D., and Pittman, J.C.U. (2007) Arsenic removal from water/wastewater using adsorbents--a critical review. *Journal of Hazardous Materials*, **142**, 1-53.
- Montgomery, D.R. (2007) *Dirt : The erosion of civilizations*. ix, 285 p. * p. University of California Press, Berkeley.
- Moore, P., and Cobby, J. (1998) *Introductory statistics for environmentalists*. x, 250p. p. Prentice Hall Europe, London.
- Moreau, E., Grimaud, P.O., and Touchard, G. (1997) Electrical decontamination of soil. *Journal of Electrostatics*, **40-41**, 675-80.
- Mukhopadhyay, B., Sundquist, J., and Schmitz, R.J. (2007) Removal of cr(vi) from cr-contaminated groundwater through electrochemical addition of fe(ii). *Journal of Environmental Management*, **82**, 66-76.

- Mulligan, C.N., Yong, R.N., and Gibbs, B.F. (2001) Remediation technologies for metal-contaminated soils and groundwater: An evaluation. *Engineering Geology*, **60**, 193-207.
- Murphy, E.M., Zachara, J.M., Smith, S.C., and Phillips, J.L. (1990) The sorption of humic acids to mineral surfaces and their roles in contaminant binding, p. Size: Pages: (15 p), United States.
- Nadal, M., Schuhmacher, M., and Domingo, J.L. (2004) Metal pollution of soils and vegetation in an area with petrochemical industry. *Science of The Total Environment*, **321**, 59-69.
- Narasimhan, B., and Sri Ranjan, R. (2000) Electrokinetic barrier to prevent subsurface contaminant migration: Theoretical model development and validation. *Journal of Contaminant Hydrology*, **42**, 1-17.
- Nyer, E.K. (2001) *In situ treatment technology*. 536 p. p. Lewis Publishers, Boca Raton, FL ; London.
- Oh, S.Y., Ye, J.C., Cha, D.K., and Chiu, P.C. (2003) Graphite-mediated reduction of organic pollutants with iron. *Abstracts of Papers of the American Chemical Society*, **225**, U804-U.
- Otsuki, N., Yodsudjai, W., and Nishida, T. (2007) Feasibility study on soil improvement using electrochemical technique. *Construction and Building Materials*, **21**, 1046-51.
- Page, M.M., and Page, C.L. (2002) Electroremediation of contaminated soils. *Journal of Environmental Engineering-Asce*, **128**, 208-19.
- Pamukcu, S. (2005) Electrically enhanced transformation of contaminants in clay rich sub-surface. In EREM, Ed. *The 5th Symposium on Elektrokinetic Remediation, EREM 2005*, Ferrara, Italy.
- . (2009) Electrochemical transport and transformations. In K.R. Reddy, and C. Cameselle, Eds. *Electrochemical remediation technologies for polluted soils, sediments and groundwater*, p. 29-64. Wiley, Haboken.
- Pamukcu, S., Weeks, A., and Wittle, J.K. (1997) Electrochemical extraction and stabilization of selected inorganic species in porous media. *Journal of Hazardous Materials*, **55**, 305-18.
- . (2003) Electro kinetically enhanced reduction of cr(vi) by aqueous fe(ii). *Abstracts of Papers of the American Chemical Society*, **225**, U811-U.
- . (2004) Enhanced reduction of cr(vi) by direct electric current in a contaminated clay. *Environmental Science & Technology*, **38**, 1236-41.
- Pamukcu, S., and Wittle, J.K. (1992) Electrokinetic removal of selected heavy-metals from soil. *Environmental Progress*, **11**, 241-50.
- PANalytical. (2006) Trace element analysis of toxic heavy metals in soils and contaminated land using minipal 4. *PAnalytical*.
- Pendergrass, A., and Butcher, D.J. (2006) Uptake of lead and arsenic in food plants grown in contaminated soil from barber orchard, nc. *Microchemical Journal*, **83**, 14-6.
- Peulon, S., Antony, H., Legrand, L., and Chausse, A. (2004) Thin layers of iron corrosion products electrochemically deposited on inert substrates: Synthesis and behaviour. *Electrochimica Acta*, **49**, 2891-9.
- Pierzynski, G.M., Sims, J.T., and Vance, G.F. (2005) *Soils and environmental quality*. 480 p. p. Boca Raton.
- Ponting, C. (2007) *A new green history of the world : The environment and the collapse of great civilizations*. x, 452 p. p. Vintage Books, London.

- Potter, H.A.B., and Yong, R.N. (1997) Influence of amorphous oxides on the fate of heavy metals. In R.N. Yong, and H.R. Thomas, Eds. *Geoenvironmental Engineering*, p. 141-50. Thomas Telford, Cardiff School of Engineering.
- . (1999) Influence of iron/aluminium ratio on the retention of lead and copper by amorphous iron-aluminium oxides. *Applied Clay Science*, **14**, 1-26.
- Potts, P.J., Ramsey, M.H., and Carlisle, J. (2002) Portable x-ray fluorescence in the characterisation of arsenic contamination associated with industrial buildings at a heritage arsenic works site near redruth, cornwall, uk. *Journal of Environmental Monitoring*, **4**, 1017-24.
- Probstein, R.F., and Hicks, R.E. (1993) Removal of contaminants from soils by electric-fields. *Science*, **260**, 498-503.
- Puppala, S.K., Alshawabkeh, A.N., Acar, Y.B., Gale, R.J., and Bricka, M. (1997) Enhanced electrokinetic remediation of high sorption capacity soil. *Journal of Hazardous Materials*, **55**, 203-20.
- Pyatt, F.B., Amos, D., Grattan, J.P., Pyatt, A.J., and Terrell-Nield, C.E. (2002) Invertebrates of ancient heavy metal spoil and smelting tip sites in southern Jordan: Their distribution and use as bioindicators of metalliferous pollution derived from ancient sources. *Journal of Arid Environments*, **52**, 53-62.
- Quincke, G. (1861) Ueber die festsetzung materieller theilchen durch stromende electricitaet. Quoted in: Barratt and harris (1912) observations on electro-osmosis, *biochemical journal*, 6, 3. *Ann. d. Physik. u. Chemie*, **113**, 513, **6**, 315-32.
- Rajeshwar, K., and Ibanez, J.G. (1997) *Environmental electrochemistry : Fundamentals and applications in pollution abatement*. xvi, 776p. p. Academic Press, San Diego ; London.
- Ramsey, M.H. (1998) Sampling as a source of measurement uncertainty: Techniques for quantification and comparison with analytical sources. *Journal of Analytical Atomic Spectrometry*, **13**, 97-104.
- . (2004) Improving the reliability of contaminated land assessment using statistical methods: Part 1 - basic principles and concepts. *Cl:air Contaminated Land in Real Environments*, p. 4.
- Ramsey, M.H., and Argyraki, A. (1997) Estimation of measurement uncertainty from field sampling: Implications for the classification of contaminated land. *Science of the Total Environment*, **198**, 243-57.
- Ramsey, M.H., Argyraki, A., and Thompson, M. (1995) Estimation of sampling bias between different sampling protocols on contaminated land. *Analyst*, **120**, 1353-6.
- Ranjan, R.S. (2009) Electrokinetic barriers: Modeling and validation. In K.R. Reddy, and C. Cameselle, Eds. *Electrochemical remediation technologies for polluted soils, sediments and groundwater*. Wiley, Hoboken, New Jersey.
- Rasmussen, W.O., and Budhu, M. (1996) Electrode placement for subsurface electric field generation. *Journal of Environmental Engineering*, **122**, 764-8.
- Raudkivi, A.J., and Callander, R.A. (1976) *Analysis of groundwater flow*. xii,214p. p. Arnold, London.
- Reddy, K.R., and Ala, P.R. (2005) Electrokinetic remediation of metal-contaminated field soil. *Separation Science and Technology*, **40**, 1701-20.
- Reddy, K.R., and Cameselle, C. (2009) *Electrochemical remediation technologies for polluted soils, sediments, and groundwater*. Wiley-Blackwell, Oxford.

- Reddy, K.R., Chaparro, C., and Saichek, R.E. (2003) Removal of mercury from clayey soils using electrokinetics. *Journal of Environmental Science and Health Part a-Toxic/Hazardous Substances & Environmental Engineering*, **38**, 307-38.
- Reddy, K.R., and Chinthamreddy, S. (1999) Electrokinetic remediation of heavy metal-contaminated soils under reducing environments. *Waste Management*, **19**, 269-82.
- . (2003) Sequentially enhanced electrokinetic remediation of heavy metals in low buffering clayey soils. *Journal of Geotechnical and Geoenvironmental Engineering*, **129**, 263-77.
- Reddy, K.R., Parupudi, U.S., Devulapalli, S.N., and Xu, C.Y. (1997) Effects of soil composition on the removal of chromium by electrokinetics. *Journal of Hazardous Materials*, **55**, 135-58.
- Reddy, K.R., Xu, C.Y., and Chinthamreddy, S. (2001) Assessment of electrokinetic removal of heavy metals from soils by sequential extraction analysis. *Journal of Hazardous Materials*, **84**, 279-96.
- Rees, M.J. (2003) *Our final century : Will civilisation survive the twenty-first century?* 288 p. p. Heinemann, London.
- Reuss, F.F. (1808) Sur un nouvel effet de l'électricité galvanique. *Mémoires de la Société Impériale des Naturalistes de Moscow* **2**, 327-36.
- Robison, W.L., Conrado, C.L., Bogen, K.T., and Stoker, A.C. (2003) The effective and environmental half-life of ¹³⁷Cs at coral islands at the former us nuclear test site. *Journal of Environmental Radioactivity*, **69**, 207-23.
- Röhrs, J., Ludwig, G., and Rahner, D. (2002) Electrochemically induced reactions in soils--a new approach to the in-situ remediation of contaminated soils?: Part 2: Remediation experiments with a natural soil containing highly chlorinated hydrocarbons. *Electrochimica Acta*, **47**, 1405-14.
- Rose, J. (1993) Croatia: Environmental effects of war. *Environmental science and technology*, **27**.
- Royal Society of Chemistry. (2008) *Journal of analytical atomic spectroscopy*, **2008**. RSC.
- Sacuta, A. (1980) Enhanced oil recovery using electrical means, p. Pages: v, United States.
- Saichek, R.E., and Reddy, K.R. (2003a) Effect of ph control at the anode for the electrokinetic removal of phenanthrene from kaolin soil. *Chemosphere*, **51**, 273-87.
- . (2003b) Effects of system variables on surfactant enhanced electrokinetic removal of polycyclic aromatic hydrocarbons from clayey soils. *Environmental Technology*, **24**, 503-15.
- Scalenghe, R., Certini, G., and Ugolini, F.C. (2006) *Soils : Basic concepts and future challenges*. xvii, 310 p. p. Cambridge University Press, Cambridge.
- Schultz, D.S. (1997) Electroosmosis technology for soil remediation: Laboratory results, field trial, and economic modeling. *Journal of Hazardous Materials*, **55**, 81-91.
- Schwertmann, W. (1991) Solubility and dissolution of iron oxides. *Plant and Soil*, **130**, 1-25
- Selim, H.M.E., and Amacher, M.C. (1997) *Reactivity and transport of heavy metals in soils*. 201p. p. CRC/Lewis, Boca Raton, Fla ; London.
- Shapiro, A. (1996) Development of an integrated in-situ remediation technology topical report for tasks no. 2-4 entitled "electrokinetic modeling". Monsanto and General Electric.

- Shapiro, A.P., and Probstein, R.F. (1993) Removal of contaminants from saturated clay by electroosmosis. *Environ. Sci. Technol.*, **27**, 283-91.
- Smedley, P.L., and Kinniburgh, D.G. (2002) A review of the source, behaviour and distribution of arsenic in natural waters. *Applied Geochemistry*, **17**, 517-68.
- Smedley, P.L., Nicolli, H.B., Macdonald, D.M.J., Barros, A.J., and Tullio, J.O. (2002) Hydrogeochemistry of arsenic and other inorganic constituents in groundwaters from la pampa, argentina. *Applied Geochemistry*, **17**, 259-84.
- Sogorka, D.B., Gabert, H., and Sogorka, B. (1998) Emerging technologies for soils contaminated with metals - electrokinetic remediation. *Hazardous and Industrial Wastes*, **30**, 673-85.
- Sparks, D.L.P.D. (1995) *Environmental soil chemistry*. xii, 267 p. p. Academic, San Diego, Calif. ; London.
- Spencer, K.L., Cundy, A.B., and Croudace, I.W. (2003) Heavy metal distribution and early-diagenesis in salt marsh sediments from the medway estuary, kent, uk. *Estuarine, Coastal and Shelf Science*, **57**, 43-54.
- Terzaghi, K., and Peck, R.B. (1967) *Soil mechanics in engineering practice*. 749p. p. Wiley, New York ; London.
- Trushinskii. (1993) Electrochemical soil stabilization method *Soil Mechanics and Foundation Engineering*, **30**.
- . (1996) Electrochemical anchors and piles in foundation engineering *Soil Mechanics and Foundation Engineering*, **33**.
- U.S. Environmental Protection Agency. (1997) Resource guide for electrokinetics laboratory and field processes applicable to radioactive and hazardous mixed wastes in soil and groundwater from 1992 to 1997. In C.f.R.T.a. Tools, Ed.
- UK-Treasury. (2006) Investing in britain's potential : Building our long-term future : Pre-budget report : December 2006, p. 266 p. HM Treasury, London.
- Van Camp, L., Bujarrabal, B., Gentile, A-R., Jones, R.J.A., Montanarella, L., Olazabal, C., Selvaradjou, S.K. (2004) Reports of the technical working groups established under the thematic strategy for soil protection., p. 872 pp. Office for Official Publications of the European Communities Luxembourg.
- Van Cauwenberghe, L. (1997) Electrokinetics: Technology overview report. *Groundwater Remediation*, p. 1-17. Technologies Analysis Centre, Pittsburgh.
- Vereda-Alonso, C., Miguel Rodriguez-Maroto, J., Garcia-Delgado, R.A., Gomez-Lahoz, C., and Garcia-Herruzo, F. (2004) Two-dimensional model for soil electrokinetic remediation of heavy metals: Application to a copper spiked kaolin. *Chemosphere*, **54**, 895-903.
- Virkutyte, J., Sillanpaa, M., and Latostenmaa, P. (2002) Electrokinetic soil remediation - a critical overview. *The Science of The Total Environment*, **289**, 97-121.
- Walker, C.H. (1996) *Principles of ecotoxicology*. xxii, 321p. p. Taylor & Francis, London.
- Wang, J.-Y., Huang, X.-J., Kao, J.C.M., and Stabnikova, O. (2006) Removal of heavy metals from kaolin using an upward electrokinetic soil remedial (uesr) technology. *Journal of Hazardous Materials*, **136**, 532-41.
- . (2007) Simultaneous removal of organic contaminants and heavy metals from kaolin using an upward electrokinetic soil remediation process. *Journal of Hazardous Materials*, **144**, 292-9.
- Warren, G.P., Alloway, B.J., Lepp, N.W., Singh, B., Bochereau, F.J.M., and Penny, C. (2003) Field trials to assess the uptake of arsenic by vegetables from contaminated soils and soil remediation with iron oxides. *Science of the Total Environment*, **311**, 19-33.

- Watts, P., and Hosford, M. (2009) *Contaminants in soil : Updated collation of toxicological data and intake values for humans : Nickel*. viii, 40 p. p. Environment Agency, Bristol.
- White, K. (2000) Peconic river remedial alternatives: Electrochemical remediation. *Technology Fact Sheet*. Brookhaven National Laboratory.
- White, R.E. (2006) *Principles and practice of soil science : The soil as a natural resource*. xi, 363 p. p. Oxford : Blackwell Science, 2006.
- Wittle, J.K., Zanko, L.M., Doering, F., and Harrison, J. (2008) Enhanced stabilization of dikes and levees using direct current technology. In K.R. Reddy, M.V. Khire, and A.N. Alshwabkeh, Eds. *GeoCongress 2008: Geosustainability and Geohazard Mitigation (GSP 178)*, p. 1203. Sponsored by GEO Institute of ASCE, Orleans, Louisiana, U.S.
- Wong, J.S.H., Hicks, R.E., and Probst, R.F. (1997) Edta-enhanced electroremediation of metal-contaminated soils. *Journal of Hazardous Materials*, **55**, 61-79.
- Xu, Y., and Marcantonio, F. (2004) Speciation of strontium in particulates and sediments from the mississippi river mixing zone. *Geochimica et Cosmochimica Acta*, **68**, 2649-57.
- Ye, J., and Chiu, P.C. (2005) Roles of graphite and atomic hydrogen in the reduction of azoaromatics with zero-valent iron. *Abstracts of Papers of the American Chemical Society*, **230**, U1569-U70.
- Yeung, A.T. (2006a) Contaminant extractability by electrokinetics. *Environmental Engineering Science*, **23**, 202-24.
- . (2006b) Fundamental aspects of prolonged electrokinetic flows in kaolinites. *Geomechanics and Geoengineering*, **1**, 13 - 25.
- . (2009) Geochemical processes affecting electrochemical remediation. In K.R. Reddy, and C. Cameselle, Eds. *Electrochemical remediation technologies for polluted soils, sediments, and groundwater*, p. 1 v. Wiley-Blackwell, Oxford.
- Yeung, A.T., Hsu, C.-n., and Menon, R.M. (1997a) Physicochemical soil-contaminant interactions during electrokinetic extraction. *Journal of Hazardous Materials*, **55**, 221-37.
- Yeung, A.T., and Mitchell, J.K. (1993) Coupled fluid, electrical and chemical flows in soil. *Geotechnique*, **43**, pp. 121-34.
- Yeung, A.T., Scott, T.B., Gopinath, S., Menon, R.M., and Hsu, C.-N. (1997b) Design, fabrication, and assembly of an apparatus for electrokinetic remediation studies. *Geotechnical testing journal*, **20**, 199-210.
- Yong, R.N., and Thomas, H.R. (1997) *Geoenvironmental engineering : Contaminated ground : Fate of pollutants and remediation*. 586p. p. Thomas Telford, London.
- Younger, P.L. (2000) Predicting temporal changes in total iron concentrations in groundwaters flowing from abandoned deep mines: A first approximation. *Journal of Contaminant Hydrology*, **44**, 47-69.
- . (2007) *Groundwater in the environment : An introduction*. xii, 318 p. p. Blackwell, Oxford.
- Younger, P.L., Banwart, S.A., and Hedin, R.S. (2002) *Mine water : Hydrology, pollution, remediation*. xvi, 442 p. p. Kluwer Academic Publishers, Dordrecht ; London.
- Yu, J.-W., and Neretnieks, I. (1997) Theoretical evaluation of a technique for electrokinetic decontamination of soils. *Journal of Contaminant Hydrology*, **26**, 291-9.

- Yuan, C., and Chiang, T.-S. (2007) The mechanisms of arsenic removal from soil by electrokinetic process coupled with iron permeable reaction barrier. *Chemosphere*, **67**, 1533-42.
- Yuan, C., and Weng, C.-H. (2004) Remediating ethylbenzene-contaminated clayey soil by a surfactant-aided electrokinetic (saek) process. *Chemosphere*, **57**, 225-32.
- Zhou, D.-M., Deng, C.-F., Alshwabkeh, A.N., Cang, L., and Deng, C.-F. (2005a) Effects of catholyte conditioning on electrokinetic extraction of copper from mine tailings. *Environment International*, **31**, 885-90.
- Zhou, D.-M., Deng, C.-F., and Cang, L. (2004) Electrokinetic remediation of a cu contaminated red soil by conditioning catholyte ph with different enhancing chemical reagents. *Chemosphere*, **56**, 265-73.
- Zhou, D.-M., Deng, C.-F., Cang, L., and Alshwabkeh, A.N. (2005b) Electrokinetic remediation of a cu-zn contaminated red soil by controlling the voltage and conditioning catholyte ph. *Chemosphere*, **61**, 519-27.

Electrokinetics and Iron Precipitation
for Ground Engineering and Metal
Removal

David W. S. Faulkner

Appendices

pH Measurement

The pH was measured throughout the project using an Oakton model pH 310 portable pH/mV/°C meter. Measurements were generally taken at the surface of an experimental cell whereby the surface was wetted with distilled water and the probe stirred into the top few millimetres of the material so that the sensing bulb was immersed into the resulting slurry. The current was temporarily switched off while the pH measurements were recorded to avoid affecting the reading. The pH meter was regularly re-calibrated using factory produced sachets of reference buffer solution rated at ± 0.01 pH or better, according to the manufacturer's literature.

XRF Sample Preparation and Analysis

The initial sampling of material to be analysed by XRF varied in method depending on the experiment (see individual experiments for details). However, after the initial sampling, a general procedure was adhered to for sample preparation method.

The sample was first dried for 24hrs in an oven at 80°C. Next, the sample was homogenised and ground down into a fine powder in a Phillips minimill II, Planetary mono-mill. Depending on the sample being prepared, the speed and duration of the milling was adjusted to generate a completely homogenous fine powder, free from coarse granules or lumps. Approximately 10 grams of the ground material was weighed and transferred to a glass beaker. 10 drops of the binding agent dilute polyvinyl alcohol (0.8%) was then added to the beaker and stirred thoroughly using a glass rod. This mixture was then transferred to the pellet press assembly and subjected to 200KN of force for a few moments to compress the mixture into a disk shaped pellet ready for insertion in the XRF spectrometer. All the apparatus used was carefully cleaned using first water and then acetone, after each pressed powder pellet was produced, to prevent cross contamination between samples.

XRD Analysis

The sample preparations for the XRD at the University of Brighton involved a dry sample of approximately 2 grams being disaggregated and ground using a pestle and mortar into powder which was then transferred to sample holder which was

pH Meter Specification

Oakton 310 portable waterproof pH/mV/°C Meter

Mode	pH	Temperature	mV
Range	-2.00 to 16.00 pH	-10.0 to 110.0°C (also 14.0 to 230.0°F for pH 310 meter)	-2000 to 2000mV
Resolution	0.01 pH	0.1°C	0.1 mV between ±199.9 mV 1 mV beyond ±199.9 mV
Accuracy	±0.01 pH	±0.5°F	±0.2 mV between ±199.9 mV ±2 mV beyond ±199.9mV
Input	BNC connector	6-pin plug	BNC connector

NIST 2710 Certified Reference Material

Table 1. Certified Values

Element	Mass Fraction (%)	Element	Mass Fraction (mg/kg)
Aluminum	6.44 ± 0.08	Antimony	38.4 ± 3
Calcium	1.25 ± 0.03	Arsenic	626 ± 38
Iron	3.38 ± 0.10	Barium	707 ± 51
Magnesium	0.853 ± 0.042	Cadmium	21.8 ± 0.2
Manganese	1.01 ± 0.04	Copper	2950 ± 130
Phosphorus	0.106 ± 0.015	Lead	5532 ± 80
Potassium	2.11 ± 0.11	Mercury	32.6 ± 1.8
Silicon	28.97 ± 0.18	Nickel	14.3 ± 1.0
Sodium	1.14 ± 0.06	Silver	35.3 ± 1.5
Sulfur	0.240 ± 0.006	Vanadium	76.6 ± 2.3
Titanium	0.283 ± 0.010	Zinc	6952 ± 91

Fibre Sand Datasheet

Quartz silica sand for man-made fibres. Used in filtering hot, molten pre-spun textile filament, 18/36 grade.

Description: Washed, dried and graded, non-staining, closely graded, hard quartz material. Lower Greensand extraction, free from clay, silt or organic matter.

Particle Shape: Semi-rounded to sub-angular.

Colour: Silver-grey to off white.

Particle size:

Coarse Grades				Fine Grades
14/18	18/36	25/36	36/60	60/85
1.2-850µm	850-420µm	600-420µm	420-250µm	250-180µm
Max<12%	Max<10%	Max<10%	Max<10%	Max<10%
Max<12%	Max<10%	Max<10%	Max<10%	Max<10%
*76%	*80%	*80%	*80%	*80%
4150	4151		4152	4154

Diffusion Coefficients and Ionic Mobilities

Absolute Values of Diffusion Coefficients and Ionic Mobilities for Representative Cations as Infinite Dilution at 25°C

Cation	$D_i \times 10^6$ cm^2s^{-1}	$U_i \times 10^5$ $\text{cm}^2\text{V}^{-1}\text{sec}^{-1}$	Cation	$D_i \times 10^6$ cm^2s^{-1}	$U_i \times 10^5$ $\text{cm}^2\text{V}^{-1}\text{sec}^{-1}$
Ag ⁺	16.47	64.1	K ⁺	19.58	76.2
Al ³⁺	5.41	63.2	La ³⁺	6.18	72.0
Ba ²⁺	8.50	66.2	Li ⁺	10.30	40.1
Be ²⁺	5.99	46.6	Mg ²⁺	7.07	55.0
Ca ²⁺	7.93	61.7	Mn ²⁺	7.12	55.4
Cd ²⁺	7.19	56.0	NH ⁴⁺	19.58	76.2
Ce ³⁺	6.21	72.5	N ₂ H ⁵⁺	15.7	61.1
Co ³⁺	4.70	54.9	Na ⁺	13.3	51.9
Co(NH ₃) ₆ ³⁺	8.87	103.6	Nd ³⁺	6.18	72.1
Co(en) ₃ ³⁺	6.63	77.4	Ni ²⁺	6.65	51.8
Cr ³⁺	5.94	69.4	Pb ²⁺	9.46	73.6
Cs ⁺	20.84	80.1	Pr ³⁺	6.1	72.1
Cu ²⁺	7.32	57.0	Ra ²⁺	8.89	69.2
D ⁺ (18°)	55.57	221.5	Rb ⁺	20.71	80.6
Dy ³⁺	5.83	68.1	Sc ³⁺	5.74	67.0
Er ³⁺	5.86	68.4	Sm ³⁺	6.08	71.0
Eu ³⁺	6.03	70.4	Sr ²⁺	7.91	61.6
Fe ²⁺	7.19	56.0	Tl ⁺	20.25	78.8
Fe ³⁺	6.04	70.5	Tm ³⁺	5.82	67.9
Gd ³⁺	15.98	69.8	UO ₂ ²⁺	4.27	33.2
H ⁺	93.13	362.5	Y ³⁺	5.50	64.2
Hg ²⁺	7.05	54.9	Yb ³⁺	5.79	67.6
Ho ³⁺	5.88	68.7	Zn ²⁺	7.03	54.7

Absolute **Values** of Diffusion Coefficients and Ionic Mobilities for Representative Anions as Infinite Dilution at 25°C

Anion	$D_i \times 10^6$ cm^2s^{-1}	$U_i \times 10^5$ $\text{cm}^2\text{V}^{-1}\text{sec}^{-1}$	Anion	$D_i \times 10^6$ cm^2s^{-1}	$U_i \times 10^5$ $\text{cm}^2\text{V}^{-1}\text{sec}^{-1}$
$\text{Au}(\text{CN})_2^-$	13.31	51.83	HS^-	17.32	67.4
$\text{Au}(\text{CN})_4^-$	9.58	37.3	HSO_3^-	13.31	51.8
$\text{B}(\text{C}_6\text{H}_3)_4^-$	5.60	21.8	HSO_4^-	13.31	51.8
Br^-	20.78	80.9	H_2SbO_4^-	8.25	32.1
Br_3^-	11.46	44.6	I^-	20.45	49.6
BrO_3^-	14.85	57.8	IO_3^-	10.79	42.0
Cl^-	20.32	79.1	IO_4^-	14.52	56.5
ClO_2^-	13.85	53.9	$\text{N}(\text{CN})_2^-$	14.52	56.5
ClO_3^-	17.19	66.9	NO_2^-	19.11	74.4
ClO_4^-	18.09	70.4	NO_3^-	19.01	74.0
CN^-	20.76	80.8	NH_2SO_3^-	12.95	50.4
CO_3^{2-}	9.58	74.6	N_3^-	18.37	71.5
$\text{Co}(\text{CN})_6^{3-}$	8.78	102.5	OCN^-	17.19	66.9
CrO_4^{2-}	11.32	88.1	OH^-	52.87	205.8
F^-	14.49	56.4	PF_6^-	15.16	59.0
$\text{Fe}(\text{CN})_6^{4-}$	7.39	115.0	PO_3F^{2-}	8.43	65.6
$\text{Fe}(\text{CN})_2^{3-}$	8.97	104.7	PO_4^{3-}	6.12	71.5
H_2AsO_4^-	9.04	35.2	$\text{P}_2\text{O}_7^{4-}$	5.42	84.3
HCO_3^-	11.84	46.1	$\text{P}_3\text{O}_9^{3-}$	7.42	86.6
HF_2^-	19.96	77.7	$\text{P}_3\text{O}_{10}^{5-}$	5.81	113.0
HPO_4^{2-}	7.59	59.1	ReO_4^-	14.57	56.7
H_2PO_4^-	8.79	34.2	SCN^-	17.57	68.4
H_2PO_2^-	12.25	47.7	SeCN^-	17.21	67.0

(Dean, 1985, cited in, Acar *et al.*, 1997)

Cast Iron Grade 250 BS1452 Specifications

BS1452 GRADE 250

(CAST IRON)

GENERAL:

A CLOSE GRAINED PREDOMINANTLY PEARLITIC GREY CAST IRON

USES:

SUITABLE FOR GLASS MOULDS, PUMP ROTORS AND HYDRAULIC PISTONS
ETC.

CHEMICAL ANALYSIS LIMITS:				
C	SI	MN	S	P
2.8% - 3.5%	2% - 3%	0.4% - 1.0%	0.125% MAX	0.7% MAX

HEAT TREATMENT & CONDITION

NOT APPLICABLE

SECTIONS

COMMERCIALY AVAILABLE IN ROUNDS, SQUARES AND FLATS.

RELATED SPECIFICATIONS

ASTM A48 CLASS 35B, DIN 1691 GG25, NFA32-101 Ft25D.

EPSRC Grant Abstract

Electrokinetic Soil and Sediment Remediation, and Pollutant Containment by Iron Precipitation

Grant Number: GR/S27924/01

Abstract:

This proposal seeks to develop a low-cost low-energy technique to generate bands of iron-stone in situ in fine grained contaminated sediments by inserting electrodes and applying a low-voltage electric current. Iron band formation occurs between electrode pairs, and is accompanied by sediment dewatering, permeability reduction, and the enforced migration of heavy metal contaminants. Accordingly, iron-band formation potentially represents a means of physically confining waste spills, promoting and controlling effluent migration, and cleaning contaminated sediment and research programme will provide a base-line study into the effectiveness of iron-band formation with respect to these three roles.

Starts: 01 September 2003 Ends: 31 August 2006 Value (£): 101,223

EPSRC Research Topic Classifications: Assessment/Remediation of Contaminated Land and Groundwater

EPSRC Industrial Sector Classifications: Environment

Land Filling Hazardous Waste

The Landfill Directive is setting tighter standards on wastes that can go to landfill. These are called waste acceptance criteria (WAC) and apply to hazardous waste from 16th July 2005. This means greater sampling, testing and treatment of hazardous waste. As a result of intensive efforts to publicise these changes, landfill operators and most hazardous waste producers are well prepared and will be able to meet the requirements. However, a very limited number of waste streams have been identified as not being able to meet WAC. This note explains how waste producers and managers should deal with these wastes. It also sets out our approach to regulating these activities to ensure protection of human health and the environment. This note applies only in England and Wales.

From the 16th July 2005 WAC will apply to all hazardous waste going to landfill, including stable non-reactive hazardous waste going to separate cells in non-hazardous landfills. The WAC set leaching and other limit values that components of the waste stream must meet in order to be landfilled. Application of these uniform standards across Europe represents a significant change in the way waste going to landfill is handled and we have been working closely with waste producers and landfill operators to help them prepare for these changes. We have already seen a reduction in the amount of hazardous waste going to landfill as a result of the Landfill Directive and we welcome these further changes which will encourage greater waste minimisation and recovery.

Despite extensive discussions, a very limited number of waste streams from specific industrial processes are not able to meet the WAC from 16th July. The following

guidance should be followed to ensure the continued safe management of those waste streams.

SUMMARY Council Directive 1999/31/EC of 26 April 1999 on the landfill of waste [See amending acts].

The Directive is intended to prevent or reduce the adverse effects of the landfill of waste on the environment, in particular on surface water, groundwater, soil, air and human health.

It defines the different categories of waste (municipal waste, hazardous waste, non-hazardous waste and inert waste) and applies to all landfills, defined as waste disposal sites for the deposit of waste onto or into land. Landfills are divided into three classes:

- landfills for hazardous waste;
- landfills for non-hazardous waste;
- landfills for inert waste.

On the other hand, the Directive does not apply to:

- the spreading on the soil of sludges (including sewage sludges and sludges resulting from dredging operations);
- the use in landfills of inert waste for redevelopment or restoration work;
- the deposit of unpolluted soil or of non-hazardous inert waste resulting from prospecting and extraction, treatment and storage of mineral resources as well as from the operation of quarries;
- the deposit of non-hazardous dredging sludges alongside small waterways from which they have been dredged and of non-hazardous sludges in surface water, including the bed and its subsoil.

A standard waste acceptance procedure is laid down so as to avoid any risks:

- waste must be treated before being landfilled;
- hazardous waste within the meaning of the Directive must be assigned to a hazardous waste landfill;
- landfills for non-hazardous waste must be used for municipal waste and for non-hazardous waste;
- landfill sites for inert waste must be used only for inert waste.

The following wastes may not be accepted in a landfill:

- liquid waste;
- flammable waste;
- explosive or oxidising waste;
- hospital and other clinical waste which is infectious;
- used tyres, with certain exceptions;
- any other type of waste which does not meet the acceptance criteria laid down in Annex II.

The Directive sets up a system of operating permits for landfill sites. Applications for permits must contain the following information:

- the identity of the applicant and, in some cases, of the operator;
- a description of the types and total quantity of waste to be deposited;
- the capacity of the disposal site;
- a description of the site;
- the proposed methods for pollution prevention and abatement;
- the proposed operation, monitoring and control plan;
- the plan for closure and aftercare procedures;
- the applicant's financial security;
- an impact assessment study, where required under Council Directive 85/337/EEC on the assessment of the effects of certain public and private projects on the environment.

Member States must ensure that existing landfill sites may not continue to operate unless they comply with the provisions of the Directive as soon as possible.

Member States must report to the Commission every three years on the implementation of the Directive.

On the basis of these reports, the Commission must publish a Community report on the implementation of the Directive;

Act	Entry into force	Deadline for transposition in the Member States	Official Journal
Directive 1999/31/EC	16.07.1999	16.07.2001	OJ L 182 of 16.07.1999
Amending act(s)	Entry into force	Deadline for transposition in the Member States	Official Journal
Regulation (EC) No 1882/2003	20.11.2003	-	OJ L 284 of 31.10.2003

Electrokinetic generation of reactive iron-rich barriers in wet sediments: implications for contaminated land management

D. W. S. FAULKNER^{1,*}, L. HOPKINSON¹ AND A. B. CUNDY²

¹ Division of Civil Engineering and Geology, University of Brighton, Brighton BN2 4GJ, UK

² Centre for Environmental Research, University of Sussex, Brighton BN1 9QJ, UK

ABSTRACT

Here we describe preliminary research into the *in situ* electrokinetic generation of continuous iron-rich precipitates to act as sub-surface barriers for the containment of contaminated sites. This is achieved using sacrificial iron electrodes emplaced either side of a soil/sediment mass to introduce iron into the system, and their dissolution and re-precipitation under the influence of an applied (DC) electric field. Continuous vertical and horizontal iron-rich bands (up to 2 cm thick) have been generated over a timescale of 300–500 h, at voltages of <5 V with an electrode separation of between 15 and 30 cm. The thickness of the iron-rich band increases as the applied voltage is increased. Geotechnical tests in sand indicate that the iron-rich band produced is practically impervious (coefficient of permeability of 10^{-9} ms⁻¹ or less), and has significant mechanical strength (unconfined compressive strength of 10.8 N mm⁻²). By monitoring the current, the integrity of the iron-rich band may be assessed, and by continued application of current, the barrier may 'self heal'. The iron-rich barrier is composed of amorphous iron, goethite, lepidocrocite, maghemite and native iron.

KEYWORDS: electrokinetics, horizontal barriers, iron, contaminated land.

Introduction

ELECTROKINETIC remediation is an emerging technology that has generated considerable interest as a technique for the *in situ* remediation of contaminated clay-rich soils and sediments. The technique involves the forced movement of contaminants under the influence of an electric field, and has been demonstrated to be effective for the removal of both organic and inorganic species (including radionuclides) (Acar and Alshawabkeh, 1993; Probstein and Hicks, 1993; Acar *et al.*, 1995; Kovalick, 1995; Mulligan *et al.*, 2001; Virkutyte *et al.*, 2001). By passing a current between electrodes inserted into the soil or sediment either side of the area of contaminated land to be treated, three phenomena occur: (1) electromigration – movement of ions towards the electrode of opposite charge; (2) electroosmosis – net movement of water

towards the cathode (negative electrode); and (3) electrophoresis – movement of charged particles or colloids towards the oppositely charged electrode (Van Cauwenberghe, 1997). Existing electrokinetic methods deal mainly with remediation of low-permeability soils and sediments and have demonstrated considerable success, often removing up to 90% of a specific contaminant (Virkutyte *et al.*, 2001). However, these levels of removal efficiency invariably involve the use of complicated pH management systems and high-voltage equipment (Acar and Alshawabkeh, 1993; Virkutyte *et al.*, 2001). In addition, high remediation efficiencies are often achieved under strictly controlled laboratory conditions, using purified soils which have been artificially 'spiked' (e.g. Reddy and Chinthamreddy, 1999). It follows that, frequently, these conditions do not necessarily reflect those found in real-life contamination situations. In many cases effective containment by constructing physical barriers may be a more realistic and cost effective method to deal with contaminated land.

* E-mail: d.w.s.faulkner@brighton.ac.uk
DOI: 10.1180/0026461056950285

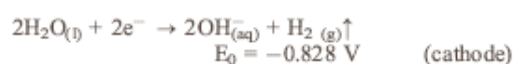
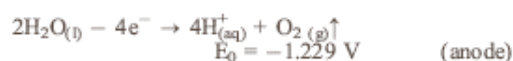
Current technology for the production of barriers for contaminant containment may be classified broadly into three categories (e.g. Cairney and Hobson, 1998). Driven barriers are formed when steel or concrete barriers are driven into the soil and are joined to form a suitably impermeable wall. These may also provide structural support. Injected barriers are formed when grout is injected into the subsurface. This technique tends to be relatively costly and may result in a discontinuous grout curtain that leaves un-grouted flow paths, along which contaminants may preferentially migrate. Cut and fill barriers are constructed by excavating a trench and filling it with concrete, grout or other material so that a suitable aquiclude is reached (Cairney and Hobson, 1998). It is very labour intensive and often expensive to install a horizontal barrier beneath an existing contaminated site (such as a landfill), because these generally require large-scale excavations or horizontal drilling, which may also be unfeasible if surface structures are close by.

Electrokinetic methods are already being used on a large scale for the stabilization of soils, either by utilizing the de-watering of the area around the anode, or by mobilizing additives such as cements and grouts to the required areas (e.g. Ingles and Metcalf, 1972). Stabilization of soils through controlled electroosmosis or by dissolving and re-precipitating aluminium electrodes to induce cementation of soils electrokinetically have been successfully demonstrated (Casagrande, 1947, 1952; Masliyeh, 1994; Lamont-Black, 2001), and have been achieved on a relatively large scale (e.g. the stabilization of a ~100 m railway cutting; Cassagrande, 1947). Until now, the materials and additives used have proved too damaging to the environment, and the high-energy costs have prevented widespread adoption of electrokinetic techniques for soil strengthening and cementation. Utilizing electrokinetic phenomena for the strategic precipitation of iron compounds within a given body of sediment, to form a barrier *in situ*, may potentially represent a new and cost-effective method for the containment of contaminated land. Here we discuss the experimental electrokinetic creation of subsurface iron-rich barriers within wet sediments.

Experimental rationale

The promoting factor for the production of an *in situ* iron-rich barrier is the generation within a soil

of an Eh/pH gradient between iron-rich electrodes, across which a DC current is applied. The passing of electric current through the soil medium causes the dissociation of water into H⁺ and OH⁻ ions according to the following reactions:



where E_0 is the standard reduction potential (at 25°C, 1 atm, pH 7) (Acar and Alshwabkeh, 1993).

These reactions result in extremes of pH being generated around the anode and cathode electrodes due to the formation of excess H⁺ and OH⁻ ions, respectively. The soil around the anode typically develops a pH of <3, whereas the soil around the cathode develops a high pH, typically >12. The sacrificial anodic iron electrodes progressively dissolve, mobilizing iron into the now acidic soil medium. The acid and the alkali fronts produced migrate towards each other until they eventually meet. The abrupt change in pH (and Eh) conditions at this 'pH jump' causes the spontaneous precipitation of iron compounds (Fig. 1). Other inorganic species in the soil that are remobilized by the acid or alkaline conditions generated by the technique may also be precipitated or sorbed onto the iron compounds (e.g. Probststein and Hicks, 1993; Cundy and Hopkinson, 2005). The generation of an acid and alkali front, and consequent iron-rich band formation, has been demonstrated in various natural media, including estuarine sediments and a range of contaminated soils, using both high ionic strength electrolyte (seawater) and tap water (Cundy and Hopkinson, 2005). The implications of this for the controlled migration of metals and radionuclides for remediation purposes have been demonstrated (Hopkinson and Cundy, 2003; Cundy and Hopkinson, 2005). However, strategic precipitation of iron for the purposes of *in situ* barrier formation and contaminant containment may also prove to be a promising avenue of research.

Experimental methods

A series of controlled bench-scale experiments were carried out to examine the formation, mechanical strength and mineralogy of electro-

ELECTROKINETIC REMEDIATION IN WET SEDIMENTS

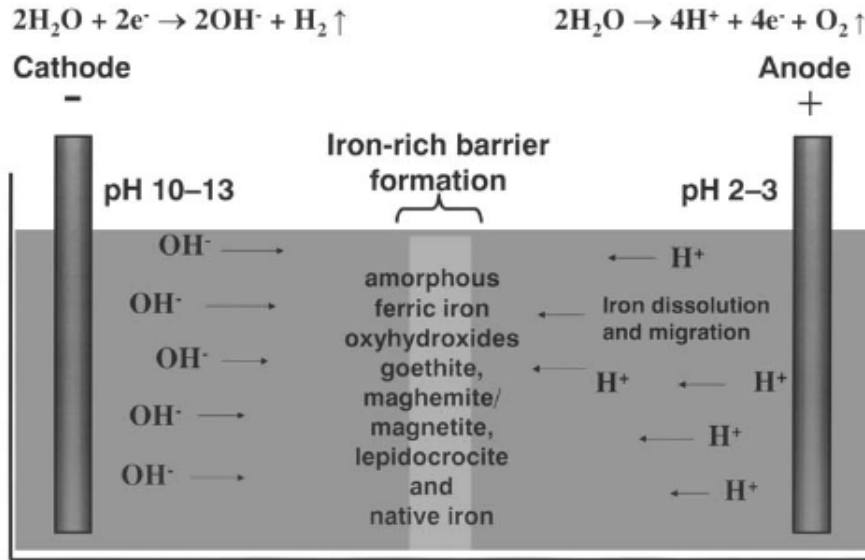


FIG. 1. The movement of ions and the dissociation of water as a result of applying a potential difference between electrodes (adapted from Alshwabkeh *et al.*, 1999). Iron derived from the sacrificial anode electrode precipitates and forms the iron-rich band on reaching the high pH front.

kinetically-generated iron-rich barriers in wet sands, the role of applied voltage on iron-barrier formation, and the potential for growth of continuous iron barriers to a desired geometry (specifically, the growth of a horizontal iron barrier). All experiments were conducted using electrodes fabricated from cast iron rods (grade 250) with composition: C 3.48%, Si 2.87%, Mn 0.812%, S 0.099%, P 0.364%, Fe 92.38%. Experiments were conducted on siliciclastic sand composed of 90% quartz and accessory clays, feldspars and carbonates (see Table 1).

Six identical Perspex cells (dimensions 200 × 150 × 180 mm) were filled with sand and

seawater added as an electrolyte. Two cast iron electrodes were inserted into each cell at 15 cm electrode separation, and a range of voltages (between 2 and 8 V DC) applied for ~300 h, to examine iron-barrier growth under different applied voltages. The resultant iron-rich bands were measured at four points as viewed through the Perspex cell (0, 2, 4 and 6 cm from the base of the cell) and the mean thickness calculated.

The potential for growth of a continuous horizontal barrier was examined using a 400 × 200 × 50 mm cell, filled with siliclastic sand. A potential difference of 3 V DC was applied between: (a) vertically emplaced anodic

TABLE 1. XRD analyses of pre-treatment quartz sand and the post-treatment iron-rich barrier region.

Pre-treatment siliciclastic sand mineralogy	Modal abundance	Post-treatment iron-rich barrier mineralogy	Modal abundance
Quartz	90%	Quartz and feldspar	65%
Clay (mica)	3.5%	Goethite	4%
K-feldspar	3.5%	Native iron	5%
Plagioclase	1.5%	Maghemite/magnetite	5%
Calcite	1%	Lepidocrocite	5%
Dolomite	0.5%	Amorphous ferric Fe oxyhydroxides	As much as 20%

electrodes partially sheathed with PU insulation, emplaced into seawater soaked sand such that the exposed electrode tips act as a single anode layer at depth, and (b) a cathode layer constructed from steel mesh, positioned at approximately 5 mm depth (Fig. 2). The current was monitored throughout. Following iron-band growth (i.e. after 400 h), a secondary investigation into the ability of the iron-rich band to re-heal when damaged was carried out whereby the iron band was deliberately point-ruptured using a glass rod.

Samples were removed from the iron-rich bands from all three experiments for geotechnical testing and mineralogical characterization. The point load and uniaxial compressive strength (UCS) of the precipitated iron band, and its permeability compared to the untreated sand, were determined following the methods of Head (1982) and Franklin and Brook (1985). Four samples from the iron-rich barriers, and the sand test medium itself, were analysed by X-ray diffraction (XRD) at the Southampton Oceanography Centre, University of

Southampton, UK, using a Philips Analytical X'Pert Diffractometer. Semi-quantitative analysis was performed using the internal standard method. Three grams of the sample and one gram of the internal standard (corundum) were ground together under iso-propanol for 8 min in a micronizing mill. The sample was side-loaded into a rotating sample holder and scanned from 3 to $76^{\circ}2\theta$ at $1.2^{\circ}2\theta \text{ min}^{-1}$ using Fe-filtered $\text{Co-K}\alpha$ radiation. Areas of selected peaks were ratioed to the areas of the peaks of the internal standard, and the values compared with those obtained for a pure mineral standard. Because of preferred orientation, clay minerals were not determined individually, but were estimated on the basis of 'total phyllosilicates' using non basal 020 and 060 reflections. Error is estimated to be 5% of the amount present or 2% absolute, whichever is the larger, except for 'total phyllosilicates' where the error is probably twice this.

The lack of appropriate mineral standards and the likelihood that poorly crystalline and X-ray amorphous iron compounds are generated by the

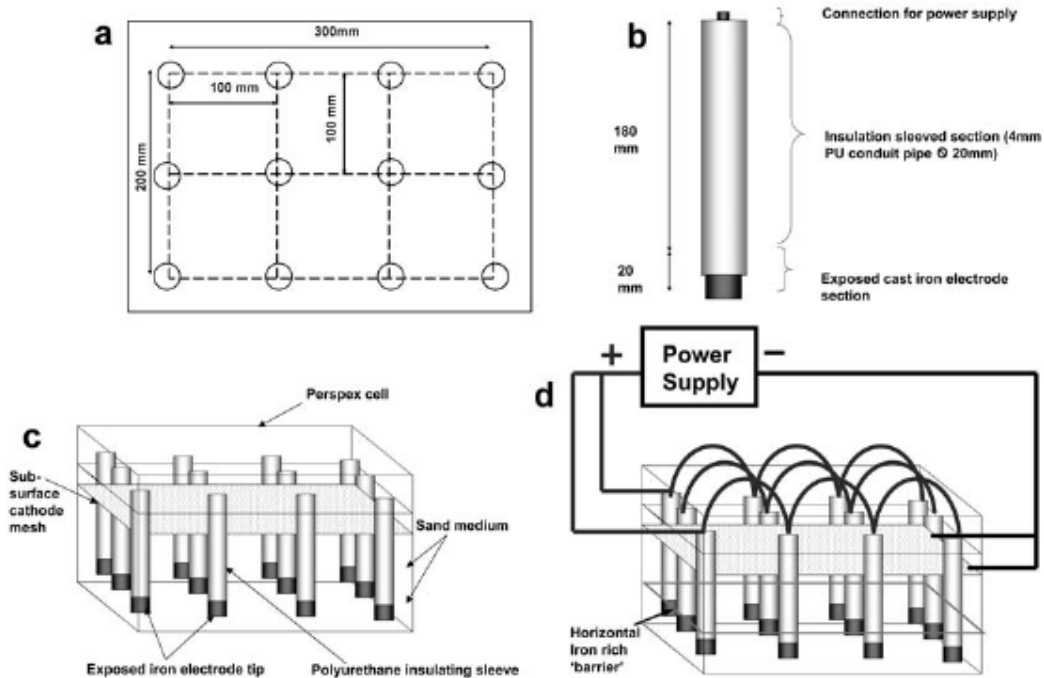


FIG. 2. Experimental configuration of cell used for growth of horizontal iron-rich band. (a) Schematic plan of anode electrode spacing as viewed from above. (b) Electrode construction and dimensions. (c) Experimental set up with vertical anode electrodes, surface cathode mesh, and sand in Perspex container. (d) Generation of the horizontal iron-rich band in the sub-surface.

electrokinetic process (Hopkinson and Cundy, 2003) prohibited quantitative analyses of the iron compounds in the iron-rich barriers.

Results

Geotechnical characteristics

By inserting cast iron electrodes vertically into the wetted sand and applying a current, the dissolution and re-precipitation of iron from the electrodes results in a sub-vertical, continuous band or curtain of iron precipitates that form a distinct cemented zone within the sand. The coefficient of permeability, (k) of this iron-rich barrier was found to be 10^{-9} ms^{-1} . This is classified according to Terzaghi and Peck (1967) as 'practically impermeable'. The co-efficient (k), for the clean, untreated sand, was measured as 10^{-2} ms^{-1} , demonstrating a dramatic decrease in the permeability of the material. The approximate uniaxial compressive strength of the iron-rich band was measured as 10.8 N mm^{-2} comparable to, for example, a strong chalk or moderately lithified sandstone (Cundy and Hopkinson, 2005). Hence the mechanical properties of the sand seem to be significantly improved due to the iron precipitation within the cell.

Iron-rich barrier mineralogy

The XRD analyses of the iron-rich bands revealed the presence of goethite, lepidocrocite, maghemite/magnetite and native iron (Fig. 3). Quantitative analyses of iron compounds were not possible (see above). However, based on the sizes of peaks it is likely that the iron-rich barriers have an approximate composition of ~65% cemented quartz (and feldspar), with ~4% goethite, ~5% native iron, 5% maghemite/magnetite, 5% lepidocrocite, and possibly as much as 20% X-ray amorphous ferric iron oxyhydroxides (Table 1).

Role of applied voltage

Data from the six Perspex cells, run over 300 h at a range of voltages, indicate a clear, directly proportional relationship between the voltages applied and iron-rich band thickness as measured at different vertical heights through the visible portion through the Perspex container (Fig. 4). Increasing the voltage apparently increases the input of iron into the system due to accelerated dissolution of the cast iron anode electrode, suggesting that increasing the applied voltage may be an effective means of increasing the

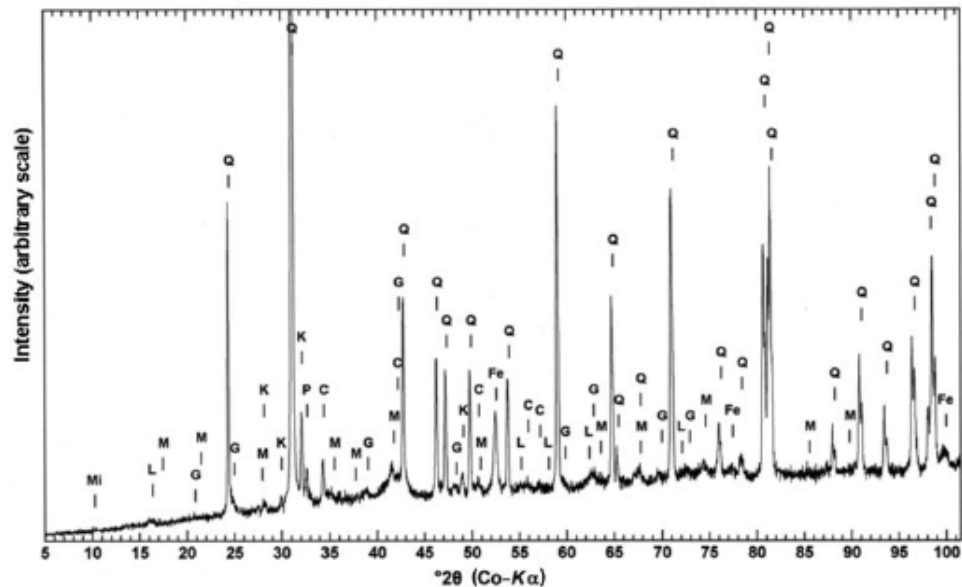


FIG. 3. XRD trace of the iron-rich band formed in quartz sand showing the presence of native iron. C = calcite, Fe = native iron, G = goethite, K = k-feldspar, L = lepidocrocite, M = maghemite and/or magnetite, Mi = mica, P = plagioclase feldspar, Q = quartz.

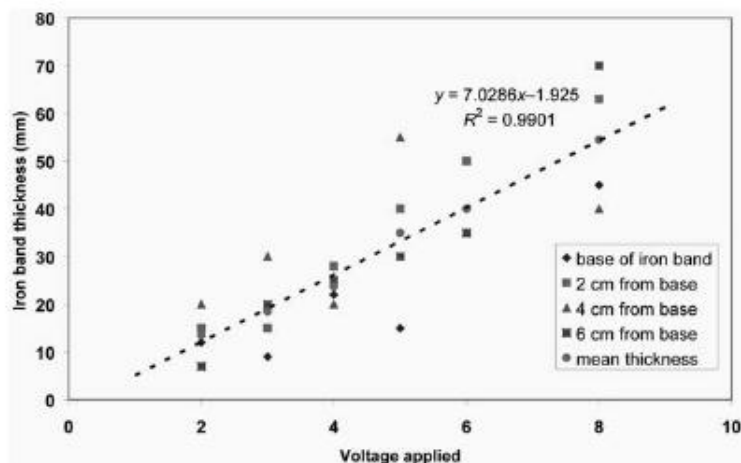


FIG. 4. Relationship between iron-rich barrier thickness (in mm) and applied voltage (see text for details).

formation rate of the iron barrier. However, at greater voltages (>100 V) soil heating and the formation of significant amounts of hydrogen gas at the anode becomes problematic (e.g. Virkutye *et al.*, 2001).

Controlling the iron barrier geometry

The straightforward parallel linear electrode arrangement of oppositely charged electrodes on either side of the sand results in the generation of a continuous, sub-vertical iron-rich barrier approximately half way between the two sets of electrodes of opposite polarity. However, by insulating the upper section of the anode electrodes and incorporating a shallow surface cathode electrode, a continuous horizontal iron-rich barrier of ~5 mm was generated in the sub-surface over a ~400 h period, without any excavation required (Fig. 5). The current through the cell shows an initial increase from

0.48 A to 0.74 A within the first ~20 h (Fig. 6a), since the water is unevenly distributed throughout the sand profile at the beginning of the experiment (it is gravitationally influenced to give a saturated water table at depth, with a drier upper region). Over time, the water becomes more evenly distributed as it is electroosmotically mobilized towards the surface cathode, allowing for more efficient ion movement and thus increased current flow. The current shows a progressive drop from a maximum of 0.74 A down to 0.14 A as the iron-rich barrier forms, due to impedance of ion flow by the precipitated iron compounds.

Resealing the iron band

After 400 h, the horizontal iron-rich layer was ruptured using a glass rod (diameter 4 mm). The current immediately increased from a steady 0.14 A to 0.17 A (Fig. 6a,b). Over the course of the next few hours the current gradually decreased

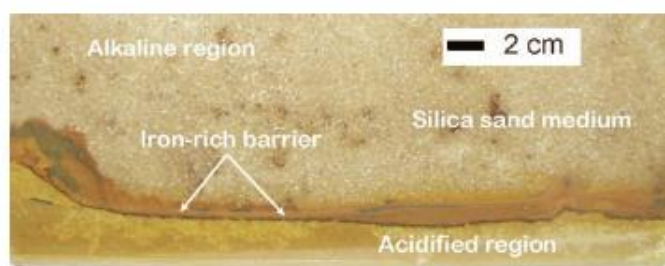


FIG. 5. Horizontal iron-rich band formed over 300 h at 3 V in siliciclastic sand using partially insulated anode electrodes and a surface mesh cathode at a separation of 20 cm. Seawater was the electrolyte added.

ELECTROKINETIC REMEDIATION IN WET SEDIMENTS

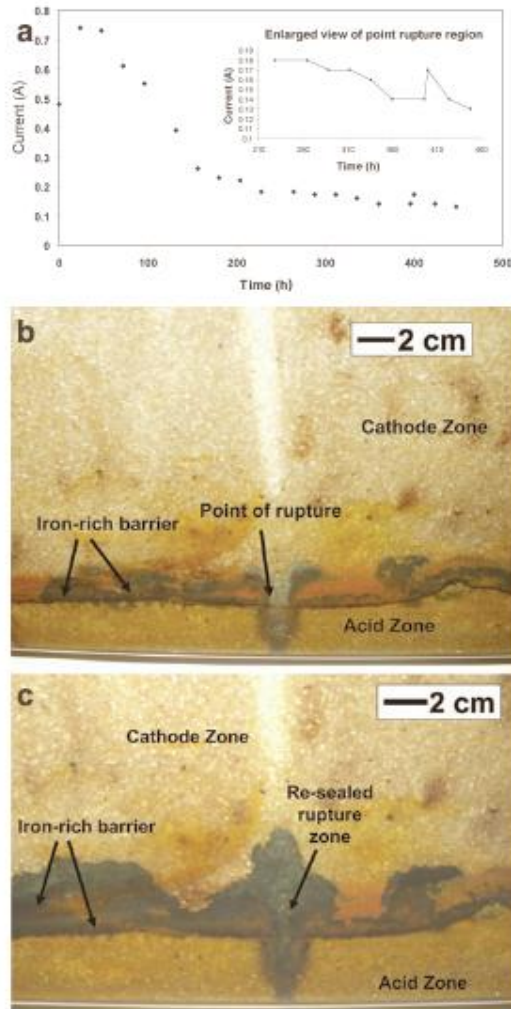


FIG. 6. Behaviour of iron-rich band. (a) As the iron-rich band forms, the current drops steadily with time and reaches a stable value. At 400 h the iron band is physically ruptured and an immediate increase in current is evident. (b) Horizontal iron-rich band immediately after rupture induced with 4 mm diameter glass rod. (c) Iron-rich band 24 h after rupture induced. The point-rupture is now blocked with freshly precipitated Fe compounds demonstrating the 'self-healing' process. Note the additional mineralization on either side of the damaged region due to ion migration.

until it returned to its pre-damage level of 0.14 A. Within 24 h the damaged section had visibly reformed, indicating that the barrier can self-heal

due to the flow path between opposite polarity electrodes created by the rupture (Fig. 6c).

Discussion

The data presented here suggest that it is possible to electrokinetically generate an impermeable, resealable iron-rich barrier to a required three-dimensional geometry in wet sediments, at low voltages and using a simple electrode array. Whilst these experiments were conducted at bench scale, the system's potential for successful up-scaling is strengthened due to the use of low voltages and inexpensive sacrificial electrodes. In addition, similar iron 'pans' have been noted to have formed naturally in (heterogeneous) geological systems over considerable spatial scales, when changes in redox conditions result in an electro-chemical gradient being formed (e.g. Jacob *et al.*, 1994). The apparent capacity of the system for *in situ* monitoring of barrier integrity, *in situ* self healing, combined with the ability to control iron-rich band geometry in three dimensions, as documented here, offer potential advantages over traditional physical barrier techniques by eliminating the need for excavations to emplace a barrier. The barrier could also be formed beneath existing structures. Since the method requires no chemical additives, and utilizes relatively low-toxicity iron as the strengthening material, any environmental impact should also be minimal. The experiments conducted so far have an energy requirement in the region of 11 kW m^{-3} of soil. Up-scaled experiments will be required to establish the technique's energy requirements for application in real environment situations but the initial findings are that the technology offers a low-cost approach.

In 'real' groundwater environments there is typically a net movement of water in a given direction. Since the rate of migration of the H^+ and OH^- ions under the influence of the electric field is many orders of magnitude greater than typical groundwater flow-rates, the technique is expected to be applicable even under significant hydraulic gradients. The use of seawater as a high ionic strength electrolyte improves current flow (e.g. Casagrande, 1947), but iron-rich barriers have also been created using distilled water. In addition to providing a physical barrier (or indeed a method of locally stabilizing and strengthening soil), the electrokinetically generated iron barrier also has the potential to act as a reactive surface

for the adsorption of contaminants from leachates. The affinity of freshly-precipitated iron compounds for sorption of a range of contaminants has been widely reported (e.g. Bendell-Young and Harvey, 1992), and evidence of the sorptive capacity of iron barriers generated using electrokinetic techniques was presented by Cundy and Hopkinson (2005) for a range of inorganic species. Notably, it has also been shown that iron compounds are significant in the catalysis of the dechlorination of contaminants such as PCBs, organic pesticides and other chlorinated hydrocarbons by acting as electron donors (McGuire, 2003). The apparent presence of zero-valent iron in the iron-rich barrier, as well as large amounts of Fe^{2+} , suggests that the technique may have important applications as a reactive surface for the degradation of chlorinated hydrocarbons through iron-mediated dechlorination of the hydrocarbon (Helland *et al.*, 1994; Johnson *et al.*, 1998).

Acknowledgements

We are grateful to the technical staff at the University of Brighton for their valuable assistance in carrying out this research, and to Mr Benjamin Kyambadde for his work on the geotechnical properties of the iron-rich barrier material, and to Conor Ryan and Emma Matthewson. Trevor Clayton (University of Southampton) is thanked for his assistance with XRD analyses. The technique and ideas described here are the subject of a World Patent application filed by the Universities of Sussex and Brighton. This work was completed using funding provided by the EPSRC grant number GR/S27924/01.

References

- Acar, Y.B. and Alshawabkeh, A.N. (1993) Principles of electrokinetic remediation. *Environmental Science and Technology*, **27**, 2638–2647.
- Acar, Y.B., Gale, R.J., Alshawabkeh, A.N., Marks, R.E., Puppala, S., Bricka, M. and Parker, R. (1995) Electrokinetic remediation – basics and technology status. *Journal of Hazardous Materials*, **40**, 117–137.
- Alshawabkeh, A.N., Yeung, A.T. and Bricka, M.R. (1999) Practical aspects of in situ electrokinetic extraction. *Journal of Environmental Engineering*, **125**, 27–35.
- Bendell-Young, L. and Harvey, H.H. (1992) The relative importance of manganese and iron oxides and organic matter in the sorption of trace metals by surficial lake sediments. *Geochimica et Cosmochimica Acta*, **56**, 1175–1186.
- Cairney, T. and Hobson, D.M. (1998) In-ground barriers. Pp. 128–139 in: *Contaminated Land: Problems and Solutions*, 2nd edition. E. and F.N. Spoon, London.
- Casagrande, L. (1947) *The application of electro-osmosis to practical problems in foundations and earthwork*. Building Research Technical paper no.30, Dept. of Scientific and Industrial Research, HMSO, London.
- Casagrande, L. (1952) Electrical stabilisation in earthwork and foundation engineering. *Proceedings of the M.I.T. conference on soil stabilisation 1952*. Pp. 26–36 in: *Methods of Treatment of Unstable Ground* (F.G. Bell, editor), Newnes Butterworths, London 1975.
- Cundy, A. and Hopkinson, L. (2005) Electrokinetic iron pan generation in unconsolidated sediments: implications for contaminated land remediation and soil engineering. *Applied Geochemistry*, **20**, 841–848.
- Franklin, J.A. and Brook, N. (1985) Method for determining point load strength index – International Society for Rock Mechanics Commission on testing methods (Revision of the Point Load Test method). *International Journal of Rock Mechanics and Mining Science*, **22**, 51–60.
- Head, K.H. (1982) *Manual of Soil Laboratory Testing*. Volume 2, Pentech Press, Plymouth, UK, pp. 450–455.
- Helland, B.R., Alvarez, P.J.J. and Schnoor, J.L. (1994) Reductive dechlorination of carbon tetrachloride with elemental iron. *Journal of Hazardous Materials*, **41**, 205–216.
- Hopkinson, L. and Cundy, A. (2003) *FIRS (ferric iron remediation and stabilisation): a novel electrokinetic technique for soil remediation and engineering*: CLAIRE research bulletin RB2, May edition.
- Ingles, O.G. and Metcalf, J.B. (1972) *Soil Stabilization – Principles and Practice*. Butterworths, London.
- Jacob, K.H., Dietrich, S. and Krug, H.J. (1994) Self organised mineral fabrics. Pp. 259–268 in: *Fractals and Dynamic Systems in Geoscience* (J.H. Kruhl, editor). Springer Verlag, Berlin.
- Johnson, T.L., Fish, W., Gorby, Y. and Tratneyek, P. (1998) Degradation of carbon tetrachloride by iron metal: Complexation effects on the oxide surface. *Journal of Contaminant Hydrology*, **29**, 379–398.
- Kovalick, W.W. (1995) *In Situ Remediation Technology: Electro-kinetics*. US Environmental Protection Agency, Office of Solid Waste and Emergency Response Technology Innovation Office, Washington.
- Lamont-Black, J. (2001) EKG: The next generation of geosynthetics. *Ground Engineering*, **34**, 22–23.
- Masliyah, J.H. (1994) *Electrokinetic Transport Phenomena*. Austra Technical Publications Series

ELECTROKINETIC REMEDIATION IN WET SEDIMENTS

- no. 12, Alberta Oil Sands Technology and Research Authority, Edmonton, Canada.
- McGuire, M.M. (2003) Applications of surface analysis in the environmental sciences: dehalogenation of chlorocarbons with zero-valent iron and iron-containing mineral surfaces. *Analytica Chimica Acta*, **496**, 301–313.
- Mulligan, C.N., Yong, R.N., and Gibbs, B.F. (2001) Remediation technologies for metal-contaminated soils and groundwater: an evaluation. *Engineering Geology*, **60**, 193–207.
- Probstein, R.F. and Hicks, R.E. (1993) Removal of contaminants from soils by electric fields. *Science*, **260**, 498–503.
- Reddy, K.R. and Chinthamreddy, S. (1999) Electrokinetic remediation of heavy metal-contaminated soils under reducing environments. *Waste Management*, **19** 269–282.
- Terzaghi, K. and Peck, R.B. (1967) *Soil Mechanics in Engineering Practice*, 2nd edition. John Wiley, New York
- Van Cauwenberghe, L. (1997) *Electrokinetics: Technology overview report: Groundwater Remediation*. Technologies Analysis Centre, Pittsburgh, PA, USA.
- Virkutyte, J., Sillanpaa, M. and Latostenmaa, P. (2001) Electrokinetic soil remediation – a critical overview. *Science of the Total Environment*, **289**, 97–121.
- [Manuscript received 11 February 2005:
revised 8 August 2005]

10 Appendix 2- Experimental Data

Loss on Ignition Test Hythe Sediment

Loss on ignition test 07/10/2007
 Hythe Sediment
 David Faulkner

sample	vessel mass	dry sample and jar		Sample Mass	post furnace jar and sample	Loss on ignition	% loss
A	148.39	160.73	12.34	159.41	1.32	10.69692	
B	149.63	161.29	11.66	159.91	1.38	11.83533	
C	151.06	163.72	12.66	162.21	1.51	11.92733	
D	148.62	158.9	10.28	157.15	1.75	17.02335	
E	150.07	158.71	8.64	157.82	0.89	10.30093	
Mean (2dp)						12.36	

Penetrometer Data

Kgf/cm²

	Anode	cathode	iron mineralised zone	mid point	Average Anode 1.99	Average Cathode 1.4	Average Iron Mineral zone	Average Midpoint
1	2	1.25	4.25	1.3	1.99	1.375	3.54	1.302
2	1.5	1.5	3.5	1.25	1.99	1.375	3.54	1.302
3	3	1.25	2.9	1.72	1.99	1.375	3.54	1.302
4	1.75	1.25	3	1.25	1.99	1.375	3.54	1.302
5	2	1.25	3.5	1.5	1.99	1.375	3.54	1.302
6	1.75	1.25	3.25	1.5	1.99	1.375	3.54	1.302
7	2	1.75	3	1.25	1.99	1.375	3.54	1.302
8	1.75	1.5	4	1	1.99	1.375	3.54	1.302
9	2	1.5	4.5	1	1.99	1.375	3.54	1.302
10	2.15	1.25	3.5	1.25	1.99	1.375	3.54	1.302
average=	1.99	1.375	3.54	1.302				
	0.40263	0.176777	0.549646	0.222701				

Two-Sample T-Test and CI: C1, C2

Two-sample T for C1 vs C2

	N	Mean	StDev	SE Mean
C1	30	0.876	0.960	0.18
C2	30	1.035	0.841	0.15

Difference = mu (C1) - mu (C2)

Estimate for difference: -0.159

95% CI for difference: (-0.626, 0.308)

T-Test of difference = 0 (vs not =): T-Value = -0.68 P-Value = 0.498 DF = 57

Uncertainty and Error

The uncertainty estimated for each element was calculated from the use of multiple analyses of certified reference materials for the bias, whilst the random uncertainty was estimated from robust ANOVA analysis of the randomly selected samples identified for inclusion in a balanced experimental design; s

Detection Limit

Table 1

Precision and limits of detection for X-ray fluorescence analysis of Seine and Medway sediment samples

Element	Zn (ppm)	Cu (ppm)	Pb (ppm)	Ni (ppm)	Co (ppm)	Fe ₂ O ₃ (wt%)	MnO (wt%)	TiO ₂ (wt%)	CaO (wt%)	K ₂ O (wt%)	Zr (ppm)	Sr (ppm)	Rb (ppm)	Br (ppm)
Precision (1 SD)	3	4	3	4	2	0.03	<0.01	0.03	0.64	0.04	9	4	2	4
Limit of detection	15	6	6	9	4	0.03	0.01	0.09	0.3	0.03	36	10	6	11

Calculated detection limits (Cundy *et al.*, 2005).

The detection limit was also calculated from the analysis of a ‘blank’ boric acid which was run for multiple analyses. Boric acid in its crystalline form is an x-ray absorber and so gives an indication of the noise associated with the measurement of an element’s x-ray fluorescence signature at zero concentration.

This was compared with the equipment manufacturer’s published values for the detection limits of a selection of elements.

Boric Acid Replicate	1	2	3	4	5			
Compound	Conc ppm	mean	stdev	3s				
Mo	2.5	2.4	2.6	2.7	2.6	2.56	0.114018	0.342053
Zr	30.6	28.5	26.8	28.6	30.6	29.02	1.609969	4.829907
Y	15.7	25.3	13.2	21.7	16.1	18.4	4.952777	14.85833
Sr	-4.1	-0.8	-2.5	-1.9	-0.2	-1.9	1.524795	4.574385
Rb	-6	-4.2	-4.8	-9.9	-5.6	-6.1	2.236068	6.708204
Ga	7.4	8	8	8.4	8.7	8.1	0.489898	1.469694
Br	-9.1	-8.5	-7.2	-7.1	-7.1	-7.8	0.938083	2.814249
Se	-5.1	-3.2	-7.4	-7.3	-1.6	-4.92	2.541063	7.623188
Zn	1.6	8	8	9.9	9.9	7.48	3.421549	10.26465
Cu	7.7	11.5	10.3	8.5	11.8	9.96	1.810525	5.431574
Ni	22.7	22.8	22.1	23.4	21.4	22.48	0.759605	2.278815
Co	19.6	19.9	19	21	17.9	19.48	1.143241	3.429723
Fe2O3	0.57	0.57	0.57	0.57	0.57	0.57	0	0
MnO	0	0	0.01	0	0.01	0.004	0.005477	0.016432
Cr	-48.9	-37.2	-37.2	-49.3	-44.9	-43.5	6.002916	18.00875
V	74.6	99.2	82.5	85.2	87.9	85.88	8.953044	26.85913
TiO2	-0.01	0.01	0	0.01	0.01	0.004	0.008944	0.026833
CaO	-0.14	-0.13	-0.16	-0.17	-0.16	-0.152	0.016432	0.049295
K2O	-0.02	-0.02	-0.03	-0.02	-0.02	-0.022	0.004472	0.013416
U	-43.8	-38.1	-41.1	-32.5	-35	-38.1	4.540374	13.62112
Th	-30.8	-27.4	-32.1	-22.2	-30.3	-28.56	3.948797	11.84639
Bi	3.7	2.4	2.6	2.2	2	2.58	0.664831	1.994492
Pb	-52.8	-40.5	-50.5	-41.8	-43.7	-45.86	5.467449	16.40235
Ba	258.5	205.8	181	122.4	47.9	163.12	80.88941	242.6682
W	6.9	2.2	7.4	-2.9	5.8	3.88	4.300814	12.90244
Nb	6.4	8.1	-4.5	7.5	7.1	4.92	5.302075	15.90623
As1	12.6	9.6	12.2	10	10.6	11	1.334166	4.002499
Ce	160.3	186.5	203.1	175	109.2	166.82	35.82258	107.4677
La	51.7	56.3	47.2	49.2	55.3	51.94	3.883684	11.65105
Sn	5.6	5.8	5.7	5.8	5.6	5.7	0.1	0.3

Arsenic

--- element 1

Classical results: Mean = 29.037502

Sums of Squares are - 25750.812 12990.666 1090.4999

Sigma values (geochemical, sampling, analysis) - 22.665 27.890 8.256

Percent variance (geochemical, sampling, analysis) - 37.78 57.21 5.01

sigma (total) - 36.874

Robust results:

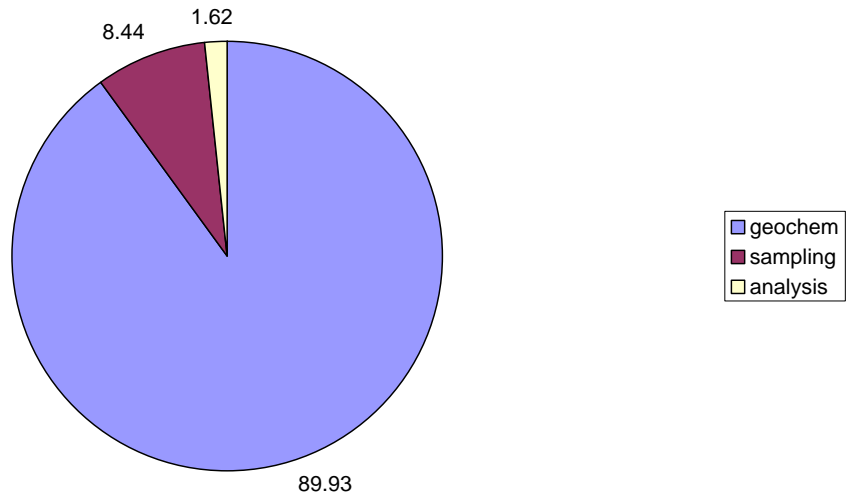
mean = 22.102868

Sigma values (geochemical, sampling, analysis) - 15.401 2.521 2.853

Percent variances (geochemical, sampling, analysis) - 94.24 2.53 3.23

sigma (total) - 15.864

Arsenic



SUMMARY OUTPUT As

Regression Statistics	
Multiple R	0.983872267
R Square	0.968004638
Adjusted R Square	0.957339518
Standard Error	82.53286723
Observations	5

ANOVA					
	df	SS	MS	F	Significance F
Regression	1	618252.0089	618252.0089	90.76359103	0.002452677
Residual	3	20435.02252	6811.674173		
Total	4	638687.0314			

	Coefficients	Standard Error	t Stat	P-value	Lower 95%	Upper 95%	Lower 95.0%	Upper 95.0%
Intercept	-44.04029619	46.96377061	-0.937750432	0.417551264	-193.4999744	105.419382	-193.4999744	105.419382
X Variable 1	1.501758307	0.157631935	9.526992759	0.002452677	1.000103136	2.003413477	1.000103136	2.003413477

$C_{meas} = 1.502 * C_{cert} - 44.040$
 bias = + 50.2%

Barium

--- element 1

Classical results: Mean = 132.60313

Sums of Squares are - 210671.70 102394.96 238883.33

Sigma values (geochemical, sampling, analysis) - 65.758 0.000 122.189

Percent variance (geochemical, sampling, analysis) - 22.46 0.00 77.54

sigma (total) - 138.760

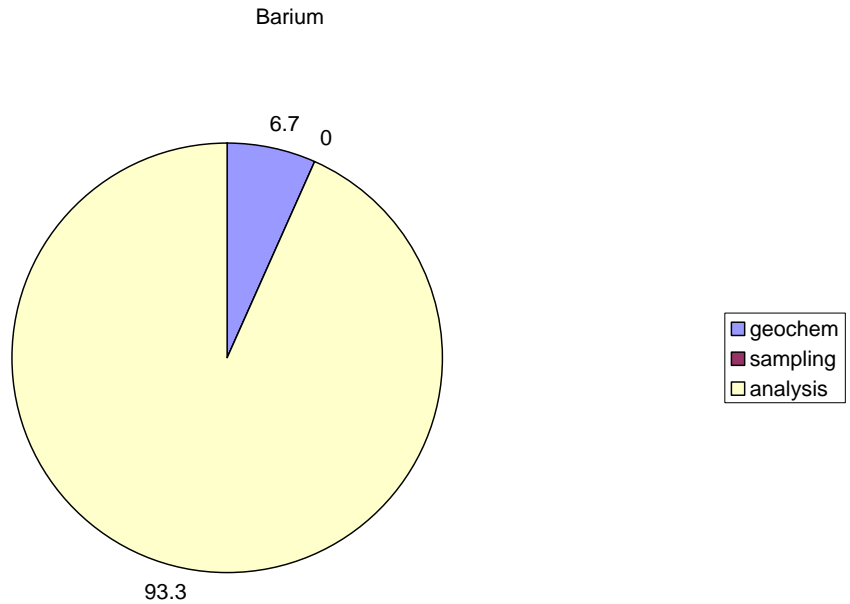
Robust results:

mean = 137.74167

Sigma values (geochemical, sampling, analysis) - 36.407 0.000 135.861

Percent variances (geochemical, sampling, analysis) - 6.70 0.00 93.30

sigma (total) - 140.655



SUMMARY OUTPUT Ba

Regression Statistics
 Multiple R 0.979039673
 R Square 0.958518682
 Adjusted R Square 0.944691576
 Standard Error 60.22321173
 Observations 5

ANOVA

	df	SS	MS	F	Significance F
Regression	1	251418.4344	251418.4344	69.32171395	0.003631289
Residual	3	10880.50569	3626.835231		
Total	4	262298.9401			

	Coefficients	Standard Error	t Stat	P-value	Lower 95%	Upper 95%	Lower 95.0%	Upper 95.0%
Intercept	-17.59916202	46.21905563	-0.380777188	0.728732484	-164.6888248	129.4905008	-164.6888248	129.4905008
X Variable 1	0.573189534	0.068843605	8.325966247	0.003631289	0.354098457	0.792280611	0.354098457	0.792280611

$C_{meas} = 0.573 * C_{cert} - 17.599$
 $(1 - 0.573) * 100$
 bias = -42.7 %

Bismuth

--- element 1

Classical results: Mean = 1.0656251

Sums of Squares are - 15.319690 6.947500 0.5650000

Sigma values (geochemical, sampling, analysis) - 0.574 0.645 0.188

Percent variance (geochemical, sampling, analysis) - 42.21 53.28 4.52

sigma (total) - 0.884

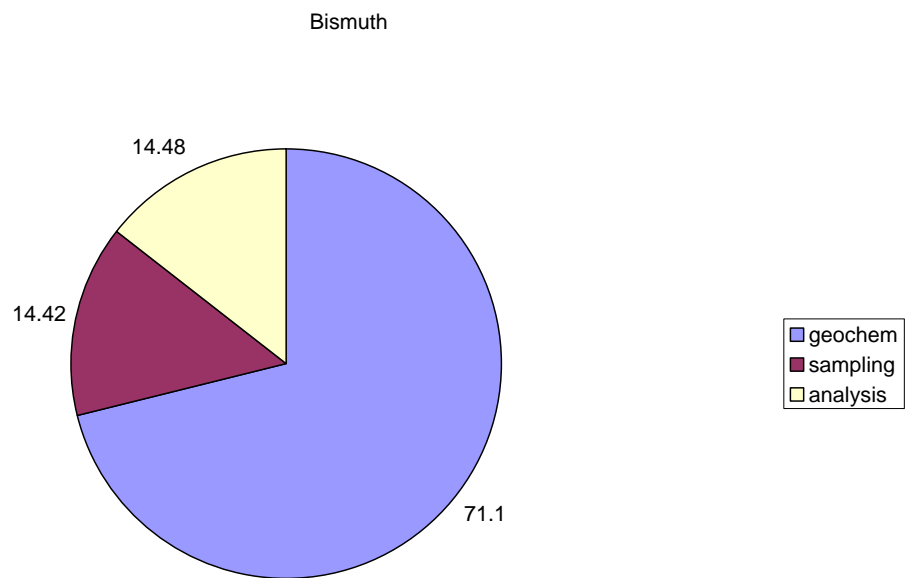
Robust results:

mean = 0.9211857

Sigma values (geochemical, sampling, analysis) - 0.430 0.194 0.194

Percent variances (geochemical, sampling, analysis) - 71.11 14.42 14.48

sigma (total) - 0.510



SUMMARY OUTPUT Bi

Regression Statistics
 Multiple R 0.999394096
 R Square 0.99878856
 Adjusted R Square 0.998182839
 Standard Error 0.194321182
 Observations 4

ANOVA

	df	SS	MS	F	Significance F
Regression	1	62.26468689	62.26468689	1648.927356	0.000605904
Residual	2	0.075521443	0.037760722		
Total	3	62.34020833			

	Coefficients	Standard Error	t Stat	P-value	Lower 95%	Upper 95%	Lower 95.0%	Upper 95.0%
Intercept	0.698686628	0.113369971	6.162889695	0.02533262	0.210895011	1.186478244	0.210895011	1.186478244
X Variable 1	0.187855609	0.004626189	40.60698654	0.000605904	0.167950723	0.207760496	0.167950723	0.207760496

$$C_{\text{meas}} = 0.188 * C_{\text{cert}} + 0.69$$

rotational bias = - 81.2%

translational bias = + 0.699 mg/kg

Bromine

--- element 1

Classical results: Mean = 73.90313

Sums of Squares are - 21737.958 927.1077 42.92498

Sigma values (geochemical, sampling, analysis) - 27.338 7.523 1.638

Percent variance (geochemical, sampling, analysis) - 92.65 7.02 0.33

sigma (total) - 28.402

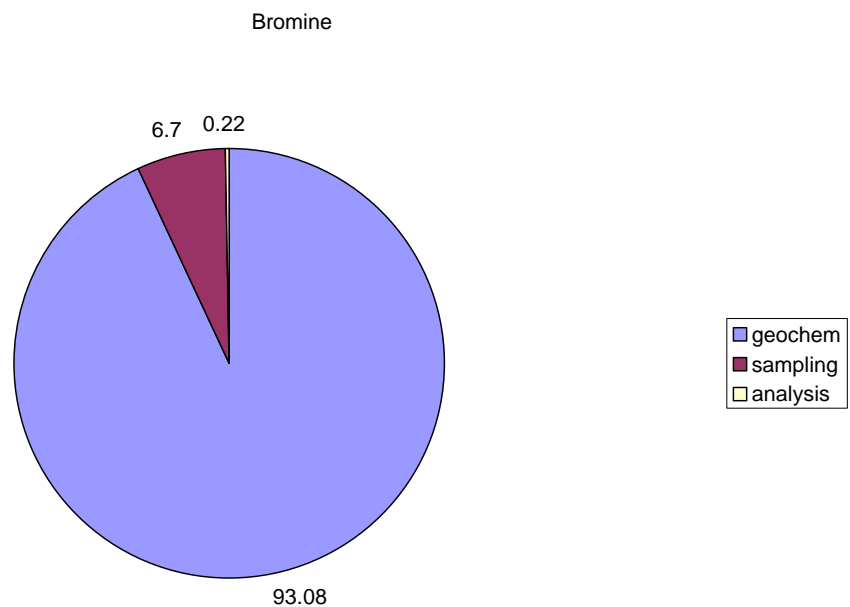
Robust results:

mean = 73.90313

Sigma values (geochemical, sampling, analysis) - 31.017 8.325 1.508

Percent variances (geochemical, sampling, analysis) - 93.08 6.70 0.22

sigma (total) - 32.150



SUMMARY OUTPUT Br

Regression Statistics	
Multiple R	0.018985844
R Square	0.000360462
Adjusted R Square	-0.499459307
Standard Error	1.00594088
Observations	4

ANOVA					
	df	SS	MS	F	Significance F
Regression	1	0.000729779	0.000729779	0.000721184	0.981014156
Residual	2	2.02383411	1.011917055		
Total	3	2.024563889			

	Coefficients	Standard Error	t Stat	P-value	Lower 95%	Upper 95%	Lower 95.0%	Upper 95.0%
Intercept	4.288871591	1.27186729	3.372106214	0.077815811	-1.183531675	9.761274858	-1.183531675	9.761274858
X Variable 1	-0.006674807	0.248550997	-0.026854878	0.981014156	-1.076103431	1.062753818	-1.076103431	1.062753818

$$C_{\text{meas}} = -0.007 * C_{\text{cert}} + 4.289$$

gradient not statistically different from zero

In all the CRMs the concentration of Bromine was much lower than the concentrations found in the experiments. This means that the bias values obtained for bromine are unlikely to be representative since the CRMs chosen to assess the bias component of the systematic error in analysis should cover a range of concentrations but particularly in the region of the measured values. The precision of the measurements is good when subjected to a visual inspection since there is good agreement between samples at a given distance across the cell such that across the entire treated zone there is a broad range of concentrations from below 50 ppm to over 450 ppm. For this reason there was no calculable bias for the available CRMs for bromine.

Calcium

--- element 1

Classical results: Mean = 3.186563

Sums of Squares are - 166.80598 7.929776 0.1941499

Sigma values (geochemical, sampling, analysis) - 2.389 0.700 0.110

Percent variance (geochemical, sampling, analysis) - 91.92 7.88 0.20

sigma (total) - 2.492

Robust results:

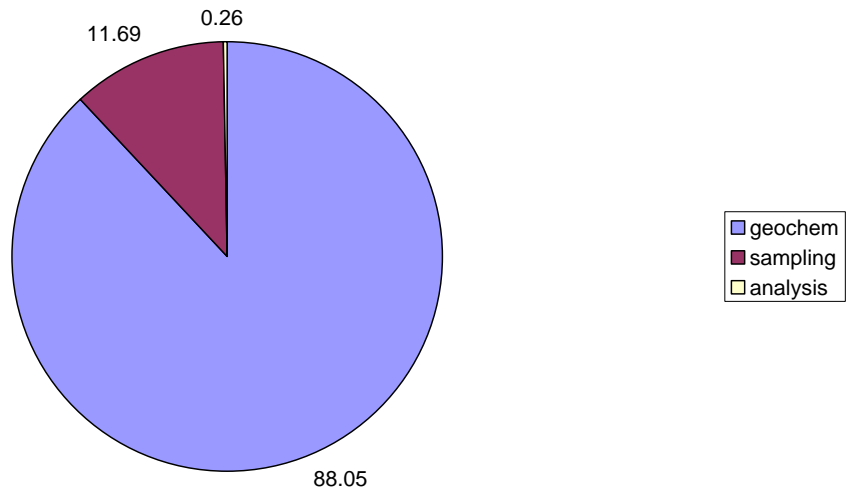
mean = 2.827035

Sigma values (geochemical, sampling, analysis) - 1.821 0.663 0.099

Percent variances (geochemical, sampling, analysis) - 88.05 11.69 0.26

sigma (total) - 1.940

Calcium



SUMMARY OUTPUT Ca

Regression Statistics	
Multiple R	0.99682348
R Square	0.993657051
Adjusted R Square	0.991542734
Standard Error	0.34849512
Observations	5

ANOVA					
	df	SS	MS	F	Significance F
Regression	1	57.07684342	57.07684342	469.966113	0.00021481
Residual	3	0.364346547	0.121448849		
Total	4	57.44118997			

	Coefficients	Standard Error	t Stat	P-value	Lower 95%	Upper 95%	Lower 95.0%	Upper 95.0%
Intercept	0.035570775	0.193963038	0.183389449	0.86618694	-0.58170618	0.652847729	-0.58170618	0.652847729
X Variable 1	1.110517043	0.051226178	21.67870183	0.00021481	0.947492482	1.273541605	0.947492482	1.273541605

$C_{meas} = 1.111 * C_{cert} + 0.036$
 bias = + 11 %

Cerium

--- element 1

Classical results: Mean = 168.27189

Sums of Squares are - 21880.133 23439.085 71530.21

Sigma values (geochemical, sampling, analysis) - 6.997 0.000 66.863

Percent variance (geochemical, sampling, analysis) - 1.08 0.00 98.92

sigma (total) - 67.228

Robust results:

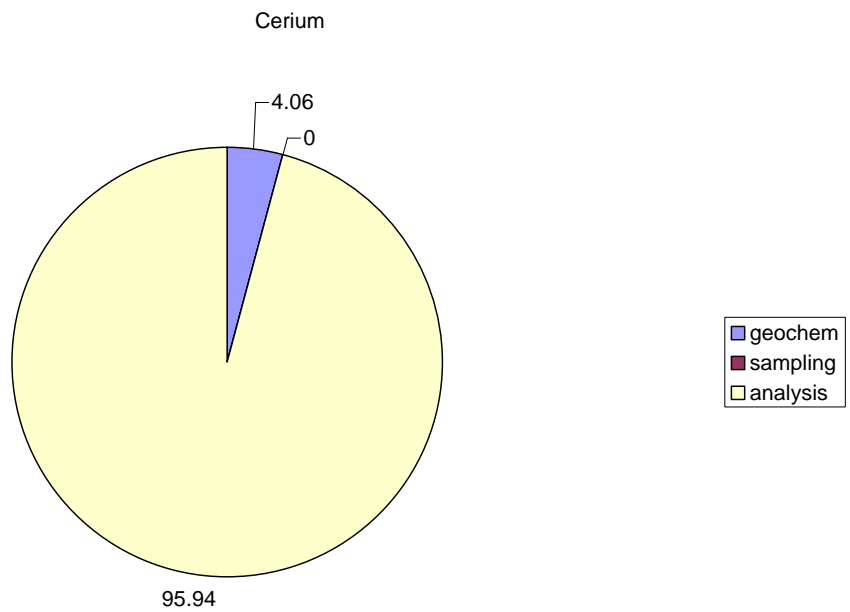
mean = 168.27188

Sigma values (geochemical, sampling, analysis) - 12.661 0.000 61.565

Percent variances (geochemical, sampling, analysis) - 4.06 0.00 95.94

sigma (total) - 62.853

—



SUMMARY OUTPUT Ce

Regression Statistics	
Multiple R	0.691184548
R Square	0.477736079
Adjusted R Square	0.216604118
Standard Error	19.63090374
Observations	4

ANOVA					
	df	SS	MS	F	Significance F
Regression	1	705.0316253	705.0316253	1.829481454	0.308815452
Residual	2	770.7447636	385.3723818		
Total	3	1475.776389			

	Coefficients	Standard Error	t Stat	P-value	Lower 95%	Upper 95%	Lower 95.0%	Upper 95.0%
Intercept	37.00696924	23.14524746	1.598901429	0.250957117	-62.57899293	136.5929314	-62.57899293	136.5929314
X Variable 1	0.369398881	0.273106206	1.352583252	0.308815452	-0.805682283	1.544480045	-0.805682283	1.544480045

no useful correlation

Cobalt

--- element 1

Classical results: Mean = 44.20938

Sums of Squares are - 15225.908 2622.548 498.2150

Sigma values (geochemical, sampling, analysis) - 21.490 12.179 5.580

Percent variance (geochemical, sampling, analysis) - 72.01 23.13 4.86

sigma (total) - 25.324

Robust results:

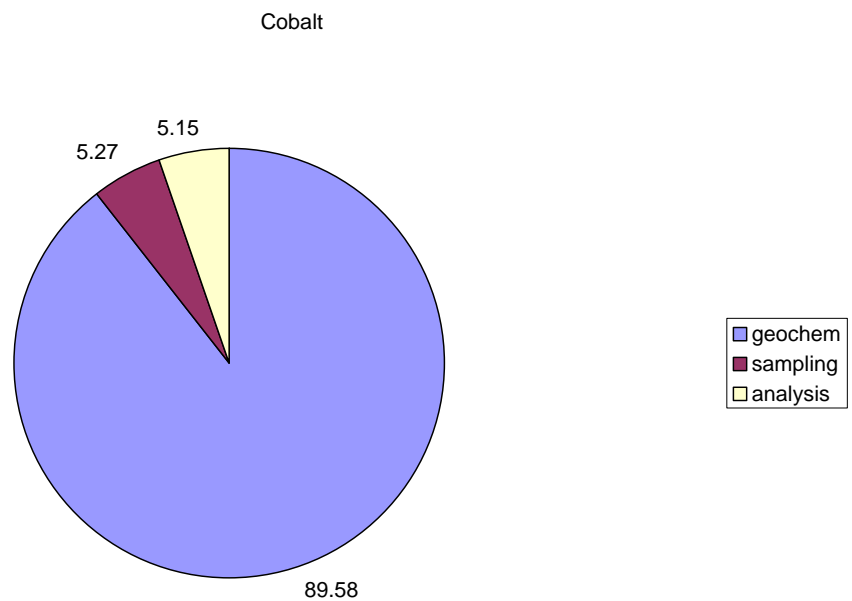
mean = 44.20938

Sigma values (geochemical, sampling, analysis) - 25.869 6.274 6.203

Percent variances (geochemical, sampling, analysis) - 89.58 5.27 5.15

sigma (total) - 27.332

—



SUMMARY OUTPUT Co

Regression Statistics	
Multiple R	0.753403587
R Square	0.567616965
Adjusted R Square	0.351425448
Standard Error	12.19871026
Observations	4

ANOVA					
	df	SS	MS	F	Significance F
Regression	1	390.7010248	390.7010248	2.625528384	0.246596412
Residual	2	297.6170641	148.8085321		
Total	3	688.3180889			

	Coefficients	Standard Error	t Stat	P-value	Lower 95%	Upper 95%	Lower 95.0%	Upper 95.0%
Intercept	4.857088654	12.97318622	0.37439443	0.744079473	-50.96202643	60.67620374	-50.96202643	60.67620374
X Variable 1	1.552544882	0.958155077	1.620348229	0.246596412	-2.570063675	5.67515344	-2.570063675	5.67515344

$$C_{\text{meas}} = 1.552 * C_{\text{cert}} + 4.857$$

no relationship between cert and meas

Chromium

--- element 1

Classical results: Mean = 218.10004

Sums of Squares are - 63866.28 7954.198 24950.204

Sigma values (geochemical, sampling, analysis) - 45.082 0.000 39.489

Percent variance (geochemical, sampling, analysis) - 56.58 0.00 43.42

sigma (total) - 59.931

Robust results:

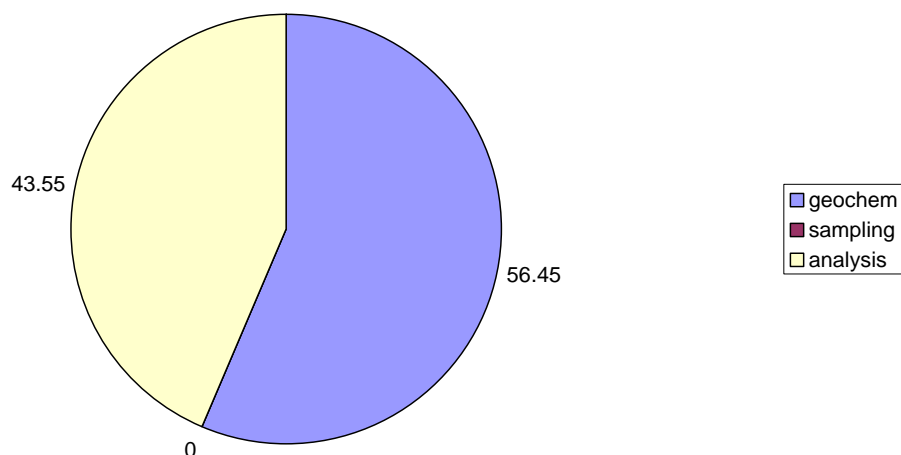
mean = 224.71234

Sigma values (geochemical, sampling, analysis) - 35.859 0.000 31.493

Percent variances (geochemical, sampling, analysis) - 56.45 0.00 43.55

sigma (total) - 47.725

Chromium



SUMMARY OUTPUT Cr

Regression Statistics	
Multiple R	0.977425749
R Square	0.955361094
Adjusted R Square	0.933041641
Standard Error	54.07059642
Observations	4

ANOVA					
	df	SS	MS	F	Significance F
Regression	1	125142.9317	125142.9317	42.80396543	0.022574251
Residual	2	5847.258795	2923.629398		
Total	3	130990.1905			

	Coefficients	Standard Error	t Stat	P-value	Lower 95%	Upper 95%	Lower 95.0%	Upper 95.0%
Intercept	19.5506975	38.2775621	0.510761303	0.660312545	-145.1443595	184.2457545	-145.1443595	184.2457545
X Variable 1	1.301163076	0.198879367	6.542473953	0.022574251	0.445454226	2.156871926	0.445454226	2.156871926

$$C_{\text{meas}} = 1.301 * C_{\text{cert}} + 19.551$$

bias = + 30 %

Copper

--- element 1

Classical results: Mean = 43.66875

Sums of Squares are - 3726.955 639.5849 716.4300

Sigma values (geochemical, sampling, analysis) - 10.636 4.194 6.692

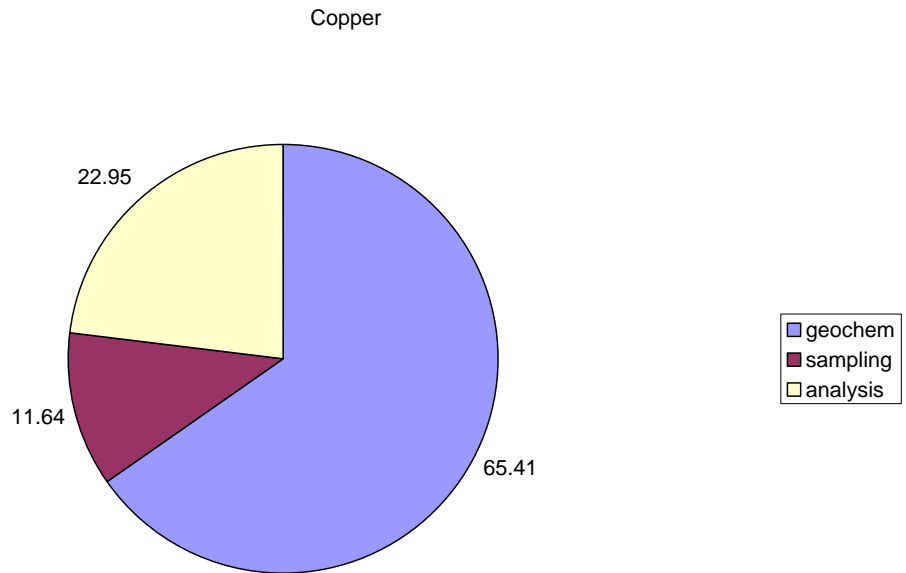
Percent variance (geochemical, sampling, analysis) - 64.46 10.02 25.52

sigma (total) - 13.247

Robust results:

mean = 43.66875

Sigma values (geochemical, sampling, analysis) - 12.054 5.085 7.141
 Percent variances (geochemical, sampling, analysis) - 65.41 11.64 22.95
 sigma (total) - 14.905



SUMMARY OUTPUT Cu

Regression Statistics	
Multiple R	0.999879604
R Square	0.999759223
Adjusted R Square	0.999678964
Standard Error	26.67081436
Observations	5

ANOVA					
	df	SS	MS	F	Significance F
Regression	1	8860826.25	8860826.25	12456.66163	1.58578E-06
Residual	3	2133.997016	711.3323388		
Total	4	8862960.247			

	Coefficients	Standard Error	t Stat	P-value	Lower 95%	Upper 95%	Lower 95.0%	Upper 95.0%
Intercept	-14.04608375	13.89797978	-1.01065651	0.386619223	-58.27565815	30.18349066	-58.27565815	30.18349066
X Variable 1	1.165456691	0.010442279	111.6094155	1.58578E-06	1.132224698	1.198688684	1.132224698	1.198688684

$$C_{\text{meas}} = 1.165 \cdot C_{\text{cert}} - 14.046$$

rotational bias = +16.5 %
 translational bias = -14.05 mg/kg

Iron

--- element 1

Classical results: Mean = 15.842814

Sums of Squares are - 2426.125 280.4813 1.4470519

Sigma values (geochemical, sampling, analysis) - 8.825 4.181 0.301

Percent variance (geochemical, sampling, analysis) - 81.59 18.32 0.09

sigma (total) - 9.770

Robust results:

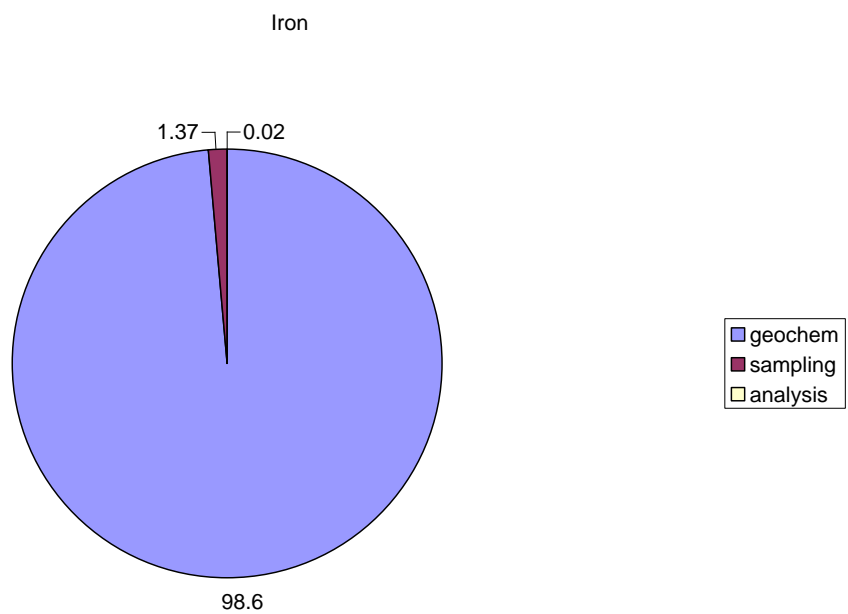
mean = 15.674115

Sigma values (geochemical, sampling, analysis) - 10.159 1.199 0.157

Percent variances (geochemical, sampling, analysis) - 98.60 1.37 0.02

sigma (total) - 10.230

-



SUMMARY OUTPUT Fe

Regression Statistics
 Multiple R 0.959203182
 R Square 0.920070744
 Adjusted R Square 0.893427659
 Standard Error 1.09051356
 Observations 5

ANOVA					
	<i>df</i>	<i>SS</i>	<i>MS</i>	<i>F</i>	<i>Significance F</i>
Regression	1	41.06755486	41.06755486	34.53319062	0.009830999
Residual	3	3.567659471	1.189219824		
Total	4	44.63521433			

	<i>Coefficients</i>	<i>Standard Error</i>	<i>t Stat</i>	<i>P-value</i>	<i>Lower 95%</i>	<i>Upper 95%</i>	<i>Lower 95.0%</i>	<i>Upper 95.0%</i>
Intercept	0.988683426	1.019021024	0.970228683	0.403496695	-2.254296266	4.231663117	-2.254296266	4.231663117
X Variable 1	0.930608075	0.158361083	5.876494756	0.009830999	0.426632431	1.434583719	0.426632431	1.434583719

$$C_{\text{meas}} = 0.931 * C_{\text{cert}} + 0.989$$

$$(1 - 0.931) * 100$$

Bias = -6.9%

Gallium

--- element 1

Classical results: Mean = 15.371876

Sums of Squares are - 413.6572 68.98250 92.02499

Sigma values (geochemical, sampling, analysis) - 3.552 1.198 2.398

Percent variance (geochemical, sampling, analysis) - 63.71 7.25 29.04

sigma (total) - 4.450

Robust results:

mean = 15.704783

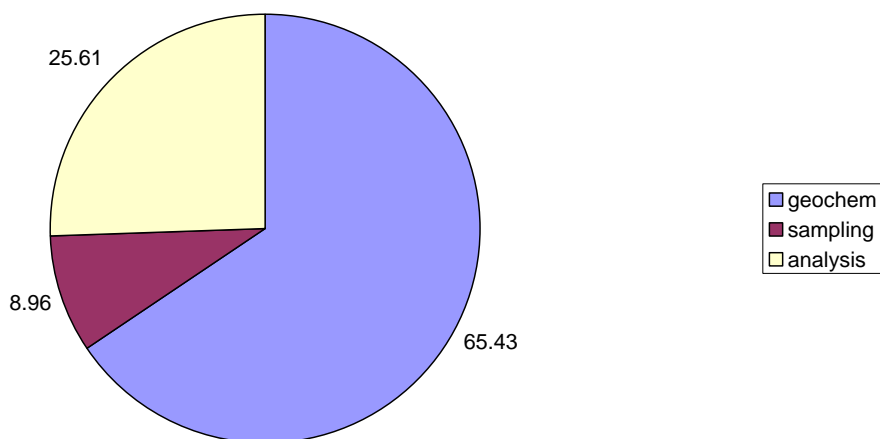
Sigma values (geochemical, sampling, analysis) - 3.327 1.231 2.082

Percent variances (geochemical, sampling, analysis) - 65.43 8.96 25.61

sigma (total) - 4.113

—

Galium



SUMMARY OUTPUT Ga

Regression Statistics	
Multiple R	0.675349215
R Square	0.456096563
Adjusted R Square	0.184144844
Standard Error	5.801761235
Observations	4

ANOVA					
	df	SS	MS	F	Significance F
Regression	1	56.45269704	56.45269704	1.677123296	0.324650784
Residual	2	67.32086685	33.66043343		
Total	3	123.7735639			

	Coefficients	Standard Error	t Stat	P-value	Lower 95%	Upper 95%	Lower 95.0%	Upper 95.0%
Intercept	10.1085654	8.483310869	1.191582574	0.3556536	-26.39217526	46.60930607	-26.39217526	46.60930607
X Variable 1	0.461404898	0.356286777	1.295037951	0.324650784	-1.071573377	1.994383173	-1.071573377	1.994383173

$$C_{\text{meas}} = 0.461 * C_{\text{cert}} + 10.108$$

gradient not statistically different from zero

Potassium

--- element 1

Classical results: Mean = 2.009375

Sums of Squares are - 7.042388 0.2909000 2.8499987E-02

Sigma values (geochemical, sampling, analysis) - 0.492 0.131 0.042

Percent variance (geochemical, sampling, analysis) - 92.71 6.61 0.68

sigma (total) - 0.511

Robust results:

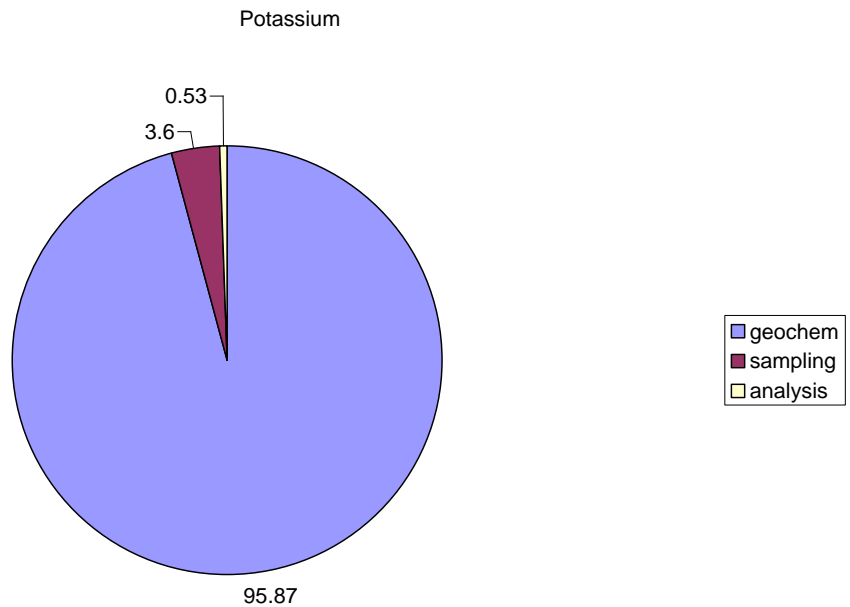
mean = 2.009375

Sigma values (geochemical, sampling, analysis) - 0.563 0.109 0.042

Percent variances (geochemical, sampling, analysis) - 95.87 3.60 0.53

sigma (total) - 0.575

—



SUMMARY OUTPUT K

Regression Statistics	
Multiple R	0.954741896
R Square	0.911532089
Adjusted R Square	0.882042785
Standard Error	0.275957762
Observations	5

ANOVA					
	df	SS	MS	F	Significance F
Regression	1	2.353925274	2.353925274	30.91060054	0.011479102
Residual	3	0.22845806	0.076152687		
Total	4	2.582383333			

	Coefficients	Standard Error	t Stat	P-value	Lower 95%	Upper 95%	Lower 95.0%	Upper 95.0%
Intercept	0.011833435	0.395913399	0.029888948	0.97803284	-1.2481397	1.27180657	-1.2481397	1.27180657
X Variable 1	1.058451366	0.190378187	5.559730258	0.011479102	0.452583008	1.664319723	0.452583008	1.664319723

$$C_{\text{meas}} = 1.058 * C_{\text{cert}} + 0.012$$

bias = + 5.8%

Lanthanum

--- element 1

Classical results: Mean = 39.63125

Sums of Squares are - 2046.3338 1316.6952 2391.180

Sigma values (geochemical, sampling, analysis) - 5.651 2.751 12.225

Percent variance (geochemical, sampling, analysis) - 16.90 4.01 79.09

sigma (total) - 13.746

Robust results:

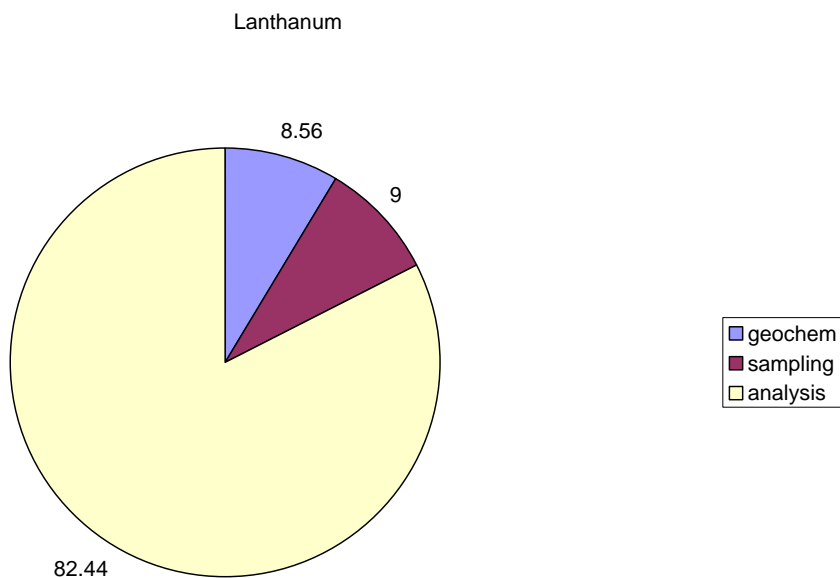
mean = 40.32417

Sigma values (geochemical, sampling, analysis) - 4.089 4.194 12.692

Percent variances (geochemical, sampling, analysis) - 8.56 9.00 82.44

sigma (total) - 13.979

—



SUMMARY OUTPUT La

Regression Statistics
 Multiple R 0.842667723
 R Square 0.710088892
 Adjusted R Square 0.565133337
 Standard Error 6.023573644
 Observations 4

ANOVA					
	df	SS	MS	F	Significance F
Regression	1	177.7404628	177.7404628	4.898666321	0.157332277
Residual	2	72.56687888	36.28343944		
Total	3	250.3073417			

	Coefficients	Standard Error	t Stat	P-value	Lower 95%	Upper 95%	Lower 95.0%	Upper 95.0%
Intercept	46.63768377	7.88830424	5.91225723	0.027436475	12.69705	80.57831754	12.69705	80.57831754
X Variable 1	0.496507166	0.224329605	2.213293094	0.157332277	-0.468705222	1.461719554	-0.468705222	1.461719554

$$C_{\text{meas}} = 0.497 * C_{\text{cert}} + 46.638$$

gradient not statistically different from 0 (95 % confidence)
 translational bias = + 46.637

Manganese

--- element 1

Classical results: Mean = 9.7812509E-02

Sums of Squares are - 0.1387219 2.2874994E-02 3.4999999E-04

Sigma values (geochemical, sampling, analysis) - 0.065 0.038 0.005

Percent variance (geochemical, sampling, analysis) - 74.64 24.98 0.39

sigma (total) - 0.075

Robust results:

mean = 8.7102806E-02

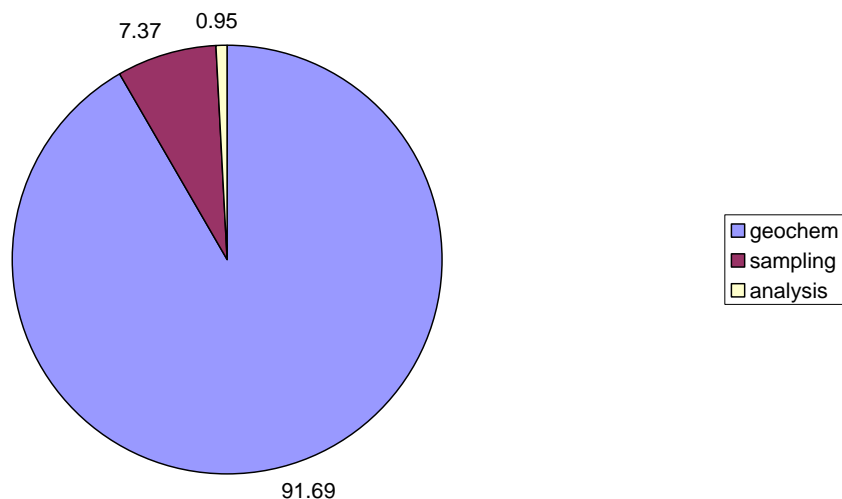
Sigma values (geochemical, sampling, analysis) - 0.052 0.015 0.005

Percent variances (geochemical, sampling, analysis) - 91.69 7.37 0.95

sigma (total) - 0.054

—

Manganese



SUMMARY OUTPUT Mn

Regression Statistics	
Multiple R	0.992660194
R Square	0.985374261
Adjusted R Square	0.978061391
Standard Error	0.013650583
Observations	4

ANOVA					
	df	SS	MS	F	Significance F
Regression	1	0.025108212	0.025108212	134.7452256	0.007339806
Residual	2	0.000372677	0.000186338		
Total	3	0.025480889			

	Coefficients	Standard Error	t Stat	P-value	Lower 95%	Upper 95%	Lower 95.0%	Upper 95.0%
Intercept	-0.019225269	0.014860162	-1.293745597	0.325017597	-0.083163387	0.044712848	-0.083163387	0.044712848
X Variable 1	1.241444354	0.106947482	11.60798112	0.007339806	0.781286478	1.70160223	0.781286478	1.70160223

$C_{\text{meas}} = 1.241 * C_{\text{cert}} - 0.019$
 bias = + 24.1%

Molybdenum

--- element 1

Classical results: Mean = 1.5406252

Sums of Squares are - 0.1646876 4.7499993E-02 0.2250001

Sigma values (geochemical, sampling, analysis) - 0.066 0.000 0.119

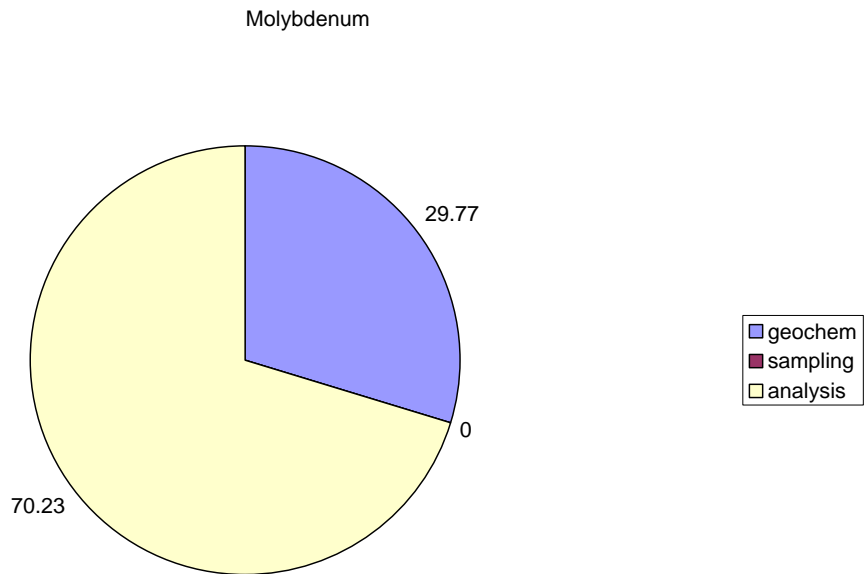
Percent variance (geochemical, sampling, analysis) - 23.82 0.00 76.18

sigma (total) - 0.136

Robust results:

mean = 1.5406250

Sigma values (geochemical, sampling, analysis) - 0.085 0.000 0.130
 Percent variances (geochemical, sampling, analysis) - 29.77 0.00 70.23
 sigma (total) - 0.155



SUMMARY OUTPUT Mo

Regression Statistics	
Multiple R	0.533937872
R Square	0.285089651
Adjusted R Square	-0.072365523
Standard Error	0.431524384
Observations	4

ANOVA					
	df	SS	MS	F	Significance F
Regression	1	0.148515078	0.148515078	0.797553571	0.466062128
Residual	2	0.372426589	0.186213294		
Total	3	0.520941667			

	Coefficients	Standard Error	t Stat	P-value	Lower 95%	Upper 95%	Lower 95.0%	Upper 95.0%
Intercept	1.978777123	0.280727567	7.048745324	0.019538929	0.770903892	3.186650354	0.770903892	3.186650354
X Variable 1	0.027288736	0.030556491	0.893058549	0.466062128	-0.104185235	0.158762706	-0.104185235	0.158762706

$$C_{\text{meas}} = 0.027C_{\text{cert}} + 1.979$$

No useful correlation between the CRM values and the measured values, so no bias calculation possible.

Nb

--- element 1

Classical results: Mean = 13.328126

Sums of Squares are - 35.59717 25.312498 128.81502

Sigma values (geochemical, sampling, analysis) - 0.693 0.000 2.837

Percent variance (geochemical, sampling, analysis) - 5.63 0.00 94.37

sigma (total) - 2.921

Robust results:

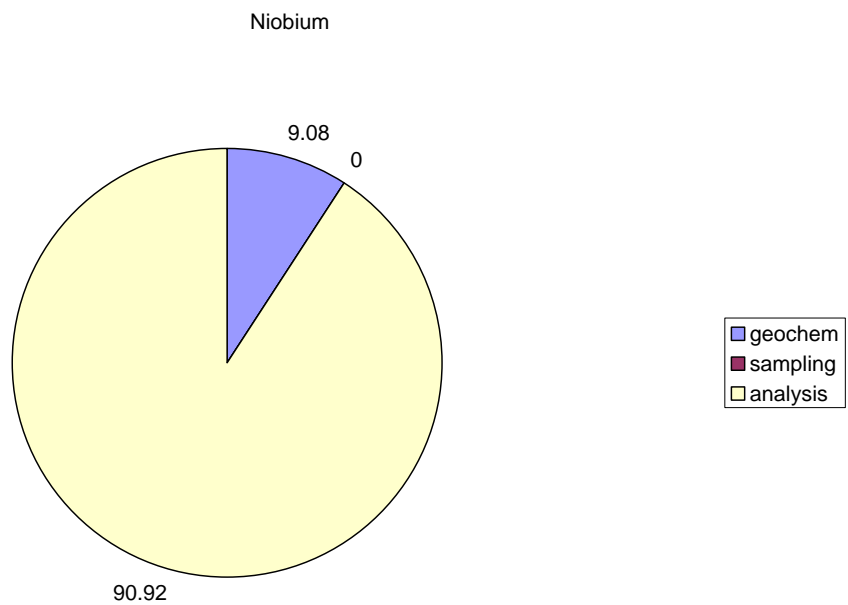
mean = 13.328126

Sigma values (geochemical, sampling, analysis) - 0.785 0.000 2.485

Percent variances (geochemical, sampling, analysis) - 9.08 0.00 90.92

sigma (total) - 2.606

-



SUMMARY OUTPUT Nb

Regression Statistics	
Multiple R	0.996078973
R Square	0.992173321
Adjusted R Square	0.988259982
Standard Error	1.465341868
Observations	4

ANOVA					
	df	SS	MS	F	Significance F
Regression	1	544.399802	544.399802	253.5362376	0.003921027
Residual	2	4.294453583	2.147226792		
Total	3	548.6942556			

	Coefficients	Standard Error	t Stat	P-value	Lower 95%	Upper 95%	Lower 95.0%	Upper 95.0%
Intercept	-3.809182077	1.648334886	-2.310927294	0.147043538	-10.90139467	3.283030517	-10.90139467	3.283030517
X Variable 1	1.053117525	0.066138877	15.92282128	0.003921027	0.768544903	1.337690146	0.768544903	1.337690146

$C_{\text{meas}} = 1.053 * C_{\text{cert}} - 3.809$

bias = + 5.3 %

Nickel

--- element 1

Classical results: Mean = 33.17812

Sums of Squares are - 2254.372 1521.6776 987.9850

Sigma values (geochemical, sampling, analysis) - 5.741 8.014 7.858

Percent variance (geochemical, sampling, analysis) - 20.74 40.41 38.85

sigma (total) - 12.607

Robust results:

mean = 32.81250

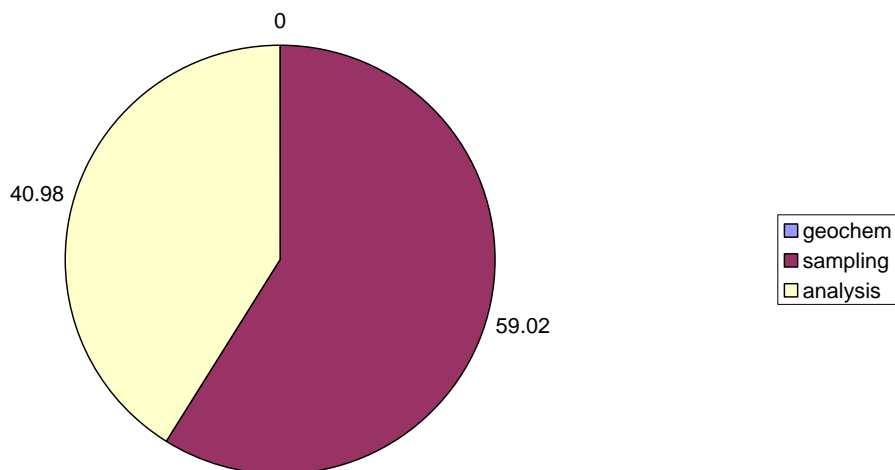
Sigma values (geochemical, sampling, analysis) - 0.000 8.424 7.019

Percent variances (geochemical, sampling, analysis) - 0.00 59.02 40.98

sigma (total) - 10.965

—

Nickle



SUMMARY OUTPUT Ni

Regression Statistics	
Multiple R	0.985171178
R Square	0.970562249
Adjusted R Square	0.960749666
Standard Error	2.949370841
Observations	5

ANOVA					
	df	SS	MS	F	Significance F
Regression	1	860.3968112	860.3968112	98.90996033	0.002162845
Residual	3	26.09636507	8.698788356		
Total	4	886.4931762			

	Coefficients	Standard Error	t Stat	P-value	Lower 95%	Upper 95%	Lower 95.0%	Upper 95.0%
Intercept	10.43835474	2.592313481	4.026656041	0.027525372	2.188456279	18.68825319	2.188456279	18.68825319
X Variable 1	0.634859636	0.063834829	9.945348678	0.002162845	0.431708719	0.838010553	0.431708719	0.838010553

$C_{meas} = 0.635 * C_{cert} + 10.438$
 rotational bias = 36.52%
 translational bias = +10.44 mg/kg

Lead

--- element 1

Classical results: Mean = 21.031254

Sums of Squares are - 133992.47 47441.84 1989.5403

Sigma values (geochemical, sampling, analysis) - 57.471 53.879 11.151

Percent variance (geochemical, sampling, analysis) - 52.18 45.86 1.96

sigma (total) - 79.562

Robust results:

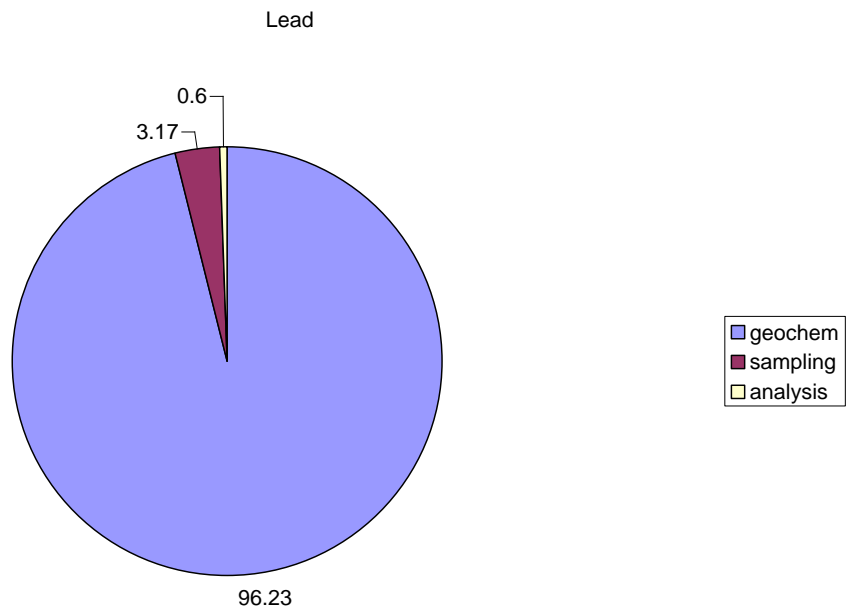
mean = 32.45846

Sigma values (geochemical, sampling, analysis) - 49.226 8.939 3.889

Percent variances (geochemical, sampling, analysis) - 96.23 3.17 0.60

sigma (total) - 50.182

—



SUMMARY OUTPUT Pb

Regression Statistics	
Multiple R	0.999978359
R Square	0.999956719
Adjusted R Square	0.999942292
Standard Error	19.36915181
Observations	5

ANOVA					
	df	SS	MS	F	Significance F
Regression	1	26003076.47	26003076.47	69311.21741	1.20849E-07
Residual	3	1125.492126	375.1640419		
Total	4	26004201.96			

	Coefficients	Standard Error	t Stat	P-value	Lower 95%	Upper 95%	Lower 95.0%	Upper 95.0%
Intercept	-16.98602565	9.875711249	-1.719979982	0.183923977	-48.41494643	14.44289512	-48.41494643	14.44289512
X Variable 1	1.049162627	0.003985117	263.2702365	1.20849E-07	1.036480207	1.061845047	1.036480207	1.061845047

$C_{\text{meas}} = 1.049 * C_{\text{cert}} - 16.986$

bias = + 4.9 %

Rb

--- element 1

Classical results: Mean = 117.56876

Sums of Squares are - 2171.018 212.11969 166.07002

Sigma values (geochemical, sampling, analysis) - 8.421 2.840 3.222

Percent variance (geochemical, sampling, analysis) - 79.36 9.03 11.62

sigma (total) - 9.453

Robust results:

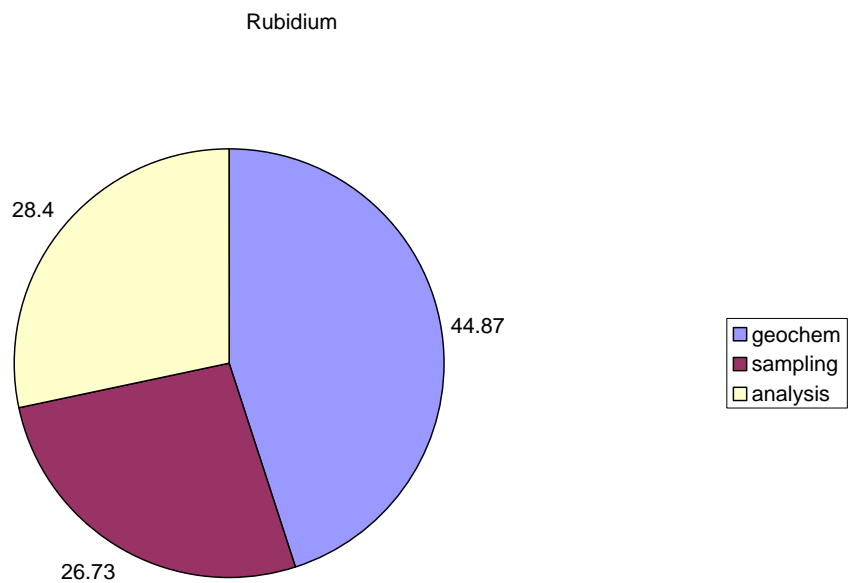
mean = 119.38641

Sigma values (geochemical, sampling, analysis) - 4.294 3.314 3.416

Percent variances (geochemical, sampling, analysis) - 44.87 26.73 28.40

sigma (total) - 6.410

—



SUMMARY OUTPUT Rb

Regression Statistics	
Multiple R	0.999793896
R Square	0.999587834
Adjusted R Square	0.999381752
Standard Error	1.941303881
Observations	4

ANOVA					
	df	SS	MS	F	Significance F
Regression	1	18279.58011	18279.58011	4850.418033	0.000206104
Residual	2	7.53732152	3.76866076		
Total	3	18287.11743			

	Coefficients	Standard Error	t Stat	P-value	Lower 95%	Upper 95%	Lower 95.0%	Upper 95.0%
Intercept	-2.842679315	2.053919599	-1.384026578	0.300562076	-11.67998208	5.994623455	-11.67998208	5.994623455
X Variable 1	1.022827689	0.014686317	69.64494262	0.000206104	0.959637568	1.08601781	0.959637568	1.08601781

$$C_{\text{meas}} = 1.022 * C_{\text{cert}} - 2.843$$

$$(1 - 1.022) * 100$$

Bias = +2.2%

Selenium

--- element 1

Classical results: Mean = 8.7500000E-02

Sums of Squares are - 3.480000 0.3850000 0.7299999

Sigma values (geochemical, sampling, analysis) - 0.335 0.035 0.214

Percent variance (geochemical, sampling, analysis) - 70.54 0.79 28.67

sigma (total) - 0.399

Robust results:

mean = 8.7500011E-02

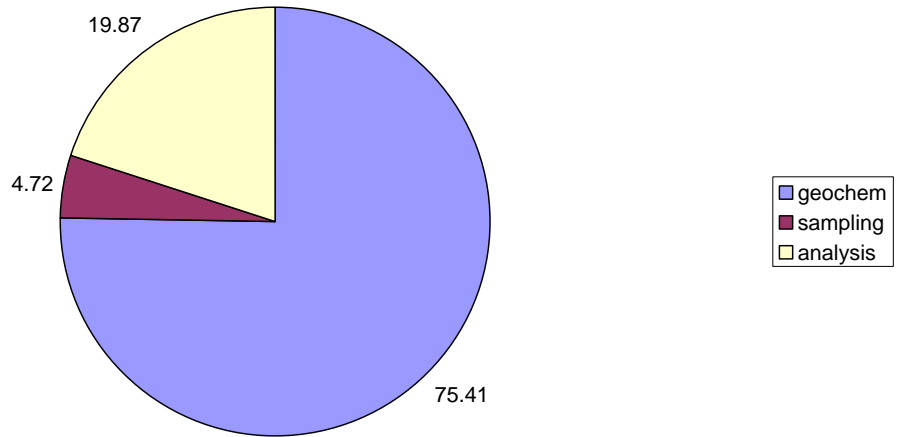
Sigma values (geochemical, sampling, analysis) - 0.381 0.095 0.196

Percent variances (geochemical, sampling, analysis) - 75.41 4.72 19.87

sigma (total) - 0.439

—

Selenium



SUMMARY OUTPUT Se

Regression Statistics	
Multiple R	0.9963075
R Square	0.992628635
Adjusted R Square	0.988942953
Standard Error	0.054542443
Observations	4

ANOVA					
	df	SS	MS	F	Significance F
Regression	1	0.801194688	0.801194688	269.3201789	0.0036925
Residual	2	0.005949756	0.002974878		
Total	3	0.807144444			

	Coefficients	Standard Error	t Stat	P-value	Lower 95%	Upper 95%	Lower 95.0%	Upper 95.0%
Intercept	0.656441141	0.039757788	16.51100775	0.003648138	0.485377187	0.827505095	0.485377187	0.827505095
X Variable 1	-0.875160322	0.053327739	-16.41097739	0.0036925	-1.104611064	-0.645709579	-1.104611064	-0.645709579

$C_{meas} = 0.461 * C_{cert} + 10.108$
 No useful correlation

Tin

--- element 1

Classical results: Mean = 4.084375

Sums of Squares are - 24.749693 26.357501 20.274995

Sigma values (geochemical, sampling, analysis) - 0.245 1.007 1.126

Percent variance (geochemical, sampling, analysis) - 2.57 43.30 54.13

sigma (total) - 1.530

Robust results:

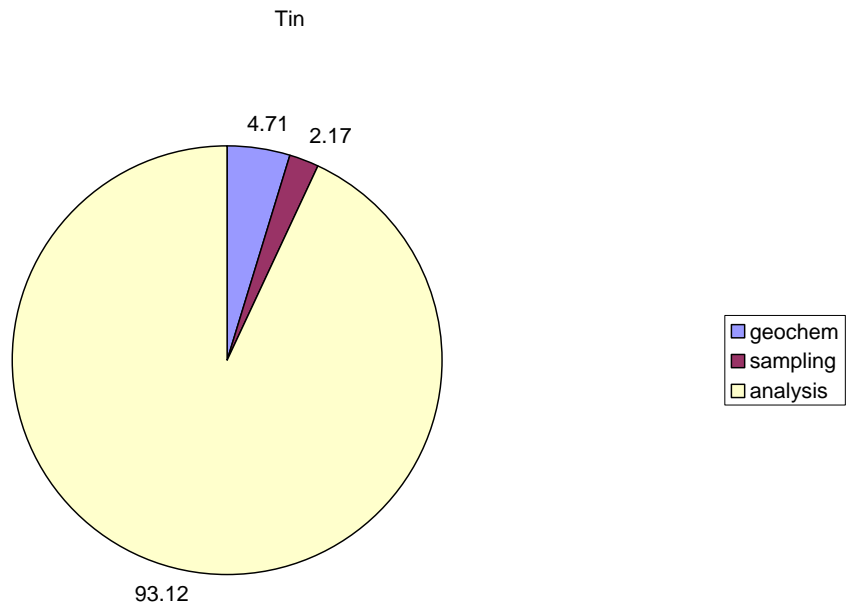
mean = 4.230881

Sigma values (geochemical, sampling, analysis) - 0.282 0.191 1.255

Percent variances (geochemical, sampling, analysis) - 4.71 2.17 93.12

sigma (total) - 1.300

—



SUMMARY OUTPUT Sn

Regression Statistics
 Multiple R 0.770284061
 R Square 0.593337534
 Adjusted R Square 0.390006301
 Standard Error 0.369377552
 Observations 4

ANOVA

	<i>df</i>	<i>SS</i>	<i>MS</i>	<i>F</i>	<i>Significance F</i>
Regression	1	0.398142671	0.398142671	2.918083591	0.229715939
Residual	2	0.272879551	0.136439776		
Total	3	0.671022222			

	<i>Coefficients</i>	<i>Standard Error</i>	<i>t Stat</i>	<i>P-value</i>	<i>Lower 95%</i>	<i>Upper 95%</i>	<i>Lower 95.0%</i>	<i>Upper 95.0%</i>
Intercept	4.892285	0.22550969	21.69434489	0.002117998	3.921995115	5.862574885	3.921995115	5.862574885
X Variable 1	0.010652932	0.006236204	1.70823991	0.229715939	-0.016179286	0.03748515	-0.016179286	0.03748515

No useful correlations

Strontium

--- element 1

Classical results: Mean = 106.28439

Sums of Squares are - 89175.29 6371.573 144.25502

Sigma values (geochemical, sampling, analysis) - 54.642 19.842 3.003

Percent variance (geochemical, sampling, analysis) - 88.11 11.62 0.27

sigma (total) - 58.210

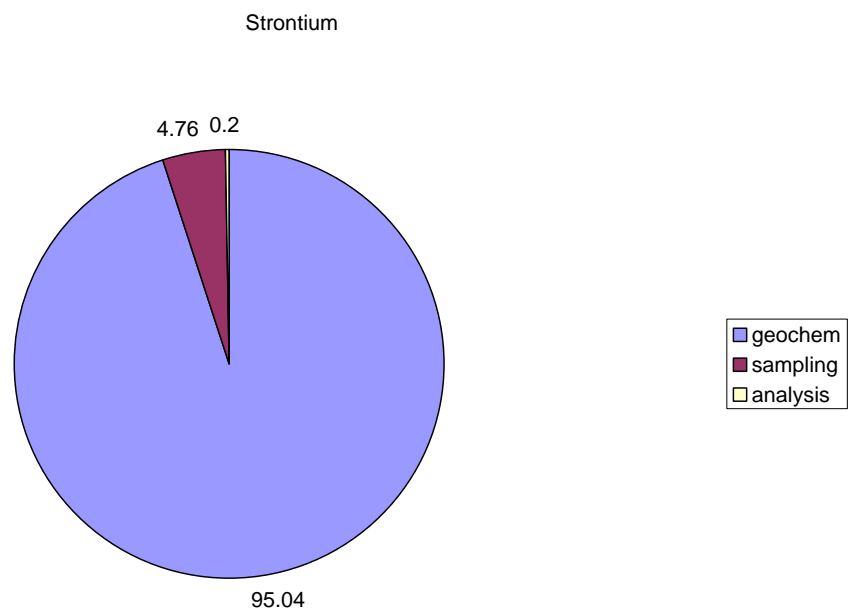
Robust results:

mean = 102.54283

Sigma values (geochemical, sampling, analysis) - 54.907 12.082 3.195

Percent variances (geochemical, sampling, analysis) - 95.07 4.60 0.32

sigma (total) - 56.311



SUMMARY OUTPUT Sr

Regression Statistics	
Multiple R	0.999553516
R Square	0.999107232
Adjusted R Square	0.998660848
Standard Error	5.947811084
Observations	4

ANOVA					
	df	SS	MS	F	Significance F
Regression	1	79180.43494	79180.43494	2238.224015	0.000446484
Residual	2	70.75291339	35.37645669		
Total	3	79251.18785			

	Coefficients	Standard Error	t Stat	P-value	Lower 95%	Upper 95%	Lower 95.0%	Upper 95.0%
Intercept	-3.679618766	4.994303754	-0.73676311	0.537970109	-25.16837344	17.80913591	-25.16837344	17.80914
X Variable 1	1.037288445	0.021925412	47.30987228	0.000446484	0.942951011	1.131625879	0.942951011	1.131626

$$C_{\text{meas}} = 1.037C_{\text{cert}} - 3.680$$

$$(1 - 1037) \cdot 100$$

$$\text{Bias} = +3.7\%$$

Thorium

--- element 1

Classical results: Mean = 0.8656254

Sums of Squares are - 1722.0997 242.71751 101.03502

Sigma values (geochemical, sampling, analysis) - 7.343 3.466 2.513

Percent variance (geochemical, sampling, analysis) - 74.63 16.63 8.74

sigma (total) - 8.500

Robust results:

mean = 0.8656251

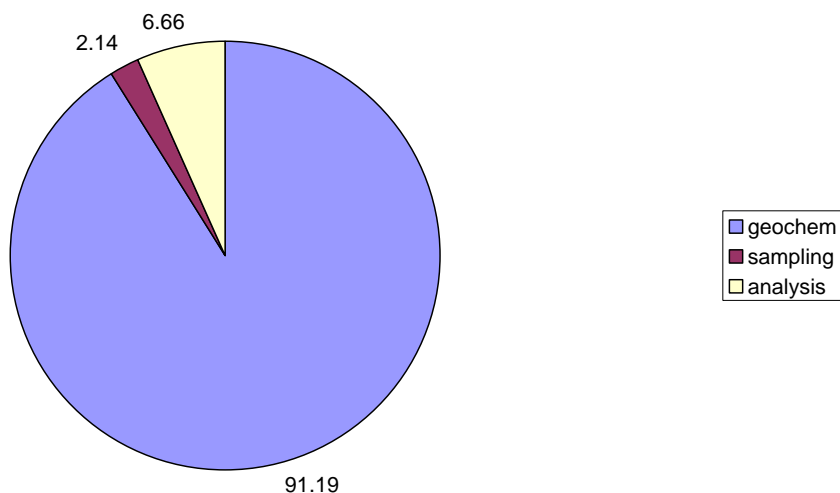
Sigma values (geochemical, sampling, analysis) - 8.758 1.343 2.367

Percent variances (geochemical, sampling, analysis) - 91.19 2.14 6.66

sigma (total) - 9.171

—

Thorium



SUMMARY OUTPUT Th

Regression Statistics
 Multiple R 0.974175556
 R Square 0.949018014
 Adjusted R Square 0.923527021
 Standard Error 3.146739977
 Observations 4

ANOVA

	df	SS	MS	F	Significance F
Regression	1	368.6459078	368.6459078	37.22954274	0.025824444
Residual	2	19.80394497	9.901972485		
Total	3	388.4498528			

	Coefficients	Standard Error	t Stat	P-value	Lower 95%	Upper 95%	Lower 95.0%	Upper 95.0%
Intercept	-3.374612658	3.534339099	-0.954807268	0.440441347	-18.58164643	11.83242111	-18.58164643	11.83242111
X Variable 1	1.139259351	0.186714803	6.101601653	0.025824444	0.335890394	1.942628307	0.335890394	1.942628307

$C_{meas} = 1.139 * C_{cert} - 3.37$
 Bias = + 13.93%

Titanium

--- element 1

Classical results: Mean = 0.6809376

Sums of Squares are - 0.5066969 4.8725005E-02 3.2500034E-03

Sigma values (geochemical, sampling, analysis) - 0.129 0.054 0.014

Percent variance (geochemical, sampling, analysis) - 84.04 14.93 1.03

sigma (total) - 0.140

Robust results:

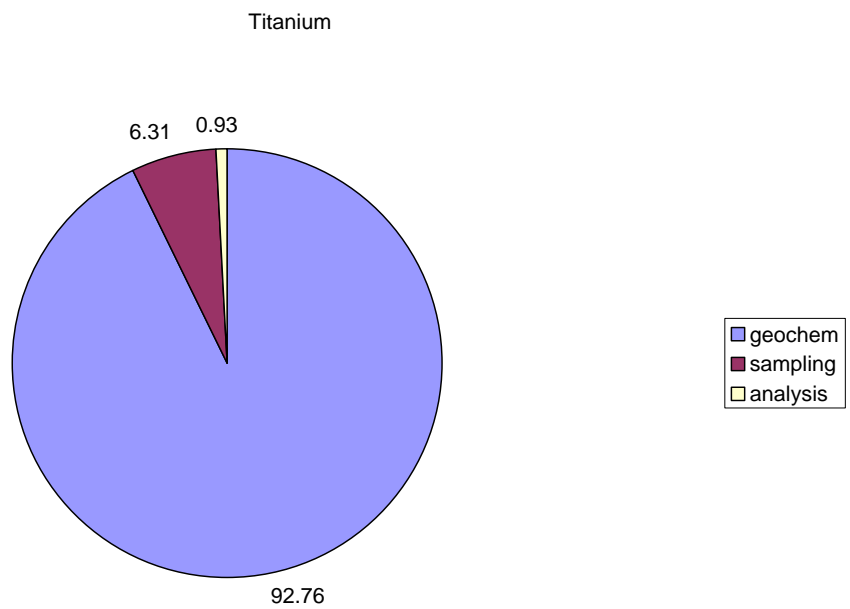
mean = 0.6858485

Sigma values (geochemical, sampling, analysis) - 0.139 0.036 0.014

Percent variances (geochemical, sampling, analysis) - 92.76 6.31 0.93

sigma (total) - 0.145

—



SUMMARY OUTPUT Ti

Regression Statistics	
Multiple R	0.992332716
R Square	0.984724218
Adjusted R Square	0.979632291
Standard Error	0.077922916
Observations	5

ANOVA					
	df	SS	MS	F	Significance F
Regression	1	1.17425611	1.17425611	193.3892975	0.000805
Residual	3	0.018215943	0.006071981		
Total	4	1.192472053			

	Coefficients	Standard Error	t Stat	P-value	Lower 95%	Upper 95%	Lower 95.0%	Upper 95.0%
Intercept	0.147589451	0.060179204	2.452499224	0.091475706	-0.043927634	0.339106536	-0.043927634	0.339106536
X Variable 1	0.892344676	0.064167692	13.90644805	0.000805	0.688134442	1.096554911	0.688134442	1.096554911

$$C_{\text{meas}} = 0.892 * C_{\text{cert}} + 0.148$$

$$(1 - 0.892) * 100$$

$$\text{bias} = -10.8 \%$$

Uranium

--- element 1

Classical results: Mean = 0.3312501

Sums of Squares are - 636.1838 339.2350 572.0500

Sigma values (geochemical, sampling, analysis) - 3.481 1.824 5.979

Percent variance (geochemical, sampling, analysis) - 23.67 6.50 69.83

sigma (total) - 7.155

Robust results:

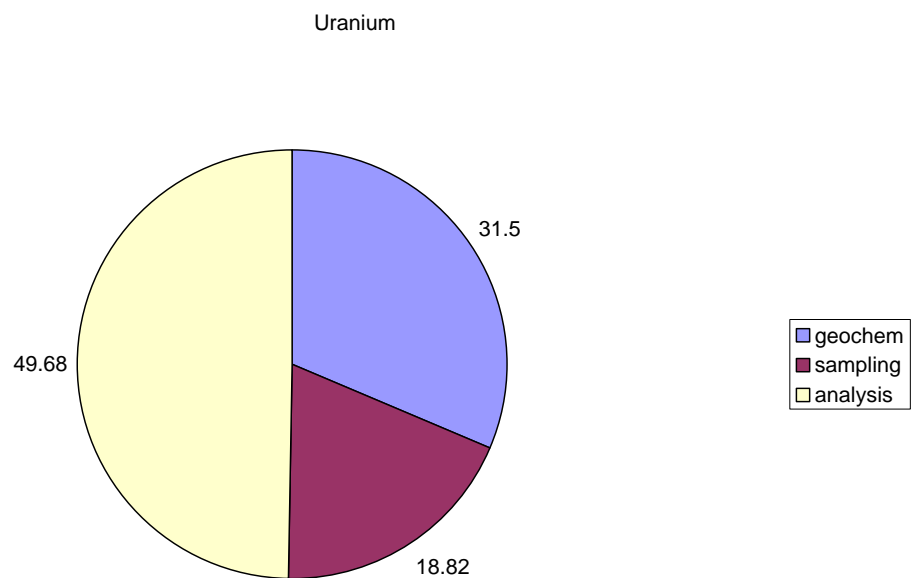
mean = 0.3376070

Sigma values (geochemical, sampling, analysis) - 4.142 3.201 5.202

Percent variances (geochemical, sampling, analysis) - 31.50 18.82 49.68

sigma (total) - 7.380

—



SUMMARY OUTPUT U

Regression Statistics	
Multiple R	0.98978538
R Square	0.979675099
Adjusted R Square	0.969512648
Standard Error	1.044375786
Observations	4

ANOVA					
	df	SS	MS	F	Significance F
Regression	1	105.1470779	105.1470779	96.40146186	0.01021462
Residual	2	2.181441564	1.090720782		
Total	3	107.3285194			

	Coefficients	Standard Error	t Stat	P-value	Lower 95%	Upper 95%	Lower 95.0%	Upper 95.0%
Intercept	-6.542589944	1.080422306	-6.055585774	0.02620306	-11.19127193	-1.893907961	-11.19127193	-1.893907961
X Variable 1	2.134886577	0.217436774	9.818424612	0.01021462	1.199331646	3.070441508	1.199331646	3.070441508

$C_{\text{meas}} = 2.135 * C_{\text{cert}} - 6.543$
 rotational bias = + 113.5%
 translational bias = -6.543 mg/kg

Vanadium

--- element 1

Classical results: Mean = 102.72501

Sums of Squares are - 25068.536 2502.365 3687.559

Sigma values (geochemical, sampling, analysis) - 28.585 6.416 15.181

Percent variance (geochemical, sampling, analysis) - 75.05 3.78 21.17

sigma (total) - 32.996

Robust results:

mean = 102.72501

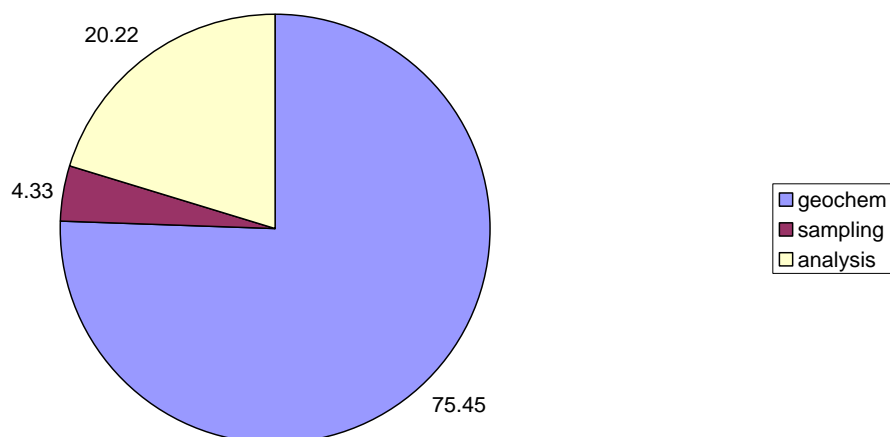
Sigma values (geochemical, sampling, analysis) - 32.397 7.760 16.774

Percent variances (geochemical, sampling, analysis) - 75.45 4.33 20.22

sigma (total) - 37.298

—

Vanadium



SUMMARY OUTPUT V

Regression Statistics	
Multiple R	0.941122394
R Square	0.88571136
Adjusted R Square	0.847615147
Standard Error	22.31624027
Observations	5

ANOVA					
	df	SS	MS	F	Significance F
Regression	1	11578.50432	11578.50432	23.24932801	0.016997534
Residual	3	1494.04374	498.0145799		
Total	4	13072.54806			

	Coefficients	Standard Error	t Stat	P-value	Lower 95%	Upper 95%	Lower 95.0%	Upper 95.0%
Intercept	28.23381606	18.5525524	1.521829204	0.225408968	-30.80868577	87.27631789	-30.80868577	87.27631789
X Variable 1	0.660794762	0.13704443	4.821755698	0.016997534	0.224658222	1.096931302	0.224658222	1.096931302

$C_{\text{meas}} = 0.661 * C_{\text{cert}} + 28.234$
 $(1 - 0.661) * 100$
 bias = - 33.1%

Tungsten

--- element 1

Classical results: Mean = 24.865628

Sums of Squares are - 4053.025 1161.3722 612.5351

Sigma values (geochemical, sampling, analysis) - 10.414 7.311 6.187

Percent variance (geochemical, sampling, analysis) - 54.18 26.70 19.12

sigma (total) - 14.149

Robust results:

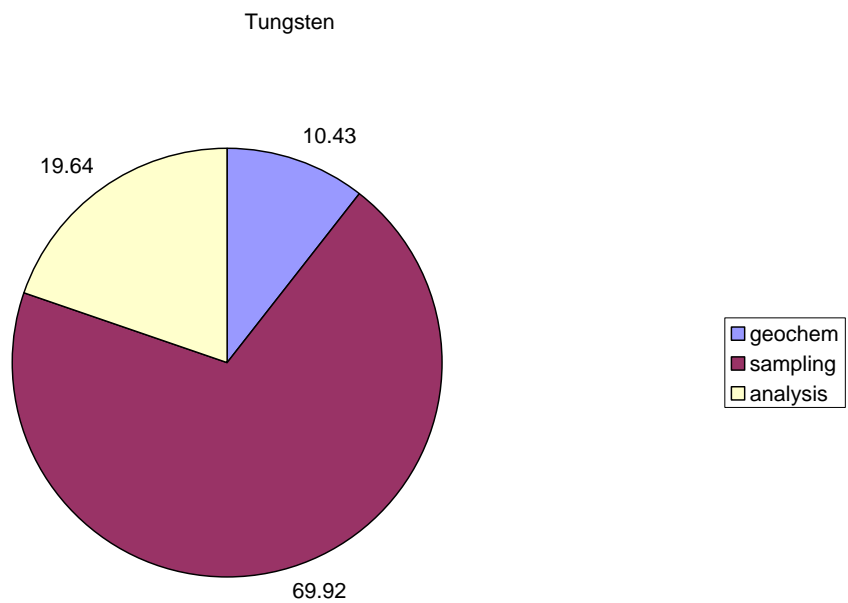
mean = 22.223998

Sigma values (geochemical, sampling, analysis) - 2.984 7.724 4.094

Percent variances (geochemical, sampling, analysis) - 10.43 69.92 19.64

sigma (total) - 9.237

—



SUMMARY OUTPUT W

Regression Statistics	
Multiple R	0.985403169
R Square	0.971019406
Adjusted R Square	0.956529109
Standard Error	4.966679264
Observations	4

ANOVA					
	df	SS	MS	F	Significance F
Regression	1	1653.038061	1653.038061	67.01169803	0.014596831
Residual	2	49.33580582	24.66790291		
Total	3	1702.373867			

	Coefficients	Standard Error	t Stat	P-value	Lower 95%	Upper 95%	Lower 95.0%	Upper 95.0%
Intercept	3.962492023	2.968327688	1.334924051	0.313572743	-8.809191206	16.73417525	-8.809191206	16.73417525
X Variable 1	0.538573389	0.065791468	8.186067311	0.014596831	0.255495548	0.82165123	0.255495548	0.82165123

$C_{meas} = 0.539 * C_{cert} + 3.962$
 $(1 - 0.539) * 100$
 bias = - 46.1 %

Yttrium

--- element 1

Classical results: Mean = 22.287502

Sums of Squares are - 2242.100 1236.3651 1564.5299

Sigma values (geochemical, sampling, analysis) - 6.437 5.327 9.889

Percent variance (geochemical, sampling, analysis) - 24.72 16.93 58.34

sigma (total) - 12.946

Robust results:

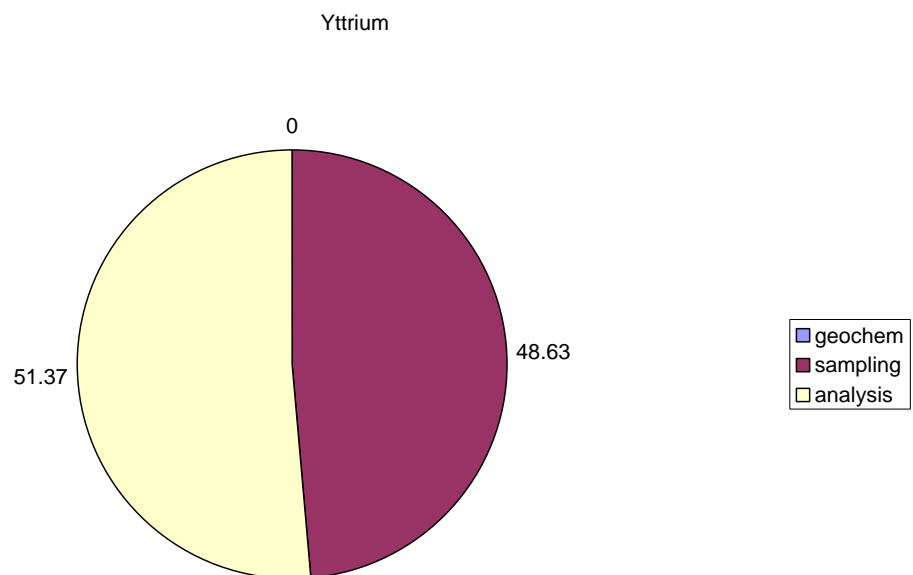
mean = 24.090746

Sigma values (geochemical, sampling, analysis) - 0.000 7.468 7.676

Percent variances (geochemical, sampling, analysis) - 0.00 48.63 51.37

sigma (total) - 10.710

—



SUMMARY OUTPUT Y

Regression Statistics	
Multiple R	0.985007348
R Square	0.970239476
Adjusted R Square	0.955359214
Standard Error	2.867086011
Observations	4

ANOVA						
	df	SS	MS	F	Significance F	
Regression	1	535.9815106	535.9815106	65.20311813	0.014992652	
Residual	2	16.44036439	8.220182194			
Total	3	552.421875				

	Coefficients	Standard Error	t Stat	P-value	Lower 95%	Upper 95%	Lower 95.0%	Upper 95.0%
Intercept	-1.399173554	4.145799522	-0.337491851	0.767875493	-19.23710918	16.43876208	-19.23710918	16.43876208
X Variable 1	1.269158527	0.157174356	8.074844774	0.014992652	0.592891855	1.945425199	0.592891855	1.945425199

$$C_{\text{meas}} = 1.269C_{\text{cert}} - 1.399$$

$$*1-1.269* 100$$

$$\text{Bias} = +26.9\%$$

Zinc

--- element 1

Classical results: Mean = 141.18438

Sums of Squares are - 20593.643 3525.404 540.0851

Sigma values (geochemical, sampling, analysis) - 25.006 14.264 5.810

Percent variance (geochemical, sampling, analysis) - 72.50 23.59 3.91

sigma (total) - 29.369

Robust results:

mean = 133.01745

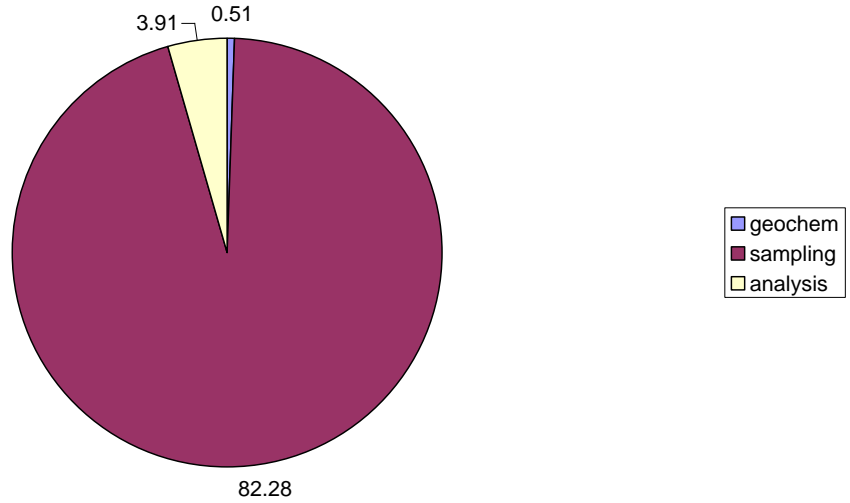
Sigma values (geochemical, sampling, analysis) - 0.682 8.652 3.956

Percent variances (geochemical, sampling, analysis) - 0.51 82.28 17.20

sigma (total) - 9.538

—

Zinc



SUMMARY OUTPUT Zn

Regression Statistics	
Multiple R	0.999998968
R Square	0.999997936
Adjusted R Square	0.999997248
Standard Error	5.431964581
Observations	5

ANOVA					
	df	SS	MS	F	Significance F
Regression	1	42879581.12	42879581.12	1453237.765	1.25882E-09
Residual	3	88.51871764	29.50623921		
Total	4	42879669.64			

	Coefficients	Standard Error	t Stat	P-value	Lower 95%	Upper 95%	Lower 95.0%	Upper 95.0%
Intercept	-9.280583944	2.757251315	-3.365882498	0.043543252	-18.0553882	-0.505779684	-18.0553882	-0.505779684
X Variable 1	1.068450933	0.000886311	1205.503117	1.25882E-09	1.065630295	1.071271571	1.065630295	1.071271571

C_{meas} = 1.068 * C_{cert} - 9.280
 Rotational Bias = + 6.8%
 Translational Bias = -9.28 mg/kg

Zirconium

--- element 1

Classical results: Mean = 126.28439

Sums of Squares are - 46418.49 4770.014 515.1053

Sigma values (geochemical, sampling, analysis) - 38.843 16.794 5.674

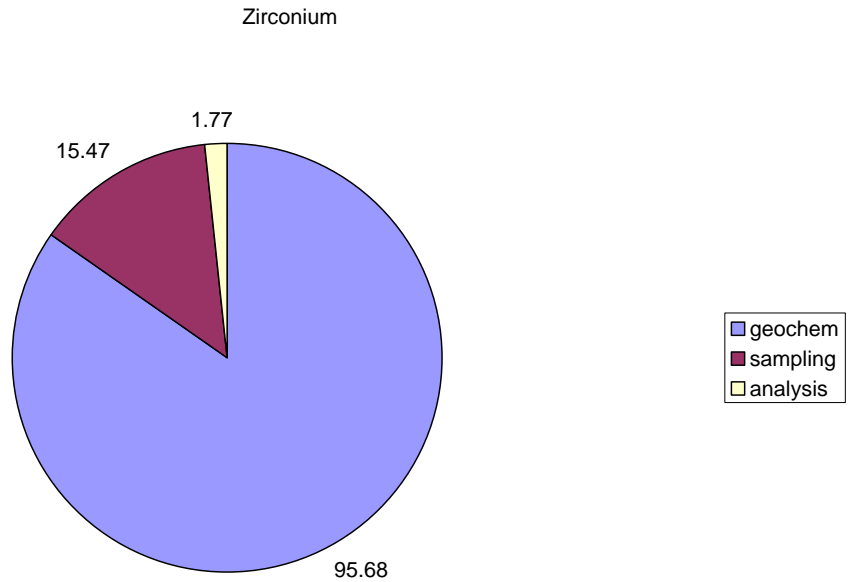
Percent variance (geochemical, sampling, analysis) - 82.76 15.47 1.77

sigma (total) - 42.696

Robust results:

mean = 126.95389

Sigma values (geochemical, sampling, analysis) - 44.300 8.199 4.628
 Percent variances (geochemical, sampling, analysis) - 95.68 3.28 1.04
 sigma (total) - 45.290



SUMMARY OUTPUT Zr

Regression Statistics	
Multiple R	0.993837396
R Square	0.98771277
Adjusted R Square	0.981569155
Standard Error	16.89871333
Observations	4

ANOVA

	df	SS	MS	F	Significance F
Regression	1	45910.7036	45910.7036	160.7706143	0.006162604
Residual	2	571.1330244	285.5665122		
Total	3	46481.83662			

	Coefficients	Standard Error	t Stat	P-value	Lower 95%	Upper 95%	Lower 95.0%	Upper 95.0%
Intercept	38.53806795	24.63564601	1.564321388	0.258198909	-67.46056158	144.5366975	-67.46056158	144.5366975
X Variable 1	0.800605544	0.063141553	12.67953526	0.006162604	0.52892937	1.072281719	0.52892937	1.072281719

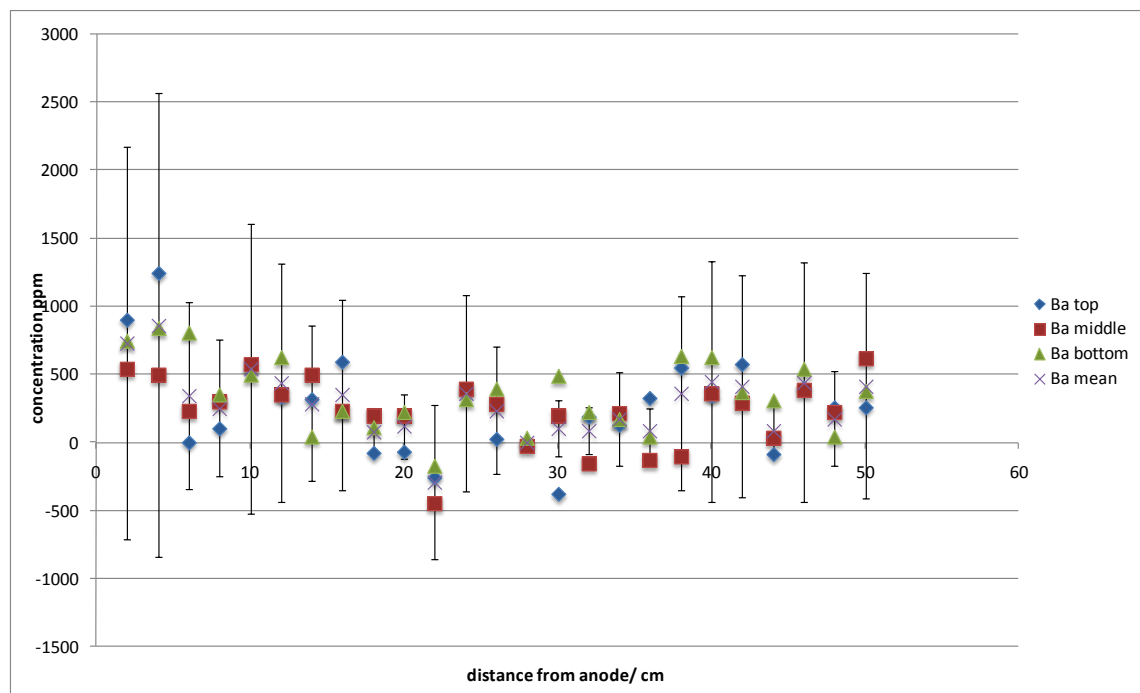
RESIDUAL OUTPUT

Observation	Predicted Y	Residuals
1	235.4870319	17.67963477
2	214.6712877	-16.0379544
3	438.8408402	-0.820840186
4	438.8408402	-0.820840186

$C_{\text{meas}} = 0.800C_{\text{cert}} + 38.538$
 $(1 - 0.800) \times 100$
 gives -20% Bias

Barium, Uranium, Niobium, Lanthanum and Cerium acetic

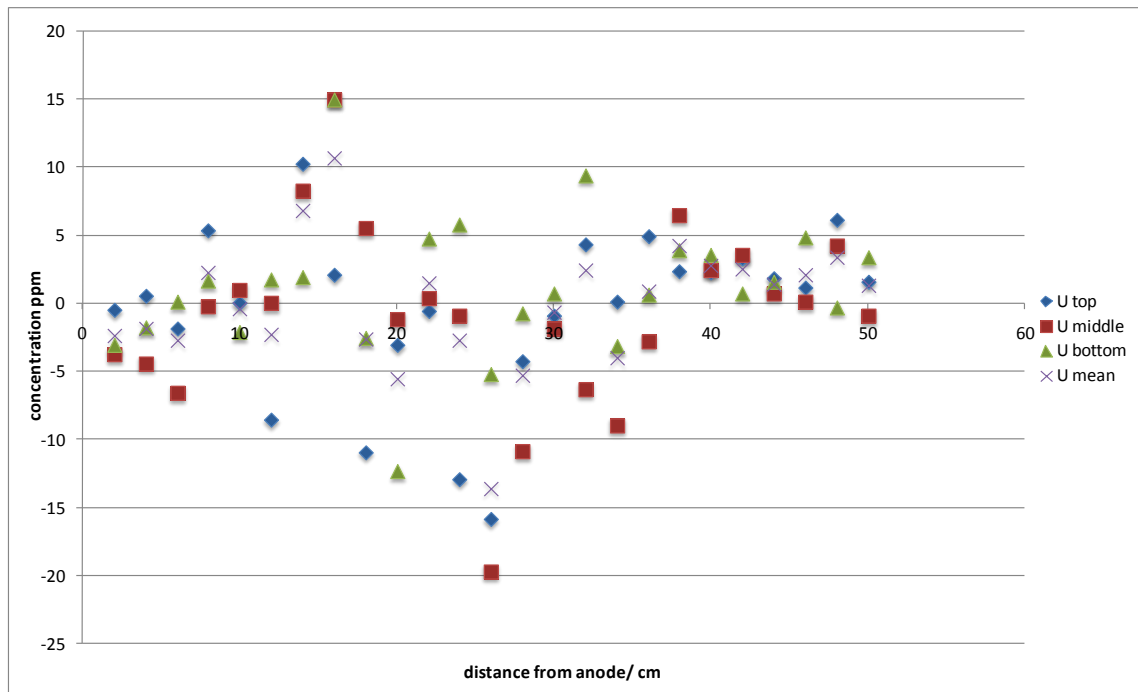
The analysis for barium, uranium, niobium, lanthanum and cerium gave results which were either too low to be reliably measured or were found to have uncertainties which were so large as to make useful interpretation of the data impossible. This may be attributed to the problems associated with finding exact matrix matches for both analyte and the standard reference materials. It might also be due to concentrations being at or below the detection limits of the machine. For completeness these are included in the Appendix.



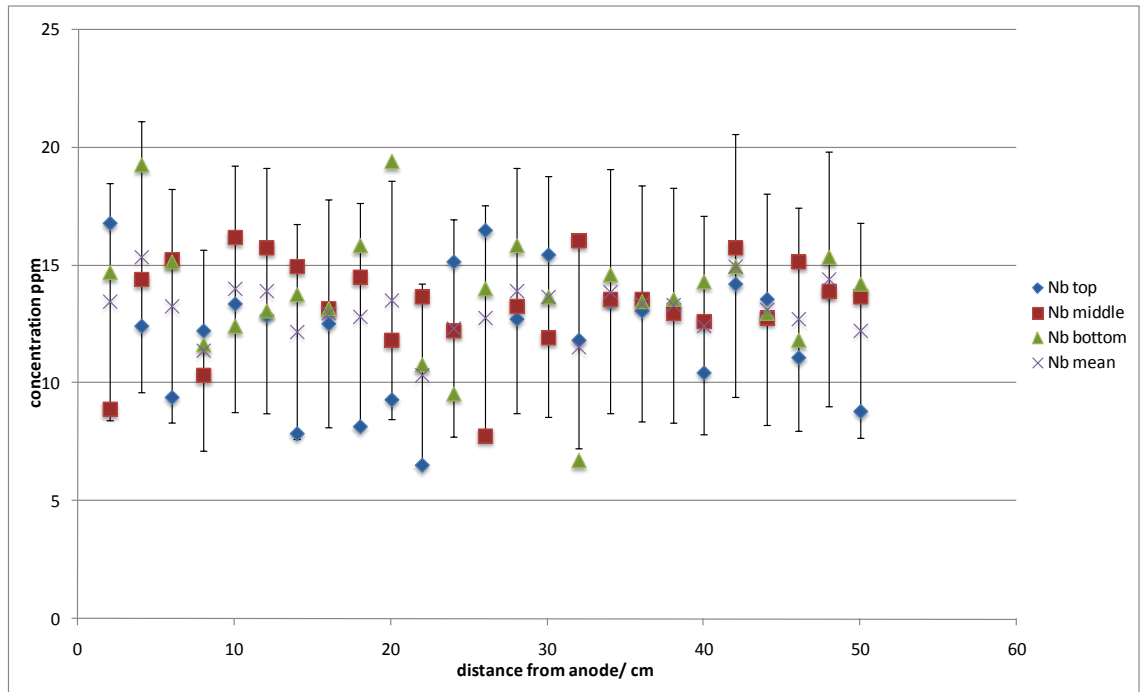
Barium concentration across treated material in the experiment conducted with acetic acid electrolyte.

The bias estimated for the barium measurements was -42.7%. This systematic error was obtained by a good range of certified concentrations and the regression analysis gave an R^2 value of 0.958. So although significantly off the 'true' value the bias adjusted values are reliable. This consistent systematic error might be due to matrix effects, or drift in the detector. The random uncertainty was significantly higher and was estimated at 197.27% which suggests significant introduced errors. However the robust ANOVA analysis gives a sigma value of zero to the sampling but the percentage variance of the analysis is 93%. This might indicate matrix problems with the analysis of the sediment

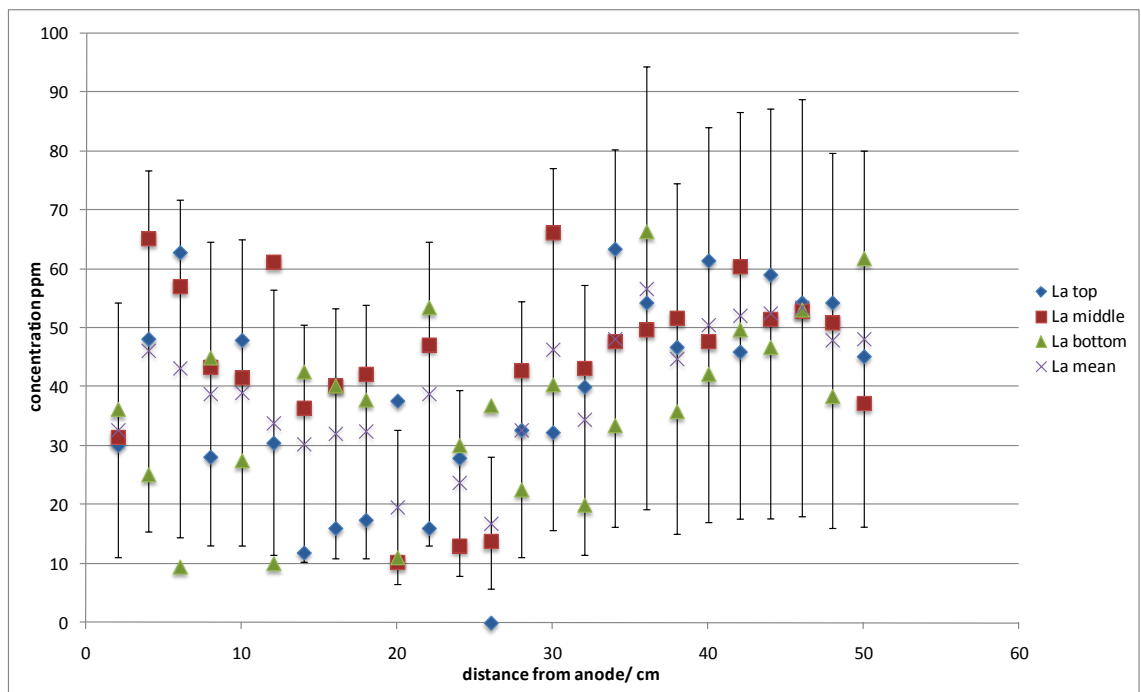
which are less significant in the matrices of the reference materials. Whilst ever effort has been made to use matrix matched reference materials it is not possible to obtain perfect matches. It may be that the discrepancy between the precision of the values for the bias measurements and the variance of the data from the treated material is simply down to matrix interference. With levels of uncertainty of this magnitude useful interpretation of the data is not possible for this element.



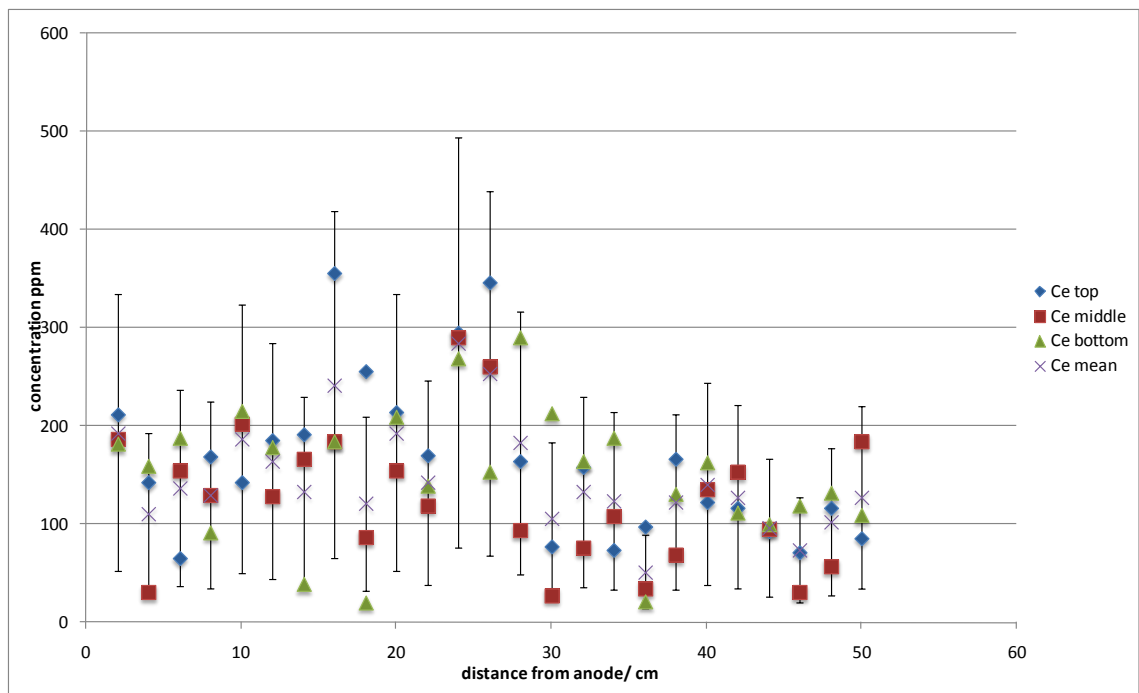
Uranium concentration across treated material in the experiment conducted with acetic acid electrolyte.



Niobium concentration across treated material in the experiment conducted with acetic acid electrolyte.



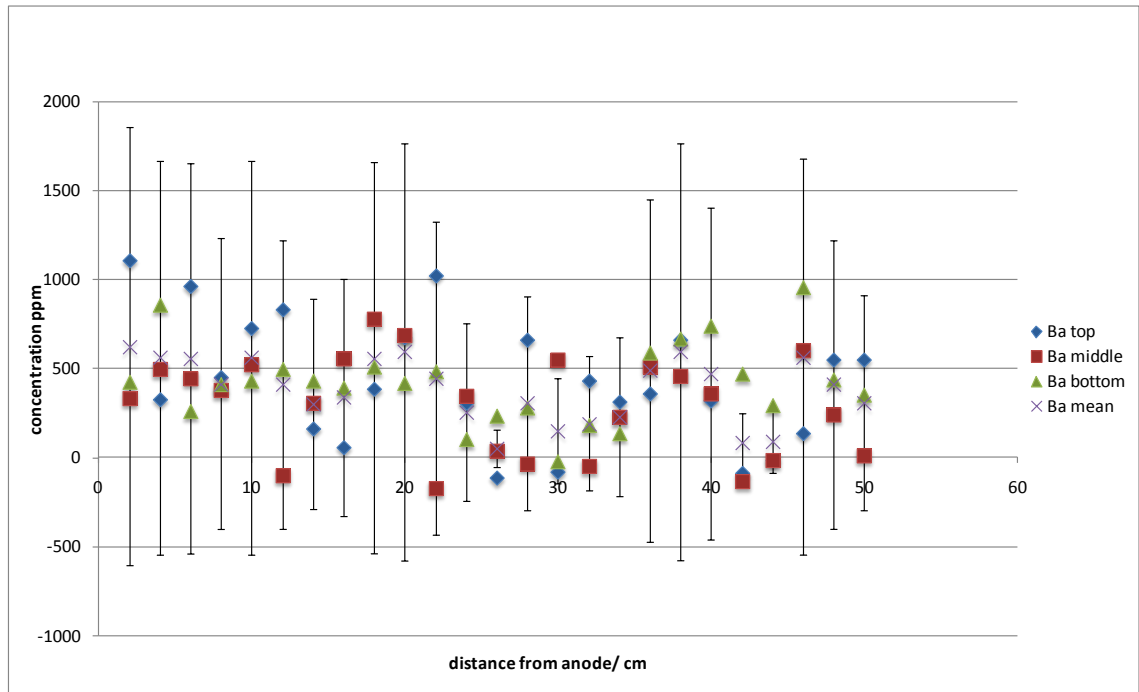
Lanthanum concentration across treated material in the experiment conducted with acetic acid electrolyte.



Cerium concentration across treated material in the experiment conducted with acetic acid electrolyte.

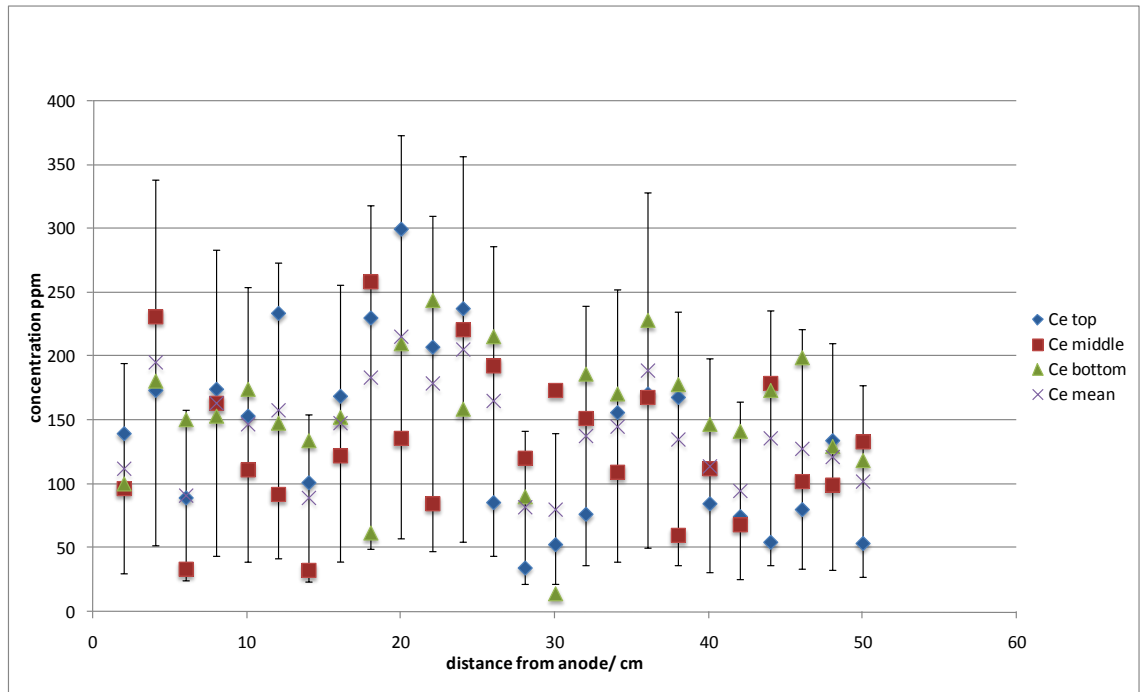
Barium, Uranium, Niobium, Lanthanum, and Cerium tap water.

The relatively high precision observed for the majority of the data obtained is in contrast to that obtained for the elements, barium, uranium, niobium lanthanum and cerium as observed in the acetic acid experiments, where the data shows very poor precision and no clear trends.

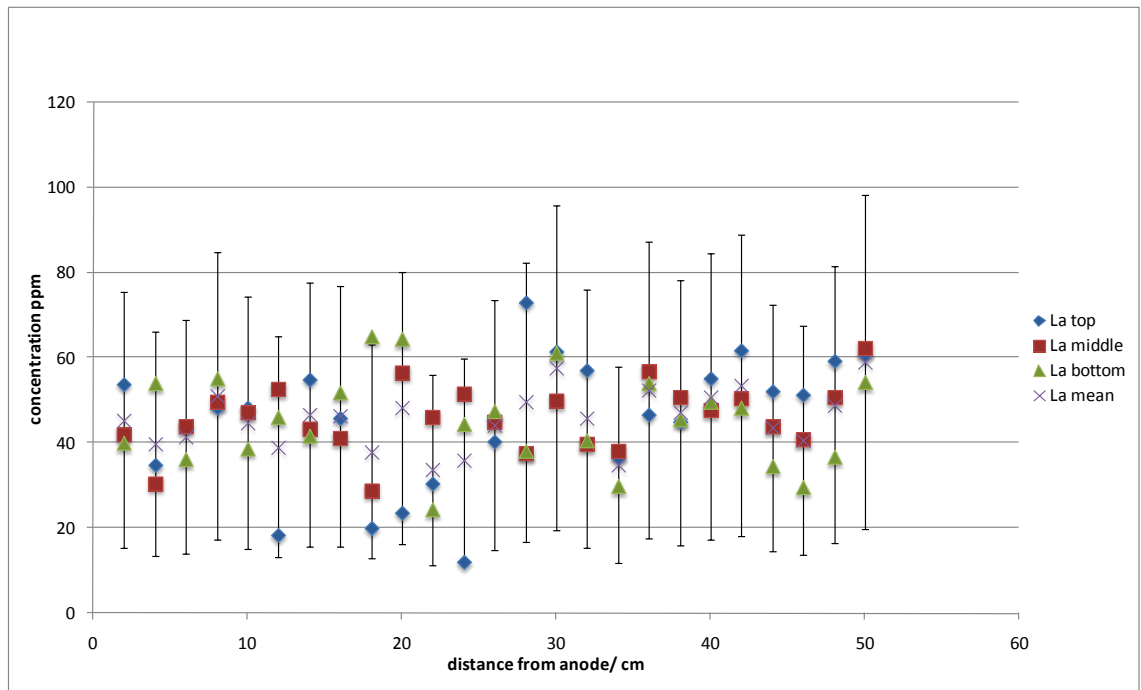


Barium concentration across treated material in the experiment conducted with tap water electrolyte.

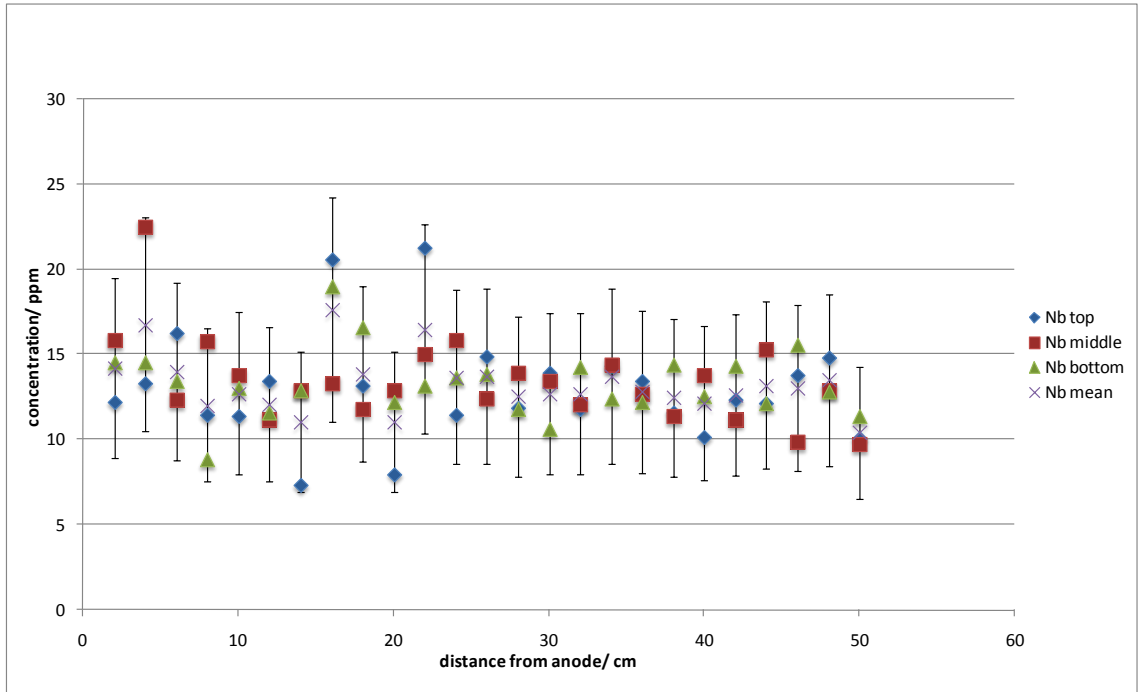
There are values of over 600 ppm and negative values in an apparently random distribution. The reasons for this are likely to be analytical since the other elements analysed for have shown good precision and bias, see section.



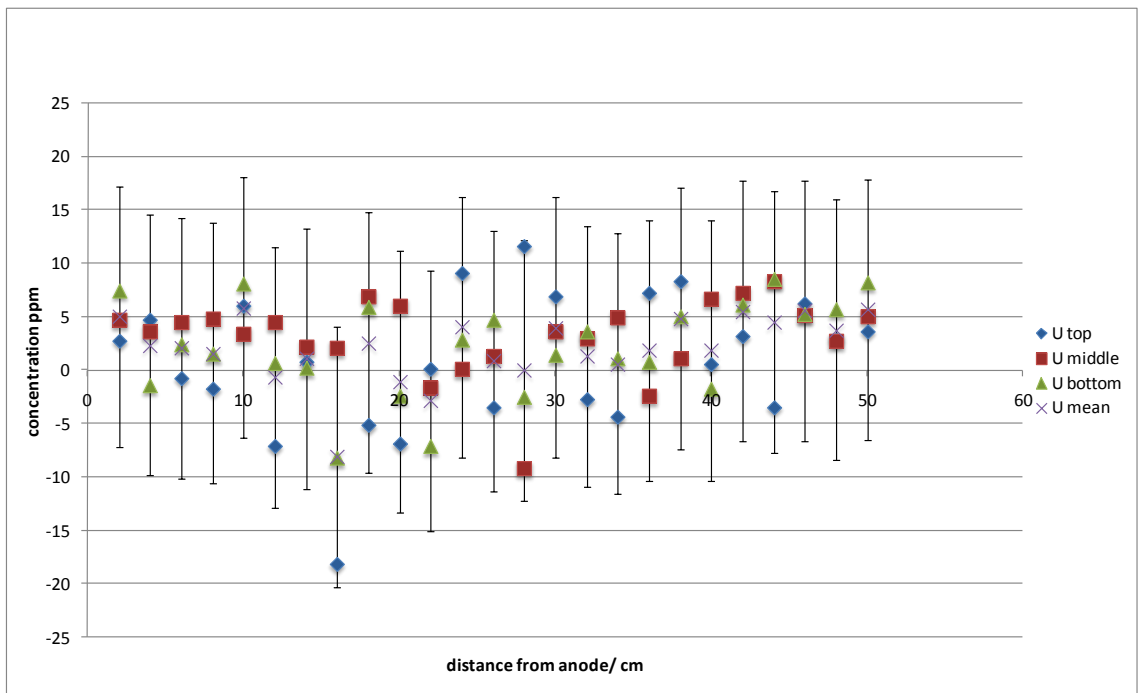
Cerium concentration across treated material in the experiment conducted with tap water electrolyte.



Lanthanum concentration across treated material in the experiment conducted with tap water electrolyte.



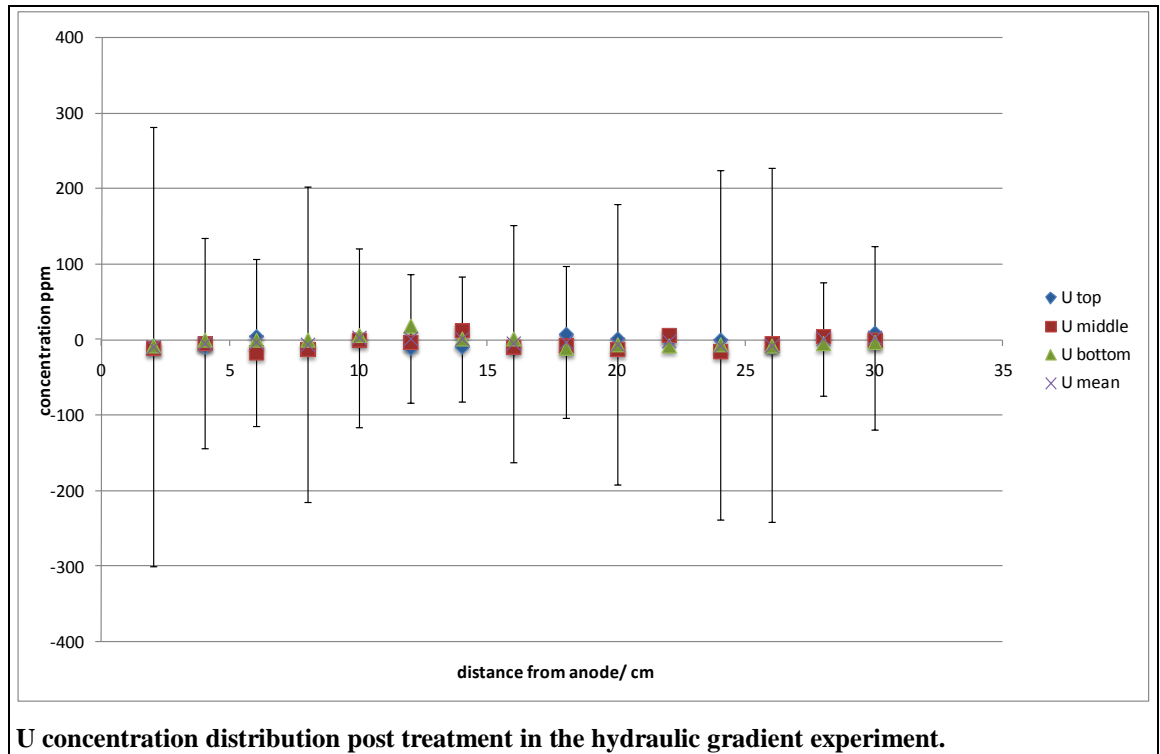
Niobium concentration across treated material in the experiment conducted with tap water electrolyte.



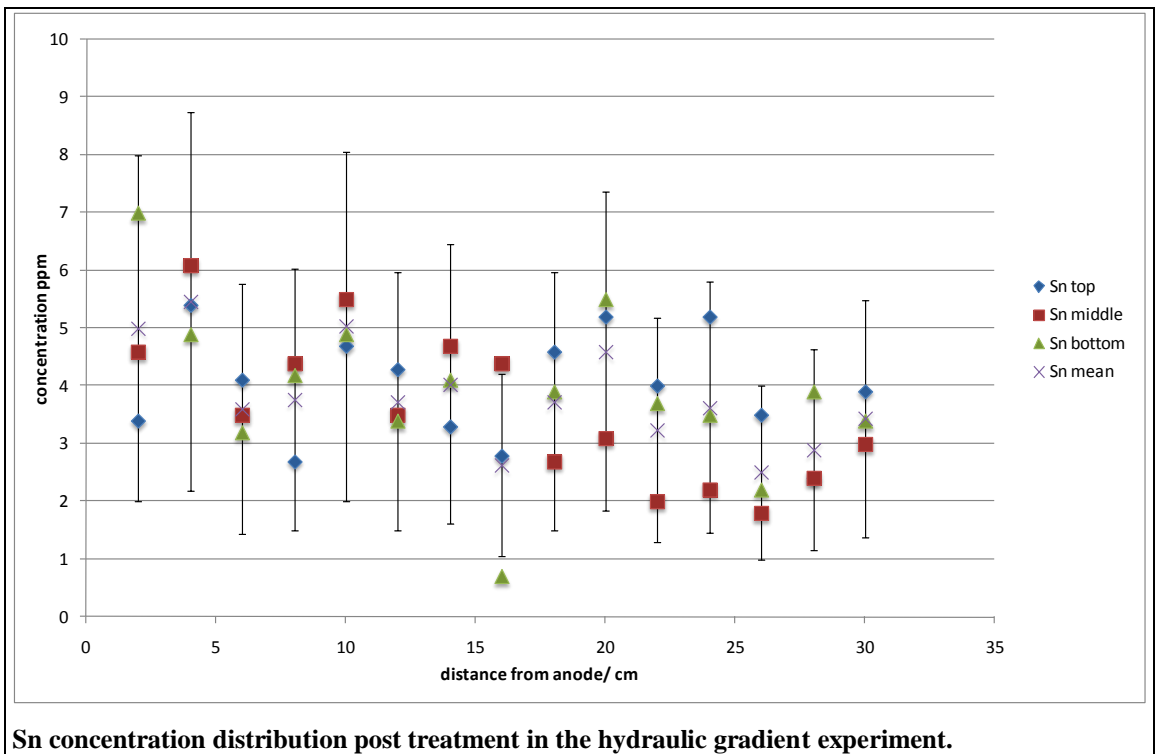
Uranium concentration across treated material in the experiment conducted with tap water electrolyte.

Remediation Under a Hydraulic Head Supplemental Results

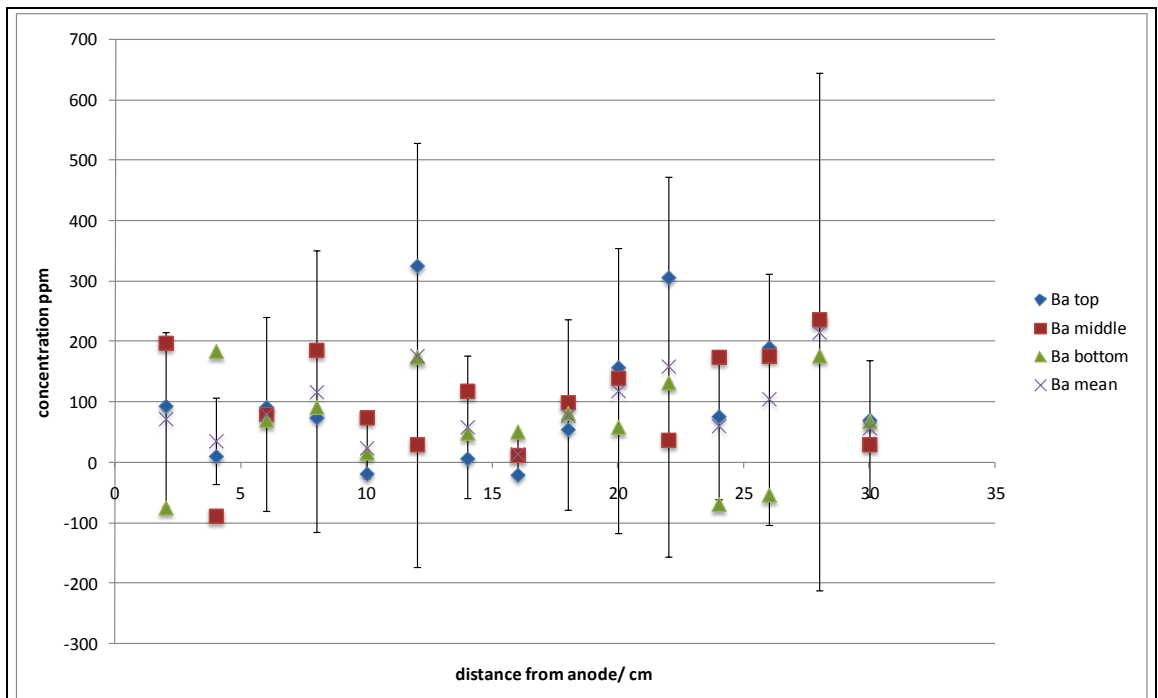
U



Sn

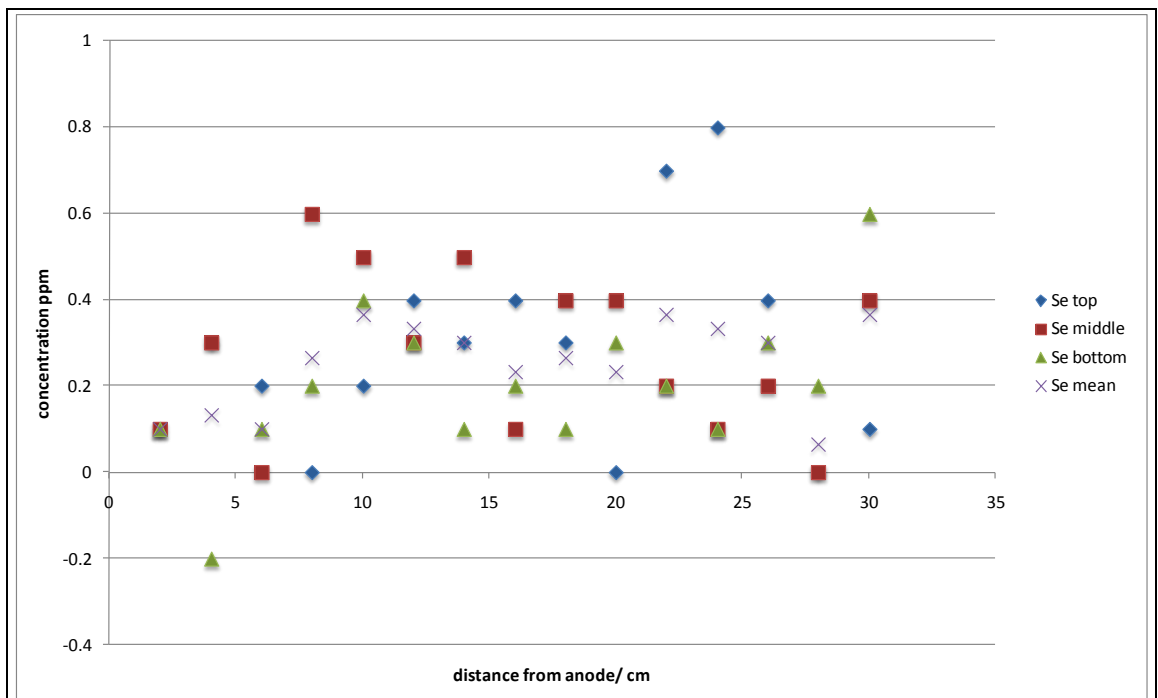


Ba



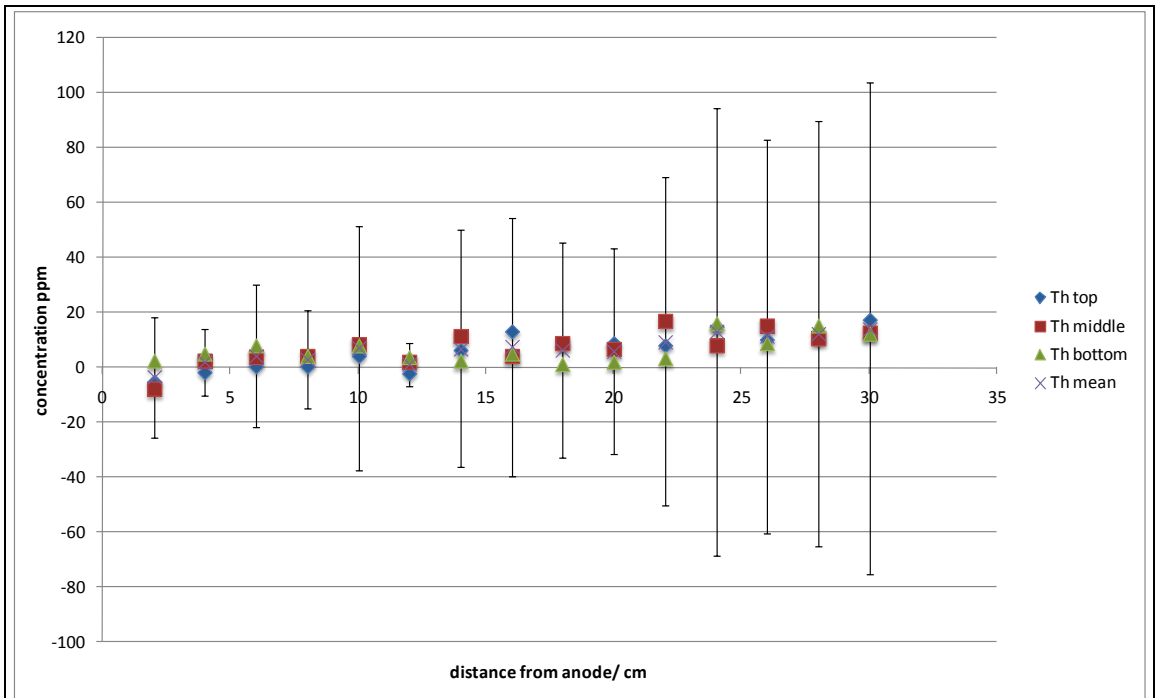
Ba concentration distribution post treatment in the hydraulic gradient experiment.

Se



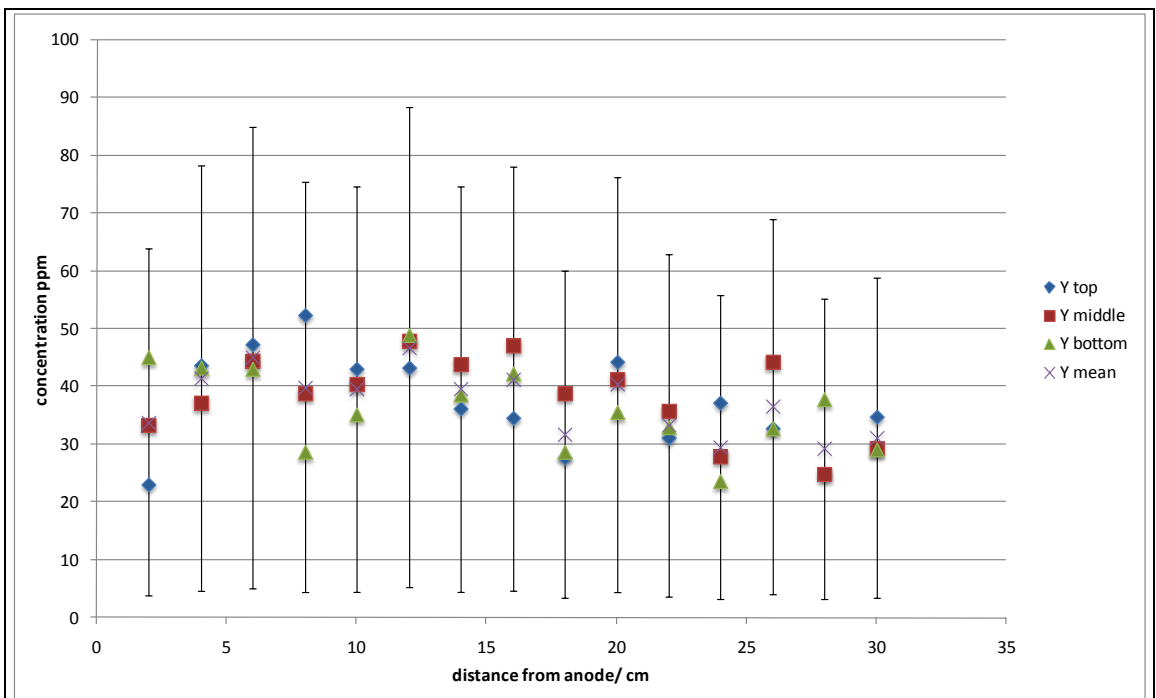
Se concentration distribution post treatment in the hydraulic gradient experiment.

Th



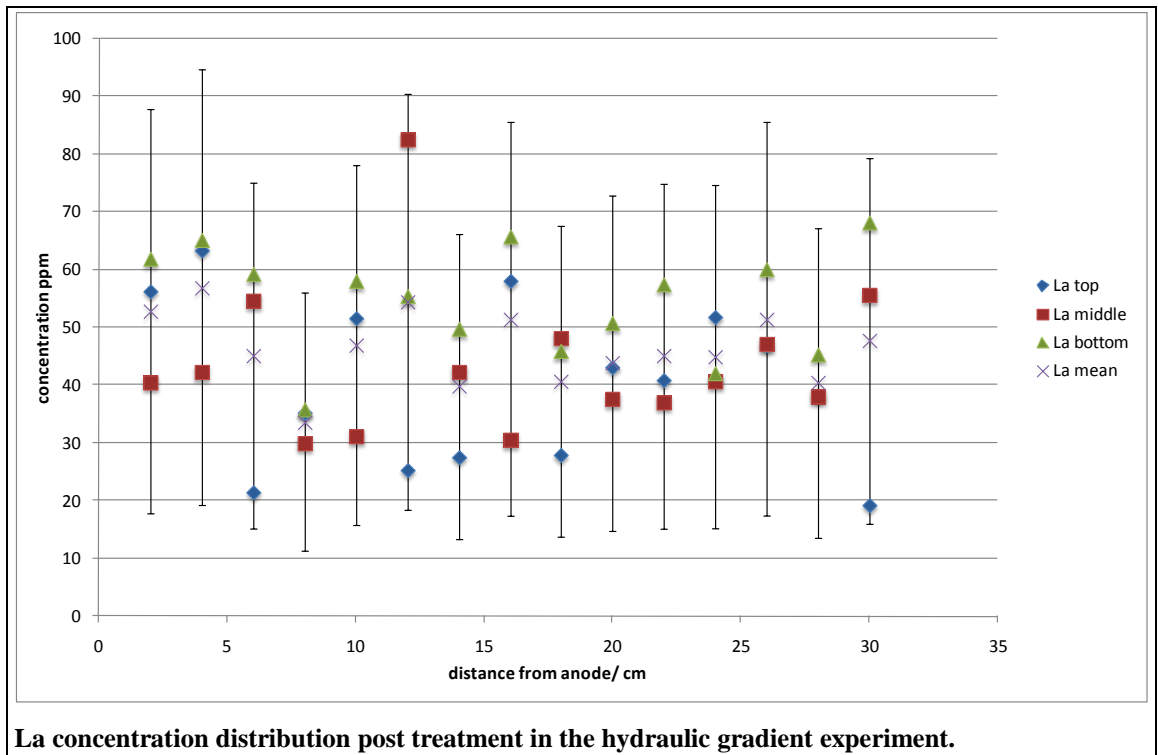
Th concentration distribution post treatment in the hydraulic gradient experiment.

Y



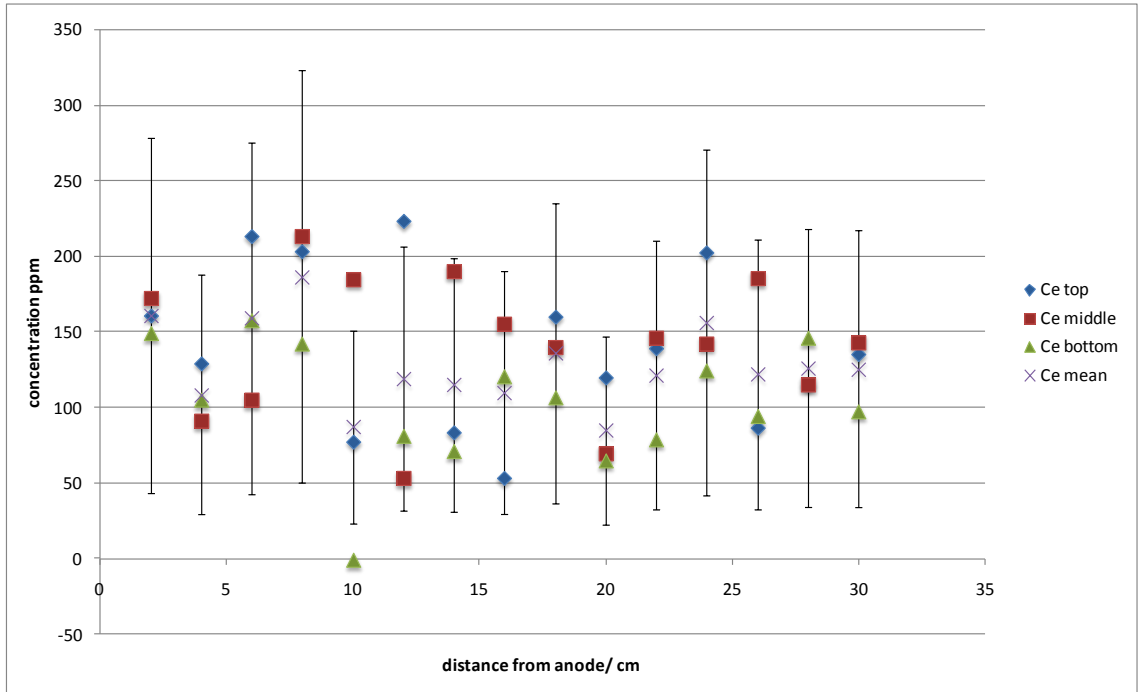
Y concentration distribution post treatment in the hydraulic gradient experiment.

La



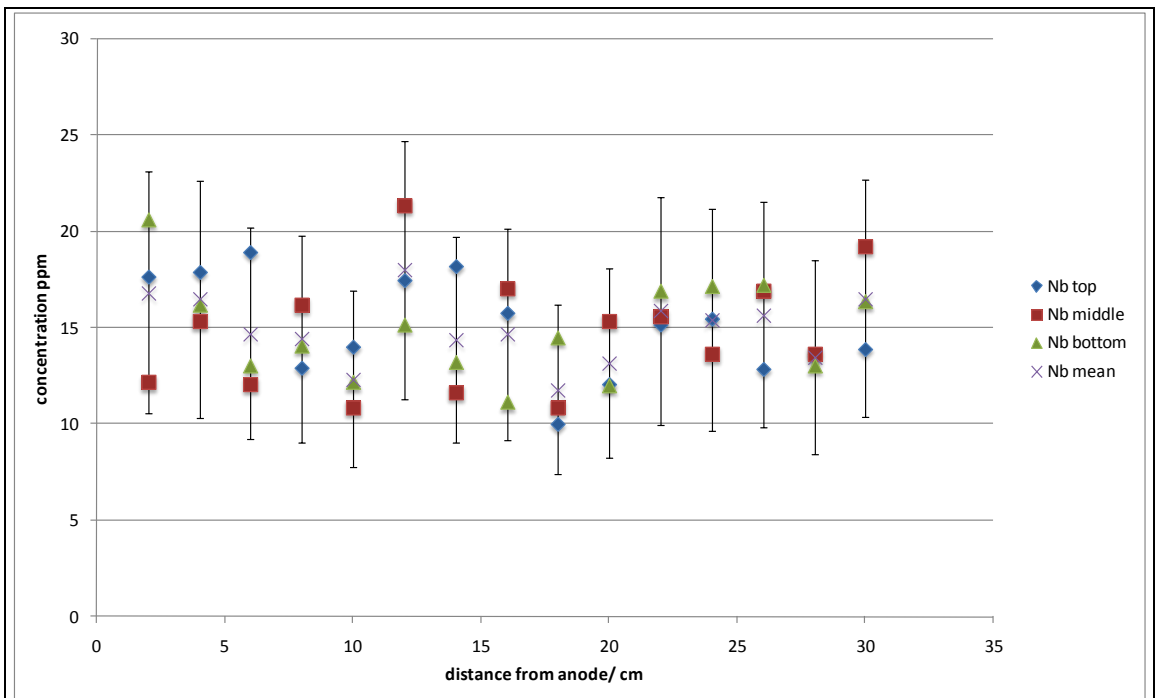
La concentration distribution post treatment in the hydraulic gradient experiment.

Ce



Ce concentration distribution post treatment in the hydraulic gradient experiment.

Nb



Nb concentration distribution post treatment in the hydraulic gradient experiment.

Two-sample T test

Two-Sample T-Test and CI Summarised Data

Sample	N	Mean	StDev	SE Mean
1	5	61.4	11.8	5.3
2	15	41.38	5.69	1.5

Difference = mu (1) - mu (2)

Estimate for difference: 20.06

95% lower bound for difference: 8.40

T-Test of difference = 0 (vs >): T-Value = 3.67 P-Value = 0.011 DF = 4

Pre-treatment Metal Concentrations in Estuarine Sediment

Compound	start ing material A1	starting material A2	hh strating material	Hythe remediation start 1	Hythe remediation start 2		
	Conc	Conc	Conc	Conc	Conc	AVERAGE	st. dev.
Mo	1.3	1.4	1.5	1.6	1.6	1.48	0.130384
Zr	174.3	179.1	207.5	204	190.9	191.16	14.67678
Y	23.2	24.7	21	27.9	23.8	24.12	2.515353
Sr	105.6	104.1	103.6	97	99.5	101.96	3.57673
Rb	122	122	108.4	114.2	118.1	116.94	5.766108
Ga	16.2	18.8	15.4	15.7	16.6	16.54	1.344619
Br	158.8	158.5	147.2	165	167.6	159.42	7.883654
Se	0.2	0.2	0.5	0	0.6	0.3	0.244949
Zn	129.4	138.6	129.8	138.8	149.1	137.14	8.088758
Cu	47.7	50.4	66.5	67.8	74.8	61.44	11.78147
Ni	22.8	31.8	24.7	29.7	33	28.4	4.457017
Co	24.8	24.4	18.1	17.7	17	20.4	3.856812
Fe2O3	4.72	4.88	5.61	5.6	5.72	5.306	0.467739
MnO	0.02	0.02	0.02	0.02	0.02	0.02	0
Cr	148.8	169.6	318.2	233.8	242.8	222.64	66.94825
V	14.8	9	104.7	115.9	132.2	75.32	58.75004
TiO2	0.39	0.42	0.76	0.78	0.79	0.628	0.204132
CaO	0.92	0.97	2.49	1.86	1.85	1.618	0.667061
K2O	0.74	0.86	2.27	2.33	2.43	1.726	0.84831
U	6.8	-5.1	5.1	-0.9	3	1.78	4.801771

Th	13.9	14.5	12.3	12	9.2	12.38	2.065672
Bi	0.8	0.6	0.8	0.8	0.4	0.68	0.178885
Pb	81.6	78.2	53.7	66.6	65.8	69.18	11.10549
Ba	272.1	317.4	303.1	263.7	310.4	293.34	23.95231
W	44.9	32.9	69.3	101.6	102.9	70.32	31.96626
Nb	13.7	14.4	13.6	11.8	13.2	13.34	0.963328
As1	24	27	24.5	24.4	26.8	25.34	1.438054
Ce	148.8	140.9	147.9	139.7	138.5	143.16	4.823692
La	31.3	22.8	30.8	34.9	34.9	30.94	4.943986
Sn	5	5	4.3	4.2	5.6	4.82	0.576194

Pre-treatment mean concentrations	
Mo	1.48
Zr	191.16
Y	24.12
Sr	101.96
Rb	116.94
Ga	16.54
Br	159.42
Se	0.3
Zn	137.14
Cu	61.44
Ni	28.4
Co	20.4
Fe2O3	5.306
MnO	0.02
Cr	222.64
V	75.32
TiO2	0.628
CaO	1.618
K2O	1.726
U	1.78
Th	12.38
Bi	0.68
Pb	69.18
Ba	293.34
W	70.32
Nb	13.34
As1	25.34
Ce	143.16
La	30.94
Sn	4.82

Iron-rich Precipitate Barriers

The creation of a continuous iron-rich precipitate in a soil or sediment mass acts in a number of ways; as an obstruction to ion, and therefore current flow; it is impermeable to groundwater and dissolved species. The straightforward parallel linear electrode arrangement of oppositely charged electrodes on either side of the sediment results in the generation of a continuous circum vertical iron-rich barrier approximately half way between the two sets of electrodes of opposite polarity. However, by insulating the upper section of the anode electrodes and incorporating a shallow surface cathode electrode, a continuous horizontal iron-rich barrier of approximately 5 mm was generated in the sub-surface over a \approx 400 hour period, without any excavation required. The current shows an initial increase from 0.48 Amps to 0.74 Amps within the first \sim 20 hours, since the water is unevenly distributed throughout the sand profile at the beginning of the experiment (it is gravitationally influenced to give a saturated water table at depth, with a drier upper region). When the current was applied the water became more evenly distributed as it was electroosmotically mobilised towards the surface cathode, allowing for more efficient ion movement and thus increased current flow. The current shows a progressive drop from a maximum of 0.74 Amps down to 0.14 Amps as the iron-rich barrier forms, due to ion-flow being impeded by the precipitated iron phases.

X-Ray Fluorescence Spectroscopy

As has been stated earlier, the effectiveness of the treatment is dependent on the specific speciation of the contaminant as a control for the level of mobility. The XRF analysis provides a robust and cost-effective method for the analysis of large numbers of samples with a high level of reliability, but comes with the limitation of no differentiation between elemental distribution associated with different compounds, instead giving overall elemental concentrations. This is useful for the technique being

investigated because the experiments are conducted in order to ascertain the overall elemental distribution of the metals of interest pre and post-treatment. Future studies should include a distinct and thorough assessment of the speciation and implied mobilities of the species of interest.

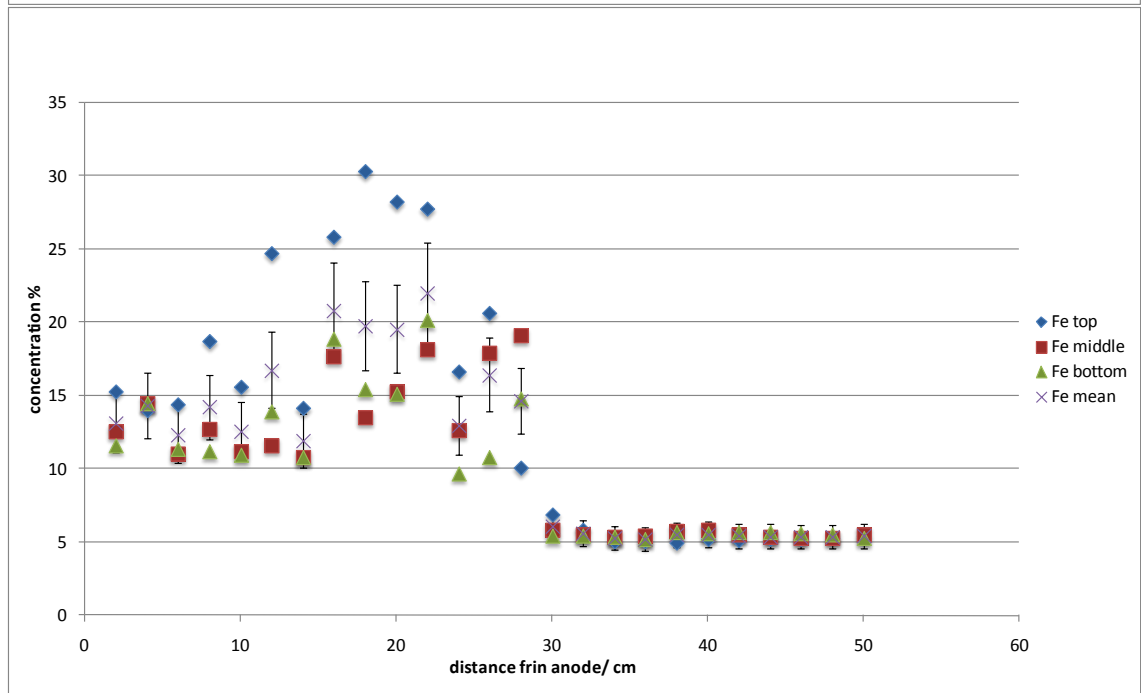
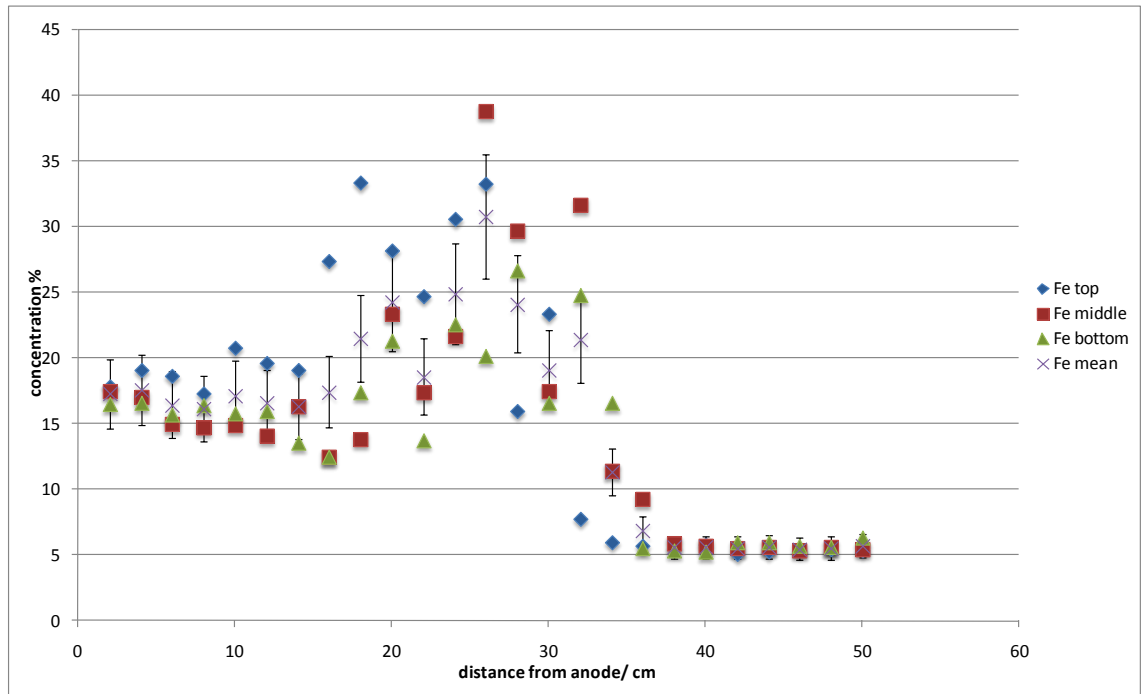
Characterisation and Composition of the Iron-Rich Precipitates

XRD analyses of the iron-rich bands revealed the presence of goethite, lepidocrocite, maghemite/magnetite and native iron. Quantitative analyses of iron mineralogy were not possible. However, based on the sizes of peaks it is likely that the iron-rich barriers have an approximate composition of ~65% cemented quartz (and feldspar), with ~4% goethite, ~5% native iron, 5% maghemite/magnetite, 5% lepidocrocite, and possibly as much as 20% x-ray amorphous ferric iron oxyhydroxides

Pre-treatment siliciclastic sand mineralogy	Modal abundance	Post-treatment iron-rich barrier mineralogy	Modal abundance
Quartz	90%	Quartz & Feldspar	65%
Clay(mica)	3.5%	Goethite	4%
K-Feldspar	3.5%	Native Iron	5%
Plagioclase	1.5%	Maghemite/magnetite	5%
Calcite	1%	Lepidocrocite	5%
Dolomite	0.5%	Amorphous ferric iron oxyhydroxides	As much as 20%

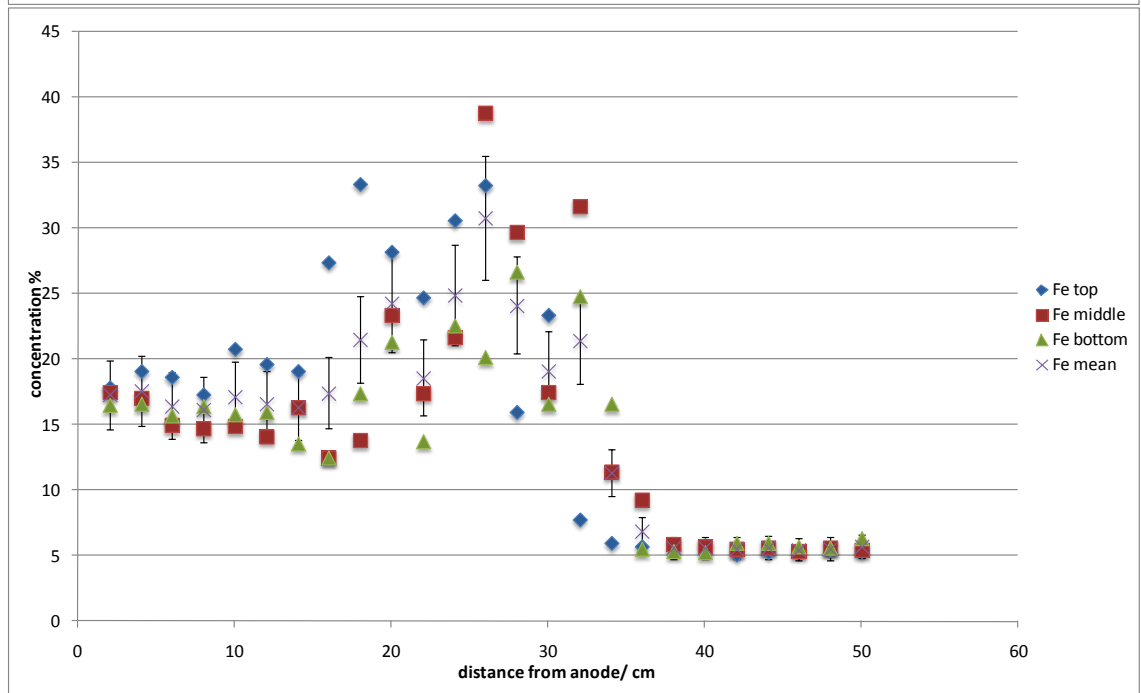
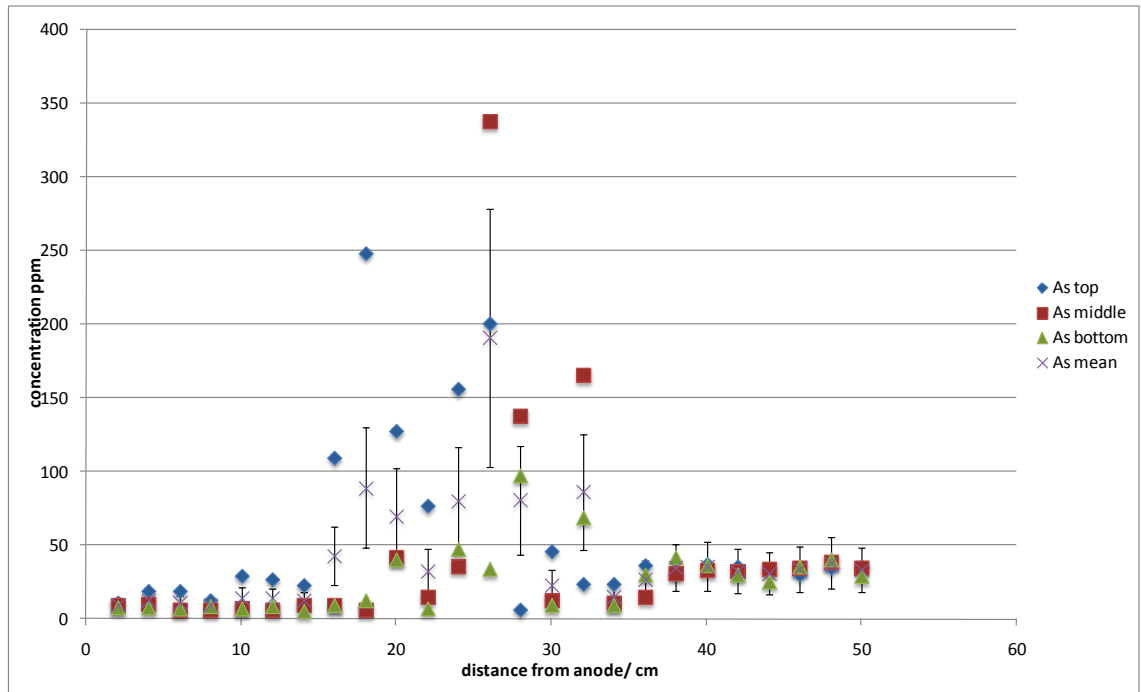
Comparison Between Tap Water and Acetic Acid Treatment

The experiments were set-up for the comparison of the results from the experiment run with tap-water influent and the experiment conducted with acetic acid influent.

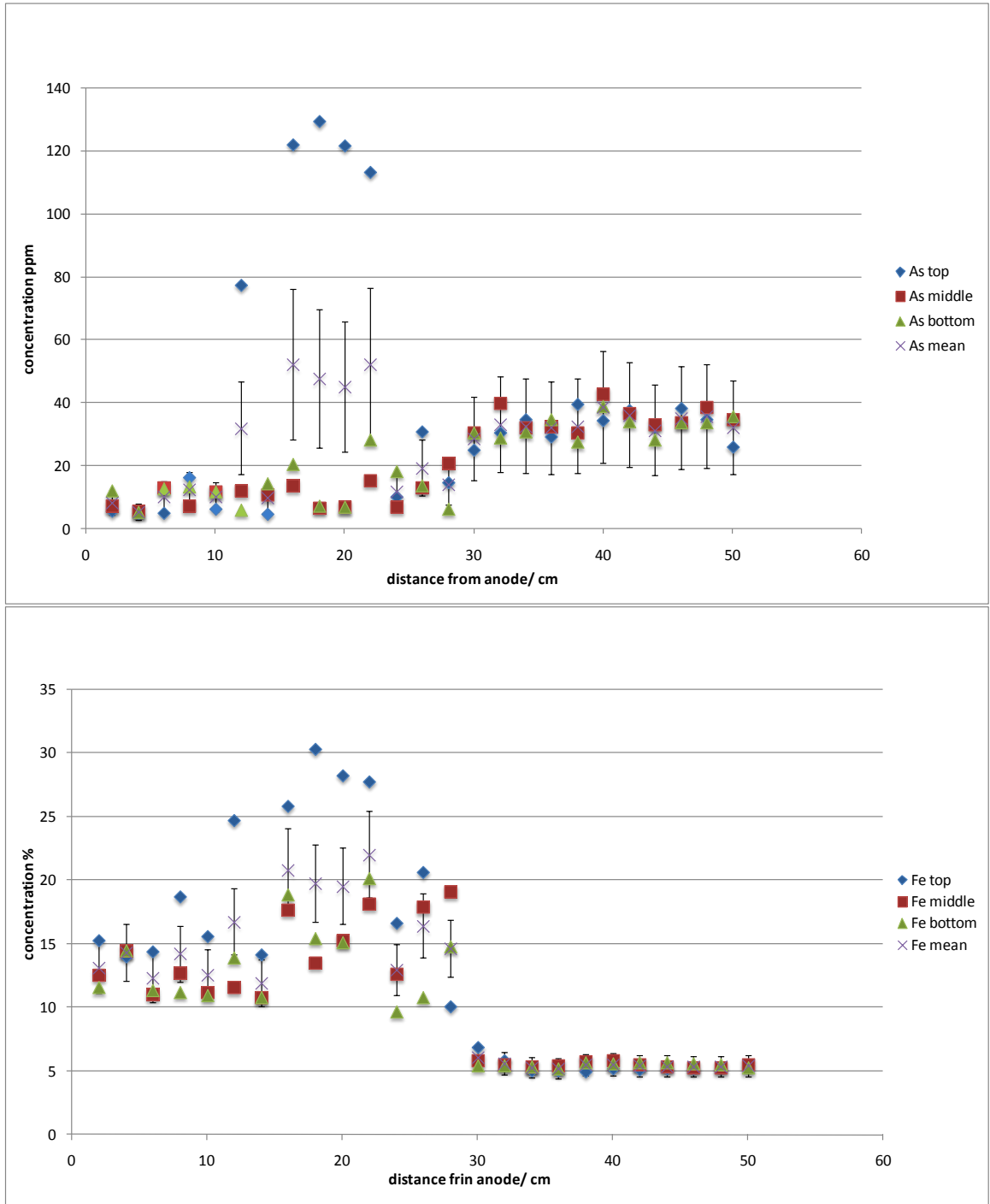


Iron concentrations in the acetic acid (top) experiments and the tap-water (bottom).

The data indicate that the iron introduced to the acetic acid experiment has progressed slightly further across the material to be treated. Other than this the distributions are markedly similar particularly in terms of the iron concentration on the cathode side of treatment cell, where all the measurements are consistently at around the 5% concentration level.

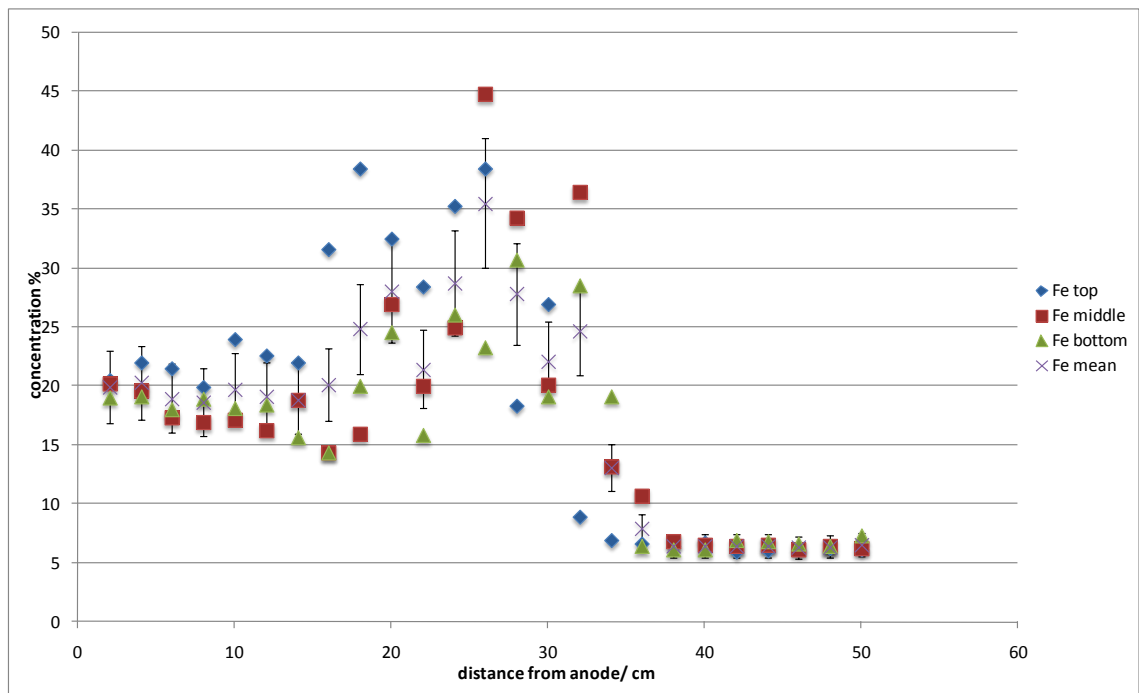


Arsenic (top) and iron (bottom) in the tap-water experiment showing the correlation between the concentration of iron and that of arsenic.



Arsenic (top) and iron (bottom) in the acetic acid experiment showing the correlation between the distributions of both.

Iron Acetic

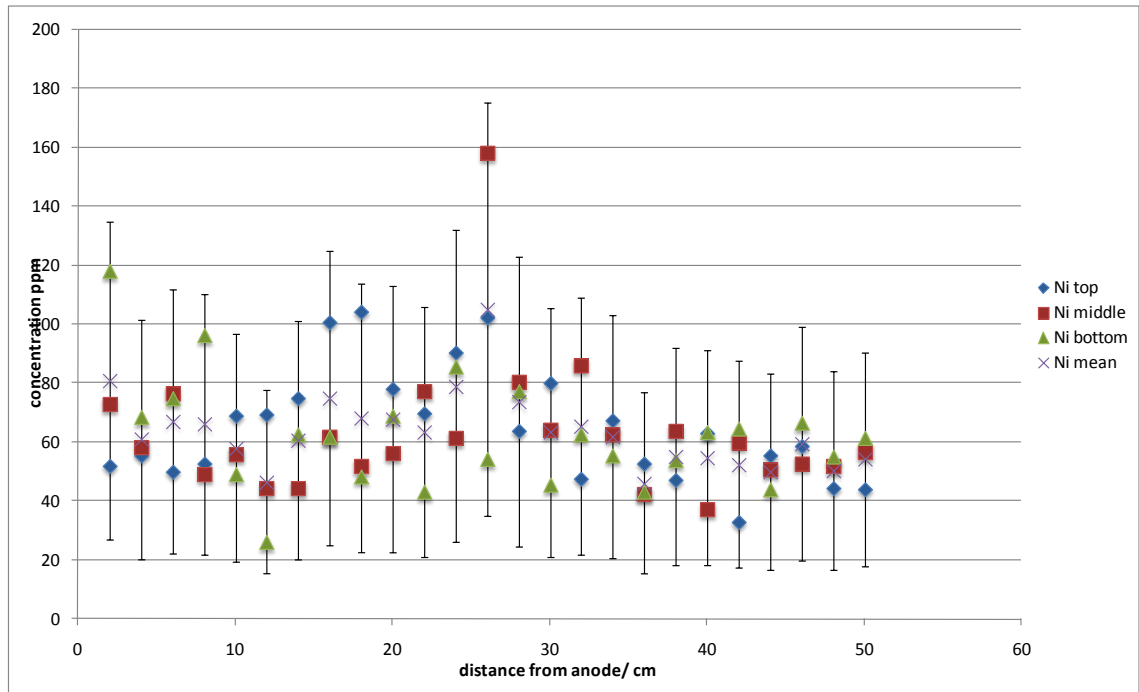


Iron concentration across treated material in the experiment conducted with acetic acid electrolyte.

The bias for the iron measurements was estimated at -6.9% with a measurement uncertainty of 15.4% demonstrating the analysis and protocol suitable for obtaining reliable data.

Nickel Acetic

The large uncertainty and the seemingly stochastic distribution of the measured values for nickel do not allow for any meaningful interpretation of the results for this element.



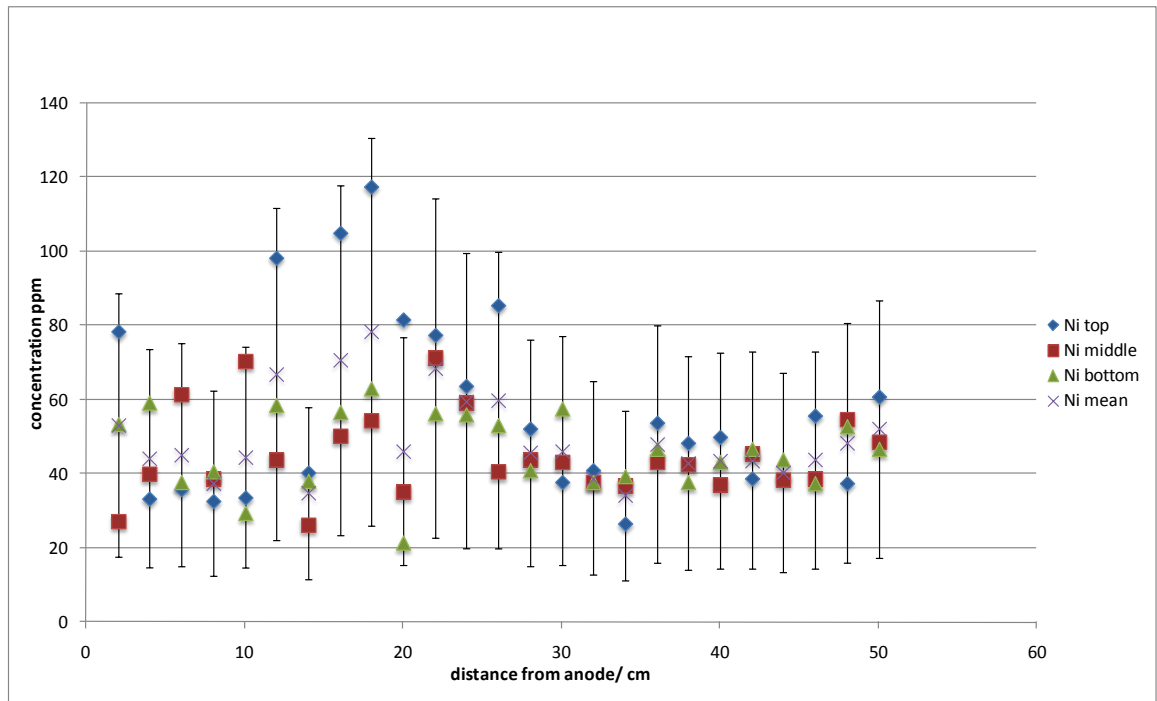
Nickel concentration across treated material in the experiment conducted with tap water electrolyte.

The bias estimate of the nickel analysis was found to have a rotational component of -36.52 mg/kg and a translational component of +10.44 mg/kg. The measurement uncertainty was estimated as 66.07%. These values are well above the normally accepted values of fitness for purpose and there is no clear concentration distribution comparable with those observed for other elements. This is somewhat unexpected since nickel is one of the elements expected to readily co-precipitate with the iron (e.g. Alloway and Ayres, 1997) and is often observed in the environment associate with iron oxides and oxyhydroxides.

Nickel Tap Water

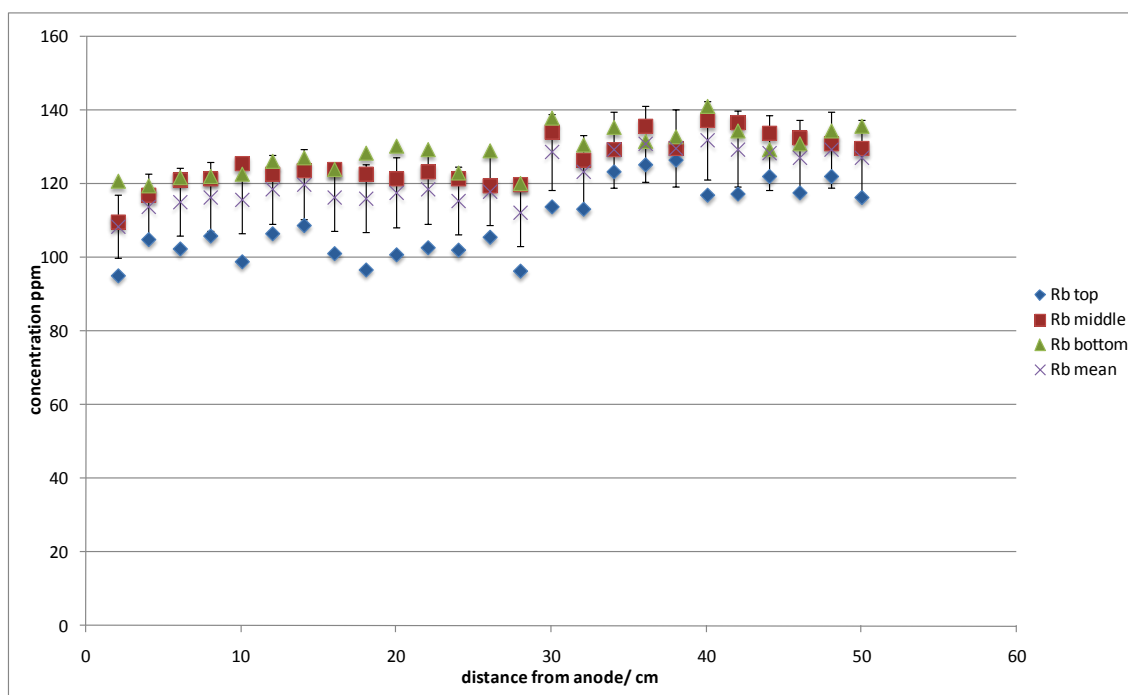
The concentration of nickel across the treated material is a less straightforward picture but it does seem clear that the area of interest once more is in the iron enriched area but the relationship is a less clear cut example than those observed for the elements dealt with so far. There appears to be significant enrichment in the iron rich precipitated region for the samples taken from the top section of the experiment. However it appears that almost the opposite is true for the middle and bottom sections since they appear to

show a decrease in concentration relative to the trend in this region. What is more apparent for this element is that the concentrations in the sections sampled on the anode half of the experiment are more widely distributed between depths and between longitudinal sections, but on the cathode side of the treated material the concentrations are much more uniform in their values. However the uncertainty is too great to reliably assert these interpretations.



Nickel concentration across treated material in the experiment conducted with tap water electrolyte.

Rubidium Acetic

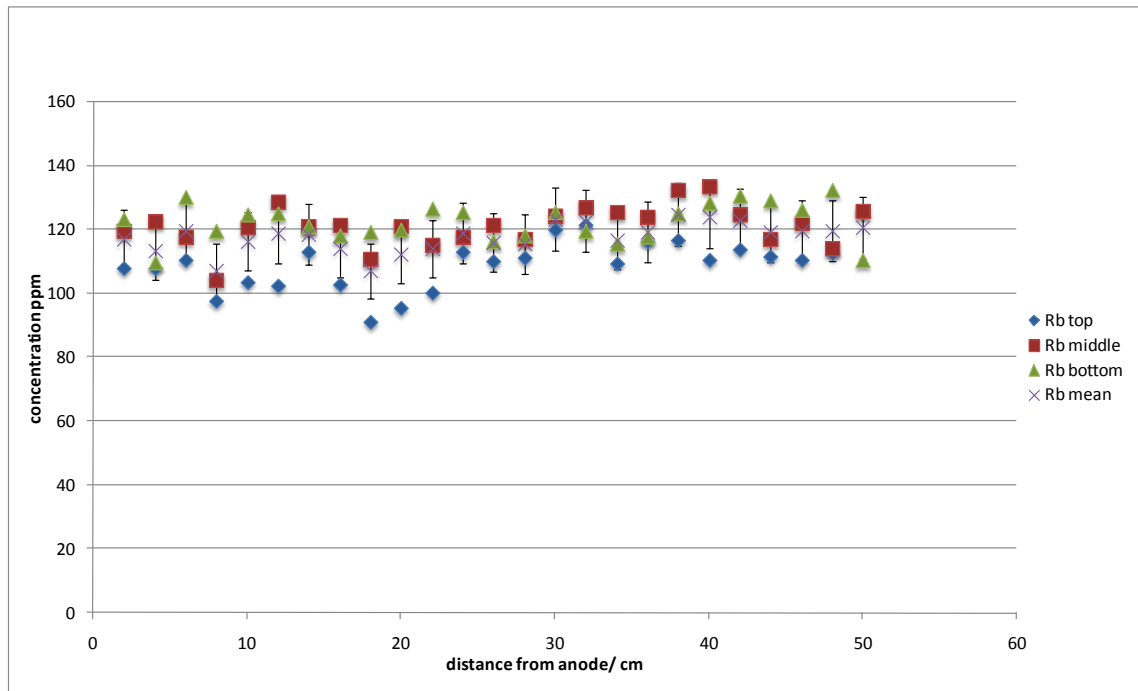


Rubidium concentration across treated material in the experiment conducted with acetic acid electrolyte.

The rubidium distribution across the cell shows a possible jump in concentration around the 30cm from the anode distance. On the anode side of this point the mean concentration measurements are generally below 120 ppm whereas the data points on the cathode side are all greater than 120 ppm. This narrow range of concentrations may indicate that the majority of the rubidium present is in an immobile form with a smaller fraction which is in a mobile form. This would explain the distribution above where the difference between the anode side and the cathode side is due to the migration of a comparatively small mobile fraction from the anode side.

The bias for this element was found to be +2.2 % and the measurement uncertainty was only 7.97 % which indicates high quality data obtained for this element.

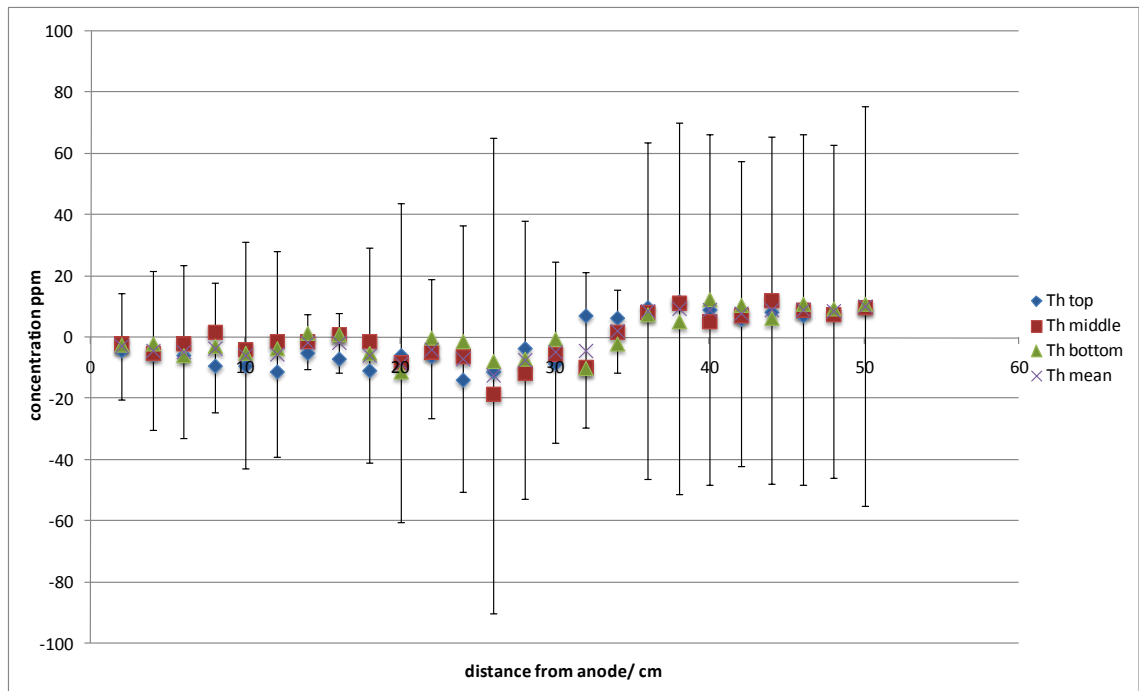
Rubidium Distribution Tap Water



Rubidium concentration across treated material in the experiment conducted with tap water electrolyte.

The distribution of the rubidium across the treated material does not show a discernable response to the treatment process with limited variation in concentration across the treated material and between depths. It appears that the acetic acid treatment enhances an otherwise limited response for this element.

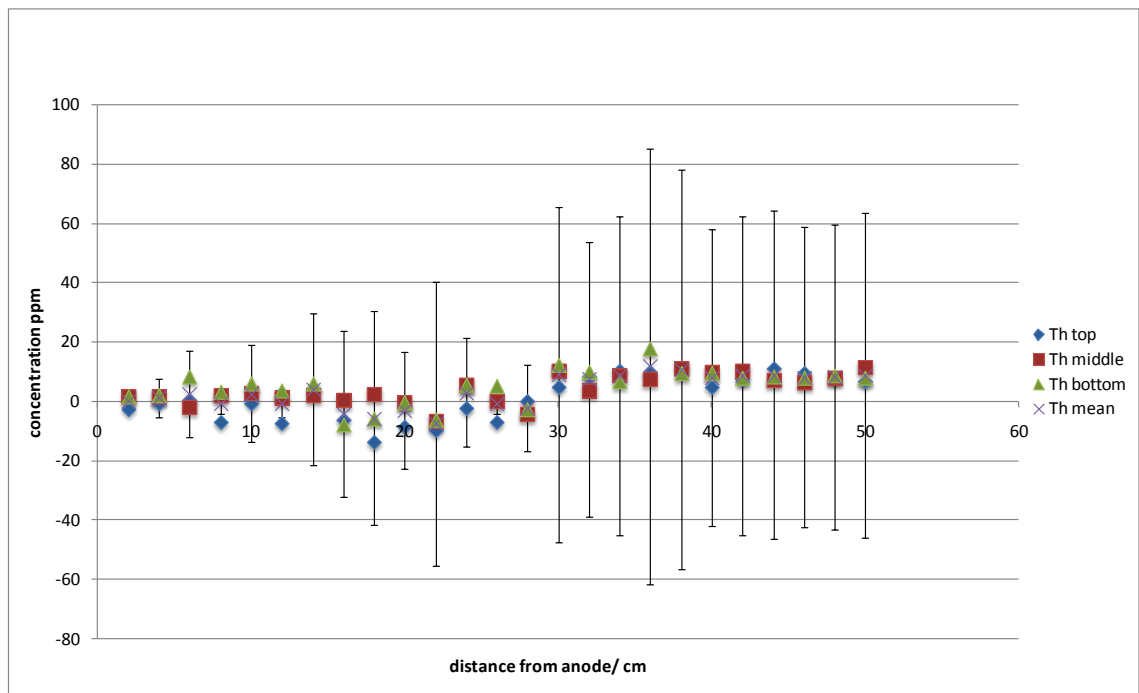
Thorium Acetic



Thorium concentration across treated material in the experiment conducted with acetic acid electrolyte.

The data for the thorium distribution shows no discernable response to the treatment. The concentrations in the test medium are below the detection limit of the equipment and the estimated uncertainty of the data is too large for any meaningful interpretation of the data. There might be some reduction in concentration on the anode side and enrichment on the cathode side but the uncertainty is too great for any meaningful level of confidence.

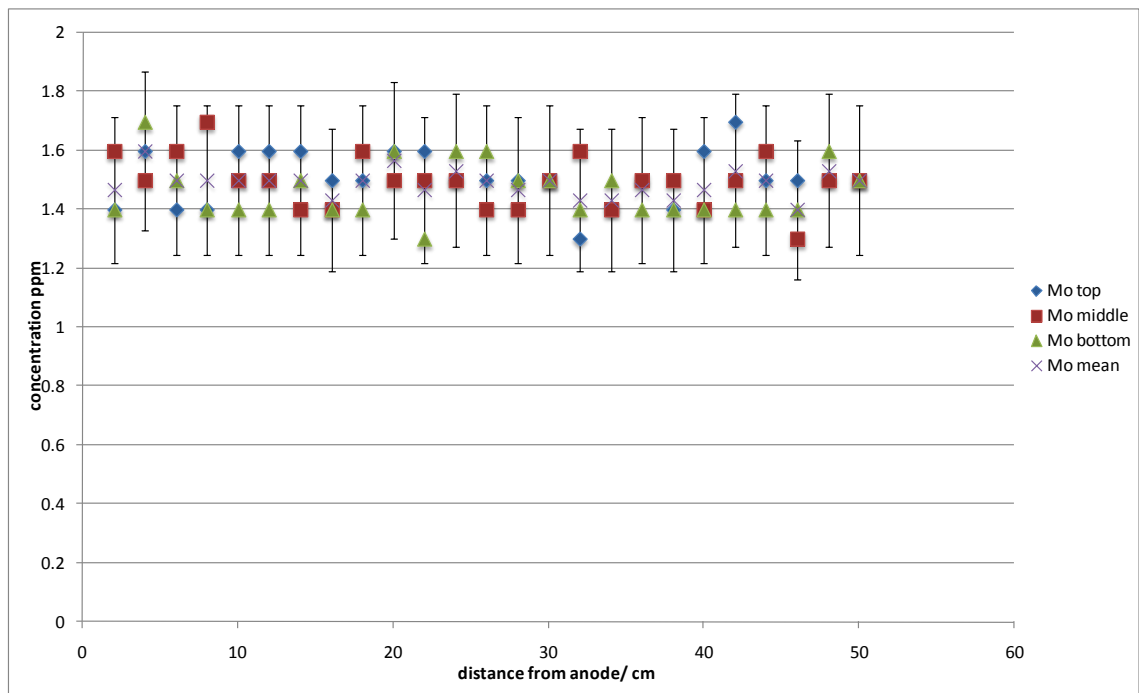
Thorium Tap Water



Thorium tap water

Thorium, is at very low concentrations with significant uncertainty resulting in negligible interpretation of any response to the treatment. This might be improved with a more suitable range of standards but the visual inspection of the data suggests that the thorium present is not in a mobile form.

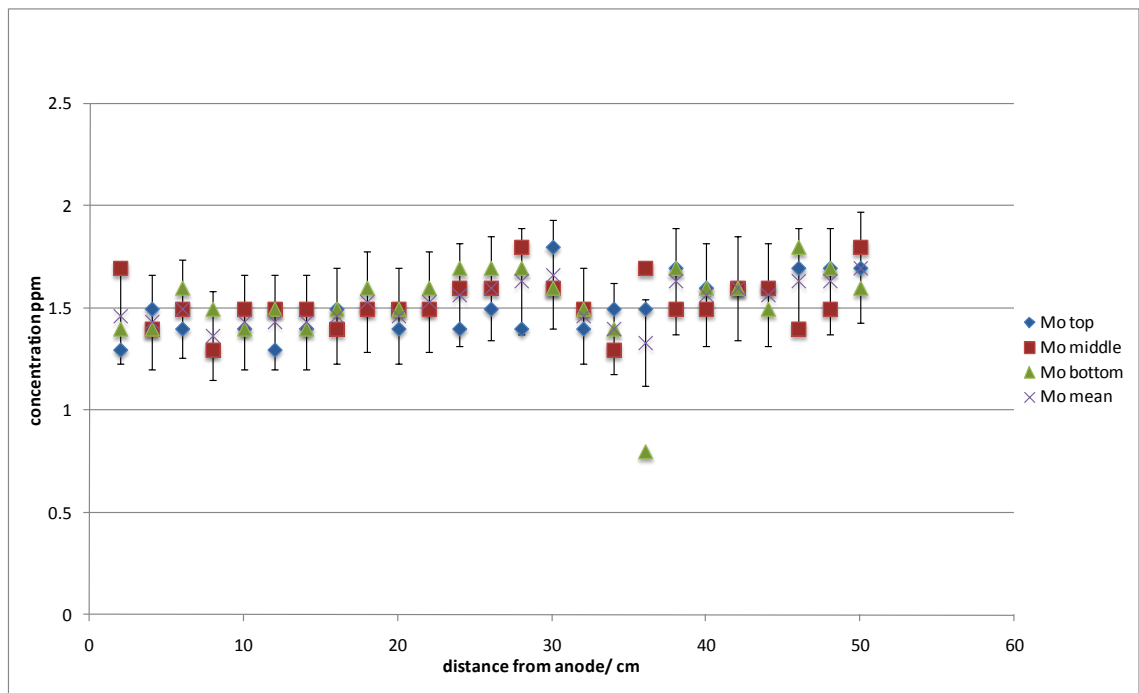
Molybdenum Acetic



Molybdenum concentration across treated material in the experiment conducted with acetic acid electrolyte.

Molybdenum shows no discernable response to the treatment. The calculated mean concentration in the sediment pre-treatment was 1.48 ppm which is the typical mean value obtained for the treated material. The molybdenum content of the standards was unsuitable for useful estimation of the bias associated with this element, but the measurement uncertainty was estimated as 16.88% which is well below the standard 20% considered fit for purpose for most applications.

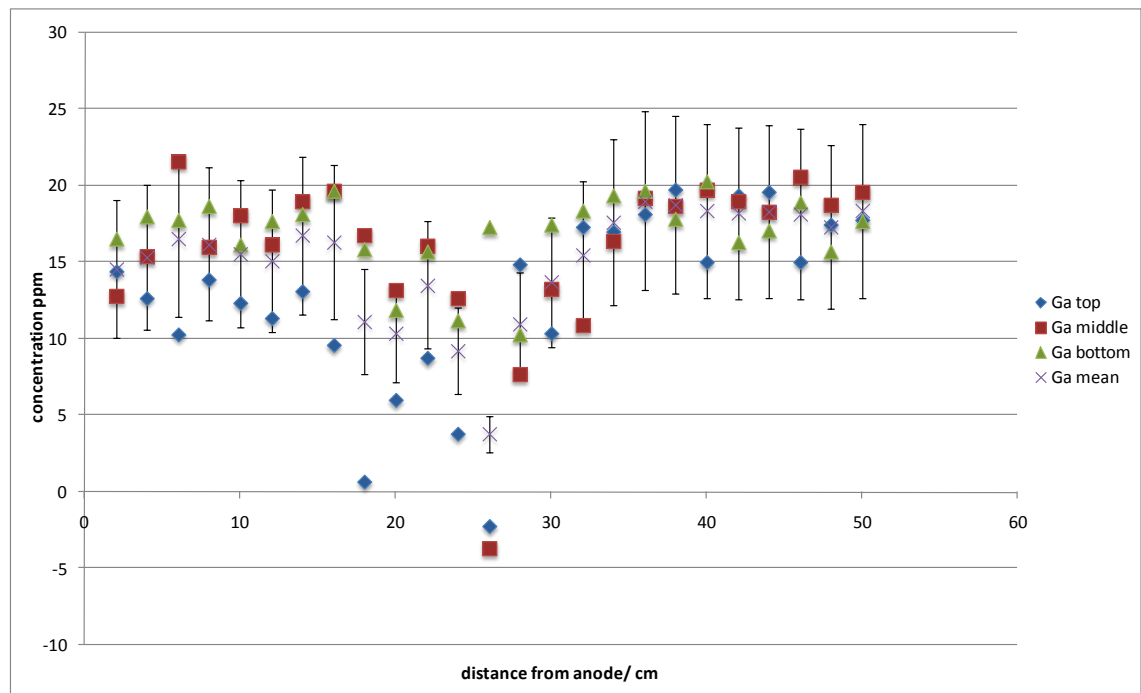
Molybdenum Tap Water



Molybdenum concentration across treated material in the experiment conducted with tap water electrolyte.

Shows the molybdenum concentration for the tap water experiment. As for the acetic acid, there is no considerable response to the treatment. The concentrations involved are low, and the mobility of the molybdenum appears negligible as a result of this treatment.

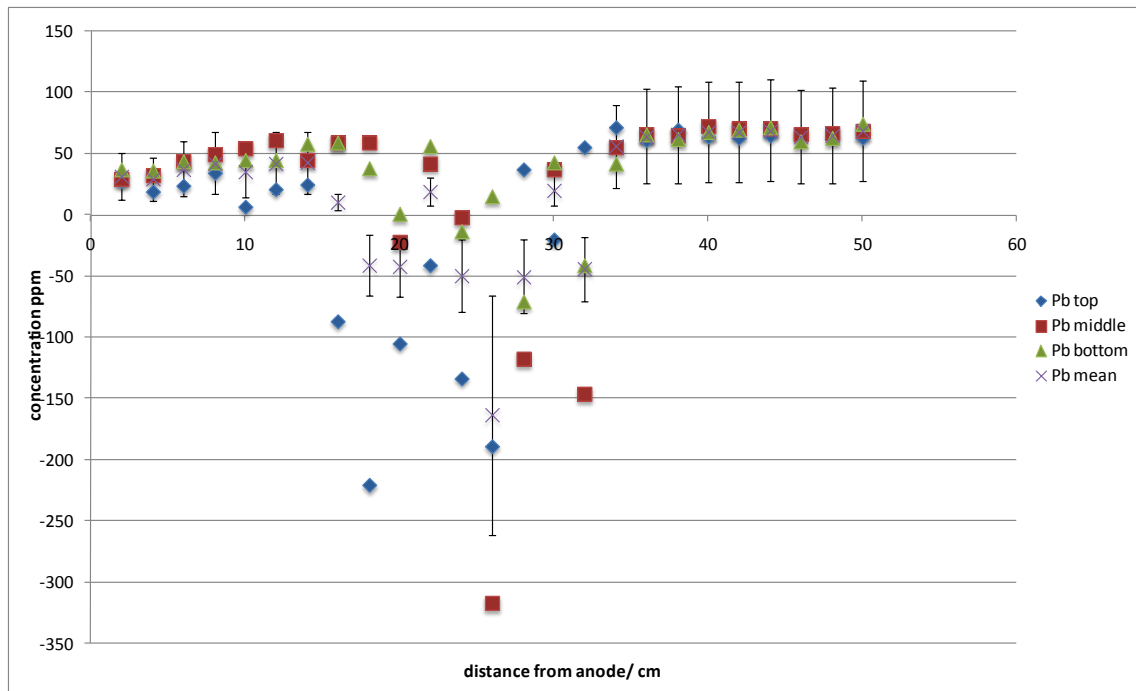
Gallium Acetic



Gallium concentration across treated material in the experiment conducted with acetic acid electrolyte.

Shows the concentration data obtained for gallium. There appears to be a drop in concentration associated with the iron mineralised zone. This is likely to indicate matrix effects/interference from the elevated iron concentration. This has resulted in some of the concentrations recording a negative value. The starting value for the gallium was found to be 16.54 ppm, consistent with the values obtained either side of the iron mineralised region. There was no estimate of bias for gallium due to unsuitable standards and the measurement uncertainty was estimated as 30.8%.

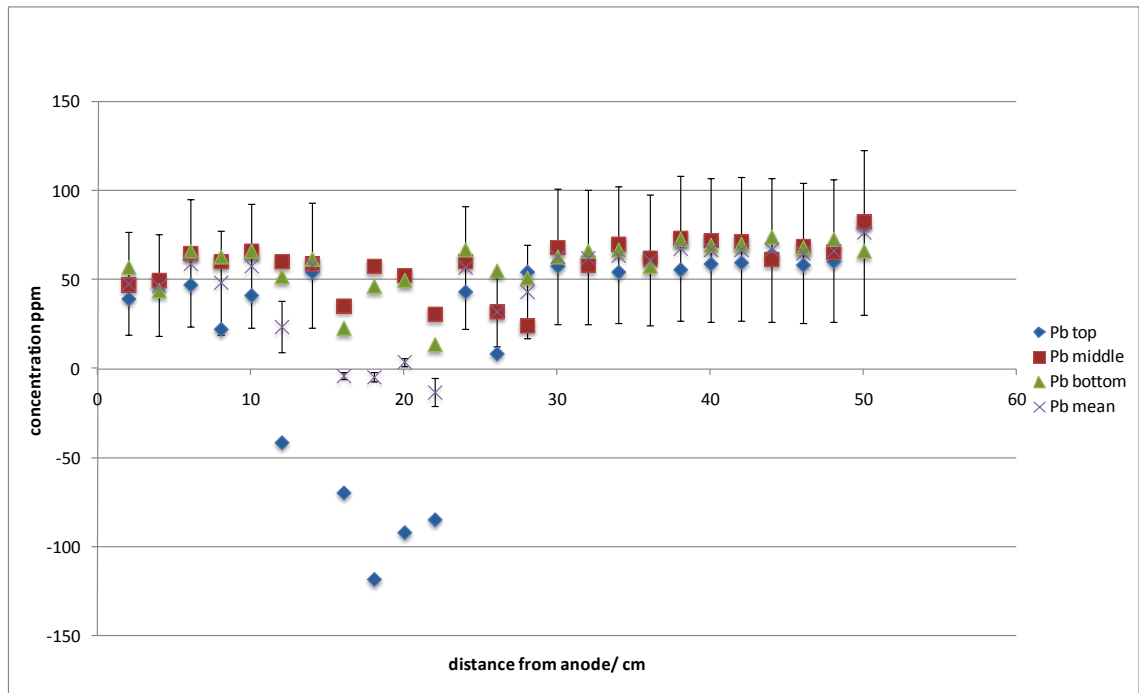
Lead Distribution Acetic



Lead concentration across treated material in the experiment conducted with acetic acid electrolyte.

The bias for the lead was calculated as + 4.9% this shows a very good level of systematic error although the random error was 60 % which, although high, does not affect the interpretation of the distribution of the lead at the concentrations found in the material.

Lead Distribution Tap Water



Lead concentration across treated material in the experiment conducted with tap water electrolyte.

In that experiment only the top section showed significantly negative values. This data shows negative values for all depths. Negative concentrations are obviously not physically achievable but arise due to the statistical method by which the XRF spectrometer detects and measures the emitted radiation. Essentially, negative values are obtained from the situation at low concentrations where the background radiation at a given energy is subtracted from a spectral peak to give a negative value (e.g. McNeill *et al.*, 2000).

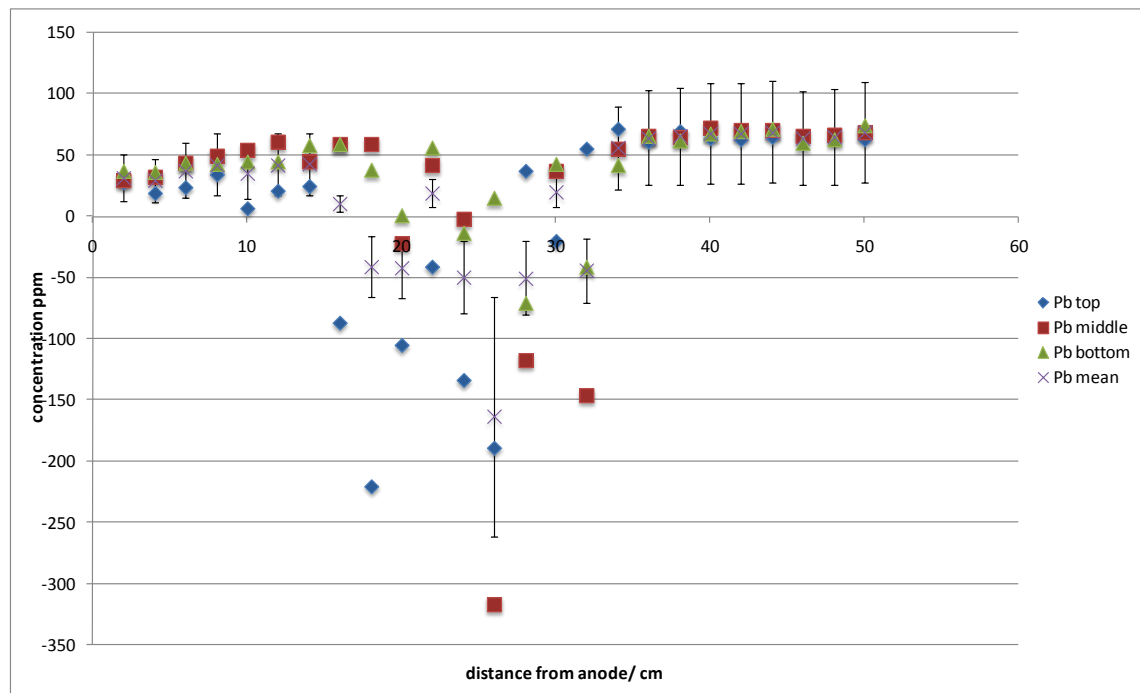
These values are therefore below the detection limit of the machine. There could also be matrix effects exacerbating the problems with detection of some elements in this region due to the expected high levels of iron and other metals which have accumulated here. The distribution of lead in the treated material demonstrates an overall depletion from around the anode zone but with negative values obtained for the region of iron deposition at the pH jump. The negative values are only obtained for the top section measurements. There are lower concentrations in the middle and bottom sections in the

iron mineralisation zone. The lead in the material has not responded to the treatment to the same extent as some of the species looked at.

The negative values can be ignored in this instance due to them being below the detection limit of the apparatus for the matrix. Since the proposed mechanism would result in a decrease in concentration of lead in the acidified region on the anode side with subsequent deposition at the point of pH jump the data obtained describes a distribution where there is very little lead present in the area of precipitation and fairly steady concentration gradients on either side of this region. This does not fit with the model and likely indicates that the lead measurements are subject to matrix effects in the precipitate region. Why lead appears to be particularly affected in this way is not clear, and should be verified with alternative analyses in future experiments.

The negative values measured in the region where these values were obtained correlate to the area of maximum metals concentration which suggests that there is interference issue.

Lead Acetic

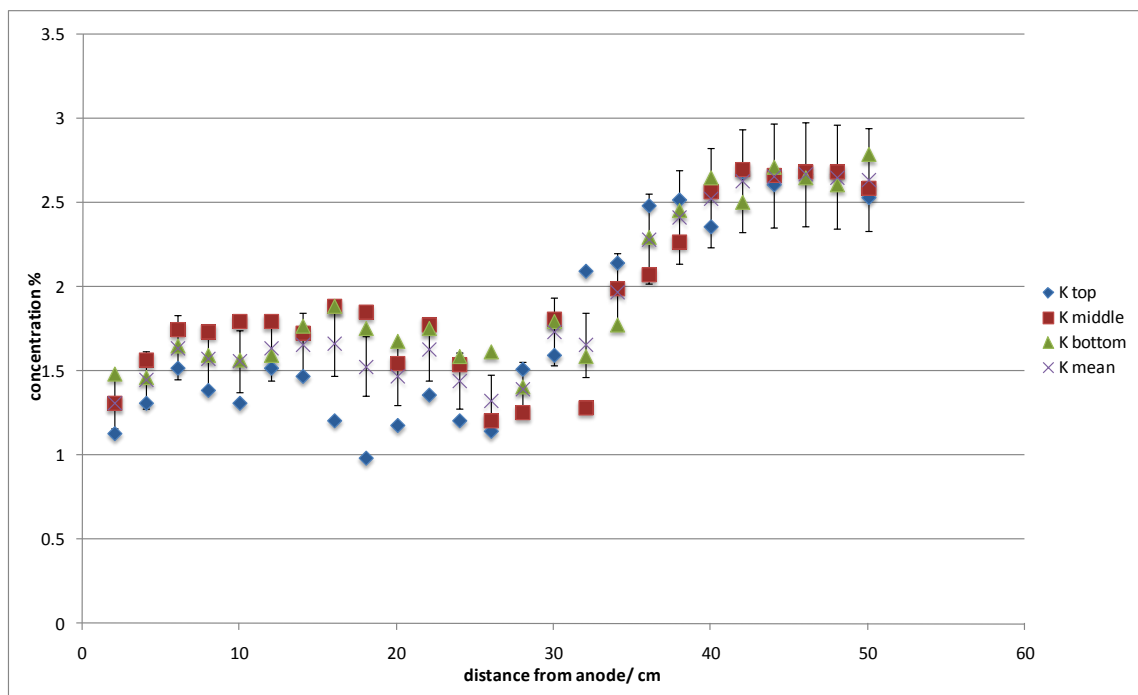


Lead concentration across treated material in the experiment conducted with acetic acid electrolyte.

The bias of the measurements calculated from the certified reference material was estimated as +4.9% and the measurement uncertainty was 60.07%. The disparity between these figures, with excellent agreement with the measured and certified values while having a large uncertainty associated with random error appears to be due to a large amount of localised variation of the lead content of the sediment. This is surprising as the samples are taken over such a small scale. The ANOVA analysis gives a percentage variance of 96.23% contributed to geochemical variations between the duplicates, with only 3.17% and 0.6% attributed to sampling and analysis respectively. This suggests significant geochemical variation between the duplicate samples taken. This might be affected by outliers which robust ANOVA can be susceptible to (Ramsey, 1998) and future work could confirm this. The sample area is currently used by fisherman and has, presumably, a long history of this kind of use, it may be that traces of a discarded lead fishing weight might have affected the localised concentrations of lead in the sample despite the measured levels of lead being fairly low.

Potassium Acetic

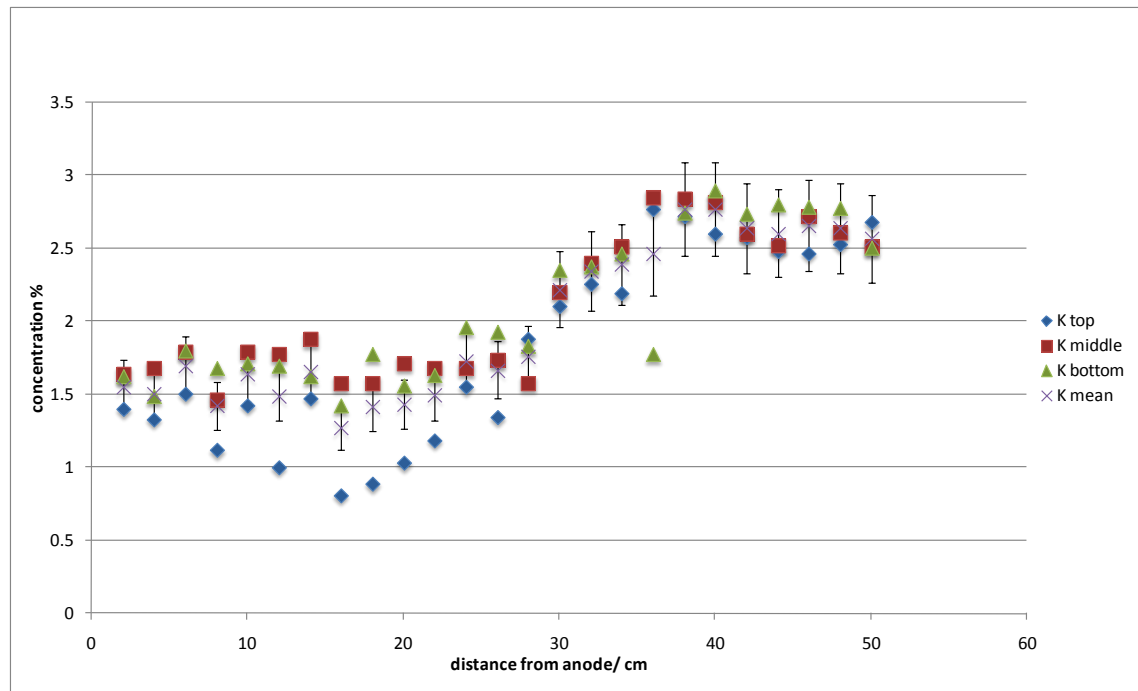
This might indicate that the response of the potassium is not particularly enhanced by the acetic acid conditioning agent, although there is enrichment at the cathode but no association with the region of iron mineralisation. The pre-treatment concentration of potassium in the material was calculated to be 1.73 %. Confirming that there is evidence for a significant response to the treatment.



Potassium concentration across treated material in the experiment conducted with acetic acid electrolyte.

The measurement uncertainty for the potassium measurements was good at 11.63% and the bias was +5.8% so the data can be considered high quality. The distribution of concentrations across the treated material in both the acetic and the tap water experiments are very similar in both cases.

Potassium Tap Water



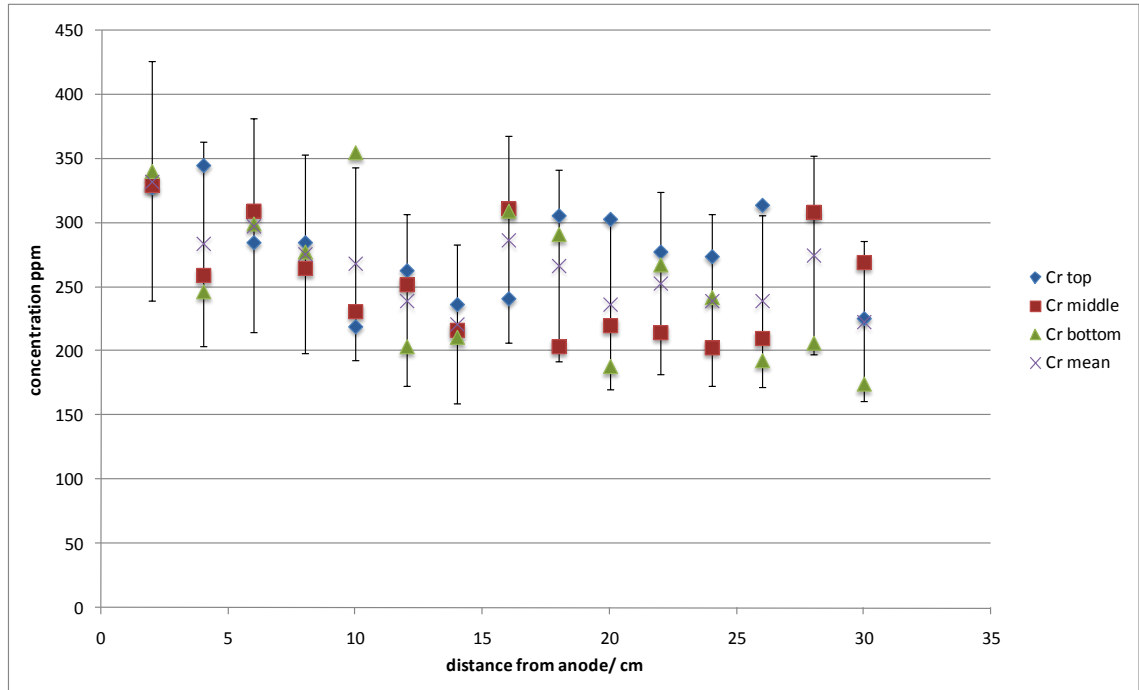
Potassium concentration across treated material in the experiment conducted with tap water electrolyte.

The distribution for the concentration of potassium for the tap water electrolyte. The distributions are similar between the two experiments with a visible reduction in the anode region and enrichment in the cathode region. Both experiments show a significant depth dependent distribution with greater reduction in the top layer on the anode side evidenced by lower concentrations for almost all measurements on the anode side.

There does not appear to be an association with the region of iron mineralisation. There is depletion and enrichment on the anode and cathode sides respectively for both experiments although interestingly there is no significant difference between the depletion and enrichment values obtained between the tap water and the acetic acid experiments suggesting in this case that the use of the acetic acid as a conditioning agent has a negligible effect on the efficiency of the treatment.

Hydro head supplemental elements.

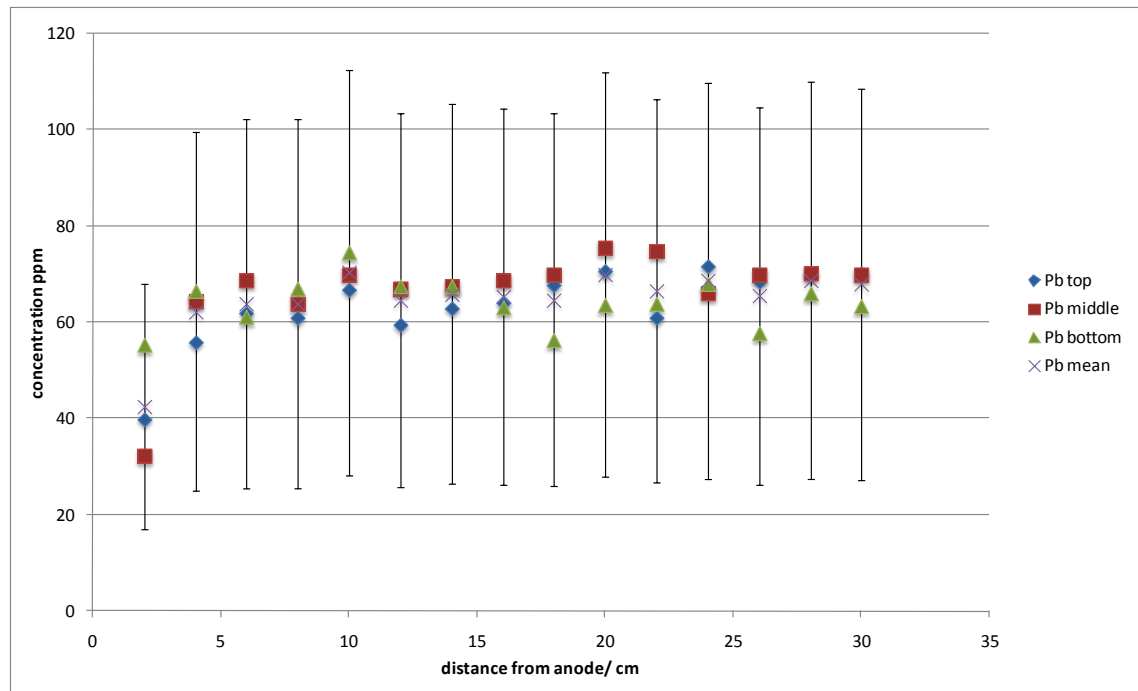
Cr



Cr concentration distribution post treatment in the hydraulic gradient experiment.

Chromium concentration post-treatment, as with previous experiments there is not a decisive change in concentration as a result of the treatment. The starting concentration for chromium pre-treatment was found to be 222.64 ppm so the data shows no significant response to the treatment.

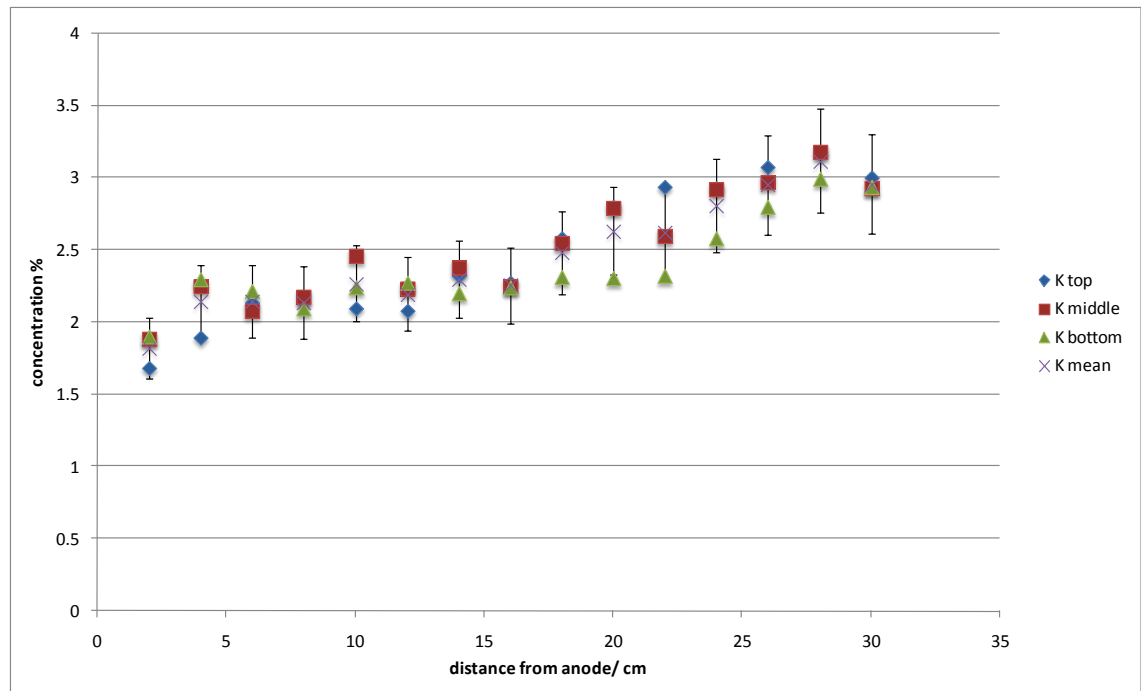
Pb



Pb concentration distribution post treatment in the hydraulic gradient experiment.

The measurements taken closest to the anode have a mean concentration of 40 ppm for the lead experiments. The mean concentration for the sediment pre-treatment was 61.44 ppm with a standard deviation of 11.1 ppm. This suggests that there has been a significant drop in the concentration in the area immediately adjacent to the anode electrode. But contrary to the results of the previously conducted experiments there is no apparent significant enrichment in the area where the iron precipitate was formed.

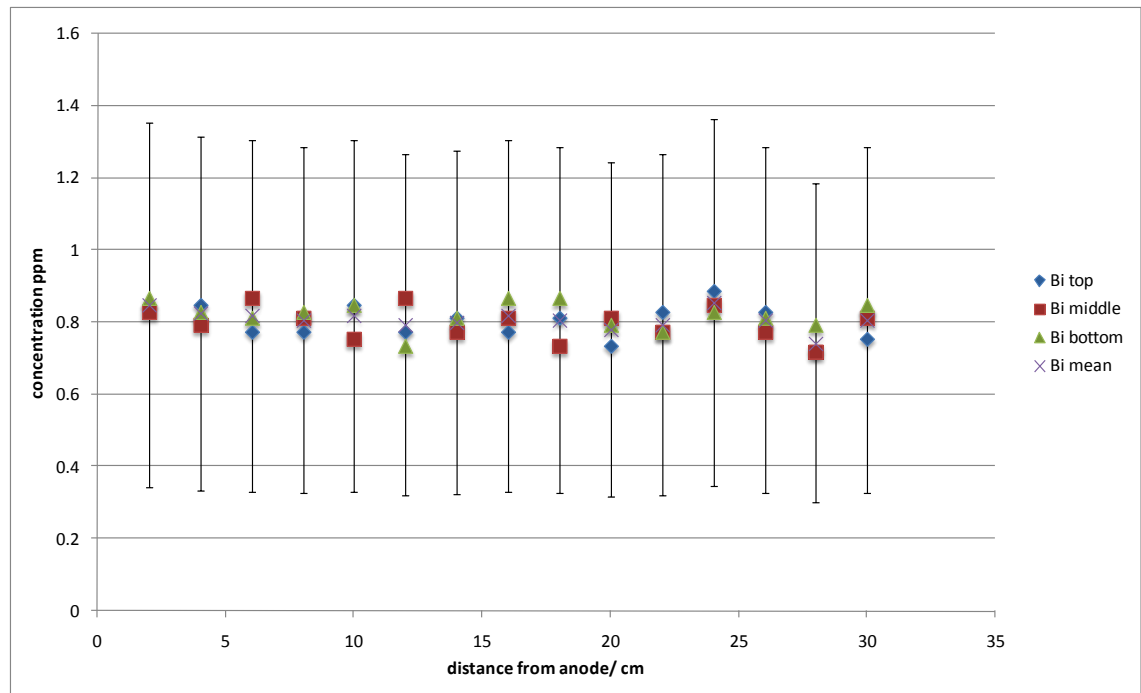
K



K concentration distribution post treatment in the hydraulic gradient experiment.

Shows a fairly familiar distribution graph for potassium with a definite but somewhat limited enrichment towards the cathode. The starting concentration was calculated to be 1.73 %, the associated error is also small. Once again though we see that there is enrichment against the direction of gravitational flow, but both the enrichment and depletion is relatively small with a maximum enrichment of around 25 % of the starting value.

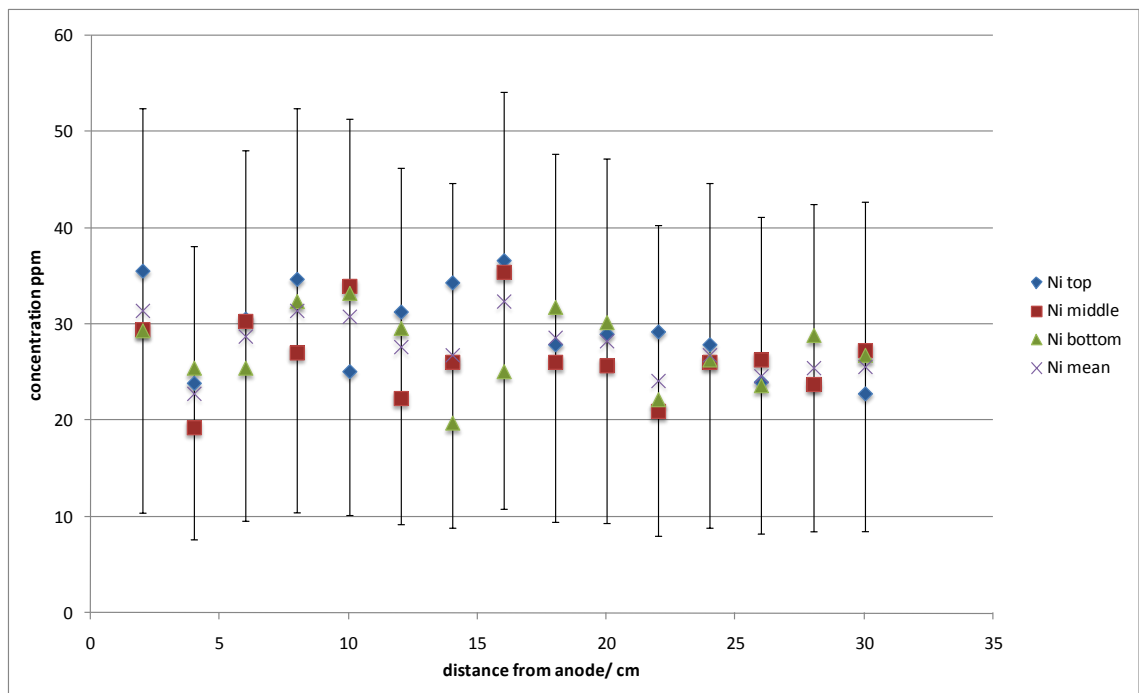
Bi



Bi concentration distribution post treatment in the hydraulic gradient experiment.

Bismuth appears to have no discernable response to the treatment, even though there was a more positive response in the previous tap water and acetic acid experiments. The previous experiments also indicated a depth dependent response with the top section showing the greatest mobilisation and enrichment which is not seen in the hydraulic head experiment.

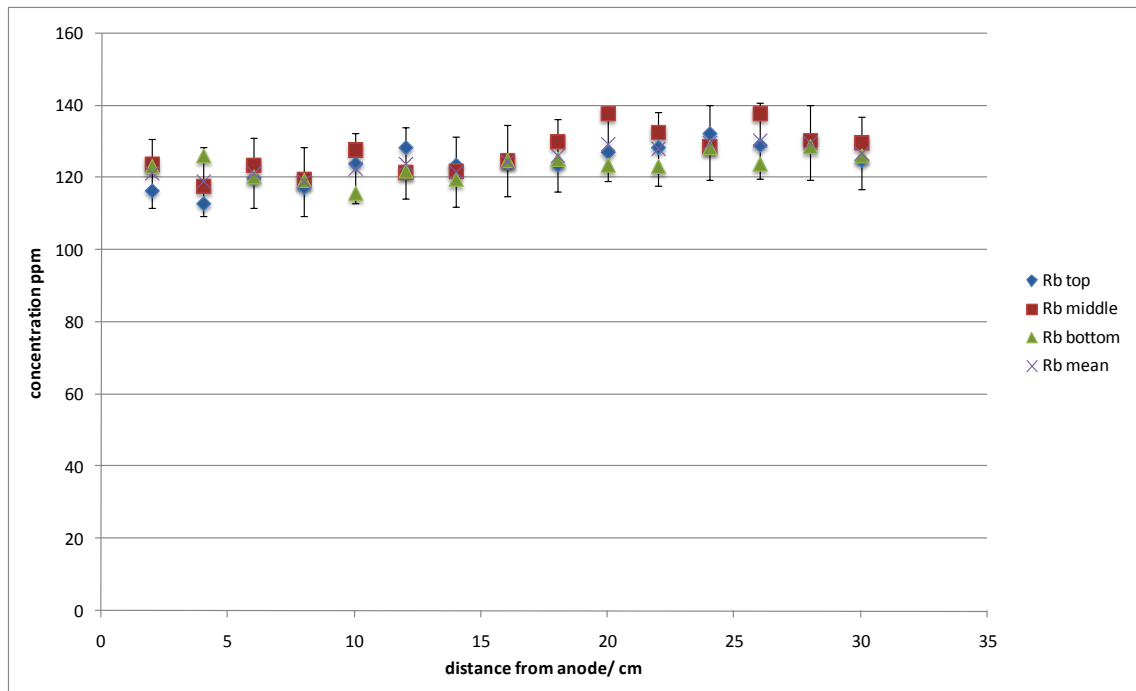
Ni



Ni concentration distribution post treatment in the hydraulic gradient experiment.

In the previous experiments on estuarine sediment the response of the nickel present was not particularly strong and in addition the measurement uncertainty is large. In the hydraulic head experiment there is also no appreciable response to the treatment

Rb

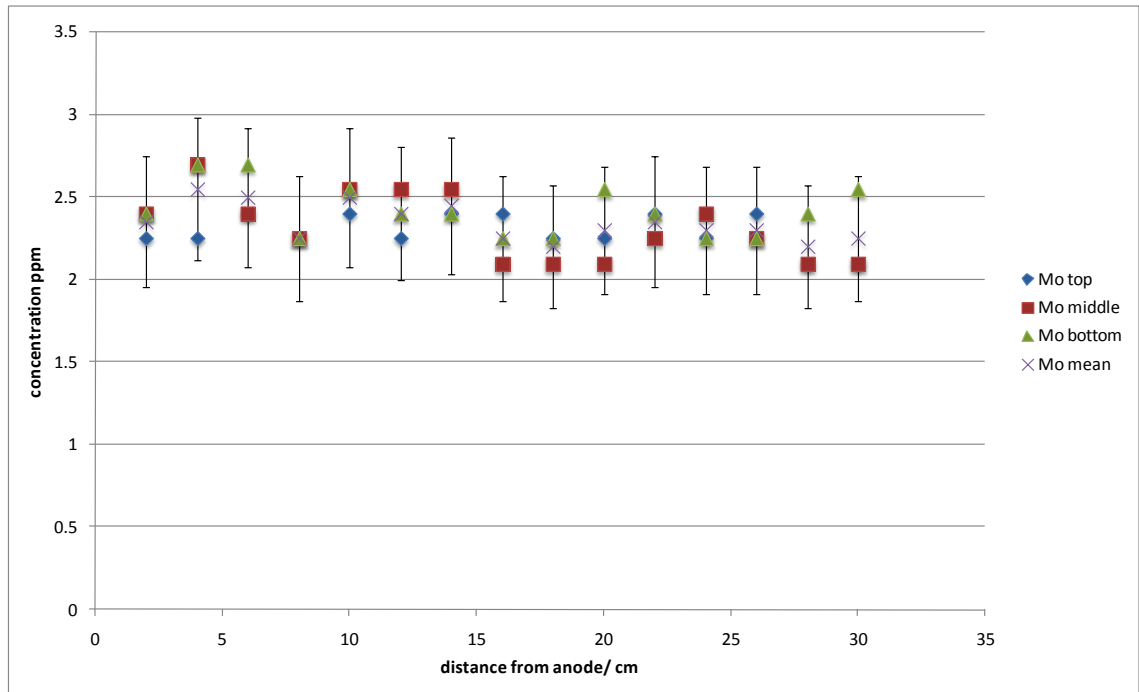


Rb concentration distribution post treatment in the hydraulic gradient experiment.

The rubidium present seems to have shown a minimal response if any at all, given that the starting concentration, pre-experiment was 116.94 ppm. It does however serve to indicate that the level of geochemical heterogeneity is low for this element.

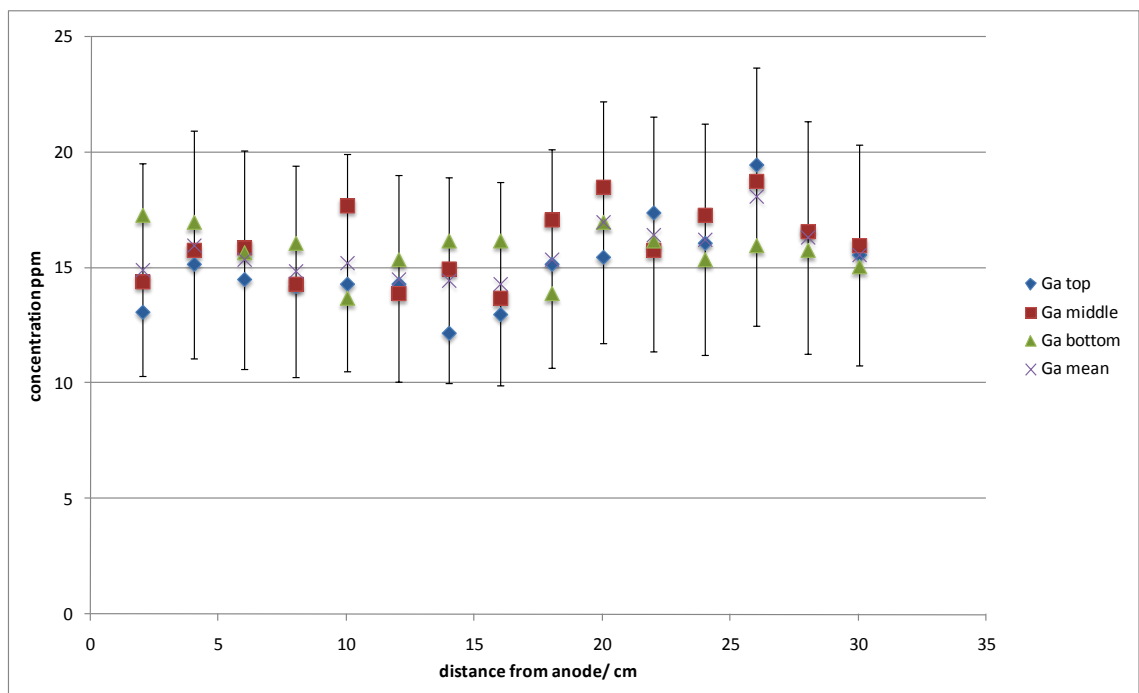
Mo

shows the distribution of the molybdenum after the experiment and, as observed in the tap water and acetic acid experiments described previously, there is no significant response to the treatment. The average starting concentration in the pre-treatment material for molybdenum was 1.48 and as the graph shows, there is no determinable deviation from this value in the treated material.



Mo concentration distribution post treatment in the hydraulic gradient experiment.

Ga

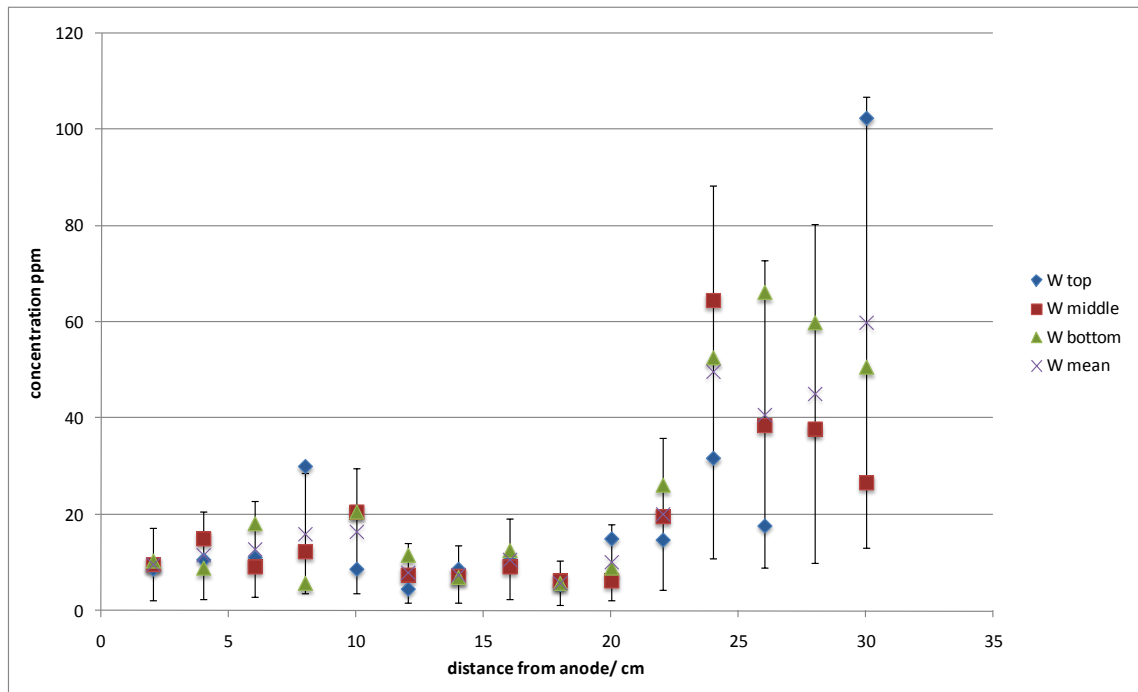


Ga concentration distribution post treatment in the hydraulic gradient experiment.

shows a similarly consistent output for gallium, with no discernable response to the treatment evident at this level of uncertainty. The pre-treatment average concentration

for gallium was calculated to be 16.54 ppm, considering the calculated uncertainty, there are no meaningful inferences to be made from this data.

W



W concentration distribution post treatment in the hydraulic gradient experiment.

Analysis of variance data for the hydraulic head and the static head experiments.

Strontium Analysis of Variance for lambda, using Adjusted SS for Tests

Source	DF	Seq SS	Adj SS	Adj MS	F	P
depth	2	0.0001530	0.0000458	0.0000229	0.23	0.795
treatment	1	0.0011024	0.0011024	0.0011024	11.10	0.001
distance	4	0.0299033	0.0269456	0.0067364	67.83	0.000
depth*treatment	2	0.0004519	0.0004519	0.0002260	2.28	0.109
depth*distance	8	0.0007508	0.0007513	0.0000939	0.95	0.484
treatment*distance	4	0.0022697	0.0022697	0.0005674	5.71	0.000
depth*treatment*distance	8	0.0005560	0.0005560	0.0000695	0.70	0.691
Error	90	0.0089381	0.0089381	0.0000993		
Total	119	0.0441252				

Arsenic Analysis of Variance for lambda, using Adjusted SS for Tests

Source	DF	Seq SS	Adj SS	Adj MS	F	P
depth	2	20.186	13.153	6.576	4.63	0.012
treat	1	15.425	15.425	15.425	10.86	0.001
distance zone	4	103.734	92.251	23.063	16.24	0.000
depth*treat	2	11.450	11.450	5.725	4.03	0.021
depth*distance zone	8	50.694	30.141	3.768	2.65	0.012
treat*distance zone	4	13.054	13.054	3.263	2.30	0.065
depth*treat*distance zone	8	41.612	41.612	5.201	3.66	0.001
Error	90	127.775	127.775	1.420		
Total	119	383.929				

S = 1.19152 R-Sq = 66.72% R-Sq(adj) = 56.00%

Iron Analysis of Variance for lambda, using Adjusted SS for Tests

Source	DF	Seq SS	Adj SS	Adj MS	F	P
depth	2	0.0000213	0.0000296	0.0000148	0.22	0.805
treat	1	0.0007419	0.0007419	0.0007419	10.88	0.001
distance zone	4	0.0214423	0.0193300	0.0048325	70.86	0.000
depth*treat	2	0.0003278	0.0003278	0.0001639	2.40	0.096
depth*distance zone	8	0.0010005	0.0009608	0.0001201	1.76	0.095
treat*distance zone	4	0.0011421	0.0011421	0.0002855	4.19	0.004
depth*treat*distance zone	8	0.0003791	0.0003791	0.0000474	0.69	0.695
Error	90	0.0061378	0.0061378	0.0000682		
Total	119	0.0311928				

S = 0.00825818 R-Sq = 80.32% R-Sq(adj) = 73.98%

Bromine Analysis of Variance for lambda, using Adjusted SS for Tests

Source	DF	Seq SS	Adj SS	Adj MS	F	P
depth	2	0.0033732	0.0025951	0.0012975	12.51	0.000
treat	1	0.0044137	0.0044137	0.0044137	42.57	0.000
distance zone	4	0.0818186	0.0677736	0.0169434	163.41	0.000
depth*treat	2	0.0004510	0.0004510	0.0002255	2.17	0.120
depth*distance zone	8	0.0006698	0.0007891	0.0000986	0.95	0.479
treat*distance zone	4	0.0076529	0.0076529	0.0019132	18.45	0.000
depth*treat*distance zone	8	0.0005715	0.0005715	0.0000714	0.69	0.700
Error	90	0.0093319	0.0093319	0.0001037		
Total	119	0.1082825				

S = 0.0101827 R-Sq = 91.38% R-Sq(adj) = 88.61%

Calcium Analysis of Variance for lambda, using Adjusted SS for Tests

Source	DF	Seq SS	Adj SS	Adj MS	F	P
depth	2	0.09448	0.09918	0.04959	1.42	0.246
treat	1	0.07483	0.07483	0.07483	2.15	0.146
distance zone	4	5.10582	5.35266	1.33817	38.40	0.000
depth*treat	2	0.00507	0.00507	0.00253	0.07	0.930
depth*distance zone	8	0.29519	0.26008	0.03251	0.93	0.494
treat*distance zone	4	0.54591	0.54591	0.13648	3.92	0.006
depth*treat*distance zone	8	0.12892	0.12892	0.01612	0.46	0.879
Error	90	3.13646	3.13646	0.03485		
Total	119	9.38668				

S = 0.186680 R-Sq = 66.59% R-Sq(adj) = 55.82%

Cobalt Analysis of Variance for lambda, using Adjusted SS for Tests

Source	DF	Seq SS	Adj SS	Adj MS	F	P
distance	4	0.1451951	0.1283663	0.0320916	60.72	0.000
treatment	1	0.0078696	0.0078696	0.0078696	14.89	0.000
depth1	2	0.0008491	0.0004570	0.0002285	0.43	0.650
distance*treatment	4	0.0101434	0.0101434	0.0025359	4.80	0.001
distance*depth1	8	0.0095291	0.0079499	0.0009937	1.88	0.073
treatment*depth1	2	0.0024260	0.0024260	0.0012130	2.30	0.107
distance*treatment*depth1	8	0.0027308	0.0027308	0.0003413	0.65	0.737
Error	90	0.0475651	0.0475651	0.0005285		
Total	119	0.2263081				

S = 0.0229891 R-Sq = 78.98% R-Sq(adj) = 72.21%

Manganese Analysis of Variance for lambda, using Adjusted SS for Tests

Source	DF	Seq SS	Adj SS	Adj MS	F	P
depth1	2	3.3389	1.5655	0.7828	1.78	0.175
treatment	1	3.6014	3.6014	3.6014	8.19	0.005
distance	4	151.3935	136.4084	34.1021	77.53	0.000
depth1*treatment	2	4.3145	4.3145	2.1572	4.90	0.010
depth1*distance	8	1.6356	2.1784	0.2723	0.62	0.760
treatment*distance	4	5.9526	5.9526	1.4881	3.38	0.013
depth1*treatment*distance	8	2.9931	2.9931	0.3741	0.85	0.561
Error	90	39.5849	39.5849	0.4398		
Total	119	212.8145				

S = 0.663198 R-Sq = 81.40% R-Sq(adj) = 75.41%

Copper Analysis of Variance for lambda, using Adjusted SS for Tests

Source	DF	Seq SS	Adj SS	Adj MS	F	P
depth1	2	5.514	0.871	0.436	0.22	0.806
treatment	1	190.311	190.311	190.311	94.23	0.000
distance	4	63.937	24.606	6.152	3.05	0.021
depth1*treatment	2	28.748	28.748	14.374	7.12	0.001
depth1*distance	8	67.936	44.149	5.519	2.73	0.010
treatment*distance	4	131.112	131.112	32.778	16.23	0.000
depth1*treatment*distance	8	40.616	40.616	5.077	2.51	0.016
Error	90	181.762	181.762	2.020		
Total	119	709.936				

S = 1.42112 R-Sq = 74.40% R-Sq(adj) = 66.15%

Zinc Analysis of Variance for lambda (1), using Adjusted SS for Tests

Source	DF	Seq SS	Adj SS	Adj MS	F	P
depth1	2	1112.6	540.5	270.2	0.89	0.415
treatment	1	3552.1	3552.1	3552.1	11.69	0.001
distance	4	2593.9	1691.0	422.7	1.39	0.243
depth1*treatment	2	3026.9	3026.9	1513.5	4.98	0.009
depth1*distance	8	1971.8	1695.7	212.0	0.70	0.693
treatment*distance	4	8557.1	8557.1	2139.3	7.04	0.000
depth1*treatment*distance	8	1897.3	1897.3	237.2	0.78	0.621
Error	90	27349.5	27349.5	303.9		
Total	119	50061.3				

S = 17.4322 R-Sq = 45.37% R-Sq(adj) = 27.76%

Vanadium Analysis of Variance for lambda, using Adjusted SS for Tests

Source	DF	Seq SS	Adj SS	Adj MS	F	P
depth1	2	4626.3	2936.3	1468.2	4.47	0.014
treatment	1	14603.2	14603.2	14603.2	44.47	0.000
distance	4	46339.3	36571.0	9142.8	27.84	0.000
depth1*treatment	2	2192.6	2192.6	1096.3	3.34	0.040
depth1*distance	8	8823.0	6465.7	808.2	2.46	0.019
treatment*distance	4	6979.8	6979.8	1745.0	5.31	0.001
depth1*treatment*distance	8	3890.6	3890.6	486.3	1.48	0.175
Error	90	29553.4	29553.4	328.4		
Total	119	117008.3				

S = 18.1210 R-Sq = 74.74% R-Sq(adj) = 66.60%

Zirconium Analysis of Variance for lambda, using Adjusted SS for Tests

Source	DF	Seq SS	Adj SS	Adj MS	F	P
depth1	2	6881.8	6350.3	3175.2	11.87	0.000
treatment	1	15517.1	15517.1	15517.1	57.99	0.000
distance	4	48465.8	41430.2	10357.6	38.71	0.000
depth1*treatment	2	19.6	19.6	9.8	0.04	0.964
depth1*distance	8	2052.9	1567.1	195.9	0.73	0.663
treatment*distance	4	3014.2	3014.2	753.5	2.82	0.030
depth1*treatment*distance	8	1833.6	1833.6	229.2	0.86	0.556
Error	90	24082.3	24082.3	267.6		
Total	119	101867.4				

S = 16.3579 R-Sq = 76.36% R-Sq(adj) = 68.74%

Titanium Analysis of Variance for lambda, using Adjusted SS for Tests

Source	DF	Seq SS	Adj SS	Adj MS	F	P
depth1	2	0.065221	0.047218	0.023609	6.37	0.003
treatment	1	0.174600	0.174600	0.174600	47.12	0.000
distance	4	1.052724	0.898439	0.224610	60.61	0.000
depth1*treatment	2	0.016168	0.016168	0.008084	2.18	0.119
depth1*distance	8	0.059287	0.055914	0.006989	1.89	0.072
treatment*distance	4	0.054311	0.054311	0.013578	3.66	0.008
depth1*treatment*distance	8	0.018239	0.018239	0.002280	0.62	0.763
Error	90	0.333517	0.333517	0.003706		
Total	119	1.774066				

S = 0.0608749 R-Sq = 81.20% R-Sq(adj) = 75.14 (8)